Dissertation

INDEPENDENT GENERATION AND CHARACTERIZATION OF 5,6-DIHYDRO-2-DEOXYURIDIN-6-YL

Submitted by
Kenneth Nolan Carter
Department of Chemistry

In partial fulfillment of the requirements
For the Degree of
Doctor of Philosophy

Colorado State University
Fort Collins, Colorado
Fall 2003

COLORADO STATE UNIVERSITY

August 1, 2003

WE HEREBY RECOMMEND THAT THE DISSERTATION PREPARED UNDER OUR SUPERVISION BY KENNETH NOLAN CARTER ENTITLED INDEPENDENT GENERATION AND CHARACTERIZATION OF 5,6-DIHYDRO-2-DEOXYURIDIN-6-YL BE ACCEPTED AS FULFILLING IN PART REQUIREMENTS FOR THE DEGREE OF DOCTOR OF PHILOSOPHY.

Committee on Graduate Work

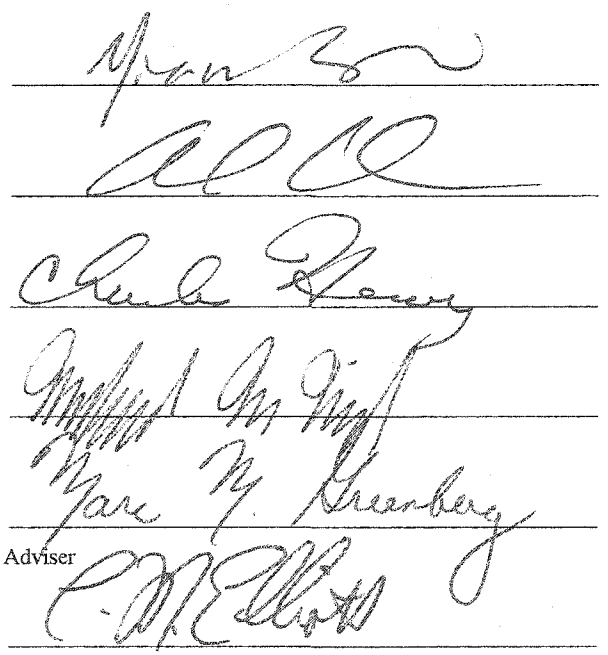

Adviser

Department Chair

Abstract of Dissertation

INDEPENDENT GENERATION AND CHARACTERIZATION OF 5,6-DIHYDRO-2'-DEOXYURIDIN-6-YL.

Design of a photolabile precursor (**122**) enabled the independent generation of 5,6-dihydro-2'-deoxyuridin-6-yl (**123**), a model for nucleobase radicals (**2, 15**) produced in DNA by ionizing radiation. Prior to generation in DNA, the reactivity of monomeric radical **123** was characterized. Using competitive kinetic methods, rate constants for the reaction of **123** with thiol and 2-deoxyribose sugar models were estimated. Under aerobic conditions, 2'-deoxyuridine C6-hydrate (**140**) is the major product of 5,6-dihydro-2'-deoxyuridin-6-yl. 2-Deoxyribonolactone (**133**) is produced in modest yield, the product of an intramolecular hydrogen atom abstraction reaction by the nucleobase peroxyl radical (**145**).

Incorporation of the radical precursor (**122**) into synthetic oligonucleotides allowed investigation of the role of a 5,6-dihydropyrimidin-6-yl in DNA damage. Generation of 5,6-dihydro-2'-deoxyuridin-6-yl (**123**) in DNA resulted in oxygen-dependent alkali-labile lesion formation at the site of the radical and at adjacent nucleotides. The mechanism of the DNA damage amplification process was elucidated by deuterium isotope effect measurements and examining the effects of modified nucleotides upon transfer of damage. It was determined that the nucleobase peroxyl radical (**158**) results in alkali-labile lesion formation at adjacent nucleotides by three distinct mechanisms: C1' hydrogen atom abstraction, C5 methyl hydrogen abstraction,

and addition to the nucleobase. The yield of tandem alkali-labile lesions was estimated to be ~ 65 % in duplex DNA, suggesting that the significance of this class of damage in the ionizing radiation mediated damage of nucleic acids may be vastly underestimated.

.

Kenneth Nolan Carter
Chemistry Department
Colorado State University
Ft. Collins, CO 80523
Fall, 2003

Table of Contents

List of Figures

List of Tables

List of Abbreviations

BME	2-mercaptoethanol
CIAP	calf intestinal alkaline phosphatase
CD	circular dichroism
CDTA	*trans*-1,2-diaminocyclohexane-*N, N, N', N'*-tetraacetic acid
dHT	5,6-dihydrothymidine
dHdU	5,6-dihydro-2'-deoxyuridine
DMEDA	*N, N'*-dimethylethylenediamine
DMTHF	2,5-dimethyltetrahydrofuran
DSB	double strand-break
DNA	deoxyribonucleic acid
EPR	electron paramagnetic resonance spectroscopy
EtOAc	ethyl acetate
Fpg	formamidopyrimidine DNA glycosylase
KIE	kinetic isotope effect
GSHOEt	glutathione ethyl ester
HPLC	high pressure liquid chromatography
LDA	lithiumdiisopropylamide
MALDI-TOF MS	matrix assisted laser desorption ionization time of flight mass spectrometry
NBS	N-bromosuccinimide

PAGE	polyacrylamide gel electrophoresis
polyT	polythymidylic acid
THF	tetrahydrofuran
Tris	tris(hydroxymethyl)aminomethane

1 Introduction.

The ability of ionizing radiation to damage DNA is the basis for its usefulness as a therapeutic agent in the treatment of cancer. Despite the biological significance of this process, the detailed chemical mechanisms of radiation induced nucleic acid damage remain elusive. As the major species initially formed, nucleobase radicals (**1-4**) are clearly key intermediates in this process (Figure 1).[1] One pathway by which these species can be formed is addition of radiolytically produced hydroxyl radical to the nucleobase.

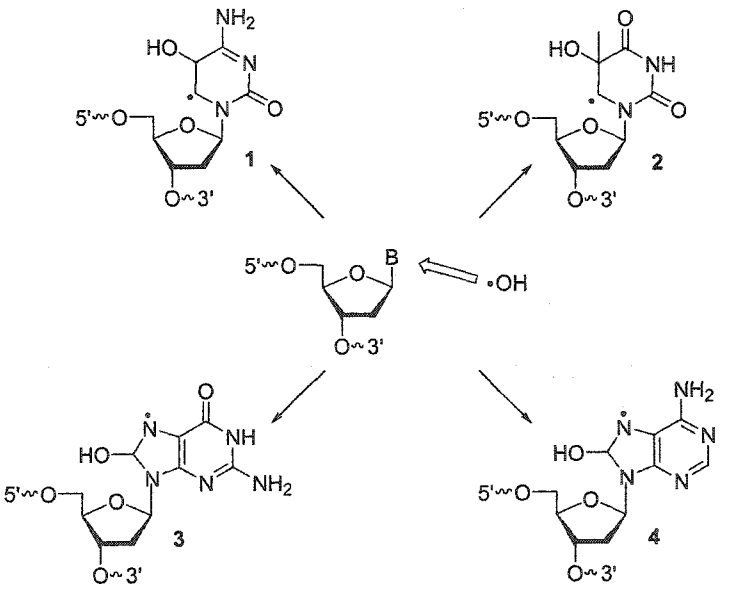

Figure 1. Products of hydroxyl radical attack on the four native nucleotides of DNA.

Purine adduct radicals (**3,4**) undergo further reactions to afford chemically modified nucleobases.[2-4] These species have deleterious biological consequences as they may lead to errors during DNA replication.[5] Although pyrimidine adduct radicals (**1,2**) can also result in the formation of modified nucleobases, these more reactive species are

believed to be capable of attacking the 2-deoxyribose sugar moiety of adjacent nucleotides, thus propagating damage along the strand in a process referred to as "DNA damage amplification" (Figure 2).[1,6-15] The resulting 2-deoxyribose sugar radical (**5**) may in turn result in the formation of direct strand breaks or alkali-labile lesions. The latter modifications represent damaged nucleotides which are converted to strand breaks upon base treatment. Radiation induced lesions which consist of two adjacent sites of damage are the subject of increasing interest due to their possible inhibition of DNA repair pathways.[16,17] In recent years, a number of these tandem lesions have been identified (Figure 3, **6-8**).[18-25]

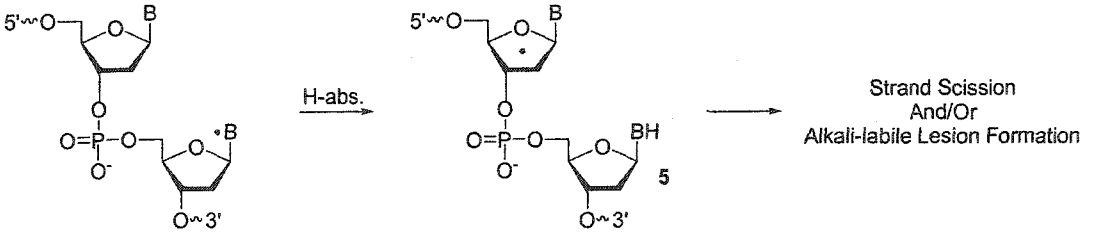

Figure 2. DNA damage amplification by a nucleobase radical.

The phenomenon of DNA damage amplification was first inferred from pulse radiolysis, ESR, and product studies.[1,6-15] Collectively, these observations provide strong evidence for a transfer of spin from initially formed nucleobase radicals to adjacent nucleotides. What remains to be clarified are the specific chemical mechanisms by which various nucleobase radicals lead to damage at neighboring sites. Furthermore, it is important to measure the extent to which DNA damage amplification occurs and assess the relative contributions of distinct reactions.

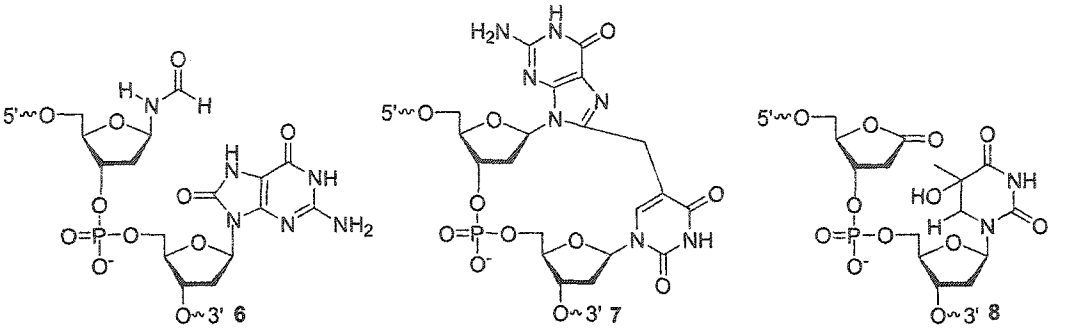

Figure 3. Tandem lesions (**6-8**) formed from nucleobase radicals.

The lack of a complete mechanistic understanding of ionizing radiation induced DNA damage is understandable in light of the complexity of this process. Mechanistic study of damage amplification pathways is impeded by the fact that γ-radiolysis of nucleic acids results in the formation of numerous reactive intermediates dispersed throughout the polymer. A strategy that has recently been adopted to facilitate the study of DNA radicals is independent generation of these species from modified nucleoside precursors.[26] These radical precursors are photolabile and upon UV irradiation produce the radical of interest. This method has been employed to study the reactivity of nucleic acid radicals in the monomeric form and in the biopolymer.[26] Generation of the radical of interest site-specifically enables detailed investigation of subsequent reactions.

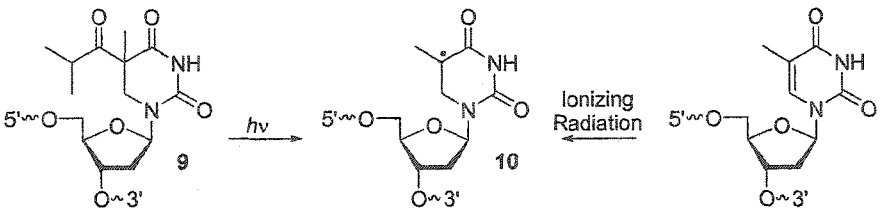

Figure 4. Generation of the 5,6-dihydrothymidin-5yl (**10**).

A salient example of this approach is the characterization of 5,6-dihydrothymidin-5-yl radical (**10**), a reactive intermediate generated by addition of a hydrogen atom to thymidine (Figure 4).[24] Independent generation of this species in oligonucleotides from an isopropyl ketone radical precursor (**9**) enabled the elucidation of the mechanism by which this species damages an adjacent nucleotide and led to the identification of tandem lesion **8**.

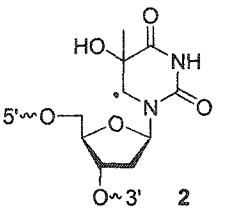

The thymidine hydroxyl radical adduct (**2**) has not been independently generated in DNA. Consequently, many questions regarding the reactivity of this and other pyrimidin-6-yl radicals remain unanswered. It has been proposed that **2** results in direct strand scission via a DNA damage amplification process.[1,6] Moreover, the intermediacy of **2** in the formation of tandem lesion **6** has been proposed.[20,23]

The monomeric hydroxyl radical adduct of thymidine (**12**) has been generated from a *m*-trifluorobenzoate precursor (**11**, Figure 5).[27] Independent generation of this

radical enabled the estimate of an upper limit for intramolecular hydrogen atom abstraction.[28] There are significant limitations associated with the use of this radical precursor (**11**). Most importantly, the photoinduced electron transfer conditions used to generate the nucleobase radical (**12**) are incompatible with the generation of this reactive intermediate in DNA. Furthermore, the presence of O_2 interferes with generation of **12**. This severely restricts the scope of mechanistic studies performed with the *m*-trifluorobenzoate radical precursor (**11**). Given the indirect evidence that hydroxyl radical adduct **2** and other 5,6-dihydropyrimidin-6-yl radicals are responsible for strand scission in DNA subjected to ionizing radiation, it was desirable to develop a new precursor to this class of nucleobase radical.

Independent generation of a 5,6-dihydropyrimidin-6-yl radical in DNA would enable detailed investigation of the mechanism(s) by which this reactive intermediate damages the biopolymer. Furthermore, the potential role of this type of nucleobase radical in the formation of tandem lesions could be investigated. The present research is aimed at developing a precursor capable of generating a 5,6-dihydropyrimidin-6-yl in DNA and elucidating the mechanism(s) by which this reactive intermediate further damages the biopolymer.

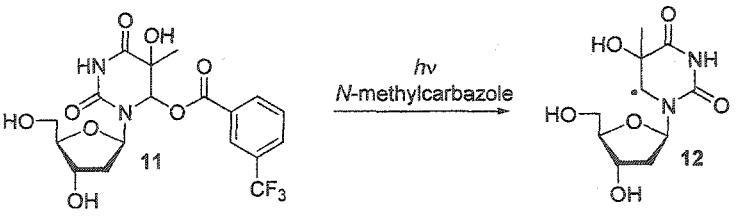

Figure 5. Independent generation of the hydroxyl radical adduct of thymidine.

2 Background

2.1 The Role of Nucleobase Radicals in DNA Damage.

Nucleobase radicals and radical ions (Figure 6, **2**, **10**, **13-17**) play a key role in ionizing radiation mediated nucleic acid damage. The direct strand breaks and alkali-labile lesions observed in nucleic acids subjected to ionizing radiation are believed to result largely from the reactions of these species.[1] Radical ions are formed via ionization of the nucleobase, a process which constitutes the so-called direct effect of ionizing radiation. Neutral radicals (**10**, **17**) may be formed via hydration/protonation of these species. Thymidine cation radical (**14**) can generate neutral nucleobase radicals by deprotonation reactions which are described below (Section 2.1.1). Alternatively, nucleobase radicals (**2**, **10**, **15-17**) may be formed by the so-called indirect effect of ionizing radiation. This refers to the reactions carried out by species derived from the radiolysis of water (H·, OH·, e_{aq}^-), which react primarily by addition to the nucleobase.

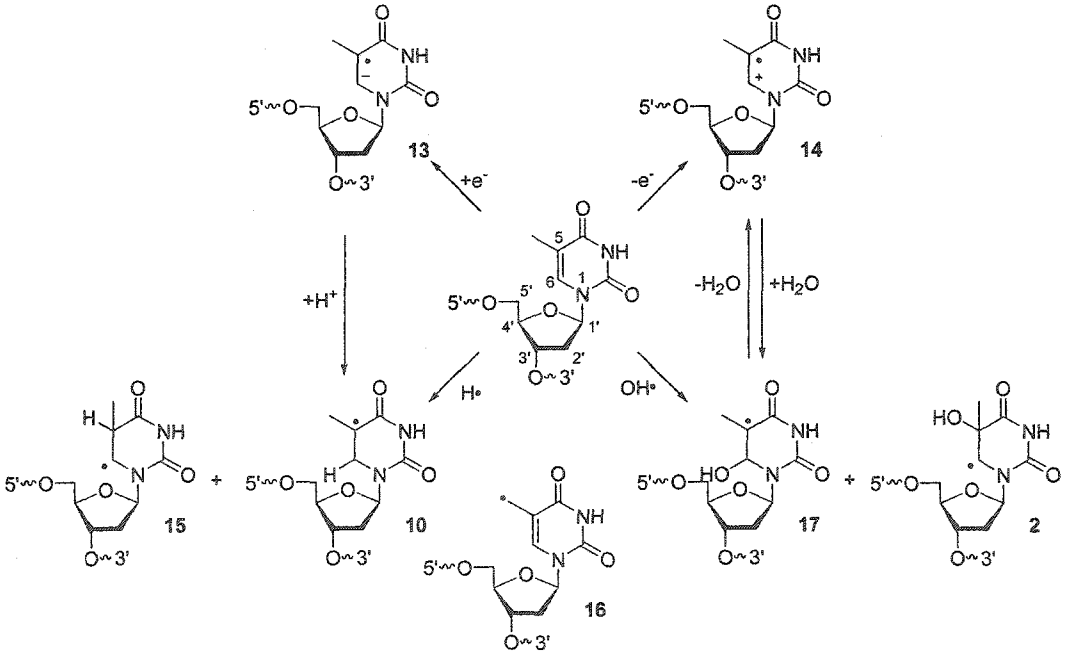

Figure 6. The direct and indirect effect of ionizing radiation upon thymidine.

2.1.1 The Direct Effect of Ionizing Radiation.

Ionization of DNA as a result of irradiation constitutes the so-called direct effect. It has been proposed that this process results in up to 50 % of the observed strand scission.[29,30] Irradiation of DNA gives rise to damage resulting from both the direct and indirect effects, the relative contributions of which are difficult to assess. In order to gain greater insight into the direct effect, researchers have utilized other methods of ionizing nucleic acids such as UV photolysis, photosensitization, and chemical oxidation.[31-35]

Experimental as well as computational studies indicate that purines are oxidized more readily than pyrimidines; the most easily oxidized base is 2'-deoxyguanosine.[2,36,37] UV-laser photolysis of DNA has been used to ionize the nucleobases and thereby model the direct effect of ionizing radiation.[38] The dG cation radical (**18**) can react by deprotonation or hydration (Figure 7). The major product of the hydration reaction is 8-oxo-2'-deoxyguanosine (**19**, 8-oxo-dG).[39] This reaction is favored in duplex DNA.[40] Deprotonation of the dG cation radical (**18**) to yield **20** followed by peroxyl radical (**21**) formation leads to the formation of an oxazolone lesion (**22**).[41]

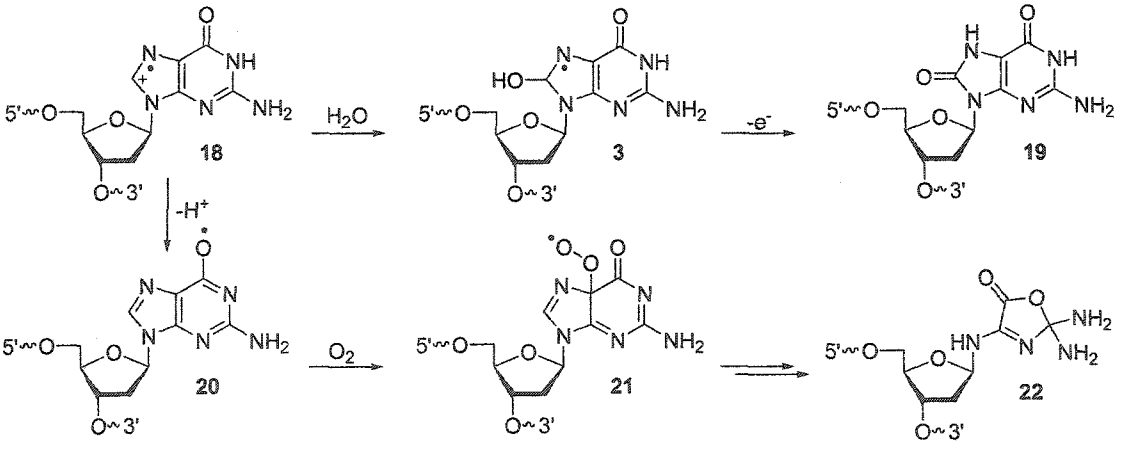

Figure 7. Products of the dG radical cation.

Oxidation by radiolytically produced $SO_4^{\cdot-}$ as well as photoinduced electron transfer have been utilized to investigate the reactivity of thymidine cation radicals. Pulse radiolysis studies by Deeble and co-workers using $SO_4^{\cdot-}$ as an oxidant indicated that under anoxic conditions formation of monomeric cation radical **23** is followed by hydration or deprotonation (Figure 8).[33] Hydration of the cation radical occurs exclusively at C6 to afford 5,6-dihydropyrimidin-5-yl **24**. Nucleobase radicals **25** and **26** are formed by deprotonation at N3 or the C5 methyl group. The presence of O_2 does not affect the rate of decay of the radical cation. However, the product radicals (**24-26**) are trapped to generate the corresponding peroxyl radicals. An alternative method of generating the thymidine cation radical (**23**), photosensitization of thymidine with menadione (MQ), has also been utilized to generate this species.[34,35]

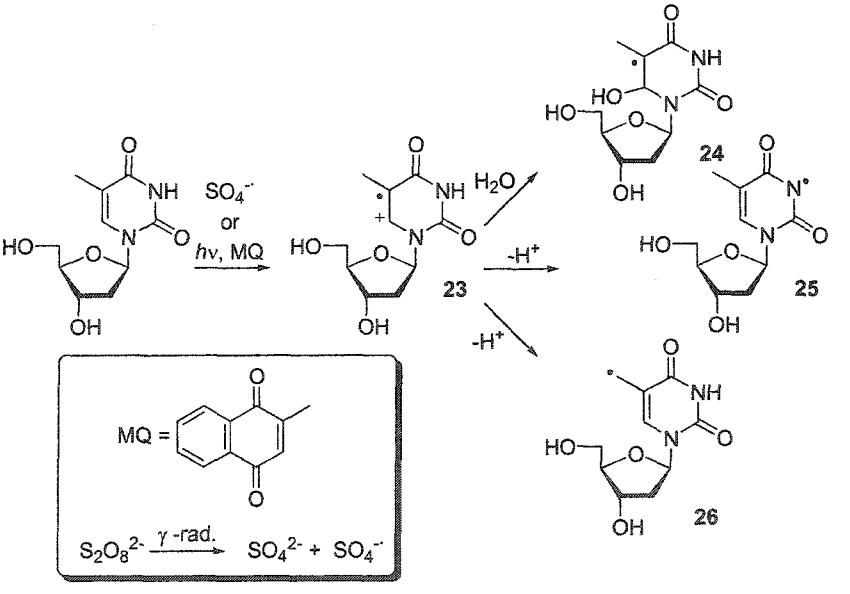

Figure 8. Generation of thymidine cation radical (**23**) by photosensitization or $SO_4^{\cdot-}$ oxidation.

Pyrimidine radical cations have been generated in polynucleotides under anaerobic conditions by laser ionization. O'Neill and co-workers used this technique to

ionize polyU as a model for the direct effect (Figure 9).[32] Transient absorption spectra of this process indicated that two pathways led to strand scission. The slow component of strand scission was proposed to result from the nucleobase cation radical (**27**) due to the fact that the rate of decay of this species correlated with the slow component of strand scission. A mechanism which was proposed to account for this process was deprotonation of the initially formed cation radical at N3 to generate neutral radical **28**. This species was then proposed to carry out an intranucleotidyl hydrogen atom abstraction reaction to generate a sugar centered radical (**29**), which in turn resulted in strand scission. Internucleotidyl hydrogen atom abstraction by the highly reactive N3 radical (**28**) was not ruled out.[42] The more rapid component of strand scission was proposed to result from direct ionization of a phosphate linkage.

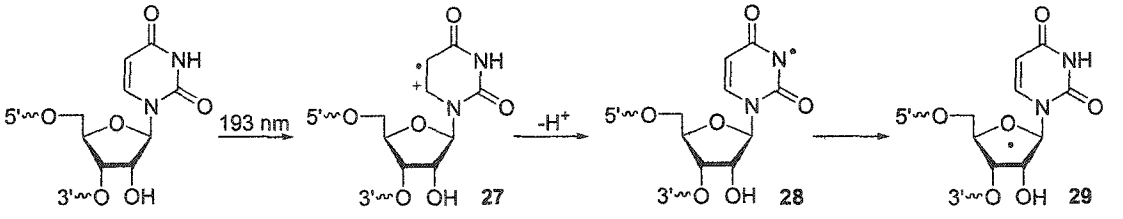

Figure 9. Photoionization of polyU induced by irradiation at 193 nm.

Formation of a one electron oxidized phosphate could result in the formation of a sugar radical by intramolecular hydrogen atom abstraction or deprotonation (Figure 10). Model studies by Steenken and co-workers using ribose-5-phosphate (**30**) indicate that the oxidized phosphate radical (**31**) can carry out an intramolecular C4' hydrogen atom abstraction with a rate constant of $> 10^7$ s^{-1} to generate a C4' ribose radical (**32**).[31] In nucleic acids, C4' radicals are known to result in strand scission.[43,44] In a recent low

temperature EPR study, Bernhard and co-workers concluded that a C3' radical (**34**) observed in a short oligonucleotide was formed via deprotonation of a nucleotide bearing an oxidized phosphate (**33**).[45] In addition to forming a 2-deoxyribose sugar radical, the oxidized phosphate could also react by oxidation of a neighboring nucleobase to generate a base cation radical (**35**).

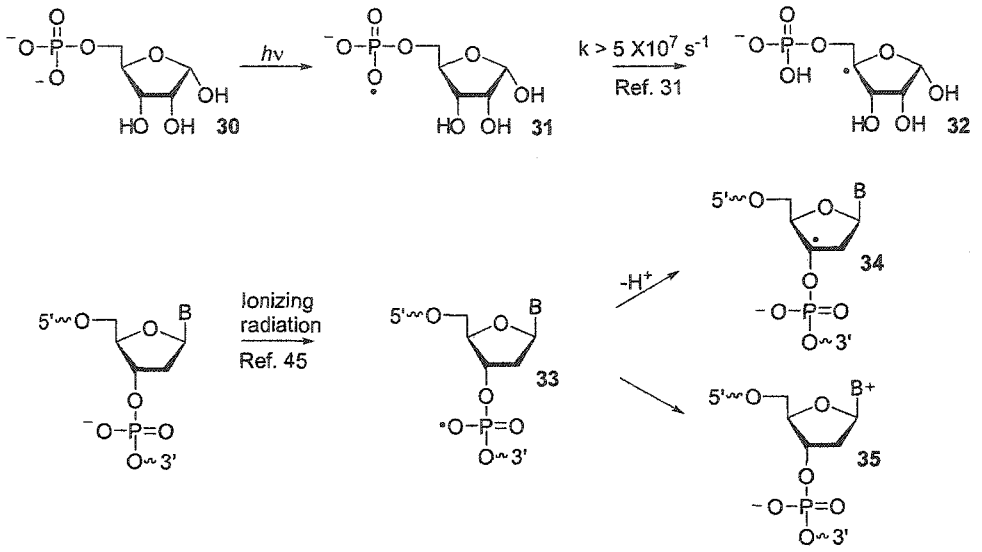

Figure 10. The reaction pathways of oxidized phosphates.

2.1.2 The Indirect Effect of Ionizing Radiation.

The attack of radiolytically produced reactive species such as hydrogen atoms, hydroxyl radicals, and solvated electrons produced from the ionization of water on DNA constitutes the "indirect effect". These species react primarily at the nucleobase. Purine nucleobase radicals result in base modifications while pyrimidine radicals are more reactive and are believed to result in direct strand scission.[3,6,10,11,14,46,47]

The major product of hydroxyl radical addition to dG is the C4 adduct radical (**39**, Figure 11). This accounts for up to 70 % of the reactions of hydroxyl radical with dG and can result in the formation of oxazolone **41**.[3,4] However, it should be noted that reduction of the strongly oxidizing dG radical (**40**) results in the reconstitution of dG. Addition to C8 accounts for ~ 17 % of the reactions of hydroxyl radical with dG. The products derived from the C8 adduct radical (**36**) vary depending upon the reaction conditions: under oxidizing conditions, 8-oxo-dG (**37**) is the major product, while formamidopyrimidine **38** is formed under reducing conditions. The remaining ~ 13 % of hydroxyl radical reactions consist of hydrogen atom abstraction from the 2-deoxyribose sugar.[4]

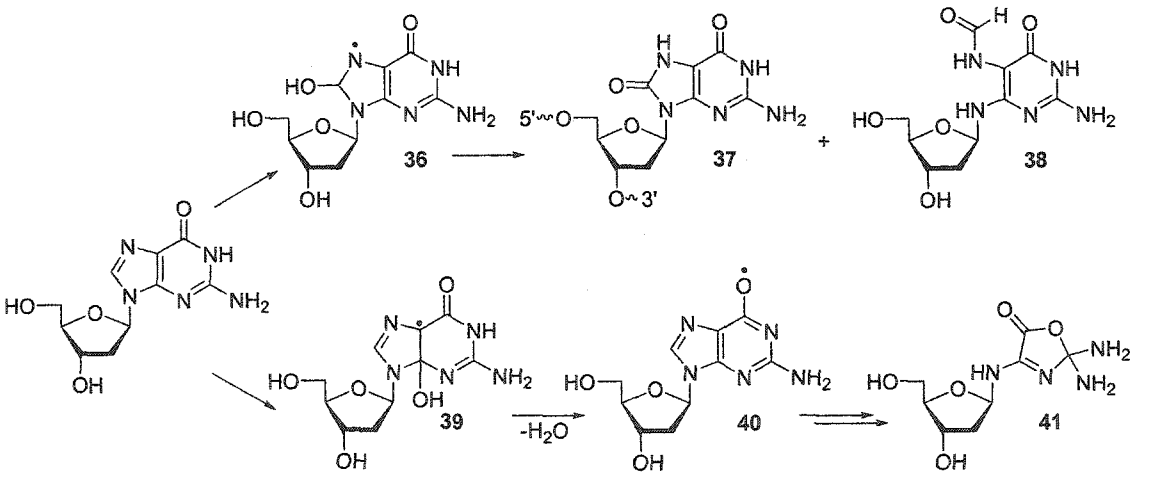

Figure 11. The reaction of hydroxyl radical with dG.

In reactions with thymidine, hydroxyl radical adds preferentially at C5 to form adduct radical **2** in a reaction that occurs with rates approaching diffusion control.[1] This species can undergo dehydration to afford cation radical **14** (Figure 12), a species also

generated by the direct effect, although this reaction may be slow at neutral pH.[10,28] Hydroxyl radical adduct **2** can undergo hydrogen atom transfer from a donor such as thiol to afford thymidine C5-hydrate **42** (Figure 12). Radical **2** is often referred to as reducing due to the fact that it is easily oxidized.[1] Formation of the C6 cation (**45**) followed by hydration affords thymidine glycol (**46**), a pyrimidine oxidation product commonly observed in DNA subjected to γ-radiolysis.[1,48,49] Alkyl radicals typically react very rapidly with O_2, and nucleobase radicals are no exception. The hydroxyl radical adduct (**2**) reacts with O_2 to afford a C6 peroxyl radical (**43**). Peroxyl radical **43** may eliminate superoxide as this process has been observed for related nucleobase radicals.[50,51] Alternatively, the peroxyl radical (**43**) may undergo reduction to generate a C6 hydroperoxide (**44**).

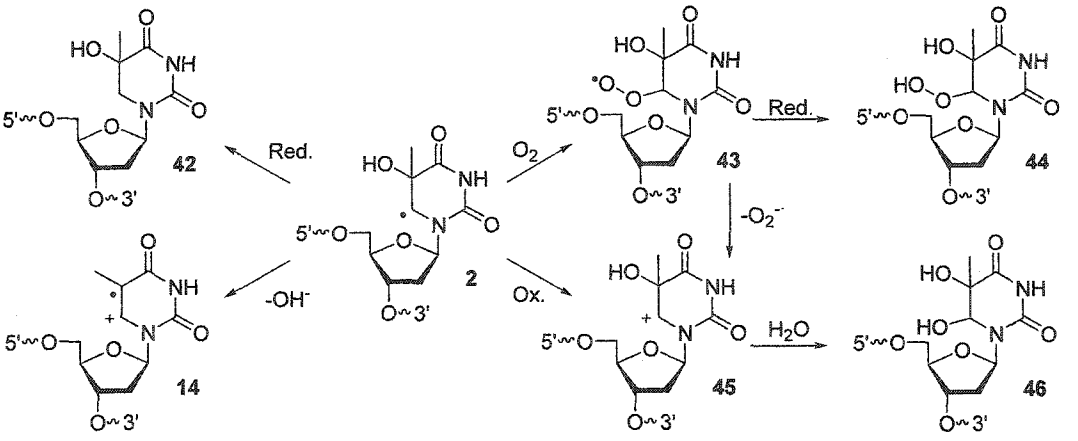

Figure 12. The reactions of the thymidine C5 hydroxyl radical adduct (**2**).

Monomeric nucleoside hydroperoxide **44** has a half-life of ~ 1-10 h in neutral aqueous solution, depending upon the stereochemistry at the C5 position. The principal

mechanism of decomposition is believed to be elimination of H_2O to form a barbituric acid derivative (**47**) followed by ring opening to afford tartonoylurea **48** (Figure 13).[52]

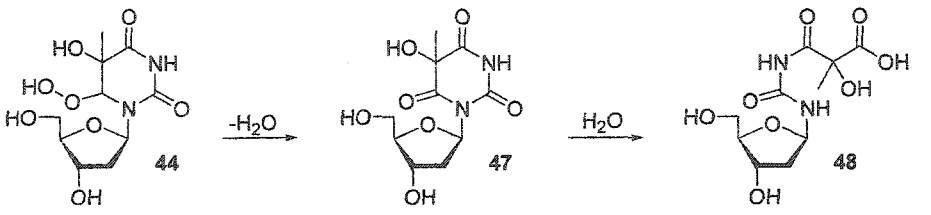

Figure 13. Decomposition of 5-hydroxy-6-hydroperoxyl-5,6-dihydrothymidine (**44**).

The C6 hydrogen atom adduct of thymidine (**10**, Figure 14) can undergo reactions analogous to those of the C5 hydroxyl radical adduct (**2**). In contrast to **2**, radical **10** is easily reduced due to the fact that the resulting anion (**52**) is stabilized.[1,49] Reduction of **10** followed by protonation, or hydrogen atom transfer affords 5,6-dihydro-2'-deoxyuridine (**49**). Formation of the C5 peroxyl radical and subsequent hydrogen atom transfer generates C5 hydroperoxide **51**.

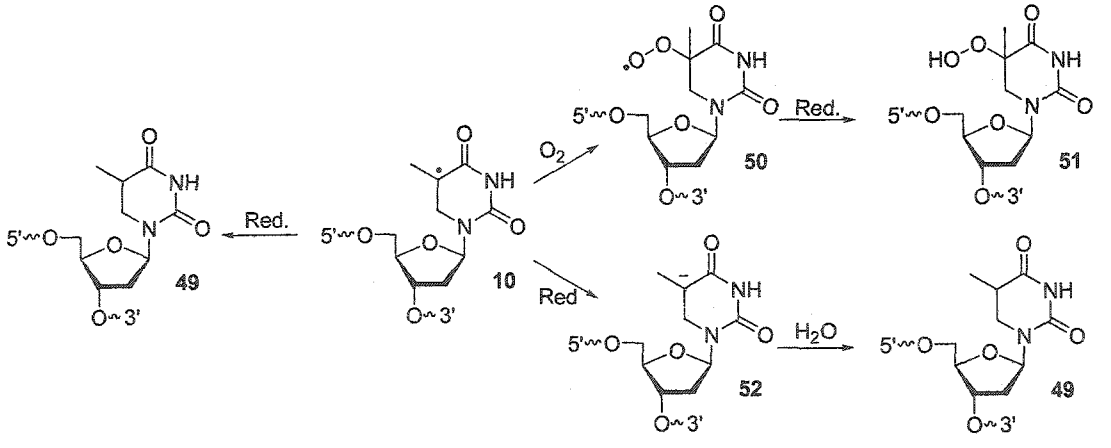

Figure 14. Reactivity of the C5 hydrogen atom adduct of thymidine (**10**).

Methyl radical **16** is the thymidine nucleobase radical formed in lowest yield. In addition to being formed from cation radical **14** which results from the direct effect, abstraction of a hydrogen atom from the methyl group of thymidine can also generate this reactive intermediate.[33,49] In the presence of oxygen, hydroperoxide **53** is formed. The hydroperoxide (**53**) can decompose to form hydroxymethyl thymidine (**54**) and 5'-formyl-2'-deoxyuridine (**55**, Figure 15).[49,53,54]

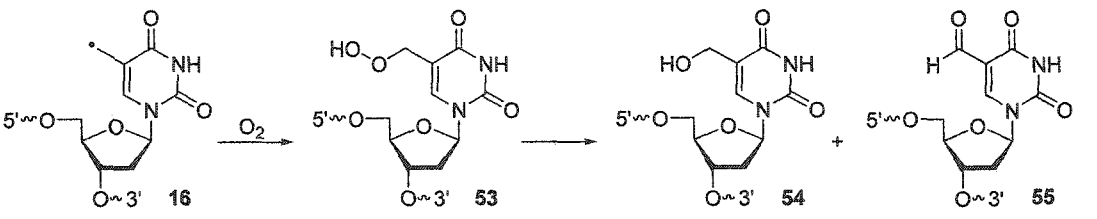

Figure 15. Products formed from the thymidine methyl radical (**16**) in the presence of oxygen.

2.2 Nucleobase Radicals and DNA Damage Amplification.

Nucleobase radicals/radical ions, and the peroxyl radicals derived thereof react with the 2-deoxyribose sugar moieties or nucleobases of adjacent nucleotides, resulting in two damaged sites from one initial chemical event.[1] This mode of reactivity is unique to nucleobase radicals. Furthermore, this process is apparently exclusive to pyrimidine radicals. Numerous studies have been conducted to determine the mechanism by which this occurs.[6-15]

A number of studies have focused on the radiation induced strand scission of polyuridylic acid, which has frequently been used as a model for DNA. Schulte-Frohlinde and co-workers estimated the efficiency of strand break formation induced by

hydroxyl radical at 41 %.[7] It is accepted that direct strand scission results from 2-deoxyribose sugar radicals, which implies that these species are formed efficiently by hydroxyl radical.[1] However, abstraction of a hydrogen atom from the sugar accounts for only ~ 7 % of the reactions of hydroxyl radical.[9] In order to reconcile these observations, it was concluded that initially formed nucleobase radicals react by hydrogen atom abstraction from the sugars of adjacent nucleotides. High yields of intact uracil were released upon irradiation. Presumably, uracil was released from nucleotides which had sustained damage to the ribose sugar moiety. This was interpreted as additional evidence that the ultimate yield of sugar centered radicals exceeded that which was initially formed by ionizing radiation, implying that nucleobase radicals abstract hydrogen atoms from adjacent sugar moieties (Figure 16).

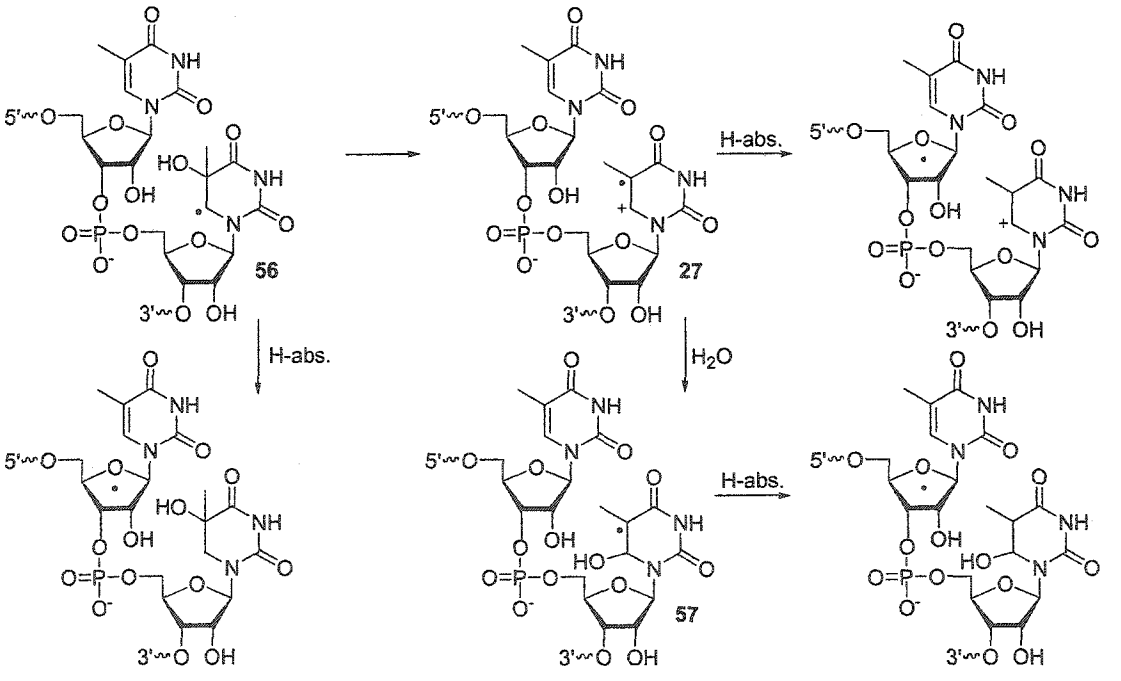

Figure 16. Radiolysis of polyuridylic acid.

Time resolved ESR studies of the hydroxyl radical induced strand scission of polyU under anaerobic conditions implicated the involvement of the uridine radical cation (Figure 16).[10] It was found that the rate of disappearance of the uridine hydroxyl radical adduct (**56**) was equal to that of strand scission. This is consistent with the notion that a rate limiting hydrogen atom abstraction reaction by the initially formed nucleobase radical results in strand scission. An increasing rate of strand scission with decreasing pH suggests that the radical cation (**27**) or a species derived thereof (**57**) leads to strand scission as well.

Product studies indicate that neutral nucleobase radicals can also result in strand scission. Dizdaroglu and co-workers subjected N_2O saturated solutions of poly-T and thymidine 5'-phosphate to γ-radiolysis and analyzed the relative amounts of 5-hydroxy-6-hydrothymine and thymine glycol liberated upon acid hydrolysis (Figure 17).[6] A significant difference in product distribution was observed between the mono- and polynucleotide. The major product of the radiolysis of thymidine was found to be thymidine glycol. This product is formed via oxidation of the C6 radical followed by hydration. In contrast, the major product observed in poly-T was 5-hydroxy-5,6-dihydrothymidine, the product of hydrogen atom abstraction by initially formed hydroxyl radical adduct. This product was proposed to result from intrastrand hydrogen atom abstraction from an adjacent 2-deoxyribose sugar. Moreover, the ratio of 5-hydroxy-5,6-dihydrothymidine to thymidine glycol was essentially the same in polyT and TpT. This indicates that the majority of internucleotidyl hydrogen atom abstraction occurs within one nucleotide of the initially formed radical. The position of the 2-deoxyribose sugar from which the hydrogen atom abstraction occurs is not apparent from this experiment.

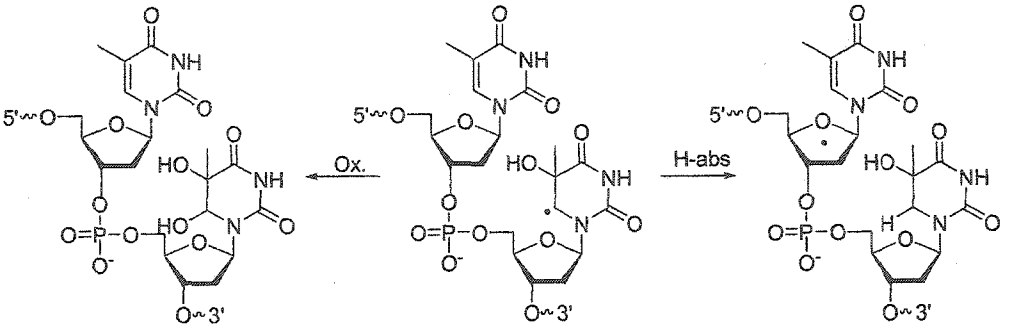

Figure 17. Competition between oxidation and hydrogen atom abstraction in polythymidylic acid.

In the presence of oxygen, intranucleotidyl hydrogen atom abstraction by peroxyl radicals is believed to result in strand scission (Figure 18). Von Sonntag and co-workers suggested that the strand scission resulting from the radiolysis of polyU in oxygenated solution resulted from abstraction of a hydrogen atom from the C3' position.[12] ESR studies indicate that the rate of strand scission is approximately equal to that of peroxyl

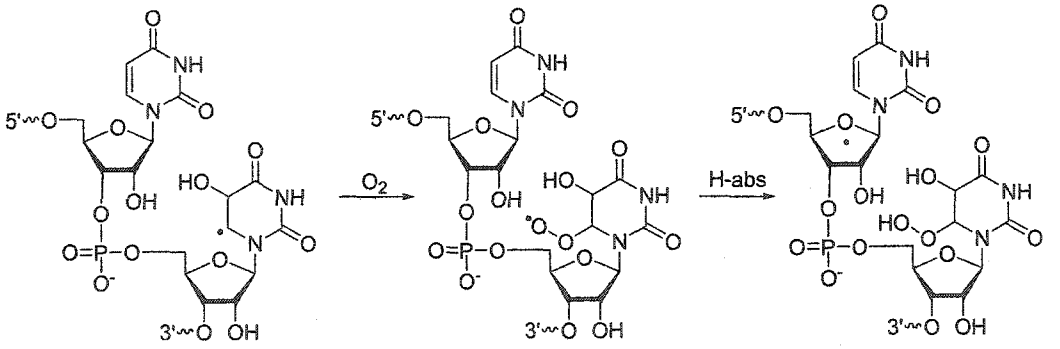

Figure 18. Radiolysis of polyU under aerobic conditions.

radical decay.[15] This reinforces the hypothesis that an internucleotidyl hydrogen atom abstraction reaction results in strand scission. Moreover, the presence of oxygen enhances strand breakage by a factor of ~ 1.6.[14]

2.3 2-Deoxyribose Radical Formation.

The above γ-radiolysis studies provide indirect evidence that initially formed nucleobase radicals and/or peroxyl radicals derived thereof react by abstraction of hydrogen atoms from the 2-deoxyribose sugar of adjacent nucleotides. Formation of 2-deoxyribose radicals can result in the formation of alkali-labile lesions or direct strand breaks. One of the unresolved questions regarding the mechanism by which radiolytically produced nucleobase radicals induce strand scission, is which position(s) of the 2-deoxyribose ring is attacked.

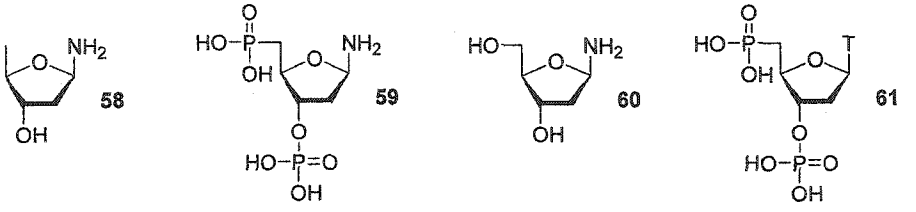

Figure 19. Models used in the computational study of DNA radicals.

Consideration of the stabilities of regioisomeric sugar radicals provides information with regard to which C-H hydrogen atom abstraction reactions are most thermodynamically feasible. Researchers have investigated the stabilities of DNA radicals by computational studies using model compounds (Figure 19).[55-59] Osman and co-workers estimated relative rate constants for hydrogen atom abstraction from 2-deoxyribose and determined that the expected order of hydrogen atom abstraction in a nucleoside was H1' > H4' ≈ H3' > H2'.[55] As this estimate was based upon calculations using **58** which lacks a C5' hydroxyl group, a value for C5' hydrogen atom abstraction

was not estimated. Direct abstraction of H1' by a diffusible species is disfavored in duplex DNA based upon the poor accessibility, but is feasible by a nucleobase radical which is formed within the duplex. A related study by Sevilla and co-workers using **59** as a nucleoside model, concluded that the relative energies of sugar radicals were C1' < C4' < C5' ~ C3' < C2'.[56] In this model, it was concluded that the presence of the phosphate groups resulted in destabilization of the C3' radical. On the basis of density functional theory calculations using **60** as a nucleoside model, Boyd and co-workers concluded that the C4' radical was the most stable of the 2-deoxyribose sugar radicals.[57] A recent *ab initio* study on thymidine diphosphoric acid (**61**) concluded that the relative order of radical stability was C4' > C5' > C1' > C3' > C2'.[58]

The fact that H2' is consistently predicted to be the poorest substrate for hydrogen atom abstraction in 2-deoxyribose points out a limitation associated with γ-radiolysis studies which use polyuridylic acid as a model for DNA. Calculations by Osman and co-workers indicate that the C-H bond strengths of ribose are very similar to one another, suggesting that experiments using RNA are biased towards H2' abstraction.[59]

Radicals formed at different positions of the 2-deoxyribose ring result in distinct types of DNA damage.[43] The sugar radical may react to produce an alkali-labile lesion, a DNA modification that renders the sugar phosphate backbone labile to base, or produce a strand break. Thus, the type of DNA damage observed provides information regarding the initially formed sugar radical.

2.3.1 C1' 2-Deoxyribose Sugar Radicals.

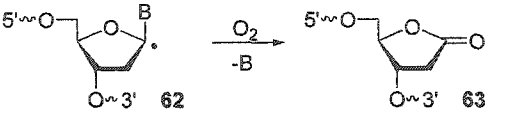

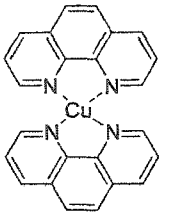

64

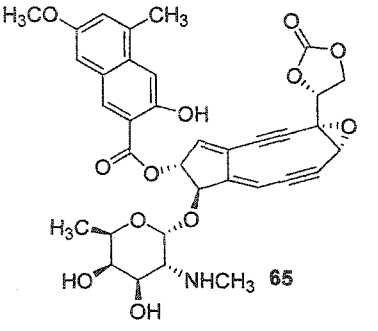

65

Generation of the C1' radical (**62**) in the presence of O_2 results in the formation of 2-deoxyribonolactone (**63**).[43] Although direct abstraction of the hydrogen atom from the C1' position of the 2-deoxyribose sugar is disfavored due to the inaccessibility of this position, this reaction has been observed for DNA cleaving agents such as copper phenanthroline (**64**) and neocarzinostatin (**65**).[60-62] Model studies in which a monomeric C1' radical (**66**) was generated independently indicate that generation of this reactive intermediate is followed by trapping with oxygen to generate the C1' peroxyl radical (**67**). Elimination of superoxide anion results in a C1' carbocation (**68**) which is trapped by water. Hydrolysis of **69** affords 2-deoxyribonolactone (**70**, Figure 20).[50, 63-66]

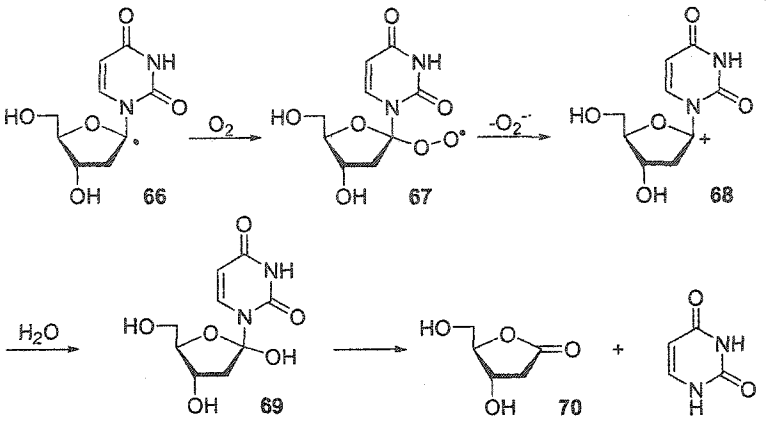

Figure 20. Mechanism of 2-deoxyribonolactone formation from a C1' radical.

2.3.2 C2' 2-Deoxyribose Sugar Radicals.

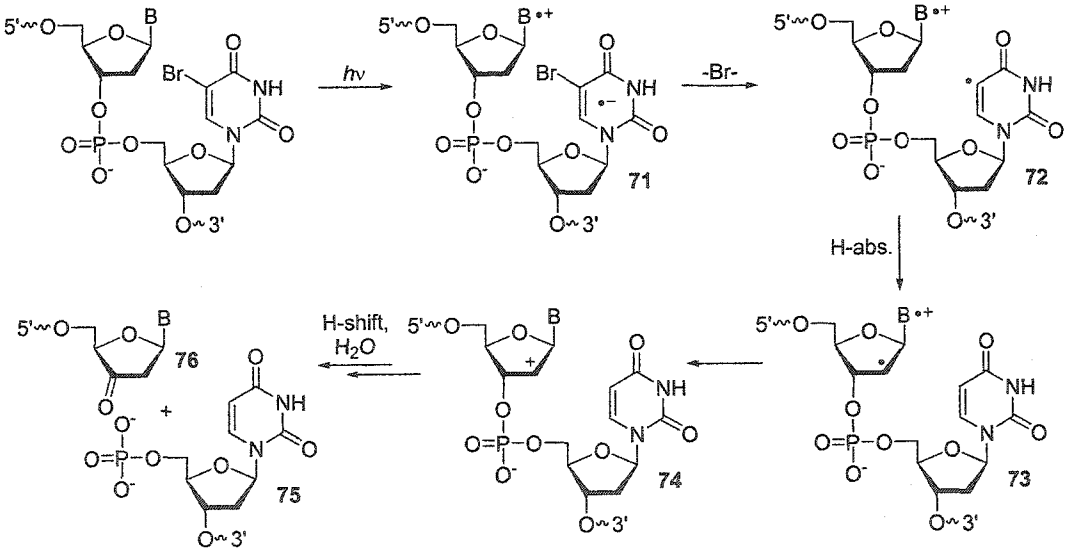

Figure 21. Direct strand breakage from a C2' radical under anaerobic conditions.

Abstraction of H2' is not a common pathway for DNA damaging agents.[43] This can be rationalized in terms of the calculated low stability of the C2' radical, relative to

other 2-deoxyribose radicals.[55-58] The reactivity of C2' radicals has been studied primarily in the context of DNA damage induced by 5-halo-2'-deoxyuridine species. The mechanism of this process has been the subject of several studies.[67-72]

Upon photolysis, 5-bromo-2'-deoxyuridine undergoes photoinduced electron transfer with a neighboring nucleotide to produce a nucleobase radical anion (**71**) which eliminates bromide to generate a highly reactive 2'-deoxyuridin-5-yl-radical (**72**, Figure 21). The sigma radical reacts in part by hydrogen atom abstraction from the C2' position of a neighboring nucleotide.[71] Under anaerobic conditions, this can result in the formation of a direct strand break.[67,68] It is proposed that the C2' radical (**73**) is oxidized by the nucleobase radical cation to generate a C2' carbocation (**74**). A subsequent hydride shift generates a C3' carbocation which reacts with water to give a phosphate fragment (**75**) as well as an unusual keto-nucleotide end-group (**76**, Figure 21). The generality of this mechanism for direct strand scission is limited by the requirement for a

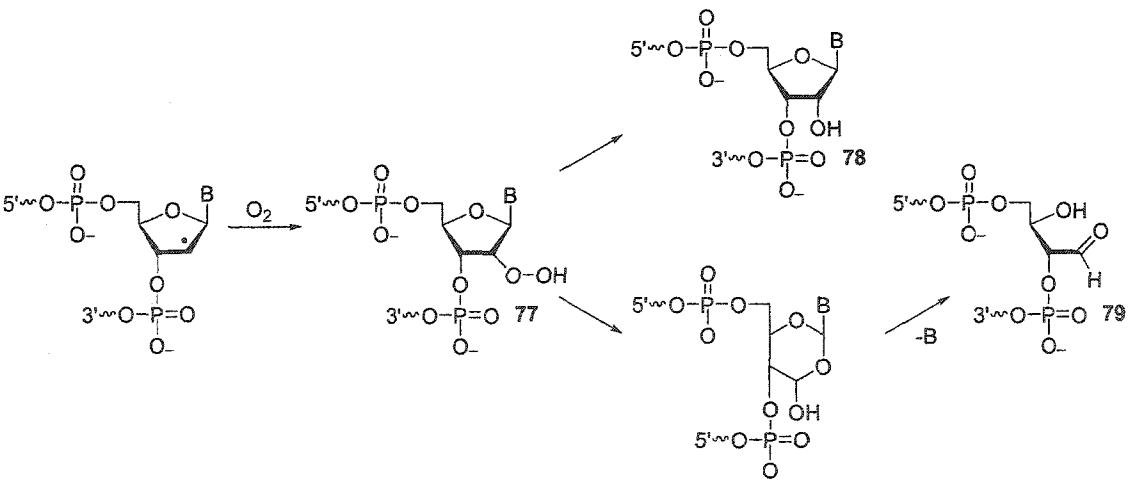

Figure 22. The formation of a C2' oxidized abasic site (**79**) from a C2' radical in the presence of oxygen.

a strong oxidant (in this case, a nucleobase cation radical) to produce the requisite C2' cation. Therefore, C2' radicals produced by other processes (viz.; hydrogen atom abstraction by an adjacent nucleobase radical) are unlikely to undergo this fragmentation.

Generation of a C2' radical in the 5-bromo-2'-deoxyuridine system under aerobic conditions results in alkali-labile lesion formation (Figure 22).[70] Reaction with oxygen converts the initially formed C2' radical to the C2' hydroperoxide (**77**). This species can either produce a C2' hydroxylated site (**78**) or undergo a Criegee-type ring expansion and subsequent hydrolysis to form abasic site **79**. Formation of the abasic site (**79**) is generally favored relative to C2' hydroxylation (**78**).[72]

2.3.3 C3' 2-Deoxyribose Sugar Radicals.

The reactivity of the C3' 2-deoxyribose radical has not been extensively studied owing to the paucity of DNA damaging reagents which react by abstraction of H3'. The only DNA damaging agents thus far for which this represents a major pathway are the photoactive complexes of Rh (III) such as **80** studied by Barton and co-workers.[73-75] These species bind in the major groove of the duplex and produce direct strand breaks by both oxygen independent and dependent pathways.

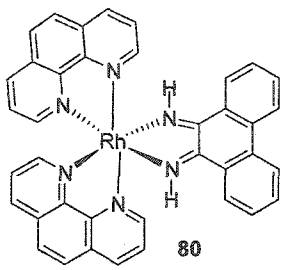

80

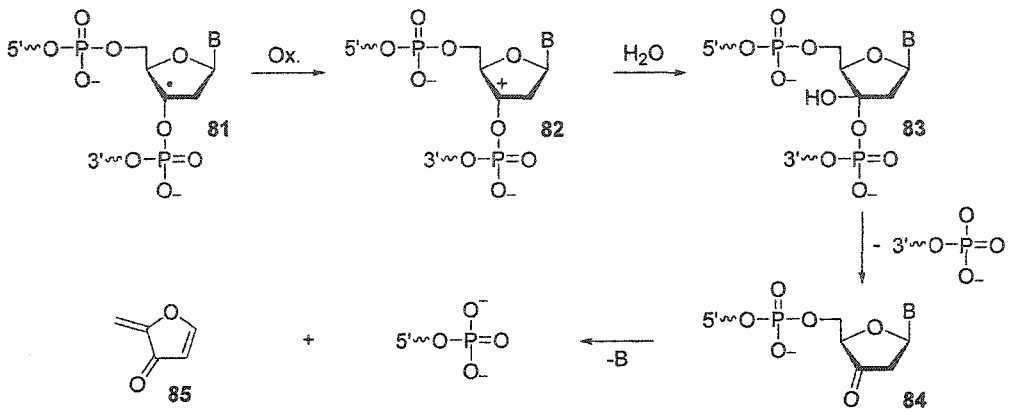

Figure 23. Oxygen independent direct strand break formation from a C3' radical.

Based upon the analysis of end-groups by PAGE, Barton and co-workers proposed that formation of direct strand breaks proceeded by a mechanism originally proposed by Stubbe and Kozarich for damage resulting from a C3' radical.[73,76] Under anoxic conditions, the C3' radical (**81**) is oxidized to the carbocation (**82**) which is trapped by water to afford **83** (Figure 23). Subsequent hydrolysis of **83** results in

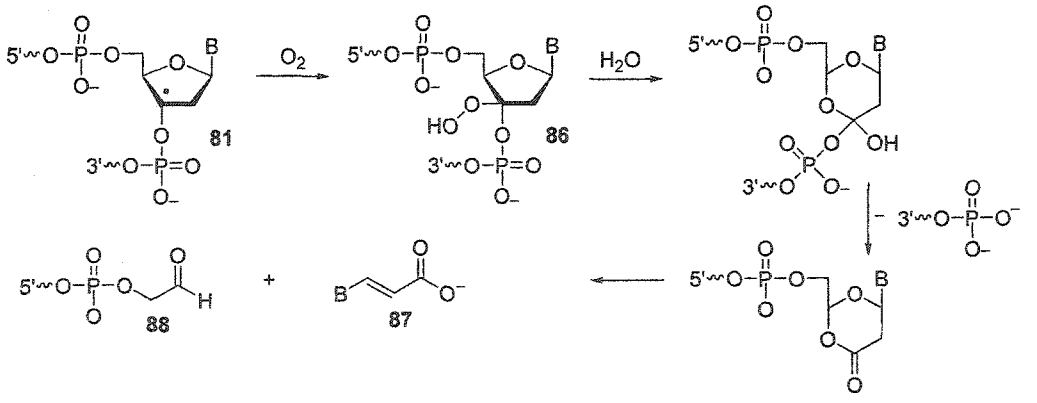

Figure 24. Oxygen dependent direct strand break formation from a C3' radical.

strand scission and the release of a phosphate fragment and sugar fragment **84**. In the presence of O_2, a C3' hydroperoxide is formed (**86**, Figure 24). This species undergoes a fragmentation to release a base propenoic acid (**87**) as well as a fragment with a 3'-phosphoglycaldehyde terminus (**88**).

2.3.4 C4' 2-Deoxyribose Sugar Radicals.

Based upon thermochemical considerations, H4' is predicted to be a favorable position of the 2-deoxyribose sugar for hydrogen atom abstraction.[55-58] Due to the accessibility of this position in the minor groove of duplex DNA, H4' is the target of a number of DNA damaging agents such as bleomycin (**89**). Therefore, the mechanisms by which the C4' radical leads to direct strand break and alkali-labile lesion formation have been the subject of numerous studies.[44,76-83]

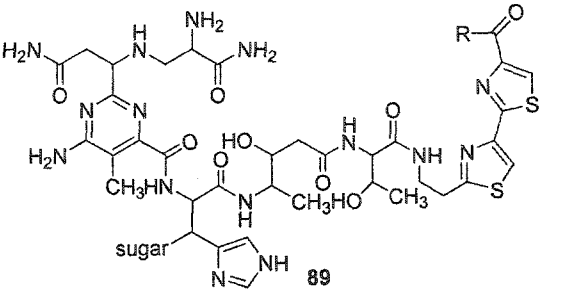

Generation of the nucleotide C4' radical under anoxic conditions results in direct strand break formation via a cation radical intermediate (**91**) which is generated by heterolytic elimination of the 3'-phosphate group (Figure 25).[1,44,80-82] This mechanism, which was proposed by Schulte-Frohlinde and co-workers based upon model studies, was later confirmed by Giese and co-workers.[44,84] Bleomycin mediated DNA cleavage in the absence of oxygen results in alkali-labile lesion formation. This occurs via oxidation of

the initially formed C4' radical (**90**) followed by hydration of the incipient carbocation (**92**).[76,82] Hydrolysis affords an alkali-labile abasic site (**93**).

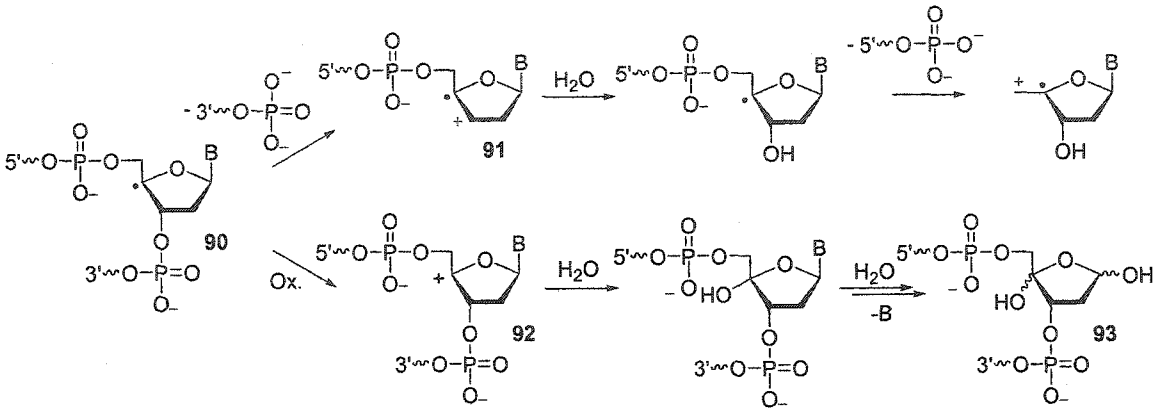

Figure 25. Mechanism of direct strand breakage and alkali-labile lesion formation from a C4' radical under anoxic conditions.

Under aerobic conditions, the C4' radical reacts with O_2 to form a peroxyl radical (**94**, Figure 26). In the presence of a reducing agent such as glutathione, this species is converted to the corresponding C4' hydroperoxide (**95**).[80] The addition of O_2 is reversible and allows the cation radical mediated direct strand scission pathway to compete in the absence of a reducing agent.[83] The C4' hydroperoxide (**95**) can undergo decomposition to produce a strand break. The 3'-phosphosglycolate (**96**) produced in this process is a signature of C4' radical chemistry which can be detected in PAGE experiments.[80,81]

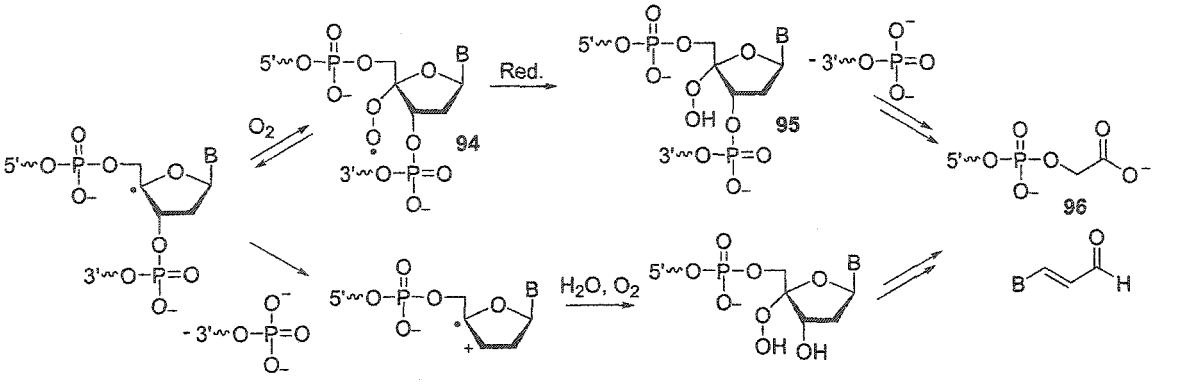

Figure 26. Mechanism of direct strand breakage and alkali-labile lesion formation under aerobic conditions

2.3.5 C5' 2'-Deoxyribose Sugar Radicals.

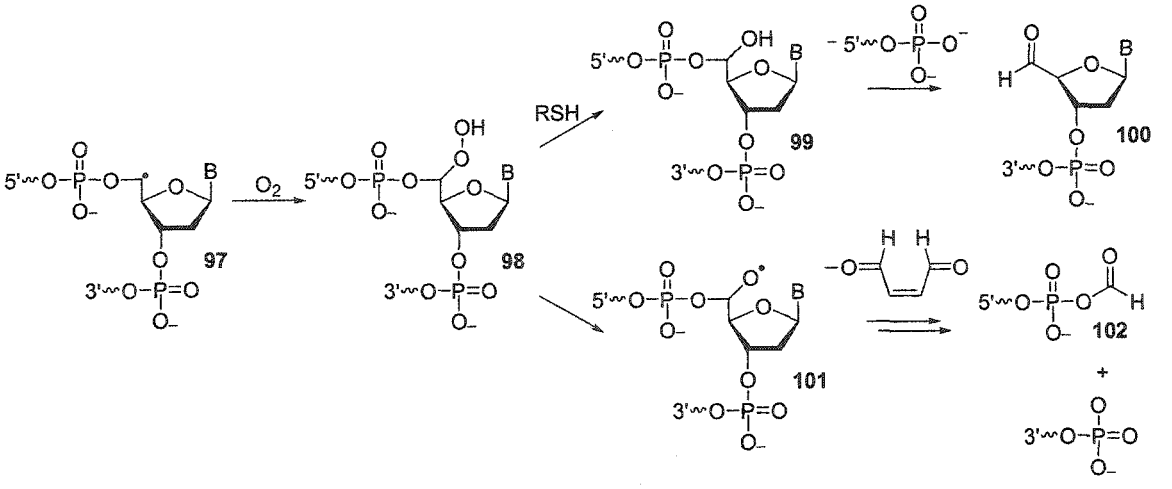

Figure 27. Pathway for direct strand scission from a C5' radical under aerobic conditions.

The C5' position of the 2-deoxyribose sugar of DNA is quite accessible and is the target of abstraction by agents such as enediynes and hydroxyl radical.[62,85] DNA cleavage mediated by NCS (**65**) involves the formation of a C5' radical intermediate which leads to direct strand breaks (Figure 27).[62,86-89] Reaction of the C5' radical (**97**) with oxygen generates a C5' hydroperoxide (**98**). Reduction of this species affords an

unstable C5' hydroxylated nucleotide (**99**) which gives rise to 5'-aldehyde **100**. The 5'-aldehyde is indicative of a C5' radical intermediate and is readily observed in PAGE experiments due to its anomalous migratory aptitude. A minor pathway involves formation of an alkoxy radical (**101**) which undergoes β-scission to result in strand scission with concomitant formation of a 3'-formyl phosphate fragment (**102**).

In addition to direct strand scission, C5' radicals also react by intranucleotidyl addition to the nucleobase to form cyclonucleosides (Figure 28, **106-109**).[90-92] One of the reactive intermediates formed from the irradiation of oxygenated solutions of dC is the C5' radical (**103**). This reactive intermediate can undergo intramolecular cyclization to form **104** which reacts with oxygen to form the C5 hydroperoxide (**105**). Reduction of the hydroperoxide followed by hydrolysis of the nucleobase affords cyclonucleoside **106**. Related cyclonucleosides (**107-109**) are formed from the irradiation of T, dG, and dA under anoxic conditions. Independent synthesis of oligonucleotides containing **106** and **107** revealed that they are only weakly alkali-labile.[93,94] Dizdaroglu and co-workers measured cyclodeoxyguanosine (**108**) and cyclodeoxyadenosine (**109**) in DNA which had been irradiated under anoxic conditions.[91,92] Using an HPLC/MS assay, it was determined that these lesions represent a significant fraction of the observed purine modifications.

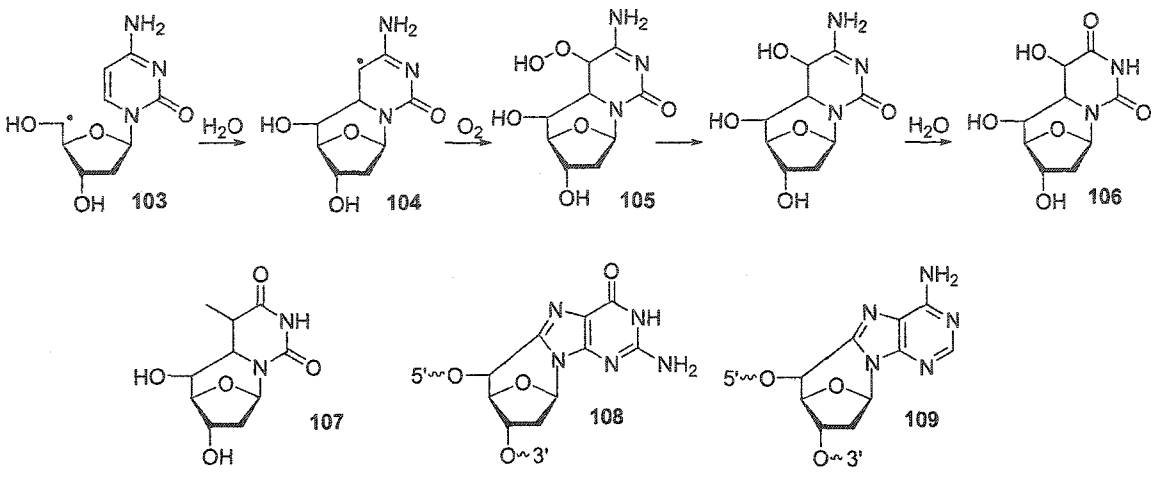

Figure 28. Cyclic lesions formed from C5' radicals.

2.4 Clustered DNA Damage.

Ionizing radiation can result in closely spaced sites of damage, either on the same or opposite strands of the duplex (Figure 29). Damaged sites located within two helical turns (~ 20 bp) of one another constitute so-called clustered damage. Two closely spaced single-strand breaks result in the formation of a double-strand break (DSB), an extremely deleterious type of damage. In addition to DSBs, there is a growing appreciation for the importance of other types of closely spaced damage.[16,95-100,102] This type of damage can consist of two oxidatively damaged bases or abasic sites in the same or opposing strands. Alternatively, non-DSB clustered damage may consist of a SSB opposed to an abasic site or damaged nucleotide.

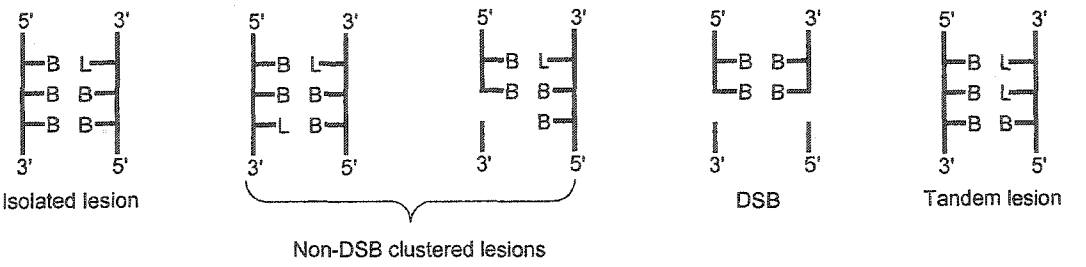

Figure 29. General types of DNA damage produced by ionizing radiation.

In a number of recent studies, significant amounts of non-DSB clustered damage has been detected in irradiated DNA. Detection of this type of damage is enabled by DNA repair enzymes such as Fpg and endonuclease III which create nicks at the sites of oxidized purines and pyrimidines, respectively. When two closely opposed lesions are nicked, this results in the formation of a DSB which can be detected in an electrophoresis experiment.[95-100] Irradiation of plasmid DNA followed by treatment with endonuclease III and Fpg revealed that the majority of clustered damage was non-DSB.[96]

Formation of clustered damage in vivo has also been detected. Sutherland and co-workers subjected extracts of irradiated human cells to the DNA repair enzymes in order to introduce nicks at damaged sites. Based upon the enhancements in strand breakage, it was concluded that non-DSB clustered damage constituted ~ 80 % of the total observed damage.[95] This value is in good agreement with a subsequent study by O'Neill and co-workers in which the amount of non-DSB and DSB clustered damage in irradiated mammalian cells was measured.[100]

2.4.1 Tandem Lesions.

While the above studies provide information with regard to the abundance of closely spaced lesions on opposing strands, they do not detect closely spaced or adjacent lesions located on the same DNA strand.[18-25] Exposure of nucleic acids to ionizing radiation can result in the formation of so-called tandem lesions, two modified nucleotides adjacent to one another in same DNA strand. This class of DNA damage is believed to result from an initially formed nucleobase radical propagating damage to an adjacent nucleotide. It is noteworthy that this type of damage may be underrepresented owing to difficulties in detection. Hydrolysis of bases followed by GC/MS analysis, a common method for assessing nucleobase modifications, is clearly unsuitable for the detection of tandem lesions.[48]

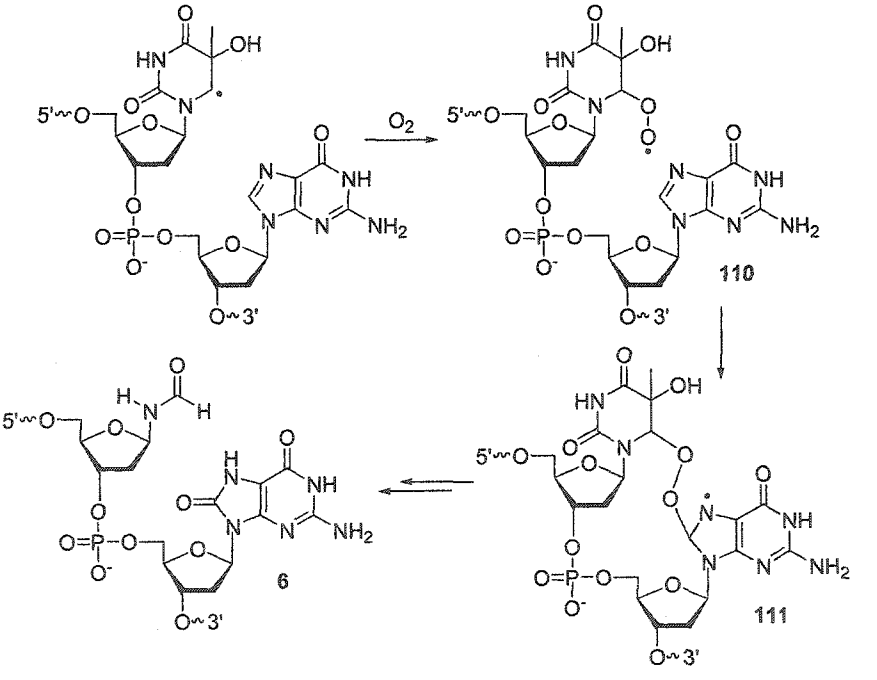

Figure 30. Tandem lesion formation between the hydroxyl radical adduct of thymidine and an adjacent 2'-deoxyguanosine .

A well characterized tandem lesion formed in the radiolysis of oligonucleotides is a modification in which an 8-oxo-2'-deoxyguanosine nucleotide is adjacent to a formamido fragment derived from a pyrimidine (**6**, Figure 30).[18-23] This type of modification was first observed by Box and coworkers upon irradiation of short oligonucleotides.[18-20] As the yield of this lesion shows a linear dependence upon the radiation dose, it was proposed that this type of lesion is the result of one initial radical event. By using enzymatic digestion followed by HPLC/MS, lesion **6** was detected in irradiated oxygenated solutions of DNA.[21] Based upon ^{18}O labeling studies, it was concluded that this product is formed via an initial addition of a thymidine C6 peroxyl radical (**110**) to an adjacent 2-deoxyguanosine nucleotide, forming an adduct radical (**111**).[23] A subsequent fragmentation process, which has not been investigated, gives rise to the observed tandem lesion **6**.

A second type of tandem lesion (**7**) is formed by the addition of a thymidine methyl radical (**112**) to an adjacent purine (Figure 31). The product of this reaction is crosslinked tandem lesion **7**, which was first identified by Box and co-workers as a product of the irradiation of short oligonucleotides under anoxic conditions.[19] An analogous tandem lesion resulting from the addition of the methyl radical to an adjacent dA has also been observed. Enzymatic digestion followed by HPLC/MS analysis of photolysates has demonstrated this class of tandem lesion is generated in irradiated calf thymus DNA.[22]

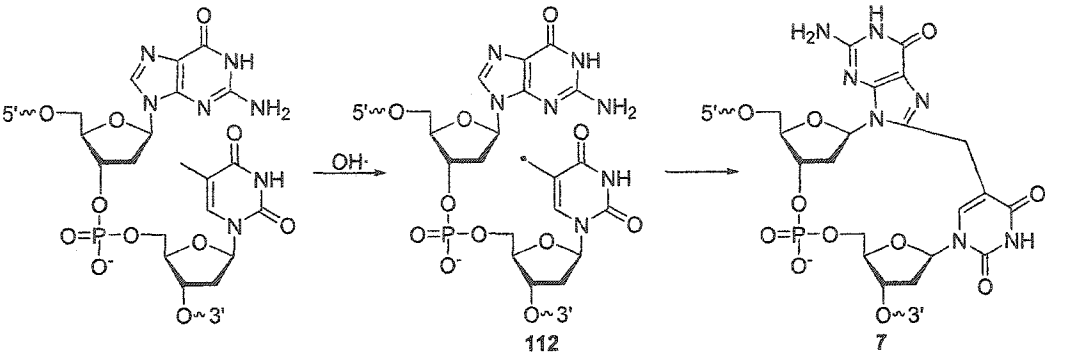

Figure 31. Tandem lesion formed between the thymidine methyl radical and an adjacent 2'-deoxyguanosine

A third type of tandem lesion in which 2-deoxyribonolactone is formed adjacent to a thymidine C5 hydrate (**8**) has been observed in a model system (Figure 32).[25] This lesion is proposed to result from abstraction of the C1' hydrogen atom from an adjacent

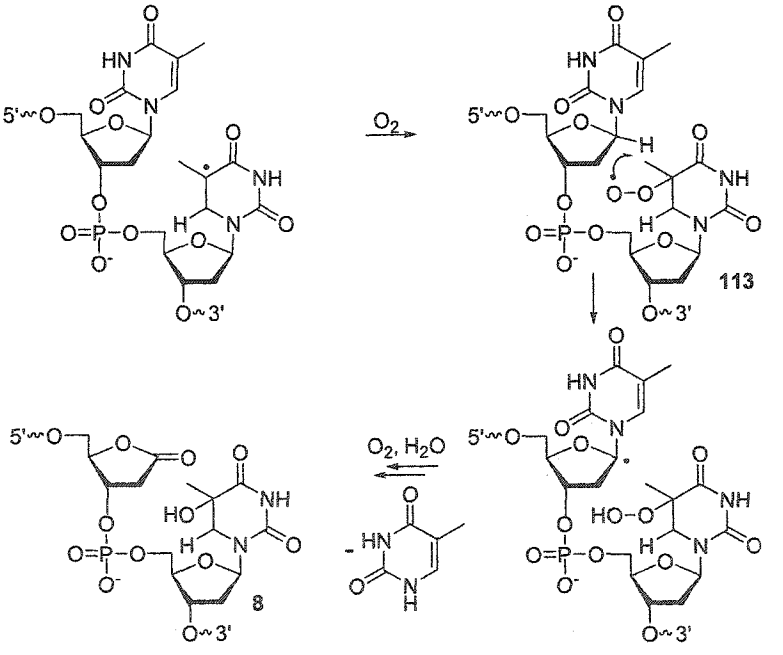

Figure 32. Tandem lesion formed between a nucleobase peroxyl radical and an adjacent nucleotide.

nucleotide by the thymidine C5 peroxyl radical (**113**). Deuterium isotope effect measurements indicate that **113** abstracts the C1' hydrogen atom in oligonucleotides as well.[24]

2.4.2 Biological Significance of Clustered DNA Damage.

The formation of clustered lesions in DNA may have deleterious biological consequences.[5,101,102] Damage which is located on opposite strands can be potentially converted to a double-strand break by enzymatic repair pathways. Indeed, this is the basis for the above studies in which repair enzymes are used as a probe for clustered damage.[95-100] Conversely, closely spaced lesions may inhibit repair proteins. Wallace and co-workers evaluated the ability of Fpg to cleave at an 8-oxo-dG or abasic site with a closely opposed single nucleotide gap (strand break).[103] They found that when the opposed lesions were > 3 nucleotides distant, Fpg efficiently cleaved at the 8-oxo-dG or abasic site, thereby generating a double strand break. This suggests that two lesions which would be repairable when isolated can be converted to more severe damage by DNA repair mechanisms.

In a related study, O' Neill and co-workers measured the efficiency with which an abasic site with closely opposed damage is incised by the major human AP endonuclease (HAP1).[104] It was found that base damage (8-oxo-dG or dHT) on the opposite strand had no effect upon the incision efficiency of HAP1. Some inhibition of incision was observed in a sequence containing an abasic site opposite another abasic site or single strand break, although this was sequence dependent. Again, this suggests that DNA repair enzymes may convert clustered damage to double strand breaks.

The presence of clustered damage may also inhibit repair enzymes. In a recent study, Dianov and co-workers evaluated the ability of human cell extracts to repair a duplex containing an abasic site opposed to thymine glycol.[105] It was found that this type of clustered damage significantly inhibited repair.

2.4.3 Repair of Tandem Lesions.

It has been proposed that tandem lesions are inhibitory to base excision repair pathways and thus contribute to the deleterious biological effects of ionizing radiation. Kow and co-workers evaluated the ability endonucleases III and VIII to recognize a tandem lesion in which two 5,6-dihydro-2'-deoxyuridine (dHdU) nucleotides were present adjacent to one another on the same DNA strand (**114**).[17] Although this tandem lesion has not been identified as a product formed from the treatment of DNA with ionizing radiation, the dHdU nucleobase was proposed to serve as a model for damage which consists of two neighboring dihydropyrimidines. These researchers observed that endonuclease III and VIII recognized a single dHdU in a DNA duplex. However, the model tandem lesion (**114**) was not efficiently removed by either enzyme.

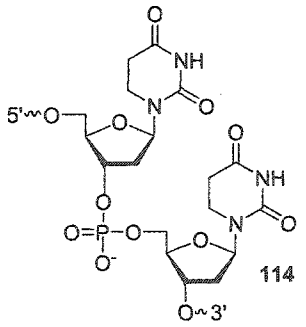

114

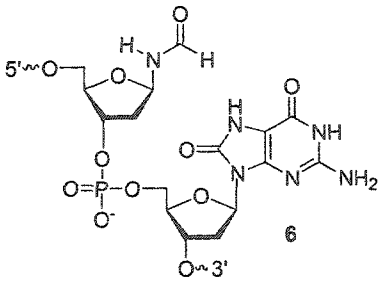

6

In order to evaluate the enzymatic processing of **6**, Cadet and co-workers prepared synthetic oligonucleotides containing this tandem lesion.[106] It was determined that **6** inhibited digestion by phosphodiesterases I and II. In contrast, tandem lesion **6** is cleaved by the repair enzymes endonuclease III and Fpg, which recognize modified pyrimidines and purines respectively.[5,101-105]

The effect of non-DSB clustered damage upon base excision repair has been studied primarily in the context of closely opposed lesions.[5,101,103-105] Tandem lesions represent another subset of non-DSB clustered damage. The above studies notwithstanding, the effects of this type of damage upon DNA repair are largely unknown. Given the difficulty of detecting this type of clustered damage, it is reasonable to assume that there are other presently unidentified tandem lesions formed in nucleic acids as a result of ionizing radiation. The formation of tandem lesions such as **6** is initiated by generation of a single nucleobase radical. In order to identify additional tandem lesions, the reactivity of nucleobase radicals must be more fully characterized.

2.5 Site-Specific Generation of Reactive Intermediates in DNA.

Upon γ-radiolysis, a wide variety of reactive intermediates are generated throughout nucleic acids. The presence of multiple reactive intermediates does not prevent global analysis of damage (i.e., measurement of the relative amounts of different types of nucleobase damage). This is often achieved by GC/MS analysis of derivatized nucleobases which have been hydrolyzed from the polymer.[46] This technique is sensitive and facile. However, it gives little information regarding the mechanism(s) by which lesions are formed and may underestimate damage products sensitive to the conditions

required for hydrolysis and/or derivatization. Furthermore, this technique gives no information regarding the original location of the DNA lesions. Consequently, isolated and tandem lesions cannot be differentiated.

A powerful strategy which researchers have adopted in order to facilitate the study of DNA radicals is site specific generation of the reactive intermediate of interest.[26] This enables generation of one reactive intermediate per DNA molecule and is accomplished by synthesizing DNA which contains a precursor to the reactive intermediate of interest. A reaction that has been extensively used as a "chemical trigger" is the Norrish type I photochemical reaction of ketones (Figure 33). In this reaction, an excited state ketone undergoes a homolytic cleavage to generate an acyl radical and an alkyl radical. Appropriately substituted acyl radicals rapidly decarbonylate, affording alkyl radicals. Another reaction which has been utilized is the photochemical cleavage of phenyl selenides (Figure 33).[25,80]

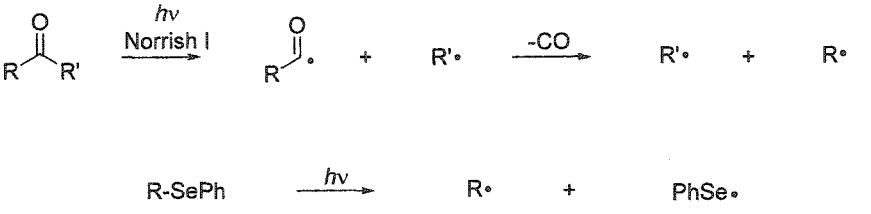

Figure 33. Photochemical generation of radicals.

The use of this strategy has enabled the generation of 2-deoxyribose as well as nucleobase centered radicals. Giese and co-workers synthesized oligonucleotides containing C4' ketone **116** and C4' phenyl selenide **115** (Figure 34).[44,80-82] Upon

photolysis these modified nucleosides generate a C4' radical which can result in the formation of direct strand breaks or alkali-labile lesions.

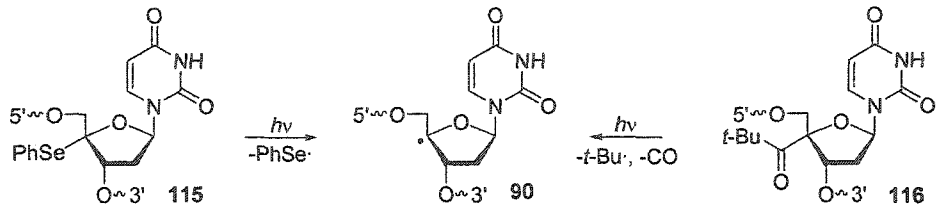

Figure 34. Photolabile precursors for the C4' radical.

Use of the Norrish I strategy also enabled generation of the C1' radical in oligonucleotides in monomeric form and in DNA (Figure 35).[63,64,107] Independent generation of the C1' radical has enabled the measurement of rate constants for the reaction of this biologically important reactive intermediate with thiols and radiosensitizers.[63,66,109,110] Photolabile radical precursor **117** enabled determination of the mechanism by which the C1' radical results in the formation of the 2-deoxyribonolactone oxidized abasic site.[63] Using precursor **117**, a PAGE assay was subsequently developed for the detection of this labile species.[111] The use of **117** to generate 2-deoxyribonolactone in DNA facilitated the discovery that this lesion irreversibly inhibits a DNA repair enzyme.[112]

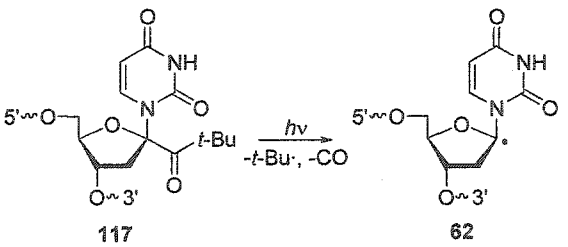

Figure 35. Ketone precursor for the C1' radical.

In addition to 2-deoxyribose centered radicals, nucleobase radicals have been generated in both nucleoside monomers and DNA. Two precursors for the 2'-deoxyuridine-5-methyl radical have been developed (Figure 36).[113,114] The use of benzyl ketone radical precursor **118** enabled measurement of the rate constants at which the methyl radical reacts with thiols as well as models of 2-deoxyribose.[113] Incorporation of phenyl sulfide **119** into short oligonucleotides enabled characterization of tandem lesions formed by this radical.[114]

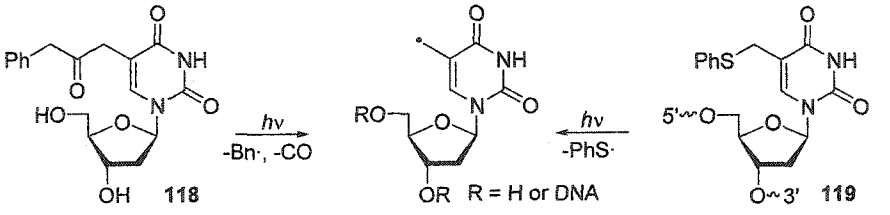

Figure 36. Photolabile precursors for the thymidine methyl radical.

Precursors for the major products of hydrogen atom and hydroxyl radical addition to the nucleobase have also been designed. The thymidine C6 hydrogen atom adduct radical has been independently generated in DNA.[24,115,116] Oligonucleotides containing the isopropyl ketone radical precursor (**9**, Figure 37) enabled elucidation of the mechanism by which this species leads to alkali-labile lesion formation at an adjacent nucleotide. The 5,6-dihydrothymidin-5-yl has also been generated from a photolabile phenyl selenide in a dinucleotide model system (**120**, Figure 37).[25] Generation of the radical in this system enabled HPLC characterization of products.

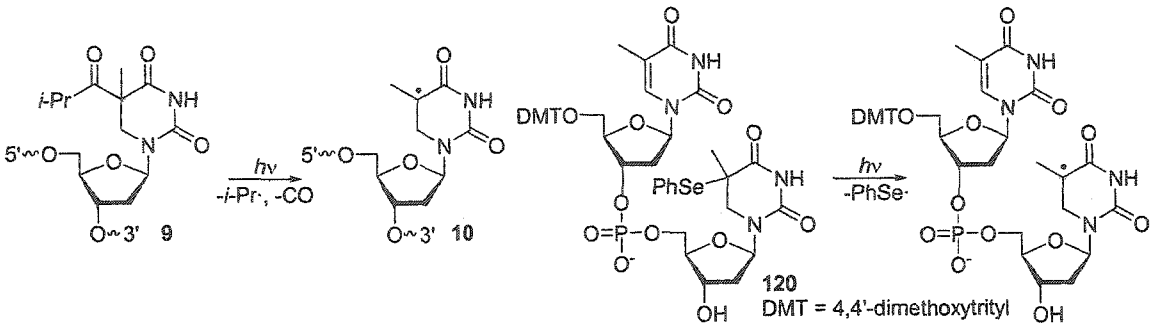

Figure 37. Precursors for the thymidine-5-yl radical.

Trifluorobenzoate **11** was used as a precursor for the monomeric hydroxyl radical adduct of thymidine (**12**, Figure 38).[27,117] Independent generation of **12** allowed investigation of the rates at which this reactive intermediate undergoes dehydration (k_{dehy}) to form cation radical **23** and intramolecular hydrogen abstraction (k_{intra}) to form a 2-deoxyribose radical (**121**). An upper limit of ~ 2 s^{-1} was estimated for k_{dehy} and k_{intra} based upon isotopic labeling experiments. This low rate constant for dehydration implies that the thymidine cation radical is not the reactive intermediate responsible for strand scission at neutral pH. Furthermore, the fact that intramolecular hydrogen abstraction by **12** is slow suggests that if the hydroxyl radical adduct results in strand scission in DNA, it is via an internucleotidyl reaction. The peroxyl radical derived from **12** could also result in strand scission, but this has not been investigated.

Unfortunately, there are several limitations associated with the use of radical precursor **11**. The photoinduced electron transfer process by which **12** is generated is not compatible with oxygen. This prevents investigation of the role of oxygen in the process by which **12** leads to strand scission. Moreover, the photoinduced electron transfer process which generates radical **12** in the monomeric form would also result in oxidation

of DNA nucleobases Therefore, a different radical precursor which was not limited in this way would be advantageous and allow more complete investigation of the mechanism by which pyrimidine C6 nucleobase radicals result in strand scission.

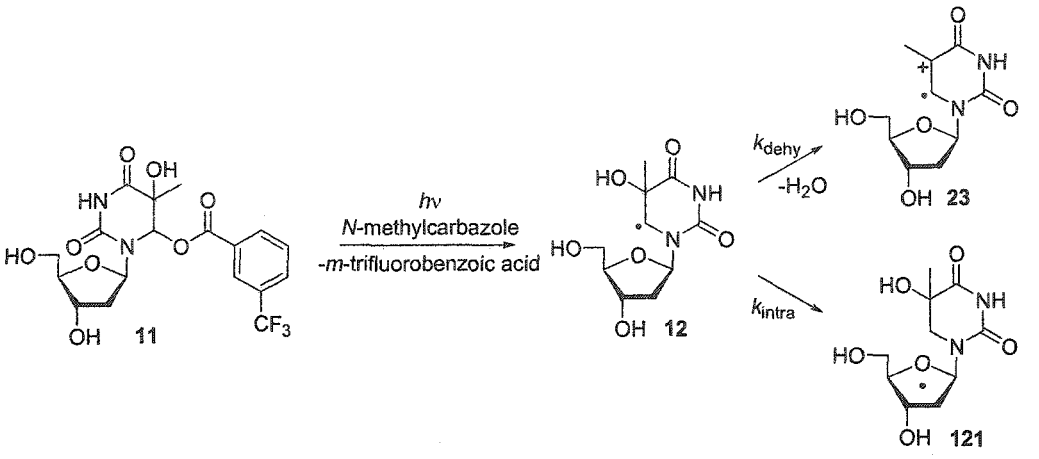

Figure 38. Generation of the hydroxyl radical adduct of thymidine by photoinduced electron transfer.

2.6 Research Objectives.

The major product of hydroxyl radical addition to thymidine is a 5,6-dihydropyrimidin-6-yl radical (**12**). There is substantial indirect evidence that in DNA this intermediate is responsible for the strand damage observed in DNA exposed to ionizing radiation. Given the incompatibility of the previously developed precursor for this class of nucleobase radical with mechanistic studies in the biopolymer, it is crucial to develop another method of generation. The goal of this research is the elucidation of the mechanism(s) by which a 5,6-dihydropyrimidin-6-yl radical leads to further strand damage. This will be realized by the design and synthesis of a pyrimidine radical precursor which can be incorporated into oligonucleotides and is compatible with O_2. The reactivity of the monomeric radical will be characterized by measuring the rate

constant for hydrogen atom abstraction from a thiol as well as 2-deoxyribose sugar models. The relative amounts of alkali-labile lesions and direct strand breaks generated by the pyrimidine C6 radical will be measured. The intermediacy of DNA peroxyl radicals will be investigated by evaluating the effect of oxygen on the observed damage. Measurement of deuterium isotope effects will enable elucidation of internucleotidyl hydrogen atom abstraction reactions carried out by the dihydropyrimidin-6-yl and respective peroxyl radical. DNA damage products will be analyzed by MS to characterize tandem lesions which may result from this reactive intermediate.

3 Results and Discussion

3.1 Synthesis of the Radical Precursor

In order to independently generate the 5,6-dihydropyrimidin-6-yl radical of interest, a C6-*t*-butyl ketone nucleoside radical precursor (**122**) was designed (Figure 39). Upon UV irradiation, it was envisioned that the radical precursor would undergo a Norrish type I photoreaction to produce the desired 5,6-dihydro-2'-deoxyuridin-6-yl (**123**, Figure 39). This radical can be used as a model for the 5,6-dihydrothymidin-6-yl radicals (**2**, **15**) produced by addition of hydrogen atom and hydroxyl radical to the nucleobase.[1]

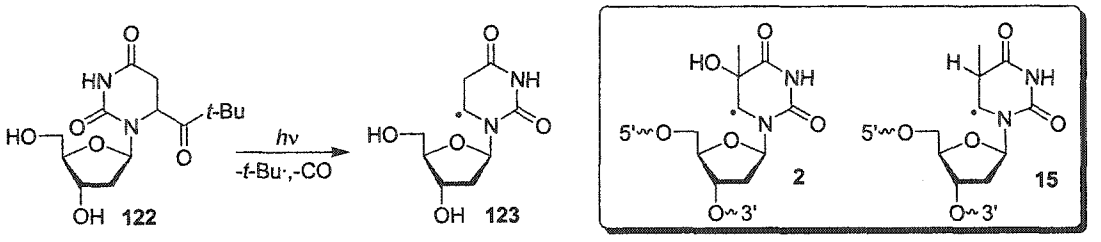

Figure 39. Independent generation of the 5,6-dihydro-2'-deoxyuridin-6-yl, a model for **2** and **15**.

The radical precursor (**122**) was synthesized in four steps from 2'-deoxyuridine (Scheme 1). Protection of the 5' and 3' hydroxyl groups as the cyclic silyl ether followed by selective lithiation and acylation of the C6 position afforded *t*-butyl acyl nucleoside **124**.[118, 119] Reduction with H_2 in the presence of Rh/Al_2O_3 afforded the cyclic silyl ether protected radical precursor (**125a, b**) as an 8.2:1 mixture of separable diastereomers.[120] Deprotection of the major (**125a**) and minor (**125b**) diastereomers with $Et_3N{\cdot}3HF$ afforded the desired radical precursors (**122a, b**).

Scheme 1

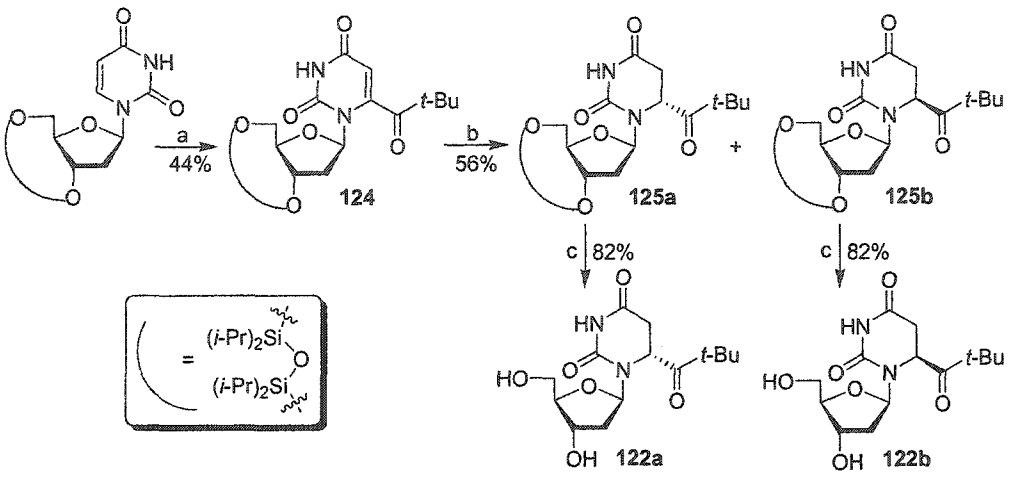

Key: a) LDA, pivaloyl chloride, THF, -78°C; b) H_2, Rh/Al_2O_3, MeOH; c) $Et_3N{\cdot}3HF$, THF.

3.2 Stereochemistry and Conformation of the 5,6-Dihydro-2'-Deoxyuridin-6-yl Precursor.

In order to determine the absolute stereochemistry of **125a** and **125b**, a combination of molecular modeling and NOE experiments was used. NOE enhancements in both diastereomers of **125** were measured to determine the proximity of the C6 hydrogen atom and *t*-butyl acyl substituent to the sugar hydrogens. The proximity of the C6 substituents to the hydrogen atoms of the 2-deoxyribose sugar varies significantly with the conformation of the dihydropyrimidine nucleobase (Figure 40). Thus, in order to correctly interpret the NOE data, it was necessary to determine the conformation of the nucleobase about the glycosidic linkage. This was accomplished by

conducting semi-empirical calculations to determine the equilibrium geometry of **125a** and **125b**.

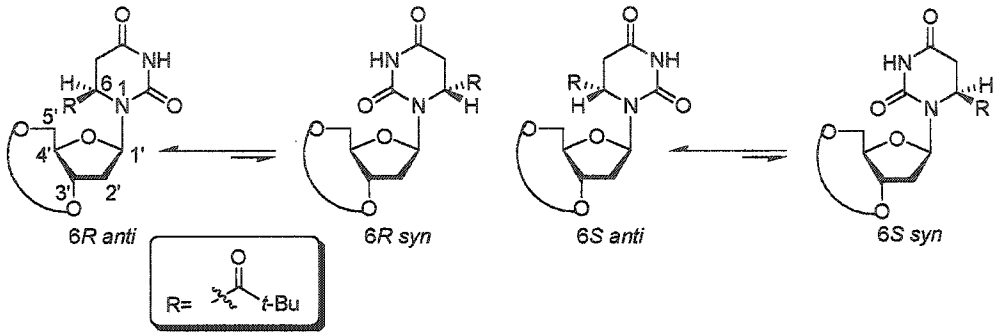

Figure 40. *Syn* and *anti* conformations of **125a** and **125b**.

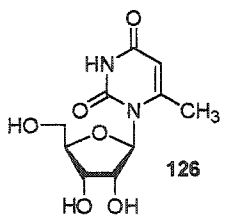

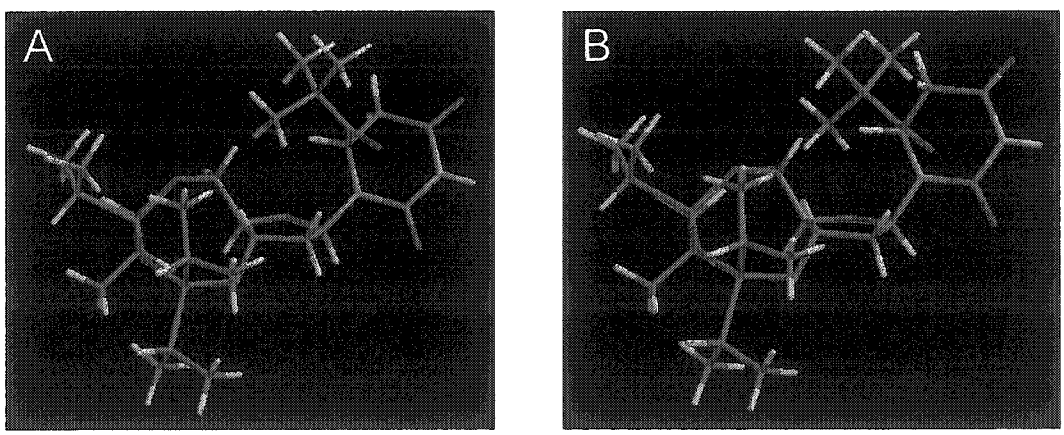

Figure 41. Energy minimized structures of protected nucleosides (A) **125a** and (B) **125b**.

In solution, pyrimidines are ordinarily in the *anti* conformation in which the C2 oxygen atom of the nucleobase is oriented away from the sugar. This conformation avoids unfavorable steric interactions between the C2 oxygen and the C5' hydrogen atoms. The introduction of substituents other than hydrogen atoms has been shown to favor the *syn* conformation in which the C2 oxygen is oriented over the sugar. For example, 5-methyluridine (**126**) has been shown to occupy the *syn* conformation.[121] Due to the presence of the large pivaloyl substituent at the C6 position of **125**, the possibility that the *syn* conformation might be favored was investigated by molecular modeling.

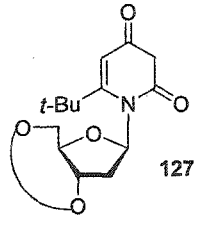

127

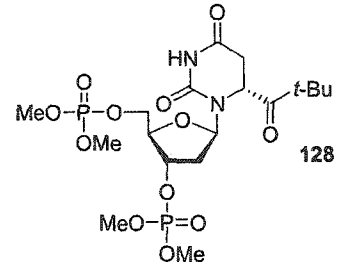

128

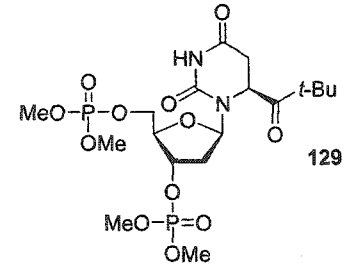

129

In order to determine the lowest energy conformation of the protected diastereomeric radical precursors (**125a, b**), molecular modeling calculations were carried out at the semi-empirical level (PM 3) to determine the equilibrium geometry. These calculations revealed that the *anti* conformation was favored for both diastereomers by 8-10 kcal/mol (Table 1). The energy minimized structures of **125a** and **125b** reveal that the acyl group is rotated such that unfavorable steric interactions with the C5' hydrogen atoms are avoided (Figure 41). Nucleoside **124** displays no conformational preference, indicating that the 5,6-dihydropyrimidine ring also provides steric relief. The cyclic silyl ether of 6-*t*-butyl-2'-deoxyuridine (**127**), which cannot

avoid unfavorable steric interactions in the *anti* conformation, displays a > 3 kcal/mol preference for the *syn* conformation.

Table 1. Calculated ΔH_f (kcal/mol) for *syn* and *anti* conformations of radical precursor **125** and related nucleosides.[a]

Compound	ΔH_f (kcal/mol) *syn*	ΔH_f (kcal/mol) *anti*	$\Delta\Delta H_{f\ (syn\text{-}anti)}$
125a (6*R*)	-510	-520	10
125b (6*S*)	-513	-521	8
124	-495	-495	0
127	-462	-459	-3
129 (6*R*)	-633	-634	1
128 (6*S*)	-637	-636	-1

[a]Calculations were performed using Spartan 02' at the semi-empirical level using a PM3 basis set.

The above calculations provide useful information regarding the preferred conformation of the diastereomeric radical precursors (**125a, b**). However, it was anticipated that the presence of the bulky disiloxane could exert considerable influence upon the equilibrium geometries of **125a** and **125b**. In order to determine if the strong preference shown by both diastereomers for the *anti* conformation could be extrapolated to the radical precursor in DNA, the relative energies of the *syn* and *anti* conformations of dimethylphosphates **128** and **129** were calculated (Table 1). The energies of the *syn* and *anti* conformations differed only by 1 kcal/mol for both diastereomers (**128, 129**). Therefore, the strong preference for the *anti* conformation displayed by the diastereomeric radical precursors (**125a, b**) is apparently the consequence of the bulky disiloxane protecting group.

While the conformational preference of **125a** and **125b** may not reflect the preferred geometry of the radical precursor in DNA, the *anti* preference of these nucleosides assists in the interpretation of NOE data. In order to establish the absolute

stereochemistry at the C6 position, the H6 and C6 *t*-butyl groups were irradiated and the enhancements at H2', H3', and H5' were measured. Comparison of the relative NOEs of both diastereomers with the calculated distances between hydrogen atoms indicates that the major diastereomer has the 6*R* configuration at the C6 position (Table 2).

Particularly diagnostic are the H3'→*t*-butyl and H6→H5' enhancements. In the 6*R* diastereomer, molecular modeling indicates that the H3' and the *t*-butyl group are in close proximity (2.3 Å), resulting in the expected NOE correlation (Table 2). The minimal NOE observed in the 6*S* diastereomer is consistent with the almost twofold greater calculated distance between these positions in this diastereomer. The H6→H5' enhancements show an analogous trend, albeit less dramatically.

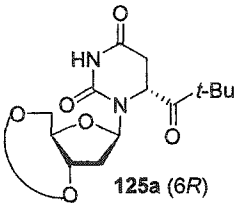

125a (6*R*)

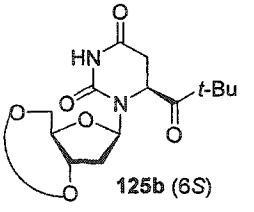

125b (6*S*)

Table 2. ^{1}H NOEs and calculated distances in **125a** and **125b**.

H Irradiated→	% Enhancement		Calculated distance (Å)[a]	
H Observed	**125a** (6*R*)	**125b** (6*S*)	**125a** (6*R*)	**125b** (6*S*)
H6→H2'	1.5	1.0	3.2	3.4
H6→H3'	1.0	1.8	3.8	3.3
H6→H5'	-	0.4	2.3	1.7
H3'→*t*-Bu	0.7	0.1	2.3	4.3

[a]Distances are from the equilibrium geometry calculated using Spartan '02.

NOE enhancements between the C6 and the C2' and C3' hydrogens are also informative. Molecular modeling calculations indicate that H6 and the C2' hydrogens

are in closer proximity in the 6*R* diastereomer. In the 6*R* diastereomer, a larger NOE is observed between these two positions. According to calculations, the C6 and C3' hydrogen atoms are more distant in the 6*R* diastereomer. This is consistent with the lesser NOE between these positions. Therefore, the NOE experiments indicate that the major diastereomer has the 6*R* configuration.

The chemical shift differences between the C2' hydrogen atoms also support this assignment. The C2' hydrogens are well resolved (0.25 ppm) in the major diastereomer (**125a**) which is consistent with the close proximity of the pro-*S* hydrogen to the carbonyl group (2.8 Å) when the C6 configuration is *R*. The lack of resolution of the C2' hydrogens in the minor diastereomer (**125b**) is consistent with the greater calculated distance (5.3 Å) between the pro-*S* C2' hydrogen atom and the carbonyl oxygen.

3.3 Synthesis of the 5'-Benzoyl Radical Precursor and Expected Products.

The overall aim of this research was identification of the types of DNA damage generated by 5,6-dihydro-2'-deoxyuridin-6-yl and elucidation of the underlying mechanism(s) of this process. However, prior to incorporation of the radical precursor (**122**) into DNA, it was necessary to characterize the reactivity of the monomeric radical (**123**). This was crucial to ensure that the radical precursor underwent the desired type I photocleavage. Moreover, understanding the reactivity of the monomeric 5,6-dihydro-2'-deoxyuridin-6-yl (**123**) provides a foundation for investigating this biologically important reactive intermediate in DNA.

To facilitate UV detection upon HPLC analysis of photolysates, 5'-benzoylated radical precursor **130** was synthesized (Scheme 2). This was accomplished via

bezoylation of radical precursor **122a** with benzoyl cyanide. Introduction of the benzoyl group was intended to provide a UV chromophore that would facilitate detection of low product yields while leaving the photochemistry of the radical precursor unaffected. In order to characterize the reactivity of the radical, it was necessary to synthesize the benzoate derivatives of the expected products (Scheme 2).

Scheme 2

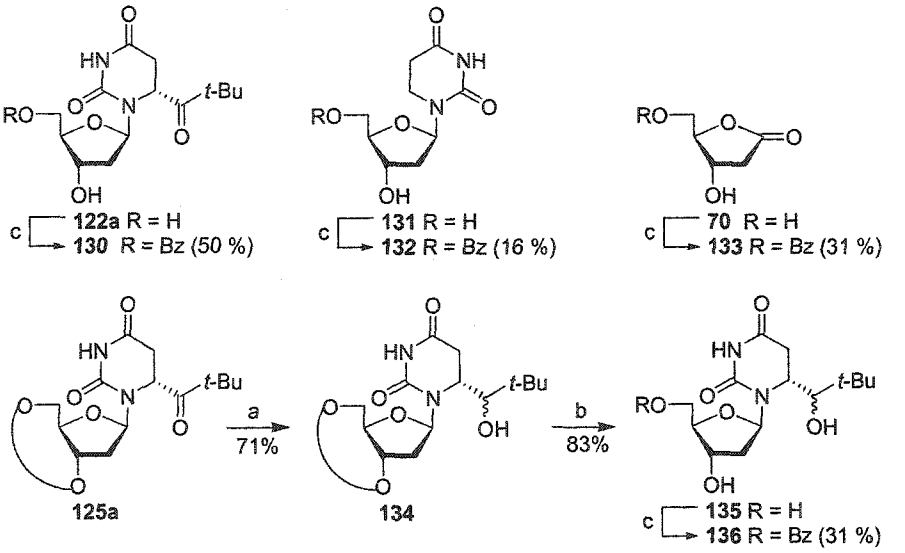

Key: a) $NaBH_4$, EtOH; b) $Et_3N{\cdot}3HF$, THF; c) BzCN, Et_3N, DMF, -40 °C

Benzoylation of 5,6-dihydro-2'-deoxyuridine (**131**) and 2-deoxyribonolactone (**70**) prepared by reported methods afforded **132** and **133** (Scheme 2).[119,122] An anticipated problem associated with the use of a ketone radical precursor was competition of photoreduction with the desired type I process (Figure 42). This reaction would result in the formation of *t*-butyl alcohol **136**. This photoreduction product (**136**) of the radical

precursor (**130**) was synthesized by $NaBH_4$ reduction of disiloxane protected radical precursor **125a** (Scheme 2). Subsequent removal of the silyl group with $Et_3N{\cdot}3HF$ afforded photoreduction product **135**. Benzoylation of **135** with benzoyl cyanide afforded protected photoreduction product **136**.

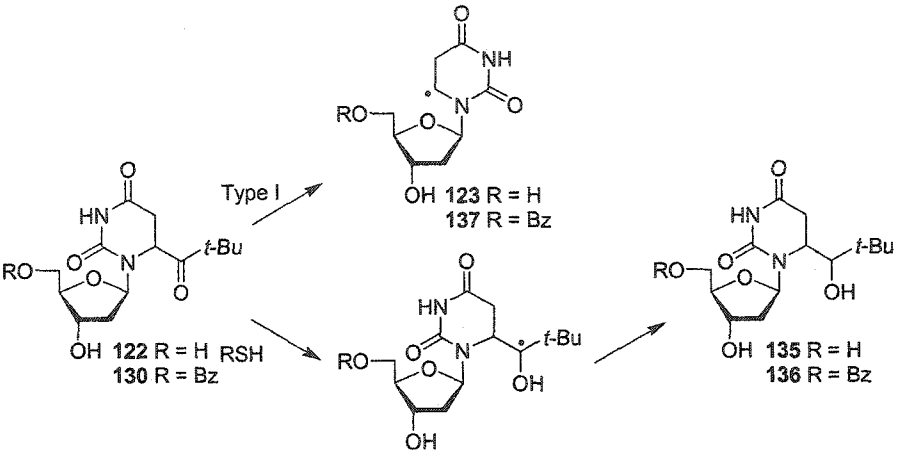

Figure 42. Competition of type I photocleavage and photoreduction.

A product which was anticipated to result from reaction of oxygen with the initially formed radical (**137**) was 5,6-dihydro-6-hydroxy-2'-deoxyuridine (2'-deoxyuridine C6 hydrate). Both diastereomers of 5'-benzoyl-2'-deoxyuridine-C6-hydrate (**140a, b**) were synthesized from 5'-benzoyl-2'-deoxyuridine (**138**, Scheme 3). This was accomplished using a modification of reported methods in which protected 2'-deoxyuridine **138** was treated with NBS to afford a separable mixture of diastereomeric bromohydrins (**139a, b**).[123] Reduction of the bromohydrins with Zn^0/AcOH afforded both diasteromers of the desired C6 hydrate (**140a, b**).

Scheme 3

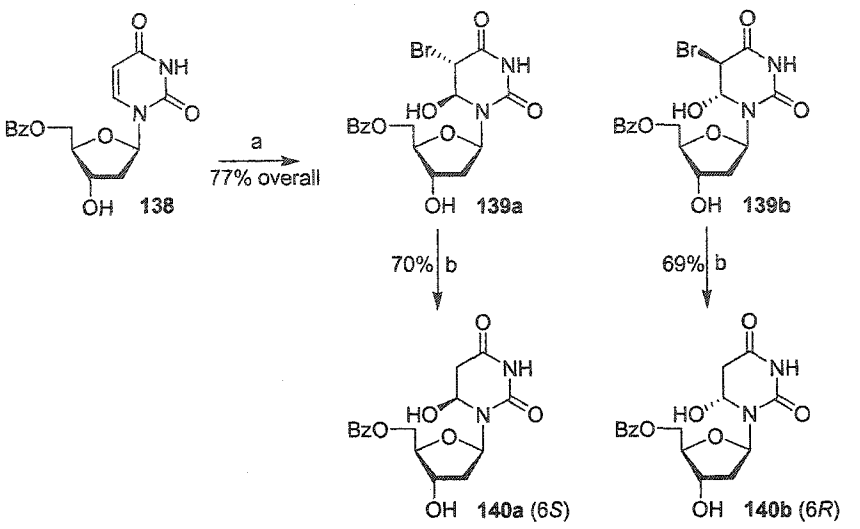

Key: a) NBS, $CaCO_3$, THF/H_2O; b) Zn^0/AcOH, THF/H_2O

The absolute stereochemistry of **139a** and **139b** was established through NOE experiments (Table 3) in conjunction with reported ^1H NMR data for related compounds. The reported ^1H NMR spectra for C6 hydrates and bromohydrins of 2'-deoxyuridine, as well as 5-hydroperoxy-6-hydroxy-5,6-dihydrothymidine and 6-hydroperoxy-5-hydroxy-5,6-dihydrothymidine, reveal a larger difference in chemical shift for the C2' hydrogens in the 6*S* diastereomers relative to the 6*R* diastereomers.[52, 123] This is due to the fact that the C2' pro-*S* hydrogen is shifted to higher field in the 6*S* diastereomers. This phenomenon can be rationalized in terms of closer proximity of C6 hydroxyl group to the pro-*S* C2' hydrogen atom in the 6*S* diastereomer, analogous to the observed chemical shift differences in the two diastereomers of the protected radical precursor (**125a**, **b**). Based upon these observations, it is proposed that the configuration of **139a** is 6*S* while the configuration of **139b** is 6*R*.

NOE experiments are consistent with this assignment (Table 3). In the 6*S* diastereomer (**139a**), a larger NOE is observed between the H6 and the C5' hydrogens relative to the 6*R* diastereomer (**139b**). This is consistent with the closer proximity of these hydrogen atoms in the 6*S* diastereomer when the nucleobase is in the *anti* conformation. The 6*R* diastereomer (**139b**) shows a greater NOE between the C6 hydrogen atom and the pro-*S* C2' hydrogen atom relative to the 6*S* diastereomer (**139a**). This again is consistent with the expected closer proximity of these hydrogen atoms in the 6*R* diastereomer when the nucleoside is in the *anti* conformation.

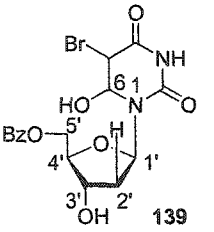

139

Table 3. NMR data for nucleoside bromohydrins

Compound	ΔH2'-Chemical Shift	NOE (H Irradiated→H Observed)	
		H6→pro-*S* H2'	H6→H5'
139a (5*S*, 6*S*)	0.26	2.27	0.96
139b (5*R*, 6*R*)	0.11	2.86	0.63

3.4 Evaluation of Pyrimidine C6 Hydrate Stability.

Generation of the 5,6-dihydro-2'-deoxyuridin-6-yl (**137**) in the presence of O_2 was anticipated to result in the formation of 2'-deoxyuridine C6-hydrate (**140**). Pyrimidine C6-hydrates are a unique class of DNA lesion which can undergo a "repair" reaction to generate the native nucleobase (Figure 43).[124-127] In order to assess the biological

importance of this class of lesion, it is necessary to have a quantitative measure of pyrimidine C6 hydrate stability.

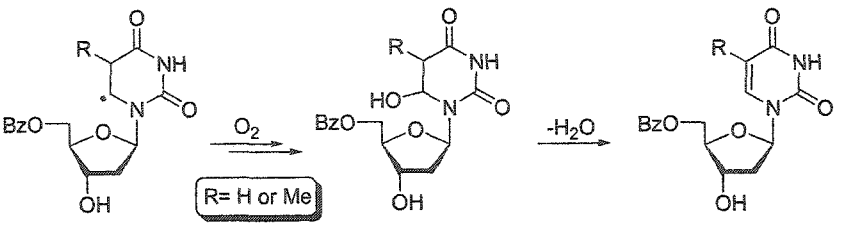

Figure 43. Formation and dehydration of pyrimidine C6-hydrates.

Radical **137** is used as a model for thymidine C6 radicals which are produced in DNA. It is likely that the 5,6-dihydrothymidin-6-yl will also result in high yields of the corresponding C6-hydrate (Figure 4A). Therefore, it is important to evaluate the stability of thymidine C6-hydrates as well. The benzyolated derivatives of the two *cis* diastereomers of thymidine C6 hydrate (**142a, b**) were prepared using the same methods described for the preparation of **140** (Scheme 4).[123] Bromination of 5'-benzoyl thymidine afforded a separable mixture of diastereomeric thymidine bromohydrins (**141a, b**). Reduction with Zn^0/AcOH yielded the desired thymidine C6-hydrates (**142a, b**).

Determination of the absolute stereochemistry of thymidine hydrates (**142a, b**) and bromohydrins (**141a, b**) was accomplished via the same methods used to assign the absolute stereochemistry of 2'-deoxyuridine C6 hydrates (**140a, b**). The C2' hydrogens of the 6*S* diastereomer were again more resolved than those of the 6*R* diastereomer (Table 4). Moreover, the 6*R* diastereomers display a greater NOE between the C6 and pro-S C2' hydrogen than is observed in the 6*S* diastereomer. In the diastereomeric bromohydrins (**141a, b**), a greater NOE between H6 and H5' is observed in the 6*S* relative to the 6*R* diastereomers. This trend is not observed in the benzoylated thymidine

C6 hydrates (**142a, b**), probably due to the poor resolution of C5' hydrogens and H3' in the 6*R* diastereomer.

Scheme 4

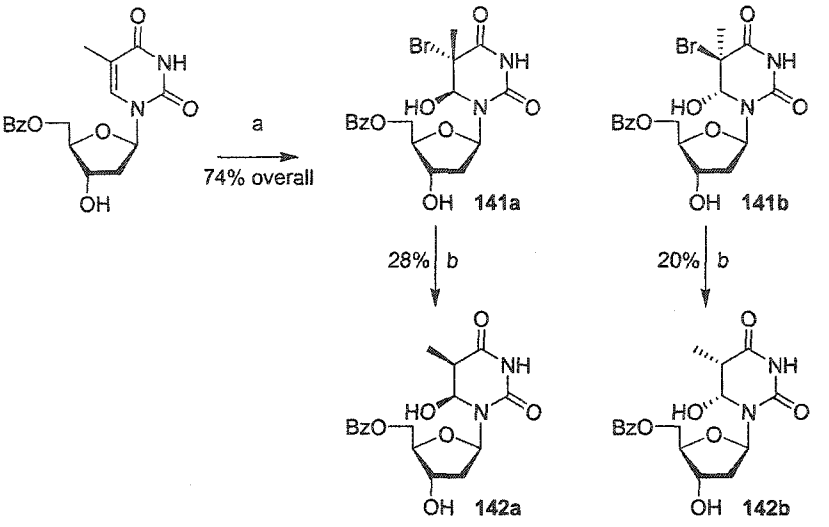

Key: a) NBS, $CaCO_3$, THF/H_2O; b) Zn^0/AcOH, THF/H_2O

Table 4. NMR data for thymidine bromohydrins (**141a, b**) and C6 hydrates (**142a, b**)

Compound	$\Delta H_{2'}$-Chemical Shift	NOE (H Irradiated→H Observed)	
		H6→pro-*S* H2'	H6→H5'
141a (5*S*, 6*S*)	0.34	2.76	0.83
141b (5*R*, 6*R*)	0.10	3.18	0.59
142a (5*R*, 6*S*)	0.33	2.28	0.60
142b (5*S*, 6*R*)	0.26	3.55	0.87[a]

[a] The enhancement could not be distinguished from that at C3'.

Direct measurements of the dehydration rates of uracil and thymine C6 hydrates have been reported.[127] The rates of dehydration of the corresponding nucleosides have not been directly measured. Indirect methods have been used to measure the dehydration

rates of 2'-deoxyuridine and thymidine C6 hydrates in DNA.[124-126] In these experiments, the amount of modified nucleobase released by endonuclease III as a function of time was measured. Endonuclease III excises a broad spectrum of modified pyrimidines. As pyrimidine hydrates undergo loss of water to resconstitute the undamaged nucleobases (which are not excised by endonuclease III), the amount of damaged nucleobases released declines over time. By measuring the amount of nucleobase release by this repair enzyme as a function of time, rate constants for the dehydration reaction may be estimated. This approach is limited. It cannot detect deglycosylation which may compete with dehydration (Figure 44). Deglycosylation of pyrimidine hydrates would be significant as it would generate an abasic site (**143**) and eliminate the possibility of the "repair" reaction. In order to directly measure the stability of pyrimidine C6 hydrates, independently synthesized nucleosides **140** and **142** were used.

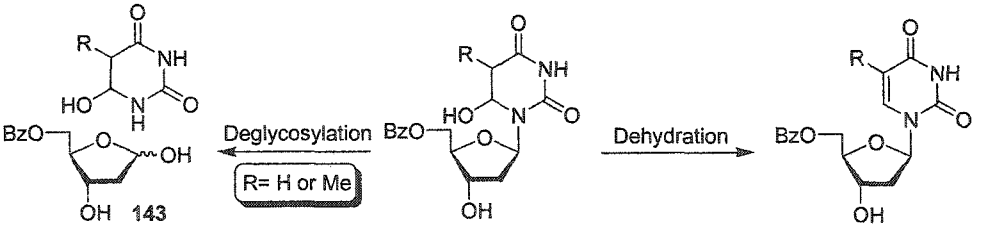

Figure 44. Deglycosylation and dehydration pathways of C6 hydrates.

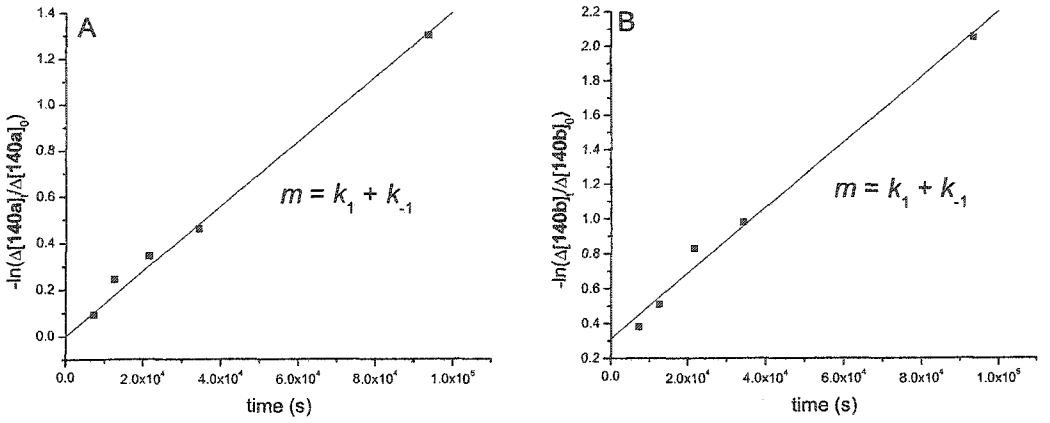

Figure 45. Epimerization of diastereomeric 5'-benzoyl C6-hydrates (A) **140a**, and (B) **140b** as a function of time. The difference between the concentration of **140** at a given time and at equilibrium is defined as Δ[**140**]. The difference between the initial and equilibrium concentration of **140** is defined as $\Delta[\mathbf{140}]_0$.

Incubation of 2'-deoxyuridine C6 hydrates (**140a, b**) at 37 °C in 2.8:1 D_2O/CH_3CN revealed that both diastereomers readily epimerize to form an equilibrium mixture (**140a:140b** = 0.67). Under these conditions, equilibrium is reached by both diastereomers in ~ 24 h. By measuring the approach to equilibrium, the epimerization rates of both diastereomers were determined (Figure 45, Table 5). Thymidine hydrates (**142a, b**) also underwent facile epimerization to four diastereomers when incubated at 37 °C. However, due to the overlapping chemical shifts of the four diastereomers, the kinetics of thymidine C6 hydrate (**142a, b**) epimerization were not measured.

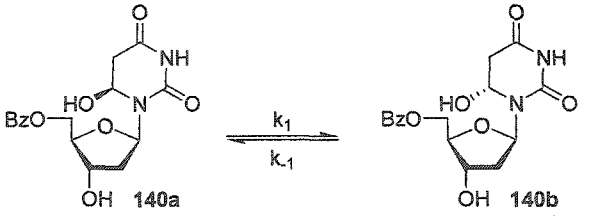

Table 5. Epimerization rates of 5'-benzoyl 2'-deoxyuridine C6 hydrates.[a]

Starting diastereomer	k_1 X 10^6 (s^{-1})	k_{-1} X 10^6 (s^{-1})
140a	11.2	7.6
140b	8.3	5.7

[a] Rate constants are the average of two identical experiments.

In order to determine the extent, if any, to which deglycosylation occurs in comptetition with dehydration of pyrimidine C6 hydrates **140** and **142**, these metastable compounds were heated for 1 h at 90 °C. The sole products observed by HPLC were the dehydrated products, benzoylated 2'-deoxyuridine and thymidine in 71 and 72% yields respectively. Heating of benzoyl protected 2-deoxyribose (**143**), one of the products of the deglycosylation reaction, under these conditions leads to significant decomposition. In order to determine the minimum amount of deglycosylation which could be detected, samples of pyrimidine hydrates **140** and **142** were spiked with protected 2-deoxyribose (**143**) prior to thermolysis. These experiments indicate that yields of **143** less than 4% are not detectable by this method. Futhermore, the fact that dehydration only accounts for ~70 % of the starting material suggests that other products may be formed. Thus, these experiments do not conclusively rule out deglycosylation.

The stabilites of the pyrimidine hydrates (**140**, **142**) at 37 °C were evaluated as a function of pH (Table 6, Figure 46). Both 2'-deoxyuridine and thymidine-C6 hydrates show a maximum stability at pH 6.0 where dehydration is extremely slow ($t_{1/2}$ > 380 h). Epimerization occurs more rapidly than dehydration under the ^{1}H NMR analysis conditions. As the pH is increased to 7.4 and 8.0, both pyrimidine hydrates dehydrate more rapidly. At a given pH, thymidine C6-hydrate **142** is more stable than 2'-deoxyuridine C6-hydrate (**140**). The half-lives of **142a**, and **140a** at pH 7.4 are 46.5 and

24.4 h, respectively. A comparable half-life (33 h) for thymidine C6-hydrate has been measured in DNA.[126]

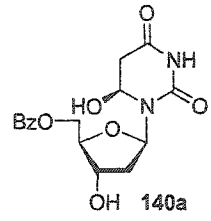

140a

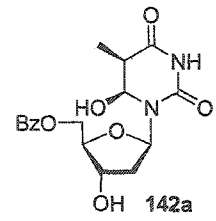

142a

Table 6. Dehydration of pyrimidine hydrates at 37 °C as a function of pH, buffer concentration and % acetonitrile.

C6-Hydrate	pH	$[KH_2PO_4]$/(mM)	% CH_3CN	k_d X 10^6 (s^{-1})	$t_{1/2}$ (h)
142a	6.0	20	5	<0.4	>785
142a	7.4	20	5	4.1	46.5
142a	8.0	20	5	11.3	17.0
142a	7.4	40	5	4.7	40.6
142a	6.0	20	50	<0.2	>1046
142a	7.4	20	50	2.9	66.3
142a	8.0	20	50	5.9	32.6
140a	6.0	20	5	~0.5	~385
140a	7.4	20	5	7.9	24.4
140a	8.0	20	5	26.8	7.2

In addition to pH, buffer concentration and organic solvent exerted a significant influence on the dehydration rates of pyrimidine hydrates. Increasing the buffer concentration from 20 to 40 mM significantly decreases the half-life of thymidine C6-hydrate (**142a**). This rate dependence upon buffer concentration suggests that the dehydration occurs via general base catalysis. This implies that the overall greater stability of thymidine C6-hydrates relative to 2'-deoxyuridine C6-hydrates is a result of differing acidities of the C5 proton in the two compounds. The influence of acetonitrile concentration upon the dehydration rate is supports this mechanism as it is consistent with the formation of a charged intermediate that is stabilized more effectively in H_2O.

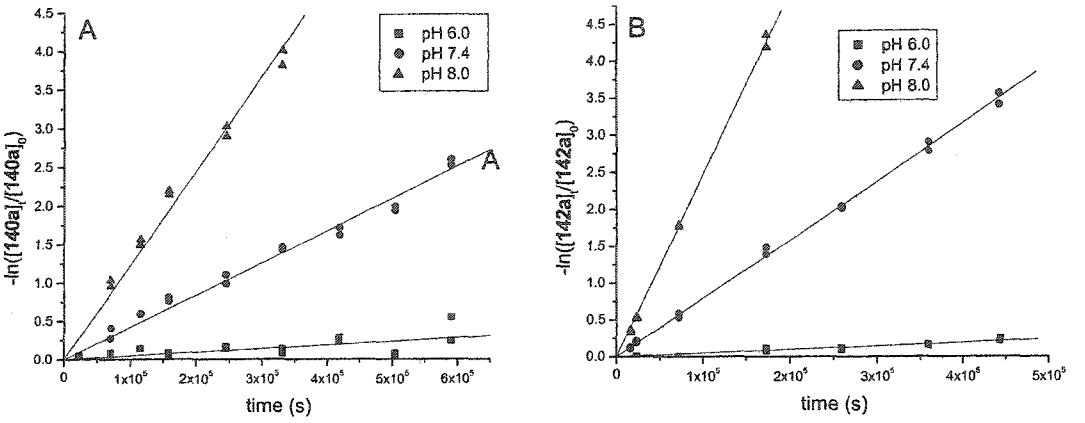

Figure 46. The dehydration of (A) 2'-deoxyuridine C6-hydrate (**140a**) and (B) thymidine C6 hydrate (**142a**) at pH 6.0, 7.4, and 8.0.

3.5 Generation of Monomeric 5,6-Dihydro-2'-deoxyuridin-6-yl

3.5.1 Reactivity of 5,6-Dihydro-2'-deoxyuridin-6-yl under anaerobic conditions

Preliminary experiments were conducted to ensure that the C6 *t*-buyl ketone radical precursor (**122a, b**) underwent the desired Norrish type I photoreaction. Photolysis of either diastereomer (1.0 mM) of the radical precursor under degassed conditions in the presence of 10 mM 2-mercaptoethanol (BME) resulted in high yields of 5,6-dihydro-2'-deoxyuridine (**131**, Table 7, Figure 47). As this product is derived from trapping of the C6 pyrimidine radical with BME, it demonstrates that both diastereomers of **122** undergo the Norrish I photocleavage efficiently. In the absence of BME, 2'-deoxyuridine (**144**) and 5,6-dihydro-2'-deoxyuridine (**131**) are formed, presumably through radical-radical disproportionation reactions.

Table 7. Products formed from 5,6-dihydro-2'-deoxyuridin-6-yl under anaerobic conditions.

Radical Precursor	[BME]	% Yield			Mass Balance
		131/132	**140**	**144/138**	
122a	-	32 ± 1	-	42 + 5	81 ± 7
122a	10 mM	104 ± 8	-	-	103 ± 2
122b	10 mM	97 ± 8	-	-	98 ± 6
130	-	11 ± 1	7.7 ± 3.3	36 ± 3	75 ± 2
130	100 mM	102 ± 1	-	-	102 ± 3

Photolysis of the benzoyl protected radical precursor (**130**) under anaerobic conditions in the presence of thiol afforded high yields of benzoyl 5,6-dihydro-2'-deoxyuridine (**132**). This indicated that the photochemical reactivity of the radical precursor was unaffected by the presence of the benzoyl group.

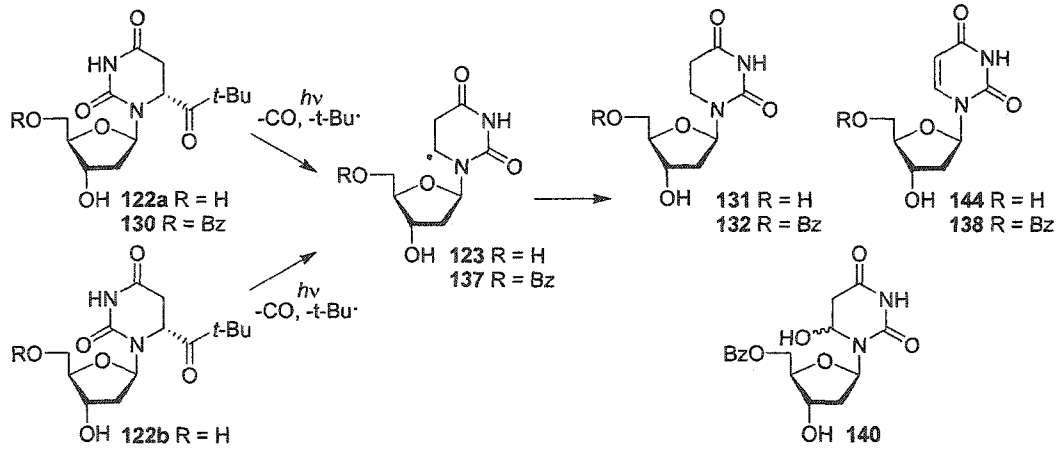

Figure 47. Generation of the 5,6-dihydro-2'-deoxyuridin-6-yl (**123**, **137**) under degassed conditions.

Generation of **137** under anaerobic conditions in the absence of BME resulted in the formation of **132** and **138**, the expected disproportionation products, as well as 2'-deoxyuridine C6 hydrate (**140**). This product could result from residual oxygen in

solution or oxidation of the radical to the respective carbocation, followed by hydration (Figure 48). Photoreduction product **136** was not observed under any photolysis conditions.

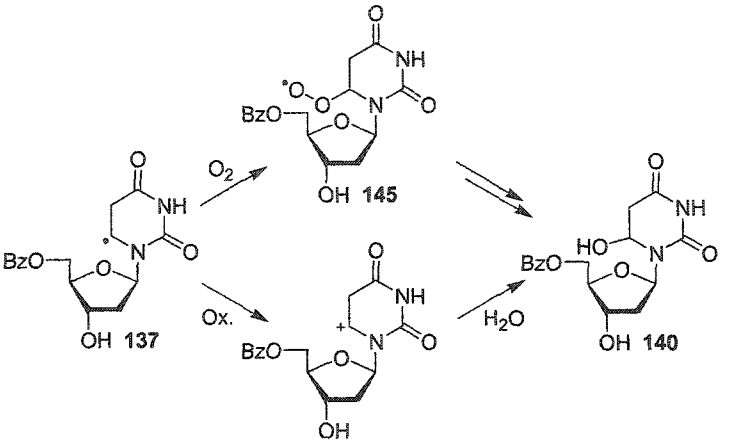

Figure 48. Possible mechanisms for the formation of 2'-deoxyuridine C6 hydrate **140**.

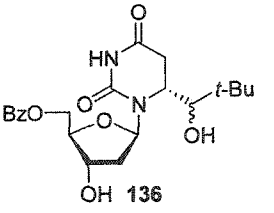

3.5.2 Reactivity of 5,6-Dihydro-2'-deoxyuridin-6-yl under aerobic conditions

Generation of 5,6-dihydro-2'-deoxyuridin-6-yl (**137**) in the presence of O_2 results in the formation of C6-hydrate (**140**) and 2'-deoxyuridine (**138**) as well as minor amounts of 2-deoxyribonolactone (**133**, Figure 49). In order to maintain oxygen in pseudo first-order excess, aerobic photolyses were conducted using low concentrations of **130** (6.2-25 μM). The identity and distribution of the products formed under aerobic conditions are

influenced by thiol concentration (Table 8). In the absence of thiol, the major observed product is C6-hydrate (**140**). Significant amounts of 2'-deoxyuridine (**138**) are also observed, presumably due to radical-radical reactions. Furthermore, 2-deoxyribonolactone (**133**) is also observed in low yield in the absence of thiol.

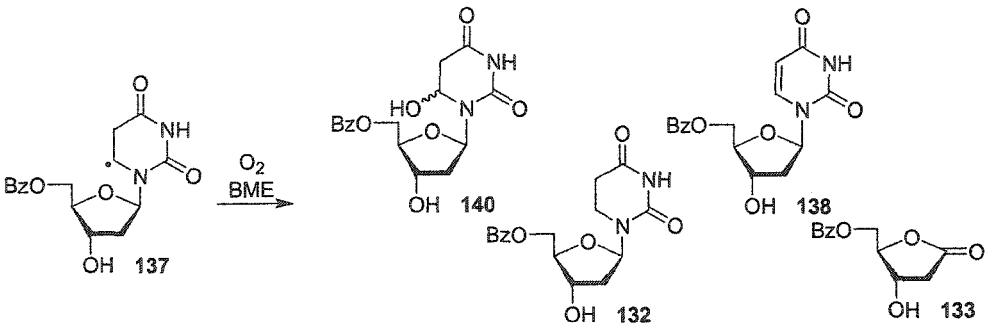

Figure 49. Products formed from radical **137** in the presence of O_2 and thiol.

Table 8. The effect of thiol on the distribution of products formed from radical **137** under aerobic conditions.

[BME]	% Yield[a]				Mass
(mM)	**132**	**140**	**138**	**133**	Balance
-	-	34 ± 7	20 ± 7	1.5 ± 0.3	71 ± 1
10	1.5 ±1.5	83 ± 3	9.1 ± 2.6	0.4 ± 0.2	96 ± 1
100	25 ± 1	67 ± 6	5.9 ± 2.3	-	99 ± 1
400	95 ± 1	14 ± 2	2.1 ± 0.7	-	104 ± 1

[a] % Yields are the average of two identical experiments and calculated based upon the amount of **130** converted.

At low BME concentration (10 mM), the yield of C6 hydrate (**140**) is increased. 2-Deoxyribonolactone (**133**) is still observed, albeit in much lower yield. A low yield of 5,6-dihydro-2'-deoxyuridine (**132**) is formed due to trapping of the C6 radical (**137**) by thiol. The amount of 2'-deoxyuridine (**138**) is reduced by half as radical-radical reactions

are suppressed. The reduction of radical-radical reactions presumably accounts for the significantly higher mass balance in the presence of thiol.

At 400 mM BME, 5,6-dihydro-2'-deoxyuridine (**132**) is formed in 95 % yield, indicating that the low concentrations (~ 0.2 mM) of O_2 in solution cannot compete with BME for radical **137**. Even at the highest BME concentration used (400 mM), photoreduction product **136** is not observed.

3.5.3 Mechanism of 2-Deoxyribonolactone Formation.

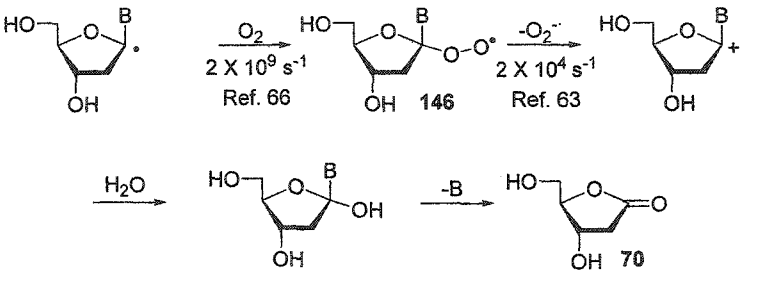

Figure 50. Mechanism for the formation of 2-deoxyribonolactone from a C1' nucleoside radical.

The formation of 2-deoxyribonolactone (**133**) from 5,6-dihydro-2'-deoxyuridin-6-yl (**137**) implies that the C1' position of nucleotides can be oxidized by an initially formed nucleobase radical. This is a significant observation because it reveals an indirect pathway for oxidation of a position which has very low accessibility within the minor groove of the DNA duplex.[55] The formation of 2-deoxyribonolactone proceeds by oxidation of a C1' sugar radical intermediate (Figure 50). Three mechanisms by which a C1' radical, and thereby **133**, could be formed from **137** were considered.

The possibility that the observation of **133** was due to an artifact introduced by the radical precursor was considered. Norrish type II photoreaction of the radical precursor

(**130**) could generate the requisite C1' radical (Figure 51). However, this mechanism was dismissed based upon the inhibition of 2-deoxyribonolactone by a low concentration of thiol. Generation of 5,6-dihydro-2'-deoxyuridin-6-yl (**137**) in the presence of 10 mM BME reduces the yield of lactone ~ 75 % (Table 8). If this pathway was inhibited by thiol, the result would be the formation of photoreduction product **136**, which is not observed. If the C1' radical was formed, formation of 2-deoxyribonolactone (**133**) would not be significantly inhibited by 10 mM thiol. This is due to the fact that oxygen (0.2 mM) reacts with the C1' radical three orders of magnitude more rapidly than thiol.[66]

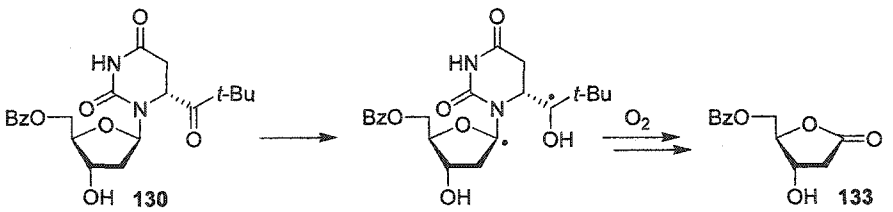

Figure 51. Formation of 2-deoxyribonolactone (**133**) by a type II photoreaction.

Another possible mechanism, β-scission of the C6 pyrimidine radical to form a C1' radical was dismissed based upon kinetic considerations (Figure 52). Since low concentrations of BME (10 mM) are sufficient to inhibit formation of 2-deoxyribonolactone (**133**), the β-scission reaction would have to occur with a rate constant of less than 10^5 s^{-1}. This rate constant is not sufficiently large for the β-scission process to compete with O_2 trapping of the pyrimidine radical (**137**). Furthermore, photolysis of **122a** or **122b** under degassed conditions results in near quantitative formation of 5,6-dihydro-2'-deoxyuridine (**131**, Table 7). The β-scission reaction would

be expected to reduce the yield of this product. Therefore, the β-scission mechanism is deemed unlikely.

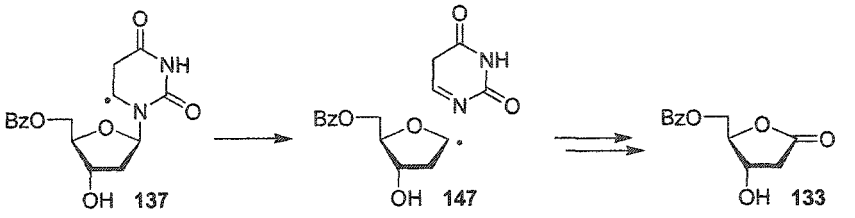

Figure 52. Formation of 2-deoxyribonolactone (**133**) by β-scission.

The mechanism which best accounts for the formation of benzoylated 2-deoxyribonolactone (**133**) is intramolecular C1' hydrogen atom abstraction by the C6 peroxyl radical (**145**, Figure 53). This pathway is consistent with the thiol effect upon formation of **133**. A similar reaction involving radiolytically produced peroxyl radical (**148**) has been reported to occur on the order of 1 s^{-1}.[128] This result is significant as it suggests that C1' radicals can be formed by ionizing radiation via a multi-step process, despite the inaccessibility of this position to a diffusible species.[55]

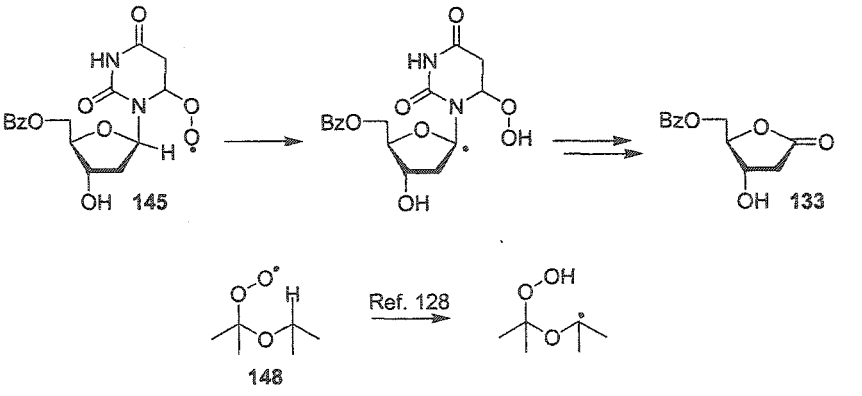

Figure 53. Formation of 2-deoxyribonolactone (**133**) by intramolecular hydrogen abstraction.

3.5.4 Mechanism of C6 Hydrate Formation.

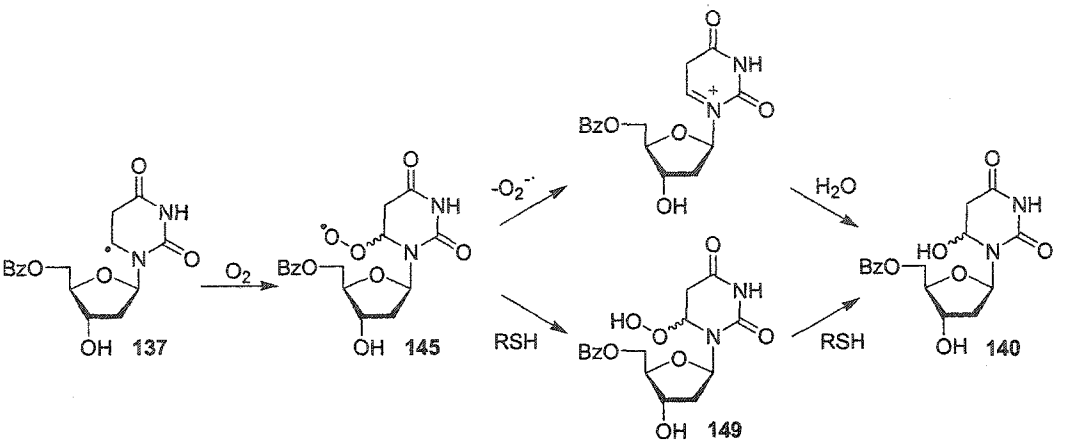

Figure 54. Mechanisms for the formation of 2'-deoxyuridine C6-hydrate (**140**).

In the presence of oxygen and thiol concentrations of up to 100 mM, 2'-deoxyuridine C6 hydrate (**140**) is the major product formed from the 5,6-dihydro-2'-deoxyuridin-6-yl (**137**, Table 8). Two mechanisms were considered for the formation of this product under aerobic conditions (Figure 54). The first was formation of the C6 peroxyl radical (**145**) followed by elimination of superoxide. Elimination of superoxide would be noteworthy because it is capable of generating species such as hydroxyl radical that are known to damage DNA. Thus, one DNA damage product, a pyrimidine C6 radical, might generate a reactive species (OH·) capable of producing further damage. Elimination of superoxide has been observed for related peroxyl radicals (**146, 150, 151**, Figure 55).[50,51,63] The most germane example is elimination from the dihydrouracil C6 peroxyl radical, although this reaction is strongly pH dependent.[51]

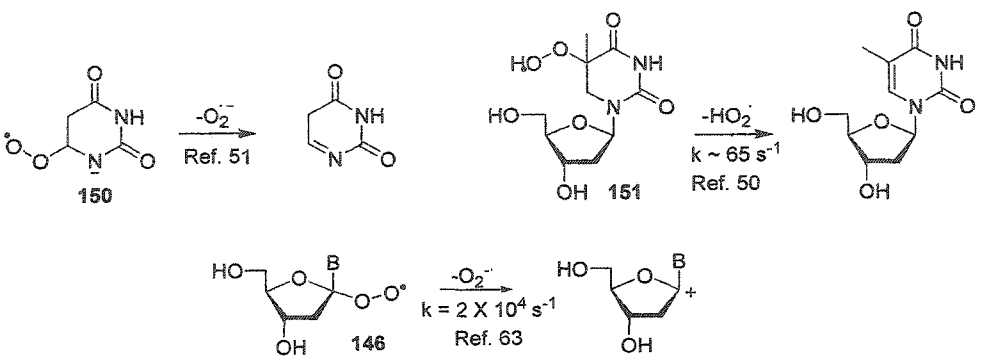

Figure 55. Elimination of superoxide from nucleobase radicals.

This mechanism was tested by generating radical **123** in the presence of cytochrome C or epinephrine which are probes for superoxide.[129,130] In order to minimize bimolecular reactions of the C6 peroxyl radical which would compete with the unimolecular elimination of interest, reactions were carried out at a low concentration of **122a** (50 μM). Reduction of cytochrome C by superoxide anion is observable by an increase in UV absorbance at 550 nm. Oxidation of epinephrine by superoxide is observed by UV at 480 nm. However, neither assay indicated the presence of superoxide anion.

Epinephrine allows qualitative measurement of superoxide release. The cytochrome c assay can provide a more quanitative measurement of superoxide production. The lack of a measureable increase in the UV absorbance at 550 nm indicates that superoxide release from the C6 peroxyl radical to form 2'-deoxyuridine C6 hydrate is not a major pathway. Assuming that the yield of 2'-deoxyuridine C6 hydrate produced from **123** under aerobic conditions is approximately equal to that of

benzoylated 2'-deoxyuridine C6 hydrate (**140**) produced from the benzoylated radical precursor (**130**) under similar conditions, the expected increase in UV absorbance can be calculated. This is carried out using the extinction coefficients for the oxidized (8900 $M^{-1}cm^{-1}$) and reduced (29, 500 $M^{-1}cm^{-1}$) forms of cytochrome c. Photolysis of benzoylated radical precursor **130** under aerobic conditions in the absence of thiol results in the formation of ~ 34 % of **140**, based upon converted starting material (Table 8). This value can be used to estimate the yield of 2'-deoxyuridine C6-hydrate produced from radical precursor **122a**. Since experiments using cytochrome c as a probe for superoxide elimination were carried out to high conversion, it is assumed that the 50 μM concentration of **122a** results in a 17 μM concentration of superoxide anion in solution. Assuming this results in quantitative reduction of cytochrome c, an increase of 0.35 AU would be observed. The lack of a noticeable increase in UV-absorbance at 550 nm indicates that superoxide elimination from **145** is not a major pathway.

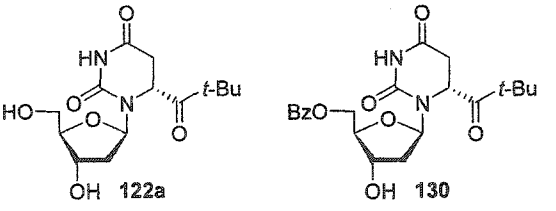

Based upon the cytochrome c and epinephrine assays, superoxide elimination from the C6 peroxyl radical is at most minor pathway. However, the observation of 2-deoxyribonolactone (**133**) formation from **137** under aerobic conditions implies that superoxide is produced from an intermediate C1' peroxyl radical (Figure 50, Figure 55). The yield of 2-deoxyribonolactone (**133**, 1.5 %) formed from the photolysis of

benzoylated radical precursor **130** was used to estimate the yield of 2-deoxyribonolactone formed from **122a**. Using the same method described above, the amount of superoxide release and expected increase in UV absorbance due to the reduction of cytochrome c was calculated. An increase of 0.015 AU was predicted. This could be decreased by incomplete conversion of the starting material or less than quantitative reduction of cytochrome c. This may explain the lack of detectable superoxide elimination.

The most likely mechanism for the formation of C6 hydrate (**140**) in the presence of oxygen and thiol was deemed to be trapping of peroxyl radical **145** with a hydrogen atom to form the C6 hydroperoxide (**149**) which was subsequently reduced to afford the pyrimidine C6 hydrate (**140**, Figure 54). This mechanism is consistent with the oxygen requirement for the formation of C6 hydrate (**140**) in the presence of thiol. Furthermore, the fact that yields of **140** are highest in the presence of moderate thiol concentrations supports this mechanism (Table 8).

3.5.5 Measurement of the Rate Constant for Hydrogen Atom Abstraction by 5,6-Dihydro-2'-deoxyuridin-6-yl from Hydrogen Atom Donors

3.5.5.1 Reaction of 5,6-Dihydro-2'-deoxyuridin-6-yl with BME

In order to gain more quantitative information regarding the reactivity of the 5,6-dihydro-2'-deoxyuridin-6-yl (**137**), competitive kinetic methods were used to measure the reaction of this species with hydrogen atom donors. In the first type of experiment, the rate constant for reaction of **137** with BME was measured using oxygen as the competitor (Figure 56). Reaction of BME with **137** affords 5,6-dihydro-2'-deoxyuridine (**132**), while trapping with oxygen yields 2'-deoxyuridine C6 hydrate (**140**).

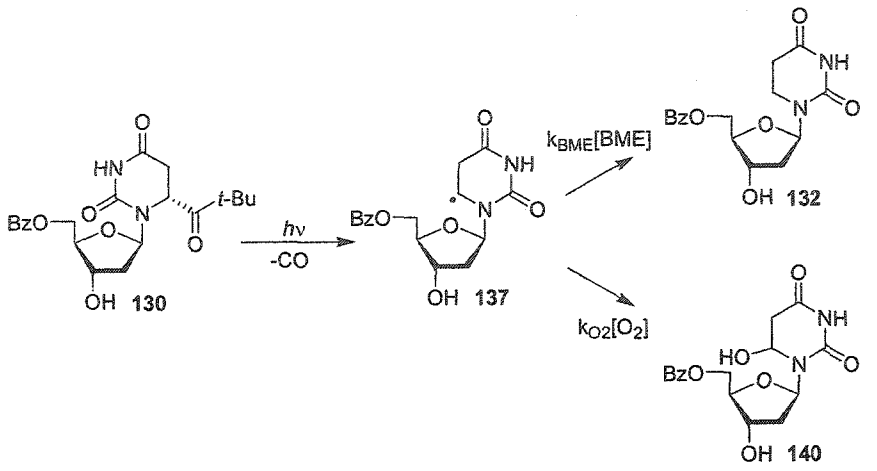

Figure 56. Competition between O_2 and BME for the 5,6-dihydro-2'-deoxyuridin-6-yl (**137**).

In order to estimate a rate constant (k_{BME}) for the reaction of **137** with BME, the ratio of these two products was meausured at multiple BME concentrations (Figure 57). By estimating the concentration of oxygen in solution at 0.2 mM and the rate constant for

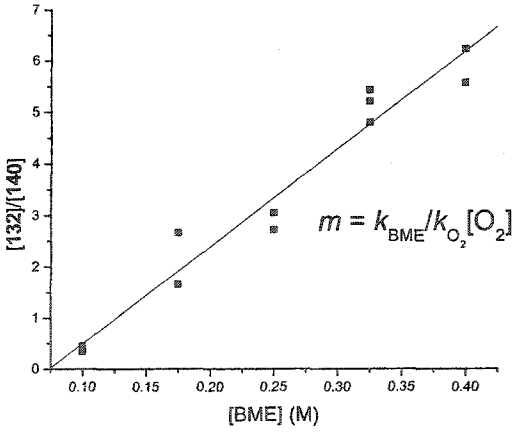

$$\frac{[132]}{[140]} = \frac{k_{BME}[BME][137]}{k_{O_2}[O_2][137]} \qquad (1)$$

Figure 57. The ratio of benzoylated 5,6-dihydro-2'-deoxyuridine (**132**) to 2'-deoxyuridine C6 hydrate (**140**) as a function of BME concentration.

the reaction of oxygen with **137** (k_{O_2}) at 2 X 10^9 $M^{-1}s^{-1}$, a value of (8.8 ± 0.5) X 10^6 M^{-1} was obtained for k_{BME} (eq 1). This rate constant is consistent with others reported for the reaction of alkyl radicals with alkyl thiols.[131]

3.5.5.2 Reaction of the 5,6-dihydro-2'-deoxyuridin-6-yl with 2-deoxyribose models.

In order to determine if the 5,6-dihydro-2'-deoxyuridin-6-yl is sufficiently reactive to abstract hydrogen atoms from the sugars of adjacent nucleotides in DNA, competitive kinetic studies were conducted to ascertain the rate at which **137** reacts with 2-deoxyribose sugar models. The hydrogen atom donors used were 2,5-dimethyltetrahydrofuran (DMTHF) and isopropanol. DMTHF was used to mimic the C1' position of the 2-deoxyribose sugar moiety while isopropanol was used to mimic the C4' position.

In these experiments, the competition measured was that between trapping of radical **137** by the hydrogen atom donor to afford 5,6-dihydro-2'-deoxyuridine (**132**) and radical-radical disproportionation to give protected 2'-deoxyuridine (**138**) as well as **132**. In order to avoid competitive trapping by oxygen, these reactions were carried out under anaerobic conditions. This method is similar to that used to measure the rate of reaction of the 2'-deoxy-5-methyleneuridin-5-yl radical with 2-deoxyribose sugar mimics, but complicated by the fact that the product of hydrogen atom trapping is also formed via disproportionation (Figure 58).[113]

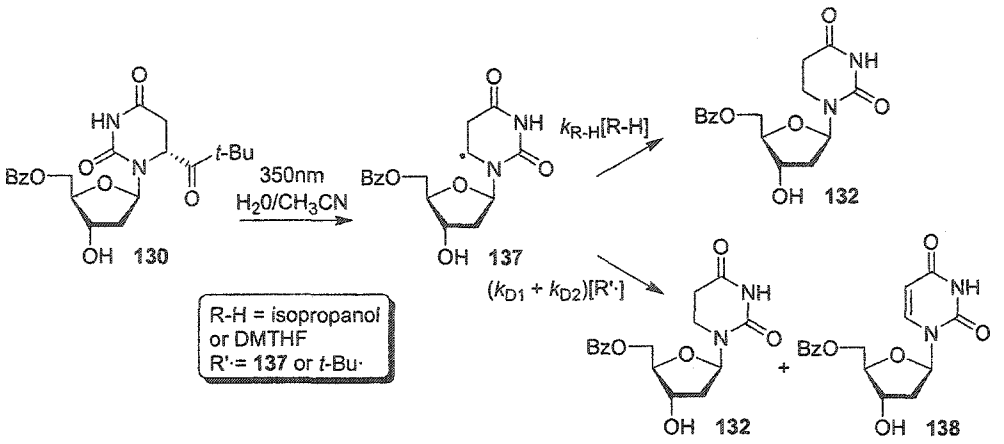

Figure 58. Measurement of the rate of hydrogen atom abstraction from 2-deoxyribose models.

$$\frac{[\mathbf{132}]}{[\mathbf{138}]} = \frac{k_{R\text{-}H}[R\text{-}H]}{k_{D2}[\mathbf{137}]} + \frac{k_{D1}}{k_{D2}} \qquad (2)$$

In order to determine the rate constant for reaction of **137** with the hydrogen atom donor of interest, the ratio of **132** to **138** was measured as a function of donor concentration. The rate constant was determined by plotting [**132**]/[**138**] versus [R-H]/k_{D2}[**137**] where R-H is the hydrogen atom donor and k_{D2} is the rate constant for radical-radical disproportionation to form **138** which was assumed to be 2 X 10^9 (eq 2, Figure 58). The rate constant for the formation of **132** by radical-radical reactions was given by k_{D1}. The steady state radical concentration ([**137**]) was calculated by dividing the amount of radical precursor (**130**) converted by the photolysis time.

Experiments conducted using DMTHF as a hydrogen atom donor revealed that C6 pyrimidine radical **137** is trapped with a rate constant of 31 ± 2.5 $M^{-1}s^{-1}$ (Table 9, Figure 59) This value is comparable to that of 46.1 ± 15.4 $M^{-1}s^{-1}$ obtained for the 2'-deoxy-5-methyleneuridin-5-yl radical (**26**).[113] Competitive kinetic studies were also carried out using isopropanol as the hydrogen atom donor. A rate constant of 8.5 ± 0.8

$M^{-1}s^{-1}$ was obtained for this reaction, which is again comparable to that of 13.6 ± 3.0 $M^{-1}s^{-1}$ measured for the 2'-deoxy-5-methyleneuridin-5-yl (**26**).

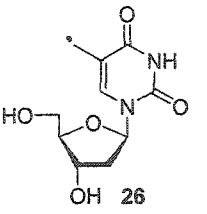

26

Due to their relative inefficiency, the hydrogen atom donors used in these experiments are present in high concentrations (up to 10 M in isopropanol experiments). This raised the concern that changing solvent composition might influence the ratio of **132** to **138** and thus skew the observed rate constant for hydrogen atom abstraction. In order to address this concern, experiments were carried out using selectively deuterated isopropanol. If a solvent effect were responsible for the increase in [**132**]/[**138**], deuteration would have no effect. The observation of a kinetic isotope effect would indicate that the change in [**132**]/[**138**] was indeed a result of hydrogen atom abstraction from isopropanol.

Table 9. Rate constants and kinetic isotope effects for the reaction of **137** with 2-deoxyribose sugar models

Hydrogen atom donor	$k_{R\text{-}H}$ ($M^{-1}s^{-1}$)	KIE
DMTHF	31 ± 2.5[a]	-
Isopropanol	8.5 ± 0.8[b]	-
Isopropanol-2D	1.3 ± 0.2[b]	6.5 ± 1.2
Isopropanol-d_8	0.19 ± 0.016[a]	45 ± 5

[a] Value is the average of two identical experiments. [b] Value is the average of four identical experiments.

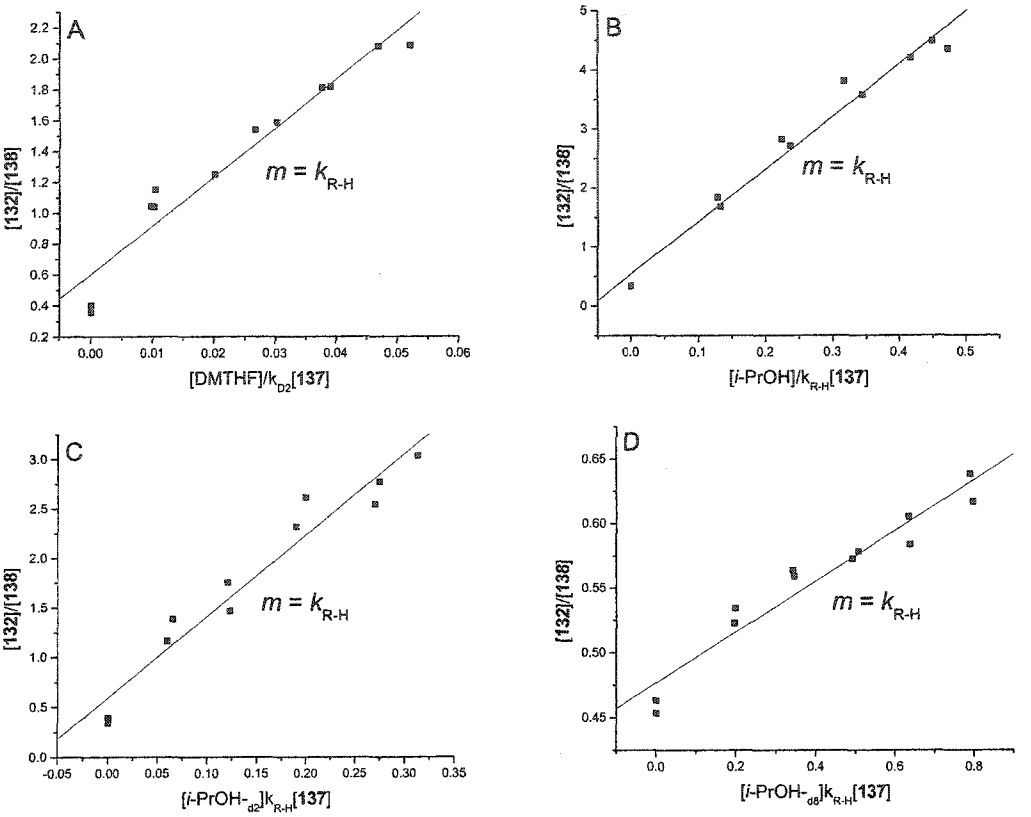

Figure 59. The ratio of benzoylated 5,6-dihydro-2'-deoxyuridine (**132**) to 2'-deoxyuridine (**138**) as a function of steady state radical concentration ([**137**]) and (A) [*i*-PrOH], (B) [DMTHF], (C) [*i*-PrOH-2D], or (D) [*i*-PrOH-d_8].

Measurement of the rate constant with which isopropanol-d_8 reacts with the C6 pyrimidine radical (**137**) gives a value of (1.9 ± 0.16) X 10^{-1} $M^{-1}s^{-1}$. This corresponds to a kinetic isotope effect of 45 ± 6. This large isotope effect is the product of the primary and six secondary isotope effects which result from hydrogen atom abstraction. The reaction of the C6 pyrimidine radical (**137**) with isopropanol-2D occurs with a rate constant of 1.3 ± 0.2 $M^{-1}s^{-1}$. This indicates that the primary kinetic isotope effect for hydrogen atom abstraction is 6.5 ± 1.2. Using this value, it is possible to extract a figure of 1.4 ± 0.3 for the individual secondary kinetic isotope effects observed in the

isopropanol-d_8 experiment. This unusually large value for a β-secondary isotope effect may be a reflection of error associated with the competitive kinetic method.

From the above competitive kinetic experiments, a number of conclusions can be drawn regarding the reactivity of the 5,6-dihydro-2'-deoxyuridin-6-yl in DNA. Based upon the rate constant measured for the reaction of **137** with BME [$(8.8 \pm 0.5) \times 10^6$ $M^{-1}s^{-1}$], it can be concluded that, at least with an efficient hydrogen atom donor, the reactivity of the pyrimidine radical parallels that of a typical alkyl radical. The rate constant for the reaction of the 5,6-dihydro-2'-deoxyuridin-6-yl with DMTHF was found to be 31 ± 2.5 $M^{-1}s^{-1}$. Assuming DMTHF is a good model for the C1' position of a nucleotide, this reaction may be feasible under anaerobic conditions. In DNA, the preorganization of substrate and radical induced by duplex structure could facilitate this reaction. Under aerobic conditions, hydrogen atom abstraction from 2-deoxyribose by the 5,6-dihydro-2'-deoxyuridin-6yl clearly cannot compete with trapping by oxygen.

3.6 Summary of the study of monomeric 5,6-dihydro-2'-deoxyuridin-6-yl.

Studies on the monomeric radical precursor (**123**, **137**) demonstrated that this modified nucleoside is an efficient tool for generating a 5,6-dihydro-pyrimidin-6-yl. The C6 pyrimidine radical reacts rapidly with thiol (k_{BME} = $(8.8 \pm 0.5) \times 10^6$ $M^{-1}s^{-1}$) , affording high yields of 5,6-dihydro-2'-deoxyuridine (**132**) under degassed conditions.

The rate constant with which 5,6-dihydro-2'-deoxyuridin-6-yl (**137**) reacts with the deoxyribose sugar mimics DMTHF and isopropanol was measured using competitive kinetic techniques. A rate constant of 31 ± 2.5 $M^{-1}s^{-1}$ was obtained when DMTHF was used as a hydrogen atom donor. Although this value is low, the effective concentration

of 2-deoxyribose sugar moieties near the 5,6-dihydro-2'-deoxyuridin-6-yl in DNA may be very high, allowing internucleotidyl hydrogen atom abstraction to occur under anaerobic conditions.

In the presence of oxygen, the major product derived from **137** is 2'-deoxyuridine C6-hydrate (**140**). This product is formed via reduction of the initially formed hydroperoxide. The stability of **140** as well at that of thymidine C6 hydrate (**142**) were directly measured as a function of pH and buffer concentration. Both 2'-deoxyuridine (**140**) and thymidine C6-hydrates (**142**) are sufficiently stable ($t_{1/2}$ > 24 h at pH 7.4) to possess significant lifetimes in DNA.

Low yields of 2-deoxyribonolactone (**133**) are also observed. This product is formed via an intramolecular C1' hydrogen atom abstraction by the C6 peroxyl radical. This process is inhibited by low thiol concentrations. The observation of 2-deoxyribonolactone (**133**) is significant as it indicates that this oxidized sugar product may be formed by pyrimidine C6 radicals in DNA.

3.2 Generation of 5,6-Dihydro-2'-deoxyuridin-6-yl in DNA.

3.2.1 Phosphoramidite and Oligonucleotide Synthesis.

In order to investigate the reactivity of the 5,6-dihydro-2'-deoxyuridin-6-yl (**123**) in DNA, oligonucleotides containing the C6 *t*-butyl ketone radical precursor (**122a, b**) were synthesized (Scheme 5). The diastereomeric C6 *t*-butyl ketone nucleosides (**122a,b**) were converted to the corresponding dimethoxytrityl derivatives (**150**, **152**) by treatment with 4,4'-dimethoxytrityl chloride in pyridine. The tritylated radical precursors were then converted to β-cyanoethyl phosphoramidites (**151**, **153**) by treatment with 2-cyanoethyl diisopropyl chlorophosphoramidite.

Scheme 5

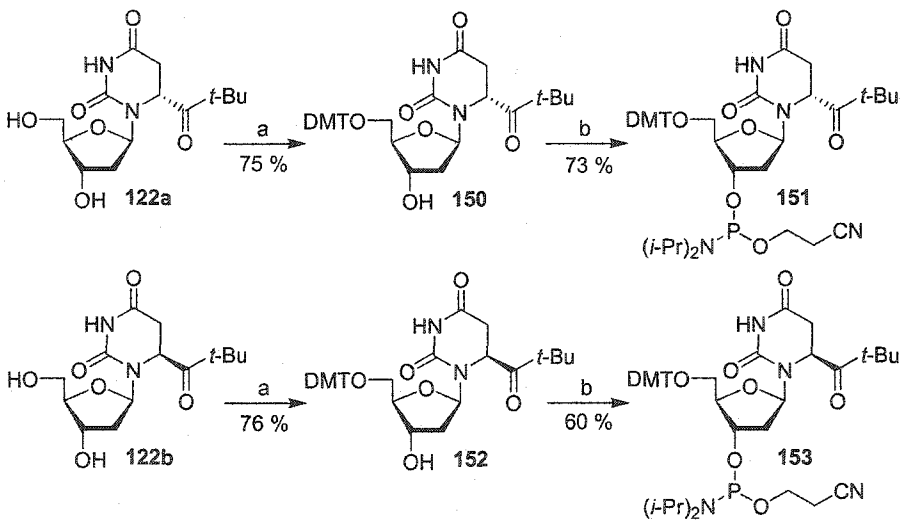

Oligonucleotides were synthesized using modifications of standard procedures for automated DNA synthesis. Instead of acetic anhydride, pivaloyl anhydride was used as a capping reagent. This was necessary to prevent acetylation of dG during the capping process of automated DNA synthesis.[133] To effect removal of oligonucleotide protecting groups, 0.05 M K_2CO_3 in methanol was used. Use of more stringent conditions (conc.

NH_4OH, 55°C) for deprotection resulted in degradation of **122**. This was ostensibly due to fragmentation of the dihydropyrimidine nucleobase, a process which has been observed for other dihydropyrimidines.[134,135]

To establish that the pyrimidine radical precursor was stable to DNA synthesis conditions and could be successfully incorporated into DNA, two oligonucleotides were initially synthesized (**154**, **155**). These were of the same sequence and differed only by the stereochemistry at the C6 position of the radical precursor.

5'-d(GAG CTA GCT CGA CCT **X**T A GGA CCT GCA GCT)
154, **X** = **122a**
155, **X** = **122b**

In order to verify that the C6 *t*-butyl ketone radical precursor (**122a**, **122b**) was successfully incorporated into oligonucleotides, enzymatic digestion was carried out. Radical precursor containing 30mers (**154**, **155**) were treated with nuclease P1 followed by phosphodiesterase I and calf intestinal alkaline phosphatase. Analysis of the digested oligonucleotides by HPLC revealed that the radical precursor (**122a**, **122b**) was not degraded by DNA synthesis or deprotection procedures (Figures 60, 61). Furthermore, the stereochemistry at the C6 position of each diasteromer was maintained without significant epimerization. All oligonucleotides, including **154** and **155** were also characterized by ESI-MS (see appendix C).

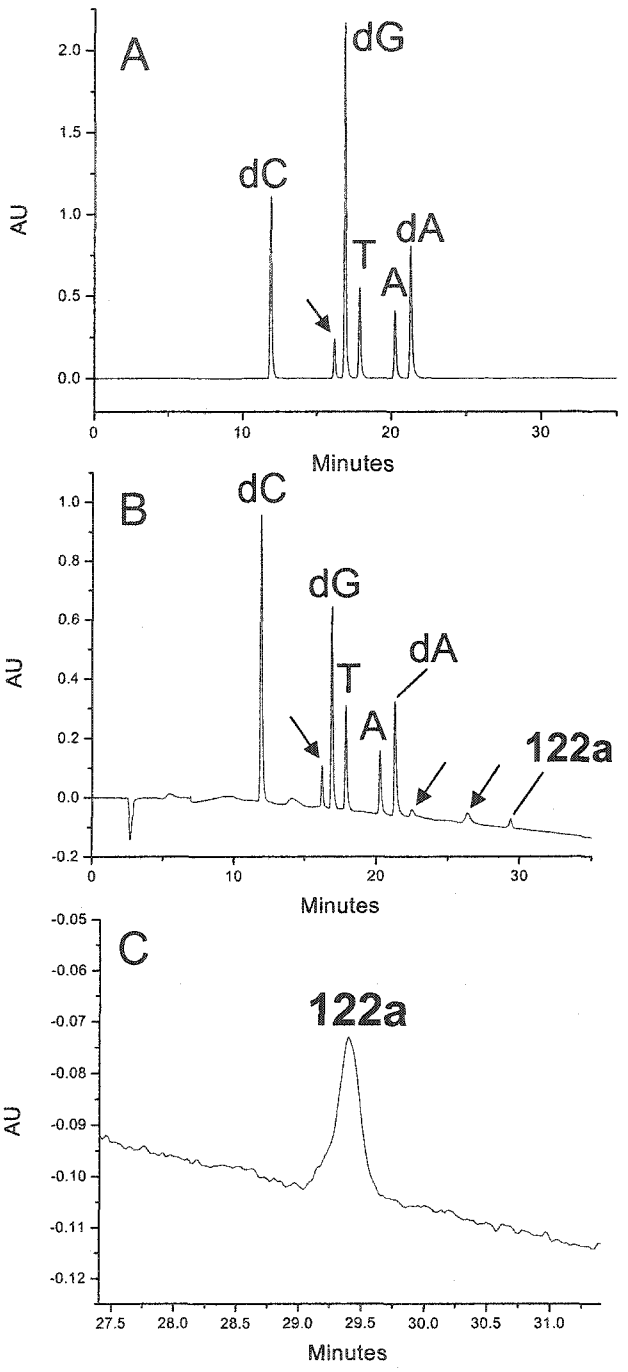

Figure 60. HPLC trace of the enzymatic digestion of **154**. (A) UV detection at 260 nm, (B) UV detection at 215 nm, and (C) expansion of region containing **122a** at 215 nm. Adenosine was added as an internal standard. Arrows denote unidentified peaks also present in the digestion of an ordinary oligonucleotide. The peak marked "**122a**" was of the same retention time as authentic material.

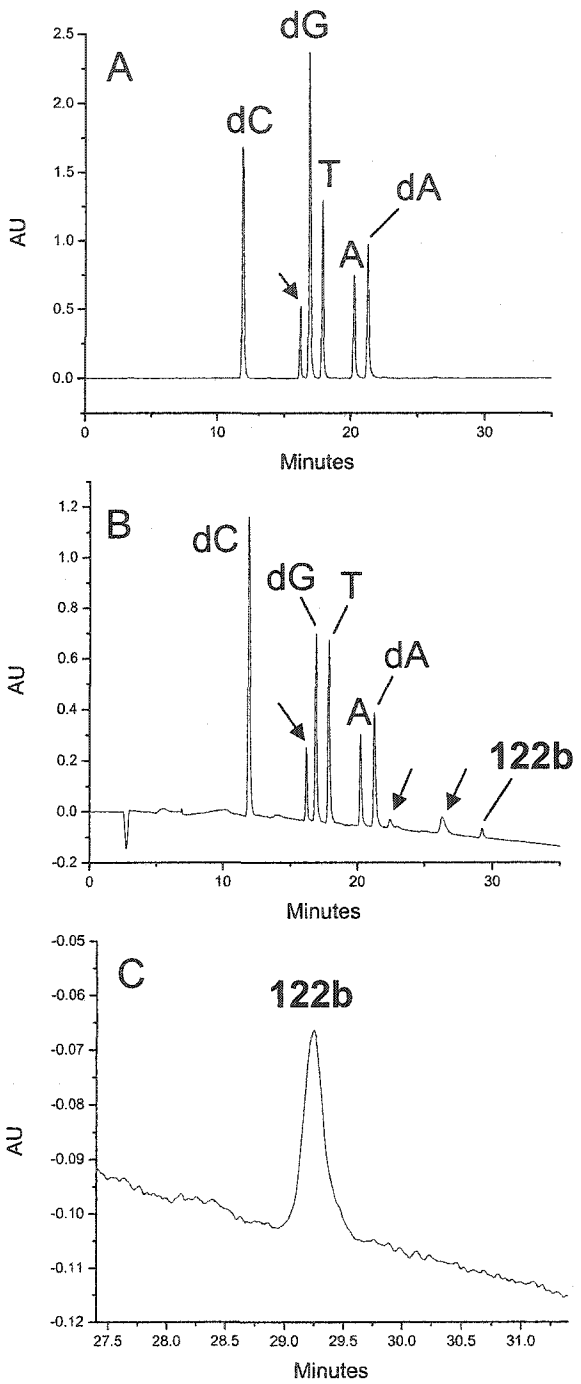

Figure 61. HPLC trace of the enzymatic digestion of **155**. (A) UV detection at 260 nm, (B) UV detection at 215 nm, and (C) expansion of region containing **122b** at 215 nm. Arrows denote unidentified peaks also present in the digestion of an ordinary oligonucleotide. The peak marked "**122b**" was of the same retention time as authentic material.

3.2.2 The Effect of the 5,6-Dihydro-2'-deoxyuridin-6-yl Radical Precursor on DNA Duplex Structure and Stability.

In order to determine the extent to which the radical precursor (**122a**) destabilizes the DNA duplex, UV-melting and CD experiments were conducted using 12mer duplex **156**. The UV absorbance of **156** (5 μM) in 100 mM NaCl as a function of temperature shows a non-sigmoidal curve indicative of non-cooperative melting (Figure 62B). Consequently, a meaningful melting temperature cannot be determined. The UV-melting curve of an oligonucleotide in which the radical precursor has been replaced with dU (**157**) is shown for comparison (Figure 62A). Based upon the melting curve of **156**, it can be concluded that the presence of the radical precursor perturbs DNA structure. The CD spectrum does show a conservative couplet characteristic of B-DNA with a positive band at 281 nm and a negative band at 253 nm (Figure 63).[136] Based upon these observations, it can be concluded that although the presence of the modified nucleotide destabilizes the double helix, duplex structure persists.

5'-d(AGT GCA **X**AA GCT)
3'-d(TCA CGT ATT CGA)
156 X = 122a
157 X = dU

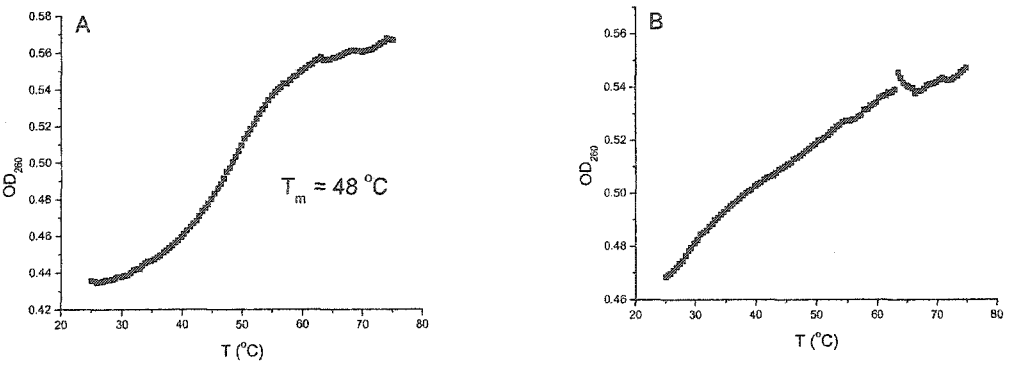

Figure 62. UV melting curve of duplexes containing (A), dU (**157**) and (B), the radical precursor (**156**). Melting studies were conducted at 5 μM duplex concentration in 10 mM PIPES, 10 mM $MgCl_2$, 100 mM NaCl, pH 7.2.

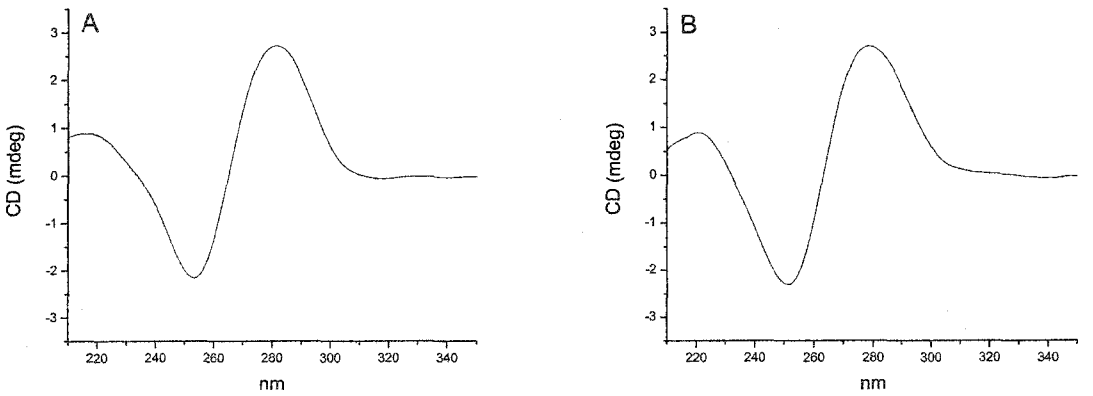

Figure 63. CD spectra of duplexes containing (A), the radical precursor (**156**) and (B), dU (**157**). Measurements were taken using 10 μM duplex in 10 mM KH_2PO_4, 100 mM NaCl, pH 7.2.

The perturbation of the double helical structure is ostensibly due to the bulky *t*-butyl group at the C6 position. Upon photolysis, this substituent is lost, with concomitant generation of the 5,6-dihydro-2'-deoxyuridin-6-yl (**123**). After generation of the radical, base pairing should be restored. DNA base pairs are known to open and reform in a dynamic process referred to as "breathing"; the lifetime of an A·T base pair is typically 0.5-7 ms.[137] In the absence of oxygen, this allows the base pair sufficient time to reform after generation of the radical. If O_2 reacts with **123** with a bimolecular rate constant of 2

X 10^9 $M^{-1}s^{-1}$, breathing is slow relative to peroxyl radical (**158**) formation (Figure 64). However, DNA peroxyl radicals are sufficiently long-lived (0.2-3.3 s) relative to breathing to permit the restoration of base pairing.[138] Therefore, regardless of the conformation in which the 5,6-dihydro-2'-deoxyuridin-6-yl (**123**) is formed, the long lifetime of the respective C6 peroxyl radical (**158**) permits conformational change to occur.

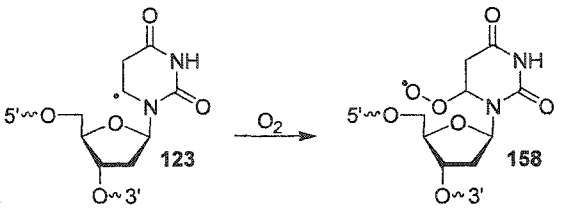

Figure 64. Formation of the C6 peroxyl radical (**158**) from 5,6-dihydro-2'-deoxyuridin-6-yl (**123**).

3.2.3 DNA Damage Induced by 5,6-Dihydro-2'-deoxyuridin-6-yl.

Independent generation of 5,6-dihydro-2'-deoxyuridin-6-yl (**123**) in DNA allows important questions regarding the reactivity of this species to be addressed. The objectives of this research were the assessment of DNA damage generated by the 5,6-dihydro-2'-deoxyuridin-6-yl radical and elucidation of the mechanism(s) by which this occurs. In addition to generating intranucleotidyl DNA damage, radical **123** could potentially damage adjacent sites. Studies in which pyrimidine C6 radicals were generated by γ-radiolysis provide evidence for this process.[6, 10-12] Moreover, the formation of tandem lesions from nucleobase radicals has been observed.[18-23] Generation of 5,6-dihydro-2'-deoxyuridin-6yl site specifically in DNA allows measurement of the

extent to which this reactive intermediate is involved in DNA damage amplification and tandem lesion formation.

3.2.3.1 Characterization of DNA Damage by PAGE.

Initial characterization of DNA damage resulting from 5,6-dihydro-2'-deoxyuridin-6-yl was carried out by using polyacrylamide gel electrophoresis (PAGE) to analyze photolyzed DNA substrates. The use of radiolabeled DNA enabled the use of picomolar amounts of material and enabled accurate measurement of the yields of cleavage products. DNA damage observed by PAGE is classified as either a "direct strand break" or an "alkali-labile lesion." A direct strand break refers to damage which severs the sugar phosphate backbone. Alkali-labile lesions are nucleotide modifications which, upon base treatment, undergo cleavage. 2-Deoxyribonolactone (**70**) and thymidine glycol (**46**) are examples of DNA lesions which are cleaved by base treatment (Figure 65). The base sensitivity of these lesions is variable: For example, the oxidized abasic site (**70**) is cleaved more readily than thymidine glycol lesion (**46**).[39,93] Therefore, the base sensitivity of a damaged site can give structural insight. In PAGE experiments, two types of base treatment were used to cleave alkali-labile lesions. The first set of conditions (1.0 M piperidine, 90 °C, 20 min) was intended to cleave extremely labile lesions such as **70**, as well as more resistant nucleobase modifications such as **46**. The second set of conditions (0.1 M NaOH, 37 °C, 20 min) was intended to selectively cleave sites abasic such as **70**, which are more sensitive to basic conditions. The two sets of conditions allow different types of damage to be distinguished. However, it is important to note that not all nucleotide modifications lead to alkali-labilty. Cyclonucleoside **106** and and 8-oxo-2'-deoxyguanosine (**19**) are examples of non alkali-labile lesions.[39,93]

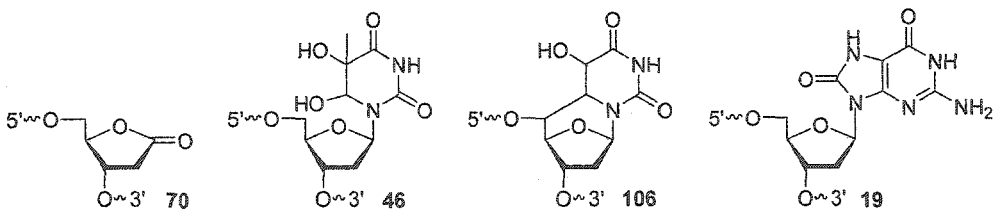

Figure 65. Alkali-labile (**70**, **46**) and non alkali-labile lesions (**106**, **19**).

3.2.3.1.1 Damage Produced by 5,6-Dihydro-2'-deoxyuridin-6yl in Single-Stranded DNA.

PAGE analysis of photolysates of radiolabeled radical precursor containing oligonucleotide **154** revealed that alkali-labile lesions are the main type of DNA damage produced by the 5,6-dihydro-2'-deoxyuridin-6-yl (Figures 66, 67). In a typical experiment, photolysis of radiolabeled **154** (~ 10 nM) under aerobic conditions followed by piperidine treatment (1.0 M, 90 °C, 20 min) resulted in 40-60 % cleavage of the oligonucleotide. As the conversion of the starting ketone is not measured in these experiments, the overall observed cleavage represents a lower limit for the yield of alkali-labile lesions.

5'-d(GAG CTA GCT CGA CCT_{15} **X** T_{17} A GGA CCT GCA GCT)
154, X = 122a

Very low levels of strand scission were observed without base treatment (< 5 %). This small amount of direct strand scission could be the result of the adventitious cleavage of alkali-labile lesions. In the presence of O_2, the major observed site of alkali-labile lesion formation in 5'-^{32}P-**154** was T_{15}, a nucleotide directly adjacent to the radical

(Table 10). Damage at this site accounted for over half of the observed alkali-labile lesions produced by the 5,6-dihydro-2'-deoxyuridin-6yl (**123**). Significant amounts of piperidine lability were also observed at T_{17} and the site of the radical. Minor amounts of alkali-lability were observed at dC_{14}

The distribution and amount alkali-labile lesions were oxygen dependent (Table 10). The overall yield of piperidine-labile lesions was reduced approximately twofold when 5'-^{32}P-**154** was photolyzed in degassed solution. Furthermore, the major site of alkali-labile lesion formation was that of the radical. Lesser amounts of alkali-lability were still observed at the 5'-adjacent nucleotide (T_{15}) as well as at T_{17} and dC_{14}.

Treatment of photolysates of 5'-^{32}P-**154** with the milder NaOH conditions (0.1 M, 37 °C, 20 min) resulted in considerably less cleavage at T_{15} and **122a** than was observed upon treatment with piperidine (1.0 M, 90 °C, 20 min). No cleavage was observed at T_{17} upon NaOH treatment of photolysates (Table 10). The observation of partial cleavage at some nucleotides upon NaOH treatment was interpreted as evidence of multiple types of damage at these sites. It was proposed that more base sensitive damage was cleaved by the milder NaOH conditions while these as well as more resistant nucleotide modifications were cleaved by piperidine treatment at elevated temperature. The observation of NaOH-induced cleavage was interpreted as evidence for the formation of a highly base labile site such as **70**.

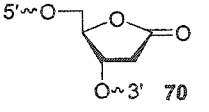

70

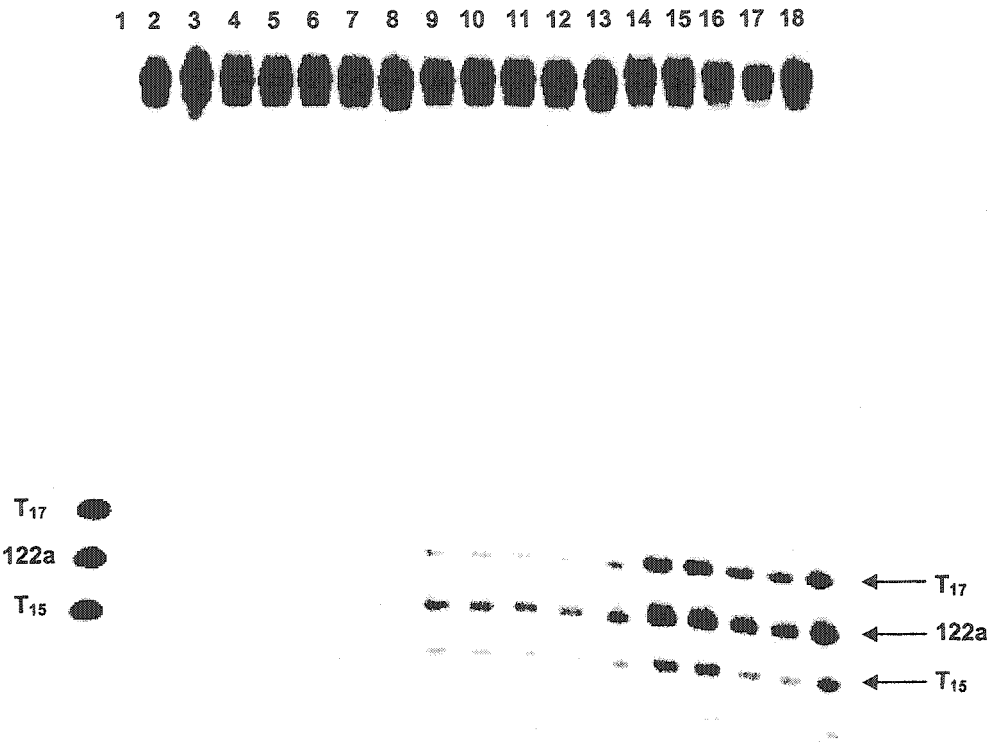

Figure 66. Phosphorimage of the aerobic photolysis of 5'-^{32}P-**154**. Lane 1, 5'-^{32}P oligonucleotide markers. Lane 2, non-photolyzed control treated with 0.1 M NaOH (37 °C, 20 min); Lane 3, non-photolyzed control treated with 1.0 M piperidine (90 °C, 20 min); lanes 4-18, photolysate treated appropriately. Lanes 4-8, no further treatment; lanes 9-13, 0.1 M NaOH (37 °C, 20 min); lanes 14-18, 1.0 M piperidine (90 °C, 20 min).

5'-d(GAG CTA GCT CGA CCT$_{15}$ **X**T$_{17}$A GGA CCT GCA GCT)
154, X = 122a

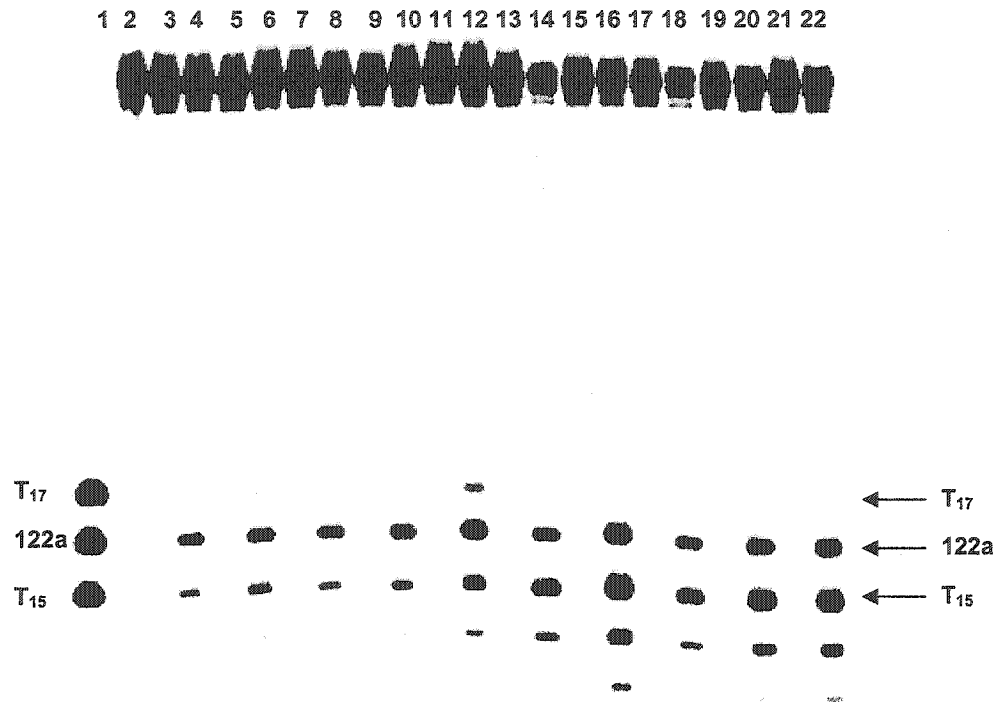

Figure 67. Phosphorimage of the photolysis 5'-^{32}P-**154** under aerobic and anaerobic conditions. The appropriate samples were treated with piperidine (1.0 M, 90 °C, 20 min). Lane 1, marker oligonucleotides;lane 2, non-photolyzed sample treated with piperidine; lanes 3 ,5 ,7 ,9 ,11 anaerobic photolysate, no further treatment; lanes 4, 6 ,8, 10, 12, anaerobic photolysate treated with piperidine; lanes 13, 15, 17, 19, 21, aerobic photolysate, no further treatment; lanes 14, 16, 18, 20, 22, aerobic pholysate treated with piperidine.

5'-d(GAG CTA GCT CGA CCT_{15} XT_{17} A GGA CCT GCA GCT)
154, X = D1a

Table 10. The distribution of alkali-labile lesions in 5'-^{32}P-**154**[a]

Oxygen[b]	Site	Percentage of total lesions (NaOH)[c]	Percentage of total lesions (Piperidine)[d]	Piperidine induced lesions/ NaOH induced lesions[e]
-	T_{17}	ND	12 ± 1	-
	122a	ND	57 ± 3	-
	T_{15}	ND	31 ± 1	-
+	T_{17}	-	6.0 ± 1.2	-
	122a	32 ± 4	37 ± 2	4.7 ± 1.1
	T_{15}	68 ± 1	57 ± 2	3.2 ± 0.4

[a] % Cleavages represent the average of multiple experiments which are presented in appendix E. The percentage alkali-lability was calculated based upon the cleavage observed at the radical precursor and the 5'- and 3'-adjacent nucleotides. [b] Anaerobic experiments were degassed using standard freeze-pump-thaw techniques. [c] Photolysates were treated with 0.1 M NaOH (37 °C, 20 min,). [d] Photolysates were treated with 1.0 M piperidine (90 °C, 20 min). [e] Enhancement in total alkali-lability upon piperidine treatment (relative to NaOH).

5'-d(GAG CTA GCT CGA CCT$_{15}$ **X**T$_{17}$A GGA CCT GCA GCT)
154, X = 122a

The amounts of strand scission as a function of base treatment and O_2 were also measured in 3'-^{32}P-**154** (Figures 68, 69). Alkali-labile lesions again comprised the vast majority of DNA damage observed (Table 11). As in experiments using 5'-^{32}P-**154**, very low amounts of direct strand scission (< 5%) were observed. In contrast to the results obtained using 5'-^{32}P-**154**, the major observed site of alkali-labile lesion formation using-3'-^{32}P-**154** was that of the radical precursor (**122a**, Table 11). A significant amount of piperidine-lability was also observed at T_{17}. This indicates that under aerobic conditions, the 5,6-dihydropyrimidin-6-yl (**123**) is capable of efficiently damaging the 3'- as well as the 5'-adjacent nucleotides.

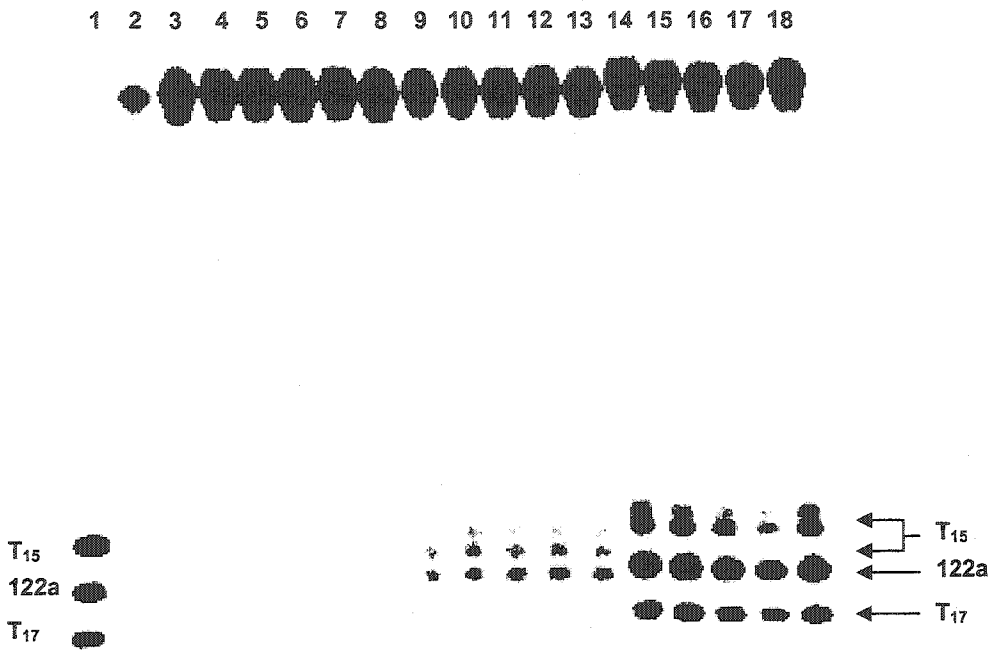

Figure 68. Phosphorimage of the aerobic photolysis of 3'-^{32}P-**154**. Lane 1, oligonucleotide markers. The appropriate samples were treated with piperidine (1.0 M, 90 °C, 20 min) or NaOH (0.1 M, 37 °C, 20 min). Lane 1, non-photolyzed control treated with NaOH; lane 2; non-photolyzed control treated with piperidine. Lanes 4-8, photolysate, no further treatment; lanes 9-13, photolysate treated with NaOH; lanes 14-18; photolysate treated with piperidine.

5'-d(GAG CTA GCT CGA CCT$_{15}$ XT$_{17}$ A GGA CCT GCA GCT)
154, X = 122a

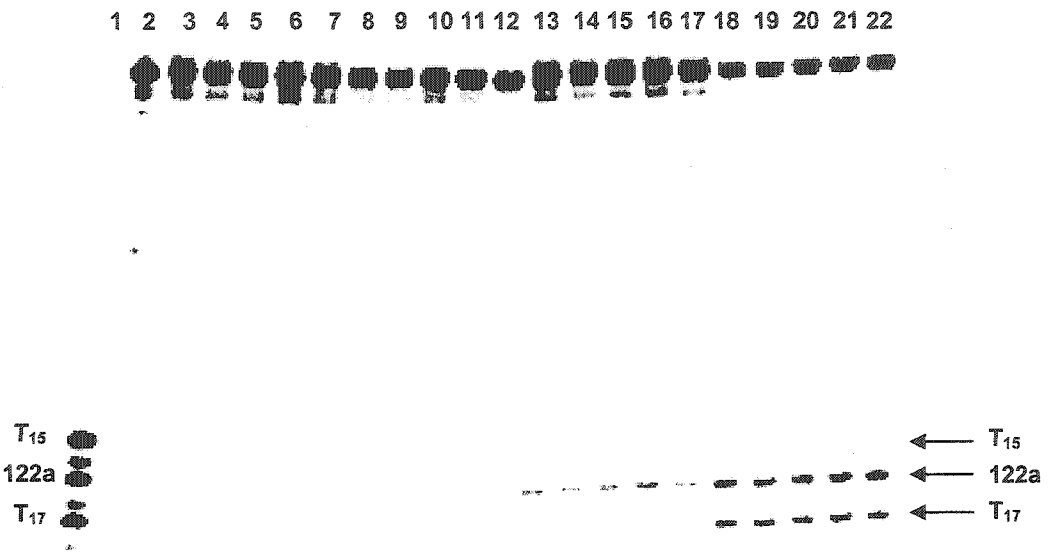

Figure 69. Phosphorimage of the photolysis of 3'-^{32}P-**154**. The appropriate samples were treated with piperidine (1.0 M, 90 °C, 20 min). Lane 1, oligonucleotide markers; lane 2, non-photolyzed control treated with piperidine. Lanes 3-7, degassed photolysis, no further treatment; lanes 8-12, aerobic photolysis, no further treatment. Lanes 13-17, degassed photolysis , treated with piperidine; lanes 18-22, aerobic photolysis treated with piperidine.

5'-d(GAG CTA GCT CGA CCT$_{15}$ **X**T$_{17}$A GGA CCT GCA GCT)
154, X = 122a

Interestingly, treatment of photolysates with the less stringent NaOH conditions resulted in no cleavage at T_{17}. This is consistent with experiments using 5'-^{32}P-**154** and implies that highly base labile lesions such as 2-deoxyribonolactone (**70**) are not formed at this site. Upon NaOH treatment, two products are observed corresponding to cleavage at T_{15}. One migrates with the same aptitude as a marker sequence of the same length having a 3'-phosphate terminus. The other migrates slightly more rapidly. Upon piperidine treatment, this product is not observed. Under degassed conditions, the major site of alkali-labile lesion formation was that of the radical (**123**), although lesser amounts of piperidine lability are observed at T_{17}.

5'-d(GAG CTA GCT CGA CCT$_{15}$ **X**T$_{17}$ A GGA CCT GCA GCT)
154, X = 122a

Table 11. The distribution of alkali-labile lesions in 3'-^{32}P-**154**[a]

Oxygen[b]	Site	Percentage of total lesions (NaOH)[c]	Percentage of total lesions (Piperidine)[d]	Piperidine induced lesions/ NaOH induced lesions[e]
-	T_{17}	ND	19 ± 5	-
	122a	ND	81 ± 7	-
	T_{15}	ND	-	-
+	T_{17}	-	33 ± 2	-
	122a	55 ± 6	49 ± 2	3.3 ± 0.6
	T_{15}	45 ± 7	16 ± 2	1.2 ± 0.2

[a] % Cleavages represent the average of multiple experiments which are presented in appendix E. The percentage alkali-lability was calculated based upon the cleavage observed at the radical precursor and the 5'- and 3'-adjacent nucleotides. [b] Anaerobic experiments were degassed using standard freeze-pump-thaw techniques. [c] Photolysates were treated with 0.1 M NaOH (37 °C, 20 min,). [d] Photolysates were treated with 1.0 M piperidine (90 °C, 20 min). [e] Enhancement in total alkali-lability upon piperidine treatment (relative to NaOH).

3.2.3.1.2 DNA damage produced by the 5,6-dihydro-2'-deoxyuridin-6yl in duplex DNA

Generation of the 5,6-dihydro-2'-deoxyuridin-6-yl in 5'-^{32}P-**159** under aerobic conditions resulted in strand damage similar to that observed in 5'-^{32}P-**154**. Alkali-labile lesions were observed primarily at the site of the radical (**123**) and T_{15} (Table 12, Figures 70, 71). The total amount of DNA piperidine-induced cleavage in the duplex was approximately equal to that observed in single stranded DNA (40-60% total alkali-labile lesion formation in a typical experiment). The distribution of alkali-labile lesions in the duplex was slightly different than that observed in single-strand oligonucleotide **154**. In duplex DNA, the major site of alkali-labile lesion formation under aerobic conditions was that of the radical precursor (**122a**). The less efficient formation of an alkali-labile lesion at T_{15} in **159** may be a consequence of the more rigid secondary structure of duplex DNA which renders internucleotidyl reactions less efficient. As in single-stranded DNA, photolyses conducted in degassed solution resulted in an approximate twofold decrease in the overall amount of alkali-labile lesions. Furthermore, damage at T_{15} was less efficient under degassed conditions (Table 12).

5'-d(GAG CTA GCT CGA CCT$_{15}$ **X**T$_{17}$ A GGA CCT GCA GCT)
3'-d(CTC GAT CGA GCT GGA A A T CCT GGA CGT CGA)
159, X = 122a

Table 12. The distribution of alkali-labile lesions in 5'-^{32}P-**159**[a]

Oxygen[b]	Site	Percentage of total lesions (NaOH)[c]	Percentage of total lesions (Piperidine)[d]	Piperidine induced lesions/ NaOH induced lesions[e]
-	T_{17}	ND	26 ± 4	-
	122a	ND	60 ± 5	-
	T_{15}	ND	14 ± 2	-
+	T_{17}	-	8.0 ± 1.4	-
	122a	63 ± 2	52 ± 2	2.4 ± 0.6
	T_{15}	37 ± 4	40 ± 4	3.3 ± 1.4

[a] % Cleavages represent the average of multiple experiments which are presented in appendix E. The percentage alkali-lability was calculated based upon the cleavage observed at the radical precursor and the 5'- and 3'-adjacent nucleotides. [b] Anaerobic experiments were degassed using standard freeze-pump-thaw techniques. [c] Photolysates were treated with 0.1 M NaOH (37 °C, 20 min,). [d] Photolysates were treated with 1.0 M piperidine (90 °C, 20 min). [e] Enhancement in total alkali-lability upon piperidine treatment (relative to NaOH).

Alkali-labile lesions generated from the aerobic photolysis of 5'-^{32}P-**159** were also treated with NaOH (0.1 M, 37 °C, 20 min) to selectively cleave highly labile lesions. The results were qualitatively similar to those observed in single stranded DNA (**154**). NaOH-lability was observed at **122a** and T_{15}, but not at T_{17}. This suggests that the 5,6-dihydro-2'-deoxyuridin-6-yl (**123**) results in the formation of a highly labile site such as 2-deoxyribonolactone (**70**) at T_{15}, but not T_{17}.

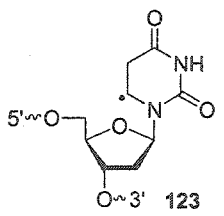

123

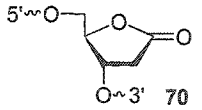

70

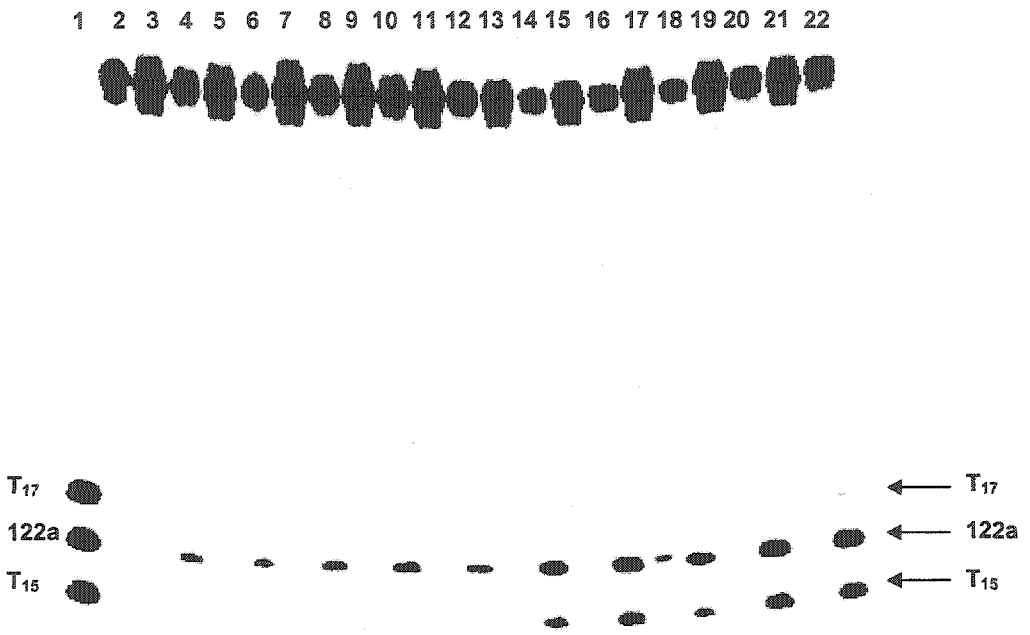

Figure 70. Phosphorimage of the photolysis of 5'-^{32}P-**159** under aerobic and anaerobic conditions. The appropriate samples were treated with piperidine (1.0 M, 90 °C, 20 min). Lane 1, marker oligonucleotides; lane 2, non-photolyzed sample treated with piperidine; lanes 3, 5, 7, 9, 11 anaerobic photolysate, no further treatment; lanes 4, 6, 8, 10, 12, anaerobic photolysate treated with piperidine; lanes 13, 15, 17, 19, 21, aerobic photolysate, no further treatment; lanes 14, 16, 18, 20, 22, aerobic photolysate treated with piperidine.

5'-d(GAG CTA GCT CGA CCT$_{15}$ **X**T$_{17}$ A GGA CCT GCA GCT)
3'-d(CTC GAT CGA GCT GGA A A T CCT GGA CGT CGA)
159, X = 122a

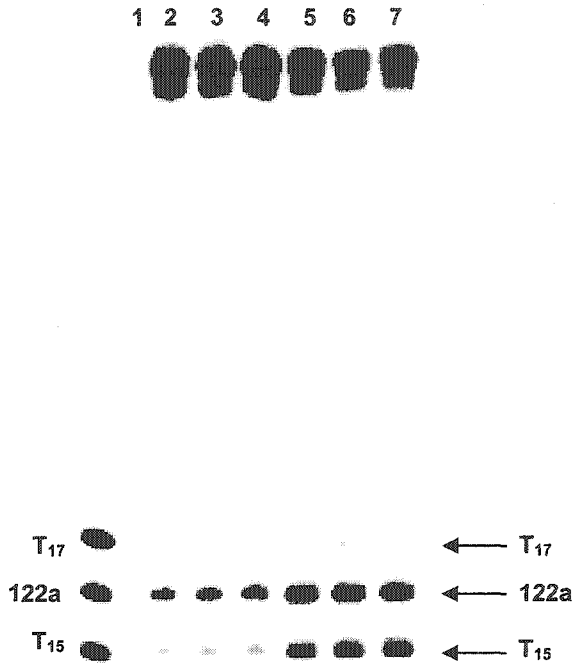

Figure 71. Phosphorimage of the aerobic photolysis of 5'-^{32}P-**159**. Lane 1, oligonucleotide markers; lanes 2-4, photolysate treated with NaOH (0.1 M, 37 °C, 20 min); lanes 5-7, photolysate treated with piperidine (1.0 M, 90 °C, 20 min).

5'-d(GAG CTA GCT CGA CCT$_{15}$ **X**T$_{17}$ A GGA CCT GCA GCT)
3'-d(CTC GAT CGA GCT GGA A A T CCT GGA CGT CGA)
159, X = 122a

The distribution of alkali-labile lesions observed in 3'-^{32}P-**159** was similar to that observed in 3'-^{32}P single stranded DNA (Table 13, Figures 72, 73). Piperidine-labile lesions were observed primarily at the site of **122a** and T_{17}, while lesser amounts were observed at T_{15}. The ratio of alkali-lability at the 3'-adjacent nucleotide (T_{17}) to **122a** is not significantly different in single-stranded and duplex DNA (Tables 11, 13). The observed piperidine-labile lesions were reduced when photolyses of 3'-^{32}P-**159** were conducted in degassed solution.

Treatment of photolysates with the milder NaOH conditions resulted in cleavage at **122a** and T_{15}. No cleavage was induced at T_{17} upon NaOH treatment,which is consistent with results obtained in single –stranded DNA (Table 13).

5'-d(GAG CTA GCT CGA CCT$_{15}$ **X**T$_{17}$A GGA CCT GCA GCT)
3'-d(CTC GAT CGA GCT GGA A A T CCT GGA CGT CGA)
159, X = 122a

Table 13. The distribution of alkali-labile lesions in 3'-^{32}P-**159**[a]

Oxygen[b]	Site	Percentage of total lesions (NaOH)[c]	Percentage of total lesions (Piperidine)[d]	Piperidine induced lesions/ NaOH induced lesions[e]
-	T_{17}	ND	38 ± 10	-
	122a	ND	62 ± 8	-
	T_{15}	ND	-	-
+	T_{17}	-	40 ± 6	-
	122a	67 ± 7	51 ± 4	2.9 ± 0.6
	T_{15}	33 ± 7	9.0 ± 4.0	0.83 ± 0.10

[a] % Cleavages represent the average of multiple experiments which are presented in appendix E. The percentage alkali-lability was calculated based upon the cleavage observed at the radical precursor and the 5'- and 3'-adjacent nucleotides. [b] Anaerobic experiments were degassed using standard freeze-pump-thaw techniques. [c] Photolysates were treated with 0.1 M NaOH (37 °C, 20 min,). [d] Photolysates were treated with 1.0 M piperidine (90 °C, 20 min). [e] Enhancement in total alkali-lability upon piperidine treatment (relative to NaOH).

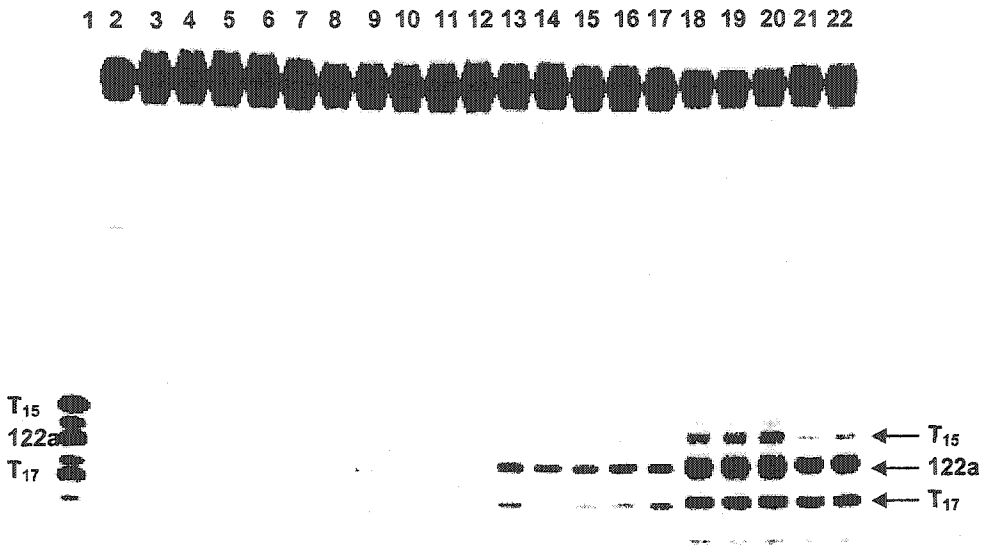

Figure 72. Phosphorimage of the photolysis of 3'-^{32}P-**159**. The appropriate samples were treated with piperidine (1.0 M, 90 °C, 20 min). Lane 1, oligonucleotide markers; lane 2, non-photolyzed control treated with piperidine. Lanes 3-7, degassed photolysis, no further treatment; lanes 8-12, aerobic photolysis, no further treatment. Lanes 13-17, degassed photolysis , treated with piperidine; lanes 18-22, aerobic photolysis treated with piperidine.

5'-d(GAG CTA GCT CGA CCT$_{15}$ **X**T$_{17}$ A GGA CCT GCA GCT)
3'-d(CTC GAT CGA GCT GGA A A T CCT GGA CGT CGA)
159, X = 122a

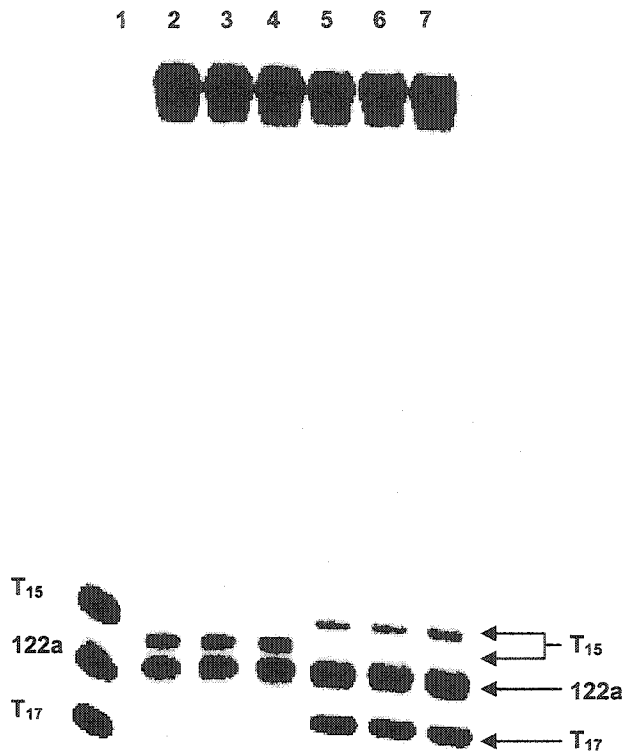

Figure 73. Phosphorimage of the aerobic photolysis of 3'-^{32}P-**159**. Lane 1, oligonucleotide markers; lanes 2-4, photolysate treated with NaOH (0.1 M, 37 °C, 20 min); lanes 5-7, photolysate treated with piperidine (1.0 M, 90 °C, 20 min).

5'-d(GAG CTA GCT CGA CCT$_{15}$ **X**T$_{17}$ A GGA CCT GCA GCT)
3'-d(CTC GAT CGA GCT GGA A A T CCT GGA CGT CGA)
159, X = 122a

In the interest of synthetic convenience, most experiments were carried out with oligonucleotides containing the major diastereomer of the radical precursor (**122a**). As both diastereomers of the radical precursor (**122**) afford the 5,6-dihydro-2'-deoxyuridin-6-yl radical of interest (**123**), the stereochemistry of the radical precursor (**122**) should not affect the distribution of damage. In order to ensure that this was the case, photolysis experiments were carried out using duplex **160**, which contains **122b**.

5'-d(GAG CTA GCT CGA CCT_{15} **X** T_{17} A GGA CCT GCA GCT)
3'-d(CTC GAT CGA GCT GGA A A T CCT GGA CGT CGA)
160, X = 122b

Table 14. The distribution of alkali-labile lesions formed under aerobic conditions in radiolabeled **160**.[a]

^{32}P-Label	Site	Percentage of total lesions (NaOH)[b]	Percentage of total lesions (Piperidine)[c]	Piperidine induced lesions/ NaOH induced lesions[d]
5'-end	T_{17}	-	12 ± 2	-
	122b	70 ± 10	57 ± 6	2.6 ± 0.3
	T_{15}	30 ± 4	31 ± 7	3.3 ± 0.8
3'-end	T_{17}	-	39 ± 4	-
	122b	73 ± 23	52 ± 7	3.0 ± 0.8
	T_{15}	27 ± 7	9.0 ± 1.0	1.4 ± 0.3

[a] % Cleavages represent the average of multiple experiments which are presented in appendix E. The percentage alkali-lability was calculated based upon the cleavage observed at the radical precursor and the 5'- and 3'-adjacent nucleotides. [b] Photolysates were treated with 0.1 M NaOH (37 °C, 20 min,). [c] Photolysates were treated with 1.0 M piperidine (90 °C, 20 min). [d] Enhancement in total alkali-lability upon piperidine treatment (relative to NaOH).

Photolysis of 5'- or 3'-^{32}P-**160**, which contains the minor diastereomer of the radical precursor (**122b**) gave a distribution of NaOH and piperidine labile lesions within error of that observed in duplex **159** which contains the major diastereomer of the radical

precursor (Table 14, Figures 74, 75) The observation of the same distribution of alkali-labile lesions, regardless of the stereochemistry of the radical precursor is consistent with the observed DNA damage resulting from the 5,6-dihydro-2'-deoxyuridin-6-yl (**123**) or a peroxyl radical derived from this reactive intermediate.

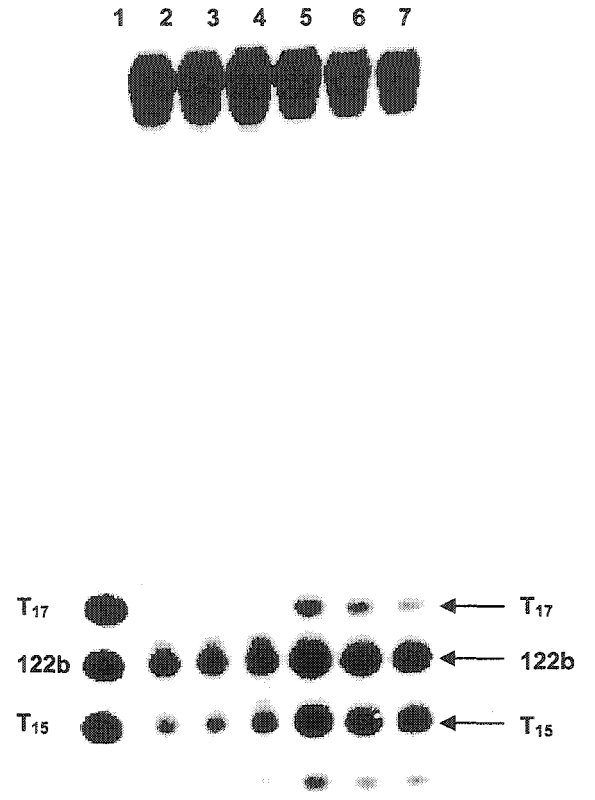

Figure 74. Phosphorimage of the aerobic photolysate of 5'-^{32}P-**160**. Lane 1, oligonucleotide markers; lanes 2-4, photolysate treated with NaOH (0.1 M, 37 °C, 20 min); lanes 5-7, photolysate treated with piperidine (1.0 M, 90 °C, 20 min).

5'-d(GAG CTA GCT CGA CCT$_{15}$ **X**T$_{17}$A GGA CCT GCA GCT)
3'-d(CTC GAT CGA GCT GGA A A T CCT GGA CGT CGA)
160, X = 122b

Figure 75. Phosphorimage of the photolysate of 3'-^{32}P-**160**. Lane 1, oligonucleotide markers; lanes 2-4, photolysate treated with NaOH (0.1 M, 37 °C, 20 min); lanes 5-7, photolysate treated with piperidine (1.0 M, 90 °C, 20 min).

5'-d(GAG CTA GCT CGA CCT_{15} **X**T_{17} A GGA CCT GCA GCT)
3'-d(CTC GAT CGA GCT GGA A A T CCT GGA CGT CGA)
160, X = 122b

3.2.3.1.3 DNA Damage Amplification by 5,6-Dihydro-2'-deoxyuridin-6-yl.

Experiments in which 5,6-dihydro-2'-deoxyuridin-6-yl (**123**) was generated in single-stranded and duplex DNA indicated that the radical is capable of damaging adjacent nucleotides, as well as the site of its generation. This indicates that the nucleobase radical (**123**), and/or the respective peroxyl radical (**158**) can participate in DNA damage amplification. Although the PAGE experiments give no detailed structural information, the transfer of damage to adjacent nucleotides indicates that **123** and/or **158** results in the formation of tandem lesions.

5'-d(GAG CTA GCT CGA CCT_{15} **X** T_{17} A GGA CCT GCA GCT)
154, X = 122a

5'-d(GAG CTA GCT CGA CCT_{15} **X** T_{17} A GGA CCT GCA GCT)
3'-d(CTC GAT CGA GCT GGA A A T CCT GGA CGT CGA)
159, X = 122a
160, X = 122b

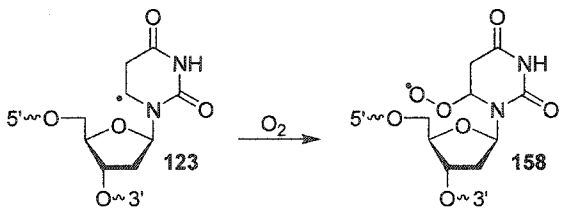

The reduced efficiency of the internucleotidyl reaction when O_2 is depleted implicates a peroxyl radical as a reactive intermediate (Figure 76). This species can then react with an adjacent nucleotide to produce an alkali-labile lesion. The fact that this reaction still occurs to a lesser extent in degassed solution is probably due to residual O_2. If degassing removes 99.9 % of the O_2 present in solution, it is still present at ~ 200 nM.

Typical experiments were conducted at DNA concentrations of ~ 10 nM. Therefore, degassed solutions may still contain O_2 in tenfold excess relative to DNA.

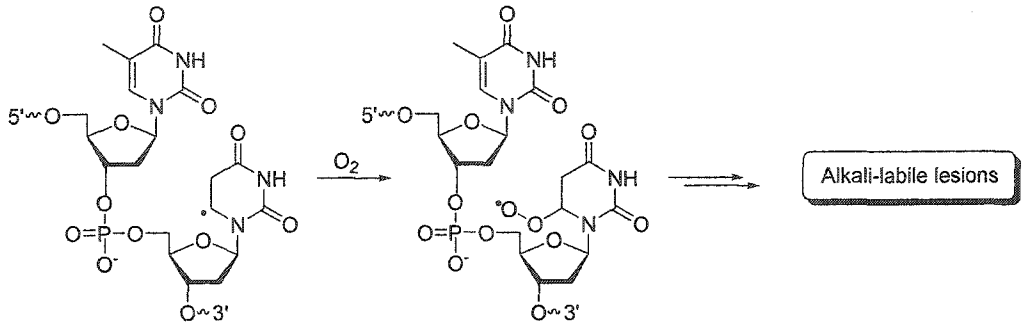

Figure 76. Alkali-labile lesion formation by the nucleobase peroxyl radical.

Photolysis of DNA containing the radical precursor (**154**, **159**, **160**) resulted in the formation of damaged sites that exhibit differing susceptibility to base induced cleavage. NaOH treatment results in cleavage at the site of the radical as well as at the 5'-adjacent nucleotide (T_{15}) in these sequences. Treatment of photolysates with piperidine at elevated temperature results in an increased amount of cleavage at these sites. This suggests that two classes of lesions are formed: those which are cleaved by treatment with NaOH (0.1 M, 37 °C, 20 min) and those which are only cleaved by piperidine (1.0 M, 90 °C, 20 min) treatment. The damage produced at T_{17} consists entirely of the latter type. While no cleavage is observed at this site upon NaOH treatment, treatment with piperidine does result in significant cleavage (Tables 10-13).

The observed distribution of alkali-labile lesions varies greatly depending upon which end of the DNA is radiolabeled. For instance, the major observed site of alkali-labile lesion formation in experiments using 5'-^{32}P-**154** is T_{15} (57 ± 2 % of the total

piperidine lability, Table 10). The amount of piperidine lability observed at this site in the same oligonucleotide labeled at the 3'-end is 16 ± 2 % of the total (Table 11). This disparity is due to the fact that only the fragment bearing the label is detected in the PAGE experiment. The formation of an alkali-labile lesion at T_{15} is proposed to also result in the formation of an alkali-labile lesion at **122**. Upon base treatment, the alkali-labile lesion at the site of the radical precursor as well as at T_{15} are *both* cleaved, leaving two fragments (Figure 77). However, only the labeled fragment is observed. For example, in a PAGE experiment using 5'-^{32}P substrate a tandem alkali-labile lesion formed between the radical and the 5'-adjacent nucleotide (T_{15}) will appear as cleavage at T_{15} (Figure 77). Conversely, the same lesion will appear as cleavage at the site of the radical if 3'-^{32}P DNA is used. Therefore, experiments using both 5'- and 3'-^{32}P DNA are necessary to detect tandem alkali-labile lesions.

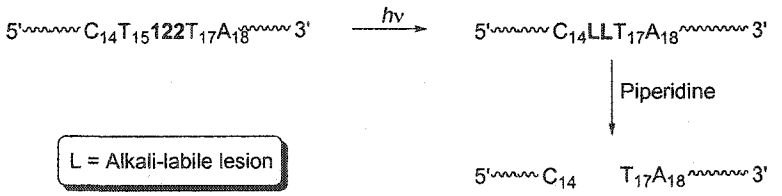

Figure 77. DNA fragments produced by tandem alkali-labile lesions.

PAGE analysis of photolyses conducted with 3'-^{32}P-**154**, **-159**, and **-160** reveals two products corresponding to cleavage at T_{15} (Figures 68, 73, 75). These may result from an initially formed tandem lesion containing a C6-hydroperoxide adjacent to 2-deoxyribonolactone (Figure 78). Decomposition of the hydroperoxide could result in the formation of dU-containing product **161**. Since dU is not alkali-labile, this product is

proposed to result in a 5'-phosphate fragment upon either NaOH or piperidine treatment. This product is proposed to represent the more slowly moving of the two gel bands corresponding to cleavage at T_{15}. This assignment is based upon the fact that this product is observed in piperidine treated photolysates as well. A possible structure for the more rapidly moving product is **162**. Due to the negatively charged carboxylate, this ring fragmentation product would be expected to migrate more rapidly in a PAGE experiment than the fragment derived from base treatment of **161**. The more rapidly moving product is not observed in piperidine treated photolysates due to the fact the hydroperoxide is cleaved under these conditions (Figure 78). Upon piperidine treatment, **162** is converted to a more rapidly moving product. This was determined by removal of this fragment of NaOH treatment from a gel, followed by treatment with piperidine (see appendix C).

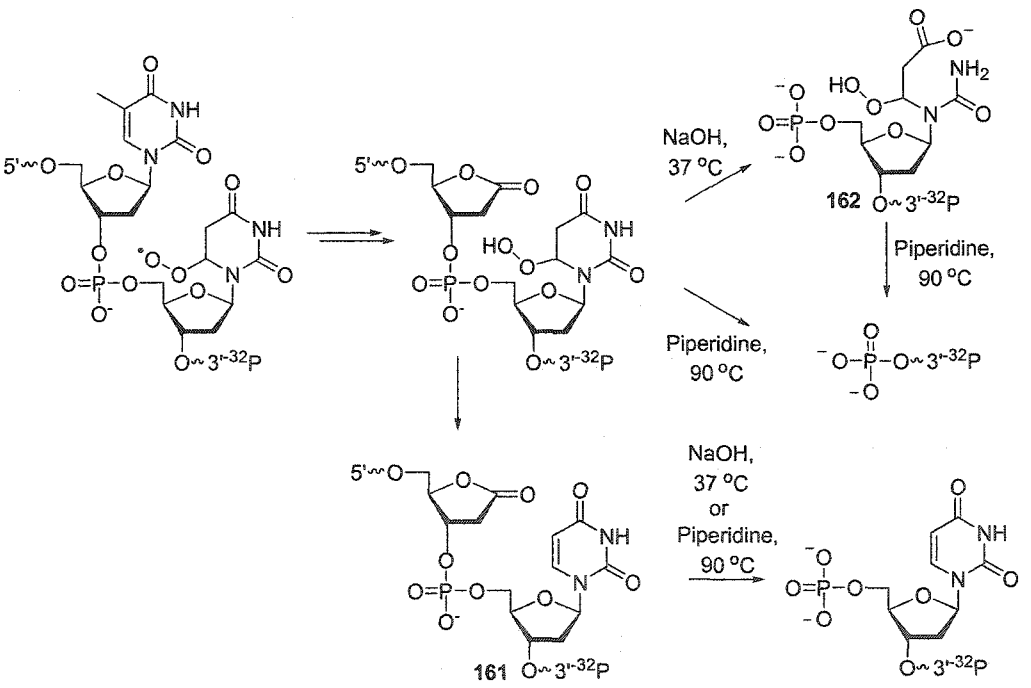

Figure 78. Proposed fragments observed in PAGE analysis of 3'-^{32}P-**154**, -**159**, and -**160**.

3.2.3.1.4 End Group Analysis of Photolysates.

In order to gain information regarding the chemical identity of end-groups produced upon base treatment of photolysates, dephosphorylation reactions were conducted (Figure 79). In these experiments, fragments produced from base treatment of photolyzed **159** were subjected to enzymatic dephosphorylation prior to PAGE analysis. Phosphate terminated fragments have a greater migratory aptitude than hydroxyl terminated ones in PAGE experiments. Therefore, a retardation in the migration of a given product upon treatment with a dephosphorylating enzyme is indicative of the presence of a phosphate end group.

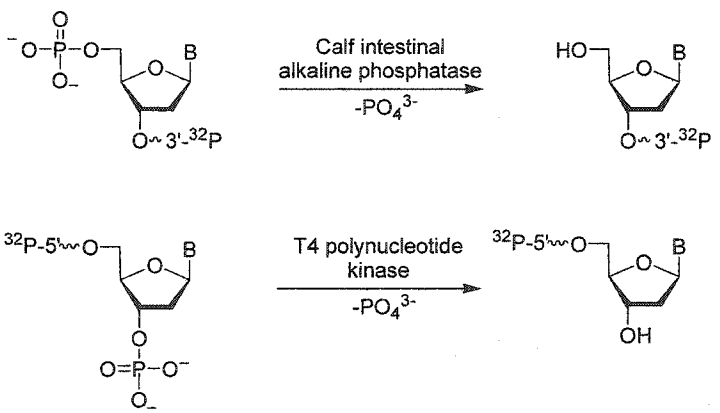

Figure 79. Enzymatic dephosphorylation of oligonucleotide fragments.

In photolysis experiments which utilized 5'-^{32}P end labeled DNA, base treated photolysates were treated with T4 polynucleotide kinase. In addition to catalyzing the phosphorylation of the 5'-hydroxyl terminus of an oligonucleotide, in the absence of ATP this enzyme also catalyzes the *dephosphorylation* of a 3' phosphate terminus. Treatment of piperidine or NaOH treated photolysates reveals that the fragments produced upon

base induced cleavage at C_{14}, T_{15}, and **122a** all possess phosphate groups at their respective 3'-termini (Figures 80, 81).

In order to determine if phosphate end-groups were produced at the 5'-termini of fragments produced by base treatment of photolysates, analogous experiments were conducted using 3'-^{32}P-**159**. Dephosphorylation of the 5' termini of DNA fragments produced by NaOH and piperidine treatment of photolysates was accomplished by using calf intestinal alkaline phosphatase. A diminished migratory aptitude upon base treatment indicates that the fragments produced by base treatment of **159** possess phosphate end groups at their 5' termini (Figures 80, 81).

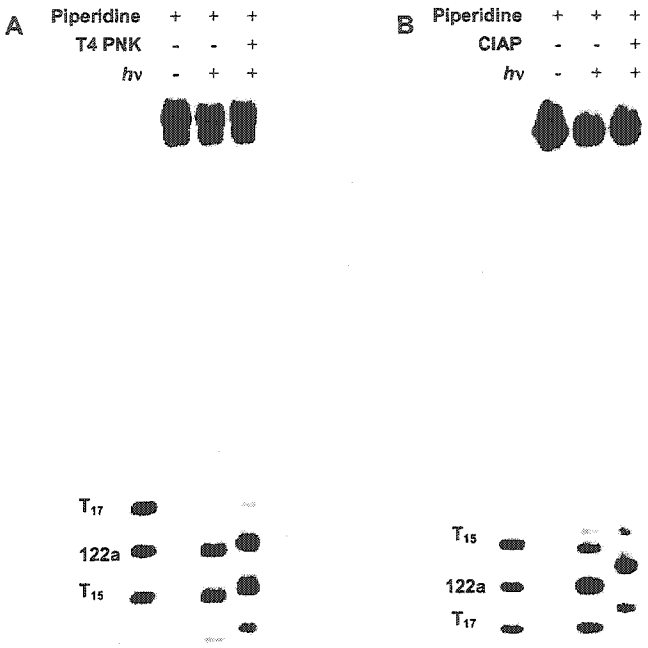

Figure 80. End-group analysis of piperidine-treated photolysates of 5'- and 3'-^{32}P-**159**. (A) 5-^{32}P-**159** dephosphorylated with T4 PNK. (B) 3'-^{32}P-**159** dephosphorylated with CIAP (Calf intestinal alkaline phosphatase).

5'-d(GAG CTA GCT CGA CCT$_{15}$ **X**T$_{17}$ A GGA CCT GCA GCT)
3'-d(CTC GAT CGA GCT GGA A A T CCT GGA CGT CGA)
159, X = 122a

Figure 81. End-group analysis of NaOH-treated photolysates of 5'- and 3'-^{32}P-**159**. (A) 5'-^{32}P-**159** dephosphorylated with T4 PNK. (B) 3'-^{32}P-**159** dephosphorylated with calf intestinal alkaline phosphatase (CIAP).

3.2.3.1.5 The Effect of Thiol upon DNA Damage Amplification by 5,6-Dihydro-2'-deoxyuridin-6-yl.

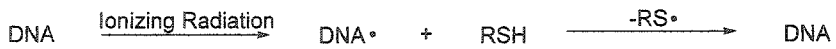

Figure 82. The radioprotecting effect of thiols.

The role of thiols as radioprotecting agents is widely accepted.[1] Thiols mitigate radical mediated DNA damage by the donation of a hydrogen atom to DNA centered radicals (Figure 82). In cells, the most abundant free thiol is glutathione, which can be present in millimolar concentrations.[141] In order to evaluate the effect of a thiol on DNA damage induced by the 5,6-dihydro-2'-deoxyuridin-6-yl (**123**), 5'-^{32}P-**154** and -**159** were photolyzed in the presence of glutathione ethyl ester (GSHOEt). At 5.0 mM GSHOEt, the amount of alkali-lability at T_{15} is reduced to ~ 18 and 31 % of the amount observed in the absence of thiol in **154** and **159** (Tables 15, 16). This presumably occurs by donation of a hydrogen atom from the glutathione to the C6 peroxyl radical (Figure 83). If GSHOEt reacts with the 5,6-dihydro-2'-deoxyuridin-6-yl in DNA at approximately the same rate measured for the reaction of thiol with the monomeric radical (8 X 10^6 $M^{-1}s^{-1}$) it cannot compete with oxygen (assuming $k_{O2}[O_2]$ = 4 X 10^5 s^{-1}). Therefore, the C6 peroxyl radical (**158**) is still formed from the alkyl radical (**123**, Figure 83) at low thiol concentrations. The peroxyl radical (**158**) may then either react with an adjacent nucleotide or abstract a hydrogen atom from GSHOEt. Alkali-labile lesion formation at the site of the radical precursor (**122a**) was undiminished in single-stranded (**154**) or duplex (**159**) DNA by thiol concentrations of up to 5.0 mM (Tables 15, 16). Therefore, it

is proposed that the alkali-labile lesion observed at the site of the initially formed radical is the C6-hydrate (**162**) or C6-hydroperoxide (**161**).

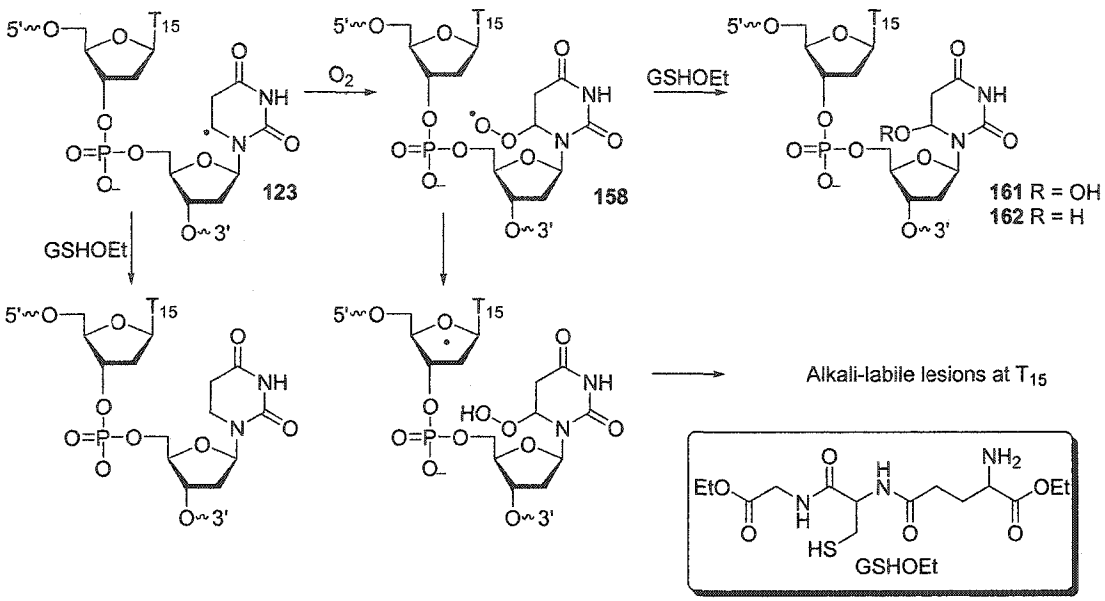

Figure 83. The effect of thiol upon DNA damage amplification under aerobic conditions.

5'-d(GAG CTA GCT CGA CCT_{15} **X** T_{17} A GGA CCT GCA GCT)
154, X = 122a

Table 15. The effect of thiol upon alkali-labile lesion formation in 5'-^{32}P-**154** under aerobic conditions.[a]

[GSHOEt] (μM)	Relative piperidine lability[b]		
	T_{15}	**122a**	T_{17}
-	1.0	1.0	1.0
5	0.73 ± 0.07	0.95 ± 0.01	0.70 ± 0.04
50	0.34 ± 0.02	1.04 ± 0.09	0.38 ± 0.01
500	0.20 ± 0.63	1.25 ± 0.23	0.45 ± 0.24
5000	0.18 ± 0.07	1.18 ± 0.02	0.43 ± 0.11

[a] % Cleavages represent the average of multiple experiments which are presented in appendix E. The percentage alkali-lability was calculated based upon the cleavage observed at the radical precursor and the 5'- and 3'-adjacent nucleotides. Photolysates were treated with 1.0 M piperidine (90 °C, 20 min). [b] Relative piperidine labilities at a given concentration of GSHOEt are calculated relative to the amount of alkali-lability observed in the absence of thiol which is defined as 1.0.

5'-d(GAG CTA GCT CGA CCT_{15} **X** T_{17} A GGA CCT GCA GCT)
3'-d(CTC GAT CGA GCT GGA A A T CCT GGA CGT CGA)
159, X = 122a

Table 16. The effect of thiol upon alkali-labile lesion formation in 5'-^{32}P-**159** under aerobic conditions.[a]

[GSHOEt] (μM)	Relative piperidine lability		
	T_{15}	**122a**	T_{17}
-	1.0	1.0	1.0
5	0.92 ± .17	0.80 ± 0.18	1.14 ± 0.12
50	0.60 ± 0.11	1.09 ± 0.28	1.02 ± 0.43
500	0.39 ± 0.063	1.06 ± 0.014	0.65 ± 0.042
5000	0.31 ± 0.071	1.17 ± 0.10	0.39 ± 0.021

[a] %. Cleavages represent the average of multiple experiments which are presented in appendix E. The percentage alkali-lability was calculated based upon the cleavage observed at the radical precursor and the 5'- and 3'-adjacent nucleotides. Photolysates were treated with 1.0 M piperidine (90 °C, 20 min). [b] Relative piperidine labilities at a given concentration of GSHOEt are calculated relative to the amount of alkali-lability observed in the absence of thiol which is defined as 1.0.

Under degassed conditions, alkali-labile lesion formation at adjacent nucleotides is less efficient (Tables 10-13). In a typical experiment using 5'-^{32}P-**159**, treatment of aerobic photolysates resulted in conversion of > 20% of the starting DNA into fragments

corresponding to cleavage at T_{15}. In degassed photolysates , this was reduced to ~ 5 %. This damage is proposed to result from trace oxygen in solution. Trace oxygen results in the formation of the C6 peroxyl radical (**158**) which reacts with adjacent nucleotides. Once **158** reacts with an adjacent nucleotide, O_2 may be required in subsequent steps which lead to alkali-labile lesion formation. When oxygen in depleted, alkali-labile lesion formation is less efficient due to more effective trapping of radicals generated at T_{15} by GSHOEt. A significant amount of alkali-lability is still observed at T_{15} under degassed conditions in the presence of 5 mM GSHOEt relative to that observed in the absence of thiol (Tables 17, 18). However, it is important to note that the damage observed at T_{15} under degassed conditions is small in absolute terms (~ 5%). Therefore, the amount of alkali-labile damage observed at T_{15} under degassed conditions in the presence of thiol is small in absolute terms.

Table 17. The effect of thiol upon alkali-labile lesion formation in 5'-^{32}P-**154** under degassed conditions.[a]

[GSHOEt] (μM)	Relative piperidine lability[b]		
	T_{15}	**122a**	T_{17}
-	1.0	1.0	1.0
5	0.94 ± 0.11	0.87 ± 0.08	1.0 ± 0.1
50	0.37 ± 0.06	0.99 ± 0.14	-
500	0.29 ± 0.09	1.01 ± 0.24	-
5000	0.32 ± 0.07	1.1 ± 0.1	-

[a] %. Raw data are presented in appendix E. The percentage alkali-lability was calculated based upon the cleavage observed at the radical precursor and the 5'- and 3'-adjacent nucleotides. Photolysates were treated with 1.0 M piperidine (90 °C, 20 min). [b] Relative piperidine labilities at a given concentration of GSHOEt are calculated relative to the amount of alkali-lability observed in the absence of thiol which is defined as 1.0.

Table 18. The effect of thiol upon alkali-labile lesion formation in 5'-^{32}P-**159** under degassed conditions.[a]

[GSHOEt] (μM)	Relative piperidine lability[b]		
	T_{15}	**122a**	T_{17}
-	1.0	1.0	1.0
5	0.82 ± 0.10	0.83 ± 0.04	0.52 ± 0.28
50	0.79 ± 0.11	0.79 ± 0.09	0.28 ± 0.15
500	0.63 ± 0.18	0.74 ± 0.12	-
5000	0.54 ± 0.07	0.73 ± 0.08	-

[a] % Raw data are presented in appendix E.. The percentage alkali-lability was calculated based upon the cleavage observed at the radical precursor and the 5'- and 3'-adjacent nucleotides. Photolysates were treated with 1.0 M piperidine (90 °C, 20 min). [b] Relative piperidine labilities at a given concentration of GSHOEt are calculated relative to the amount of alkali-lability observed in the absence of thiol which is defined as 1.0.

The fact that the addition of GSHOEt to aerobic photolysis reactions leads to a modest increase in alkali-lability at the site of **122a** suggests that the alkali-labile lesion formed at this site is in fact C6 hydrate **162**. Experiments using the benzyolated monomeric radical precursor (**130**) show that the major product under aerobic conditions in the presence of low thiol millimolar concentrations is benzoylated 2'-deoxyuridine C6 hydrate (**140**). This possibility that C6-hydrate (**162**) was the alkali-labile lesion formed at the site of the radical precursor (**122a**) was investigated by subjecting photolysates to conditions which promote dehydration of this species prior to treatment with piperidine.[125,132] Although 2'-deoxyuridine C6 hydrate (**162**) may be alkali-labile, the dehydration product, dU, is not. Therefore, dehydration should lead to a decrease in alkali-lability.

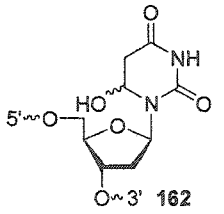

Photolysates of 5'-^{32}P-**154** were either heated at 90°C for 1 h or incubated in tris pH 8.9 for 18 h prior to treatment with piperidine to reveal alkali-labile lesions. The overall amount and distribution of alkali-labile lesions was similar to that observed in photolysates which had not been heated, which does not support the notion that the alkali-labile lesion formed at the site of **122a** is 2'-deoxyuridine C6 hydrate (Table 19). This suggests that the alkali-labile lesion observed at the site of the ketone may be C6 hydroperoxide (**161**). Upon heating, this may eliminate water to generate C6-hydroxy-2'-deoxyuridine (**163**, Figure 84) which undergoes cleavage upon piperidine treatment. Thymidine C6-hydroperoxides are known to undergo a similar decomposition reaction.[52]

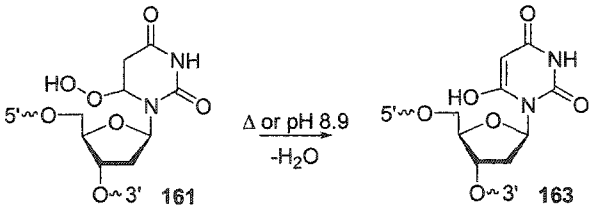

Figure 84. Decomposition of C6-hydroperoxy-2'-deoxyuridine (**161**) to C6-hydroxy-2'-deoxyuridine (**163**).

Table 19. The effect of heating and incubation at pH 8.9 upon alkali-lability in 5'-^{32}P-**154**.[a]

[GSHOEt]	Treatment	Relative piperidine lability[b]		
		T_{15}	**122a**	T_{17}
-	-	1.0	1.0	1.0
	90 °C, 1 h	1.0 ± 0.03	0.97 ± 0.05	0.74 ± 0.38
	pH 8.9, 18 h[c]	1.2 ± 0.2	1.0 ± 0.1	1.2 ± 0.2
50 mM	-	0.20 ± 0.01	1.3 ± 0.1	0.76 ± 0.24
	90 °C, 1 h	0.21 ± 0.02	1.3 ± 0.2	2.0 ± 0.9

[a]. "Treatment" denotes treatment of photolysates prior to piperidine treatment. Samples were maintained at pH 8.9 with 100 mM tris buffer. [b]. Relative piperidine labilities at a given concentration of GSHOEt are calculated relative to the amount of alkali-lability observed in samples which were photolyzed in the absence of thiol and not heated prior to photolysis which is defined as 1.0. Alkali-labile lesions were revealed by treatment with 1.0 M piperidine (90 °C, 20 min). [c] Samples were incubated in 100 mM tris pH 8.9 for 18 h.

3.2.3.1.6 Damage to the Complementary DNA Strand.

PAGE experiments using radiolabeled single-stranded and duplex DNA reveal that 5,6-dihydro-2'-deoxyuridin-6-yl results in the transfer of damage to adjacent nucleotides. The efficiency of this process is reduced under conditions in which O_2 is depleted. Moreover, low concentrations of thiol inhibit this process. Therefore, the species which carries out the internucleotidyl reaction which results in alkali-labile lesion formation is proposed to be the C6 peroxyl radical (**158**). However, a potential disadvantage to using the Norrish I strategy for radical generation is that for every C6 pyrimidine radical of interest produced, a *t*-butyl radical is also formed. The involvement of the *t*-butyl and *t*-butyl peroxyl radicals in DNA damage was therefore considered. It is well known that peroxyl radicals are capable of damaging DNA.[142-144] Since the *t*-butyl and *t*-butyl peroxyl radicals are freely diffusible, they would be expected to react with the complementary strand of a DNA duplex, as well as the strand containing the radical precursor.

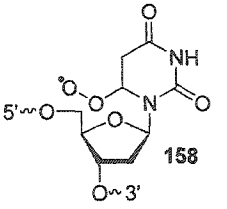

In order to investigate this possibility, the amount of alkali-lability generated on the complementary strand was generated by conducting a photolysis in which this strand was 5'-^{32}P end-labeled (Figure 85). Although the nucleobase peroxyl radical (**158**) is not well situated to react with nucleotides on the opposite strand, these sites could be attacked by a diffusible species such as *t*-butyl peroxyl radical. PAGE analysis of piperidine treated photolysates indicated that the damage to the complementary strand is minimal: < 2 % at a given nucleotide, < 8 % total. This is much less than the cleavage (40-60 %) observed in the strand in which the radical is generated. This supports the conclusion that the alkali-labile lesions which are formed in **154** and **157** are a result of the C6 peroxyl radical, not an artifact due to the diffusible *t*-butyl and *t*-butyl peroxyl

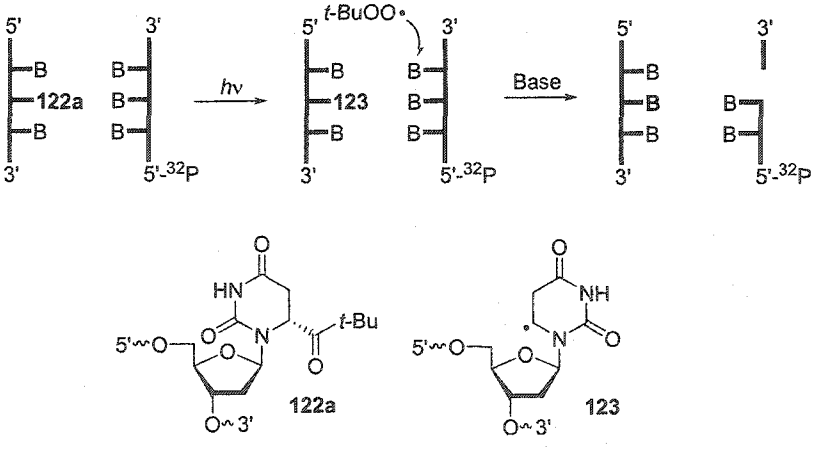

radicals.

Figure 85. Damage to the complementary DNA strand by the *t*-butyl radical.

3.2.3.1.7 The Effect of DNA Concentration upon Alkali-labile Lesion Formation.

To further investigate the possibility that the *t*-butyl peroxyl radical was responsible for the observed alkali-labile lesions, the effect of concentration upon alkali-labile lesion formation was investigated. If the alkali-labile lesion formation at nucleotides adjacent to the 5,6-dihydro-2'-deoxyuridin-6-yl was the result of an internucleotidyl hydrogen atom abstraction, the amount of alkali-lesions might decrease with increasing DNA concentration. This is due to the fact that radical-radical termination reactions would be expected to compete more effectively with the internucleotidyl (intramolecular) hydrogen atom abstraction reaction (Figure 86). The caveat is that the termination reaction reaction between the peroxyl radicals may occur slowly ($k \sim 7.5 \times 10^2\ M^{-1}s^{-1}$), thus rendering the concentration effect small.[145]

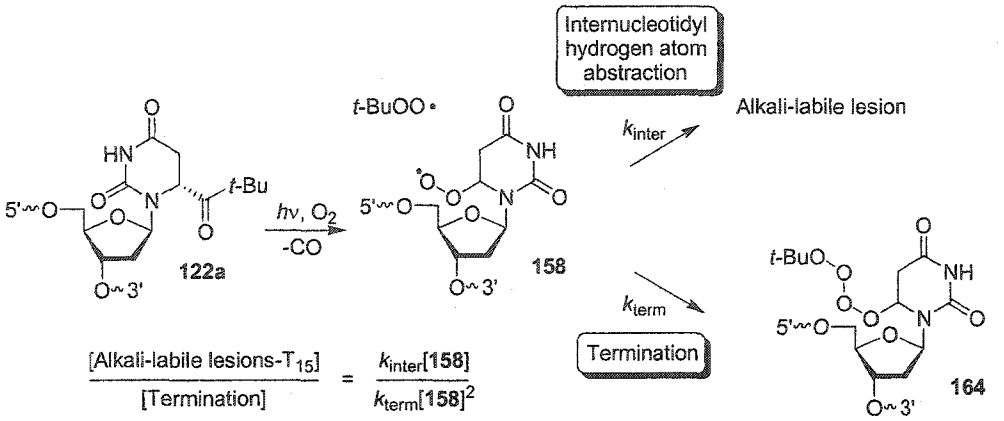

Figure 86. The effect of DNA concentration upon alkali-labile lesion formation in 5'-^{32}P-**154**.

Table 20. The effect of duplex concentration upon alkali-labile lesion formation in 5'-^{32}P-**154**.[a]

[unlabeled **154**] (nM)	Relative piperidine lability[b]		
	T_{15}	**122a**	T_{17}
-	1.0	1.0	1.0
5	1.0 ± 0.1	1.0 ± 0.1	0.93 ± 0.06
50	0.99 ± 0.11	1.03 ± 0.12	0.98 ± 0.10
500	1.0 ± 0.1	1.1 ± 0.1	1.1 ± 0.2
5000	1.2 ± 0.2	1.1 ± 0.2	0.94 ± 0.03

[a] %. [b] Relative piperidine labilities at a given concentration of unlabeled **154** are calculated relative to the amount of alkali-lability observed in the absence of unlabeled **154** which is defined as one. Alkali-labile lesions were revealed by treatment with 1.0 M piperidine (90 °C, 20 min).

Photolysis experiments were conducted in which the amount of alkali-labile lesions were measured as a function of DNA concentration (Table 20). It was found that increasing the concentration of oligonucleotide up to 5 μM resulted in no effect upon alkali-labile lesion formation at T_{15} and T_{17}. Alkali-labile lesion formation at the site of the 5,6-dihydro-2'-deoxyuridin-6-yl was unaffected as well, although this could result from cleavage of a termination product such as **164**. Although intramolecular reactions should compete less effectively with termination reactions at increasing radical

concentrations (Figure 86), the lack of an effect can be explained on the basis of the slow rate of peroxyl radical termination. Even at 5 μM DNA concentrations, the steady-state radical concentration is ~ 42 pM. If a bimolecular rate constant of 10^3 $M^{-1}s^{-1}$ is assumed for the peroxyl radical termination reaction, this gives an overall rate of 4.2 X 10^{-7} s^{-1}.[145] Assuming that the rate constant for internucleotidyl reaction is significantly higher than this value, the effect of increasing DNA concentration is expected to be minor.

3.2.3.1.8 Deuterium Isotope Effect Experiments.

A likely mechanism for DNA damage amplification by the peroxyl radical derived from 5,6-dihydro-2'-deoxyuridin-6-yl is abstraction of a hydrogen atom from the 2-deoxyribose sugar of an adjacent nucleotide. The resulting 2-deoxyribose sugar radical could then result in the formation of an alkali-labile lesion. The structurally similar C5 peroxyl radical (**113**) derived from thymidine has been shown to react via abstraction of a hydrogen atom from the C1' position of an adjacent nucleotide.[24]

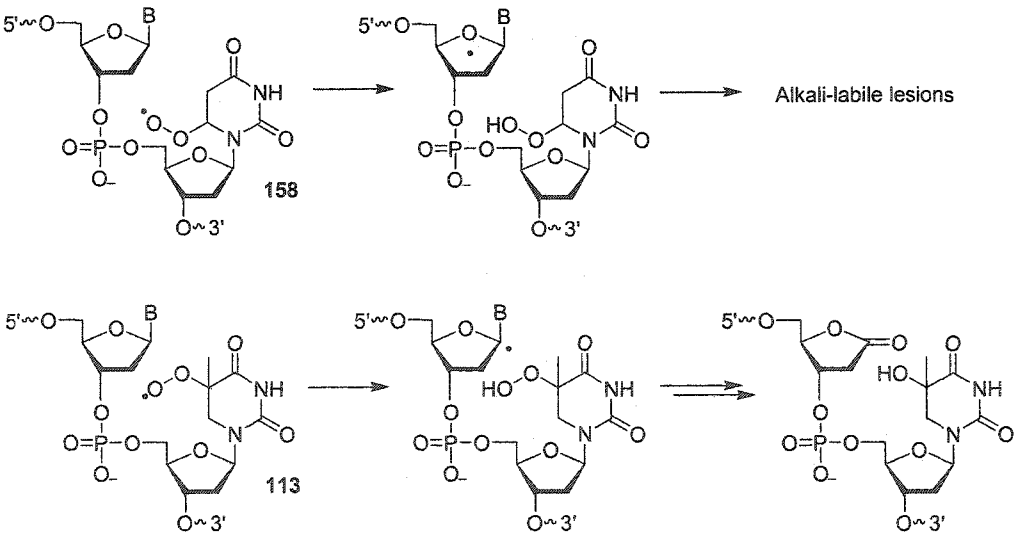

Figure 87. Intranucleotidyl hydrogen atom abstraction by nucleobase peroxyl radicals (**158**, **113**).

Hydrogen atom abstraction from C4' and C5' was also considered. Abstraction of a hydrogen atom from the C1' position would be expected to result in the formation of 2-deoxyribonolactone (**70**).[43,63-66,107] The C4' oxidized abasic site (**93**) or hydroperoxide (**95**) are alkali-labile lesions which can be formed from abstraction of H4'.[43,80,81] Cyclopyrimidine **165** could be formed by abstraction of H5' followed by reaction of the cyclized radical with oxygen.[90] Based upon known characteristics of similar compounds, it was considered unlikely that **165** would be alkali-labile.[93]

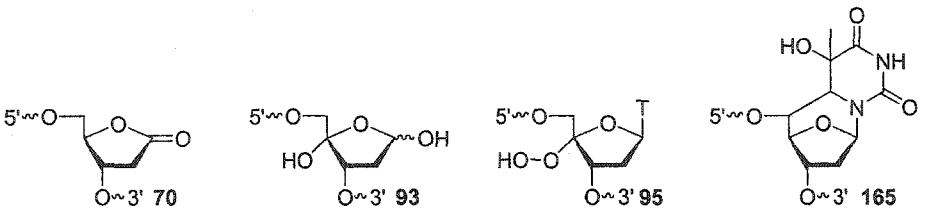

Figure 88. Anticipated products for abstraction of a hydrogen atom from the C1' (**70**), C4' (**93**, **95**), and C5' (**165**) positions of a thymidine adjacent to 5,6-dihydro-2'-deoxyuridin-6-yl (**123**).

To determine if hydrogen atom abstaction from the C1', C4', or C5' position of nucleotides adjacent to the C6 pyrimidine radical was responsible for alkali-labile lesion formation, deuterium isotope effect studies were conducted. For these experiments, oligonucleotides were synthesized in which the radical precursor (**122a**) was situated next to a selectively deuterated nucleotide. Deuteration of a position which was a target for hydrogen atom abstraction would be expected to result in a primary kinetic isotope effect which would be observed as a diminution in alkali-labile lesion formation. By comparing the amount of alkali-lability at positions adjacent to the radical precursor in DNA containing deuterated and non-deuterated nucleotides, an isotope effect can be meausured.

To measure isotope effects for hydrogen atom abstraction in DNA, oligonucleotides containing *two* radical precursors (**122a**) were used (Figure 89).[67] One oligonucleotide contained a selectively deuterated nucleotide adjacent to one radical precursor (**122a**), while the other (control) oligonucleotide was non-deuterated. The presence of two radical precursors in each oligonucleotide provides an internal reference for both the control and deuterated DNA. Therefore, the calculated isotope effect is unaffected by small variations in conversion between the control and deuterated DNA. By comparing the ratio of cleavage at the nucleotides 5'-adjacent to the radical precursors in both oligonucleotides, a kinetic isotope effect can be calculated (Figure 89).

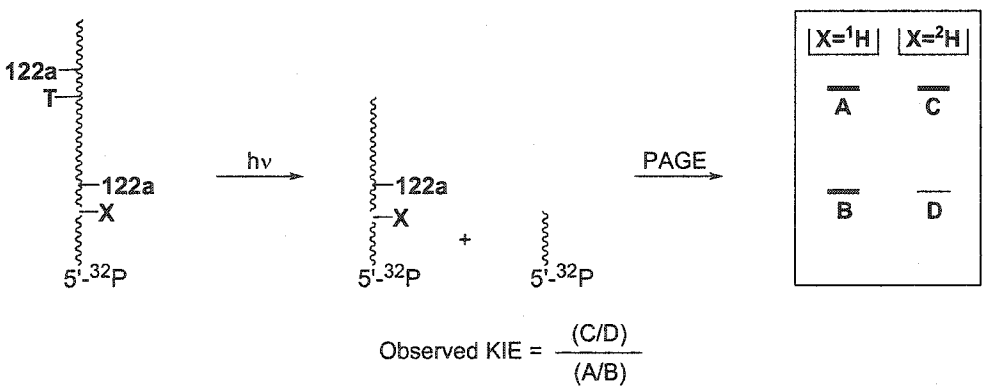

Figure 89. Isotope effect measurement using DNA containing two radical precursors.

Two general types of kinetic isotope effect experiments were conducted. In the first type of experiment, the thymidine nucleotide 5'-adjacent to a radical precursor was deuterated. Experiments utilizing these oligonucleotides were conducted using 5'-^{32}P end-labeled substrates. In the second type of experiment, the thymidine nucleotide 3'-

adjacent to a radical precursor was deuterated. These oligonucleotides were 3'-^{32}P end-labeled prior to photolysis.

3.2.3.1.8.1 Isotope Effect for C1' Hydrogen Atom Abstraction.

A likely candidate for the alkali-labile site formed at T_{15} from the C6 peroxyl radical is the 2-deoxyribonolactone (**70**, Figure 90). Abstraction from this position is favorable based upon thermodynamic considerations.[55-57,59] DNA (**167**, **168**) containing two *t*-butyl ketone radical precursors (**122a**) and one selectively deuterated thymidine was photolyzed to test this possibility.[67]

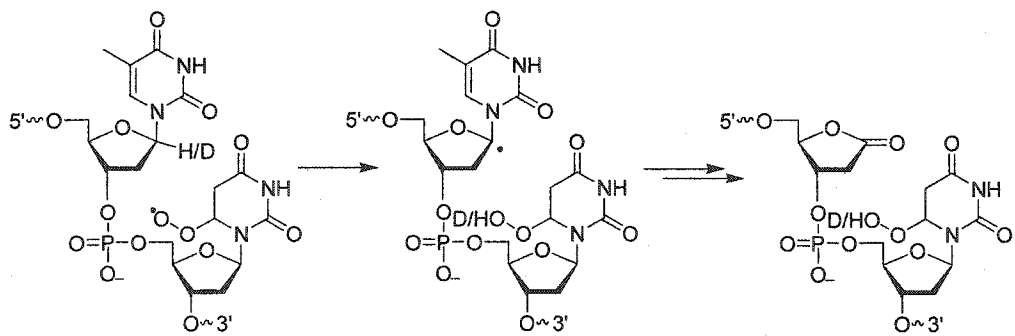

Figure 90. C1' hydrogen atom abstraction to generate 2-deoxyribonolactone.

5'-d(GAG TCA CGC CX_{11}**122a** Y_{13}AG CGT CAG CCT_{24} **122a**TA GAG CGC AGT)
166 X = Y = thymidine
167 X = C1' ^{2}H thymidine, Y = thymidine
168 X = thymidine, Y = C1' ^{2}H thymidine

5'-d(GAG TCA CGC CX_{11}**122a** Y_{13}AG CGT CAG CCT_{24} **122a**TA GAG CGC AGT)
3'-d(CTC AGT GCG GA A A TC GCA GTC GGA A A T CTC GCG TCA)
169 X = Y = thymidine
170 X = C1' ^{2}H thymidine, Y = thymidine
171 X = thymidine, Y = C1' ^{2}H thymidine

The observed isotope effect for C1' hydrogen atom abstraction from T_{11} (the nucleotide 5'-adjacent to the radical) in 5'-^{32}P-**167** and -**170** was strongly dependent upon the base treatment used to reveal alkali-labile lesions (Table 21). Treatment of photolysates with piperidine to reveal alkali-labile lesions resulted in a modest observed isotope effect in both single-stranded (**167**) and duplex DNA (**170**). Treatment of photolysates with NaOH, however, gave a much larger isotope effect (Figure 91).

The dependence of the observed kinetic isotope effect upon the type of base treatment suggests that there is more than one type of alkali-labile lesion formed at T_{11} in oligonucleotides **167** and **170**. This is consistent with previous experiments using 5'-^{32}P-**154** and -**159** (Tables 1,3) which revealed that the ratio of piperidine to NaOH-induced cleavage at the nucleotide 5'-adjacent to the radical was > 3. This suggests that distinct types of damage with differing base sensitivities are formed at the nucleotide 5'-adjacent to the radical. Treatment of photolysates with piperidine results in cleavage of all alkali-labile lesions, some of which apparently do not involve C1' hydrogen atom abstraction in the product determining step. Consequently, a lower value for the isotope effect is measured. Treatment of photolysates with 0.1 M NaOH (37 °C, 20 min) is sufficient to selectively cleave abasic sites such as the 2-deoxyribonolactone, the expected product of C1' hydrogen atom abstraction.[140] Since the product determining step of 2-deoxyribonolactone formation is C1'-hydrogen atom abstraction, selective cleavage of this lesion results in a larger observed isotope effect. Comparable values (~ 4.3) are obtained for both single-stranded (**167**) and duplex (**170**) DNA. These values are consistent with hydrogen atom abstraction by an oxygen radical.[146]

Treatment of photolysates of 3'-^{32}P-**168** or 3'-^{32}P-**171** with NaOH results in no cleavage at T_{13}, indicating that no 2-deoxyribonolactone is formed at this position. This observation is consistent with previous experiments which have demonstrated a lack of NaOH-lability at the nucleotide 3'-adjacent to 5,6-dihydro-2'-deoxyuridin-6-yl. As expected, treatment of photolysates with piperidine reveals there is no isotope effect for C1' hydrogen atom abstraction, which is consistent with the lack of NaOH-lability at this position. Therefore, the pathway leading to alkali-labile lesion formation at the thymidine nucleotide adjacent to the C6 pyrimidine radical (**123**) in the 3' direction does not involve abstraction of a hydrogen atom from the C1' position of 2-deoxyribose sugar.

Table 21. Deuterium isotope effects for C1' hydrogen atom abstraction.

DNA[a]	Base Treatment	Isotope Effect[e]
167 (ss)	Piperidine[c]	1.7 ± 0.2
170 (ds)	Piperidine[c]	2.0 ± 0.1
167 (ss)	NaOH[d]	4.3 ± 0.3
170 (ds)	NaOH[d]	4.4 ± 0.1
168 (ss)	Piperidine[c]	1.1 ± 0.2
171 (ds)	Piperidine[c]	1.1 ± 0.2

a. ss denotes single-strand DNA, ds denotes duplex DNA. b. Thymidine was selectively deuterated at the C1' position. c. Photolysates were treated with 1.0 M piperidine (90 °C, 20 min). d. Photolysates were treated with 0.1 M NaOH (37 °C, 20 min). e. Experiments were carried out with ten replicates of the control and deuterated oligonucleotides. Values for individual experiments are given in appendix D.

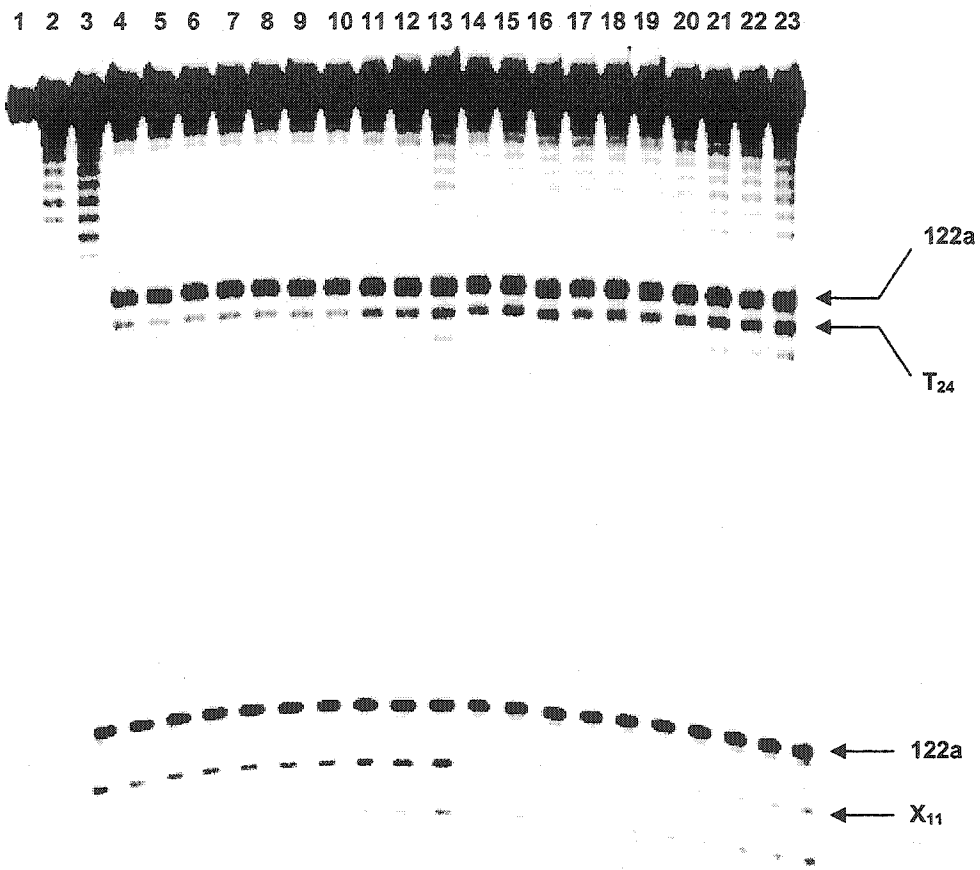

Figure 91. The deuterium isotope effect for C1' hydrogen atom abstracton. Lane 1, T selective sequencing reaction. Lanes 2-23 were treated with 0.1 M NaOH (37 °C, 20 min). Lane 2, non-photolyzed 5'-^{32}P-**169**; lane 3, non-photolyzed 5'-^{32}P-**170**. Lanes 4-13, photolyzed 5'-^{32}P-**169**; lanes 14-23, 5'-^{32}P-**170**.

5'-d(GAG TCA CGC CX_{11}**122a** Y_{13}AG CGT CAG CCT_{24} **122a**TA GAG CGC AGT)
3'-d(CTC AGT GCG GA A A TC GCA GTC GGA A A T CTC GCG TCA)
169 X = Y = thymidine
170 X = C1' ^{2}H thymidine, Y = thymidine

3.2.3.1.8.2 Isotope Effect for C4' Hydrogen Atom Abstraction.

The isotope effect for C4' hydrogen atom abstraction was measured using the appropriate selectively deuterated DNA (**174-177**). A modest isotope effect was observed for the abstraction of H4' from T_{11} in 5'-^{32}P-**174** and -**176** (Table 22). The magnitude of the isotope effect is slightly larger in single-stranded DNA and is independent of the base treatment used to reveal alkali-labile lesions. These results suggest that C4' hydrogen atom abstraction may be a minor pathway for alkali-labile lesion formation.

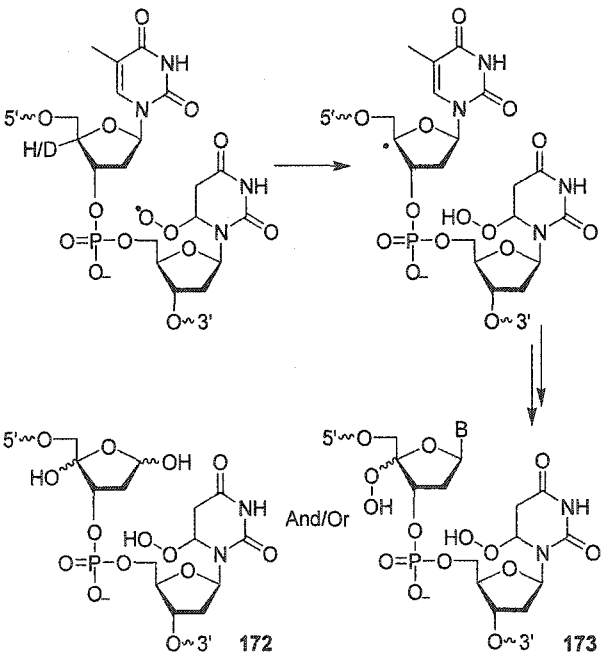

Figure 92. Possible alkali-labile lesions formed from C4' hydrogen atom abstraction.

Two possible alkali-labile lesions formed from the C4' hydrogen atom abstraction mechanism are the C4' hydroperoxide (**173**) and the C4' oxidized abasic site (**172**, Figure 92). The C4' hydroperoxide was identified as a product of the C4' radical by Giese and co-workers.[80] The oxidized abasic site is generated from the C4' radical generated by

bleomycin.[62,76,77] As no NaOH lability is observed at nucleotides 3'-adjacent to the pyrimidine C6 radical, only piperidine treatment was used to reveal alkali-labile lesions in experiments measuring the kinetic isotope effect at T_{26}. The lack of an isotope effect for C4' hydrogen atom abstraction from T_{26} in 3'-^{32}P-**175** and -**177** indicates that this is not a viable pathway for the formation of alkali-labile lesions.

5'-d(GAG TCA CGC CX_{11}**122a** TAG CGT CAG CCT **122a**Y_{26}A GAG CGC AGT)
166 X = Y = thymidine
174 X = C4' ^{2}H thymidine, Y = thymidine
175 X = thymidine, Y = C4' ^{2}H thymidine

5'-d(GAG TCA CGC CX_{11}**122a** Y_{13}AG CGT CAG CCT_{24} **122a**TA GAG CGC AGT)
3'-d(CTC AGT GCG GA A A TC GCA GTC GGA A A T CTC GCG TCA)
169 X = Y = thymidine
176 X = C4' ^{2}H thymidine, Y = thymidine
177 X = thymidine, Y = C4' ^{2}H thymidine

Table 22. Deuterium isotope effects for C4' hydrogen atom abstraction

DNA[a]	Base Treatment	Isotope Effect[e]
174 (ss)	Piperidine[c]	2.2 ± 0.2
176 (ds)	Piperidine[c]	1.6 ± 0.4
174 (ss)	NaOH[d]	2.2 ± 0.3
176 (ds)	NaOH[d]	1.6 ± 0.1
175 (ss)	Piperidine[c]	1.2 ± 0.1
177 (ds)	Piperidine[c]	1.2 ± 0.1

a. ss denotes single-strand DNA, ds denotes duplex DNA. b. Thymidine was selectively deuterated at the C1' position. c. Photolysates were treated with 1.0 M piperidine (90 °C, 20 min). d. Photolysates were treated with 0.1 M NaOH (37 °C, 20 min). e. Experiments were carried out with ten replicates of the control and deuterated oligonucleotides. Values for individual experiments are given in appendix D.

3.2.3.1.8.3 Isotope Effect for C5' Hydrogen Atom Abstraction.

An inverse isotope effect upon piperidine labile lesion formation was observed for C5' hydrogen atom abstraction from T_{11} in both single-stranded (**181**) and duplex (**183**) DNA (Table 23). This suggests that C5' hydrogen atom abstraction results in a product which is not alkali-labile. In the deuterated oligonucleotide, abstraction from the C5' position is disfavored, resulting in less of the non alkali-labile product. Other lesions, which are cleaved by base treatment, are likely formed at the expense of the C5' hydrogen atom abstraction pathway. Therefore, in the deuterated DNA, a larger fraction of the internucleotidyl hydrogen atom abstraction reactions result in the formation of alkali-labile lesions. This leads to more cleavage at the nucleotide 5'-adjacent to the radical precursor in the deuterated DNA and the observation of an inverse isotope effect.

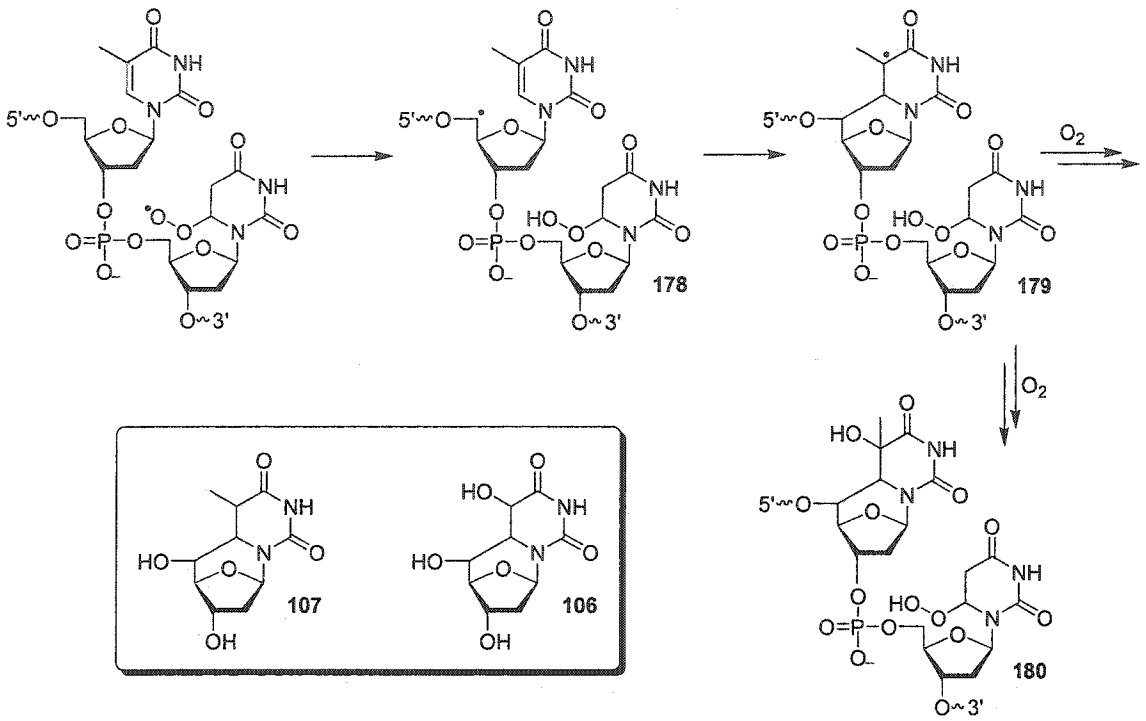

Figure 93. Formation of a non-alkali-labile lesion (**180**) from the C5' radical.

Treatment of photolysates with NaOH resulted in no isotope effect. The fact that the inverse isotope effect is only observed when piperidine is used to reveal alkali-labile lesions suggests that a large fraction of the lesions formed when the C5' hydrogen atom abstraction pathway is disfavored are not labile to NaOH. This is consistent with previous experiments which show that the ratio of piperidine to NaOH induced cleavage at the nucleotide 5'-adjacent to **122a** in 5'-^{32}P-**154** and -**159** is > 3 (Tables 10, 12). Therefore, the majority of alkali-labile damage at this site is not NaOH-labile. Although the amount of NaOH-lability would be expected to increase as well upon isotopic substitution of the C5' hydrogen atoms (and result in an inverse isotope effect upon

NaOH-labile lesion formation), the increase would be more difficult to measure due to its lower overall yield.

A pathway which is consistent with this inverse isotope effect is intranucleotidyl addition of the C5' radical (**178**) to the nucleobase (Figure 93). In the presence of oxygen, the C5 adduct radical (**179**) could react with O_2 to give rise to cyclonucleoside **180**. Structurally related cyclopyrimidines **106** and **107** are formed via the reaction of hydroxyl radical with thymidine and 2'-deoxycytidine respectively. Using independently synthesized DNA containing these lesions, Cadet and co-workers determined that they are only weakly alkali-labile.[93,94] Based upon these results, it is likely that lesion **180** would be resistant to piperidine-induced cleavage as well.

5'-d(GAG TCA CGC CX_{11}**122a** Y_{13}AG CGT CAG CCT_{24} **122a**TA GAG CGC AGT)
166 X = Y = thymidine
181 X = C5' ^{2}H thymidine, Y = thymidine
182 X = thymidine, Y = C5' ^{2}H thymidine

5'-d(GAG TCA CGC CX_{11}**122a** Y_{13}AG CGT CAG CCT_{24} **122a**TA GAG CGC AGT)
3'-d(CTC AGT GCG GA A A TC GCA GTC GGA A A T CTC GCG TCA)
169 X = Y = thymidine
183 X = C5' ^{2}H thymidine, Y = thymidine
184 X = thymidine, Y = C5' ^{2}H thymidine

Table 23. Isotope effects for C5' hydrogen atom abstraction.

DNA[a]	Base Treatment	Isotope Effect[e]
181 (ss)	Piperidine[c]	0.67 ± 0.06
183 (ds)	Piperidine[c]	0.78 ± 0.15
181 (ss)	NaOH[d]	1.1 ± 0.1
182 (ss)	Piperidine[c]	1.1 ± 0.3
184 (ds)	Piperidine[c]	1.0 ± 0.1

a. ss denotes single-strand DNA, ds denotes duplex DNA. b. Thymidine was selectively deuterated at the C1' position. c. Photolysates were treated with 1.0 M piperidine (90 °C, 20 min). d. Photolysates were treated with 0.1 M NaOH (37 °C, 20 min). e. Experiments were carried with ten replicates of the control and deuterated oligonucleotides. Values for individual experiments are given in appendix D.

To determine the extent, if any, of hydrogen atom abstraction from the C5' position of the nucleotide 3'-adjacent to the radical, 3'-^{32}P-**182** and **-184** were used. No deuterium isotope effect was observed Furthermore, isotope effect studies show no isotope effect upon alkali-labile lesion formation for hydrogen atom abstraction from the C1', C4', or C5' positions of the nucleotide 3'-adjacent to 5,6-dihydro-2'-deoxyuridin-6-yl. However, significant transfer of damage from the 5,6-dihydro-2'-deoxyuridin-6-yl to the 3'-adjacent nucleotide is observed (Tables 11, 13). This suggests that instead of abstraction of a hydrogen atom from the 2-deoxyribose sugar, an alternative mechanism must result in the transfer of damage to the 3'-adjacent nucleotide.

3.2.3.1.9 Testing for Reaction with Nucleobases.

In order to test for hydrogen atom abstraction by the C6 peroxyl radical from the adjacent nucleotide, deuterium isotope effects for hydrogen atom abstraction were measured. These studies revealed that C1' hydrogen atom abstraction to form the 2-deoxyribonolactone is a major pathway leading to alkali-labile lesion formation at the nucleotide 5'-adjacent to the 5,6-dihydro-2'-deoxyuridin-6-yl (**123**). However, in

addition to 2-deoxyribonolactone, which is cleaved by NaOH, another more robust type of product is formed. This alkali-labile lesion requires piperidine treatment to induce cleavage, which is consistent with the smaller isotope effect observed for C1' hydrogen atom abstraction in piperidine treated photolysates of deuterated oligonucleotides (Table 21). All of the alkali-labile lesions formed at the nucleotide 3'-adjacent to the C6 pyrimidine radical (**123**) require piperidine to induce cleavage. Furthermore, no kinetic isotope is observed for abstraction of the C1', C4', or C5' hydrogen atoms. These studies suggest that the C6 peroxyl radical (**158**) reacts with the nucleobase rather than the 2-deoxyribose sugar of the 3'-adjacent nucleotide. Two pathways which were considered were addition to the C5-C6 position to generate an adduct radical such as **186** or abstraction of hydrogen atom from an adjacent nucleobase to generate a thymidine C5-methyl radical (**185**, Figure 94).

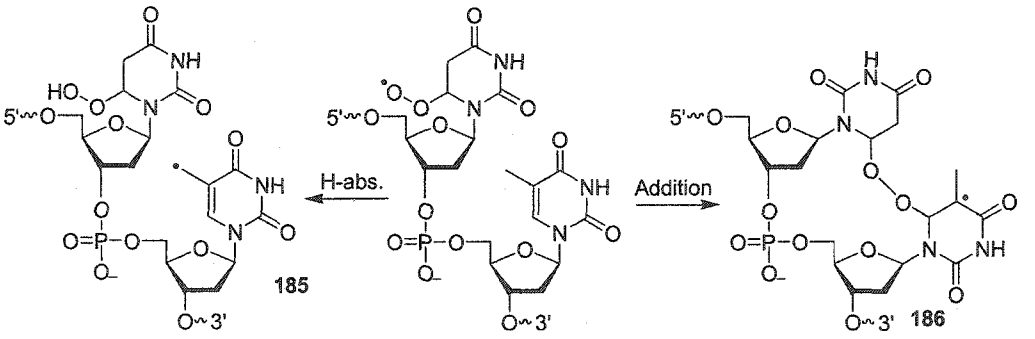

Figure 94. Reactions of the C6 peroxyl radical with the adjacent thymine nucleobase.

3.2.3.1.9.1 Testing for Addition to the Nucleobase.

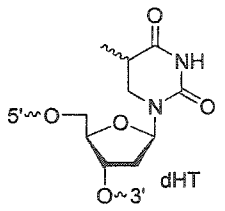

In some cases, peroxyl radical addition to alkenes can occur on the order of 10^4 $M^{-1}s^{-1}$.[147] Furthermore, addition of a nucleobase peroxyl radical to an adjacent nucleotide has been reported.[23] In order to probe for addition to the nucleobase, **187-190** were utilized. These mechanistic probes were of the same sequence at **159**, but contain 5,6-dihydrothymidine (dHT) nucleotides in place of T_{15} and/or T_{17}. Substitution of dHT for T eliminates the possibility of C6 peroxyl radical addition to the nucleobase as the C5 and C6 carbons are sp^3 hybridized. If addition to the nucleobase were indeed a major pathway, incorporation of dHT at positions adjacent to **122a** would be expected to either greatly reduce the amount of alkali-labile lesions formed at these positions or increase the amount of products formed from other pathways such as C1' hydrogen atom abstraction (Figure 95).

5'-d(GAG CTA GCT CGA CCX$_{15}$ **122a**Y$_{17}$ A GGA CCT GCA GCT)
187 X = dHT, Y = T

5'-d(GAG CTA GCT CGA CCX$_{15}$ **122a**Y$_{17}$ A GGA CCT GCA GCT)
3'-d(CTC GAT CGA GCT GGA A A T CCT GGA CGT CGA)
159 X = Y = thymidine
188 X= dHT, Y=thymidine
189 X=thymidine, Y=dHT
190 X = Y = dHT

Photolysis of 5'-^{32}P-**187** or -**188** followed by treatment with NaOH (0.1 M, 37 °C, 20 min) or piperidine (1.0 M, 90 °C, 20 min) demonstrated that substitution of T_{15} with dHT has a dramatic effect on the type of alkali-labile lesion formed at this position. The amount of alkali-lability observed at T/diHT_{15} in NaOH treated photolysates is two-fold greater in **188** than in **159** (Table 24, Figure 96). Furthermore, the amount of cleavage at T_{15} induced by piperidine treatment in 5'-^{32}P-**159** is > 3-fold higher than that induced by the milder NaOH conditions. The respective ratio of piperidine to NaOH induced strand scission at dHT_{15} is much smaller (~ 1.4) in duplex **188**. However, the overall amount of cleavage induced by piperidine treatment in 5'-^{32}P-**187** and -**188** is approximately equal to that in 5'-^{32}P-**159**.

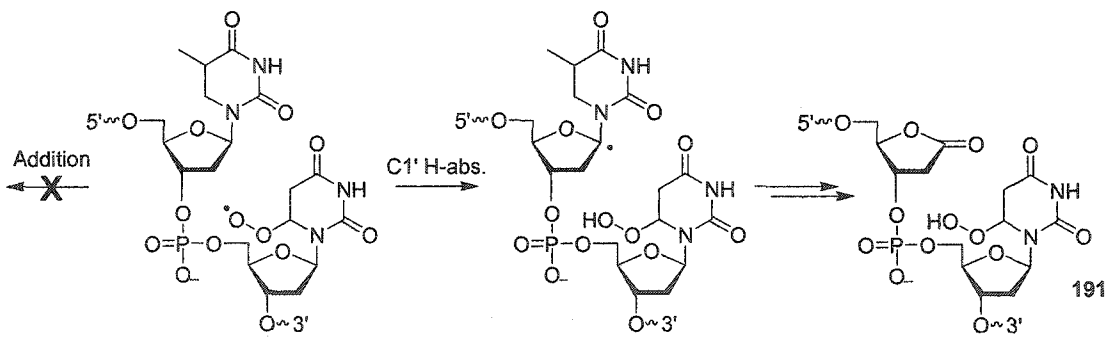

Figure 95. 2-Deoxyribonolactone formation in **187** and **188**.

This is consistent with the proposal that two types of lesions with differing alkali-labilities are formed at T_{15} in oligonucleotide **159**. The major reaction pathway is

proposed to be addition of the C6 peroxyl radical to the C5 or C6 position of the 5'-adjacent thymidine nucleotide, resulting in an adduct radical analogous to **186** (Figure 94) which subsequently produces a piperidine (but not NaOH) labile lesion at T_{15}. The minor pathway is C1' hydrogen atom abstraction which affords a lesion (**191**) containing 2-deoxyribonolactone (**70**), a highly base labile product which is cleaved under the milder NaOH conditions. Because the nucleobase addition pathway is not possible in duplex **188**, the majority of the observed DNA damage is the NaOH-labile 2-deoxyribonolactone which arises from C1' hydrogen atom abstraction (Figures 95, 96).

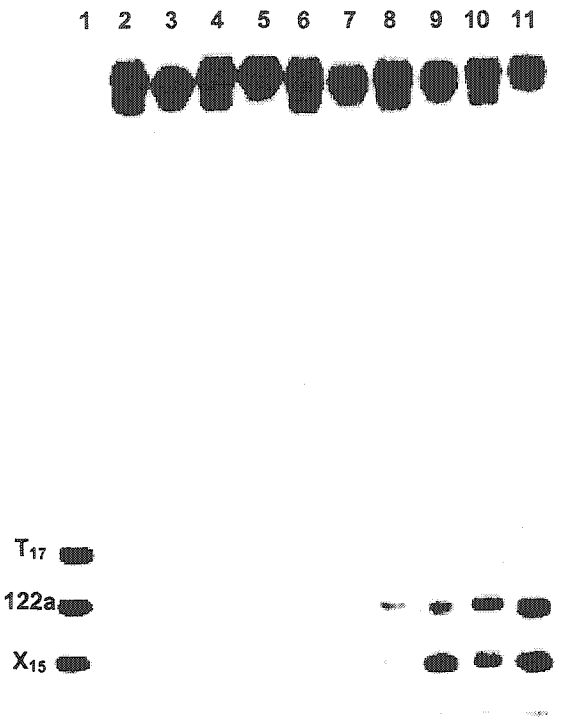

Figure 96. Phosphorimage of the photolysis of 5'-^{32}P-**159** and **188**. The appropriate lanes were treated with 1.0 M piperidine (90 °C, 20 min) or 0.1 M NaOH (37 °C, 20 min). Lane 1, oligonucleotide markers; lane 2, non-photolyzed **159** treated with NaOH; lane 3, non-photolyzed **188** treated with NaOH; lane 4, non-photolyzed **159** treated with piperidine; lane 5, non-photolyzed **188** treated with piperidine; lane 6, photolysate of **159**, no further treatment, lane 7, photolysate of **188**, no further treatment; lane 8, photolysate of **159**, treated with NaOH; lane 9, photolysate of **188** treated with NaOH; lane 10, photolysate of **E7**, treated with piperidine; lane 11, photolysate of **159**, treated with piperidine.

5'-d(GAG CTA GCT CGA CCX_{15} **122a**Y_{17} A GGA CCT GCA GCT)
3'-d(CTC GAT CGA GCT GGA A A T CCT GGA CGT CGA)
159 X = Y = thymidine
188 X= dHT, Y=thymidine

5'-d(GAG CTA GCT CGA CCX$_{15}$ **122a**Y$_{17}$ A GGA CCT GCA GCT)
187 X = dHT, Y = T

5'-d(GAG CTA GCT CGA CCX$_{15}$ **122a**Y$_{17}$ A GGA CCT GCA GCT)
3'-d(CTC GAT CGA GCT GGA A A T CCT GGA CGT CGA)
159 X = Y = thymidine
188 X= dHT, Y=thymidine
189 X=thymidine, Y=dHT
190 X = Y = dHT

Table 24. NaOH and piperidine lability in 5'-^{32}P-**159, -187-190.**[a]

DNA	Site	Percentage of total lesions (NaOH)[b]	Percentage of total lesions (Piperidine)[c]	Piperidine induced lesions/ NaOH induced lesions[d]
159	T_{17}	-	8.0 ± 1.4	-
	122a	63 ± 2	52 ± 2	2.4 ± 0.6
	T_{15}	37 ± 4	40 ± 4	3.3 ± 1.4
187	T_{17}	-	1.0 ± 0.1	-
	122a	22 ± 2	30 ± 1	2.6
	dHT_{15}	78 ± 2	69 ± 1	1.3 ± 0.2
188	T_{17}	-	3.0 ± 0.1	-
	122a	26 ± 3	38 ± 4	2.8 ± 4
	dHT_{15}	74 ± 1	59 ± 8	1.4 ± 0.1
189	dHT_{17}	-	17 ± 0.1	-
	122a	40 ± 9	40 ± 4	4.2 ± 1.1
	T_{15}	60 ± 6	43 ± 2	3.1 ± 0.3
190	dHT_{17}	-	8.0 ± 3.8	-
	122a	30 ± 8	36 ± 8	2.3 ± 0.4
	dHT_{15}	70 ± 6	56 ± 5	1.6 ± 0.2

[a] % Cleavages represent the average of multiple experiments which are presented in appendix D. The percentage alkali-lability was calculated based upon the cleavage observed at the radical precursor and the 5'- and 3'-adjacent nucleotides. [b] Photolysates were treated with 0.1 M NaOH (37 °C, 20 min,). [c] Photolysates were treated with 1.0 M piperidine (90 °C, 20 min). [d] Enhancement in total alkali-lability upon piperidine treatment (relative to NaOH).

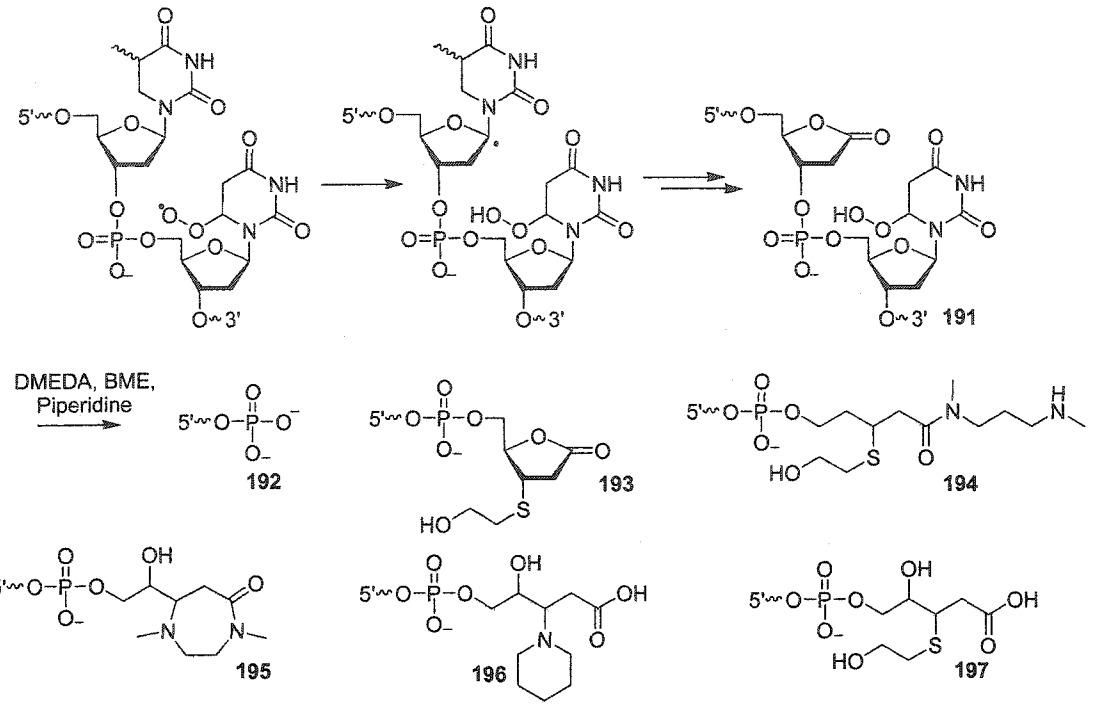

Figure 97. Adducts and cleavage products (**192-197**) formed from treatment of 2-deoxyribonolactone with BME, piperidine, and DMEDA.[111]

The larger amount of the NaOH-labile lesion formed at dHT_{15} in **188** (relative to T_{15} in **159**) enabled the use of a PAGE assay for the detection of 2-deoxyribonolactone. In this experiment, photolysates of 5'-^{32}P-**188** were treated with piperidine, DMEDA, and 2-mercaptoethanol (Figure 97).[111] This results in the conversion of the labile 2-deoxyribonolactone to stable adducts which migrate with characteristic aptitudes in a PAGE experiment. Photolysates of 5'-^{32}P-**188** displayed the characteristic products in a PAGE experiment when treated with these reagents (Figure 98). The same results were obtained using a 30mer containing 2-deoxyribonolactone independently generated from C1' radical precursor **198** (Figure 99).[107, 108, 111]

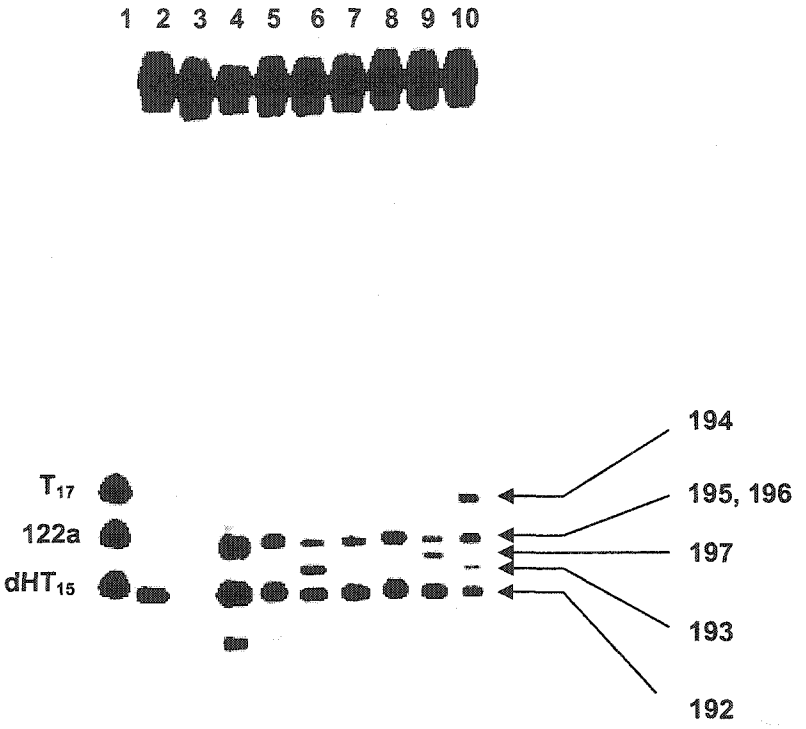

Figure 98. Adducts formed from 2-deoxyribonolactone produced in 5'-^{32}P-**188**. Lane 1, oligonucleotide markers. Lane 2, photolysate treated with 1.0 M piperidine (90 °C, 20 min); lane 3 photolysate, no further treatment; lane 4 photolysate treated with 1.0 M piperidine (90 °C, 20 min). Lanes 5-10, photolysate treated with the appropriate reagent(s) at 37 °C for 20 min. Lane 5, piperidine (100 mM); lane 6, piperidine (100 mM), BME (50 mM); lane 7, DMEDA (100 mM); lane 8, DMEDA (5 mM); lane 9, DMEDA (5 mM), BME (5 mM); lane 10, DMEDA (100 mM); BME (50 mM).

5'-d(GAG CTA GCT CGA CCX$_{15}$ **122a**Y$_{17}$ A GGA CCT GCA GCT)
3'-d(CTC GAT CGA GCT GGA A A T CCT GGA CGT CGA)
188 X= dHT, Y=thymidine

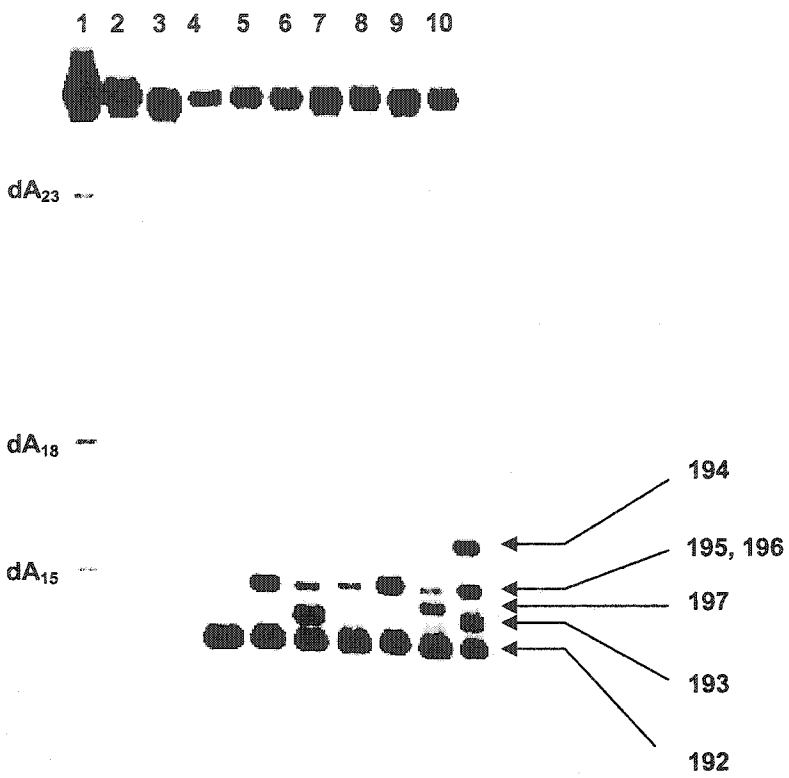

Figure 99. Adducts formed from 2-deoxyribonolactone produced in 5'-^{32}P-**199**. Lane 1, dA selective sequencing reaction. Lane 2, photolysate treated with 1.0 M piperidine (90 °C, 20 min); lane 3 photolysate, no further treatment; lane 4 photolysate treated with 1.0 M piperidine (90 °C, 20 min). Lanes 5-10, photolysate treated with the appropriate reagent(s) at 37 °C for 20 min. Lane 5, piperidine (100 mM); lane 6, piperidine (100 mM), BME (50 mM); lane 7, DMEDA (100 mM); lane 8, DMEDA (5 mM); lane 9, DMEDA (5 mM), BME (5 mM); lane 10, DMEDA (100 mM); BME (50 mM).

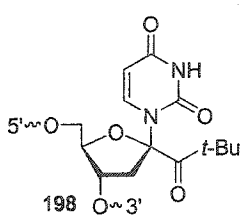

5'-d(GTC ACG TGC TGC AXA CGA CGT GCT GAG CCT)
199 X = 198

The possibility that the NaOH lability observed at dHT_{15} of 5'-^{32}P-**188** was partially due to the presence of a C4' oxidized abasic site (**93**, Figure 100) was also investigated. This lesion is a product of the C4' radical and its presence would be consistent with the modest isotope effect (~ 1.6) observed for abstraction of H4'. A PAGE assay, similar to the method described above for detection of the 2-deoxyribonolactone in DNA, for detection of the C4' oxidized abasic site was developed by Hecht and co-workers.[148] In this procedure, the labile C4' oxidized abasic site (**93**) is converted to a pyridazine fragment by treatment with hydrazine (Figure 100). The fragment containing the pyridazine end-group migrates more slowly than the corresponding phosphate terminated fragment. Treatment of photolysates of 5'-^{32}P-**188** with hydrazine under conditions used to cleave **93** resulted in no reaction, suggesting that the C4' oxidized abasic site (**93**) is not a major product formed at dHT_{15}. However, this does not rule out the presence of the C4' hydroperoxide (**95**), a base-labile product of C4' radicals which has been observed by mass spectrometry.[80]

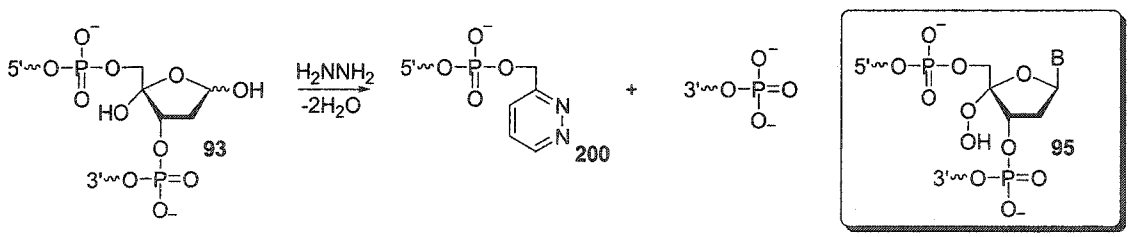

Figure 100. Derivatization of the C4' oxidized abasic site.

The C6 peroxyl radical could also react by addition to the nucleobase of T_{17}. It is likely that this process would generate a tandem alkali-labile lesion in which both the site

of the radical precursor as well as T_{17} are converted to alkali-labile lesions. In experiments utilizing 5'-^{32}P DNA, this would be observed as an alkali-labile lesion at the site of **122a**. In duplex **189**, formation of this tandem lesion is not possible due to the substitution of T_{17} with dHT. Photolysis of 5'-^{32}P-**189** followed by treatment with piperidine reveals a decrease in alkali-lability at **122a** relative to **159** (Table 24, Figure 101). This implies that reaction with the nucleobase of T_{17} leads, at least in part, to alkali-labile lesion formation at **122a**.

Duplex **190** contains radical precursor **122a** flanked by two dHT nucleotides. A similar decrease in the amount of piperidine-lability at **122a** (relative to duplex **159**) is observed in photolysates of 5'-^{32}P-**190** (Table 24, Figure 102). Again, this is presumably due to a reduction in the amount of tandem lesion formed from reaction of the C6 peroxyl radical with T_{17}. Furthermore, the amount of NaOH-lability at dHT_{15} is increased relative to **159** due to the inhibition of the base addition pathway.

The amounts of NaOH and piperidine labile lesions were also measured in 3'-^{32}P **188-190**. Generation of radical **122a** in 3'-^{32}P-**188** followed by NaOH treatment resulted in strand scission primarily at T_{15} (Figure 104, Table 25). This is consistent with experiments using 5'-^{32}P-**188** which also show a high degree of NaOH lability at this position (Table 24). Alkali-lability at this position is not enhanced by treatment with the more stringent piperidine conditions. This is consistent with the exclusive formation of 2-deoxyribonolactone at this position, a labile product which is cleaved by NaOH treatment. The amount of alkali-lability at the site of the radical precursor (**122a**) is greatly enhanced by treatment with piperidine (Table 25). Photolysis of 3'-^{32}P-**190** also

produced a NaOH-labile lesion primarily at dHT_{15}, presumably due to the formation of 2-deoxyribonolactone at this position (Figure 106, Table 25).

Photolysates of 3'-^{32}P-**189** and **190** undergo very little cleavage at dHT_{17} upon treatment with NaOH, indicating that 2-deoxyribonolactone is not formed at this site and therefore that C1' hydrogen atom abstraction does not occur at this position, even when the base addition pathway is blocked (Table 25, Figures 105, 106). This is consistent with kinetic isotope effect studies which indicate that abstraction of the C1' hydrogen of the nucleotide 3'-adjacent to **122a** does not occur.

An increase in piperidine lability at dHT_{17} in 3'-^{32}P-**189** is observed relative to 3'-^{32}P-**159**. The fact that a significant amount of cleavage (which is partially accounted for by adventitious cleavage of dHT) is still observed at dHT_{17} is inconsistent with the nucleobase addition pathway. However, this does not necessarily rule out that addition to the nucleobase in **159** leads to alkali-labile lesion formation. Replacement of T_{17} with dHT could introduce an additional pathway for alkali-labile lesion formation. The peroxyl radical derived from **122a** may react by hydrogen atom abstraction from the C5 or C6 position of the adjacent dHT. This would result in a stabilized tertiary radical. Reaction of the 5,6-dihydrothymidin-5-yl with O_2 would likely result in the formation of an alkali-labile lesion at this position (Figure 103).

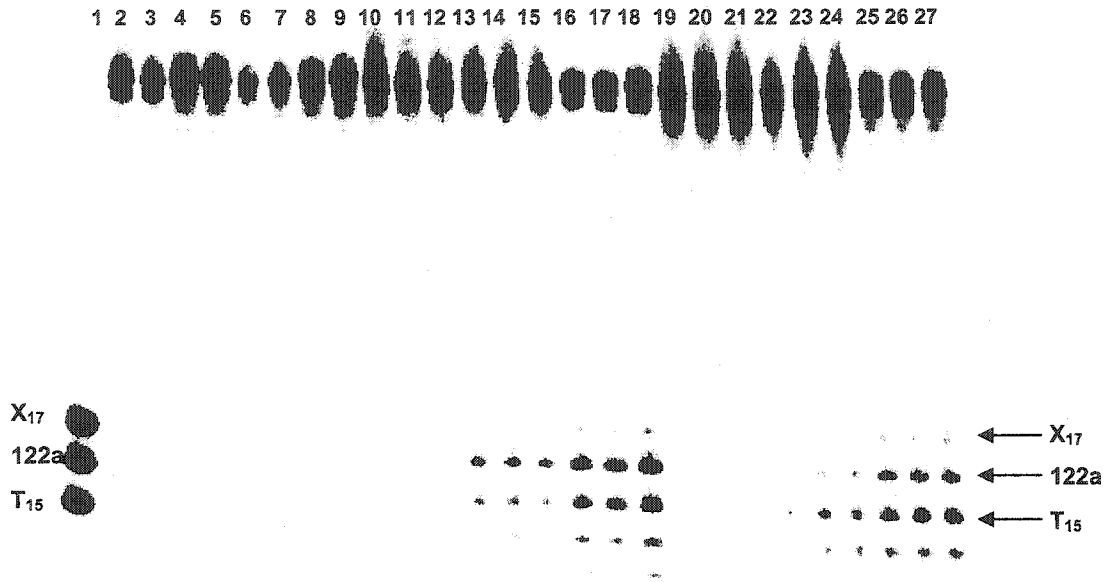

Figure 101. Photolysis of 5'-^{32}P-**189** and **159**. The appropriate lanes were treated with 0.1 M NaOH (37 °C, 20 min) or 1.0 M piperidine (90 °C, 20 min). Lane 1, oligonucleotide markers. Lanes 2-9 were non-photolyzed controls treated with the appropriate reagents. Lanes 2,3 **159**, NaOH; lanes 4,5 **189**, NaOH; lanes 6,7 **159**, piperidine; lanes 8,9 **189**, piperidine. Lanes 10-18 were photolysates of **159** treated appropriately. Lanes 10-12, no further treatment; lanes 13-15, NaOH; lanes 16-18; piperidine. Lanes 13-27 were photolysates of **189** treated appropriately. Lanes 19-21, no further treatment; lanes 22-24, NaOH; lanes 25-27, piperidine.

5'-d(GAG CTA GCT CGA CCX$_{15}$ **122a**Y$_{17}$A GGA CCT GCA GCT)
3'-d(CTC GAT CGA GCT GGA A A T CCT GGA CGT CGA)
159 X = Y = thymidine
189 X= thymidine, Y = dHT

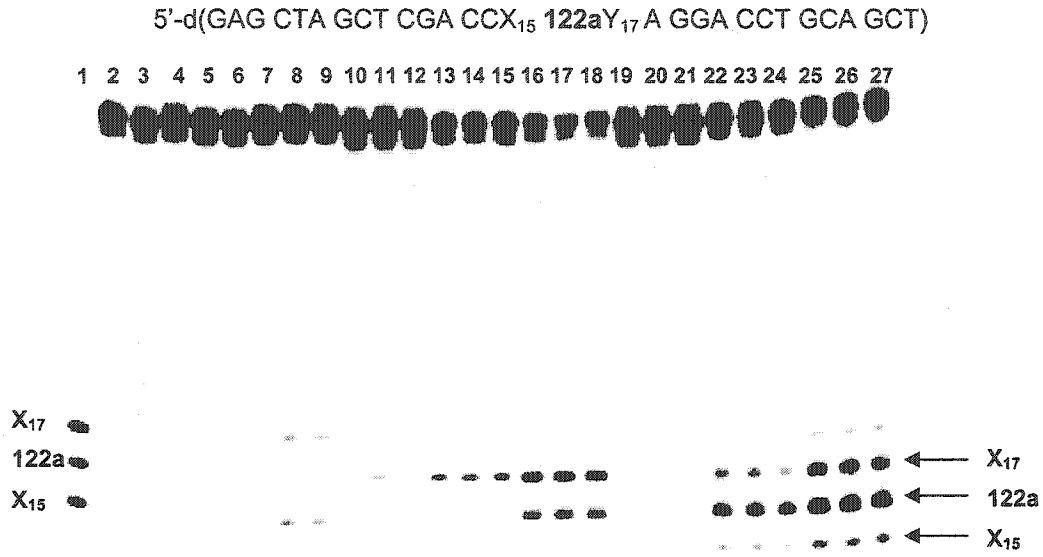

Figure 102. Photolysis of 5'-^{32}P-**190** and **159**. The appropriate lanes were treated with 0.1 M NaOH (37 °C, 20 min) or 1.0 M piperidine (90 °C, 20 min). Lane 1, oligonucleotide markers. Lanes 2-9 were non-photolyzed controls treated with the appropriate reagents. Lanes 2,3 **159**, NaOH; lanes 4,5 **190**, NaOH; lanes 6,7 **159**, piperidine; lanes 8,9 **190**, piperidine. Lanes 10-18 were photolysates of **159** treated appropriately. Lanes 10-12, no further treatment; lanes 13-15, NaOH; lanes 16-18; piperidine. Lanes 13-27 were photolysates of **190** treated appropriately. Lanes 19-21, no further treatment; lanes 22-24, NaOH; lanes 25-27, piperidine.

5'-d(GAG CTA GCT CGA CCX$_{15}$ **122a**Y$_{17}$ A GGA CCT GCA GCT)
3'-d(CTC GAT CGA GCT GGA A A T CCT GGA CGT CGA)
159 X = Y = thymidine
190 X= Y = dHT

3'-d(CTC GAT CGA GCT GGA A A T CCT GGA CGT CGA)
159 X = Y = thymidine
188 X= dHT, Y=thymidine
189 X=thymidine, Y=dHT
190 X = Y = dHT

Table 25. Piperidine and NaOH labile sites in 3'-^{32}P-**159**, -**188**-**190**.[a]

DNA	Site	Percentage of total lesions (NaOH)[b]	Percentage of total lesions (Piperidine)[c]	Piperidine induced lesions/ NaOH induced lesions[d]
159	T_{17}	-	40 ± 6	-
	122a	67 ± 7	51 ± 4	2.9 ± 0.6
	T_{15}	33 ± 7	9.0 ± 4.0	0.83 ± 0.10
188	T_{17}	-	31 ± 1	-
	122a	36 ± 9	50 ± 4	4.1 ± 0.3
	dHT_{15}	64 ± 9	19 ± 3	0.9 ± 0.2
189	dHT_{17}	23 ± 3	50 ± 1	9.9 ± 3.0
	122a	46 ± 7	34 ± 1	3.1 ± 0.7
	T_{15}	31 ± 5	16 ± 1	2.3 ± 0.6
190	dHT_{17}	-	42 ± 8	-
	122a	41 ± 2	20 ± 3	2.1 ± 0.1
	dHT_{15}	59 ± 3	38 ± 4	2.8 ± 0.1

[a] % Cleavages represent the average of multiple experiments which are presented in appendix D. The percentage alkali-lability was calculated based upon the cleavage observed at the radical precursor and the 5'- and 3'-adjacent nucleotides. [b] Photolysates were treated with 0.1 M NaOH (37 °C, 20 min,). [c] Photolysates were treated with 1.0 M piperidine (90 °C, 20 min). [d] Enhancement in total alkali-lability upon piperidine treatment (relative to NaOH).

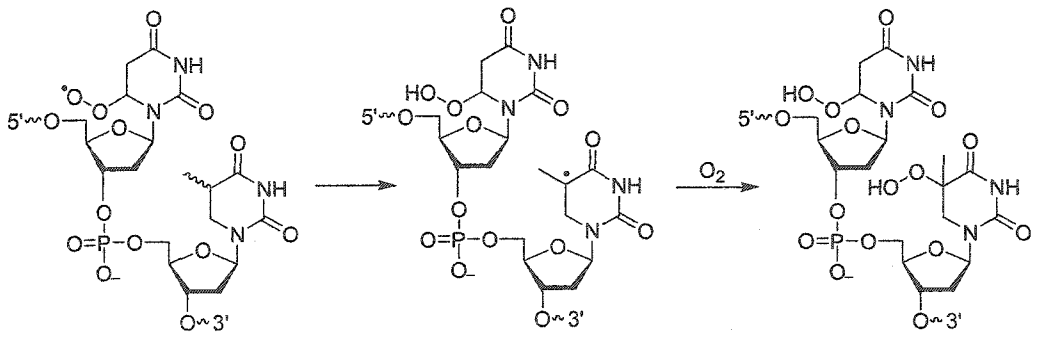

Figure 103. Hydrogen atom abstraction from dHT.

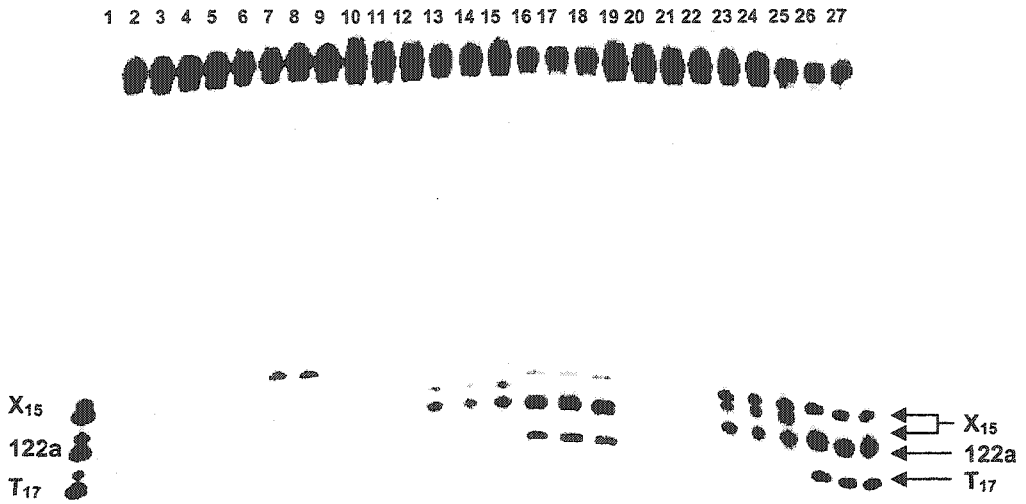

Figure 104. Photolysis of 3'-^{32}P-**188** and **159**. The appropriate lanes were treated with 0.1 M NaOH (37 °C, 20 min) or 1.0 M piperidine (90 °C, 20 min). Lane 1, oligonucleotide markers. Lanes 2-9 were non-photolyzed controls treated with the appropriate reagents. Lanes 2,3 **159**, NaOH; lanes 4,5 **188**, NaOH; lanes 6,7 **159**, piperidine; lanes 8,9 **188**, piperidine. Lanes 10-18 were photolysates of **159** treated appropriately. Lanes 10-12, no further treatment; lanes 13-15, NaOH; lanes 16-18; piperidine. Lanes 13-27 were photolysates of **188** treated appropriately. Lanes 19-21, no further treatment; lanes 22-24, NaOH; lanes 25-27, piperidine.

5'-d(GAG CTA GCT CGA CCX_{15} **122a**Y_{17} A GGA CCT GCA GCT)
3'-d(CTC GAT CGA GCT GGA A A T CCT GGA CGT CGA)
159 X = Y = thymidine
188 X= dHT, Y = T

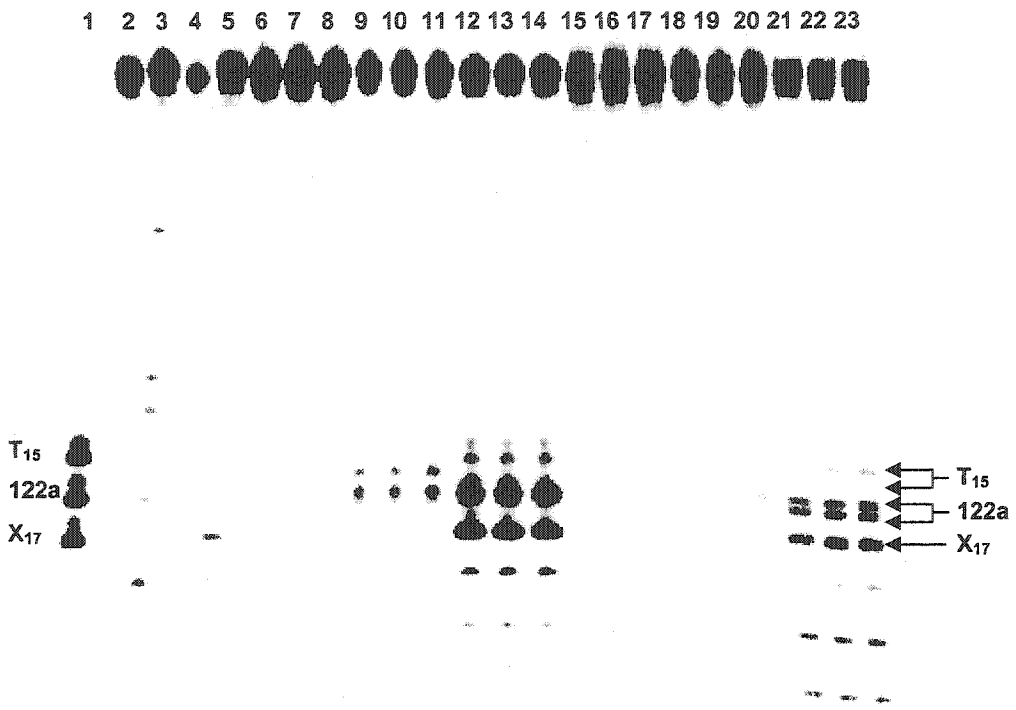

Figure 105. Photolysis of 3'-^{32}P-**189** and **159**. The appropriate lanes were treated with 0.1 M NaOH (37 °C, 20 min) or 1.0 M piperidine (90 °C, 20 min). Lane 1, oligonucleotide markers. Lanes 2-5 were non-photolyzed controls treated with the appropriate reagents. Lane 2 **159**, NaOH; lane 3 **189**, NaOH; lane 4, **159**, piperidine; lane 5 **189**, piperidine. Lanes 6-14 were photolysates of **159** treated appropriately. Lanes 6-8, no further treatment; lanes 9-11, NaOH; lanes 12-14; piperidine. Lanes 15-23 were photolysates of **189** treated appropriately. Lanes 15-17, no further treatment; lanes 18-20, NaOH; lanes 21-23, piperidine.

5'-d(GAG CTA GCT CGA CCX$_{15}$ **122a**Y$_{17}$A GGA CCT GCA GCT)
3'-d(CTC GAT CGA GCT GGA A A T CCT GGA CGT CGA)
159 X = Y = thymidine
189 X= thymidine, Y = dHT

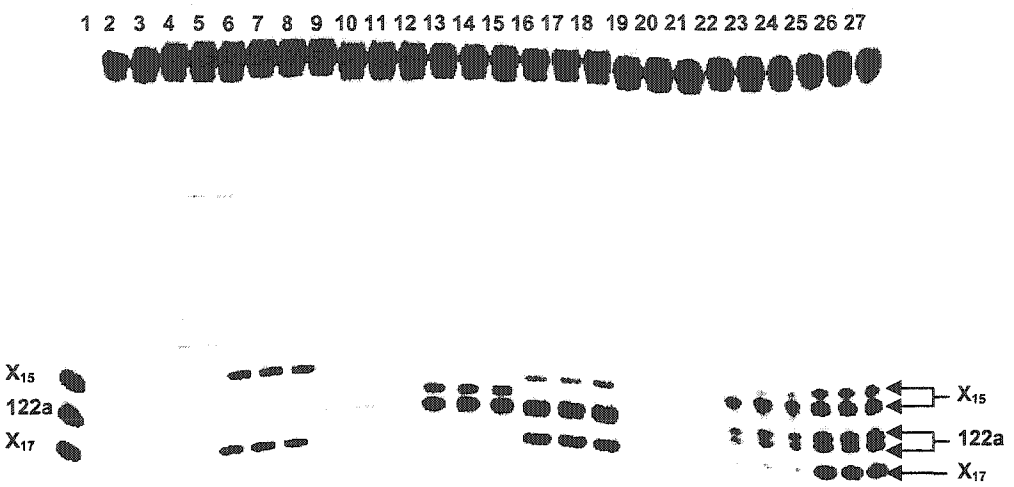

Figure 106. Phosphorimage of the photolysis of 3'-^{32}P-**190** and **159**. The appropriate lanes were treated with 0.1 M NaOH (37 °C, 20 min) or 1.0 M piperidine (90 °C, 20 min). Lane 1, oligonucleotide markers. Lanes 2-9 were non-photolyzed controls treated with the appropriate reagents. Lanes 2,3 **159**, NaOH; lanes 4,5 **190**, NaOH; lanes 6,7 **159**, piperidine; lanes 8,9 **190**, piperidine. Lanes 10-18 were photolysates of **159** treated appropriately. Lanes 10-12, no further treatment; lanes 13-15, NaOH; lanes 16-18; piperidine. Lanes 13-27 were photolysates of **190** treated appropriately. Lanes 19-21, no further treatment; lanes 22-24, NaOH; lanes 25-27, piperidine.

5'-d(GAG CTA GCT CGA CCX$_{15}$ **122a**Y$_{17}$ A GGA CCT GCA GCT)
3'-d(CTC GAT CGA GCT GGA A A T CCT GGA CGT CGA)
159 X = Y = thymidine
190 X= Y = dHT

3.2.3.1.9.2 Testing for Methyl Hydrogen Atom Abstraction.

Another mechanism which could explain alkali-labile lesion formation at nucleotides adjacent to the peroxyl radical (**158**) derived from **123** is abstraction of a hydrogen atom from the thymidine C5 methyl group (Figure 107). Solid state ESR studies indicate that methyl radical **201** is the most stable radical formed from the γ-irradiation of 1-methylthymine.[149] Abstraction of methyl hydrogen atoms from thymidine by peroxyl radicals has been detected.[144] DNA which contains dU in place of T (**202-204**) was designed as a probe for this mechanism. In these oligonucleotides, the nucleobase addition pathway is still possible, but no methyl group is present to undergo hydrogen atom abstraction. A reduction in alkali-lability upon replacement of T_{15} or T_{17} with dU would be indicative of hydrogen atom abstraction from the methyl group.

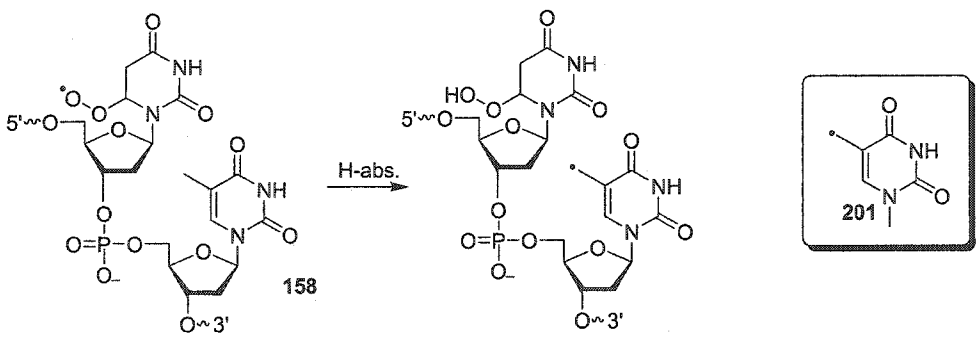

Figure 107. Methyl hydrogen atom abstraction.

5'-d(GAG CTA GCT CGA CCX_{15} **122a**Y_{17} A GGA CCT GCA GCT)
3'-d(CTC GAT CGA GCT GGA A A T CCT GGA CGT CGA)
159 X = Y = thymidine
202 X= dHT, Y=thymidine
203 X=thymidine, Y=dHT
204 X = Y = dHT

Experiments using 5'-^{32}P-**202** indicate that abstraction of a hydrogen atom from the C5 position of the 5'-adjacent thymidine methyl group is not a major pathway for alkali-labile lesion formation (Table 26, Figure 108). The distribution of alkali-labile lesions in this duplex is similar to that observed in duplex **159**. Furthermore, the major site of NaOH-labile lesions in this duplex is not dU_{15}. If abstraction of a methyl hydrogen from the 5'-adjacent nucleotide were a major pathway for the reaction of the C6 peroxyl radical (**158**), elimination of this pathway would be expected to greatly increase the amount of C1' hydrogen atom abstraction and thus the yield of 2-deoxyribonolactone. Only a small increase is observed. The piperidine enhancement (~1.6), however, is somewhat lower than that observed in 5'-^{32}P-**159**, indicating that abstraction of a hydrogen atom from the methyl group may be a minor pathway for alkali-labile lesion formation in **159**. However, this could also be a consequence of less efficient peroxyl radical addition to dU relative to T.

5'-d(GAG CTA GCT CGA CCX_{15} **122a** Y_{17} A GGA CCT GCA GCT)
3'-d(CTC GAT CGA GCT GGA A A T CCT GGA CGT CGA)
159 X = Y = thymidine
202 X= dU, Y =thymidine
203 X=thymidine, Y= dU
204 X = Y = dU

Table 26. Piperidine and NaOH lability in 5'-^{32}P-**159, -202-204**.[a]

DNA	Site	Percentage of total lesions (NaOH)[b]	Percentage of total lesions (Piperidine)[c]	Piperidine induced lesions/ NaOH induced lesions[d]
159	T_{17}	-	8.0 ± 1.4	-
	122a	63 ± 2	52 ± 2	2.4 ± 0.6
	T_{15}	37 ± 4	40 ± 4	3.3 ± 1.4
202	T_{17}	-	15 ± 1	-
	122a	53 ± 10	51 ± 2	2.2 ± 0.3
	dU_{15}	47 ± 9	34 ± 2	1.6 ± 0.2
203	dU_{17}	-	6.0 ± 0.4	-
	122a	28 ± 3	34 ± 9	4.6 ± 0.8
	T_{15}	72 ± 4	60 ± 2	3.2 ± 1.0
204	dU_{17}	-	4.0 ± 0.3	-
	122a	14 ± 1	29 ± 1	3.9 ± 0.3
	dU_{15}	86 ± 4	67 ± 2	1.5 ± 0.1

[a] % Cleavages represent the average of multiple experiments which are presented in appendix E. The percentage alkali-lability was calculated based upon the cleavage observed at the radical precursor and the 5'- and 3'-adjacent nucleotides. [b] Photolysates were treated with 0.1 M NaOH (37 °C, 20 min,). [c] Photolysates were treated with 1.0 M piperidine (90 °C, 20 min). [d] Enhancement in total alkali-lability upon piperidine treatment (relative to NaOH).

A different distribution of alkali-labile lesions was observed in 5'-^{32}P duplexes **203** and **204**, which contain dU nucleotides on the 3'-side of the radical precursor (**122a**). The major site of NaOH-labile lesions in these oligonucleotides is T/dU_{15}, indicating that a much greater amount of 2-deoxyribonolactone is formed at this position, relative to duplexes **159** and **202**.

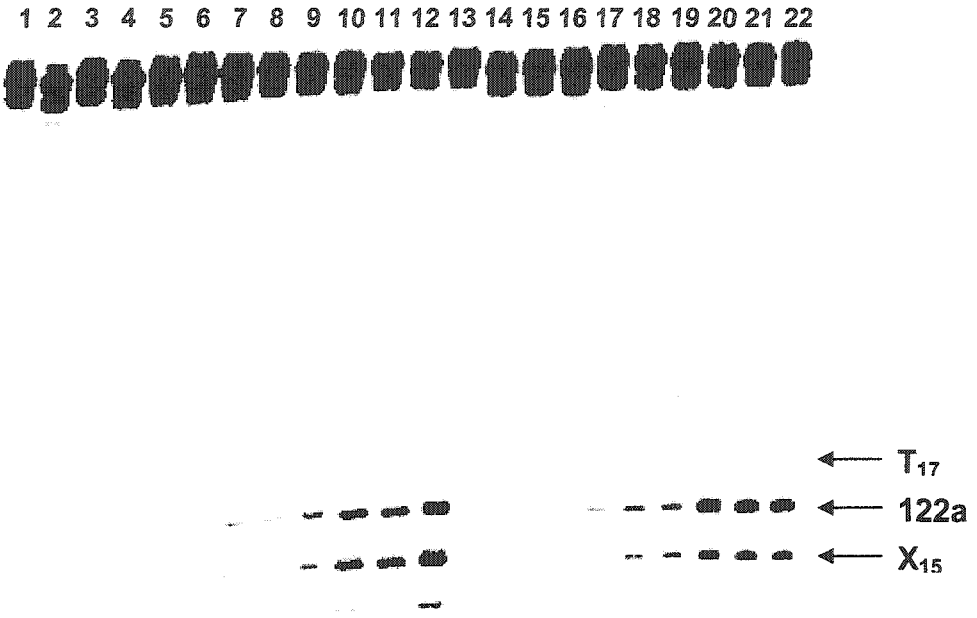

Figure 108. Phosphorimage of the aerobic photolysis of 5'-^{32}P-**159** and 5'-^{32}P-**202**. The appropriate lanes were treated with 0.1 M NaOH (37 °C, 20 min) or 1.0 M piperidine (90 °C, 20 min). Lanes 1-4 were non-photolyzed controls treated appropriately. Lane 1, **159**, NaOH; Lane 2, **202**, NaOH; Lane 3, **159** piperidine, lane 4, **202**, piperidine. Lanes 5-13 were the photolysate of **159** treated appropriately. Lanes 5-7, no further treatment; lanes 8-10, NaOH; lanes 11-13. Lanes 14-22 were the photolysate of **202** treated appropriately. Lanes 14-16, no further treatment; lanes 17-19, NaOH; lanes, 20-22, piperidine.

5'-d(GAG CTA GCT CGA CCX_{15} **122a**Y_{17} A GGA CCT GCA GCT)
3'-d(CTC GAT CGA GCT GGA A A T CCT GGA CGT CGA)
159 X = Y = thymidine
202 X= dU, Y=thymidine

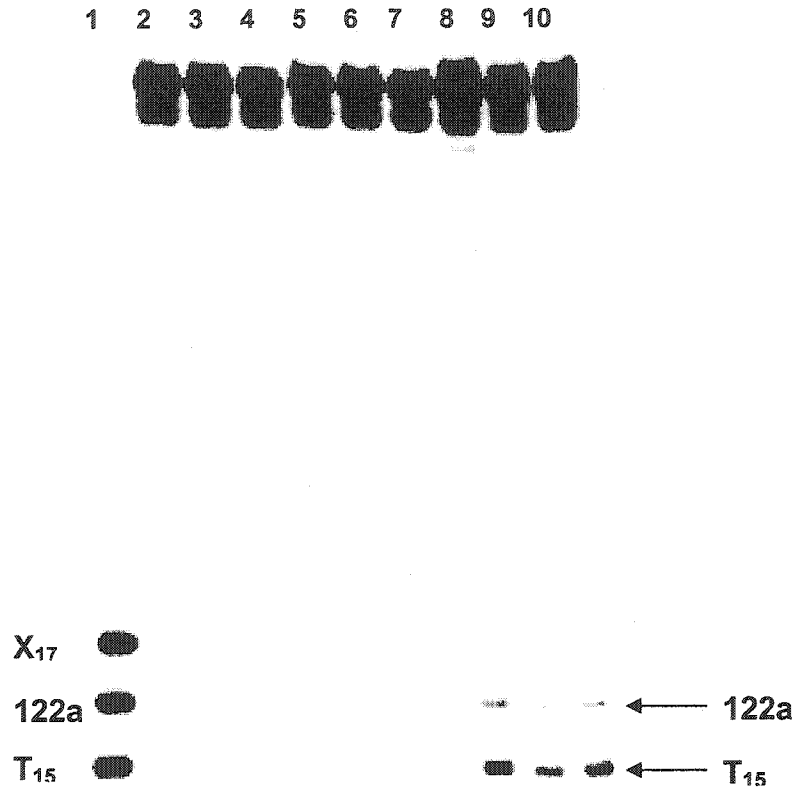

Figure 109. Photolysis of 5'-^{32}P-**203**. The appropriate lanes were treated with 0.1 M NaOH (37 °C, 20 min) or 1.0 M piperidine (90 °C, 20 min). Lanes 2-4, photolysate with no further treatment; lanes 5-7, photolysate treated with NaOH; lanes 8-10, photolysate treated with piperidine.

5'-d(GAG CTA GCT CGA CCX$_{15}$ **122a**Y$_{17}$ A GGA CCT GCA GCT)
3'-d(CTC GAT CGA GCT GGA A A T CCT GGA CGT CGA)
159 X = Y = thymidine
203 X= thymidine, Y= dU

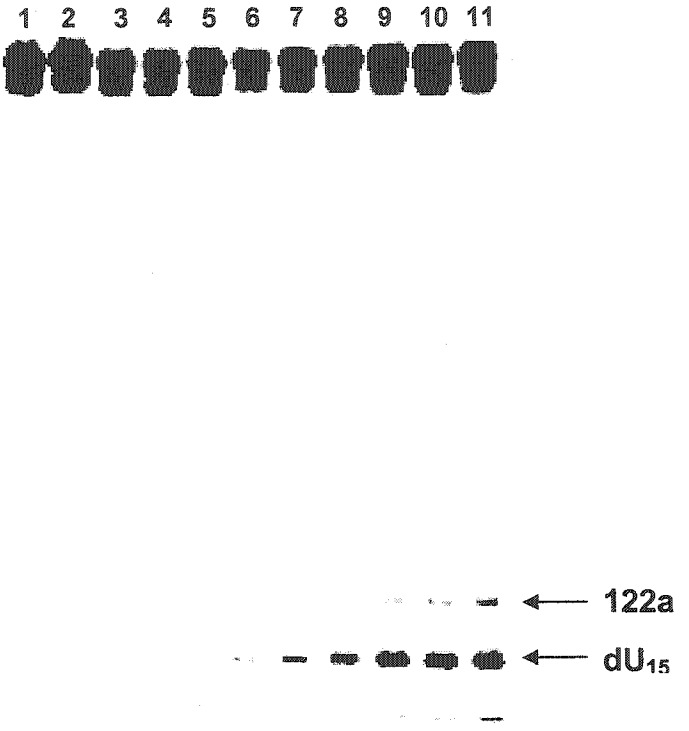

Figure 110. Phosphorimage of the aerobic photolysis of 5'-^{32}P-**204**. The appropriate lanes were treated with 0.1 M NaOH (37 °C, 20 min) or 1.0 M piperidine (90 °C, 20 min). Lanes 1 and 2 were non-photolyzed controls treated appropriately. Lane 1, NaOH; lane 2, piperidine. Lanes 4-14 were photolysate treated appropriately. Lanes 4-6, no further treatment; lanes 7-9, NaOH, lanes, 10-12, piperidine.

5'-d(GAG CTA GCT CGA CCX$_{15}$ **122a**Y$_{17}$ A GGA CCT GCA GCT)
3'-d(CTC GAT CGA GCT GGA A A T CCT GGA CGT CGA)
204 X = Y= dU

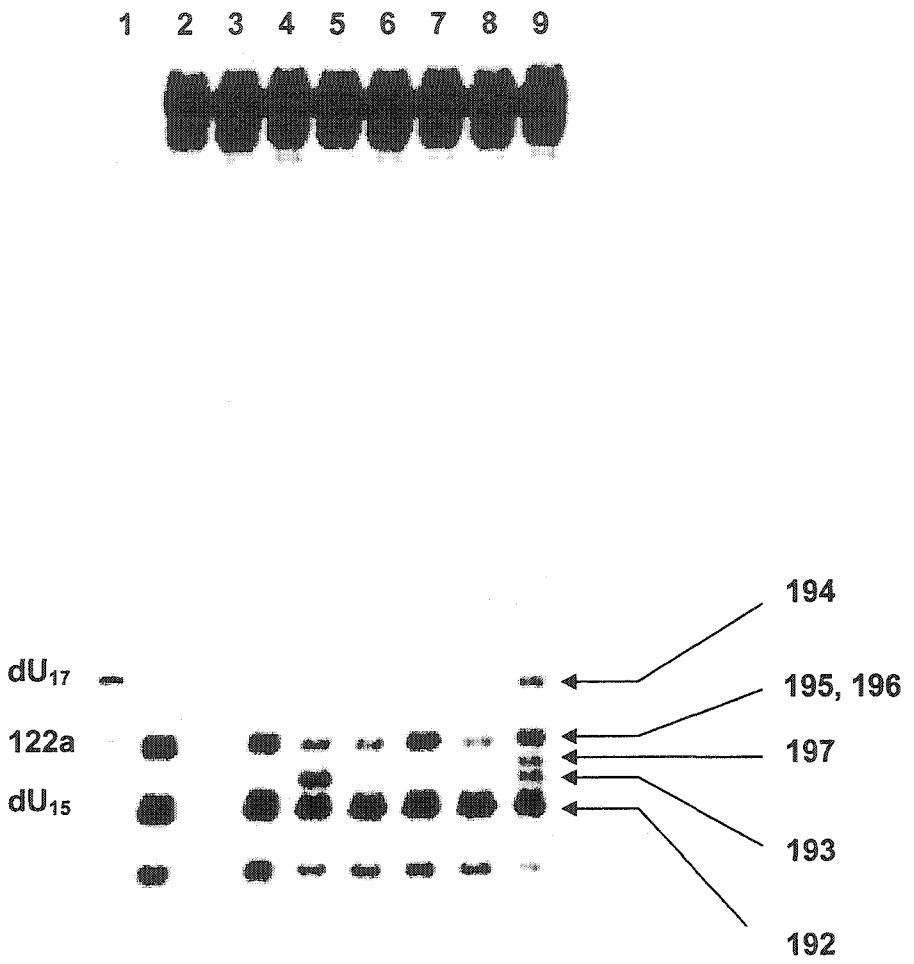

Figure 111. Adducts formed from 2-deoxyribonolactone produced in 5'-^{32}P-**204**. Lane 1, dA selective sequencing reaction. Lane 2, photolysate treated with 1.0 M piperidine (90 °C, 20 min); lane 3 photolysate, no further treatment. Lanes 4-9, photolysate treated with the appropriate reagent(s) at 37 °C for 20 min. Lane 4, piperidine (100 mM); lane 5, piperidine (100 mM), BME (50 mM); lane 6, DMEDA (100 mM); lane 7, DMEDA (5 mM); lane 8, DMEDA (5 mM), BME (5 mM); lane 9, DMEDA (100 mM); BME (50 mM).

5'-d(GAG CTA GCT CGA CCX$_{15}$ **122a**Y$_{17}$ A GGA CCT GCA GCT)
3'-d(CTC GAT CGA GCT GGA A A T CCT GGA CGT CGA)
204 X = Y= dU

The ratio of piperidine to NaOH labile lesions is still >1 at T/dU15, indicating that lesions which are only labile to piperidine are formed as well, ostensibly from the nucleobase addition pathway (Table 26, Figures 109, 110). The higher yield of the NaOH-labile lesion in 5'-^{32}P-**204** facilitated confirmation of its identity as 2-deoxyribonolactone by the set of "fingerprint" reactions used to characterize this labile product by PAGE (Figure 111).[111]

A very striking effect upon the distribution of alkali-labile lesions is observed in 3'-^{32}P-**203**, in which T_{17} is replaced with dU (Figure 112, Table 27). Alkali-lability is virtually eliminated at this position by removal of the methyl group from the nucleobase. This indicates that abstraction of a hydrogen atom from the thymidine C5 methyl group is the major pathway leading to alkali-labile lesion formation at the nucleotide 3'-adjacent to the 5,6-dihydro-2'-deoxyuridin-6-yl. A possible structure for the alkali-labile lesion formed at T_{17} in **159** is a 5-hydroperoxymethyl-2'-deoxyuridine (Figure 113).

Table 27. Piperidine and NaOH lability in 3'-^{32}P-**159** and -**203**.[a]

DNA	Site	Percentage of total lesions (NaOH)[b]	Percentage of total lesions (Piperidine)[c]	Piperidine induced lesions/ NaOH induced lesions[d]
159	T_{17}	-	40 ± 6	-
	122a	67 ± 7	51 ± 4	2.9 ± 0.6
	T_{15}	33 ± 7	9.0 ± 4.0	0.83 ± 0.10
203	dU_{17}	-	8.0 ± 4.3	-
	122a	51 ± 1	54 ± 4	3.9 ± 1.2
	T_{15}	49 ± 1	38 ± 7	2.9 ± 0.6

[a] % Cleavages represent the average of multiple experiments which are presented in appendix E. The percentage alkali-lability was calculated based upon the cleavage observed at the radical precursor and the 5'- and 3'-adjacent nucleotides. [b] Photolysates were treated with 0.1 M NaOH (37 °C, 20 min,). [c] Photolysates were treated with 1.0 M piperidine (90 °C, 20 min). [d] Enhancement in total alkali-lability upon piperidine treatment (relative to NaOH).

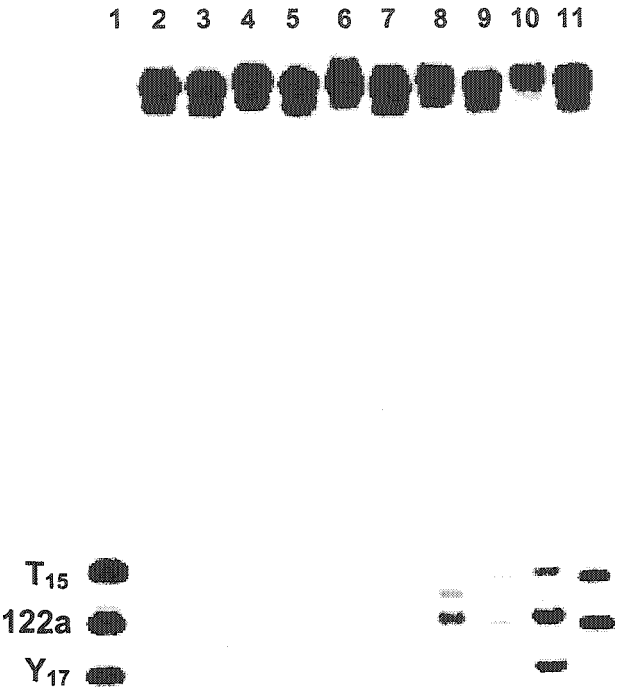

Figure 112. Phosphorimage of the aerobic photolysis of 3'-^{32}P-**159** and **203**. The appropriate lanes were treated with 1.0 M piperidine (90 °C, 20 min) or 0.1 M NaOH (37 °C, 20 min). Lane 1, oligonucleotide markers; lane 2, non-photolyzed **159** treated with NaOH; lane 3, non-photolyzed **203** treated with NaOH; lane 4, non-photolyzed E7 treated with piperidine; lane 5, non-photolyzed **203** treated with piperidine; lane 6, photolysate of **159**, no further treatment, lane 7, photolysate of **203**, no further treatment; lane 8, photolysate of **159**, treated with NaOH; lane 9, photolysate of **203** treated with NaOH; lane 10, photolysate of **159**, treated with piperidine; lane 11, photolysate of **203**, treated with piperidine.

5'-d(GAG CTA GCT CGA CCX$_{15}$ **122a**Y$_{17}$A GGA CCT GCA GCT)
3'-d(CTC GAT CGA GCT GGA A A T CCT GGA CGT CGA)
159, X = Y = thymidine
203 X = thymidine, Y= dU

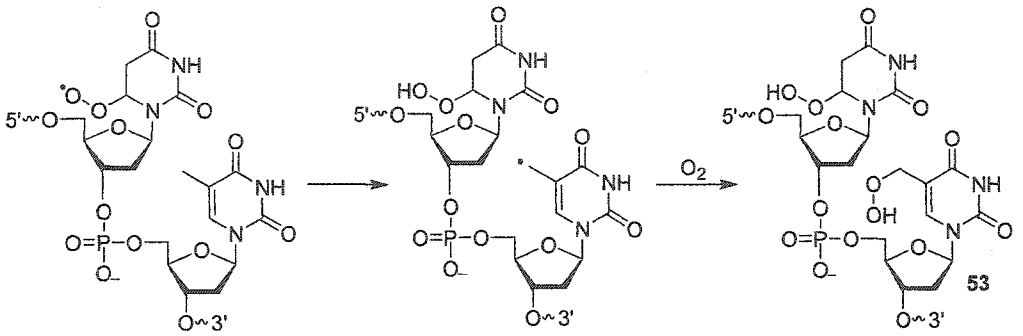

Figure 113. Formation of 5-hydroperoxylmethyl-2'-deoxyuridine (**53**).

3.2.3.2 The Structural Basis for the Reactivity of 5,6-Dihydro-2'-deoxyuridin-6-yl.

PAGE experiments using dU and dHT containing duplexes provided a great deal of information with regard to the mechanism by which the C6 peroxyl radical leads to alkali-labile lesion formation in duplex **159**. Alkali-labile lesion formation at T_{15} results primarily from addition to the nucleobase as well as C1' hydrogen atom abstraction. The C1' hydrogen atom abstraction pathway leads to formation of a NaOH-labile product, the proposed identity of which is 2-deoxyribonolactone. The nucleobase addition pathway gives rise to an unidentified piperidine-labile product. Studies using dU-containing oligonucleotides indicate that damage at T_{17} results primarily from abstraction of a hydrogen atom from the thymine nucleobase which results in a piperidine-labile lesion.

The fact that replacement of T_{17} with dU in oligonucleotides **203** and **204** affects the type of lesion formed at dU/T_{15} has significant implications with regard to the mechanism by which the C6 peroxyl radical leads to alkali-labile lesion formation. This suggests that two diasteromeric peroxyl radicals are responsible for the alkali-labile lesions which are formed at T_{15} and T_{17} in DNA duplex **159** (Figure 114). One diastereomer reacts primarily with T_{15} via abstraction of the C1' hydrogen atom or

addition to the nucleobase. The other diastereomer reacts by abstraction of a hydrogen atom from the methyl group of T_{17} to form a piperidine-labile product at this position. Experiments using 3'-^{32}P duplex **204** demonstrate that when this reaction pathway is not possible, alkali-lesion formation at the 3'-adjacent nucleotide is reduced by a factor of five (Table 27). It is proposed that the diastereomeric peroxyl radical which ordinarily reacts with T_{17} can undergo rotation about the glycosidic bond into the syn conformation and react with T_{15} by C1' hydrogen atom abstraction.

To gain insight into the reactivity of the diastereomeric peroxyl radicals in DNA, models of these reactive intermediates in B-form DNA were constructed. The energy minimized structures of the 6*R* and 6*S* diastereomers were generated in a B-form DNA duplex. The duplex structure surrounding the peroxyl radical was frozen. Therefore, this approach neglects any perturbations by the peroxyl radical upon local DNA structure. Assuming the nucleobase is in the *anti* conformation in the DNA duplex, the 6*S* peroxyl radical is oriented toward the 3'-adjacent thymidine while the 6*R* diastereomer is oriented toward the 5'-adjacent thymidine (Figures 115, 116, Table 28). The oxygen radical in the *anti*-6*S* diastereomer is in close proximity to the C5 methyl group of the 3'-adjacent thymidine (1.9 Å) but distant from the C1' hydrogen atom at this position (5.5 Å, Table 28). This is consistent with kinetic isotope effect experiments and the lack of NaOH lability at this site which indicate that C1' hydrogen atom abstraction from the nucleotide 3'-adjacent to ketone **122a** does not occur.

The *anti*-6*R* diastereomer, which is oriented toward the 5'-adjacent thymidine, is much closer to the C1' hydrogen atom of this position (1.3 Å, Figure 115). This is consistent with deuterium isotope effect studies and NaOH lability which provide

evidence of C1' hydrogen atom abstraction. The fact that abstraction of a hydrogen atom from the methyl group of this nucleotide appears to be a minor pathway leading to alkali-labile lesion formation is consistent with the greater distance (5.3 Å) to this position relative to the 6*S* diastereomer (Table 28, Figure 115).

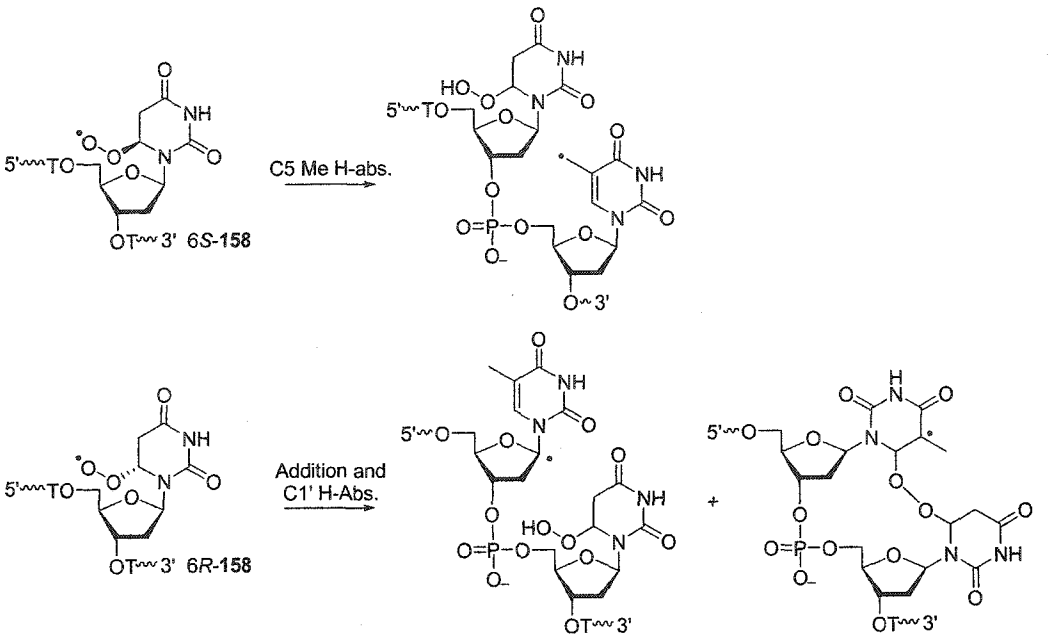

Figure 114. Reactivity of the 6*S* and 6*R* peroxyl radicals.

The greater efficiency with which 2-deoxyribonolactone is formed in **203** and **204** can also be rationalized with the aid of this model. When a thymidine nucleotide is present in the 3'-adjacent position to ketone **122a** (as in duplex **159**) the 6*S* peroxyl radical reacts via C5 methyl group hydrogen atom abstraction. This reaction cannot occur in **203** or **204**. However, DNA peroxyl radicals have long lifetimes (0.2-3.3 s).[138] Consequently, the peroxyl radical is able to rotate about the glycosidic bond into the *syn* conformation (Figure 116). In this conformation, the 6*S* peroxyl radical is in close proximity to the C1' hydrogen atom of the 5'-adjacent thymidine (1.5 Å). The C5 methyl

group of this thymidine as well as the C6 position of the nucleobase are distant (5.8 and 4.0 Å respectively).

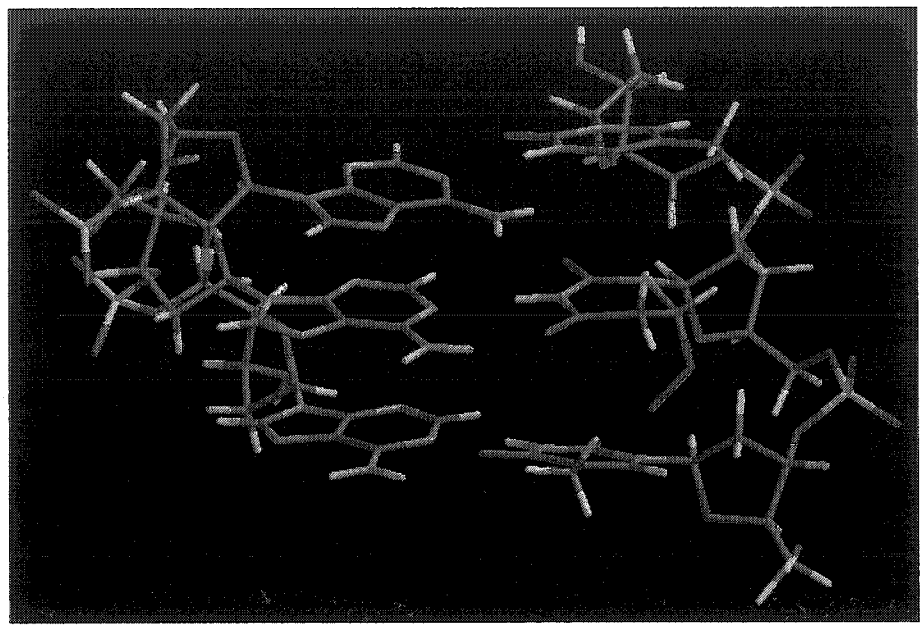

Figure 115. The *anti* 6*R* peroxyl radical (**158**) in a B-form 3mer duplex

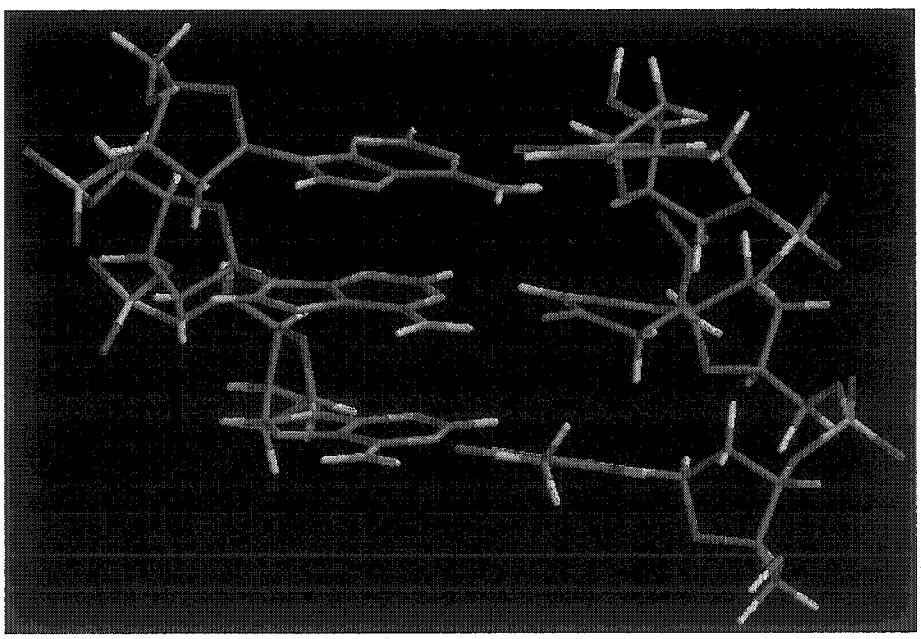

Figure 116. The *anti* 6*S* peroxyl radical (**158**) in a B-form 3mer duplex

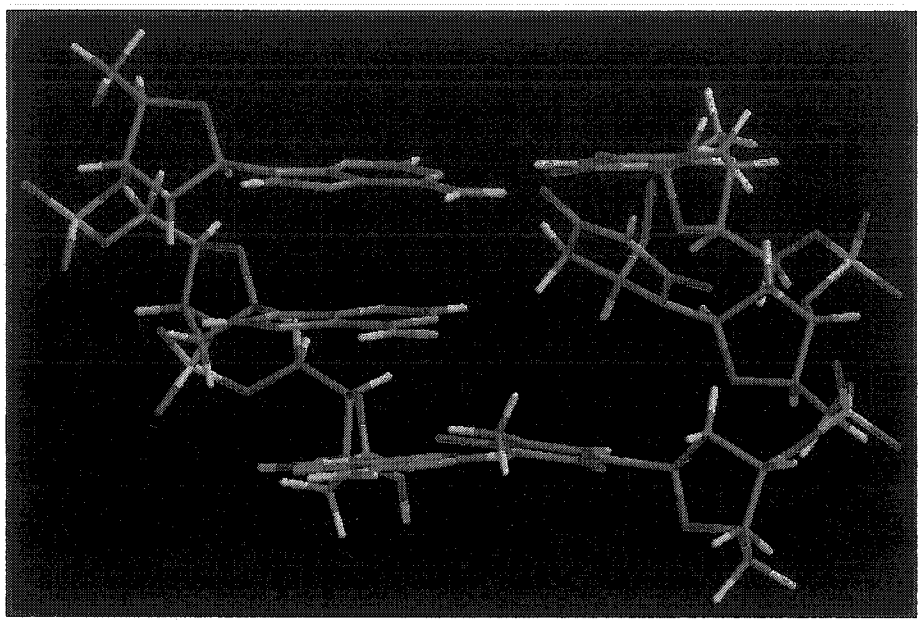

Figure 117. The *syn* 6*R* peroxyl radical (**158**) in a B-form 3mer duplex

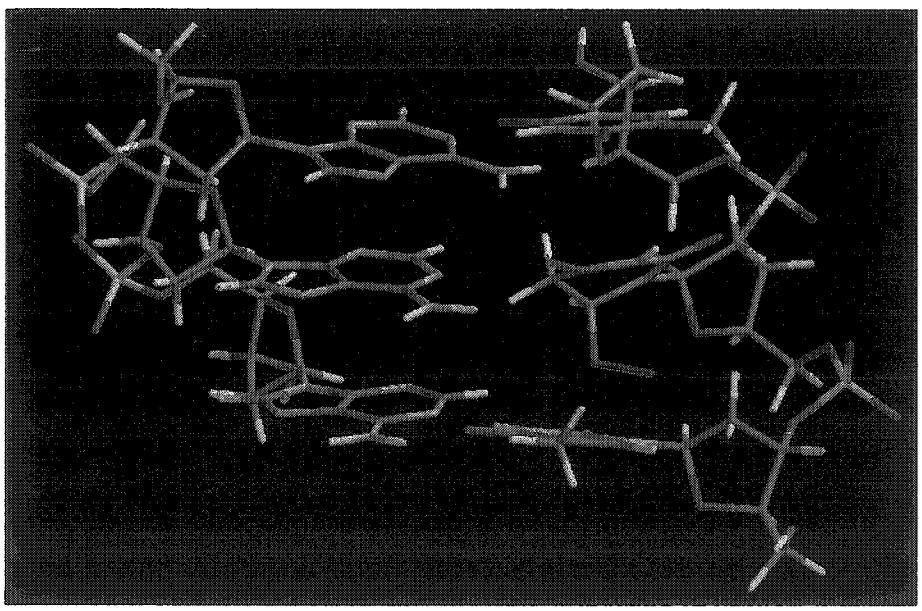

Figure 118. The *syn* 6*S* peroxyl radical (**158**) in a B-form 3mer duplex

Table 28. Calculated distances between the C6 peroxyl radical (**158**) oxygen and sites of reactivity on the adjacent thymidine nucleotides in a 3mer duplex.

Peroxyl Radical	Distance to positions of adjacent thymidines (Å)					
	5'-adjacent thymidine			3'-adjacent thymidine		
	H1'	C6	C5 Me-H	H1'	C6	C5 Me-H
6*R* anti	1.3	2.8	5.3	8.6	6.8	6.0
6*R* syn	7.1	8.4	9.3	3.1	1.0	3.3
6*S* anti	5.8	6.6	7.4	5.5	2.7	1.9
6*S* syn	1.5	3.2	5.5	8.2	6.3	6.0

The reason for the inability of the C6 peroxyl radical to react with the nucleotides of the opposite strand is also apparent from the above models. The closest C1' hydrogen atom of the complementary strand is > 9.0 Å from the peroxyl oxygen atom. The nearest dA bridgehead position is > 7.0 Å distant.

3.2.3.3 The Yield of Tandem Lesions Produced in 154 and 159.

In PAGE experiments using oligonucleotides **154** and **159** containing radical precursor **122a**, alkali-labile lesions are formed at the site of the radical, as well as at adjacent nucleotides (T_{15}, T_{17}). Using data obtained from experiments in which these sequences are 5'- and 3'-^{32}P end-labeled, the yields of isolated and tandem lesions at these sites may be estimated (Figure 119). In photolysis experiments using 5'-^{32}P-**159**, the fragments generated upon base treatment of tandem lesion **D** and isolated lesion **B** are indistinguishable. Quantitative analysis of gel experiments shows that these two products represent 40 ± 5 % of the total observed DNA damage (Table 12). Experiments utilizing 3'-^{32}P end-labeled **159** allow measurement of the yield of isolated lesion **B** (9.0 ± 4.1 %, Table 13) as the labeled fragment produced upon base treatment is distinguishable from

D. Therefore, the yield of tandem lesion **D** is 31 ± 6 %, the difference of these two quantities.

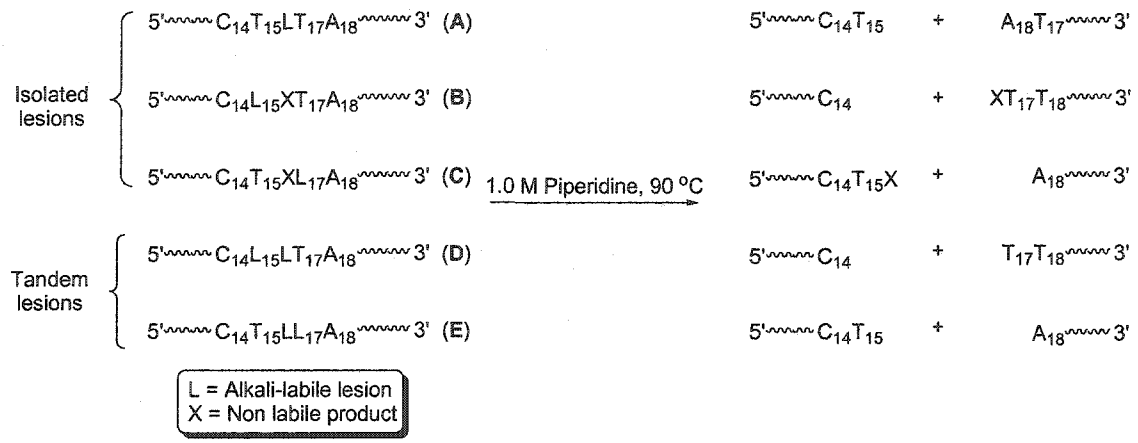

Figure 119. General types of lesions formed in duplex **154** and oligonucleotide **159**.

5'-d(GAG CTA GCT CGA CCT$_{15}$ **X**T$_{17}$ A GGA CCT GCA GCT)
154, X = 122a

5'-d(GAG CTA GCT CGA CCT$_{15}$ **X**T$_{17}$ A GGA CCT GCA GCT)
3'-d(CTC GAT CGA GCT GGA A A T CCT GGA CGT CGA)
159, X = 122a

Table 29. Distribution of tandem and isolated lesions in **154** and **159**.[a]

DNA	Percentage of total DNA damage				
	A	**B**	**C**	**D**	**E**
154	10 ± 4	16 ± 2	6.0 ± 1.2	41 ± 2.8	27 ± 2.3
159	20 ± 7	9.0 ± 4.1	8.0 ± 1.4	31 ± 6	32 ± 7

[a] The amount of each class of lesion as classified in figure 119. Values were calculated based upon data in Tables 10-13.

Similarly, photolysis experiments using 3'-^{32}P-**159** do not enable differentiation between tandem lesion **E** and isolated lesion **C**. Experiments using 3'-^{32}P-**159** show that

the sum of these products represents 40 ± 7 % of the observed alkali-labile DNA damage (Table 13). The yield of isolated lesion **C**, as determined from experiments utilizing 5'-^{32}P-**159**, is 8.0 ± 1.4 % (Table 12). Therefore, tandem lesion **E** represents approximately 32 ± 7 % of the total DNA damage. Hence, the overall percentage of DNA damage which is due to tandem lesions formed is 63 ± 9 %.

The amount of isolated lesion **C** at the site of the radical precursor can also be estimated from quantitative analysis of PAGE experiments. In experiments using 5'-^{32}P-**159**, the amount of alkali-lability at the original site of the radical precursor (**122a**) is the sum of isolated isolated lesion **C** and tandem lesion **E**. A value of ~52 ± 2 % was obtained for this sum. Since the amount of tandem lesion **E** is ~32 ± 7 %, a value of 20 ± 7 % is obtained for **C**. The yield of **C** can also be estimated by measuring the amount of alkali-lability at the site of radical precursor **122a** in an experiment using 3'-^{32}P duplex **159**. In this case, the yield of alkali-labile lesions (52 ± 2 %) formed at the site of the radical precursor (**122a**) represents the sum of isolated lesion **C** and tandem lesion **D**. By subtracting the previously determined yield of **D** (~31 ± 6 %) a value of 20 ± 7 % is again obtained for the percentage of total DNA damage represented by isolated lesion **C**.

Although the ratios of alkali-labile lesions vary somewhat, the same classes of products are formed in single-strand oligonucleotide **154**, based upon PAGE experiments (Tables 10, 11). The yield of alkali-labile lesions can be calculated in the same way used for duplex **159**. Values of 41 ± 3 and 27 ± 2 % are obtained for the yields of tandem lesions **D** and **E** respectively. The yield of isolated alkali-labile lesion at the site of the ketone (**C**) is 9.0 ± 1.4 %. Isolated lesions at T_{15} (**B**) and T_{17} (**C**) are observed in 16 ± 2 and 6.0 ± 1.2 % respectively (Table 29).

Tandem alkali-labile lesions are the major product formed from the 5,6-dihydro-2'-deoxyuridin-6-yl radical in both single-stranded and duplex DNA. Although the overall yield of tandem lesions in single-strand and duplex DNA is approximately equal, the tandem lesion involving the site of the radical precursor and T_{15} (𝔻) is favored in single-stranded DNA.

Deuterium isotope effect studies as well as PAGE experiments in which T_{15} of duplex **159** was replaced with dHT indicate that two types of tandem lesions are formed between the initially formed radical and T_{15}. One involves formation of the highly base labile 2-deoxyribonolactone lesion at T_{15}. A less labile product results from peroxyl radical addition to this position. Assuming that treatment with NaOH gives rise to cleavage of the oxidized abasic site only, while piperidine treatment results in the cleavage of both types of tandem lesion, the relative amounts of these two DNA damage products may be estimated. The ratio of piperidine labile lesions to NaOH labile lesions in **159** is 3.3:1 (Table 12), indicating that of the total amount of tandem lesions formed between the peroxyl radical and T_{15}, ~ 30 % contain 2-deoxyribonolactone.

3.2.3.4 Mass Spectral Analysis of Photolysates.

In order to gain further insight into the reactivity of the 5,6-dihydro-2'-deoxyuridin-6-yl in DNA, photolysates of oligonucleotides were analyzed by mass spectrometry. Preliminary experiments were conducted in which **205** was photolyzed under anaerobic conditions in the presence of thiol (Figure 120). After photolysis, the crude reaction was analyzed by ESI-MS. Observation of 5,6-dihydro-2'-deoxyuridine-

containing DNA (**206**) as the sole product demonstrates that 5,6-dihydro-2'-deoxyuridin-6-yl is formed efficiently from the radical precursor in DNA.

Figure 120. Photolysis of **205** under anaerobic conditions.

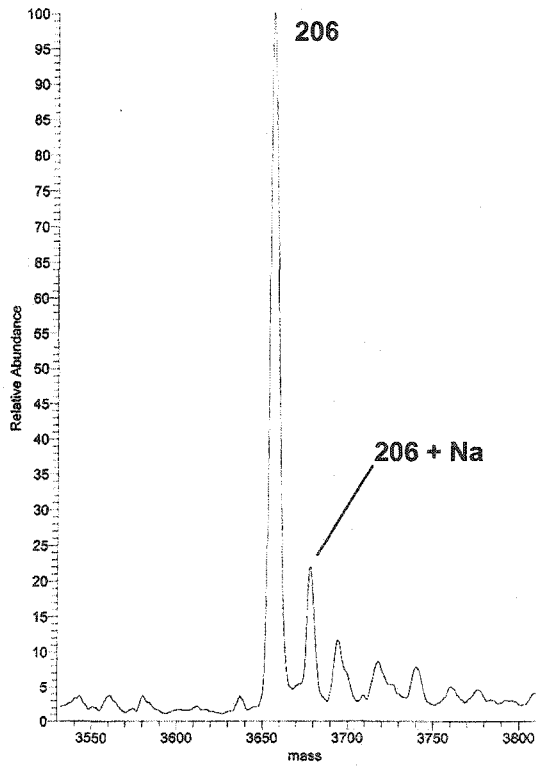

Figure 121. ESI-MS of the photolysate of **205**.

In the presence of O_2, a more complex distribution of damage products was anticipated. PAGE experiments demonstrate that tandem lesions are formed between the nucleobase radical (**123**) and adjacent thymidine nucleotides. These experiments provide evidence that tandem lesion formation in the 5'-direction occurs via C1' hydrogen atom abstraction and peroxyl radical addition to the nucleobase. In the 3'-direction, PAGE experiments provide evidence that tandem lesions are formed via abstraction of a C5 methyl hydrogen atom by the C6 peroxyl radical. These mechanisms are supported by deuterium isotope effect studies as well as experiments in which the adjacent thymidine nucleotides were replaced with 5,6-dihydrothymidine or 2'-deoxyuridine. Based upon the known reactivity of C1' nucleoside radicals, it was assumed that the product of the C1' hydrogen atom abstraction pathway was a tandem lesion containing 2-deoxyribonolactone.[43] A PAGE assay specific for this labile product supports this conclusion.[111]

Analysis of photolyses conducted under aerobic conditions in the absence of thiol did not show expected products of DNA damage amplification such as 2-deoxyribonolactone containing lesions. Spectra collected from these experiments typically exhibited extremely poor signal to noise, prohibiting identification of lesions. The presence of multiple products was thought to contribute to this difficulty. To overcome this problem, photolysates were purified by HPLC prior to analysis. Fractionation of products prior to analysis was intended to improve the quality of spectra. However, the additional purification step prior to analysis resulted in an overall loss of material. Consequently, the use of quantities of DNA which afforded sufficient analyte

for ESI-MS analysis was rendered impractical. Therefore, samples were analyzed by MALDI-TOF MS, a technique which has lower detection limits.

It was anticipated that tandem lesions containing the 2-deoxyribonolactone might be difficult to observe owing to the instability of this lesion. Furthermore, PAGE experiments using duplex **159** suggest that 2-deoxyribonolactone is not the sole product formed at the nucleotide adjacent to the 5,6-dihydro-2'-deoxyuridin-6-yl in the 5'-direction. Other lesions, which are proposed to result from addition to the nucleobase, are also produced. Substitution of dHT for T in **187** and **188** results in a much higher yield of the NaOH labile product, which is presumably 2-deoxyribonolactone (Table 24). Therefore, this oligonucleotide was used in initial MALDI experiments aimed at detecting the oxidized abasic site. To aid analysis of photolysates containing this unstable product, **187** was photolyzed then subsequently treated with DMEDA (0.1 M, 37 °C). These conditions have been shown to convert the 2'-deoxyribonolactone to a stable cyclic adduct which has been observed by MALDI-TOF MS (Figure 122).[111] MALDI analysis of photolysates revealed the expected cyclic adduct (**208**) as well as 5'- (**209**) and 3'-phosphate terminated fragments (**207**, Figure 123). The 5'-terminal dU nucleotide of 5'-phosphate fragment **209** is proposed to result from decomposition of an initially formed C6 hydroperoxide.

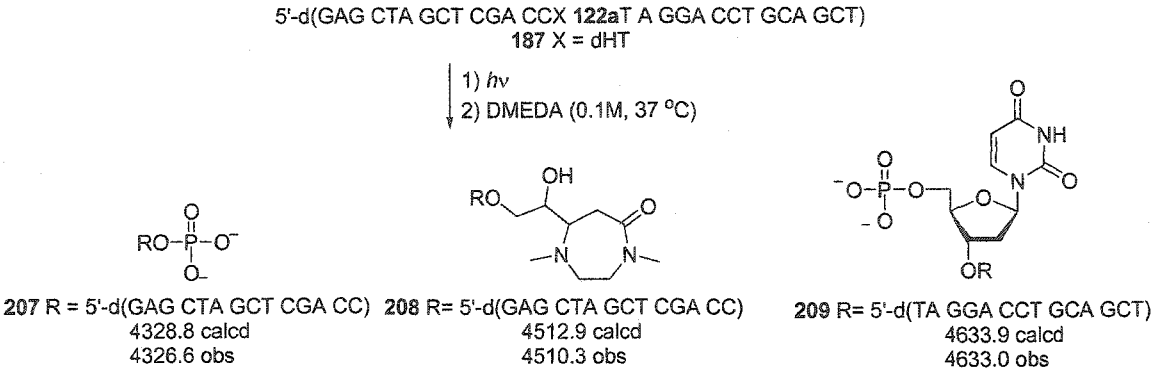

Figure 122. Formation of the cyclic adduct of the 2-deoxyribonolactone.

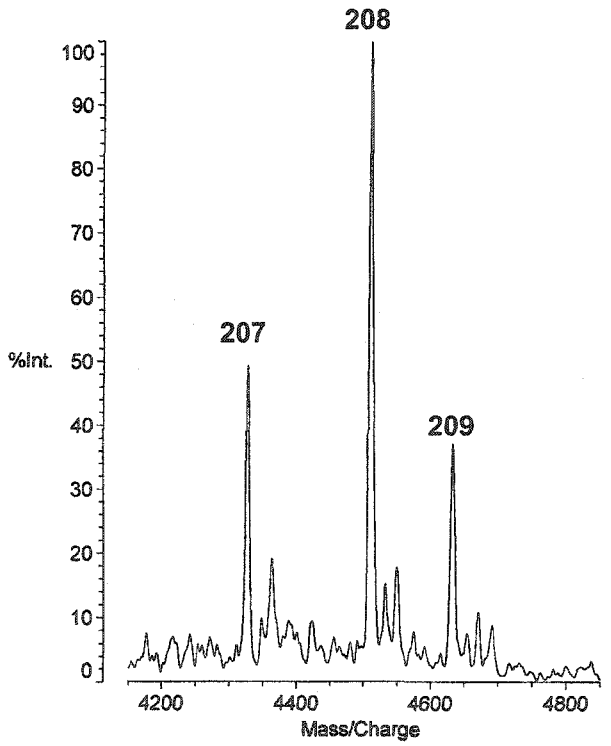

Figure 123. MALDI-TOF/MS 2-deoxyribonolactone cleavage products.

To more fully characterize the DNA damage products resulting from the 5,6-dihydro-2'-deoxyuridin-6-yl radical, additional experiments were conducted using 12mer oligonucleotide **210** (Figure 124). Although the yield of 2-deoxyribonolactone containing products was expected to be lower in this sequence, it was anticipated that

products resulting from the nucleobase addition and C5 methyl hydrogen atom abstraction pathways would be observed. Prior to mass spectral analysis of photolysates, experiments were conducted in which the yield of piperidine and NaOH labile lesions were measured in 5'- and 3'-^{32}P-**210** (see appendix E). As expected, piperidine and NaOH labile lesions were observed at T_6, while only piperidine lability is observed at T_8. Thus, the distribution and type of damage is similar to that observed in oligonucleotides such as duplex **159** which were used for PAGE characterization of the 5,6-dihydro-2'-deoxyuridin-6-yl.

5'-d(TAT CCT_6 **X**T_8A CTA)
210 X = 122a

Photolysis of **210** under aerobic conditions followed by HPLC purification and MALDI-TOF MS analysis yielded ample information regarding the products formed in DNA from the pyrimidine radical (**122**). Ions corresponding to both isolated and tandem lesions are observed in the MALDI-TOF spectra (Figure 124, Table 30, appendix E)

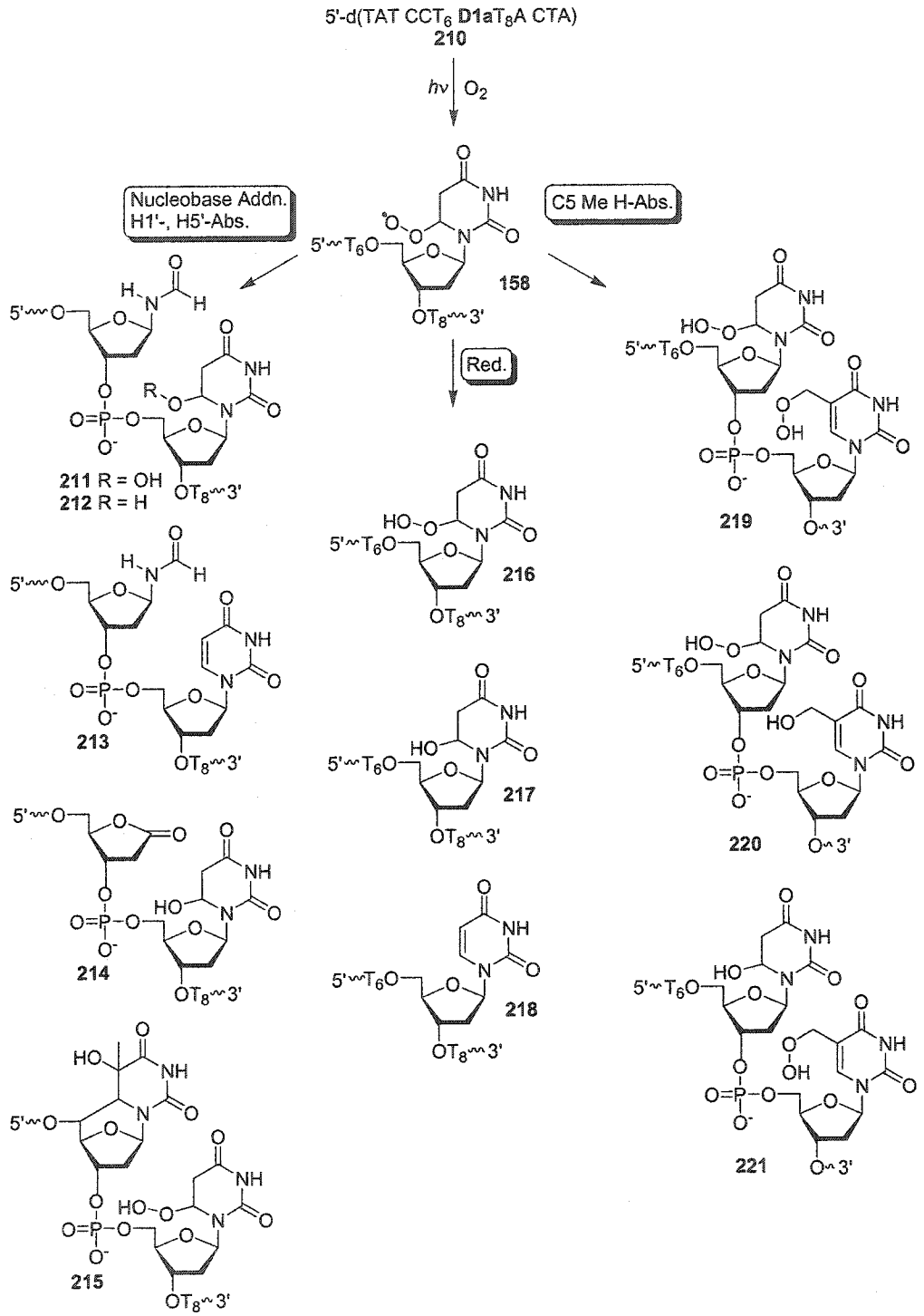

Figure 124. Structural assignments for products from the photolysis of **210** observed by MALDI-TOF/MS.

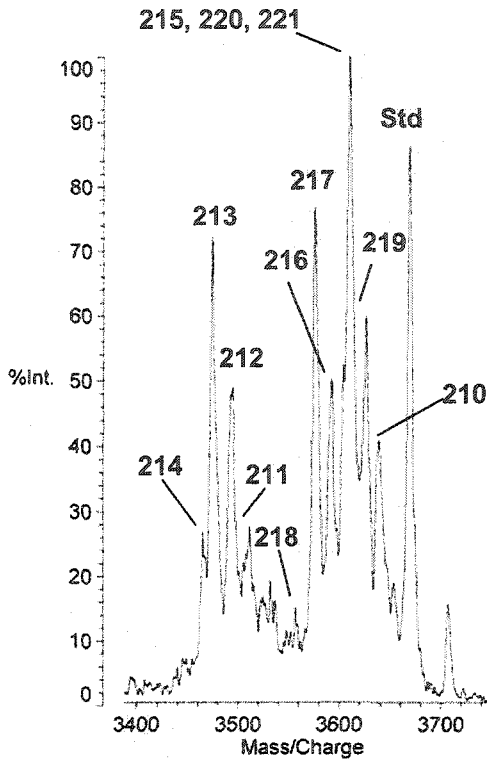

Figure 125. MALDI-TOF/MS of the photolysate of **210**. "Std" denotes an oligonucleotide of known molecular weight added for calibration purposes.

Table 30. Calculated and observed masses of DNA damage products in **210**.

Compound	Calculated Mass	Observed Mass	Obs-Calc. (% Var.)[a]
211	3509.4	3511.4	1.0 (0.028)
212	3493.4	3494.1	0.70 (0.020)
213	3475.4	3774.0	-1.4 (-0.040)
214	3464.3	3465.2	0.90 (0.026)
215, 220, 221	3606.4	3609.8	3.4 (0.094)
219	3622.4	3625.6	3.2 (0.088)
216	3590.4	3591.9	1.5 (0.041)
217	3574.4	3575.5	1.1 (0.031)
218	3556.4	3557.1	0.70 (0.019)
210	3642.5	3638.8	-3.7 (-0.10)
Std[b]	3669.4	3668.8	-0.60 (-0.016)

[a] Obs-Calc = observed mass – calculated mass. % var. = [(obs. – calc.)/(calc.)](100). [b] Std oligonucleotide sequence: 5'-d(AGT GCA TAA GCT)

A tandem lesion containing 2-deoxyribonolactone adjacent to 2'-deoxyuridine C6 hydrate (**214**) is observed. Three products which are ostensibly derived from the nucleobase addition pathway are **211-213**. One product corresponding to reaction of the

C6 peroxyl radical with T_8 is observed. As PAGE experiments indicate that the major pathway for reaction in the 3'-direction is abstraction of a hydrogen atom from the thymidine methyl group, the structure of the product which has incorporated two molecules of O_2 is proposed to be bis-hydroperoxide **219**. Isolated lesions **216** and **217**, the products of reduction of the initially formed peroxyl radical, are also observed.

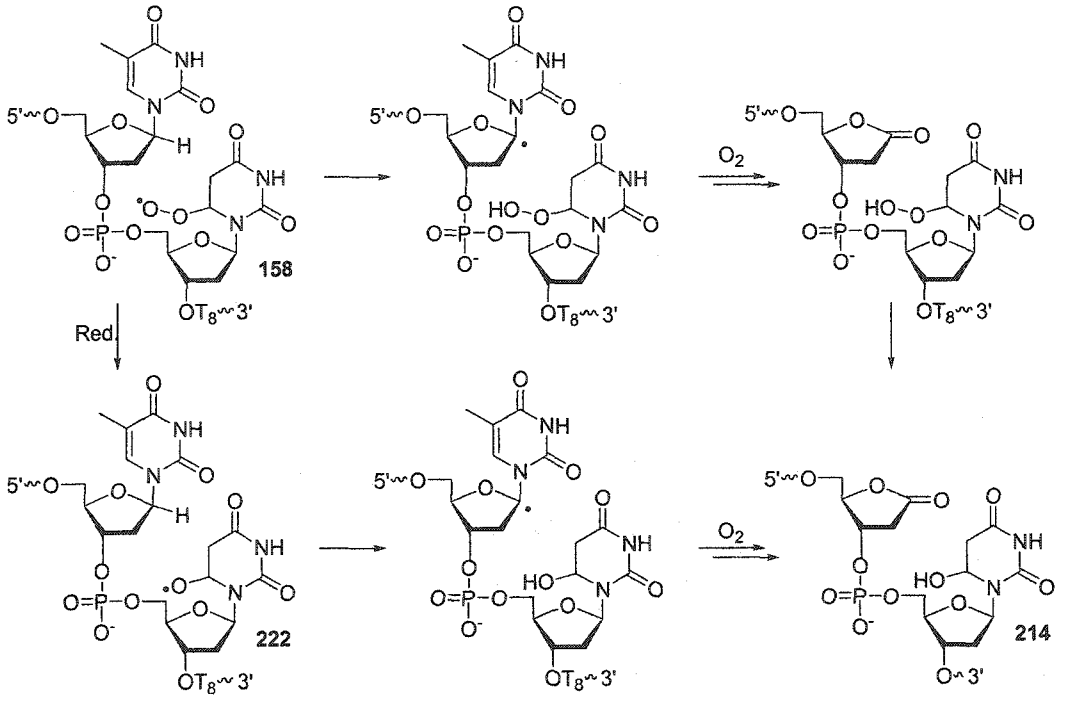

Figure 126. Mechanisms for the formation of 2-deoxyribonolactone-containing lesion **214**.

Three possible structures (**215**, **220**, **221**) were considered for the identity of the product corresponding to the addition of three oxygen atoms and one hydrogen atom to the initially formed 5,6-dihydro-2'-deoxyuridin-6-yl. The first (**215**) was the anticipated product of abstraction of H5' followed by intranucleotidyl cyclization. A related C5 hydroxylated cyclonucleoside is formed from the radiolysis of dC.[90] The other possible

structures (**220**, **221**) are products which could be derived from bis-hydroperoxide **219**. It is important to note that it is possible that each of the above lesions is formed.

The 2-deoxyribonolactone containing tandem lesion (**214**) is proposed to result from hydrogen atom abstraction by the C6 peroxyl radical (**158**) from the C1' position of T_6 (Figure 126). In the presence of O_2, the C1' radical undergoes oxidation to generate the abasic site.[50, 63-66] The C6 hydroperoxide which is formed by this reaction at the original site of the radical precursor (**122a**) is not observed in by MALDI-TOF MS. Instead, 2'-deoxyuridine C-6 hydrate is formed at the site of the radical precursor. This could plausibly occur via decomposition or reduction of the C6 hydroperoxide in solution. Fragmentation of the hydroperoxide upon laser desorption of the sample is also a possibility. Other hydroperoxide containing products (**216**, **219**) are observed in the MALDI-TOF experiment, suggesting that some of these species are at least partially stable to the analysis conditions. The possibility that an alkoxy radical derived from reduction of the peroxyl radical (or hydroperoxide) carries out the intranucleotidyl hydrogen atom abstraction cannot be discounted (Figure 126).

Formamide containing products (**211-213**) are proposed to result from addition of the C6 peroxyl radical (**158**) to the nucleobase of an adjacent thymidine nucleotide (Figure 127). A similar process involving addition of a nucleobase peroxyl radical to an adjacent 2'-deoxyguanosine has been reported.[23] Fragmentation of the resulting radical adduct was shown to afford a tandem lesion containing a formamide fragment of a pyrimidine. It is proposed that products **211-213** result from an analogous fragmentation of a radical adduct. While the mechanism of fragmentation is uncertain, it is likely that it involves formation of a nucleoside alkoxy radical intermediate. The 2-deoxyuridine

containing product (**213**) is probably derived from dehydration of **212**, either in solution or upon analysis.

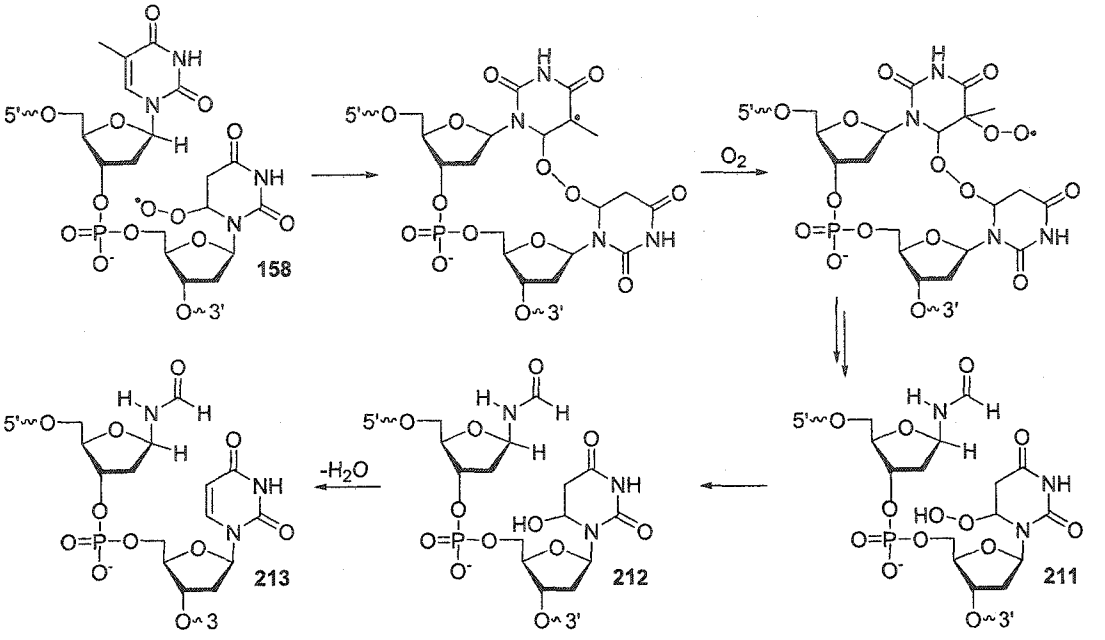

Figure 127. Mechanism for the formation of formamide containing lesions **211-213**.

A plausible structure for the product corresponding to the addition of three oxygen atoms and one hydrogen atom to the radical is cyclonucleotide containing lesion **215**. This product is proposed to result from abstraction of a C5' hydrogen atom from T_6 followed by an intranucleotidyl cyclization. Reaction of the adduct radical with O_2 produces a bis hydroperoxide. In the observed product, one hydroperoxide is reduced to the corresponding alcohol (Figure 128). Formation of a non alkali-labile lesion of this type is consistent with the inverse isotope effect observed upon deuteration of the C5' position.

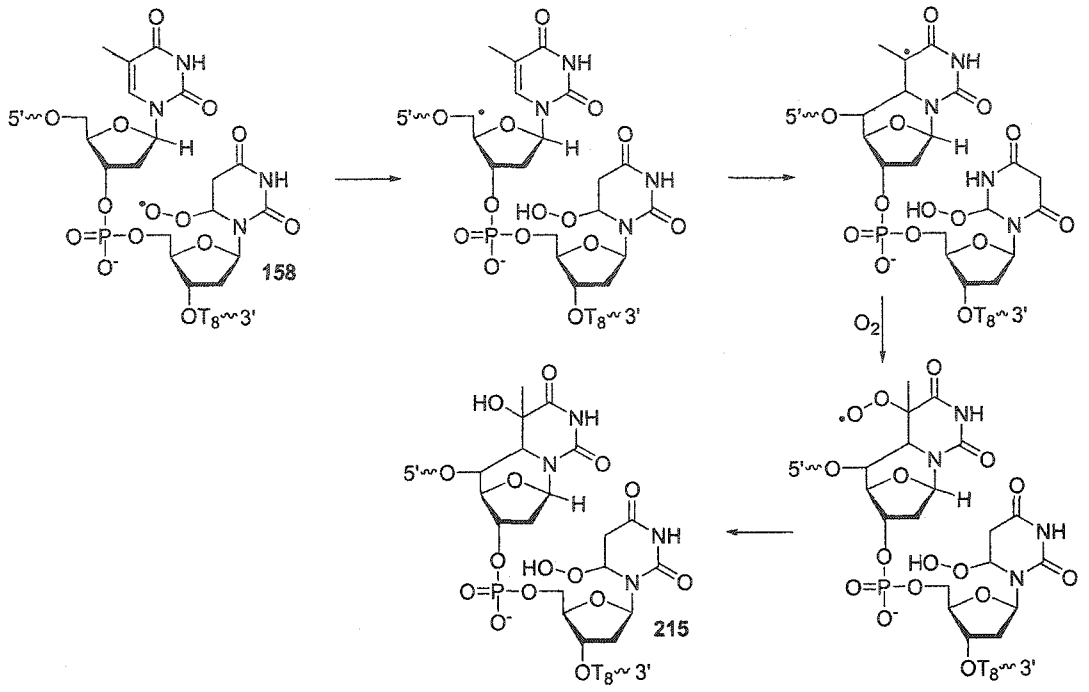

Figure 128. Formation of a cyclonucleotide containing lesion (**215**).

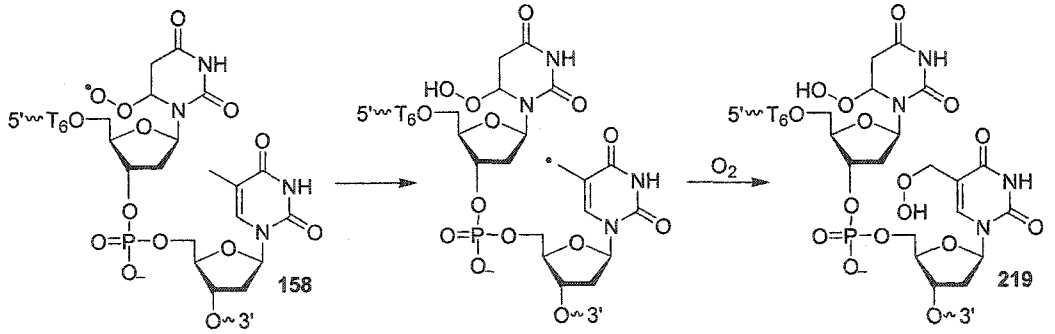

Figure 129. Proposed mechanism for the formation of bis-hydroperoxide **219**.

Bis hydroperoxide **219** is the product of hydrogen atom abstraction from the C5 methyl group of T_8 by the C6 peroxyl radical (**158**). Trapping of the resulting allylic

radical with oxygen generates a C5 methyl peroxyl radical. Reduction of this species affords tandem lesion **219** (Figure 129). Formation of this product is consistent with PAGE experiments which implicate the involvement of the thymidine methyl group in alkali-labile lesion formation.

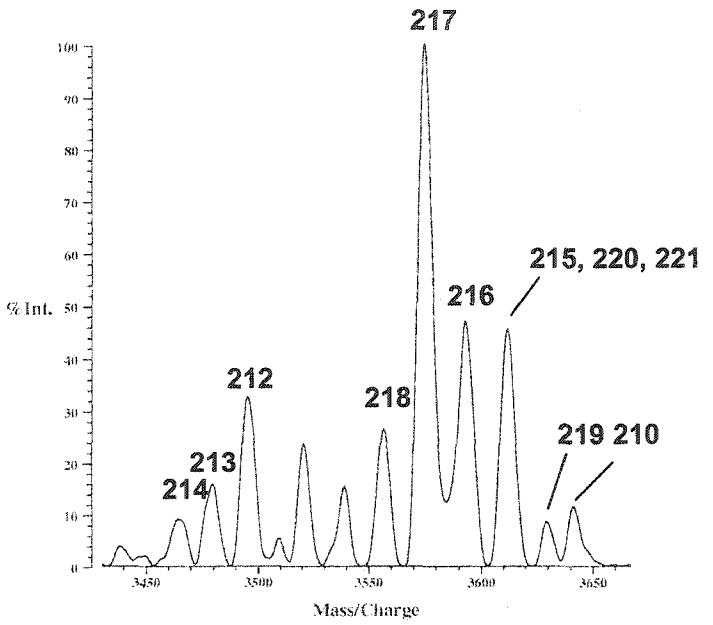

Figure 130. MALDI-TOF/MS of the photolysate of **210**. The photolysis was conducted in the presence of $^{18}O_2$.

5'-d(TAT CCT_6 **122a**T_8 CTA)
210

Table 31. Calculated and observed masses of DNA damage products generated from the photolysis of **210** in the presence of $^{18}O_2$.

Compound	Calculated Mass[a] (^{16}O)	Observed Mass	Obs. – Calc. (% Var.)[b]
212	3593.4	3594.9	1.5 (0.041)
213	3475.4	3479.9	4.5 (0.13)
214	3464.3	3464.0	-0.30 (-0.0086)
215, 220, 221	3606.4	3612.2	5.8 (0.16)
219	3622.4	3629.6	7.2 (0.20)
216	3590.4	3592.7	2.3 (0.064)
217	3574.4	3574.7	0.10 (0.0028)
218	3556.4	3556.4	0
210	3642.5	3641.0	-1.5 (0.041)

a Product molecular weights are calculated using ^{16}O rather than ^{18}O. [a] Obs-Calc = observed mass – calculated mass. % var. = [(obs. – calc.)/(calc.)](100).

Photolysis of **210** in the presence of $^{18}O_2$ resulted in the formation of a number of isotopically labeled compounds (Figure 130, Table 31). Bis hydroperoxide **219** is shifted by 7.2 mass units, which is consistent with the incorporation of two molecules of $^{18}O_2$ (Table 31). Formamide containing product **213** is observed at 4.5 mass units higher than calculated. This is puzzling as this product should contain a maximum of 1 ^{18}O atom and may reflect the imprecision of the MALDI experiment. The product corresponding to addition of three oxygen atoms and one hydrogen atom to the 5,6-dihydro-2'-deoxyuridin-6-yl was shifted by 5.8 mass units, indicating the incorporation of three oxygen atoms (Table 31). This is inconsistent with the formation of tandem lesion **221**, in which one of the oxygen atoms derived from $^{18}O_2$ is exchangeable. The oxygen atom incorporated at the C6 position at the site of the radical would be expected to exchange with H_2O.[123] Therefore, the product in which 3 ^{18}O atoms have been incorporated could be either **215** or **220**.

In order to more definitively establish that product **219** was derived from reaction of the C6 peroxyl radical with the methyl group T_8, photolysis experiments were conducted using dU containing oligonucleotide **223**. Replacement of T_8 with dU was anticipated to prevent this reaction and therefore the formation of a product corresponding to the addition of four oxygen atoms and one hydrogen atom to the 5,6-dihydro-2'-deoxyuridin-6-yl. MALDI-TOF analysis of the HPLC purified photolysate of **223** revealed no product corresponding to the incorporation of two molecules of O_2 (Figures 131, 132, Table 32). Products corresponding to reaction with T_6 via nucleobase addition and hydrogen atom abstraction were observed. Products analogous to the 2-deoxyribonolactone and formamide containing lesions from photolysis of **210** were also

observed (Figures 131, 132, Table 32). The peak assigned as the intranucleotidyl cyclization product (**227**) was also observed.

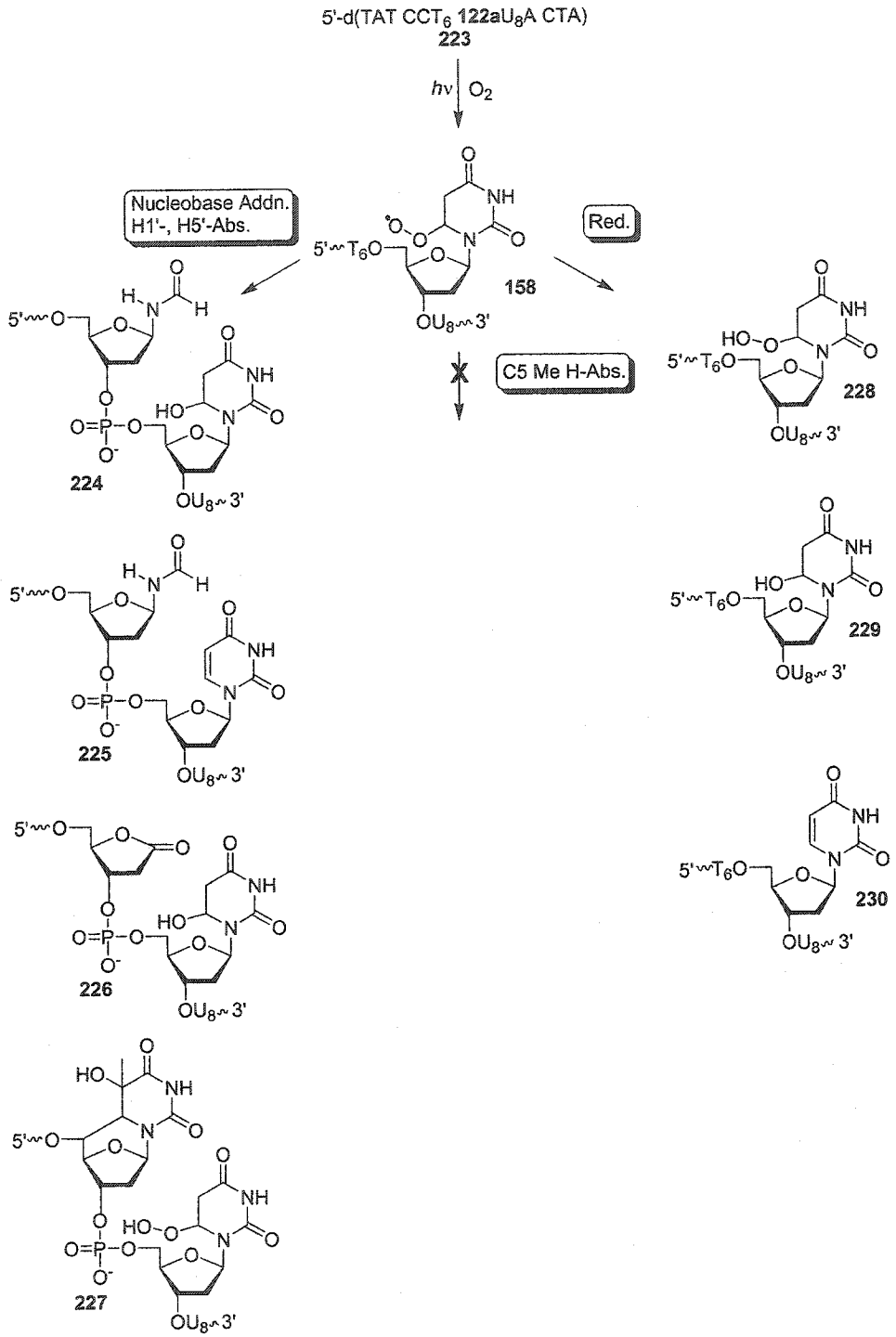

Figure 131. Structural assignments for products from the photolysis of **223** observed by MALDI-TOF/MS.

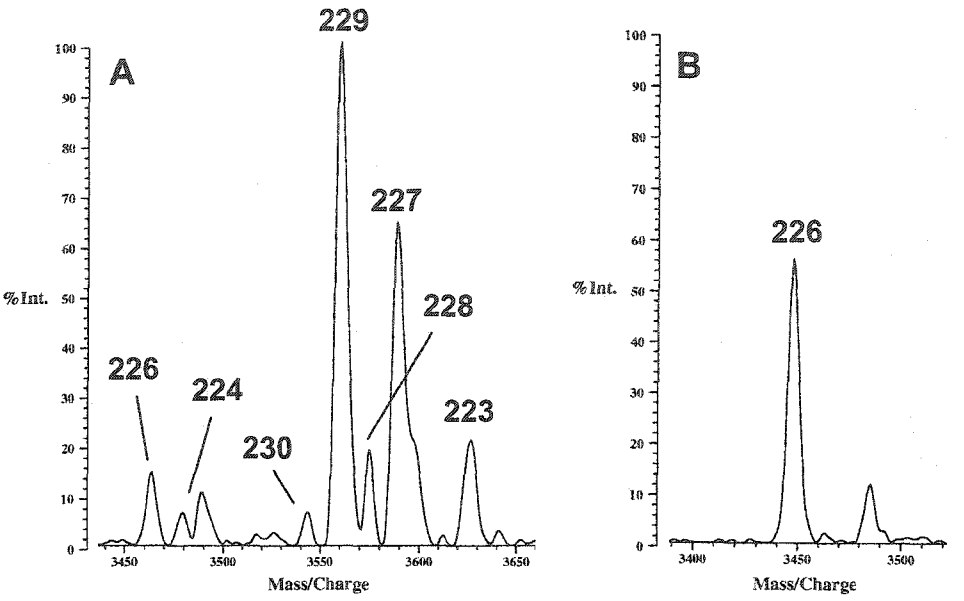

Figure 132. MALDI-TOF MS of the photolysate of **223**. "A" and "B" represent different fractionsof the HPLC purified photolysate.

Table 32. Calculated and observed masses in the photolysate of **223**.

Compound	Calculated Mass	Observed Mass	Obs. – Calc. (% Var)[a]
224	3479.4	3479.9	0.50 (0.014)
225	3461.4	3463.7	2.3 (0.066)
226	3450.2	3447.6	-2.6 (-0.075)-
227	3592.3	3588.8	-3.5 (-0.097)
228	3576.3	3574.7	-1.6 (-0.045)
229	3560.3	3560.5	0.20 (0.0056)
230	3542.3	3543.7	1.4 (0.039)
223	3628.5	3626.8	-1.7 (-0.046)

[a] Obs-Calc = observed mass – calculated mass. % var. = [(obs. – calc.)/(calc.)](100).

Photolysis of **223** in the presence of $^{18}O_2$ results in shift of the peak corresponding to **227** by 7.2 mass units (Table 33). This is consistent with the assigned cylic structure, as this lesion contains no readily exchangeable oxygen atoms (Figure 133, Table 33). Formamide containing compound **225** is shifted by almost 9 mass units. As this product would be expected to contain a maximum of one ^{18}O atom, this large increase is puzzling.

This large error could imply that the formamide structure assigned to this product is incorrect. Hydroperoxide **228** is observed 5.6 mass units greater than anticipated. This compound would be expected to contain two isotopically labeled oxygens and therefore display a molecular weight increase of four mass units.

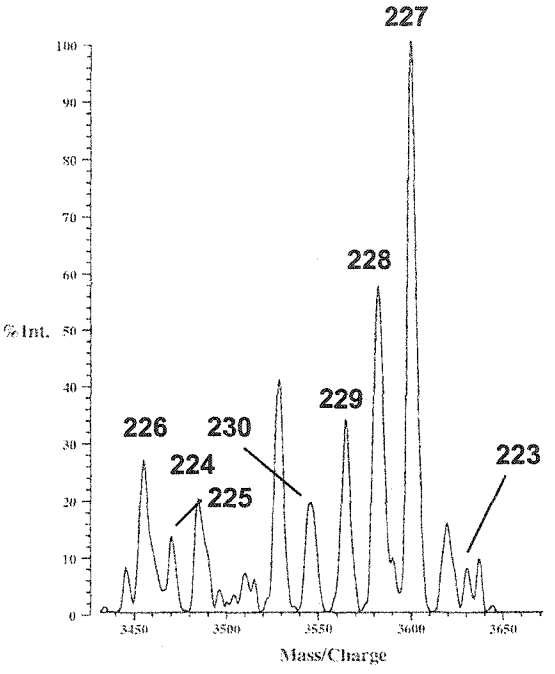

Figure 133. MALDI-TOF/MS of the photolysate of **223**. The photolysis was conducted in the presence of $^{18}O_2$.

Table 33. Calculated and observed masses of DNA damage products generated from the photolysis of **223** in the presence of $^{18}O_2$.

Compound	Calculated Mass (^{16}O)[a]	Observed Mass	Obs. – Calc. (% Var.)[b]
223	3628.5	3630.2	1.7 (0.046)
224	3479.4	3484.2	4.8 (0.14)
225	3461.4	3470.3	8.9 (0.25)
226	3450.2	3454.7	4.5 (0.13)
227	3592.3	3599.5	7.2 (0.20)
228	3576.3	3581.9	5.6 (0.16)
229	3560.3	3564.4	4.1 (0.11)
230	3542.3	3545.3	3.0 (0.084)

a Product molecular weights are calculated using ^{16}O rather than ^{18}O. [a] Obs-Calc = observed mass – calculated mass. % var. = [(obs. – calc.)/(calc.)](100).

To provide additional evidence for the formation of a lesion resulting from intranucleotidyl cyclization of a C5' radical, 12mer **231** was designed. In this sequence, T_6 is replaced with dHT (Figure 135). This change in the nucleobase was expected to inhibit the formation of cyclized product **215** as well as formamide containing products (**211-213**, Figure 124). Despite this change, a product corresponding to addition of three oxygen atoms and one hydrogen atom to the 5,6-dihydro-2'-deoxyuridin-6-yl was observed (Figure 136, Table 34). This is consistent with the formation of **235** and/or **236** (Figure 135). 2-Deoxyribonolactone-containing tandem lesion **214** (Figure 124) was observed as well. Products with a mass consistent with formamide-containing lesions (**238-240**, Figure 135) were observed. This may be a consequence of the longer lifetime of the 6*R* peroxyl radical in this oligonucleotide. Although the C6 peroxyl radical can still react at dHT by C1' hydrogen atom abstraction, the nucleobase addition pathway is no longer possible. Since this is ordinarily the major pathway for alkali-labile lesion formation, it is reasonable to assume that the rate constant for this process is greater than that for hydrogen atom abstraction. Therefore, the 6R peroxyl radical may have a lifetime sufficient to react in the 3'-direction upon rotation of the nucleobase into the *syn* conformation (Figure 134). In this conformation, a B-form duplex model indicates that the peroxyl radical is ~ 1.0 Å from the C6 position of the 3'-adjacent thymidine.

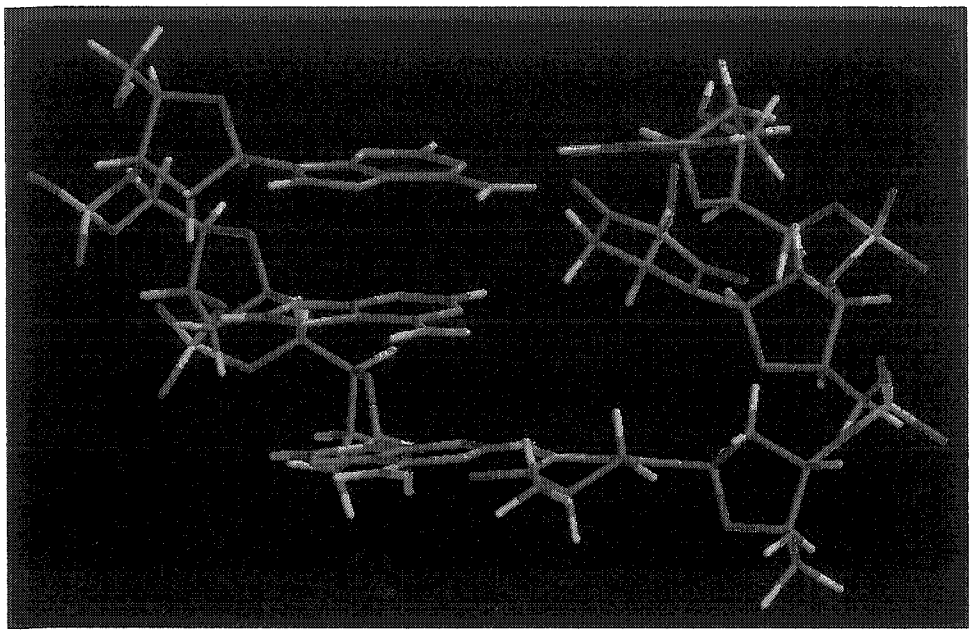

Figure 134. The *syn* 6*R* peroxyl radical in a B-form 3mer duplex

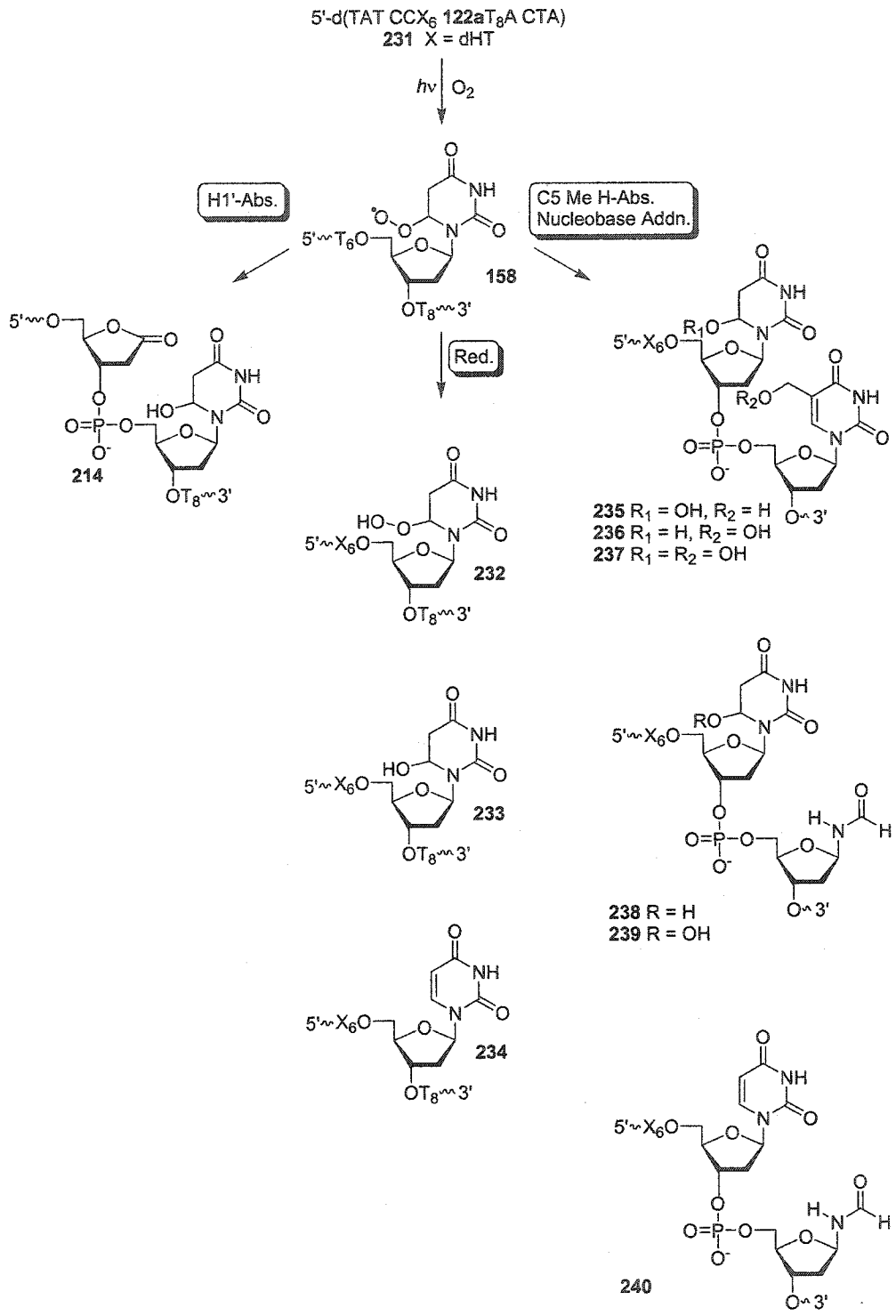

Figure 135. Structural assignments for products formed from the photolysis of **231** and observed MALDI TOF MS.

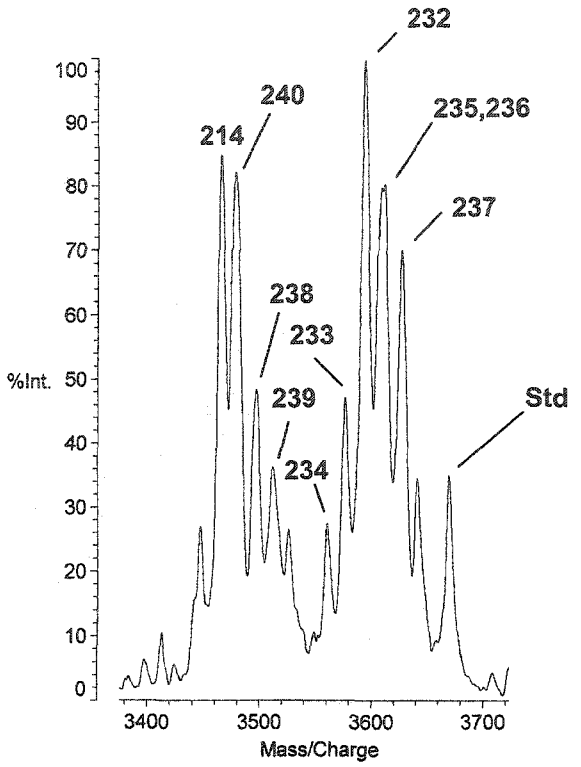

Figure 136. *MALDI-TOF MS of the photolysate of* **231**.

Table 34. Calculated and observed masses of DNA damage products in **231**.

Compound	Calculated Mass	Observed Mass	Obs. – Calc. (% Var.)[a]
214	3464.3	3464.8	0.50 (0.0149)
232	3592.4	3593.6	1.2 (0.033)
233	3576.4	3576.1	0.30 (0.0084)
234	3558.4	3560.3	1.9 (0.053)
235, 236	3608.4	3610.8	2.4 (0.066)
237	3624.4	3626.7	2.3 (0.063)
238	3495.4	3496.9	1.5 (0.043)
219	3511.4	3512.1	0.70 (0.019)
240	3477.4	3477.7	0.30 (0.086)
Std	3669.4	3668.8	0.60 (0.016)

[a] Obs-Calc = observed mass – calculated mass. % var. = [(obs. – calc.)/(calc.)](100).

3.2.3.5 Generation of 5,6-Dihydro-2'-deoxyuridin-6-yl Adjacent to 2'-Deoxyguanosine.

In order to evaluate the reactivity of the pyrimidine radical (**123**) in a different sequence context, photolysis experiments were conducted using duplexes **241** and **242**, in which the radical precursor (**122**) is positioned between two dG nucleotides. One of the major pathways of reactivity in duplex **159**, C1' hydrogen atom abstraction should be unaffected by the change in sequence. Peroxyl radical addition to an adjacent nucleobase is still possible, and if addition to the C8 position occurs, this process would be expected to result in the formation of 8-oxo-2'-deoxyguanosine.[23] Hydrogen atom abstraction from the base is also possible. The N2 and exocyclic amino hydrogens could serve as donors to the C6 peroxyl radical.

5'-d(GAG CTA GCT CGA CCG$_{15}$ **X**G$_{17}$A GGA CCT GCA GCT)
3'-d(CTC GAT CGA GCT GGC AC T CCT GGA CGT CGA)
241 X = 122a
242 X = 122b

Photolysis of radiolabeled duplex **241**, followed by treatment with NaOH or piperidine to reveal alkali-labile lesions gave rise to cleavage primarily at **122a**, dG$_{15}$, and dG$_{17}$. Photolysis of **122a** in these sequences typically resulted in less than half of the overall yield (~ 15%) of alkali-labile lesions observed in sequences in which the radical was flanked by thymidines (**154**, **159**) and may reflect quenching of the excited state radical precursor by the neighboring 2'-deoxyguanosine nucleotides.[143]

Table 35. NaOH and piperidine lability in duplex **241**.

^{32}P label	Site	Percentage of total lesions (NaOH)[a]	Percentage of total lesions (Piperidine)[b]	Piperidine induced lesions/ NaOH induced lesions[c]
5'-end	dG_{15}	81 ± 14	29 ± 16	3.1 ± 0.4
	122a	18 ± 3	40 ± 10	10 ± 1.5
	dG_{17}	-	27 ± 2	-
3'-end	dG_{15}	28 ± 9	9.0 ± 0.2	3.9 ± 1.2
	122a	40 ± 7	29 ± 5	9.6 ± 1.3
	dG_{17}	32 ± 4	62 ± 10	25 ± 2

[a] Calculated based upon total alkali-labile lesions. Photolyses were aerobic. Photolysates were treated with 1.0 M piperidine (90 °C, 20 min).. [b] Photolysates were treated with 0.1 M NaOH (37 °C, 20 min). [c] Enhancement in total alkali-lability upon piperidine treatment (relative to NaOH).

Experiments using 5'-^{32}P-**241** show piperidine-labile lesions at the site of the radical (**122a**) as well as at dG_{15} (Table 35). NaOH-lability is observed predominantly at dG_{15}. The significant enhancement (~ 3.1) at this position upon treatment with piperidine indicates the presence of two types of lesions. This ratio of piperidine to NaOH-lability at T_{15} is comparable to that observed in 5'-^{32}P-**159** (Table 12). The NaOH labile product is proposed to be 2'-deoxyribonolactone while the piperidine labile product is proposed to consist of an oxidatively modified 2'-deoxyguanosine. As C1' hydrogen atom abstraction occurs from a 5'-adjacent thymidine in **159**, it is reasonable to conclude that this pathway occurs in **241** as well. Treatment of photolysates with the set of fingerprint reactions used to identify 2-deoxyribonolactone in **188** was inconclusive, due to the low yield of NaOH-labile lesions in **241**.

To probe for hydrogen atom abstraction from the nucleobase, deuterium isotope effect studies were carried out. As the hydrogens of interest were in this case exchangeable, synthesis of isotopically labeled oligonucleotides was not required. By

conducting photolyses in D_2O, exchangeable hydrogens such as the exocyclic amino protons of dG were replaced with deuterium. Comparison of the amount of alkali-lability when photolyses were conducted in D_2O relative to H_2O allows calculation of an isotope effect. Photolyses of 5'- and 3'-^{32}P duplex **241** reveals that there is no significant isotope effect on alkali-labile lesion formation at dG_{15} or dG_{17} (Table 36)

Table 36. The effect of D_2O upon the distribution of piperidine-labile lesions in **241**.

^{32}P label	Solvent[a]	Relative piperidine-lability[b]		
		dG_{15}	**122a**	dG_{17}
5'-end	H_2O	1.0	1.0	1.0
	D_2O	0.93 ± 0.1	1.0 ± 0.1	1.1 ± 0.2
3'-end	H_2O	1.0	1.0	1.0
	D_2O	1.2 ± 0.3	1.0 ± 0.3	1.0 ± 0.2

[a] Raw data is presented in appendix E. Photolyses in D_2O were buffered with 10 mM KD_2PO_4, pD 7.2. b. The alkali-lability observed in H_2O at each site was defined as 1.0. The relative alkali-labilities observed in D_2O are calculated based upon this.

Alkali-labile lesions were observed predominantly at the site of the radical and at dG_{17} in photolysates of 3'-^{32}P-**241**. NaOH treatment resulted in virtually no strand scission at dG_{17}, indicating that abasic site formation at this site is not a major pathway. Piperidine treatment gave strand scission primarily at dG_{17}. This is consistent with experiments using 3'-^{32}P-**159**, in which the radical precursor is flanked by T. The ratio of cleavage at dG_{17} to the radical precursor is significantly greater than the ratio of T_{17} to the radical precursor observed in duplex **159**.

One of the possible products generated from the reaction of the C6 peroxyl radical with an adjacent 2'-deoxyguanosine is 8-oxo-2'-deoxyguanosine (8-oxo-dG). It has been shown that this oxidation product of dG is not alkali-labile and therefore is difficult to detect by PAGE.[39] Use of the mild oxidant Na_2IrCl_6, however, has been recently reported to efficiently convert 8-oxo-dG to an alkali-labile product, the cleavage product

of which is observable in electrophoresis experiments.[150] Exposure of photolysates of 3'-^{32}P-**241** to Na_2IrCl_6 prior to piperidine treatment resulted in no enhancement in the amount of alkali-labile lesions at dG_{17} (Table 37). However, a significant increase in alkali-lability (~ 2.5) was observed at G_{15} in oxidized photolysates of 5'-^{32}P-**241**, indicating the formation of 8-oxo-dG at this position.

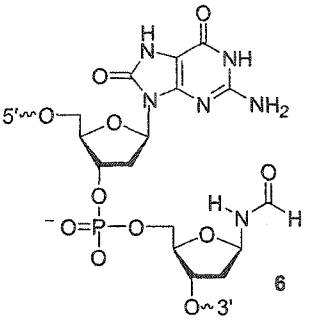

Table 37. The effect of Na_2IrCl_6 oxidation upon piperidine-lability in photolysates of **241** and **242**.

Duplex	Na_2IrCl_6 Enhancement[a]		
	dG_{15}	**122a**	dG_{17}
5'-^{32}P-**241**	3.1 ± 0.8	1.7 ± 0.1	0.6 ± 0.1
5'-^{32}P-**242**	2.4 ± 0.1	1.6 ± 0.1	0.9 ± 0.2
3'-^{32}P-**241**	1.6 ± 0.1	1.2 ± 0.1	0.90 ± 0.04
3'-^{32}P-**242**	1.6 ± 0.1	1.2 ± 0.1	0.94 ± 0.02

a. The Na_2IrCl_6 enhancement is calculated by dividing the amount of alkali-labile lesions in oxidized photolysates by that in untreated photolysates.

The 8-oxo- 7,8- dihydro -2'- deoxyguanosine – *N* - (2- deoxy - β - D -*erythro*-pentofuranosyl)formylamine (**6**, 8-oxo-dG-dβF) tandem lesion first characterized by Box and co-workers has been proposed to result from the addition of a C6 nucleotide peroxyl radical to an adjacent 2'-deoxyguanosine.[18,23] Based upon this finding, it seems likely that the 8-oxo-dG observed in duplex **241** results from an analogous reaction (Figure 137).

As in duplex **159**, in which the 5,6-dihydro-2'-deoxyuridin-6-yl is generated adjacent to thymidine, the C6 peroxyl radical reacts differently in the 5' and 3' direction. This suggests that the nature of the internucleotidyl reaction is again determined by the secondary structure of DNA. The formation of 8-oxo-dG at dG_{15} and not dG_{17} does raise the concern that this dG-oxidation is a result of sensitization by the ketone functionality of the radical precursor. Damage at dG resulting from sensitization by ketones has been reported.[143] Selective formation of 8-oxo-dG at dG_{15} could be rationalized in terms of the closer proximity of the pivaloyl substituent to this nucleotide.

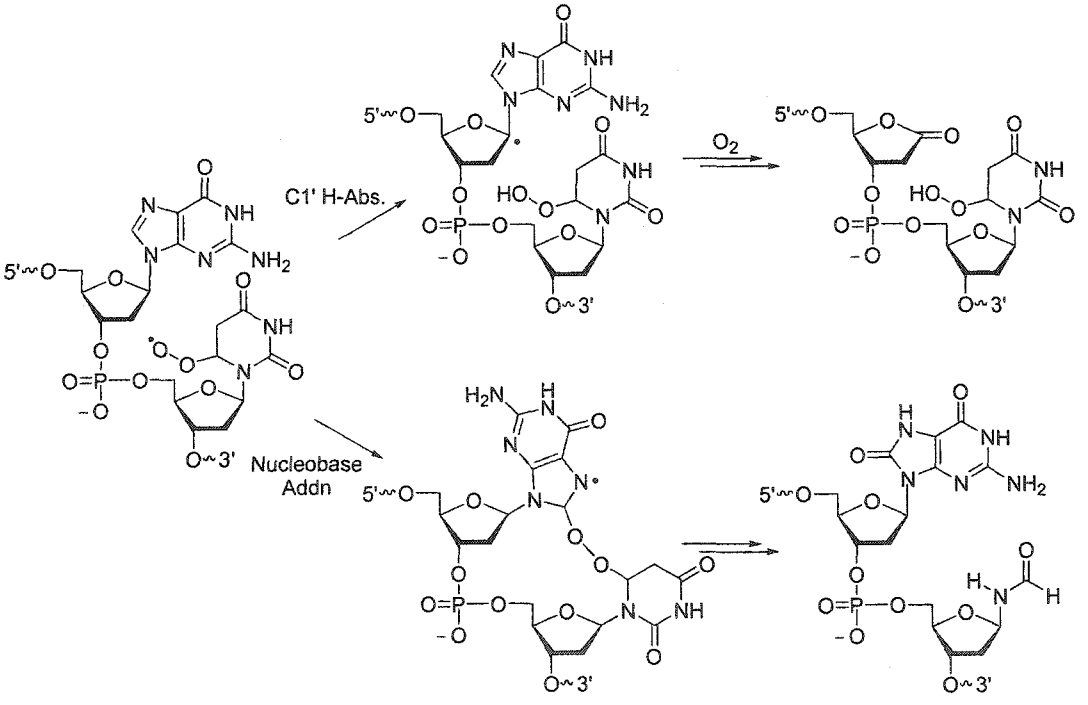

Figure 137. Competing C1' hydrogen abstraction and nucleobase addition by the C6 peroxyl radical.

In order to investigate the possible effects of the stereochemistry of the starting radical precursor, the extent and location of 8-oxo-dG formation in duplex **242** was

measured using the Ir (IV) oxidation method (Table 37).[150] Photolysis of 5'- and 3'-^{32}P end-labeled duplexes shows a distribution of alkali-labile lesions identical to that observed in duplex **241** (Table 38). Oxidation of photolysates with Na_2IrCl_6 shows an enhancement in piperidine-lability at G_{15}, but not G_{17}.

Table 38. Piperidine-labile lesions in duplex **242**.[a]

^{32}P-label	Site	% of Total Lesions
5'-end	dG_{15}	21 ± 4
	122b	46 ± 1
	dG_{17}	33 ± 7
3'-end	dG_{15}	8.0 ± 1
	122b	24 ± 1
	dG_{17}	68 ± 2

[a] Calculated based upon total alkali-labile lesions. Photolyses were aerobic. Photolysates were treated with 1.0 M piperidine (90 °C, 20 min) to cleave alkali-labile lesions.

This is consistent with the proposed mechanism for the formation of 8-oxo-dG in which C6 peroxyl radical addition to the C8 position of G_{15} is followed by a fragmentation process, but does not rule out direct photosensitization by the radical precursor. Due to the facile photooxidation of dG by ketones, it is difficult to rule out artifacts in this system.

4 Conclusions.

A photochemical precursor was developed for the independent generation of 5,6-dihydro-2'-deoxyuridin-6-yl (**123**, Figure 138). This reactive intermediate is a model for the 5,6-dihydrothymidin-6-yl radicals produced by the action of ionizing radiation upon DNA (**2**, **15**). These species have been implicated as key reactive intermediates in DNA damage processes.[1, 6-15] This is the first study in which a reactive intermediate of this class has been generated in the presence of oxygen and in biopolymers.

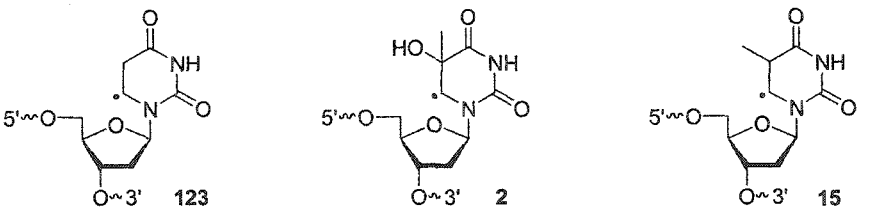

Figure 138. 5,6-Dihydropyrimidin-6-yl nucleobase radicals.

Prior to generation of 5,6-dihydro-2'-deoxyuridin-6-yl (**123**) in DNA, the reactivity of the benzoate ester of the monomeric nucleoside radical (**137**) was investigated (Figure 139).[120] An efficient precursor for the nucleobase radical (**137**), photolysis of **130** under anaerobic conditions in the presence of a hydrogen atom donor resulted in the formation of high yields of 5,6-dihydro-2'-deoxyuridine (**132**). The rate of hydrogen atom abstraction by **137** from different types of hydrogen atom donors was measured. Abstraction of a hydrogen atom from a thiol was found to occur with a rate constant typical for an alkyl radical [$(8.8 \pm 0.5) \times 10^6$ $M^{-1}s^{-1}$]. Modest rate constants (~8-30 $M^{-1}s^{-1}$, Figure 139) were observed for hydrogen abstraction from 2-deoxyribose sugar

models. This suggests that hydrogen atom abstraction from an adjacent nucleotide in DNA will be unable to compete with the very rapid addition of oxygen to 5,6-dihydro-2'-deoxyuridin-6-yl to form the corresponding peroxyl radical. In order for hydrogen atom abstraction to compete, an effective molarity of ~ 1 X 10^4 is required for DNA C-H bonds.

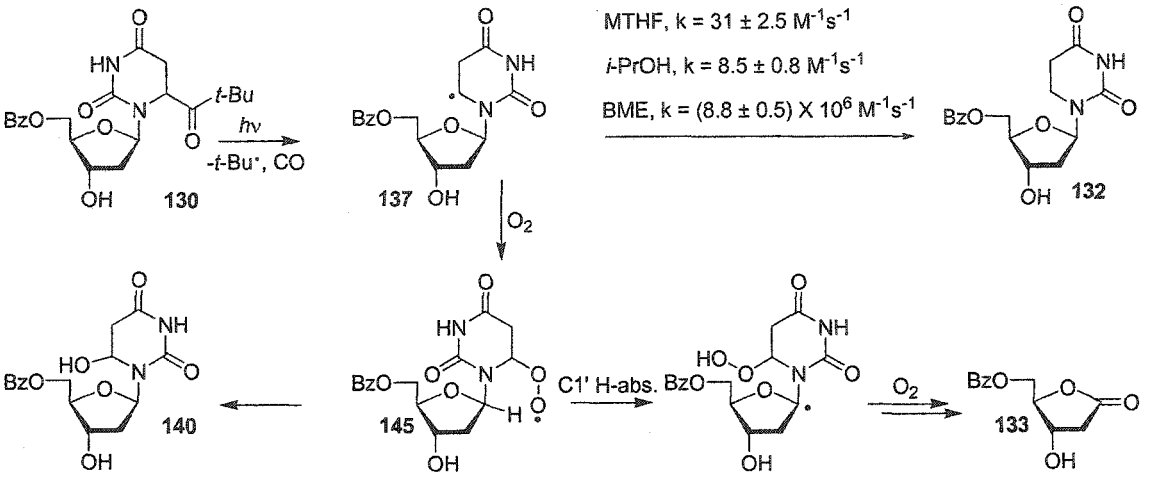

Figure 139. Reactivity of monomeric 5,6-dihydro-2'-deoxyuridin-6-yl (**137**).

In the presence of oxygen, the major product of monomeric 5,6-dihydro-2'-deoxyuridine-6-yl is 2'-deoxyuridine C6-hydrate (**140**). This metastable product results from peroxyl radical (**145**) formation and subsequent reduction. The analogous C6-hydrate would be formed from the thymidine hydrogen atom adduct (**15**) in the presence of oxygen. The dehydration rate constants of these metastable species were measured directly using the independently synthesized lesions (Figure 140, **140**, **142**). At physiological temperature (37 °C) and pH (7.4), 2'-deoxyuridine C6-hydrate (**140**) and thymidine C6-hydrate (**142**) have half-lives of ~ 46 and 24 h, respectively. The relative

longevity of these species is significant as pyrimidine C6-hydrates promote miscoding *in vitro*.[151]

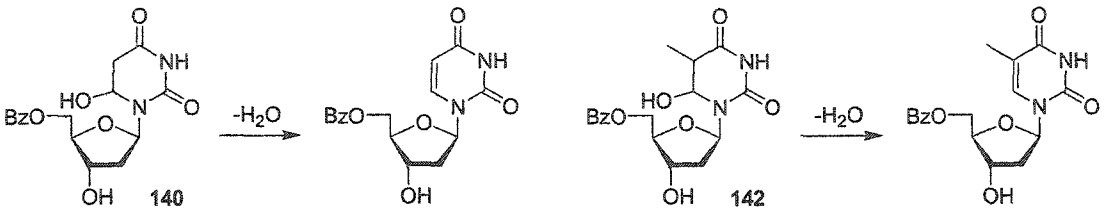

Figure 140. Dehydration of pyrimidine C6-hydrates (**140**, **142**).

Under aerobic conditions, 2-deoxyribonolactone (**133**) is formed in low yields. It is proposed that this results from an intramolecular C1' hydrogen atom abstraction by the C6 peroxyl radical (Figure 139) Although hydrogen atom abstraction from the C1' position of nucleotides in DNA is feasible thermodynamically, the extremely poor accessibility of H1' disfavors this pathway.[55] The observation of this novel intramolecular hydrogen atom abstraction pathway suggests that nucleobase radicals, the major reactive intermediates formed by ionizing radiation, can indirectly oxidize the C1' position. This implies that the yield of 2-deoxyribonolactone formed in DNA subjected to ionizing radiation may be higher than previously believed.

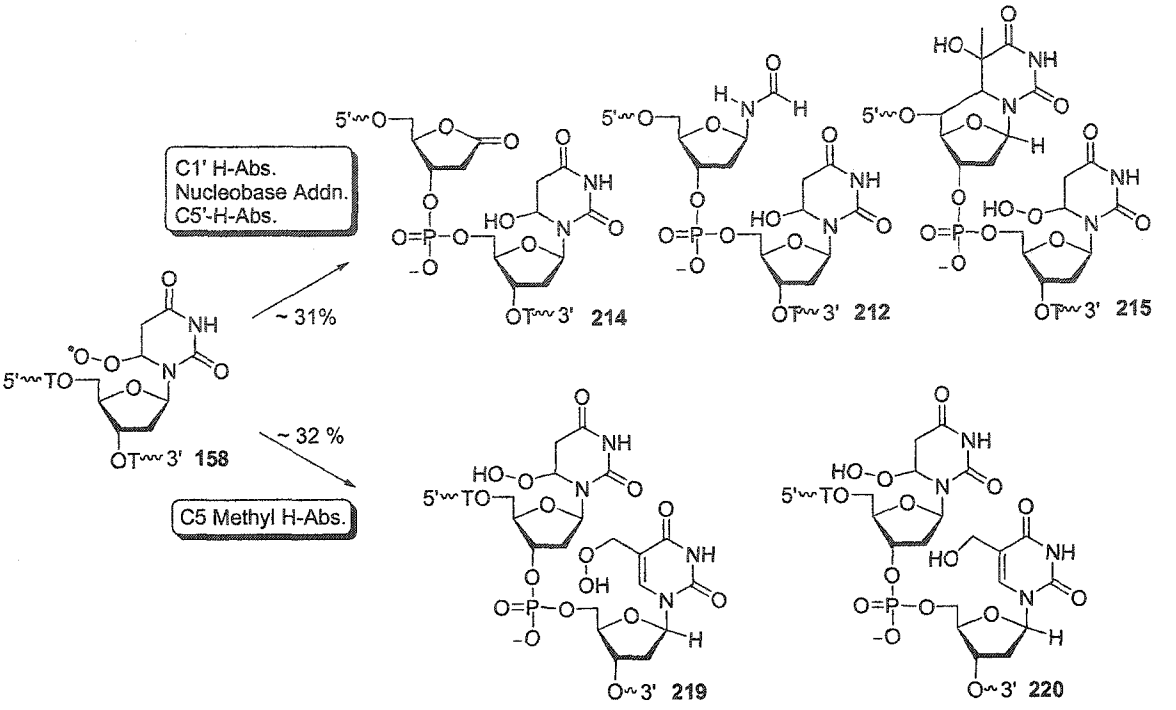

Figure 142. Tandem lesions produced by the 5,6-dihydro-2'-deoxyuridin-6-yl in DNA.

When produced in DNA, the peroxyl radical derived from 5,6-dihydro-2'-deoxyuridin-6-yl (**158**) was found to propagate damage to adjacent nucleotides, resulting in the formation of alkali-labile tandem lesions (**212, 214, 215, 219, 220**, Figure 142). Damage at adjacent nucleotides is the result of multiple pathways that are governed by the secondary structure of the DNA duplex. The use of deuterium isotope effects and selectively modified oligonucleotides as mechanistic probes enabled the elucidation of these pathways. At the thymidine nucleotide 5'-adjacent to 5,6-dihydro-2'-deoxyuridin-6-yl, alkali-labile lesion formation results from addition to the nucleobase as well as hydrogen atom abstraction from the 2-deoxyribose sugar. Abstraction of H1' results in the formation of a 2'-deoxyribonolactone containing lesion (**214**) while abstraction of H5' is proposed to lead to **215**. Although the product of this reaction has not been

determined, deuterium isotope effect studies indicate that abstraction of H4' is a minor pathway leading to alkali-labile lesion formation. The nucleobase addition pathway results in the formation of formamide-containing lesions such as **212**. Although nucleobase peroxyl radical addition to purines has been observed, the present study provides the first evidence of nucleobase peroxyl radical addition to a neighboring pyrimidine.[23] Abstraction of a hydrogen atom from the thymidine methyl group is the major reaction in the 3'-direction, giving rise to tandem lesions containing 5-hydroxymethyl- (**220**) or 5-hydroperoxymethyl-2'-deoxyuridine (**219**).

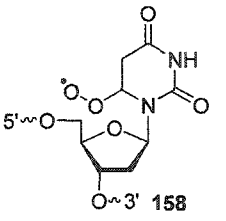

158

The addition and hydrogen atom abstraction reactions by which the nucleobase peroxyl radical (**158**) results in damage of adjacent nucleotides are well documented. Activated peroxyl radicals can react with alkenes with rate constants on the order of 10^4 M^{-1} s^{-1}. Trichloromethyl peroxyl radical (**243**) reacts with cyclohexene with a bimolecular rate constant of 9.5 X 10^4 $M^{-1}s^{-1}$ (Figure 143).[147] Intramolecular addition reactions have also been reported. Porter and co-workers estimated the rate constant for cyclization of the peroxyl radical (**244**) derived from linoleic acid at 800 s^{-1} (Figure 143).[155] Both of these processes are anticipated to be more rapid than the internucleotidyl addition by **158** as the former involves a reactive perhalogenated peroxyl radical and the latter is a 5-exo-trig ring closure. However, the secondary structure of DNA may result in a high effective molarity of the C6 position at the 5'-adjacent base, thus favoring the

addition reaction. This is consistent with a models of the peroxyl radical (**158**) in DNA which indicate that it is < 3 Å from the C6 position of the 3'-adjacent thymidine (Table 28). In a mechanistic study of the autooxidation of indene (**245**), Ingold and co-workers found that this peroxyl radical mediated process involves both addition and hydrogen atom abstraction (Figure 143).[156] The rate constants for the addition and hydrogen atom abstraction reactions were found to be 1281 and 141 $M^{-1}s^{-1}$ respectively. In the present study, the addition pathway was also found to be favored. The ratio of piperidine to NaOH induced cleavage at T_{15} in 5'-^{32}P-**159** was found to be 3.3. Assuming that the nucleobase addition pathway is the only source of piperidine labile lesions at T_{15}, it is favored over hydrogen atom abstraction (which results in a NaOH-labile site) by ~ 2.3:1.

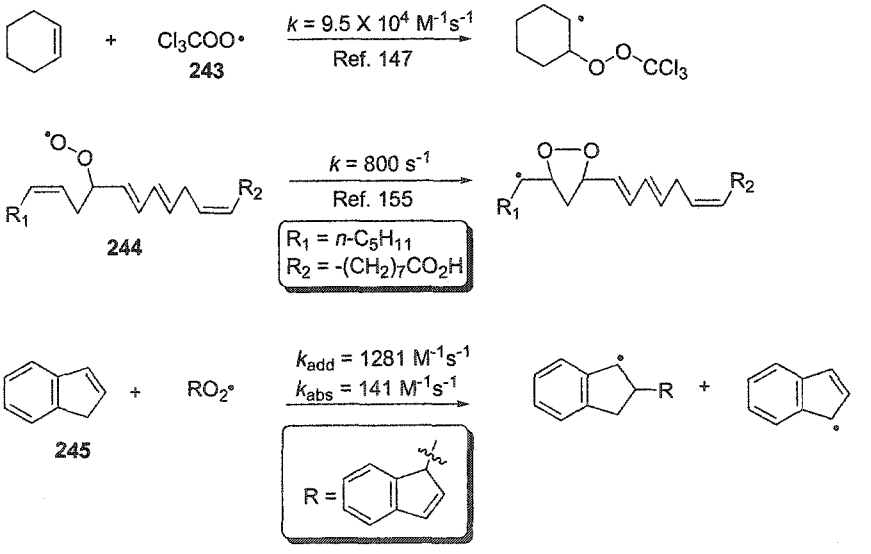

Figure 143. Addition Reactions of peroxyl radicals,

The other major pathway for alkali-labile lesion formation is abstraction of a hydrogen atom from the methyl group of the 3'-adjacent thymidine nucleotide. This results in an allylic radical which was predicted to have a stability greater than the C1'

radical in a computational study by Toure and co-workers.[58] Rate constants for hydrogen atom abstraction reactions by peroxyl radicals vary widely. Although values as high as 10^5 $M^{-1}s^{-1}$ have been reported for efficient hydrogen atom donors such as α-tocpherol, the rate constant in the present system is clearly much lower.[157] Porter and co-workers determined that the rate constant for the propogation (hydrogen-atom abstraction) step of oleate autooxidaton was 0.82 $M^{-1}s^{-1}$ (Figure 144).[158] This reaction also generates an allylic radical. As with the addition pathway, it should be noted that the secondary structure of DNA may result in a high effective concentration of the thymidine methyl group hydrogen atoms. A model of the 6*S* diastereomer of **158** in DNA indicates that this position is < 2 Å from the peroxyl radical oxygen (Table 28).

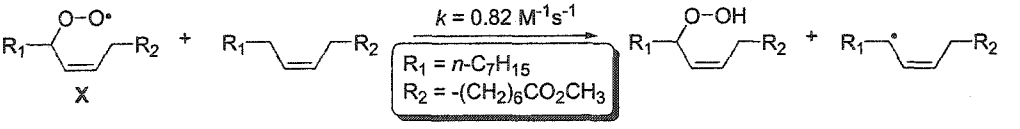

Figure 144. Allylic C-H abstraction by a peroxyl radical.

The result of peroxyl radical hydrogen atom abstraction and nucleobase addition is the formation of tandem lesions. Using data from PAGE experiments, it was estimated that this class of damage constitutes > 60 % of the observed alkali-labile lesions. The present study is the first to observe that tandem lesions are the *major* products of nucleobase radicals. Tandem lesion **8**, which was observed in a model system is formed in < 1 % yield from the thymidine C5 peroxyl radical (Figure 145).[25] The formamido

containing tandem lesion **6** has been isolated from irradiated DNA, but the yield in which it is formed has not been determined.[18,22]

The fact that tandem lesions are the major product of a 5,6-dihydro-pyrimidin-6-yl radical implies that they are formed in significant yields from other nucleobase radicals. Consequently, it is of growing importance to evaluate the biological effects of these lesions. It has been proposed that damage of this type would be resistant to repair, although there is currently scant data available.[17,101,106] Cadet and co-workers evaluated the ability of endonuclease III and Fpg to cleave an independently synthesized DNA strand containing tandem lesion **6** and found that both repair proteins give efficient cleavage.[106] In a related study, Kow and co-workers found that tandem dihydropyrimidines inhibit base excision repair proteins.[17] Using a duplex containing adjacent 5,6-dihydro-2'-deoxyuridine nucleotides (**114**) as a model tandem lesion, it was found that endonucleases III and VIII are unable to process both modified nucleotides. This suggests that certain types of tandem lesions may inhibit DNA repair pathways. The resistance of **114** to repair may be shared by other tandem pyrimidine modifications such as **219** and **220**.

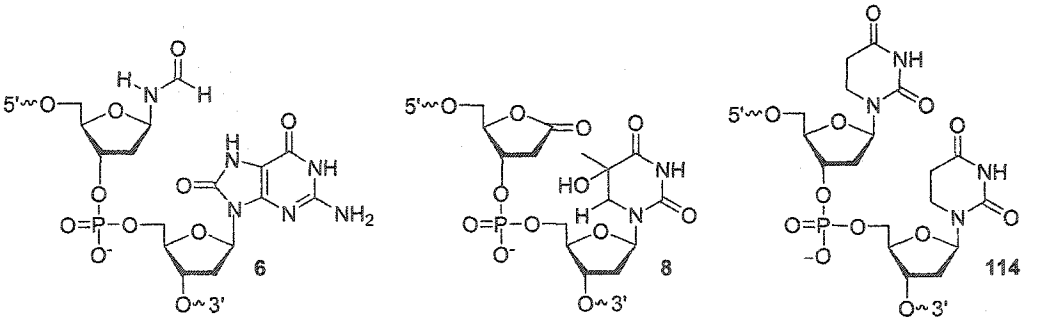

Figure 145. Tandem lesions.

The present study conflicts with proposals that 5,6-dihydropyrimidin-6-yl radicals result in direct strand scission. In this study, the DNA damage which results from the 5,6-dihydro-2'-deoxyuridin-6-yl was found to consist predominantly, if not exclusively, of alkali-labile lesions. A significant difference between the 5,6-dihydro-2'-deoxyuridin-6-yl (**123**) and the thymidine hydroxyl radical adduct (**2**) is the presence of the C5 hydroxyl group in the latter radical. The presence of a leaving group at the C5 position allows this species to form the corresponding cation radical (**14**, Figure 146). This reactive intermediate has been implicated in the direct strand scission of nucleic acids subjected to γ-radiolysis under anaerobic conditions.[10] The absence of direct strand breaks formed under anaerobic conditions in the present study is not inconsistent with this proposal, as the requisite cation radical intermediate cannot be formed from **123**.

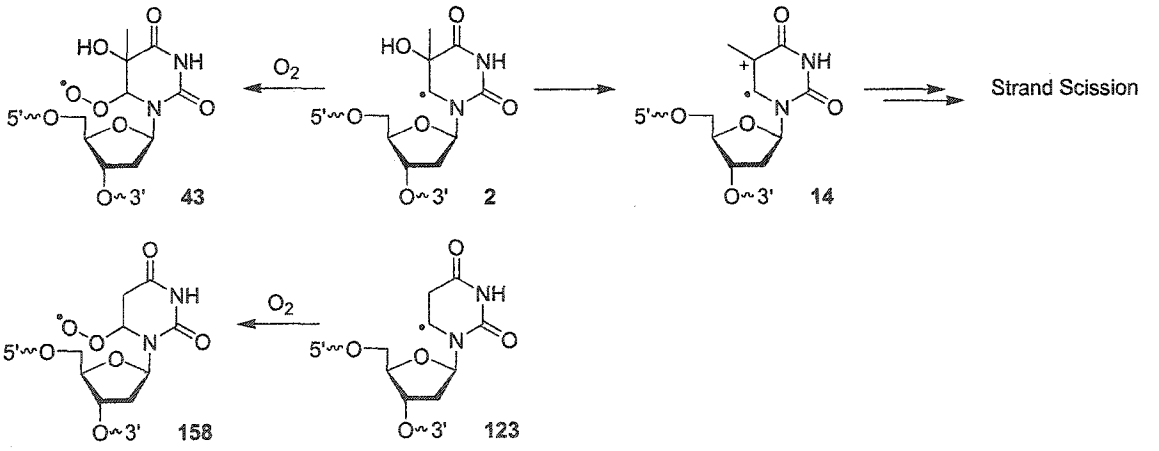

Figure 146. Cation radical versus peroxyl radical formation in nucleobase radicals.

Under aerobic conditions, the cation radical pathway is unlikely to compete with rapid conversion of the nucleobase radical (**2**) into the corresponding peroxyl radical (**43**). Experiments in which monomeric **2** was independently generated estimate the rate constant for dehydration at < 2 s^{-1}.[28] If the overall rate of oxygen (0.2 mM) trapping is 4 X 10^5 s^{-1}, dehydration clearly cannot compete. Since this pathway is not relevant under aerobic conditions, the results obtained with **123** can be safely extrapolated to **2**. This suggests that, under aerobic conditions, the thymidine hydroxyl radical adduct results primarily in the formation of alkali-labile lesions, contrary to previous studies which implicate this species in the formation of direct strand breaks.[12,14]

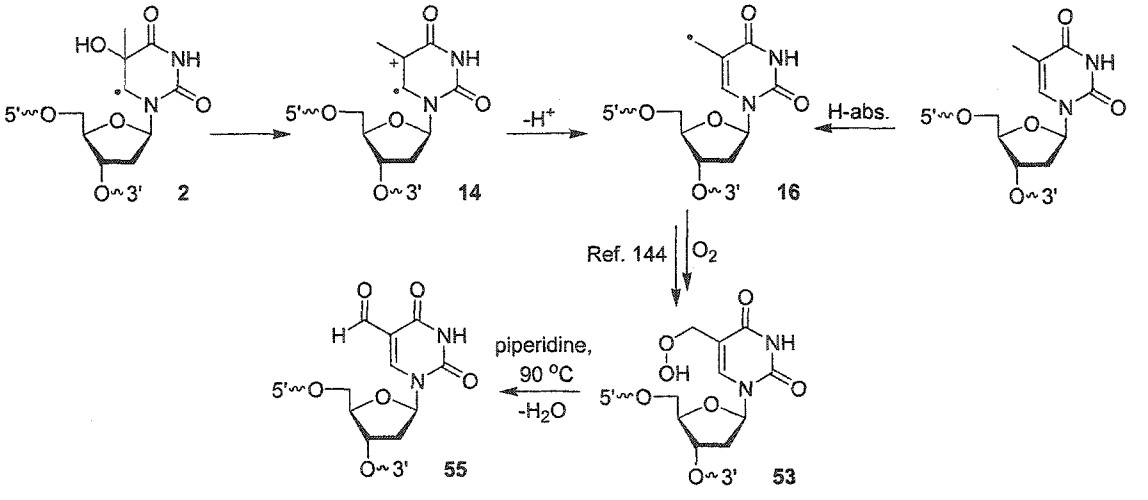

Figure 147. The formation of 5'-hydroperoxymethyl-2'-deoxyuridine (**53**) from the thymidine cation radical and methyl hydrogen atom abstraction

It is noteworthy that abstraction of a hydrogen atom from the methyl group of an adjacent thymidine nucleotide represents a major pathway of alkali-labile lesion formation (Figure 147). Characterization by MALDI-TOF MS demonstrated that methyl hydrogen atom abstraction gives rise to a tandem lesion containing 5-

hydroperoxymethyl-2'-deoxyuridine (**219**). Upon base treatment, **53** is proposed to undergo dehydration to form 5-formyl-2'-deoxyuridine which then leads to cleavage.[54] It has been proposed that modifications of the thymidine methyl group observed in cells subjected to γ-radiolysis are formed from deprotonation of the thymidine cation radical (**14**) formed by the direct effect (Figure 147).[33] Attack of the thymidine methyl group as a result of the indirect effect is thought to be minimal.[153] Abstraction by a nucleobase peroxyl radical provides an alternative pathway by which these lesions may be formed.

Independent generation of 5,6-dihydro-2'-deoxyuridin-6-yl (**123**) in DNA has enabled characterization of DNA damage pathways which begin with this reactive intermediate. In the presence of O_2, 5,6-dihydro-2'-deoxyuridin-6-yl (**123**) results in the formation of alkali-labile tandem lesions. This occurs in part by addition of a nucleobase peroxyl radical (**158**) to an adjacent pyrimidine, a pathway which has not been previously observed. Alkali-labile tandem lesions are the *major* observed products formed from 5,6-dihydro-2'-deoxyuridin-6-yl (**123**) in DNA. The observation that tandem lesions are the primary product of a nucleobase radical underscores the importance of identifying and studying this class of damage.

5 Experimental Methods

General Methods: Benzoyl cyanide, BME, and pivaloyl chloride were distilled prior to use. Diisopropylamine was distilled from NaOH. THF was distilled from Na^0/Benzophenone. Et_3N, CH_2Cl_2, Hünig's base, DMF, MeOH, pyridine, isopropanol and 2,5-dimethyltetrahydrofuran were distilled from CaH_2. CH_3CN was passed through anhydrous $CuSO_4$ prior to distillation from CaH_2. NBS was recrystallized from H_2O prior to use. Zinc dust was activated with dilute HCl then dried under vacuum. K_2CO_3 was dried overnight at 110 °C in the presence of P_2O_5.

All photolyses were carried out in Pyrex tubes using a Rayonet photoreactor fitted with an appropriate number of lamps having an output maximum at 350 nm. The lamp output was measured at 360 nm using a UVX radiometer (UVP, Inc.). The output of a typical lamp was ~ 700 $\mu W/cm^2$. All anaerobic reactions were carried out in sealed Pyrex tubes, which were degassed and sealed using standard freeze-pump-thaw degassing techniques (three cycles, three minutes each).

Oligonucleotides were synthesized using standard automated techniques using an Applied Biosystems model 394 DNA/RNA synthesizer. Pivaloyl anhydride/2,6-lutidine/THF (8:1:1) was used as a capping reagent. For introduction of the radical precursor phosphoramidite (**151**, **153**), an extended coupling time (5 min) was used. Oligonucleotides containing the radical precursor (**122a**, **b**) were deprotected using K_2CO_3 (0.05 M in dry MeOH).

Oligonucleotides were 5'- or 3'-^{32}P end-labeled according to reported methods.[154] Oligonucleotide photolyses were carried out in 10 mM potassium phosphate (pH 7.2) and 100 mM NaCl for a period of 50 min unless otherwise specified. In a typical experiment,

the DNA concentration was ~ 10 nM. In some cases, GSHOEt in phosphate buffer was added. After photolyses, samples were precipitated from 3 N NaOAc pH 5.2 and calf thymus DNA (1.3 mM in base pairs). To dehydrate any 2'-deoxyuridine C6-hydrate present, some samples were heated for 1 h at 90 °C prior to precipitation and piperidine treatment. In some cases, samples were treated with 1.0 M piperidine (100 μL, 90°C, 20 min). After piperidine treatment, samples were lyophilized and co-evaporated with H_2O (25 μL). Samples were resuspended in formamide loading buffer prior to analysis by denaturing PAGE. In some cases, precipitated photolysates were treated with 0.1 M NaOH (10 μL, 37 °C, 20 min). These samples were neutralized with 1.0 M HCl (1.0 μL) and combined with an equal volume of formamide loading buffer prior to analysis by denaturing PAGE.

Oligonucleotide separations were carried out using 20% polyacrylamide denaturing gel [5% crosslink, 45 % urea (w/w)]. Gels were sequenced using 5'- or 3'-^{32}P end-labeled markers. Analytical separations were carried out using gels of 0.4 mm thickness while preparative separations were carried out using gels of 1.5 mm thickness. Independently synthesized marker oligonucleotides were used to sequence gels. For gels using 5'-^{32}P 30mers, the following three marker sequences were used:

5'-d(GAG CTA GCT CGA CCT T)-OPO_3^{2-}

5'-d(GAG CTA GCT CGA CCT)-OPO_3^{2-}

5'-d(GAG CTA GCT CGA CC)-OPO_3^{2-}

Although these sequences were 3'-phosphorylated, upon labeling with T4 PNK they were dephosphorylated. For experiments using 3'-^{32}P 30mers, the following marker sequences were used:

3'-d(TCG ACG TCC AGG ATT)-OPO_3^{2-}

3'-d(TCG ACG TCC AGG AT)-OPO_3^{2}

3'-d(TCG ACG TCC AGG A)-OPO_3^{2}

The 5'-phospate end-groups of these marker sequences remained intact after 3' end-labeling with terminal deoxynucleotidyl transferase.

Oligonucleotide samples were precipitated from ammonium acetate (5.0 M, pH 5.6) prior to mass spectral analysis. Electrospray mass spectra were acquired in the negative mode with a Finnagan LCQ Deca instrument. The capillary temperature was set at 120 °C. Oligonucleotide samples (~1-2 nmoles) were dissolved in a matrix of 0.2% Et_3N (v/v), 2 mg/100 mL CDTA, in 1:1 *i*-PrOH/H_2O. MALDI samples were analyzed in the negative ion mode using a Kratos instrument. Samples were prepared by combining 1 μL of analyte solution (~ 10 μM) with 1 μL of 2, 6-dihydroxyacetophenone matrix solution (36 mM 2', 6'-dihydroxyacetophenone, 0.17 M ammonium tartrate in 2:1 H_2O/CH_3N) and allowing this mixture to dry on the sample plate. In some cases, an oligonucleotide of known molecular weight for purposes of calibration.

HPLC samples were analyzed with a Microsorb-MV C18 5 μm column (0.46 × 25 cm). Separations were carried out using one of the following five gradients (A-E). Gradient A: The initial conditions were 95/5 10 mM ammonium formate, pH 6.2/CH_3CN. The initial conditions were held for 5 min then ramped to 35% CH_3CN linearly over 45

min and held constant for 10 min. Gradient B was identical to gradient A except water was used in place of ammonium formate. Gradient C: The initial conditions were 95/5 10 mM ammonium formate, pH 6.2/CH_3CN. The initial conditions were held for 5 min then ramped to 35% CH_3CN linearly in 50 min and held for 10 min. Gradient D: The initial conditions were 90/10 50 mM ammonium formate pH 6.2/50 mM ammonium formate pH 6.2 (50 % CH_3CN). Over a period of 70 min, the conditions were ramped to 73.7/26.3. Gradient E: The initial conditions were 100 mM ammonium formate pH 6.2. The conditions were changed to 75/25 ammonium formate/CH_3CN over a period of 45 min.

Steady state radical concentrations ([R•]) were calculated as follows: [R•] = [**X**](fraction **X** converted)/(photolysis time in seconds), where [**X**] is the starting concentration of the photosubstrate. The fraction of **X** converted was determined by HPLC.

In some cases, response factors for compounds were calculated versus a standard (Table 39). The response factor (R) was defined using the following equation in which A_X and A_S represent the integrated areas under the peak of the compound of interest and the standard, while [X] and [S] represent the respective concentrations.

$$\frac{[X]}{[S]} = R\frac{A_X}{A_S}$$

Computer calculations were carried out using Spartan '02 (Wavefunction, Inc.; Irvine, CA). Equilibrium geometries were determined using molecular mechanics and energies were minimized using semi-empirical calculations (PM3).

Table 39. Response Factors and retention times for HPLC analysis.

Compound	Retention time (min)				Response factor
	Gradient A	Gradient B	Gradient C	Gradient D	
130	50.1	53.4	60.9	-	1.6[a]
122a	-	-	-	18.7	1.7[b]
132	34.8	37.1	41.7	-	1.4[a]
131	-	-	-	16.6	1.6[b]
140b	32.1	34.4	38.1	-	1.6[a], 0.80[c]
138	35.6	37.9	42.3	-	1.3[a], 0.64[c]
144	-	-	-	9.4	1.2[b]
133	-	-	46.1	-	1.4[a]
142a	37.2	-	-	-	0.85[c]
5'-benzoylthymidine	40.4	-	-	-	0.65[c]

[a] Response factor was calculated versus the 5'-benzoate ester of thymidine. [b] Response factor was calculated versus thymidine. [c] Response factor was calculated versus *p*-methoxybenzyl alcohol.

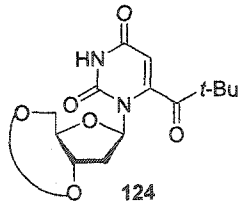

124

Preparation of 124. To a solution of diisopropylamine (1.69 g, 16.7 mmol) in THF (14.7 mL) at -78 °C was added 12.2 mL (5 equiv.) of a 1.3 M solution of *s*-BuLi in cyclohexane. The solution was allowed to warm to room temperature, then cooled to -78 °C. A solution of 3', 5'-*O*-(tetraisopropyldisiloxane-1, 3-diyl)-2'-deoxyuridine (1.50 g, 3.19 mmol) in THF (4 mL) was added and the reaction was stirred 1 h at -78 °C. A solution of pivaloyl chloride (603 mg, 4.79 mmol) in THF (4 mL) was added slowly. After 0.5 h, the reaction was quenched with glacial acetic acid, taken up in Et_2O, washed with H_2O, brine, dried over Na_2SO_4

and concentrated *in vacuo*. The crude reaction mixture was purified via silica gel flash chromatography (5-40% EtOAc/Hexanes) to afford **124** (534 mg, 30%) as a white solid (mp 66-68 °C). ^{1}H NMR ($CDCl_3$) δ 8.95 (s, 1 H), 5.48 (s, 1 H), 5.30 (dd, J = 8.7, 4.8 Hz, 1 H), 4.87 (dd, J = 6.3, 2.4 Hz, 1 H), 4.14-3.98 (m, 2 H), 3.81-3.77 (m, 1 H), 2.90-2.75 (m, 1 H), 2.39-2.35 (m, 1 H), 1.24 (s, 1 H), 1.12-0.96 (m, 28 H); ^{13}C NMR ($CDCl_3$) δ 201.1, 158.0, 148.2, 144.3, 94.4, 83.3, 82.0, 68.8, 59.4, 40.8, 35.9, 22.5, 13.1, 13.0, 12.95, 12.90, 12.7, 12.6, 8.81, 8.67, 8.28, 8.15; IR (film) 2945, 2867, 1703, 1463, 1388, 1362, 1249, 1091, 885 cm^{-1}; HRMS (FAB) calcd 555.2921 (M + H), found 555.2903.

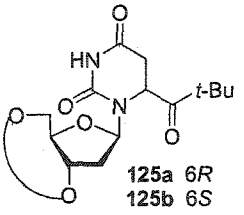

125a 6*R*
125b 6*S*

Preparation of 125a, b. To a solution of **124** (534 mg, 0.96 mmol) in MeOH (9.6 mL) was added 5% Rh/Al_2O_3 (54 mg). The reaction was pressurized with H_2 and stirred for 2 h. The reaction was monitored closely by TLC to prevent overreduction. The crude reaction mixture was filtered through celite and concentrated *in vacuo*. The crude product was purified via silica gel flash chromatography (10-40% EtOAc/Hexanes) to afford **125a** and **125b** (440 mg, 82%) as an 8.2:1 mixture. **125a**: *Rf* = 0.44 (1:1 hexanes/EtOAc); ^{1}H NMR ($CDCl_3$) δ 7.39 (s, 1 H), 5.97 (t, J = 6.0 Hz, 1 H), 4.79 (d, J = 8.1 Hz, 1 H), 4.42-4.39 (m, 1 H), 4.08-4.03 (m, 1 H), 3.84-3.70 (m, 2 H), 3.03 (dd, J = 16.9, 8.1 Hz, 1 H), 2.79 (d, J = 17.1 Hz, 1 H), 2.18-2.05 (m, 1 H), 1.95-1.80 (m, 1 H), 1.25 (s, 9 H), 1.17-0.89 (m, 28 H); ^{13}C NMR ($CDCl_3$) δ 207.5, 163.9, 148.5, 80.9, 79.7, 68.4, 59.07, 49.6, 38.8, 32.9, 29.1, 21.6, 12.2, 12.1, 12.0, 11.8, 11.7, 8.8, 8.6, 8.4, 8.0; IR (film) 3214, 3088, 2945, 2893, 2868, 1718, 1464, 1387, 1119, 1087, 1038, 972, 920 cm^{-1}; HRMS (FAB) calcd 557.3078 (M + H), found 557.3058. **125b**: *Rf* = 0.52 (1:1 hexanes/EtOAc); ^{1}H NMR ($CDCl_3$) δ 7.86 (s,

1 H), 5.66 (dd, J = 6.0, 2.7 Hz), 5.10 (dd, J = 7.2, 2.4 Hz, 1 H), 4.38 (q, J = 8.7 Hz, 1 H), 3.96 (d, J = 3.0 Hz, 1 H), 3.66-3.62 (m, 1 H), 2.88-2.84 (m, 2 H), 2.35-2.29 (m, 2 H), 1.17 (s, 9 H), 1.05-0.91 (m, 28 H); ^{13}C NMR ($CDCl_3$) 211.2, 166.8, 153.2, 84.8, 84.4, 68.1, 60.5, 52.9, 43.2, 40.7, 33.6, 27.6, 17.7, 17.6, 17.5, 17.4, 17.3, 17.2, 17.1, 17.0, 13.6, 13.3, 13.1, 12.5; IR (film) 3211, 2945, 2867, 1716, 1463, 1039 cm^{-1}; HRMS (FAB) calcd 557.3078 (M+H) 557.3087 found.

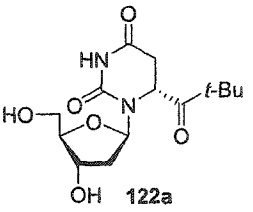

122a

Preparation of 122a. To a solution of **125a** (241 mg, 0.433 mmol) in THF (4 mL) was added Et_3N•3HF (697 mg, 4.33 mmol). The reaction was stirred overnight and concentrated *in vacuo*. The crude product was purified twice via silica gel flash chromatography (10% MeOH/$CHCl_3$) to afford **122a** (112 mg, 82%) as a white solid (mp 199-200 °C); ^{1}H NMR (MeOH-d_4) δ 6.23 (dd, J = 8.4, 4.2 Hz, 1 H), 5.30 (d, J = 7.8 Hz, 1 H) 4.25-4.23 (m, 1 H), 3.77-3.67 (m, 3 H), 3.14 (dd, J = 17.1, 8.1 Hz, 1 H), 2.84 (d, J = 17.2 Hz, 1 H), 1.79-1.71 (m, 1 H), 1.24 (s, 9 H); ^{13}C NMR (MeOH-d_4) δ 207.7, 163.9, 149.0, 81.3, 79.9, 66.8, 57.2, 48.2, 38.4, 32.2, 29.1, 22.1; IR (Film) 3261, 2965, 1711, 1465, 1371, 1289, 1226, 1092, 1049, 968, 873, 759 cm^{-1}; HRMS (FAB) calcd 315.1556 (M + H) found 315.1558.

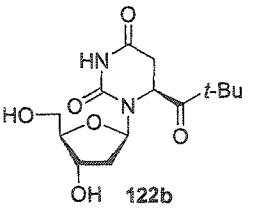

122b

Preparation of 122b. Compound **125b** (20 mg, 0.036 mmol) was deprotected with Et_3N•3HF (28 mg, 0.18 mmol) as previously described for the preparation of **122a** to afford **122b** (9.0 mg, 82%) as a clear residue; ^{1}H NMR (MeOH-d_4) δ 5.92 (t, J = 6.0 Hz, 1 H), 5.22 (d, J = 7.2 Hz, 1

H), 4.27-4.23 (m, 1 H), 3.79 (dd, J = 6.9 Hz, 3.6 Hz, 1 H), 3.65 (d, J = 3.6 Hz, 2 H), 3.10 (dd, J = 17.4, 8.1 Hz, 1H), 2.76 (d, J = 17.4 Hz, 1 H), 1.23 (s, 9 H); ^{13}C NMR (100 MHz, MeOH-d_4) δ 213.3, 170.2, 155.6, 88.5, 86.5, 72.4, 63.1, 53.9, 44.2, 41.2, 34.7, 27.9; IR (film) 3320, 2926, 2360, 1708, 1468 cm^{-1}; HRMS (FAB) calcd 315.1556 (M + H) 315.1565 found.

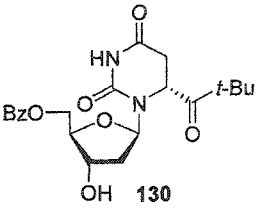

130

Preparation of 130. To a solution of C-6 *t*-butyl ketone **122a** (30 mg, 0.095 mmol) and Et_3N (12 mg, 0.12 mmol) in DMF (1.0 mL) at -40 ^{0}C was added benzoyl cyanide (15 mg, 0.11 mmol). The reaction was stirred overnight and allowed to warm to ambient temperature. The reaction was quenched with H_2O and diluted with EtOAc. The crude reaction mixture was washed with H_2O, brine, dried over Na_2SO_4 and concentrated. The crude product was purified via silica gel flash chromatography (15-25 % EtOAc/CH_2Cl_2) to afford **130** (20 mg, 50 %) as a clear oil; ^{1}H NMR ($CDCl_3$) δ 8.06-8.04 (m, 2 H), 7.81 (s, 1H), 7.62-7.57 (m, 1 H), 7.49-7.44 (m, 2 H), 6.20 (t, J = 6.0 Hz, 1 H),4.86 (d, J = 6.3 Hz, 1 H), 4.56-4.41 (m, 2 H), 4.33-4.31 (m, 1 H), 4.11-4.09 (m, 1 H), 2.99 (dd, J = 17.4, 6.3 Hz, 1 H), 2.82 (d, J = 17.4 Hz, 1 H), 2.71 (d, J = 4.2 Hz, 1 H), 2.13-2.05 (m, 1 H), 1.77-1.70 (m, 1 H), 1.17 (s, 9 H); ^{13}C NMR ($CDCl_3$) δ 211.1, 166.8, 166.7, 152.5, 133.7, 129.9, 129.8, 128.8, 84.8, 82.8, 71.8, 64.4, 52.5, 43.7, 37.0, 34.3, 27.6; IR (Film) 3227, 2965, 2360, 1716, 1457, 1370, 1276, 1090, 1026 cm^{-1}; HRMS (FAB) calcd 419.1818 (M + H) found 419.1804.

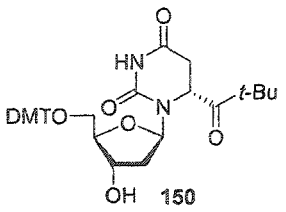

150

Preparation of 150 . C-6 *t*-butyl ketone **122a** (100 mg) was dried azeotropically with pyridine (3 X 1 mL) then redissolved in pyridine (2 mL) and cooled to 0 °C. DMT-Cl (129 mg, 0.382 mmol) was added. The reaction was stirred 20 h, then additional DMT-Cl (33 mg, 0. 097 mmol) was added. The reaction was stirred an additional 3 h, then quenched with MeOH (100 μL). The reaction was taken up in Et_2O (50 mL), washed with H_2O (3 X 50 mL), brine (50 mL), dried over Na_2SO_4 and concentrated *in vacuo*. The crude product was purified via silica gel flash chromatography (15-40% EtOAc/Hexanes) to afford **122a** (147 mg, 75%) as a white solid; ^{1}H NMR ($CDCl_3$) δ 7.45-7.41 (m, 3 H), 7.32-7.24 (m, 7 H), 6.86-6.82 (m, 4 H), 6.18 (t, J = 7.3 Hz, 1 H), 4.72 (d, J = 7.8 Hz, 1 H), 4.26-4.24 (m, 1 H), 3.91-3.89 (m, 1 H), 3.80 (s, 6 H), 3.37 (dd, J = 9.6, 4.8 Hz, 1 H), 3.14 (dd, J = 9.9, 5.7 Hz, 1 H), 3.01 (dd, J = 17.2, 7.8 Hz, 1 H), 2.79 (d, J = 16.8 Hz, 1 H), 2.05-1.95 (m, 2 H), 1.62-1.60 (m, 2 H), 1.07 (s, 9 H), ^{13}C NMR ($CDCl_3$) δ 206.2, 162.0, 154.0, 147.7, 140.0, 131.2, 125.6,123.6, 123.4, 122.5, 108.7, 81.9, 79.6, 79.2, 73.0, 72.6, 72.2, 67.8, 59.6, 50.8, 47.6, 38.8, 32.2, 29.6, 23.0; IR (Film) 3413, 3218, 3085, 2963, 2837, 1751, 1601, 1582, 1509, 1462, 1415, 1369, 1296, 1250, 1224, 1177, 1084, 1033, 968, 728 cm^{-1}, HRMS (FAB) calcd 639.2682 (M + Na) 639.2666 found.

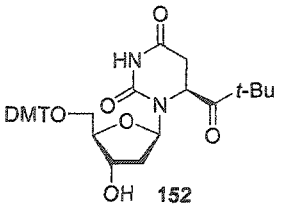

152

Preparation of 152. Compound **122b** (37 mg, 0.12 mmol) was tritylated as desribed for the preparation of **150** to afford **152** (55 mg, 76%) as a white foam; ^{1}H NMR ($CDCl_3$) δ 7.64 (s, 1H), 7.38-7.36 (m, 2 H), 7.27-7.22 (m, 8 H), 6.83-6.81 (m, 2 H), 5.68 (t, J= 6.4 Hz, 1 H), 4.81 (d,

J= 7.6 Hz, 1H), 4.30 (s, 1 H), 3.99 (d, *J*= 4.0 Hz, 1 H), 3.77 (s, 6 H), 3.32 (dd, *J*=10.0, 5.2 Hz, 1 H), 3.12 (dd, *J*= 10.0, 5.2 Hz, 1 H), 2.76 (dd, *J*= 25.2, 17.6 Hz, 1 H), 2.64 (d, *J*=17.6 Hz), 2.41-2.39 (m, 1 H), 2.24-2.15 (m, 1 H), 1.04 (s, 9 H); ^{13}C NMR ($CDCl_3$) δ 211.7, 167.6, 159.7, 154.0, 145.4, 136.5, 136.4, 131.02, 131.01, 129.1, 114,3, 87.8, 86.8, 86.2, 73.9, 65.0, 56.3, 53.6, 44.3, 42.5, 34.5, 28.4, 2.1; IR (Film) 3061, 2964, 2838, 1716, 1607, 1582; HRMS (FAB) calcd 639.2682 (M+ Na) found 639.2665.

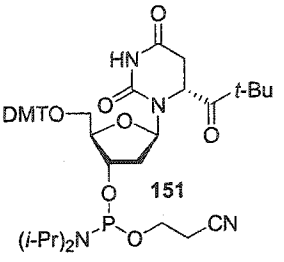

Preparation of 151. To a solution of **150** (88 mg, 0.143 mmol) and diisopropylethylamine (74 mg, 0.571 mmol) in CH_2Cl_2 (1.4 mL) was added 2-cyanoethyl diisopropyl chlorophosphoramidite (43 mg, 0.186 mmol). The reaction was stirred 2 h, diluted with EtOAc (50 mL), washed with saturated Na_2CO_3 (50 mL), brine (50 mL), dried over Na_2SO_4 and concentrated *in vacuo*. The crude product was purified via silica gel flash chromatography (1:1 Hexanes/EtOAc) to afford **151** (85 mg, 73%) as a colorless oil; ^{1}H NMR ($CDCl_3$) δ 7.48-7.26 (m, 10 H), 6.87-6.84 (m, 3 H), 6.26.25-6.20 (m, 1 H), 4.80 (t, *J* = 7.8 Hz), 4.46-4.44 (m, 1H), 4.09-4.07 (m, 1 H), 3.88-3.55 (m, 9 H), 3.26-3.20 (3.m, 2 H), 3.11-3.08 (m, 2 H), 3.05-3.02 (m, 1 H), 2.82-2.66(m, 1 H), 2.64 (t, *J* = 6.3 Hz, 1 H), 2.43 (t,*J* = 6.6 Hz, 1 H), 2.15-2.06 (m, 1 H), 1.63-1.55 (m, 2 H), 1.37-1.09 (m, 21 H); ^{32}P NMR (121 MHz, $CDCl_3$) δ 149.7, 149.0 cm^{-1}; IR (Film) 3413, 3218, 3085, 2963, 2837, 1751, 1601, 1582, 1509, 1462, 1415, 1369, 1296, 1250, 1224, 1177, 1084, 1033, 968, 728 cm^{-1}; HRMS (FAB) calcd 839.3843 (M + Na) 839.3803 found.

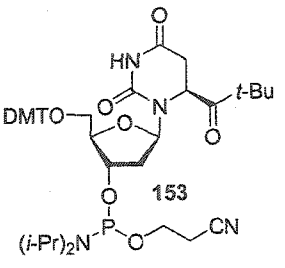

Preparation of 153. Compound **152** (40 mg, 0.065 mmol) was phosphitylated as described for the preparation of **151** to afford **153** (32mg, 60%) as a white foam; ^{1}H NMR ($CDCl_3$) δ 7.48-7.45 (m, 2 H), 7.38-7.36 (m, 4 H), 7.27-7.18 (m, 14 H), 6.82-6.78 (m, 8 H), 5.68 (t, *J*= 7.2 Hz, 1 H), 5.62 (t, *J*= 6.0 Hz, 1 H), 4.86 (d, *J*= 6.4 Hz, 1 H), 4.79 (d, *J*= 6.4 Hz, 1 H), 4.45-4.39 (m, 2 H), 3.84-3.53 (m, 20 H), 3.23 (d, *J*= 4.8 Hz, 2 H), 3.16 (t, *J*= 5.6 Hz, 2 H), 2.80-2.72 (m, 2 H), 2.65-2.43 (m, 8 H), 2.28-2.17 (m, 2 H), 1.30-1.03 (m, 44 H), ^{13}C NMR ($CDCl_3$) δ 211.9, 211.7, 167.6, 167.5, 159.7, 159.6, 154.0, 153.9, 145.5, 145.4, 136.6, 136.5, 131.2, 131.1, 131.1, 131.0, 129.2, 129.1, 128.9, 128.1, 128.0, 118.8, 118.6, 114.2, 87.7, 87.6, 87.3, 87.0, 86.5, 86.4, 86.1, 86.0, 75.5, 75.3, 74.9, 74.7, 64.9, 64.7, 59.3, 59.2, 59.1, 59.0, 56.4, 56.3, 53.6, 53.5, 44.4, 44.3, 44.2, 41.7, 41.6, 41.5, 41.4, 34.5, 28.4, 28.3, 25.8, 25.7, 25.6, 25.5, , 21.5, 21.4, 21.3, 21.2; ^{31}P NMR (100 MHz, $CDCl_3$) δ 149.0, 148.8; IR (Film) 3231, 3071, 2967, 1722, 1510; HRMS (FAB) calcd 839.3843 (M + Na) 839.3771 found.

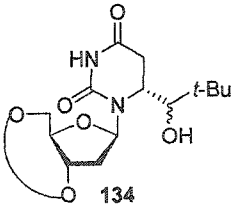

Preparation of 134. $NaBH_4$ (15.5 mg, 0.41 mmol) was added to a solution of **125a** (114 mg, 0.20 mmol) in MeOH (2.0 mL) at 0 °C. The reaction was stirred 2 h then diluted with Et_2O. The reaction mixture was washed with H_2O, brine, dried over Na_2SO_4 and concentrated *in vacuo*. The crude reaction mixture was purified via silica gel flash chromatography (2:1-1:1 Hexanes/EtOAc) to afford **134** (82 mg, 71%) as a white foam; ^{1}H NMR ($CDCl_3$) δ 6.56 (s, 1H), 5.92 (t, *J* = 6.9 Hz), 5.47 (s, 1 H), 4.50-4.47 (m, 1 H), 4.22 (d, *J* = 3.3 Hz, 1H), 4.22-3.84 (m, 3 H), 3.69-3.67 (m, 1 H), 2.86-2.80 (m, 1 H), 2.34-2.21 (m, 3 H), 1.09-0.91

(m, 37 H); ^{13}C NMR ($CDCl_3$) δ 166.4, 152.2, 80.6, 79.5, 78.1, 65.8, 57.2, 46.3, 37.1, 31.1, 30.1, 19.7, 13.1, 13.0, 12.9, 12.8, 12.6, 12.5, 12.4, 9.0, 8.8, 8.7, 8.0; IR (Film) 3390, 3182, 2945, 2868, 2360, 1744, 1688, 1633, 1453, 1367, 1328, 1279, 1081, 1039, 963, 919, 885 cm^{-1}; HRMS (FAB) calcd 581.3075 (M+H) 581.3078 found.

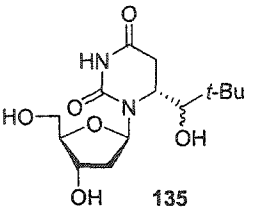

135

Preparation of 135. $Et_3N{\cdot}3HF$ (101 mg, 0.63 mmol) was added to a solution of **134** (70 mg, 0.12 mmol) in THF (1.2 mL). The reaction was stirred overnight and concentrated *in vacuo*. The crude reaction mixture was purified via silica gel flash chromatography (5-10% MeOH/$CHCl_3$) to afford **135** (33mg, 83%) as a white foam; ^1H NMR (MeOH-d_4) δ 5.77 (dd, J = 9.5, 9.3 Hz, 1 H), 4.31-4.29 (m, 1 H) 4.17-4.12 (m, 2 H), 3.80-3.65 (m, 2 H), 2.73-2.63 (m, 2 H), 2.44-2.41 (m, 1 H) 1.93-1.86 (m, 2 H) 0.92 (s, 9 H); ^{13}C NMR (MeOH-d_4) δ 168.6, 153.0, 81.9, 81.7, 79.8, 66.6, 57.4, 47.2, 36.3, 31.3, 29.6, 18.7; IR (Film) 3368, 2359, 1735, 1670, 1073, 726 cm^{-1}; HRMS (FAB) calcd 317.1725 (M+H) 317.1712 found.

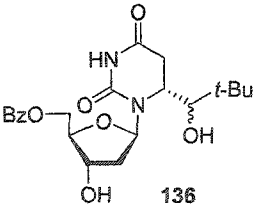

136

Preparation of 136. To a solution of **135** (24 mg, 0.075 mmol) and Et_3N (10 mg, 0.099 mmol) in DMF (1 mL) at 0 ^0C, was added benzoyl cyanide (11 mg, 0.083 mmol). After stirring 2 h at 0 ^0C, the reaction was quenched with saturated $NaHCO_3$ (1 mL), diluted with EtOAc (25 mL), washed with H_2O (25 mL), brine (25 mL), dried over Na_2SO_4 and concentrated *in vacuo*. The crude product was purified by silica gel flash chromatography (2-3% MeOH/CH_2Cl_2) to afford **136** and 3'-benzoylated material (10 mg, 31%) in a 5.8:1 ratio

as a clear oil; ^{1}H NMR (300 MHz, MeOH-d_4) δ 8.06-8.02 (m, 2 H), 7.64-7.59 (m, 1 H), 7.53-7.46 (m 2 H), 5.77 (t, J = 8.7 Hz), 4.54-4.40 (m, 3 H), 4.20-4.16 (m, 1 H), 4.09-4.04 (m, 1 H) 2.80-2.51 (m, 3 H), 1.99 (ddd, J = 13, 6.3, 3.0 Hz, 1 H), 0.90 (s, 9 H); IR (film) 3346, 2959, 1723, 1668, 1427, 1272, 1069 cm^{-1}; HRMS (FAB) calcd 421.1974 (M + H) found 421.1973.

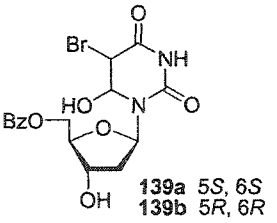

139a 5*S*, 6*S*
139b 5*R*, 6*R*

Preparation of 139a, b. $CaCO_3$ (407 mg, 4.06 mmol) and NBS (578 mg, 3.25 mmol) were added to solution of 5'-benzoyl-2'-deoxyuridine (900 mg, 2.71 mmol) in 3:1 THF/H_2O (21 mL) at 0 °C. The solution was allowed to warm to ambient temperature and stirred for 6 h. The reaction mixture was filtered through celite and concentrated. The crude mixture was subjected to silica gel flash chromatography (2-10% MeOH/$CHCl_3$) to yield **139a** (407mg, 35%) and **139b** (489 mg, 42%) as white foams: **139a**: ^{1}H NMR (MeOH-d_4) δ 8.07-8.05 (m, 2 H), 7.65-7.60 (m, 1 H), 7.52-7.47 (m, 2 H), 6.24 (t, J = 6.9 Hz, 1 H), 5.28 (d, J = 2.1 Hz, 1 H) 4.54-4.41 (m, 3 H), 4.17 (d, J = 2.1 Hz, 1 H), 4.14-4.10 (m, 1 H), 2.47-2.38 (m, 1 H), 2.19-2.14 (m, 1 H); ^{13}C NMR (MeOH-d_4) δ 168.2, 167.9, 152.3, 134.6, 131.3, 130.8, 129.8, 85.6, 84.7, 77.6, 72.4, 65.8, 41.4, 38.9; IR (film) 3396, 1698, 1452, 1276, 1090 cm^{-1}; HRMS (FAB) calcd (M + H) 431.0277 found 431.0279. **139b**: ^{1}H NMR (MeOH-d_4) δ 8.07-8.03 (m, 2 H), 7.67-7.61 (m, 1 H), 7.53-7.48 (m, 2 H), 6.25 (t, J = 6.6 Hz, 1 H), 5.31 (d, J =2.4 Hz, 1 H), 4.53 (d, J = 4.2 Hz, 2 H), 4.46-4.42 (m, 1 H), 4.21 (d, J = 2.4 Hz, 1 H), 4.14 (dd, J = 8.1, 4.2 Hz), 2.31-2.27 (m, 1H), 2.20-2.16 (m, 1 H); ^{13}C NMR (MeOH-d_4) δ 168.1, 167.9, 152.4, 134.6, 131.2,

130.7, 129.9, 86.1, 85.4, 77.9, 72.5, 66.0, 41.8, 40.2; IR (film) 3431, 1700, 1465, 1273, 1087 cm^{-1}; HRMS (FAB) calcd (M + H) 431.0277 found 431.0285.

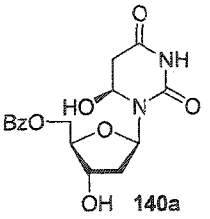

140a

Preparation of 140a. To a solution of **139a** (75 mg, 0.17 mmol) in 3:1 THF/H_2O at 0 °C was added zinc dust (66 mg, 1.0 mmol) and acetic acid (19 mg, 0.31 mmol). The reaction mixture was stirred at 0 °C for 20 min, filtered through celite, and concentrated. The crude product was purified via silica gel flash chromatography (1-6% MeOH/$CHCl_3$) to afford **140a** (42 mg, 63% overall) as a white foam; ^{1}H NMR (MeOH-d_4) δ 8.06-8.04 (m, 2 H), 7.65-7.60 (m, 1 H), 7.52-7.47 (m, 2 H), 6.23 (t, J = 6.0 Hz, 1 H), 5.31 (dd, J = 3.9 Hz, 2.1 Hz, 1 H), 4.56-4.41 (m, 3 H), 4.07 (dd, J = 9.3, 4.2 Hz, 1 H), 2.77 (dd, J = 16.8, 3.9 Hz, 1 H), 2.54-2.44 (m, 2 H), 2.18-2.10 (m, 1 H); ^{13}C NMR (MeOH-d_4) δ 174.3, 171.3, 167.9, 153.7, 134.6, 131.2, 130.8, 129.9, 85.7, 84.5, 73.1, 72.4, 65.7, 40.7, 38.7; IR (film) cm^{-1} 3392, 1700, 1472, 1274, 1067, 711 cm^{-1}.

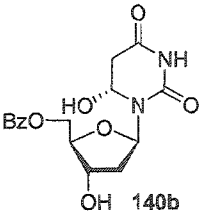

140b

Preparation of 140b. Using the same procedure described for the preparation of **140a**, **139b** (75 mg, 0.17 mmol) was reduced with zinc dust (66 mg, 1.0 mmol) and acetic acid (19 mg, 0.31 mmol). The crude reaction mixture was purified via silica gel flash chromatography (1-6% MeOH/$CHCl_3$) to afford an 11.5:1 mixture of **140b** and 5'-benzoyl-2'-deoxyuridine (42 mg, 63% overall) as a white foam; ^{1}H NMR (MeOH-d_4) δ 8.05-8.01 (m, 2 H), 7.65-7.59 (m, 1 H), 7.51-7.47 (m, 2 H), 6.17 (t, J = 6.9 Hz, 1 H), 3.52 (dd, J =4.1, 2.1 Hz, 1 H), 4.53-4.41 (m, 3

H), 4.10 (dd, J = 9.0, 4.5 Hz), 2.82 (dd, J = 17, 4.1 Hz, 1 H), 2.53 (dd, J = 17, 2.1 Hz, 1 H) 2.35-2.28 (m, 1 H), 2.21-2.16 (m, 1 H); ^{13}C NMR (MeOH-d_4) δ 171.4, 168.0, 153.9, 142.1, 134.6, 131.2, 130.7, 129.8, 86.9, 85.3, 74.5, 72.6, 65.9, 39.8; IR (Film) 3446, 1700, 1472, 1275, 1069, 757 cm^{-1}.

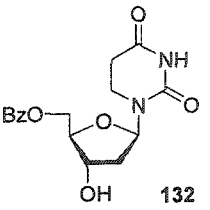

132

Preparation of 132. To a solution of 5,6-dihydro-2'-deoxyuridine[119] (100 mg, 0.43 mmol) and Et_3N (57 mg, 0.56 mmol) in DMF (4.0 mL) at -40 ^{0}C was added benzoyl cyanide (57mg, 0.43 mmol). The reaction was stirred overnight and allowed to warm to ambient temperature. The reaction was quenched with H_2O and diluted with EtOAc. The crude reaction mixture was washed with H_2O, brine, dried over Na_2SO_4 and concentrated. The crude product was purified via silica gel flash chromatography (5% MeOH/$CHCl_3$) to afford **132** (24 mg, 16 %) as a white foam; ^{1}H NMR (MeOH-d_4) δ 8.04-8.01 (m, 2 H), 7.63-7.56 (m, 2 H), 7.49-7.44 (m, 2 H), 6.34 (t, J = 7.5 Hz, 1 H), 4.54-4.43 (m, 3 H), 4.12 (dd, J = 8.4 Hz, 4.2 Hz, 1 H), 3.52-3.45 (m, 1 H), 3.33-3.25 (m, 1 H), 2.61-2.53 (m, 2 H), 2.39 (s, 1 H), 2.20-2.15 , (m, 2 H); ^{13}C NMR (MeOH-d_4) δ 172.3, 167.3, 154.4, 134.1, 130.8, 130.2, 129.4, 84.9, 84.1, 72.0, 65.2, 36.9, 36.5, 31.4; IR (Film) 3230, 1716, 1487, 1450, 1276, 1217, 1088, 1025, 712 cm^{-1}; HRMS (FAB) calcd 335.1244 (M+H) 335.1243 found.

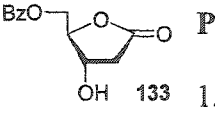

133

Preparation of 133. To a solution of 2-deoxyribonolactone[122] (230 mg, 1.74 mmol) and Et_3N (229mg, 2.26 mmol) in DMF (15 mL) at -40 ^{0}C was added benzoyl cyanide (274 mg, 2.09 mmol). The reaction was stirred overnight and

allowed to warm to ambient temperature. The reaction was quenched with H_2O and diluted with EtOAc. The crude reaction mixture was washed with H_2O, brine, dried over Na_2SO_4 and concentrated. The crude product was purified via silica gel flash chromatography (2:1-1:1 Hexanes/EtOAc) to afford **133** (127 mg, 31 %) as a clear oil; ^{1}H NMR ($CDCl_3$) δ 7.99-7.96 (m, 2 H), 7.62-7.57 (m, 1 H), 7.48-7.45 (m, 2 H), 4.70-4.68 (m, 1 H), 4.61-4.55 (m, 3 H), 3.08 (s, J = 3 Hz, 1 H), 2.95 (dd, J = 18, 6.9 Hz, 1 H), 2.62 (dd, J = 18 Hz, 3.9 Hz, 1 H); ^{13}C NMR ($CDCl_3$) δ 176.0, 167.4, 134.8, 130.7, 129.9, 129.7, 85.9, 70.0, 64.6, 38.9; IR (Film) 3461, 2950, 1601, 1451, 1781, 1720, 1176, 1164, 1026, 944 cm^{-1}; HRMS (FAB) calcd 254.1035 (M+H) 254.1028 found.

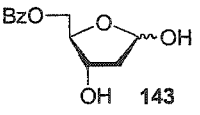

143

Preparation of 143. A toluene solution of DIBAL (2.0 mL, 1.0 M.) was added via syringe pump overnight to a solution of **133** (496 mg, 2.09 mmol) in CH_2Cl_2 (20 mL) maintained at –78 ^{0}C. The reaction was quenched while cold with MeOH (1 mL) and allowed to warm to ambient temperature. The reaction mixture was diluted with CH_2Cl_2 (80 mL) and washed with saturated Rochelle salt solution (100 mL), brine (100 mL), and concentrated *in vacuo*. The crude residue was purified via silica gel flash chromatography (1:3-1:1 EtOAc/CH_2Cl_2) to afford both anomers of **143** (22 mg, 4.4 %) as a clear oil. ^{1}H NMR ($CDCl_3$) δ 8.07-8.00 (m, 2 H), 7.60-7.54 (m, 1 H), 7.46-7.41 (m, 2 H), 5.64 (t, J = 4.5 Hz, 1H), 4.58-4.54 (m, 1 H), 4.49 (d, J = 5.1 Hz, 0.6 H), 4.37-4.32 (m, 2 H), 4.20 (q, J = 5.1 Hz, 0.4 H), 3.71 (d, J = 5.1 Hz, 0.7 H), 3.48 (s,0.3 Hz), 3.11 (d, J = 8.1 Hz, 0.7 H), 2.47 (s, 0.3 H), 2.98-2.14 (m, 2 H); ^{13}C NMR ($CDCl_3$) δ 166.9, 166.6, 133.5, 129.9, 129.8, 128.7, 99.6, 98.9, 85.3, 73.5, 72.6, 65.8,

64.8, 42.5, 41.5; IR (Film) 3418, 2926, 1715, 1468, 1385, 1277, 1070, 1026 cm^{-1}; ESI-MS, 237.1 (M-H).

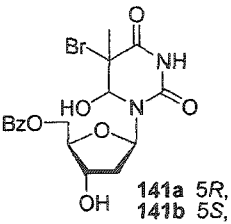

141a 5*R*, 6*R*
141b 5*S*, 6*S*

Preparation of 141 a, b.. To a solution of 5'-benzoyl thymidine (1.00 g, 2.89 mmol) in 3:1 THF/H_2O (28 mL) at 0 ^{0}C was added $CaCO_3$ (434 mg, 4.33 mmol) and NBS (616 mg, 3.46 mmol). The reaction mixture was stirred for 0.5 h at 0 ^{0}C and then allowed to warm to ambient temperature where it was stirred for an additional 2 h. The reaction mixture was filtered through celite and concentrated. The crude reaction mixture was purified via silica gel flash chromatography (2-10% MeOH/$CHCl_3$) to afford **141a** (701 mg, 55%) and **141b** (247 mg, 19%) as a partially separable mixture of diastereomers. **141a**: ^{1}H NMR (MeOH-d_4) δ 8.09-8.07 (m, 2 H), 7.67-7.63 (m, 1 H), 7.54-7.50 (m, 2 H), 6.29 (t, J = 5.2 Hz, 1 H), 5.17 (s, 1 H), 4.62 (dd, J = 9.0, 2.4 Hz, 1 H), 4.51-4.47 (m, 2 H), 4.18-4.15 (m, 1 H), 2.45-2.39 (m, 1 H), 2.22-2.16 (m, 1 H), 1.64 (s, 3 H); ^{13}C NMR (DMSO-d_6) δ 167.8, 165.6, 150.4, 133.5, 129.6, 129.4, 128.8, 83.2, 82.5, 78.8, 70.2, 64.3, 54.3, 37.1, 22.5 ; IR (film) 3396, 1700, 1452, 1275, 1087 cm^{-1}, HRMS (FAB) calcd 445.0433 (M + H) found 445.0438. **141b**: ^{1}H NMR (MeOH-d_4) δ 8.09-8.07 (m, 2 H), 7.65-7.61 (m, 1 H), 7.52-7.48 (m, 2 H), 6.25 (t, J = 5.5 Hz, 1 H), 5.15 (s, 1 H), 4.56 (dd, J = 9.0, 3.0 Hz, 1 H), 4.13-4.10 (m, 1 H), 2.48-2.42 (m, 1 H), 2.19-2.14 (m, 1 H), 1.69 (s, 3 H); ^{13}C NMR (DMSO-d_6) δ 167.7, 165.7, 150.7, 133.5, 129.6, 129.2, 128.8, 84.0, 83.1, 78.9, 70.6, 65.3, 55.3, 38.1, 22.5; IR (film) 3446, 1701, 1466, 1273, 1070 cm^{-1}; HRMS (FAB) calcd 445.0433 (M + H) found 445.0447.

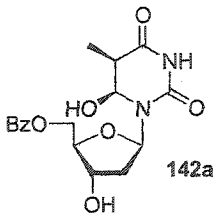

142a

Preparation of 142a. To a solution of **141a** (100 mg, 0.226 mmol) in 3:1 THF/H_2O at O °C was added zinc dust (46 mg, 1.31 mmol) in acetic acid (24 mg, 0.41 mmol). The reaction was stirred at O^0C for 20 min, filtered through celite and concentrated at ambient temperature. The crude reaction mixture was purified via silica gel flash chromatography (2% MeOH/ $CHCl_3$) to afford **142a** (23 mg, 28%) as a white residue; ^1H NMR (MeOH-d_4) δ 8.08-8.05 (m, 2 H), 7.66-7.61 (m, 1 H), 7.53-7.48 (m, 2 H), 6.27 (t, J = 6.3 Hz, 1 H), 5.10 (d, J = 3.0 Hz, 1 H), 4.56-4.43 (m, 3 H), 4.06 (dd, J = 8.7, 3.9 Hz, 1 H), 2.73-2.65 (m, 1 H), 2.53-2.43 (m, 1 H), 2.18-2.10 (m, 1H), 1.07 (d, J = 6.9 Hz, 3 H); ^{13}C NMR (MeOH-d_4) δ 173.8, 167.9, 154.0, 134.6, 131.2, 130.8, 129.9, 85.5, 84.5, 76.8, 72.5, 65.7, 43.1, 38.5, 10.5; IR (Film) 3445, 3231, 2929, 2857, 1709, 1462, 1256, 1215, 1125, 1028, 835 cm^{-1}; HRMS (FAB) calcd (M+H) 365.1349 found 365.1352.

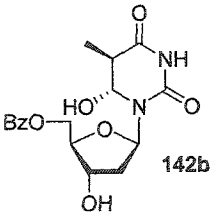

142b

Preparation of 142b. Using the same general procedure for the preparation of **142a**, **141b** (100 mg, 0.226 mmol) was treated with zinc dust (46 mg, 1.31 mmol) and acetic acid (24 mg, 0.41 mmol). Purification of the crude product by silica gel flash chromatography (2% MeOH/$CHCl_3$) afforded **142b** (16 mg, 20%) as a white solid; ^1H NMR (MeOH-d_4) δ 8.07-8.04 (m, 2 H), 7.66-7.61 (m, 1 H), 7.52-7.48 (m, 2 H), 6.19 (t, J = 6.6 Hz, 1 H), 5.10 (d, J = 3.3 Hz, 1 H), 4.62-4.44 (m, 3 H), 4.13-4.11 (m, 1 H), 2.76-2.72 (m, 1 H), 2.32-2.28 (m, 1 H), 2.22-2.19 (m, 1 H), 1.04 (d, J = 7.2 Hz, 3 H); ^{13}C NMR (MeOH-d_4) 173.9, 168.0, 154.4,

134.7, 131.3, 130.8, 129.9, 86.7, 85.3, 78.0, 72.6, 65.9, 42.6, 40.2, 10.6; IR (Film) 3417, 2924, 1714, 1472, 1276, 1251, 711 cm^{-1}; HRMS (FAB) calcd (M+H) 365.1349 found 365.1347.

Analysis of pyrimidine C6-hydrate decomposition. Aliquots were taken at appropriate times from a 1.0 mM solution (95/5 20 mM KH_2PO_4/CH_3CN) of the pyrimidine hydrate maintained at 37 °C or 90 °C. An internal standard (10 μL of 1.0 mM solution of 5'-benzoyl thymidine for 2'-deoxyuridine hydrate, *p*-methoxybenzyl alcohol for thymidine hydrates) was added and the samples were diluted with 1:1 40 mM KH_2PO_4, pH 6.0/CH_3CN to inhibit further decomposition. In some cases samples were spiked with 10 μL of a 0.2 mM (1:1 H_2O/CH_3CN) solution of **143** prior to heating at 90 °C to determine the extent of decomposition of this compound.

Photolysis of 205 under degassed conditions. A solution of **205** (60 μM) and BME (100 mM) in H_2O (100 μL) was placed in a pyrex tube and degassed using freeze-pump-thaw techniques. The solution was then photolyzed for 3.0 h using 16 lamps. After photolysis the solution was transferred to an eppendorf tube. The empty pyrex tube was rinsed with H_2O (100 μL) which was combined with the photolysate. The photolysate was precipitated from 5.0 M NH_4OAc, pH 5.6 and analyzed by ESI-MS.

MALDI-TOF MS analysis the cyclic 2-deoxyribonolactone adduct formed in 187. A solution of **187** (5.0 nmol) in H_2O (200 μL) was photolyzed 2 h using 16 lamps. The sample was transferred to an eppendorf tube and 20 μL of a 1.0 M solution of DMEDA in H_2O was added. The solution was incubated at 37 °C for 20 min then lyophilized. The residue was resuspended in H_2O (60 μL) and purified by HPLC using gradient D with UV detection at 260 nm. The appropriate fractions were lyophilized then resuspended in H_2O (1.0 mL) and desalted using a sep pack C_{18} column. After concentration, the samples were resuspended in H_2O (10 μL) and analyzed by MALDI-TOF as described above.

MALDI-TOF Analysis of oligonucleotide photolysates. The appropriate oligonucleotide (5.0 nmol) in H_2O (50 μL) was photolyzed at 350 nm in a pyrex tube for 2 h. In some cases, the photolysis was conducted in an $^{18}O_2$ saturated solution. This was accomplished by fitting the pyrex tube with a septa and flushing the DNA solution with N_2 for 30 min, then briefly (~ 2 min) bubbling the solution with $^{18}O_2$ immediately prior to photolysis. After the photolysis was complete the photolysate was transferred to an HPLC autosampler vial. The pyrex tube was rinsed with H_2O (50 μL) which was combined with the photolysates. The photolysate was then purified by HPLC using gradient D with UV detection at 260 nm. Typically, 10 μL of the 100 μL sample was analyzed first. The data from this injection was used to determine appropriate times for fraction collection. The appropriate fractions (Tables 40-42, Figures 138-40) were lyophilized then resuspended in H_2O (1.0 mL) and desalted using a sep pack C_{18} column.

After concentration, the samples were resuspended in H_2O (10 μL) and analyzed by MALDI-TOF as described above.

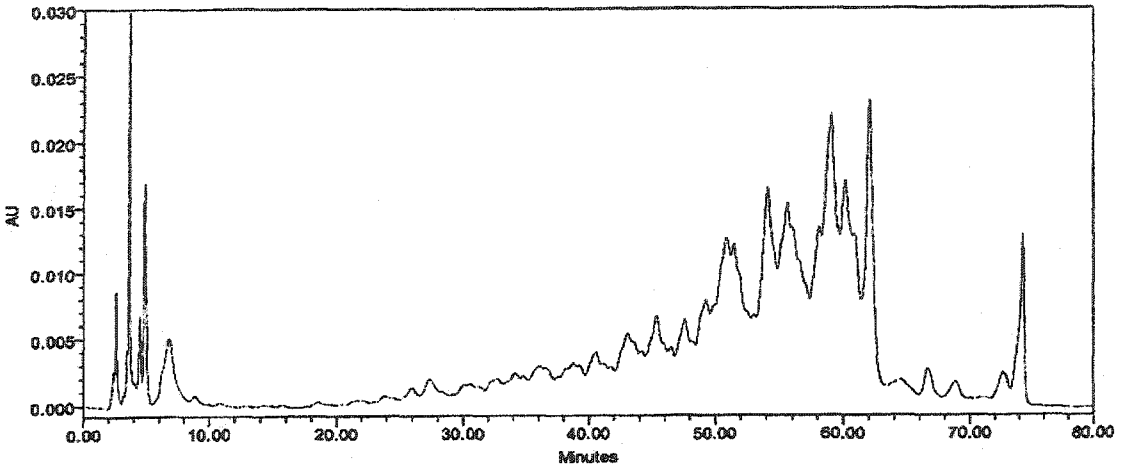

Figure 138. HPLC trace of the photolysate of **210**. Fractions were collected and analyzed by MALDI-TOF MS.

Table 40. Fractions collected of photolyzed **210** prior to MALDI-TOF MS analysis.

Fraction (min)	Products Observed
53.4-55.0	**211-213, 215, 220, 216**
55.0-57.0	**211-221**
57.0-58.4	**211, 212, 215, 216, 220**
58.4-59.5	**213, 217**
59.9-61.5	**213, 217**
61.6-62.8	**218**
72.0-73.0	**210**

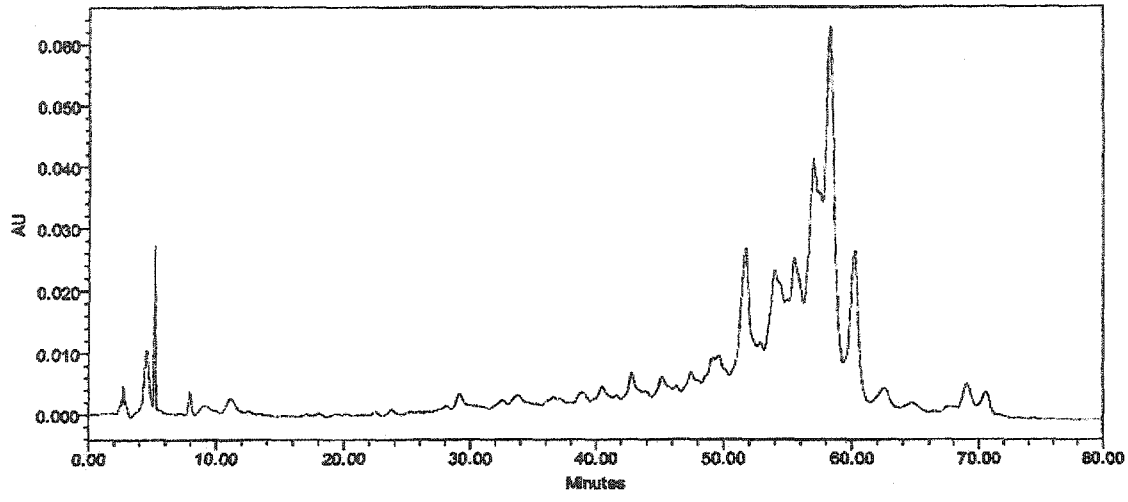

Figure 139. HPLC trace of the photolysate of **223**. Fractions were collected and analyzed by MALDI-TOF MS.

Table 41. Fractions collected of photolyzed **223** prior to MALDI-TOF MS analysis.

Fraction (min)	Products observed
59.0-61.0	**214**
63.0-65.0	**227**
65.0-68.0	**224-230**
68.0-70.0	**226, 228-230**
70.0-71.0	**228-230**

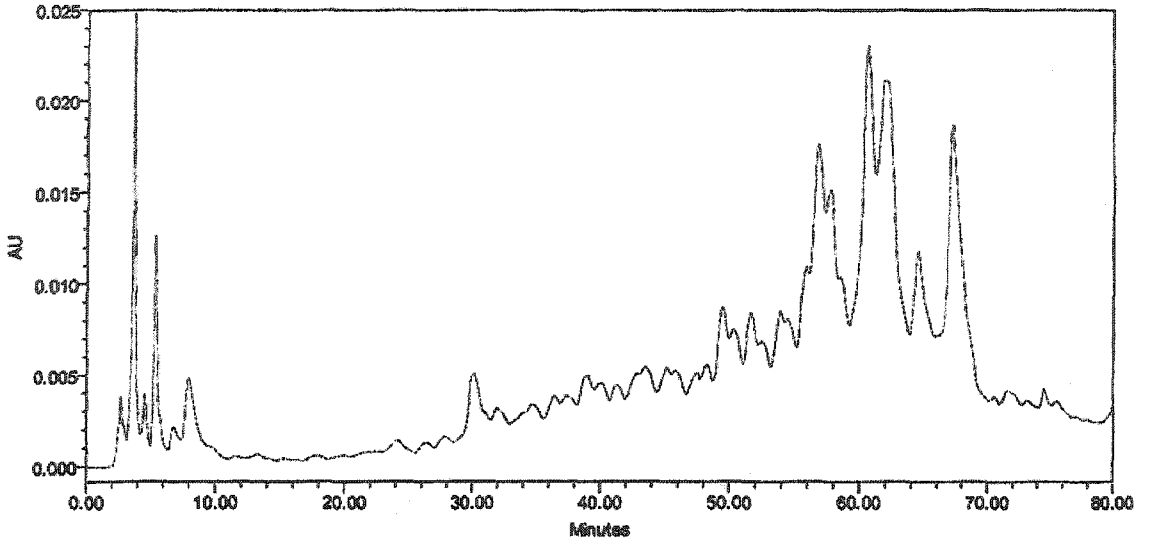

Figure 140. HPLC trace of the photolysate of **231**. Fractions were collected and analyzed by MALDI-TOF MS.

Table 42. Fractions collected of photolyzed **231** prior to MALDI-TOF MS analysis

Fraction (min)	Products observed
49.0-50.6	**214, 237-240**
50.7-52.2	**214, 237, 238**
53.3-55.1	**235, 236**
55.2-56.4	**214, 232-240**
56.5-58.0	**232-234**
58.0-59.1	**233, 234**
60.0-60.6	**234**

Competitive kinetic studies using DMTHF and *i*-PrOH. Photolyses were carried out for 2 h using 4 lamps in 9/1 CH_3CN/H_2O under degassed conditions. The concentration of **130** was 0.1 mM. The concentration of 2,5-dimethyltetrahydrofuran (MTHF) ranged from 0 to 1.0 M, while the concentration of *i*-PrOH ranged from 0 to 10.4 M. Duplicate samples were prepared for each hydrogen atom donor concentration. After photolysis, the 5' benzoate ester of thymidine was added as an internal standard and the photolysates were transferred to Eppendorf tubes. The Pyrex tubes were rinsed with 1:1 CH_3CN/ H_2O and this was then combined with the photolysates. The photolysates were lyophilized, resuspended in 1:1 CH_3CN/ H_2O, and analyzed by HPLC utilizing UV detection at 230 nm (Gradient B).

Competitive kinetic studies using BME. Photolyses were carried out in 1:1 CH_3CN/20 mM HCO_2NH_4, pH 6.2 for 3 h under aerobic conditions using 2 lamps. The concentration of **130** was 8.3 μM and the concentration of BME ranged from 100-400 mM. Low concentrations of **130** were employed in order to maintain O_2 under pseudo first-order conditions. Duplicate samples were prepared of each BME concentration. After photolysis, the 5'-benzoate ester of thymidine was added as an internal standard and the photolysates were transferred to Eppendorf tubes. The tubes were rinsed with 1:1 CH_3CN/20 mM HCO_2NH_4, pH 6.2, and this was then combined with the photolysates. BME was added to bring all samples to equal thiol concentration and the samples maintained at ambient temperature for 1 h. The photolysates were lyophilized, resuspended in 1:1 CH_3CN/20 mM HCO_2NH_4, pH 6.2, and analyzed by HPLC utilizing

UV detection at 230 nm (Gradient A). The rate of BME trapping was estimated by assuming $k_{O_2}[O_2] = 4 X 10^5\ s^{-1}$.

Measurement of 2-Deoxyribonolactone in photolysates. Photolyses were carried out in 4:1 H_2O/CH_3CN for 8 h using 2 lamps. The concentration of **130** was 25 μM and the concentration of BME ranged from 0 – 5 mM. After photolysis, the tubes were rinsed with 1:1 CH_3CN/20 mM HCO_2NH_4, pH 6.2, and this was then combined with the photolysates, which were then lyophilized. The photolysates were resuspended in 1:1 CH_3CN/H_2O mM HCO_2NH_4, pH 6.2, and analyzed by HPLC utilizing UV detection at 230 nm (Gradient C).

General procedure for cytochrome C superoxide assay. A solution of **122a** (50 μM), cytochrome C (50 μM), and catalase (1 μg) in 50 mM phosphate buffer (pH 8.0), 0.1 mM EDTA was prepared in a UV cuvette. A control sample lacking **122a** was prepared in the same way. The samples were photolyzed at 350 nM (2 lamps). The absorbance of each solution was checked by UV-Vis at 550 nm at appropriate time intervals up to 90 min.

General procedure for epinephrine superoxide assay. A photolysis cocktail containing **122a** (5 μM) and epinephrine (5 μM) was prepared in 50 mM phosphate and 1 mM desferal. A control sample was prepared without **122a**. The samples were placed in UV cuvettes and photolyzed at 350 nM (2 lamps). The absorbances were checked by UV-Vis at 480 nm at appropriate intervals.

UV Melting Measurements. UV melting experiments were carried out using quartz cells with a path length of 1 cm in a Beckman DU 640 spectrophotometer equipped with a temperature control unit. A DNA duplex concentration of 5μM in 10 mM PIPES, 10 mM $MgCl_2$, 100 mM NaCl, pH 7.0 was used. Prior to the melting experiment, the duplex was hybridized by heating at 90 °C for 5 min then allowing to cool to ambient temperature. In the melting experiment, the temperature was held at 25 °C for 10 min, then ramped linearly to 75 °C at 0.5 °C/min while monitoring the change in UV absorbance at 260 nm. The data was processed using Microcal Origin 3.5 by plotting the absorbance versus temperature and fitting the curve to the following equation:

$$y = \frac{a}{\left(1 + e^{(b-cx)}\right)} + d$$

where a,b,c, and d are constants. The melting temperature was calculated by determining the maximum value of the derivative of this function.

Circular dichroism measurements. Circular dichroism measurements were collected using a Jasco instrument. Quartz samples cells having a path length of 1.0 mM were used. Samples consisted of 10 μM duplex in 10 mM KH_2PO_4, 100 mM NaCl pH 7.2. Samples were scanned from 350-210 nm.

General procedure for kinetic isotope effect experiments.[B45] Ten 100 μL samples of the appropriate 5'- or 3'-^{32}P end-labeled deuterated oligonucleotide as well as ten

samples of the control non-deuterated oligonucleotide were prepared in pyrex tubes. The samples were photolyzed at 350 nm for 10 min then transferred to eppendorf tubes. The photolysates were precipitated from NaOAc and calf thymus DNA. Samples were treated with either 0.1 M NaOH or 1.0 M piperidine. The samples were analyzed by PAGE.

Dephosphorylation of photolysates with T4 polynucleotide kinase. The appropriate 5'-^{32}P end-labeled oligonucleotide was photolyzed and precipitated from NaOAc. The precipitated DNA was treated with either 0.1 M NaOH (37 °C, 20 min) or 1.0 M piperidine (90 °C, 20 min). The NaOH treated samples were neutralized HCl after incubation. The base treated samples were then lyophilized. The DNA pellet was resuspended in 50 μL T4 polynucleotide kinase buffer (70 mM Tris-HCl, pH 7.6, 10 mM $MgCl_2$, 5 mM dithiothreitol). T4 polynucleotide kinase (10 U) was added and the reaction was incubated at 37 °C for 2 h. The kinase treated sample was precipitated from NaOAc and calf thymus DNA prior to resuspension in formamide loading buffer and analysis by PAGE.

Dephosphorylation of photolysates with calf intestinal alkaline phosphatase. The appropriate 5'-^{32}P end-labeled oligonucleotide was photolyzed and precipitated from NaOAc. The precipitated DNA was treated with either 0.1 M NaOH (37 °C, 20 min) or 1.0 M piperidine (90 °C, 20 min). The NaOH treated samples were neutralized HCl after incubation. The base treated samples were then lyophilized. Samples were resuspended

in calf intestinal alkaline phosphatase buffer (50 mM Tris, 1 mM $MgCl_2$, pH 9.0) and calf intestinal alkaline phosphatase (50 U) was added. The dephosphorlyated sample was precipitated from NaOAc and calf thymus DNA prior to resuspension in formamide loading buffer and analysis by PAGE.

Enzymatic digestion of oligonucleotides. The appropriate oligonucleotide (10 nmol) was dissolved in 1.0 M $MgCl_2$ (10 μL). A solution of nuclease P1 (10 μL, 0.31 U) in 30 mM NaOAc, pH 5.3, 200 mM $ZnCl_2$ was added and the digestion sample was incubated at 37 °C for 2 h. Calf intestinal alkaline phosphatase buffer (10 μL, 500 mM Tris, 10 mM $MgCl_2$, pH 9.0) and calf intestinal alkaline phosphatase (50U) were added to the sample. Snake venom phosphodiesterase (0.18 U) which had been reconstituted from lyophilized solid into 110 mM Tris, pH 8.9, 110 mM NaCl, 15 mM $MgCl_2$, with 50% glycerol was added and the digestion sample was incubated at 37 °C for an additional 12 h. The reaction mixture was passed through a Microcon cellulose filter (10,000 molecular weight cutoff, Amicon Inc.) by centrifugation at 12,000 RPM. The filter was washed with H_2O (2 X 200 μL) and the combined filtrate was lyophilized. The sample was resuspended in H_2O (75 μL) and analyzed by HPLC (Gradient E) with UV detection at 260 and 215 nm. Typically, adenosine (3μL of a 2mM solution) was added to a 25 μL portion of the resuspended digested oligonucleotide and the sample was diluted to 30 μL prior to analysis. The retention times of the nucleosides liberated by enzymatic digestion had retention times identical to authentic samples (Table 142).

Table 142. The retention times of nucleosides produced by enzymatic digestion of oligonucleotides.

Nucleoside	Retention time (min)
dC	11.9
dG	16.9
T	17.9
A	20.2
dA	21.3
122a	29.4
122b	29.2

Oxidation of photolysates using Na_2IrCl_6.[150] To a 30 μL volume of the appropriate radiolabeled photolysate was added 50 μL of a 1.0 mM solution of Na_2IrCl_6 and 20 μL of H_2O. The reaction was allowed to stand at ambient temperature for 1 h then precipitated from sodium acetate and calf thymus DNA as usual. The resulting pellet was resuspended in 100 μL of 1.0 M piperidine and heated at 90 °C for 30 min (not the typical 20 min), lyophilized, and analyzed by gel electrophoresis.

Analysis of pyrimidine hydrate decomposition. Aliquots were taken at appropriate times from a 1 mM solution (95/5 20 mM KH_2PO_4/CH_3CN) of the respective pyrimidine hydrate maintained at 37 °C or 90 °C. An internal standard (10 μL of a 1 mM solution of 5'-benzoyl thymidine for 2'-deoxyuridine hydrates, *p*-methoxybenzyl alcohol for

thymidine hydrates) was added and the samples were diluted with 1:1 40 mM KH_2PO_4, pH 6.0/ CH_3CN to inhibit further decomposition.

^{1}H NMR analysis of 2'-deoxyuridine hydrate epimerization. C6-Hydrate **140a** or **140b** (10 mg, 0.028 mmol) and internal standard (*i*-PrOH, 0.3 mg, 0.005 mmol) were dissolved in 2.8:1 D_2O/ CD_3CN (0.95 mL). Samples were placed in NMR tubes and incubated in a 37 ^{0}C bath. ^{1}H NMR spectra were collected at appropriate time intervals. The extent of epimerization was determined by observing the change in integration of the C-6 hydrogen peaks (δ 5.29 for **140a**, δ 5.22 for **140b**). The rate of epimerization was deterimined by plotting the following equation:

$$-\ln\frac{\Delta[\mathbf{140}]_t}{\Delta[\mathbf{140}]_0} = (k_1 + k_{-1})t$$

where $\Delta[\mathbf{140}]_t$ is the difference between the concentration of **140** at time t and its equilibrium concentration. The difference between the initial concentration of **7** and its equilibrium concentration is given by $\Delta[\mathbf{140}]_0$. The individual rate constants for epimerization , k_1 and k_{-1}, obtained from the plot were obtained using the equilibrium constant for the two diastereomers.

5 References

1 von Sonntag, C. *The Chemical Basis of Radiation Biology*; Taylor and Francis: London, 1987.

2 Steenken, S. "Purine Bases, Nucleosides, and Nucleotides: Aqueous Solution Redox Chemistry and Transformation Reactions of Their Radical Cations and e- and OH· adducts." *Chem. Rev.*, **1989**, *89*, 503.

3 Burrows, C. J.; Muller, J. G. "Oxidative Nucleobase Modifications Leading to Strand Scission." *Chem. Rev.* **1998**, *98*, 1109.

4 Candeias, L. P.; Steenken, S. "Reaction of HO· with Guanine Derivatives in Aqueous Solution: Formation of Two Different Redox-Active OH-Adduct Radicals and Their Unimolecular Transformation Reactions. Properties of G(-H)·." *Chem. Eur. J.* **2000**, **7**, 475.

5 Wallace, S. S. "Enzymatic Processing of Radiation-Induced Free Radical Damage in DNA." *Radiat. Res.* **1998**, *150*, S60.

6 Karam, L. R.; Dizdaroglu, M.; Simic, M. "Intramolecular H Atom Abstraction from the Sugar Moiety by Thymine Radicals in Oligo- and Polydeoxynucleotides." *Radiation Res.* **1988**, *116*, 210.

7 Lemaire, D. G. E.; Bothe, E.; Schulte-Frohlinde, D. "Yields of Radiation-Induced Main Chain Scission of Poly U in Aqueous Solution: Strand Break Formation via Base Radicals." *Int. J. Radiat. Biol.* **1984**, *45*, 351.

8 Deeble, D. J.; von Sonntag, C. "γ-Radiolysis of PolyU in Aqueous Solution. The Role of Primary Sugar and Base Radicals in the Release of Undamaged Uracil." *Int. J. Radiat. Biol.* **1984**, *46*, 247.

9 Deeble, D. J.; Schulz, D.; von Sonntag, C. "Reactions of OH Radicals with PolyU in Deoxygenated Solutions: Sites of OH Radical Attack and the Kinetics of Base Release." *Int. J. Radiat. Biol.* **1986**, *49*, 915.

10 Hildenbrand, K.; Schulte-Frohlinde, D. "E.S.R. Studies on the Mechanism of Hydroxyl Radical-Induced Strand Breakage of Polyuridylic Acid." *Int. J. Radiat. Biol.* **1989**, *55*, 725.

11 Schulte-Frohlinde, D.; Bothe, E.; Behrens, G. "Radiation Chemistry of Polyuridylic Acid in Aqueous Solution." *Radiat. Phys. Chem.* **1985**, *26*, 481.

12 Deeble, D. J.; von Sonntag, C. "Radiolysis of PolyU in Oxygenated Solution." *Int. J. Radiat. Biol.* **1986**, *49*, 927.

[13] Teoule, R.; Bonicel, A.; Bert, C.; Cadet, J.; Polverelli, M. "Identification of Radioproducts Resulting from the Breakage of Thymine Moiety by Gamma Irradiation of *E. Coli*. DNA in an Aerated Aqueous Solution." *Radiation Res.* **1974**, *57*, 46.

[14] Jones, G. D. D.; O' Neill, Peter. "Kinetics of Radiation-Induced Strand Break Formation in Single-Stranded Pyrimidine Polynucleotides in the Presence and Absence of Oxygen; a Time-Resolved Light-Scattering Study." *Int. J. Radiat. Biol.* **1991**, *59*, 1127.

[15] Bothe, E.; Behrens, G.; Bohm, E.; Sethuram, B.; Schulte-Frohlinde, D. "Hydroxyl Radical-Induced Strand Break Formation of PolyU in the Presence of Oxygen: Comparison of the Rates as Determined by Conductivity, ESR, and Rapid-Mix Experiments with a Thiol." *Int. J. Radiat. Biol.* **1986**, *49*, 57.

[16] Lomax, M. E.; Gulston, M. K.; O' Neill, P. "Chemical Aspects of Clustered DNA Damage Induction by Ionising Radiation." *Radiat. Prot. Dosimetry* **2002**, *99*, 63.

[17] Venkhataraman, R.; Donald. C. D.; Roy, R.; You, H. J.; Doetsch, P. W.; Kow, Y. W. "Enzymatic Processing of DNA Containing Tandem Dihydrouracil by Endonucleases III and VIII." *Nucleic Acids Res.* **2001**, *29*, 407.

[18] Box, H. C.; Freund, H. G.; Budzinski, E. E.; Wallace, J. C.; Maccubbin, A. E. "Free Radical-Induced Double Base Lesions." *Radiat. Res.* **1995**, *141*, 91.

[19] Box, H. C.; Patzyc, H. B.; Dawidzik, J. B.; Wallace, J. C.; Freund, H. G.; Iijima, H.; Budzinski. "Double Base Lesions in DNA X-Irradiated in the Presence or Absence of Oxygen." *Radiat. Res.* **2000**, *153*, 442.

[20] Maccubbin, A. E.; Iijima, H.; Ersing, N.; Dawidzic, J. B.; Patrzyc, H. B.; Wallace, J. C.; Budzinski, E. E.; Freund, H. G.; Box, H. C. "Double-Base Lesions Are Produced by Free Radicals." *Arch. Biochem. Biophys.* **2000**, *375*, 119.

[21] Bourdat, A.; Douki, T.; Frelon, S.; Gasparutto, D.; Cadet, J. "Tandem Base Lesions Are Generated by Hydroxyl Radical within Isolated DNA in Aerated Aqueous Solution." *J. Am. Chem. Soc.* **2000**, *122*, 4549.

[22] Bellon, S.; Ravanat, J.; Gasparutto, D.; Cadet, J. "Cross-Linked Thymine-Purine Base Tandem Lesions: Synthesis, Characterization, and Measurement in γ-Irradiated Isolated DNA." *Chem. Res. Toxicol.* **2002**, *15*, 598.

[23] Douki, T.; Rivière, J.; Cadet, J. "DNA Tandem Lesions Containing 8-Oxo-7,8-dihydroguanine and Formanido Residues Arise from Intramolecular

Addition of Thymine Peroxyl Radical to Guanine." *Chem. Res. Toxicol.* **2002**, *15*, 445.

[24] Greenberg, M. M.; Barvian, M. R.; Cook, G. P.; Goodman, B. K.; Matray, T. J.; Tronche, C.; Venkatesan, H. "DNA Damage Induced via 5,6-Dihydrothymid-5-yl in Single-Stranded Oligonucleotides." *J. Am. Chem. Soc.* **1997**, *119*, 1828.

[25] Tallman, K. A.; Greenberg, M. M. "Oxygen-Dependent DNA Damage Amplification Involving 5,6-Dihydrothymidin-5-yl in a Structurally Minimal System." *J. Am. Chem. Soc.* **2001**, *123*, 5181.

[26] Greenberg, M. M. "Investigating Nucleic Acid Damage Processes via Independent Generation of Reactive Intermediates." *Chem. Res. Toxicol.* **1998**, *11*, 1235.

[27] Barvian, M. R.; Greenberg, M. M. "Independent Generation of the Major Adduct of Hydroxyl Radical and Thymidine. Examination of Intramolecular Hydrogen Atom Transfer in Competition with Thiol Trapping." *Tetrahedron Lett.* **1992**, *33*, 6057.

[28] Barvian, M. R.; Barkley, R. M.; Greenberg, M. M. "Reactivity of 5,6-Dihydro-5-hydroxythymid-6-yl Generated via Photoinduced Single Electron Transfer and the Role of Cyclohexa-1,4-diene in the Photodeoxygenation Process." *J. Am. Chem. Soc.* **1995**, *117*, 4894.

[29] Krisch, R. E.; Flick, M. B.; Trumbore, C. N. "Radiation Chemical Mechanisms of Single- and double-strand break formation in irradiated SV40 DNA." *Radiat. Res.* **1991**, *126*, 251.

[30] deLara, C. M.; Jenner, T. J.; Stewart Townsend, K. M.; Marsden, S. J.; O' Neill, P. "The Effect of Dimethyl Sulfoxide on the Induction of DNA Double-Strand Breaks in V79-4 Mammalian Cells by Alpha Particles." *Radiat. Res.* **1995**, *144*, 43.

[31] Steenken, S.; Goldbergerova, L. "Photoionization of Organic Phosphates by 193 nm Laser Light in Aqueous Solution: Rapid Intramolecular H-Transfer to the Primarily Formed Phosphate Radical. A model for Ionization-Induced Chain-Breakage in DNA?" *J. Am. Chem. Soc.* **1998**, *120*, 3928.

[32] Melvin, T.; Botchway, S. W.; Parker, A. W.; O' Neill, P. "Induction of Strand Breaks in Single-Stranded Polyribonucleotides and DNA by Photoionization: One Electron Oxidized Nucleobase Radicals as Precursors." *J. Am. Chem. Soc.* **1996**, *118*, 10031.

33 Deeble, D. J.; Schuchmann, M. N.; Steenken, S.; von Sonntag, C. "Direct Evidence for the Formation of Thymine Radical Cations from the Reaction of $SO_4^{\cdot-}$ with Thymine Derivatives: A Pulse Radiolysis Study with Optical and Conductance Detection." *J. Phys. Chem.* **1990**, *94*, 8186.

34 Wagner, J. R.; van Lier, J. E.; Johnston, L. J. "Quinone Sensitized Electron Transfer Photooxidation of Nucleic Acids: Chemistry of Thymine and Thymidine Radical Cations in Aqueous Solution." *Photchem. Photobiol.* **1990**, *52*, 333.

35 Krishna, C. M.; Decarroz, C.; Wagner, J. R.; Cadet, J.; Riesz, P. "Menadione Sensitized Photooxidation of Nucleic Acid and Protein Constituents. An ESR and Spin-Trapping Study." *Photochem. Photobiol.* **1987**, *46*, 175.

36 Jovanovic, S. V.; Simic, M. G. "One-Electron Redox Potentials of Purines and Pyrimidines." *J. Phys. Chem.* **1986**, *90*, 974.

37 Steenken, S.; Jovanovic, S. V. "How Easily Oxidizable is DNA? One-Electron Reduction Potentials of Adenosine and Guanosine Radicals in Aqueous Solution." *J. Am. Chem. Soc.* **1997**, *119*, 617.

38 Angelov, D.; Spassky, A.; Berger, M.; Cadet, J. "High-Intensity UV Laser Photolysis of DNA and Purine 2'-Deoxyribonucleotides: Formation of 8-Oxopurine Damage and Oligonucleotide Strand Cleavage as Revealed by HPLC and Gel Electrophoresis Studies." *J. Am. Chem. Soc.* **1997**, *119*, 11373.

39 Cullis, P. M.; Malone, M. E.; Merson-Davies, L. A. "Guanine Radical Cations Are Precursors of 7,8-Dihydro-8-oxo-2'-deoxyguanosine But Are Not of Immediate Strand Breaks in DNA." *J. Am. Chem. Soc.* **1996**, *118*, 2775.

40 Spassky, Annick; Angelov, D. "Influence of the Local Helical Conformation on the Guanine Modifications Generated from One-Electron DNA Oxidation." *Biochemistry* **1997**, *36*, 6571.

41 Cadet, J.; Berger, M.; Buchko, G. W.; Joshi, P. C.; Raoul, S.; Ravanat, J. "2,2-Diamino-4-[(3,5-di-*O*-acetyl-2-deoxy-β-D-*erythro*-pentofuranosyl)amino]-5-(2*H*)-oxazolone: A novel and Predominant Radical Oxidation Product of 3',5'-Di-*O*-acetyl-2'-deoxyguanosine." *J. Am. Chem. Soc.* **1994**, *116*, 7403.

42 Sutcliffe, R.; Anpo, M.; Stolow, A.; Ingold, K. U. "Kinetic Applications of Electron Paramagnetic Resonance Spectroscopy. 39. Bimolecular Self-Reactions of Some *N*-Alkylcarboxamidyl, *N*-Alkylsulfonamidyl, *N*-Alkyl-*N*-(alkoxycarbonyl)aminyl Radicals. Intermolecular Hydrogen Atom

Abstraction by N-Ethylpropionamidyl Radical." *J. Am. Chem. Soc.* **1982**, *104*, 6064.

[43] Pogozelski, W. K.; Tullius, T. D. "Oxidative Strand Scission of Nucleic Acids: Routes Initiated by Hydrogen Abstraction from the Sugar Moiety." *Chem. Rev.* **1988**, *98*, 1089.

[44] Giese, B.; Dussy, A.; Elie, C.; Erdmann, P.; Schwitter, U. "Synthesis and Selective Radical Cleavage of C4' Modified Oligonucleotides." *Angew. Chem. Int. Ed. Engl.* **1994**, *33*, 1861.

[45] Debije, M. G.; Bernhard, W. A. "Electron Paramagnetic Resonance Evidence for a C3' Sugar Radical in Crystalline d(CTCTCGAGAG) X-Irradiated at 4 K." *Radiation Res.* **2001**, *155*, 687.

[46] Önal, A. M.; Lemaire, D. G. E.; Bothe, E.; Schulte-Frohlinde, D. "γ-Radiolysis of Poly(A) in Aqueous Solution: Efficiency of Strand Break Formation by Primary Water Radicals." *Int J. Radiat. Biol.* **1988**, *53*, 787.

[47] Steenken, S.; Jovanovic, S. V.; Candeias, L. P.; Reynisson. "Is 'Frank' DNA-Strand Breakage via the Guanine Radical Thermodynamically and Sterically Possible?" *Chem. Eur. J.* **2001**, *7*, 2829.

[48] Dizdaroglu, M.; Jaruga, P.; Birincioglu, M.; Rodriguez, H. "Free Radical-Induced Damage to DNA: Mechanisms and Measurement." *Free Radic. Biol. Med.* **2002**, *32*, 1102.

[49] Breen, A. P.; Murphy, J. A. "Reactions of Oxyl Radicals with DNA." *Free Radic. Biol. Med.* **1995**, *18*, 1033.

[50] Tallman, K. A.; Tronche, C.; Yoo, D. J.; Greenberg, M. M. "Release of Superoxide from Nucleoside Peroxyl Radicals, a Double-Edged Sword?" *J. Am. Chem. Soc.* **1998**, *120*, 4903.

[51] Al-Sheikhly, M. I.; Hissung, A.; Schuchmann, H.; Schuchmann, M. N.; von Sonntag, C. "Radiolysis of Dihydrouracil and Dihydrthymidine in Aqueous Solutions Containing Oxygen; First- and Second-Order Reactions of the Organic Peroxyl Radicals; the Role of Isopyrimidines as Intermediates." *J. Chem. Soc. Perkin Trans. 2* **1984**, 601.

[52] Wagner, J. R.; van Lier, J. E.; Berger, M.; Cadet, J. "Thymidine Hydroperoxides: Structural Assignment, Conformational Features, and Thermal Decomposition in Water." *J. Am. Chem. Soc.* **1994**, *116*, 2235.

[53] Bjelland, S.; Eide, L.; Time, R. W.; Stote, R.; Eftedal, I.; Volden, G.; Seeberg, E. "Oxidation of Thymine to 5-Formyluracil in DNA: Mechanisms of formation, Structural Implications, and Base Excision by Human Cell Free Extracts." *Biochemistry* **1995**, *34*, 14758.

[54] Tofigh, S.; Frenkel, K. "Effect of Metals on Nucleoside Hydroperoxide, a Product of Ionizing Radiation in DNA." *Free Radic. Biol. Med.* **1989**, *7*, 131.

[55] Miaskiewicz, K.; Osman, R. "Theoretical Study on the Deoxyribose Radicals Formed by Hydrogen Abstraction." *J. Am. Chem. Soc.* **1994**, *116*, 232.

[56] Colson, A.; Sevilla, M. D. "Structure and Relative Stability of Deoxyribose Radicals in a Model DNA Backbone: *Ab Initio* Molecular Orbital Calculations." *J. Phys. Chem.* **1995**, *99*, 3867.

[57] Wetmore, S. D.; Boyd, R. J.; Eriksson, L. A. "A Comprehensive Study of Sugar Radicals in Irradiated DNA." *J. Phys. Chem. B.* **1998**, *102*, 7674.

[58] Toure, P.; Villena, F.; Melikyan, G. G. "Thymidine 3',5'-Diphosphoric Acid Derived Cations and Radicals: *Ab Initio Study*." *Org. Lett.* **2002**, *4*, 3989.

[59] Luo, N.; Litvin, R.; Osman, R. "Theoretical Studies of Ribose and Its Radicals Produced by Hydrogen Abstraction from Ring Carbons." *J. Phys. Chem. A.* **1999**, *103*, 592.

[60] Sigman, D. S.; Graham, D. R.; D'Aurora, V.; Stern, A. M. "Oxygen-Dependent Cleavage of DNA by the 1,10-Phenanthroline-Cuprous Complex." *J. Biol. Chem.* **1979**, *254*, 12269.

[61] Sigman, D. S.; Mazumder, A.; Perrin, D. M. "Chemical Nucleases." *Chem. Rev.* **1993**, *93*, 2295.

[62] Dedon, P. C.; Goldberg, I. H. "Free-Radical Mechanisms Involved in the Formation of Sequence-Dependent Bistranded DNA Lesions by the Antitumor Antibiotics Bleomycin, Neocarzinostatin, and Calicheamicin." *Chem. Res. Toxicol.* **1992**, *5*, 311.

[63] Emmanuel, C. J.; Newcomb, M.; Ferreri, C.; Chatgilialoglu, C. "Kinetics of 2'-Deoxyuridin-1'-yl Radical Reactions." *J. Am. Chem. Soc.* **1999**, *121*, 2927.

[64] Chatgilialoglu, C.; Gimisis, T. "Fate of the C1' Peroxyl Radical in the 2'-Deoxyuridine System." *Chem. Commun.* **1998**, 1249.

[65] Hwang, J.; Greenberg, M. M. "Kinetics and Stereoselectivity of Thiol Trapping of Deoxyuridin-1'-yl in Biopolymers and Their Relationship to the

Formation of Premutagenic α-Deoxynucleotides." *J. Am. Chem. Soc.* **1999**, *121*, 4311.

66 Chatgilialoglu, C.; Ferreri, C.; Bazzanini, R.; Guerra, M.; Choi, S.; Emanuel, C. J.; Horner, J. H.; Newcomb, M. "Models of DNA C1' Radicals. Structural, Spectral, and Chemical Properties of the Thyminylmethyl Radical and the 2'-Deoxyuridin-1'-yl Radical." *J. Am. Chem. Soc.* **2000**, *122*, 9525.

67 Cook, G. P.; Greenberg, M. M. "A Novel Mechanism for the Formation of Direct Strand Breaks upon Anaerobic Photolysis of Duplex DNA Containing 5-Bromodeoxyuridine." *J. Am. Chem. Soc.* **1996**, *118*, 10025.

68 Cook, G. P.; Chen, T.; Koppisch, A. T.; Greenberg, M. M. "The Effects of Secondary Structure and O_2 on the Formation of Direct Strand Breaks upon UV Irradiation of 5-Bromodeoxyuridine-Containing Oligonucleotides." *Chem. Biol.* **1999**, *6*, 451.

69 Chen, T.; Cook, G. P.; Koppisch, A. T.; Greenberg, M. M. "Investigation of the Origin of the Sequence Selectivity for the 5-Halo-2'-deoxyuridine Sensitization of DNA to damage by UV-Irradiation." *J. Am. Chem. Soc.* **2000**, *122*, 3861.

70 Sugiyama, H.; Tsutsumi, Y.; Fujimoto, K.; Saito, I. "Photoinduced Deoxyribose C2' Oxidation in DNA. Alkali-Dependent Cleavage of Erythrose-Containing Sites via a Retroaldol Reaction." *J. Am. Chem. Soc.* **1993**, *115*, 4443.

71 Sugiyama, H.; Fujimoto, K.; Saito, I. "Evidence for Intrastrand C2' Hydrogen Abstraction in Photoirradiation of 5-Halouracil-Containing Oligonucleotides by Using Stereospecifically C2'-Deuterated Deoxyadenosine." *Tetrahedron Lett.* **1996**, *37*, 1805.

72 Kawai, K.; Saito, I.; Sugiyama, H. "Conformation-Dependent Photochemistry of 5-Halouracil-Containing DNA: Stereospecific 2' α-Hydroxylation of Deoxyribose in Z-form DNA." *J. Am. Chem. Soc.* **1999**, *121*, 1391.

73 Sitlani, A.; Long, E. C.; Pyle, A. M.; Barton, J. K. "DNA photocleavage by Phenanthrenequinone Diimine Complexes of Rhodium (III): Shape-Selective Recognition and Reaction." *J. Am Chem. Soc.* **1992**, *114*, 2303.

74 Pyle, A. M.; Long, E. C.; Barton, J. K. "Shape-Selective Targeting of DNA by (Phenanthrenequinone Diimine) Rhodium (III) Photocleaving Agents. *J. Am. Chem. Soc.* **1989**, *111*, 4520.

75 Barton, J. K. "Metals and DNA: Molecular Left-Handed Complements." *Science* **1986**, *233*, 727.

76 Stubbe, J.; Kozarich, J. W. "Mechanisms of Bleomycin-Induced DNA Degradation." *Chem. Rev.* **1997**, *87*, 1107.

77 Rabow, L. E.; Stubbe, J.; Kozarich, J. W. "Identification and Quantitation of the Lesion Accompanying Base Release in Bleomycin-Mediated DNA Degradation." *J. Am. Chem. Soc.* **1990**, *112*, 3196.

78 Absalon, M. J.; Wu, W.; Kozarich, J. W.; Stubbe, J. "Sequence-Specific Double-Strand Cleavage of DNA by Fe-Bleomycin. 2. Mechanism and Dynamics." *Biochemistry* **1995**, *34*, 2076.

79 Kozarich, J. W.; Worth, L., Jr.; Frank, B. L.; Christner, D. F.; Vanderwall, D. E.; Stubbe, J. "Sequence-Specific Isotope Effects on the Cleavage of DNA by Bleomycin." *Science* **1989**, *245*, 1396.

80 Giese, B.; Beyrich-Graf, X.; Erdmann, P.; Petretta, M.; Schwitter, U. "The Chemistry of Single-Stranded 4'-DNA Radicals: Influence of the Radical Precursor on Anaerobic and Aerobic Strand Cleavage." *Chem. Biol.* **1995**, *2*, 367.

81 Giese, B.; Beyrich-Graf, X.; Erdmann, P.; Giraud, L.; Imwinkelreid, P.; Müller, S. N.; Schwitter, U. "Cleavage of Single-Stranded 4'-Oligonucleotide Radicals in the Presence of O_2." *J. Am. Chem. Soc.* **1995**, *117*, 6146.

82 Beyrich-Graf, X.; Müller, S. N.; Giese, B. "Oxidation of 4'-Deoxyribonucleoside Radicals to 4'-Deoxyribonucleoside Cations. A Model for the Function of Bleomycin." *Tetrahedron Lett.* **1998**, *39*, 1553.

83 Dussy, A.; Meggers, E.; Giese, B. "Spontaneous Cleavage of 4'-DNA Radicals under Aerobic Conditions: Apparent Discrepancy between Trapping Rates and Cleavage Products." *J. Am. Chem. Soc.* **1998**, *120*, 7399.

84 Dizdaroglu, M.; von Sonntag, C.; Schulte-Frohlinde, D. "Strand Breaks and Sugar Release by γ-Irradiation of DNA in Aqueous Solution." *J. Am. Chem. Soc.* **1975**, *97*, 2277.

85 Sy, D.; Savoye, C.; Begusova, M.; Michalik, V.; Charlier, M.; Spotheim-Maurizot, M. "Sequence-Dependent Variations of DNA Structure Modulate Radiation-Induced Strand Breakage." *Int. J. Radiat. Biol.* **1997**, *72*, 147.

86 Kappen, L. S.; Goldberg, I. H. "Deoxyribonucleic Acid Damage by Neocarzinostatin Chromophore: Strand Breaks Generated by Selective Oxidation of C5' of Deoxyribose." *Biochemistry* **1983**, *22*, 4872.

[87] Kappen, L. S.; Goldberg, I. H.; Frank, B. L.; Worth, L., Jr; Christner, D. F.; Kozarich, J. W.; Stubbe, J. "Neocarzinostatin-Induced Hydrogen Atom Abstraction from C4' and C5' of the T Residue at a d(GT) Step in Oligonucleotides: Shuttling between Deoxyribose Attack Sites Based on Isotope Selection Effects." *Biochemistry* **1991**, *30*, 2034.

[88] Frank, B. L.; Worth, L., Jr.; Christner, D. F.; Kozarich, J. W.; Stubbe, J.; Kappen, L. S.; Goldberg, I. H. "Isotope Effects on the Sequence-Specific Cleavage of DNA by Neocarzinostatin: Kinetic Partitioning between 4'- and 5'-Hydrogen Abstraction at Unique Thymidine Sites." *J. Am. Chem. Soc.* **1991**, *113*, 2271.

[89] Chin, D.; Kappen, L. S.; Goldberg, I. H. "3'-Formyl Phosphate-Ended DNA: High-Energy Intermediate in Antibiotic-Induced DNA Sugar Damage." *Proc. Natl. Acad. Sci. USA* **1987**, *84*, 7070.

[90] Wagner, J. R.; Decarroz, C.; Berger, M.; Cadet, J. "Hydroxyl-Radical-Induced Decomposition of 2'-Deoxycytidine in Aerated Aqueous Solution." *J. Am. Chem. Soc.* **1999**, *121*, 4101.

[91] Jaruga, P.; Birincioglu, M.; Rodriguez, H.; Dizdaroglu, M. "Mass Spectrometric Assays for the Tandem Lesion 8,5'-Cyclo-2'-deoxyguanosine in Mammalian DNA." *Biochemistry* **2002**, *41*, 3703.

[92] Dizdaroglu, M.; Jaruga, P.; Rodriguez, H. "Identification and Quantification of 8,5'-Cyclo-2'-deoxyadenosine in DNA by Liquid Chromatography/Mass Spectrometry." *Free Radic. Biol. Med.* **2001**, *30*, 774.

[93] Muller, E.; Gasparutto, D.; Cadet, J. "Chemical Synthesis and Biochemical Properties of Oligonucleotides that Contain the (5'*S*, 5*S*, 6*S*)-5', 6-Cyclo-5-hydroxy-5,6-dihydro-2'-deoxyuridine DNA Lesion." *Chem. Biochem.* **2002**, *3*, 534.

[94] Romieu, A.; Gasparutto, D.; Cadet, J. "Synthesis and Characterization of Oligodeoxynucleotides Containing the Two 5*R* and 5*S* Diastereomers of (5'*S*, 6*S*)-5', 6-Cyclo-5-hydroxy-5,6-dihydrothymidine; Radiation Induced Tandem Lesions of Thymidine." *J. Chem. Soc., Perkin Trans. 1*, **1999**, 1257.

[95] Sutherland, B. M.; Bennett, P. V.; Sidorkina, O.; Laval, J. "Clustered DNA Damages Induced in Isolated DNA and in Human Cells by Low Doses of Ionizing Radiation." *Proc. Natl. Acad. Sci. USA* **2000**, *97*, 103.

[96] Sutherland, B. M.; Bennett, P. V.; Sidorkina, O.; Laval, J. "Clustered Damages and Total Lesions Induced in DNA by Ionizing Radiation: Oxidized Bases and Strand Breaks." *Biochemistry* **2000**, *39*, 8026.

97 Milligan, J. R.; Aguilera, J. A.; Nguyen, T.-T. D.; Paglinawan, R. A.; Ward, J. F. "DNA Strand-Break Yields After Post-Irradiation Incubation with Base Excision Repair Endonucleases Implicate Hydroxyl Radical Pairs in Double-Strand Break Formation." *Int. J. Radiat. Biol.* **2000**, *76*, 1475.

98 Jenner, T. J.; Fulford, J.; O' Neill, P. "Contribution of Base Lesions to Radiation-Induced Clustered DNA Damage: Implication for Models of Radiation Response." *Radiat. Res.* **2001**, *156*, 590.

99 Prise, K. M.; Pullar, C. H. L.; Michael, B. D. "A study of Endonuclease III-Sensitive Sites in Irradiated DNA: Detection of α-Particle-Induced Oxidative Damage." *Carcinogenesis* **1999**, *20*, 905.

100 Gulston, M.; Fulford, J.; Jenner, T.; de Lara, C.; O' Neill, P. "Clustered DNA Damage Induced by γ Radiation in Human Fibroblasts (HF19), Hamster (V79-4) Cells and Plasmid DNA is Revealed as Fpg and Nth Sensitive Sites." *Nucleic Acids Res.* **2002**, *30*, 3464.

101 Weinfeld, M.; Rasouli-Nia, A.; Chaudhry, M. A.; Britten, R. A. "Response of Base Excision Repair Enzymes to Complex DNA Lesions." *Radiat. Res.* **2001**, *156*, 584.

102 Chaudhry, M. A.; Weinfeld, M. "The Action of Escherichia coli Endonuclease III on Multiply Damaged Sites in DNA." *J. Mol. Biol.* **1995**, *249*, 914.

103 Harrison, L.; Hatahet, Z.; Wallace, S. S. "In Vitro Repair of Synthetic Ionizing Radiation-Induced Multiply Damaged DNA Sites." *J. Mol. Biol.* **1999**, *290*, 667.

104 David-Cordonnier, M.; Cunniffe, S. M. T.; Hickson, I. D.; O' Neill, P. "Efficiency of Incision of an AP Site within Clustered DNA Damage by the Major Human AP Endonuclease." *Biochemistry* **2002**, *41*, 634.

105 Budworth, H.; Dianov, G. L. "Mode of Inhibition of Short-Patch Base Excision Repair by Thymine Glycol within Clustered DNA Lesions." *J. Biol. Chem.* **2003**, *278*, 9378.

106 Bourdat, A.; Gasparutto, D.; Cadet, J. "Synthesis and Enzymatic Processing of Oligodoxynucleotides Containing Tandem Base Damage." *Nucleic Acids Res.* **1999**, *27*, 1015.

107 Goodman, B. K.; Greenberg, M. M. "Independent Generation and Reactivity of 2'-Deoxyuridin-1'-yl." *J. Org. Chem.* **1996**, *61*, 2.

[108] Tronche, C.; Goodman, B. K.; Greenberg, M. M. "DNA Damage Induced via Independent Generation of the Radical Resulting from Formal Hydrogen Atom Abstraction From the C1'-position of a Nucleotide." *Chem. Biol.* **1998**, *5*, 263.

[109] Hwang, J.; Greenberg, M. M, Fuchs, T.; Gates, K. S. "Kinetics and Stereoselectivity of Thiol Trapping of Deoxyuridin-1'-yl in Biopolymers and Their Relationship to the Formation of Premutagenic α-Deoxynucleotides." *J. Am. Chem. Soc.* **1999**, *121*, 4311.

[110] Hwang, J.; Greenberg, M. M. "Reaction of Hypoxia-Selective Antitumor Agent Tirapazamine with a C1'-Radical in Single-Stranded and Double-Stranded DNA: The Drug and Its Metabolites Can Serve as Surrogates for Molecular Oxygen in Radical-Mediated DNA Damage Reactions." *Biochemistry* **1999**, *38*, 14248.

[111] Hwang, J.; Tallman, K. A.; Greenberg, M. M. "The Reactivity of the 2-Deoxyribonolactone Lesion in Single-Stranded DNA and its Implication in Reaction Mechanisms of DNA Damage and Repair." *Nucleic Acids Res.* **1999**, *27*, 3805.

[112] Hashimoto, M.; Greenberg, M. M.; Kow. Y. W.; Hwang, J.; Cunningham, R. R. "The 2-Deoxyribonolactone Lesion Produced in DNA by Neocarzinostatin and Other Damaging Agents Forms Cross-Links with the Base-Excision Repair Enzyme Endonuclease III." *J. Am. Chem. Soc.* **2001**, *123*, 3161.

[113] Anderson, A. S.; Hwang, J.; Greenberg, M. M. "Independent Generation and Reactivity of 2'-Deoxy-5-methyleneuridin-5-yl, a Significant Reactive Intermediate Produced from Thymidine as a Result of Oxidative Stress." *J. Org. Chem.* **2000**, *65*, 4648.

[114] Romieu, A.; Bellon, S.; Gasparutto, D.; Cadet, J. "Synthesis and UV Photolysis of Oligodeoxynucleotides That Contain 5-(Phenylthiomethyl)-2'-deoxyuridine: A Specific Photolabile Precursor of 5-(2'-Deoxyuridilyl)methyl Radical." *Org. Lett.* **2000**, *2*, 1085.

[115] Barvian, M. R.; Greenberg, M. M. "Independent Generation of 5,6-Dihydrothymid-5-yl in Single-Stranded Polythymidylate. O_2 is Necessary for Strand Scission." *J. Am. Chem. Soc.* **1995**, *117*, 8291.

[116] Barvian, M. R.; Greenberg, M. M. "Independent Generation of 5,6-Dihydrothymid-5-yl and Investigation of Its Ability to Effect Nucleic Acid Strand Scission via Hydrogen Atom Abstraction." *J. Org. Chem.* **1995**, *60*, 1916.

[117] Barvian, M. R.; Barkley, R. M.; Greenberg, M. M. "Reactivity of 5,6-Dihydro-5-hydroxythymid-6-yl Generated via Photoinduced Single Electron Transfer and the Role of Cyclohexa-1,4-diene in the Photodeoxygenation Process." *J. Am. Chem. Soc.* **1995**, *117*, 4894.

[118] Tanaka, H.; Hayakawa, H.; Iijima; S.; Haraguchi, K.; Miyasaka, T. "Lithiation of 3',5'-*O*-(Tetraisoproyldisiloxane-1,3-Diyl)-2'-Deoxyuridine: Synthesis of 6-Substituted 2'-Deoxyuridine." *Tetrahedron* **1985**, *41*, 861.

[119] Hanze, A. R. "Nucleic Acids IV. The Catalytic Reduction of Pyrimidine Nucleosides (Human Liver Deaminase Inhibitors)." *J. Am. Chem. Soc.* **1967**, *89*, 6720.

[120] Carter, K. N.; Greenberg, M. M. "Independent Generation and Study of 5,6-Dihydro-2'-deoxyuridin-6-yl, a Member of the Major Family of Reactive Intermediates Formed in DNA from the Effects of γ-Radiolysis." *J. Org. Chem.* **2003**, *68*, 4275.

[121] Schweizer, M. P.; Banta, E. B.; Witkowski, J. T.; Robins, R. K. "Determination of Pyrmidine Nucleoside *Syn*, *Anti* Conformational Preference in Solution by Proton and Carbon-13." *J. Am. Chem. Soc.* **1973**, *95*, 3770.

[122] Overend, R. E.; Stacey, M.; Teece, E. G.; Wiggins, L. F. "Desoxy Sugars V. A Reinvestigation of the Glycal Method for the Synthesis of 2-Desoxy-D and –L-Ribose" *J. Chem. Soc.* **1949**, 1879.

[123] Cadet, J.; Ducolomb, R.; Teoule, R. "Preparation, Isomerization Et Configuration Abolue Des 'Hydrates' De Thymidine." *Tetrahedron* **1977**, *33*, 1603.

[124] Boorstein, R. J.; Hilbert, T. P.; Cunningham, R. P.; Teebor, G. W. "Formation and Stability of Repairable Pyrimidine Photohydrates in DNA." *Biochemistry* **1990**, *29*, 10455.

[125] O'Donnell, R. E.; Boorstein, R. J.; Cunningham, R. P.; Teebor, G. W. "Effect of pH and Temperature on the Stability of UV-Induced Repairable Pyrimidine Hydrates in DNA." *Biochemistry* **1994**, *33*, 9875.

[126] Ganguly, T.; Duker, N. J. "Stability of DNA Thymine Hydrates." *Nucleic Acids Res.* **1991**, *19*, 3319.

[127] Fisher, G. J.; Johns, H. E. *Photochemistry & Photobiology of Nucleic Acids*; Wang, S. Y., Ed.; Academic: New York, 1976.

128 Schuchmann, M. N.; von Sonntag, C. "Hydroxyl Radical-Induced Oxidation of Diisopropyl Ether in Oxygenated Aqueous Solution. A Product and Pulse Radiolysis Study." *Z. Naturforsch* **1987**, 42b, 495.

129 Misra, H. P.; Fridovich, I. "Role of Superoxide Anion in the Autoxidation of Epinephrine and a Simple Assay for Superoxide Dismutase." *J. Biol. Chem.* **1972**, *247*, 3170.

130 Armitage, B.; Yu, C.; Devadoss, C.; Schuster, G. B. "Cationic Anthraquinone Derivatives as Catalytic DNA Photonucleases: Mechanisms for DNA Damage and Quinone Recycling." *J. Am. Chem. Soc.* **1994**, *116*, 9847.

131 Newcomb, M. "Competition Methods and Scales for Alkyl Radical Reaction Kinetics." *Tetrahedron* **1993**, *49*, 1151.

132 Carter, K. N.; Greenberg, M. M. "Direct Measurement of Pyrimidine C6-Hydrate Stability." *Bioorg. Med. Chem.* **2001**, *9*, 2341.

133 Zhu, Q.; Delaney, M. O.; Greenberg, M. M. "Observation and Elimination of *N*-Acetylation of Oligonucleotides Prepared Using Fast-Deprotecting Phosphoramidites and Ultra-Mild Deprotection." *Bioorg. Med. Chem. Lett.* **2001**, *11*, 1105.

134 House, C. J.; Miller, S. J. "Hydrolysis of Dihydrouridine and Related Compounds." Biochemistry **1996**, *35*, 315.

135 Matray, T. J.; Haxton, K. J.; Greenberg, M. M. "The Effects of the Ring Fragmentation Product of Thymidine C5-Hydrate on Phosphodiesterases and Klenow (Exo-) Fragment." *Nucleic Acids Res.* **1995**, *23*, 4642.

136 Gray, D. M.; Ratliff, R. L.; Vaughan, M. R. "Circular Dichroism Spectroscopy of DNA." *Methods Enzymol.* **1992**, *211*, 389.

137 Guéron, M.; Leroy, J. "Studies of Base Pair Kinetics by NMR Measurement of Proton Exchange." *Methods Enzymol.* 1995, 261, 383.

138 Schulte-Frohlinde, D.; Behrens, G.; Önal, A. "Lifetime of peroxyl radicals of poly(U), poly(A), and single- and double-stranded DNA and the rate of their reaction with thiols." *Int. J. Radiat. Biol.* **1986**, *50*, 103.

139 Iwai, S. "Synthesis of Thymine Glycol Containing Oligonucleotides from a Building Block with the Oxidized Base." *Angew. Chem. Int. Ed.* **2000**, *39*, 3874.

140 Roupioz, Y.; Lhomme, J.; Kotera, M. "Chemistry of the 2-Deoxyribonolactone Lesion in Oligonucleotides: Cleavage Kinetics and Products Analysis." *J. Am. Chem. Soc.* **2002**, *124*, 9129.

141 Apontoweil, P.; Berends, W. "Glutathione Biosynthesis in *E. Coli* K_{12}, Properties of the Enzymes and Regulation." *Biochim. Biophys. Acta.* **1975**, *399*, 1.

142 Paul, T.; Young, M. J.; Hill, I. E.; Ingold, K. U. "Strand Cleavage of Supercoiled DNA by Water-Soluble Peroxyl Radicals. The Overlooked Importance of Peroxyl Radical Charge." *Biochemistry* **2000**, *39*, 4129.

143 Adam, W.; Arnold, M. A.; Nau, W. M.; Pischel, U.; Saha-Möller, C. R. "A Comparative Photomechanistic Study (Spin Trapping, EPR Spectroscopy, Transient Kinetics, Photoproducts) of Nucleoside Oxidation (dG and 8-oxo-dG) by Triplet-Excited Acetophenones and by the Radicals Generated from α-Oxy-Substituted Derivatives through Norrish-Type I Cleavage." *J. Am. Chem. Soc.* **2002**, *124*, 3893.

144 Martini, M.; Termini, J. "Peroxy Radical Oxidation of Thymidine." *Chem. Res. Toxicol.* **1997**, *10*, 234.

145 Bennett, J. E. "Kinetic Electron Paramagnetic Resonance Study of the Reactions of *t*-Butylperoxyl Radicals in Aqueous Solution." *J. Chem. Soc. Faraday Trans.* **1990**, *86*, 3247.

146 Green, M. M.; Boyle, B. A.; Vairamani, T. M.; Saunders, W. H. Jr.; Bowen, P.; Allinger, N. L. "Temperature-Dependent Stereoselectivity and Hydrogen Deuterium Kinetic Isotope Effect for γ-Hydrogen Transfer to 2-Hexyloxy Radical. The Transition State for the Barton Reaction." *J. Am. Chem. Soc.* **1986**, *108*, 2381.

147 Shoute, L. C. T.; Alfassi, Z. B.; Neta, P.; Huie, R. E. "Rate Constants for Reactions of (Perhaloalkyl)peroxyl Radicals with Alkenes in Methanol." *J. Phys. Chem.* **1994**, *98*, 5701.

148 Sugiyama, H.; Xu, C.; Murugesan, N.; Hecht, S. M. "Chemistry of the Alkali-Labile Lesion Formed from Iron (II) Bleomycin and d(CGCTTTAAAGCG)." *Biochemistry* **1988**, *27*, 58.

149 Schmidt, J. "An ESR Analysis of a Heat-Stable Radical in γ-Irradiated Single Crystals of 1-Methylthymine." *J. Chem. Phys.* **1975**, *62*, 370.

150 Muller, J. G.; Duarte, V.; Hickerson, R. P.; Burrows, C. J. "Gel Electrophoretic Detection of 7,8-Dihydro-8-oxoguanine and 7,8-dihydro-8-oxoadenine via Oxidation by Ir (IV)." *Nucleic Acids Res.* **1998**, *26*, 2247.

151 Lecomte, P.; Boiteaux, S.; Doubleday, O. "Mechanism of Ultraviolet-Induced Mutagenesis: The Coding Properties of Ultraviolet-Irradiated Poly(dC) Replicated by *E. coli* DNA Polymerase I." *Nucleic Acids Res.* **1981**, *9*, 3491

152 Teebor, G. W.; Frenkel, K., Goldstein, M. S. "Ionizing Radiation and Tritium Transmutation Both Cause Formation of 5-Hydroxymethyl-2'-deoxyuridine in Cellular DNA." *Proc. Natl. Acad. Sci. USA* **1984**, *81*, 318.

153 Fujita, S.; Steenken, S. "Pattern of OH Radical Addition to Uracil and Methyl- and Carboxyl-Substituted Uracils. Electron Transfer of OH Adducts with *N, N, N', N'*-Tetramethyl-p-phenlenediamine and Tetranitromethane." *J. Am. Chem. Soc.* **1981**, *103*, 2540.

154 Sambrook, J.; Fritsch, E. F.; Maniatis, T. *Molecular Cloning: A Laboratory Manual* Cold Spring Harbor Laboratory Press: New York, 1989.

155 Porter, N. A.; Lehman, L. S.; Weber, B. A.; Smith, K. J. "Unified Mechanism for Polyunsaturated Fatty Acid Autoxidation. Competition of Peroxy Radical Hydrogen Atom Abstraction, β-Scission and Cyclization." *J. Am. Chem. Soc.* **1981**, *103*, 6447.

156 Howard, J. A.; Ingold, K. U. "Absolute Rate Constants for Hydrocarbon Autoxidation. III. α-Methylstyrene, β-methylstyrene, and Indene." *Can J. Chem.* **1966**, *44*, 1113.

157 Burton, G. W.; Ingold, K. U. "Autoxidation of Biological Molecules. 1. The Antioxidant Activity of Vitamin E and Related Chain-Breaking Phenolic Antioxidants *In Vitro*." *J. Am. Chem. Soc.* **1981**, *103*, 6472.

158 Porter, N. A.; Mills, K. A.; Carter, R. L. "A Mechanistic Study of Oleate Autoxidation: Competing Peroxyl H-Atom Abstraction and Rearrangement." *J. Am. Chem. Soc.* **1994**, *116*, 6690.

Appendix A: Representative Phosphorimages

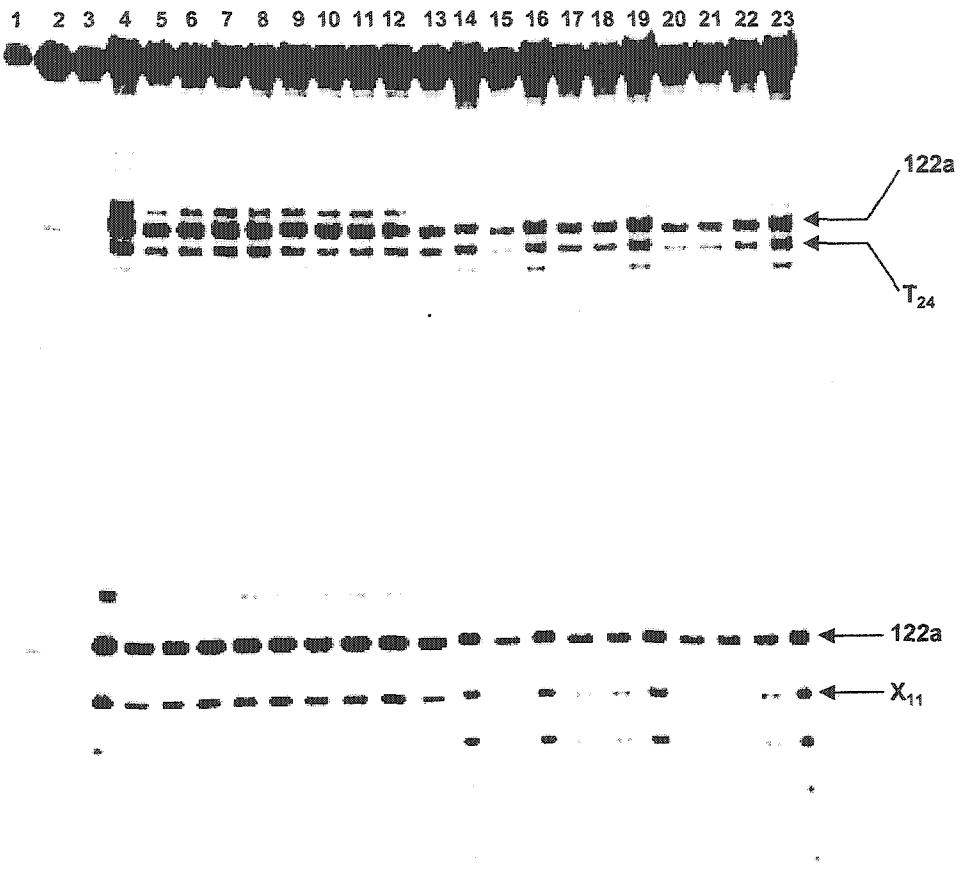

Supplementary Figure. The deuterium isotope effect for C1' hydrogen atom abstraction. Lane 1, T selective sequencing reaction. Lanes 2-23 were treated with 1.0 M piperidine (90 °C, 20 min). Lane 2, non-photolyzed 5'-^{32}P-**166**; lane 3, non-photolyzed 5'-^{32}P-**167**. Lanes 4-13, photolyzed 5'-^{32}P-**166**; lanes 14-23, 5'-^{32}P-**167**.

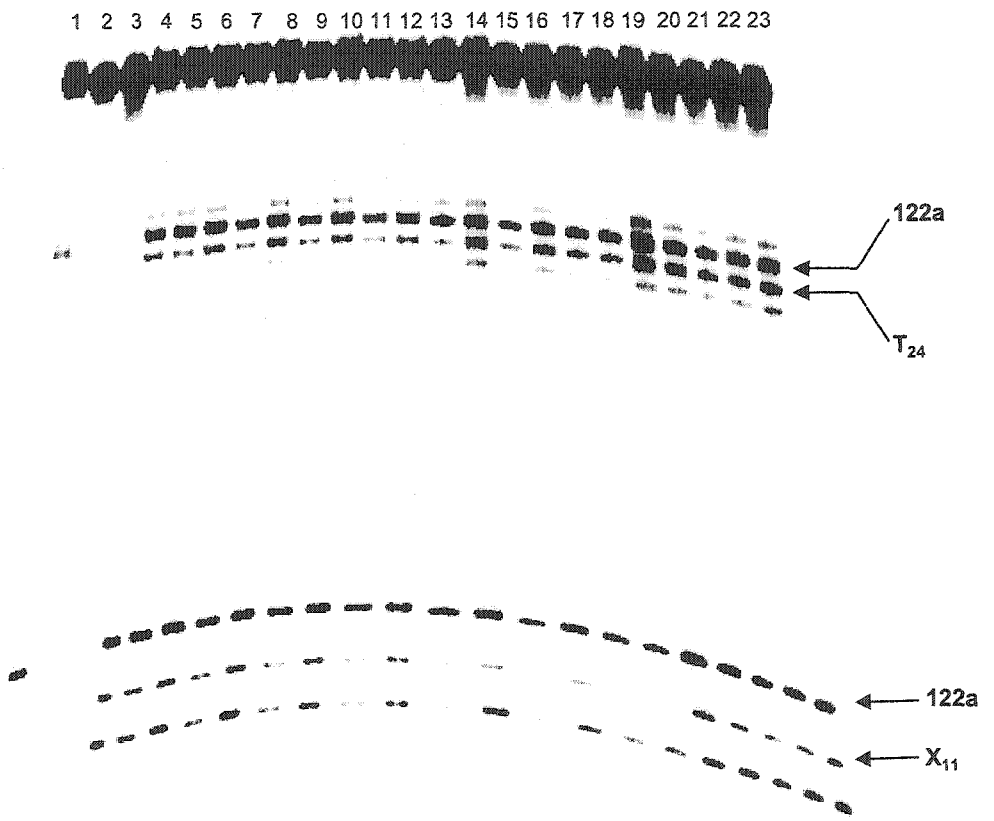

Supplementary Figure. The deuterium isotope effect for C1' hydrogen atom abstraction. Lane 1, T selective sequencing reaction. Lanes 2-23 were treated with 1.0 M piperidine (90 °C, 20 min). Lane 2, non-photolyzed 5'-^{32}P-**169**; lane 3, non-photolyzed 5'-^{32}P-**170**. Lanes 4-13, photolyzed 5'-^{32}P-**169**; lanes 14-23, 5'-^{32}P-**170**.

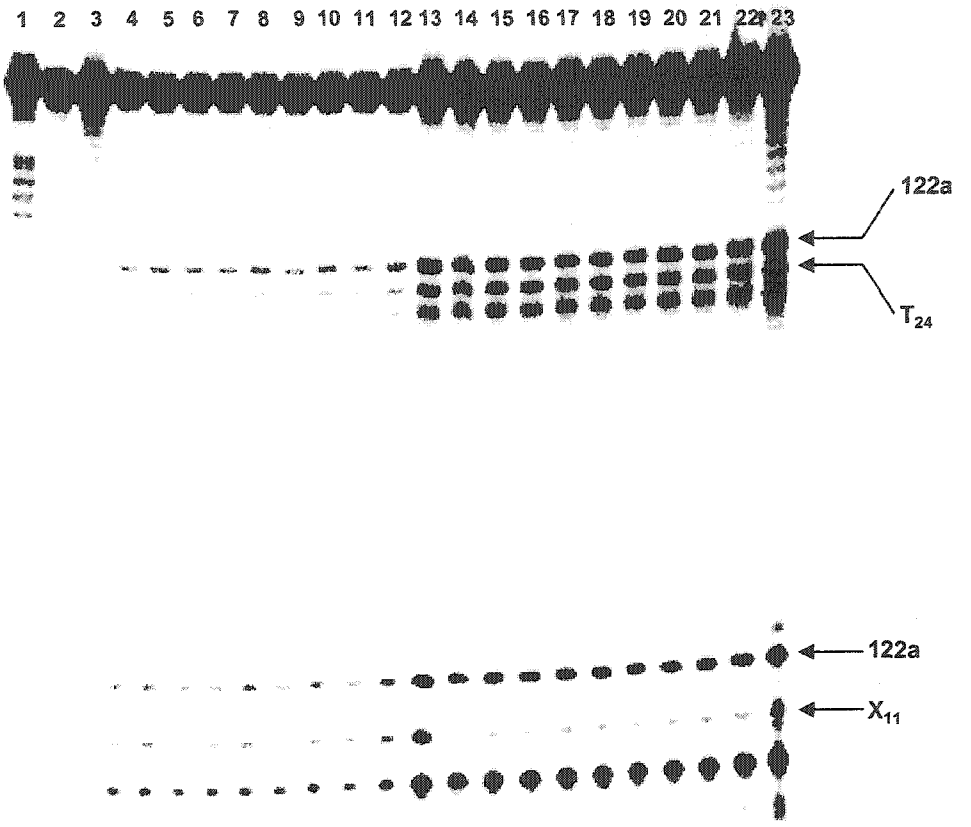

Supplementary Figure. The deuterium isotope effect for C1' hydrogen atom abstraction. Lane 1, T selective sequencing reaction. Lanes 2-23 were treated with 0.1 M NaOH (37 °C, 20 min). Lane 2, non-photolyzed 5'-^{32}P-**166**; lane 3, non-photolyzed 5'-^{32}P-**167**. Lanes 4-13, photolyzed 5'-^{32}P-**166**; lanes 14-23, 5'-^{32}P-**167**.

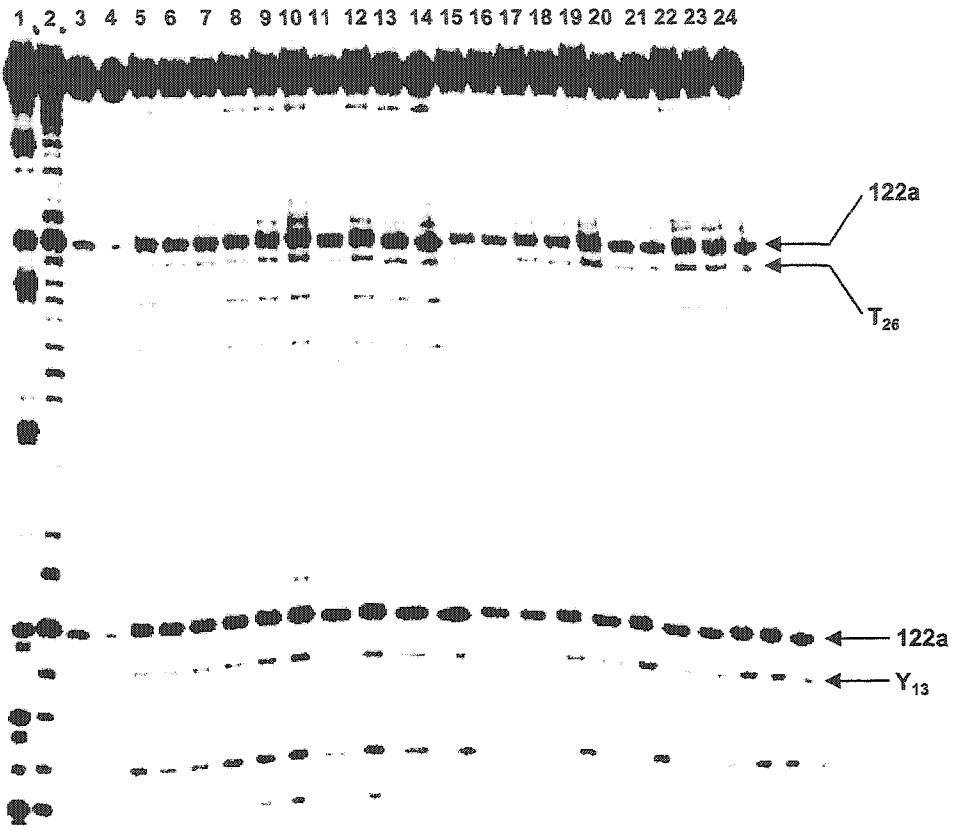

Supplementary Figure. The deuterium isotope effect for C1' hydrogen atom abstraction. Lane 1, T selective sequencing reaction. Lane 2, dC > T sequencing reaction. Lanes 3-24 were treated with 1.0 M piperidine (90 °C, 20 min). Lane 3, non-photolyzed 3'-^{32}P-**166**; lane 4, non-photolyzed 3'-^{32}P-**168**. Lanes 5-14, photolyzed 3'-^{32}P-**166**; lanes 15-24, 3'-^{32}P-**168.**

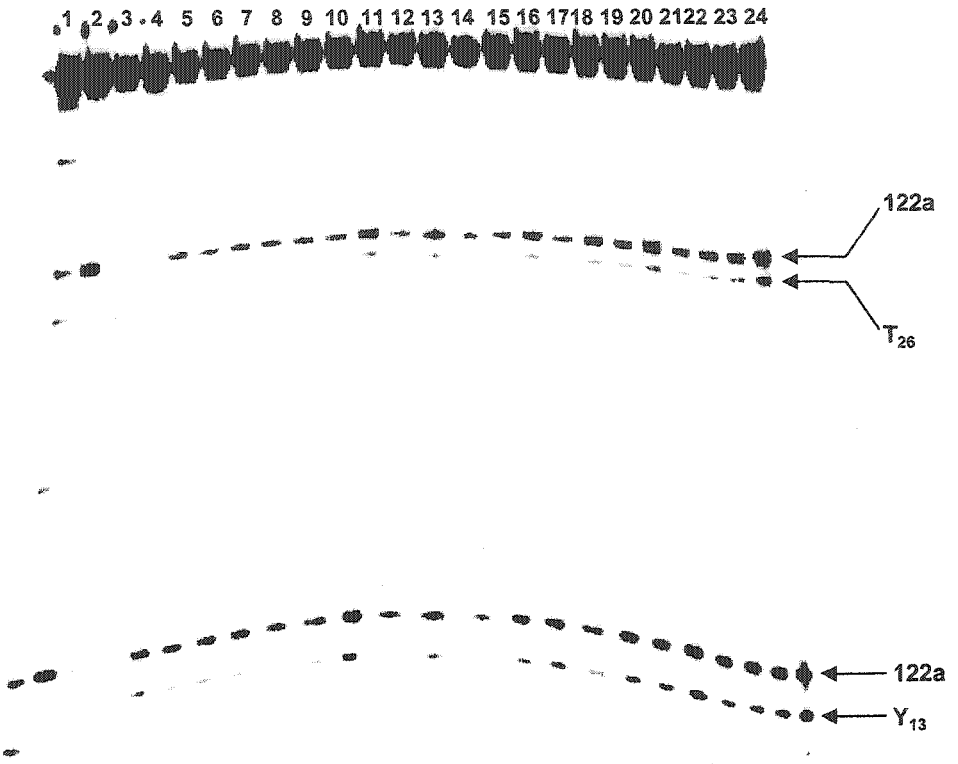

Supplementary Figure. The deuterium isotope effect for C1' hydrogen atom abstraction. Lane 1, T selective sequencing reaction. Lane 2 dC > T sequencing reaction. Lanes 3-24 were treated with 1.0 M piperidine (90 °C, 20 min). Lane 3, non-photolyzed 3'-^{32}P-**169**; lane 4, non-photolyzed 3'-^{32}P-**171**. Lanes 5-14, photolyzed 3'-^{32}P-**169**; lanes 15-24, 3'-^{32}P-**171**.

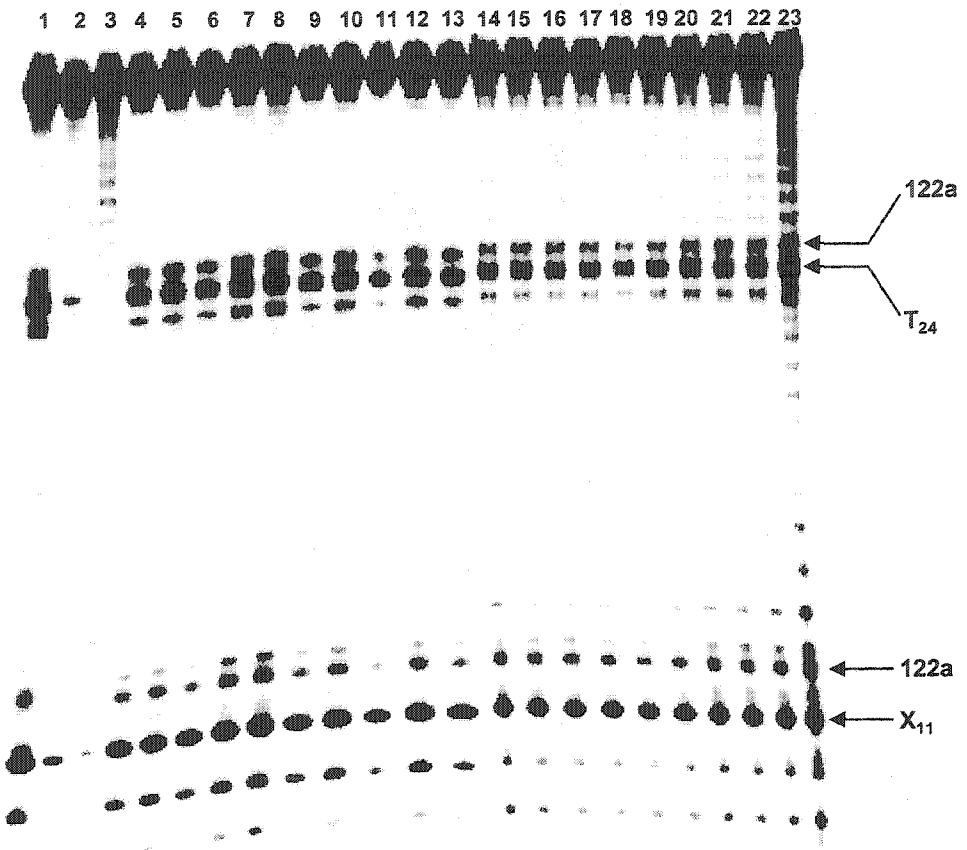

Supplementary Figure. The deuterium isotope effect for C4' hydrogen atom abstraction. Lane 1, T selective sequencing reaction. Lanes 2-23 were treated with 1.0 M piperidine (90 °C, 20 min). Lane 2, non-photolyzed 5'-^{32}P-**166**; lane 3, non-photolyzed 5'-^{32}P-**174**. Lanes 4-13, photolyzed 5'-^{32}P-**166**; lanes 14-23, 5'-^{32}P-**174.**

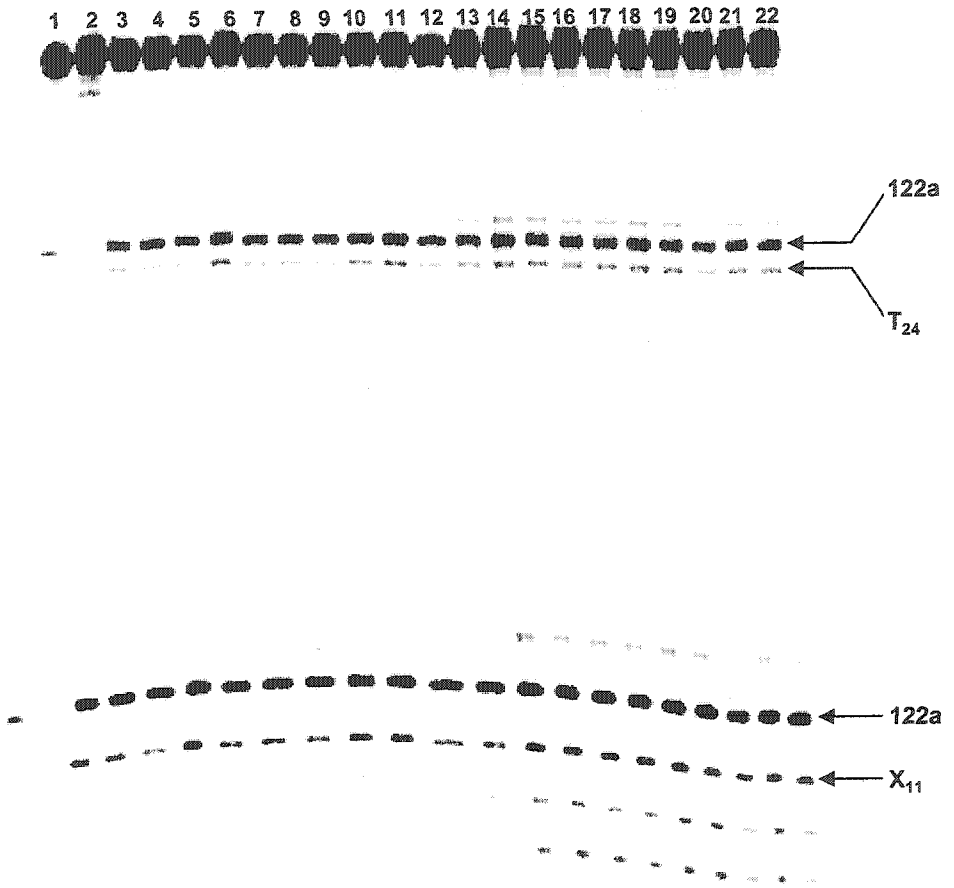

Supplementary Figure. The deuterium isotope effect for C4' hydrogen atom abstraction. Lane 1, T selective sequencing reaction. Lanes 2-23 were treated with 1.0 M piperidine (90 °C, 20 min). Lane 2, non-photolyzed 5'-^{32}P-**169**; lane 3, non-photolyzed 5'-^{32}P-**176**. Lanes 4-13, photolyzed 5'-^{32}P-**169**; lanes 14-23, 5'-^{32}P-**176**.

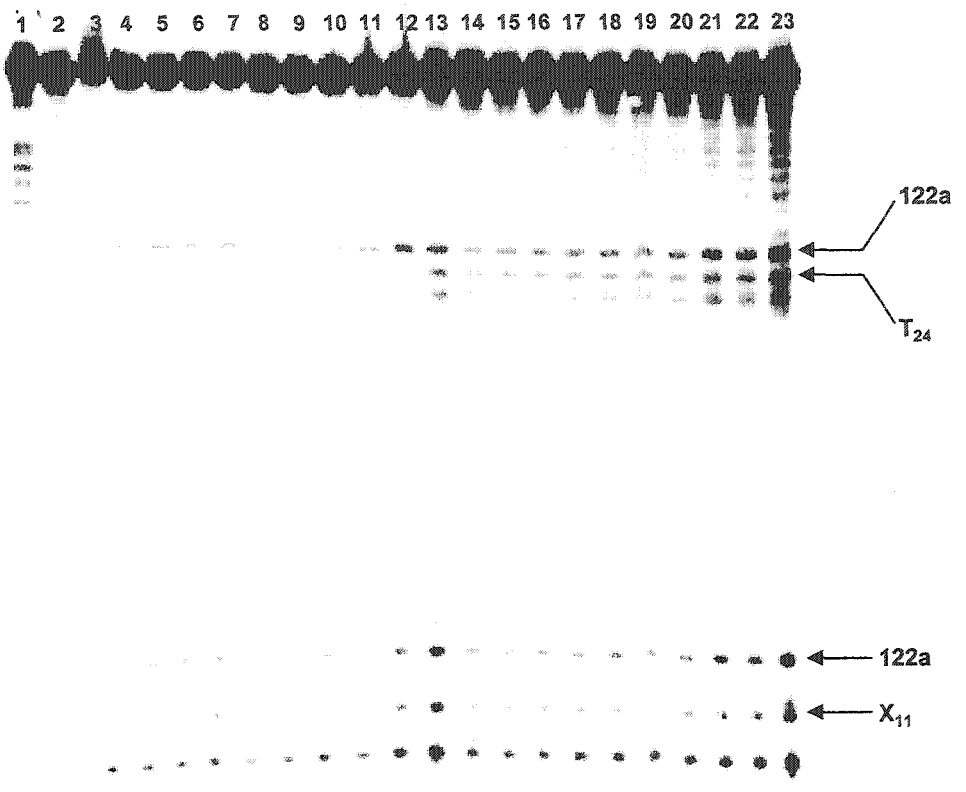

Supplementary Figure. The deuterium isotope effect for C4' hydrogen atom abstraction. Lane 1, T selective sequencing reaction. Lanes 2-23 were treated with 0.1 M NaOH (37 °C, 20 min). Lane 2, non-photolyzed 5'-^{32}P-**166**; lane 3, non-photolyzed 5'-^{32}P-**174**. Lanes 4-13, photolyzed 5'-^{32}P-**166**; lanes 14-23, 5'-^{32}P-**174**.

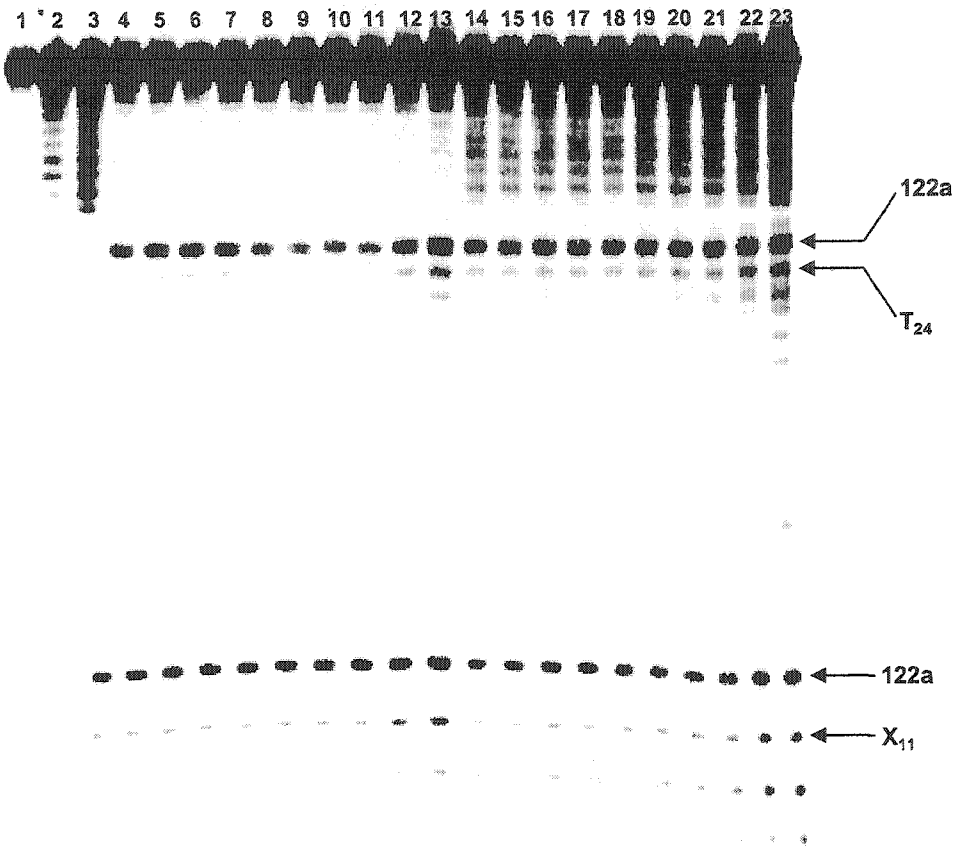

Supplementary Figure. The deuterium isotope effect for C4' hydrogen atom abstraction. Lane 1, T selective sequencing reaction. Lanes 2-23 were treated with 0.1 M NaOH (37 °C, 20 min). Lane 2, non-photolyzed 5'-^{32}P-**169**; lane 3, non-photolyzed 5'-^{32}P-**176**. Lanes 4-13, photolyzed 5'-^{32}P-**169**; lanes 14-23, 5'-^{32}P-**176**.

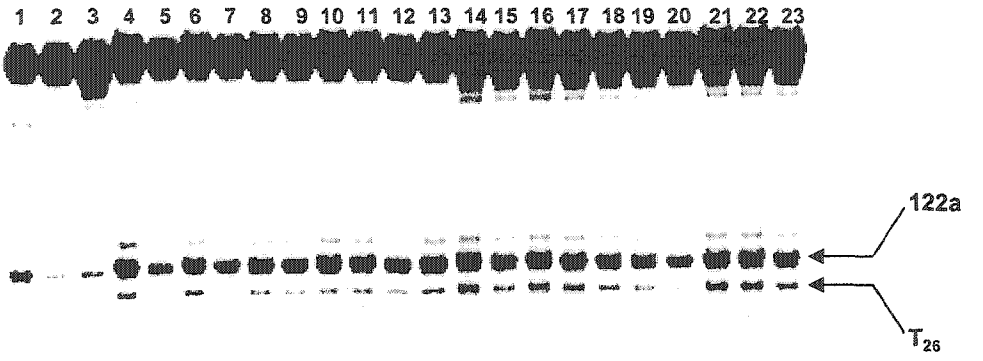

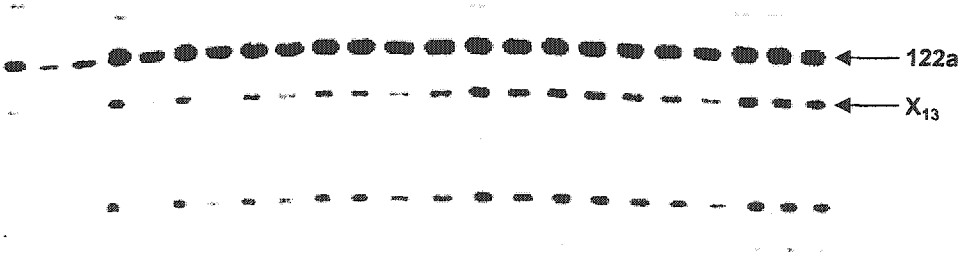

Supplementary Figure. The deuterium isotope effect for C4' hydrogen atom abstraction. Lane 1, T selective sequencing reaction. Lanes 2-23 were treated with 1.0 M piperidine (90 °C, 20 min). Lane 2, non-photolyzed 3'-^{32}P-**166**; lane 3, non-photolyzed 3'-^{32}P-**175**. Lanes 4-13, photolyzed 3'-^{32}P-**166**; lanes 14-23, 3'-^{32}P-**175**.

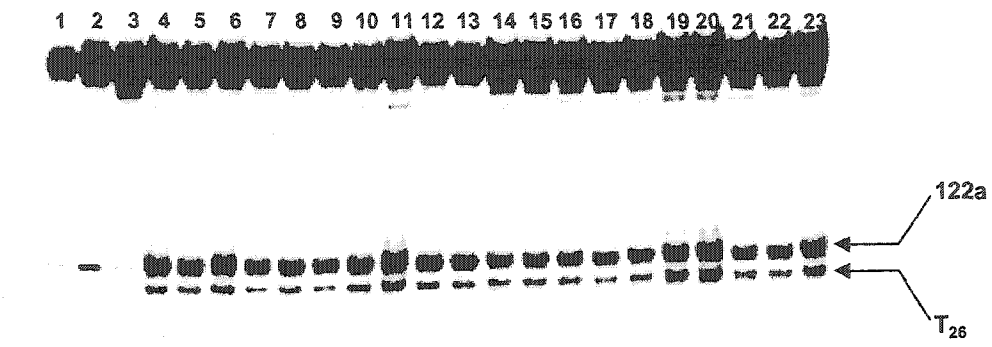

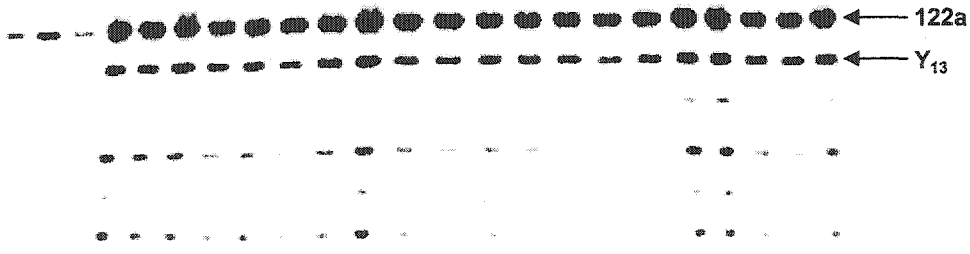

Supplementary Figure. The deuterium isotope effect for C4' hydrogen atom abstraction. Lane 1, T selective sequencing reaction. Lanes 2-23 were treated with 1.0 M piperidine (90 °C, 20 min). Lane 2, non-photolyzed 3'-^{32}P-**169**; lane 3, non-photolyzed 3'-^{32}P-**177**. Lanes 4-13, photolyzed 3'-^{32}P-**169**; lanes 14-23, 3'-^{32}P-**177**.

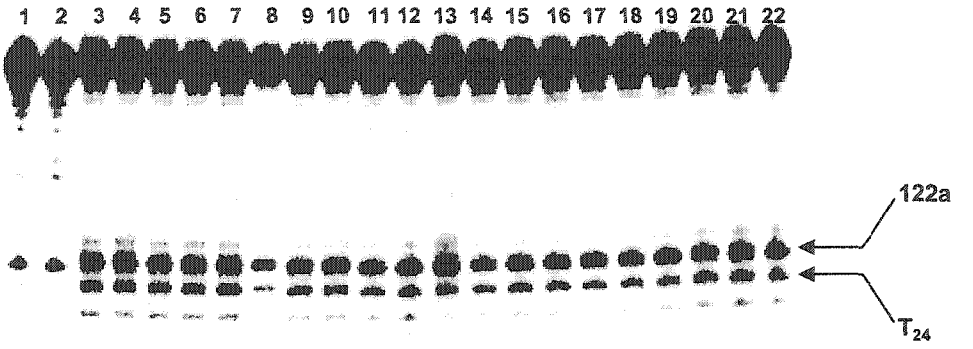

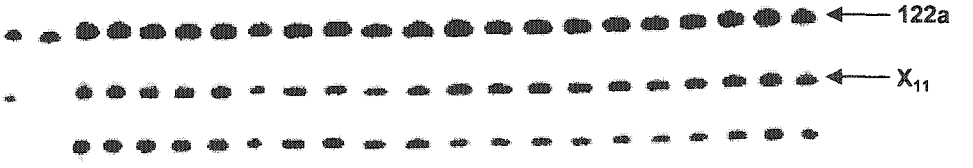

Supplementary Figure. The deuterium isotope effect for C5' hydrogen atom abstraction. Lanes 1-22 were treated with 1.0 M piperidine (90 °C, 20 min). Lane 1, non-photolyzed 5'-^{32}P-**166**; lane 2, non-photolyzed 5'-^{32}P-**181**. Lanes 3-12, photolyzed 5'-^{32}P-**166**; lanes 13-22, 5'-^{32}P-**181**.

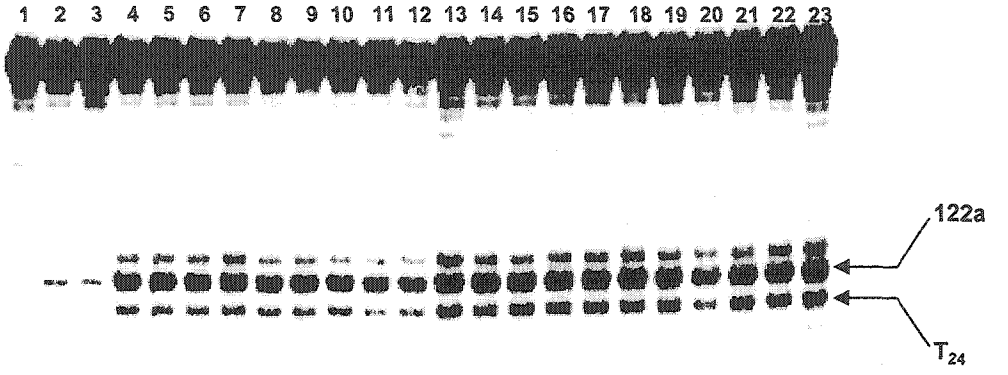

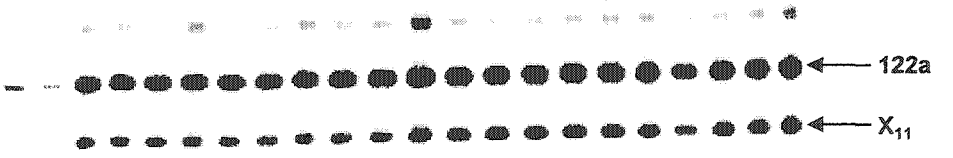

Supplementary Figure. The deuterium isotope effect for C5' hydrogen atom abstraction. Lane 1, T selective sequencing reaction. Lanes 2-23 were treated with 1.0 M piperidine (90 °C, 20 min). Lane 2, non-photolyzed 5'-^{32}P-**169**; lane 3, non-photolyzed 5'-^{32}P-**183**. Lanes 4-13, photolyzed 5'-^{32}P-**169**; lanes 14-23, 5'-^{32}P-**183**.

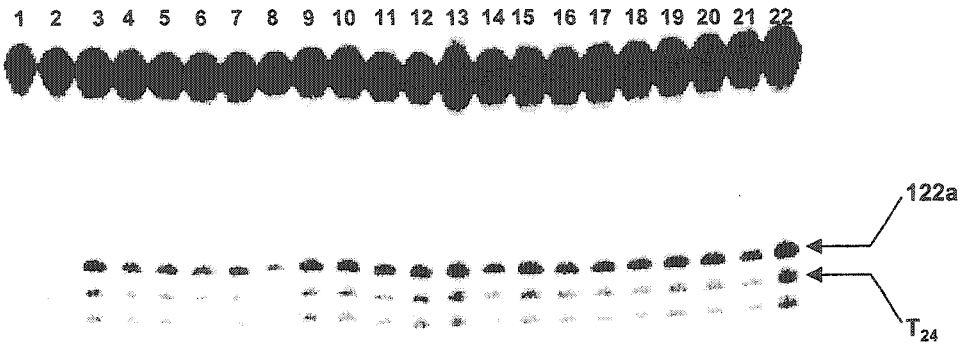

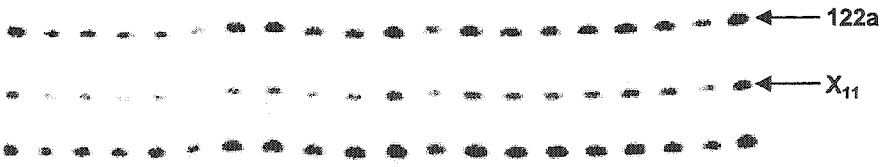

Supplementary Figure. The deuterium isotope effect for C5' hydrogen atom abstraction. Lanes 1-22 were treated with 0.1 M NaOH (37 °C, 20 min). Lane 1, non-photolyzed 5'-^{32}P-**166**; lane 2, non-photolyzed 5'-^{32}P-**181**. Lanes 3-12, photolyzed 5'-^{32}P-**166**; lanes 13-22, 5'-^{32}P-**181.**

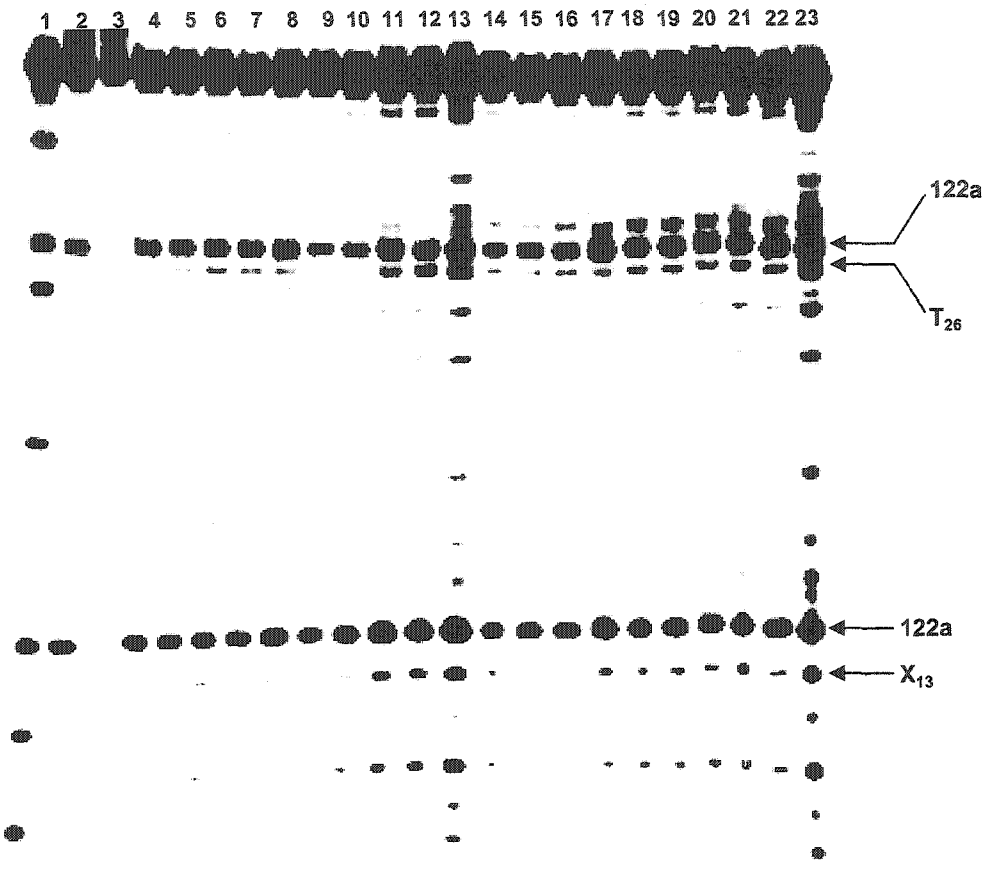

Supplementary Figure. The deuterium isotope effect for C5' hydrogen atom abstraction. Lane 1, T selective sequencing reaction. Lanes 2-23 were treated with 1.0 M piperidine (90 °C, 20 min). Lane 2, non-photolyzed 3'-^{32}P-**166**; lane 3, non-photolyzed 3'-^{32}P-**182**. Lanes 4-13, photolyzed 3'-^{32}P-**166**; lanes 14-23, 3'-^{32}P-**182**.

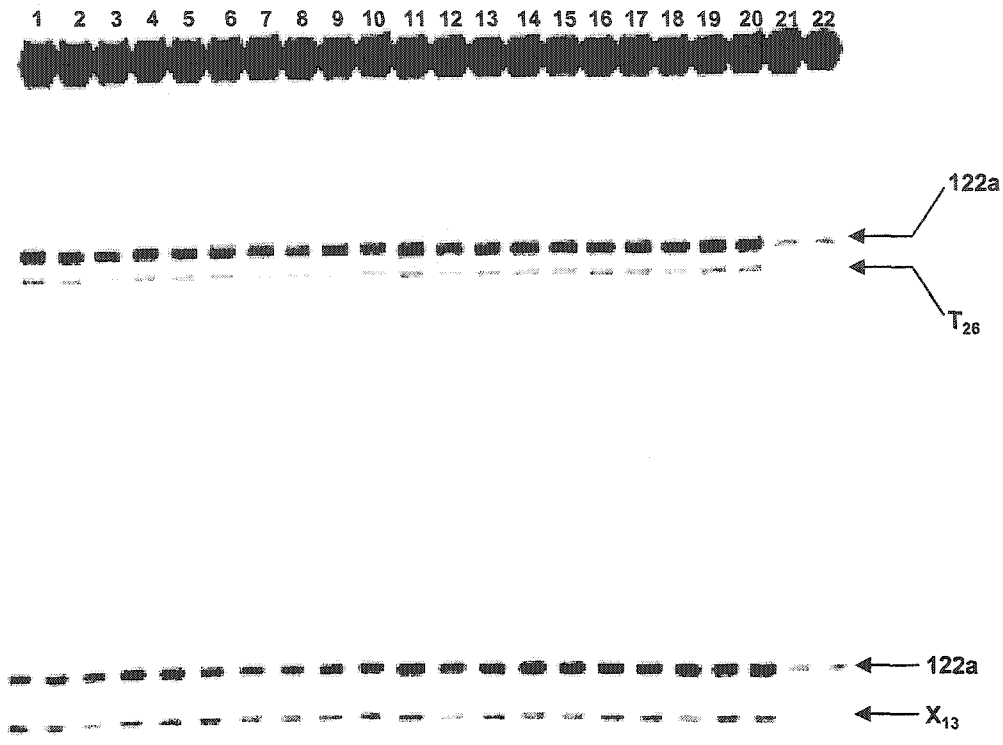

Supplementary Figure. The deuterium isotope effect for C5' hydrogen atom abstraction. Lanes 1-22 were treated with 1.0 M piperidine (90 °C, 20 min). Lane 1, non-photolyzed 3'-^{32}P-**169**; lane 2, non-photolyzed 3'-^{32}P-**184**. Lanes 3-12, photolyzed 3'-^{32}P-**169**; lanes 13-22, 3'-^{32}P-**184**.

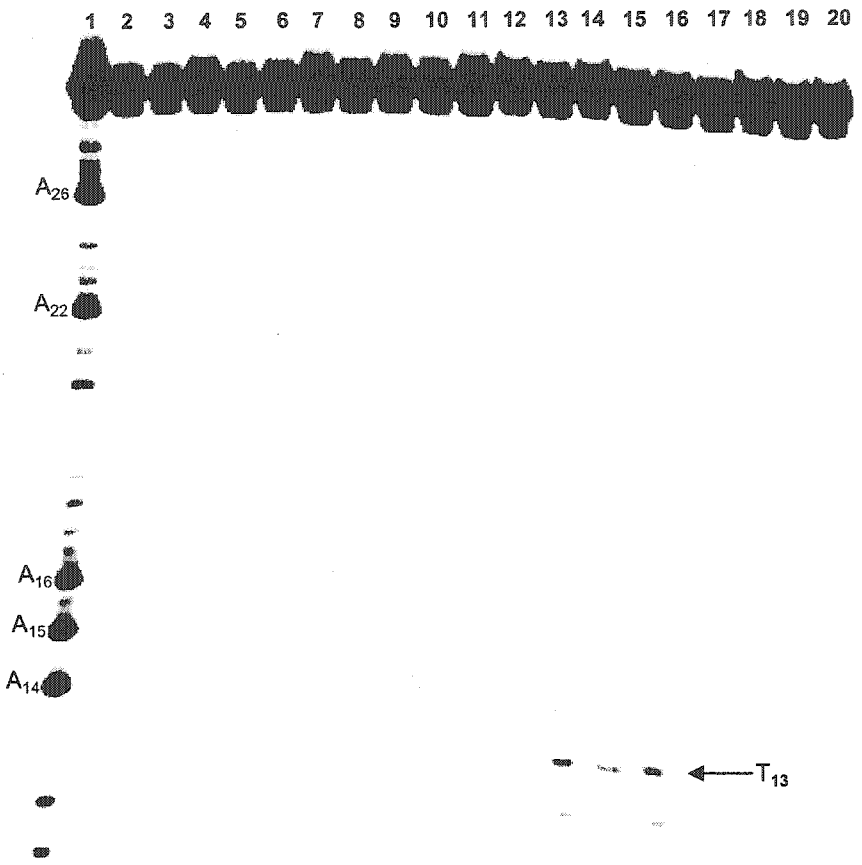

Supplementary Figure. Alkali-labile lesion formation on the complementary strand of 5'-^{32}P-**159**. Lane 1, dA selective sequencing reaction. Lane 2, non photolyzed DNA treated with 1.0 M piperidine (90 °C, 20 min); lanes 3-5, photolysate with no further treatment. Lanes 6-8, photolysis conducted in the presence of 50 μM GSHOEt, no further treatment; lanes 9-11, photolysis conducted in the presence of 10 mM GSHOEt, no further treatment. Lanes 12-20, photolysates treated with piperidine (1.0 M, 90 °C, 20 min). Lanes 15-17, photolysis conducted in the presence of 50 μM GSHOEt; lanes 18-20 photolysis conducted in the presence of 10 mM GSHOEt.

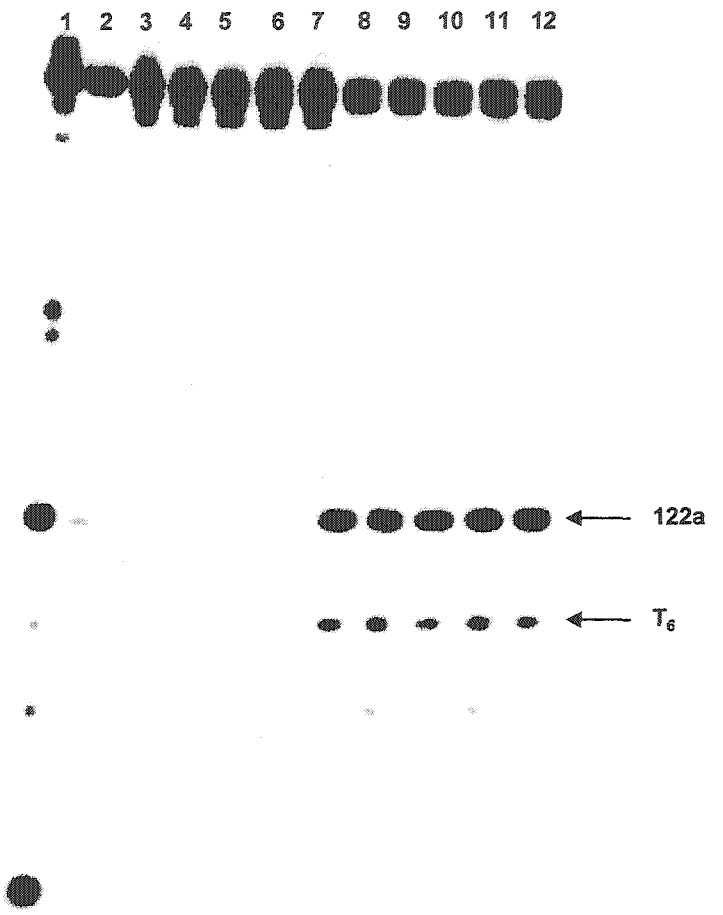

Supplementary Figure. Alkali-labile lesion formation in 5'-^{32}P-**210**. Lane 1, T selective sequencing reaction. Lanes 2, non-photolyzed DNA treated with 1.0 M piperidine (90 °C, 20 min); lanes 3-7, photolysate with no further treatment. Lanes 8-12, photolysate treated with 1.0 M piperidine (90 °C, 20 min.)

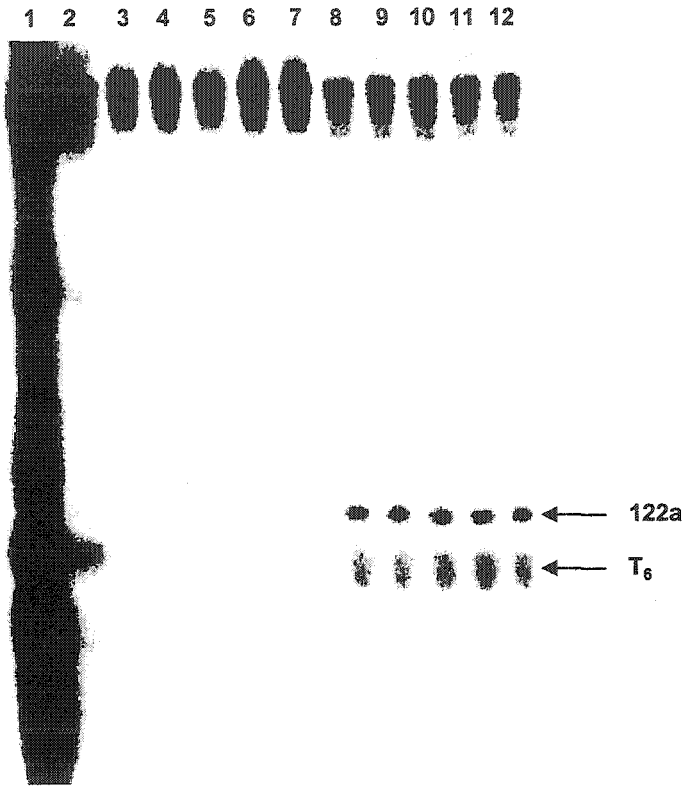

Supplementary Figure. Alkali-labile lesion formation in 3'-^{32}P-**210**. Lane 1, T selective sequencing reaction. Lanes 2, non-photolyzed DNA treated with 1.0 M piperidine (90 °C, 20 min); lanes 3-7, photolysate with no further treatment. Lanes 8-12, photolysate treated with 1.0 M piperidine (90 °C, 20 min.)

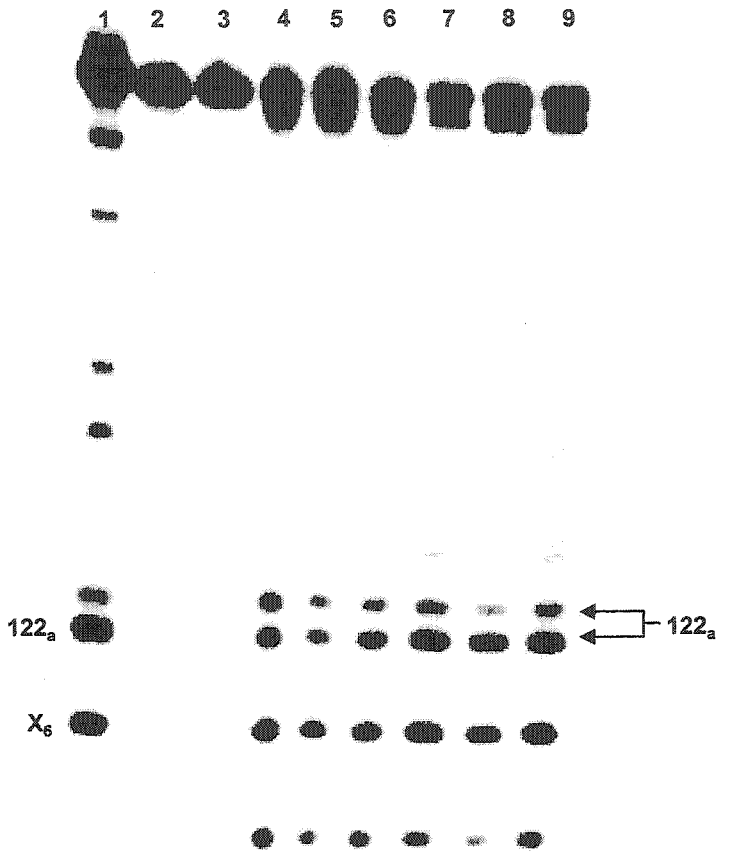

Supplementary Figure. Alkali-labile lesion formation in 5'-^{32}P-**223**. Lane 1, T selective sequencing reaction. Lane 2, non-photolyzed DNA treated with 0.1 M NaOH (37 °C, 20 min). Lane 3, non-photolyzed DNA treated with 1.0 M piperidine (90 °C, 20 min). Lanes 4-6, photolysate treated with 0.1 M NaOH (37 °C, 20 min). Lanes 7-9, photolysate treated with 1.0 M piperidine (90 °C, 20 min).

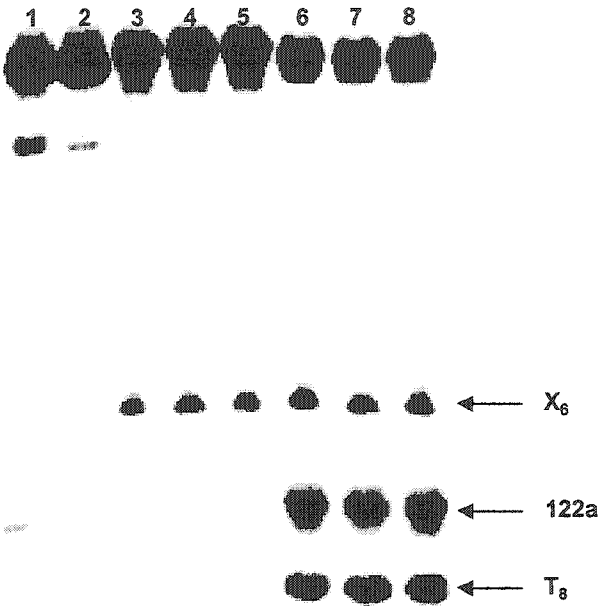

Supplementary Figure. Alkali-labile lesion formation in 3'-^{32}P-**223**. Lane 1, non-photolyzed DNA treated with 0.1 M NaOH (37 °C, 20 min). Lane 2, non-photolyzed DNA treated with 1.0 M piperidine (90 °C, 20 min). Lanes 3-5, photolysate treated with 0.1 M NaOH (37 °C, 20 min). Lanes 6-8, photolysate treated with 1.0 M piperidine (90 °C, 20 min).

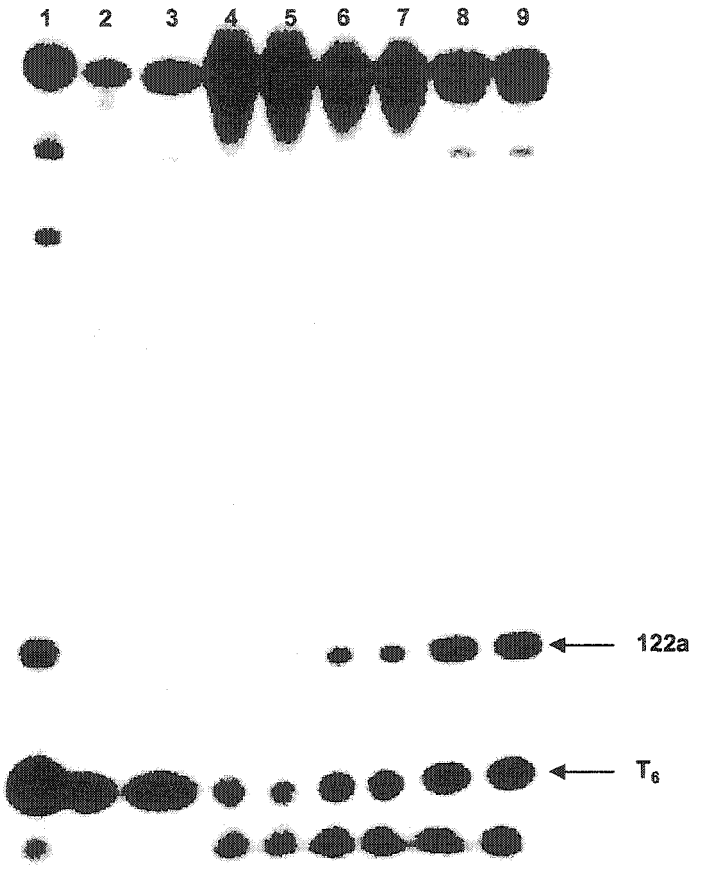

Supplementary Figure. Alkali-lability in 5'-^{32}P-**231**. Lane 1, T selective sequencing reaction. Lane 2, non-photolyzed DNA treated with 0.1 M NaOH (37 °C, 20 min). Lane 3, non-photolyzed DNA treated with 1.0 M piperidine (90 °C, 20 min). Lanes 4-9, photolysate treated appropriately. Lanes 4,5, no further treatment. Lanes 6,7, 0.1 M NaOH (37 °C, 20 min). Lanes 8,9, 1.0 M piperidine (90 °C, 20 min).

VII042

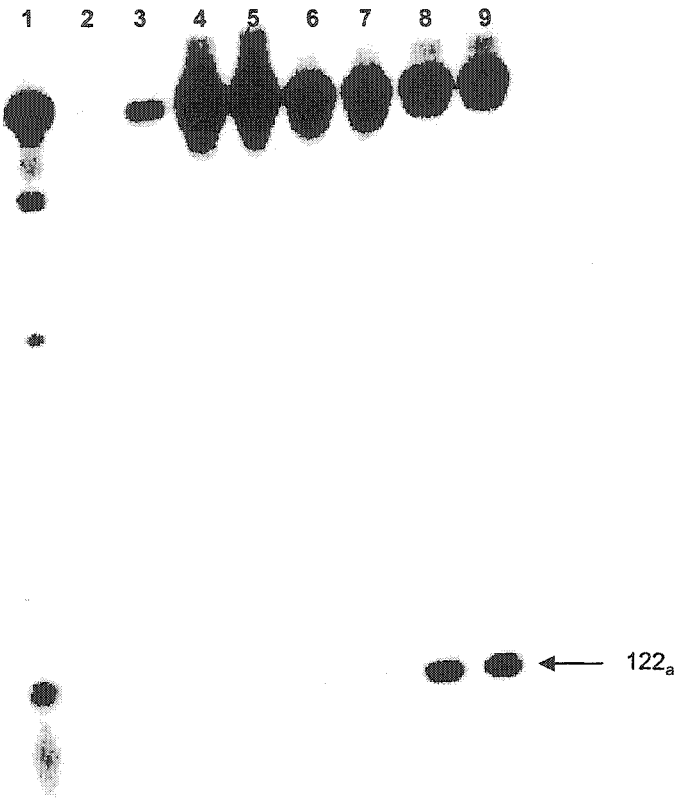

Supplementary Figure. Alkali-lability in 3'-^{32}P-**231**. Lane 1, T selective sequencing reaction. Lane 2, non-photolyzed DNA treated with 0.1 M NaOH (37 °C, 20 min). Lane 3, non-photolyzed DNA treated with 1.0 M piperidine (90 °C, 20 min). Lanes 4-9, photolysate treated appropriately. Lanes 4,5, no further treatment. Lanes 6,7, 0.1 M NaOH (37 °C, 20 min). Lanes 8,9, 1.0 M piperidine (90 °C, 20 min).

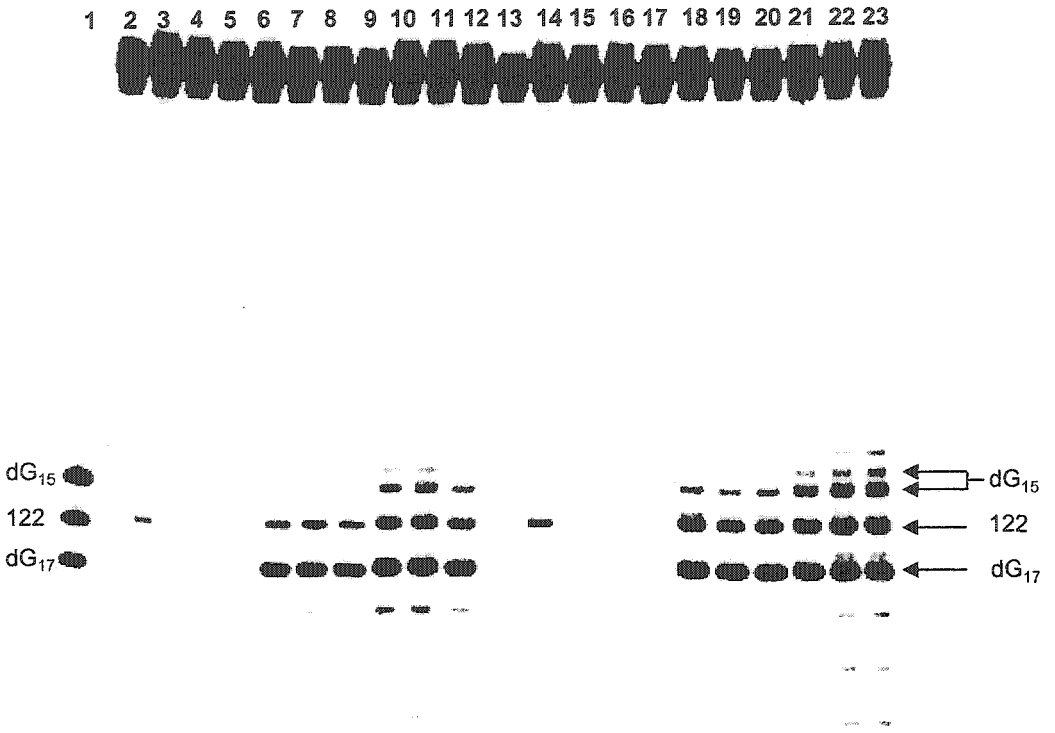

Supplementary Figure. Alkali-lability and the effect of Ir (IV) oxidation in the photolysates of 3'-^{32}P-**241** and **242**. Lane 1, oligonucleotide markers. The appropriate samples in lanes 2-23 were treated with 1.0 M piperidine (90 °C, 20 min) and/or 0.5 mM Na_2IrCl_6 (RT, 1 h) Lanes 2-5, non-photolyzed controls. Lane 2, 3'-^{32}P **241** treated with piperidine. Lane 3, 3'-^{32}P-**242** treated with piperidine. Lane 4, 3'-^{32}P-**241** treated with Ir (IV) prior to piperidine treatment. Lane 5, 3'-^{32}P-**242** treated with Ir (IV) prior to piperidine treatment. Lanes 6-14, photolysate of 3'-^{32}P-**241** treated appropriately. Lanes 6-8, no further treatment; lanes 9-11, piperidine, lanes 12-12; Ir (IV) then piperidine. Lanes 6-14, photolysate of 3'-^{32}P-**242** treated appropriately. Lanes 15-17, no further treatment; lanes 18-20, piperidine, lanes 21-23; Ir (IV) then piperidine.

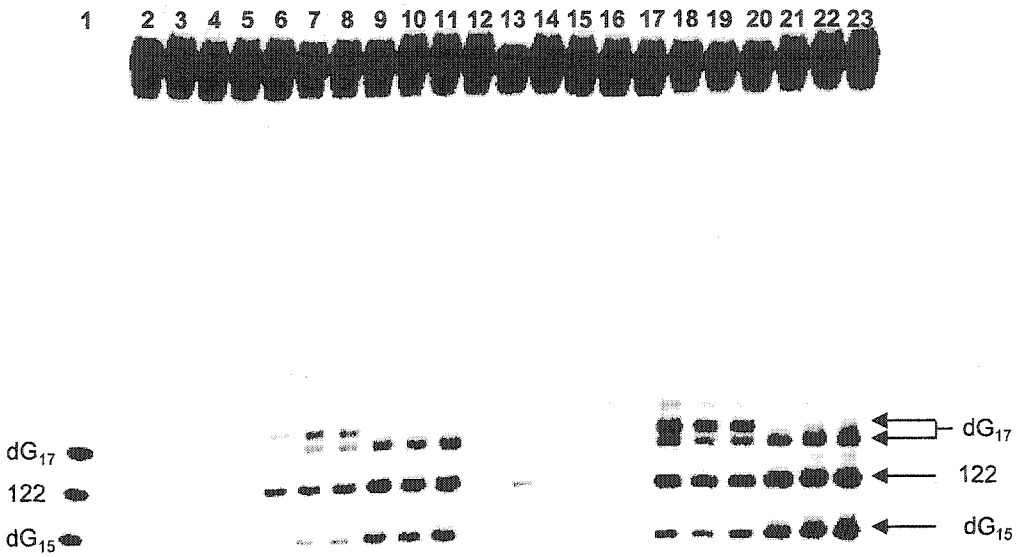

Supplementary Figure. Alkali-lability and the effect of Ir (IV) oxidation in the photolysates of 5'-^{32}P-**241** and **242**. Lane 1, oligonucleotide markers. The appropriate samples in lanes 2-23 were treated with 1.0 M piperidine (90 °C, 20 min) and/or 0.5 mM Na_2IrCl_6 (RT, 1 h) Lanes 2-5, non-photolyzed controls. Lane 2, 5'-^{32}P **241** treated with piperidine. Lane 3, 5'-^{32}P-**242** treated with piperidine. Lane 4, 5'-^{32}P-**241** treated with Ir (IV) prior to piperidine treatment. Lane 5, 5'-^{32}P-**242** treated with Ir (IV) prior to piperidine treatment. Lanes 6-14, photolysate of 5'-^{32}P-**241** treated appropriately. Lanes 6-8, no further treatment; lanes 9-11, piperidine, lanes 12-12; Ir (IV) then piperidine. Lanes 6-14, photolysate of 5'-^{32}P-**242** treated appropriately. Lanes 15-17, no further treatment; lanes 18-20, piperidine, lanes 21-23; Ir (IV) then piperidine.

Appendix B: NMR, IR, and Mass Spectral Data

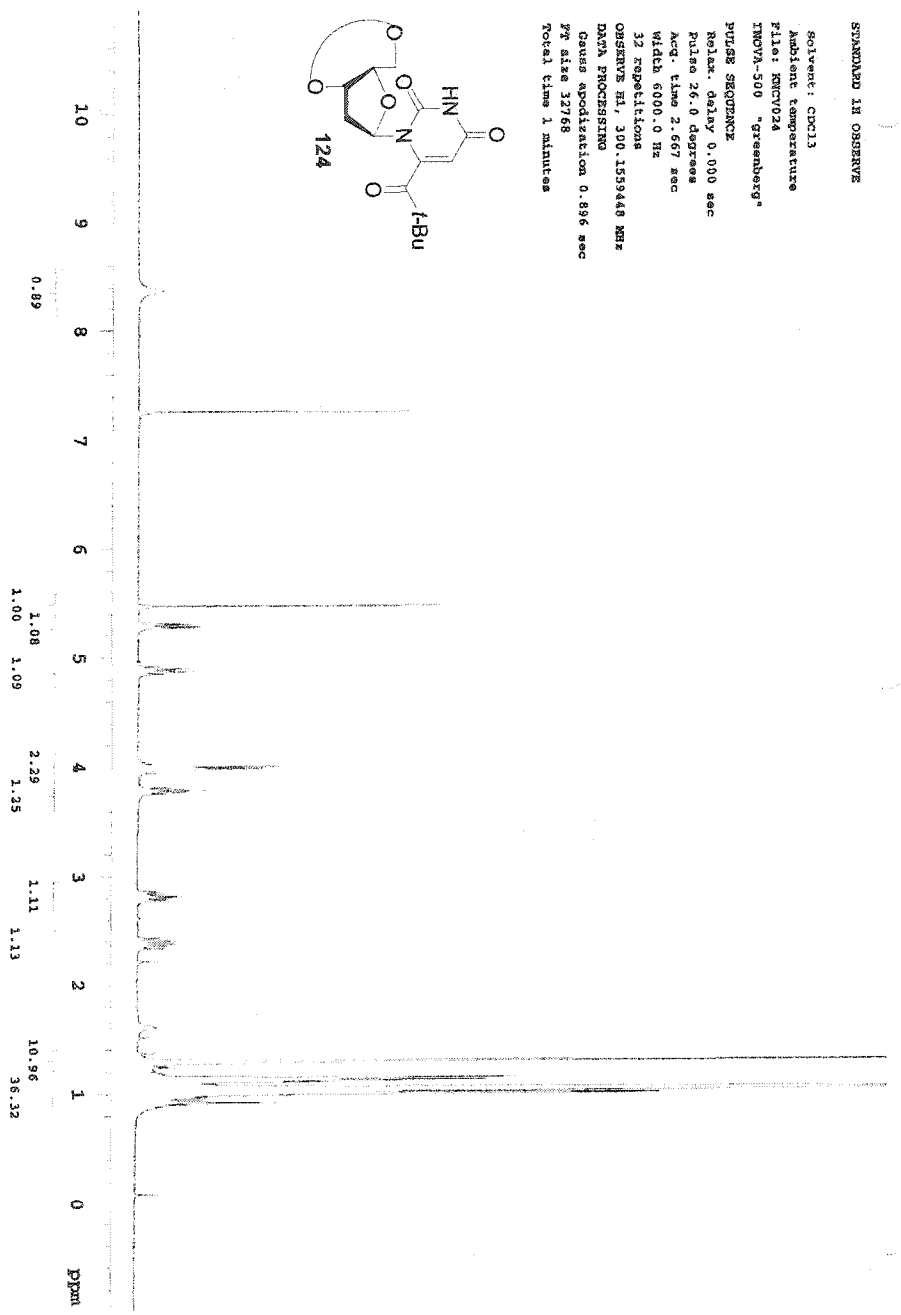

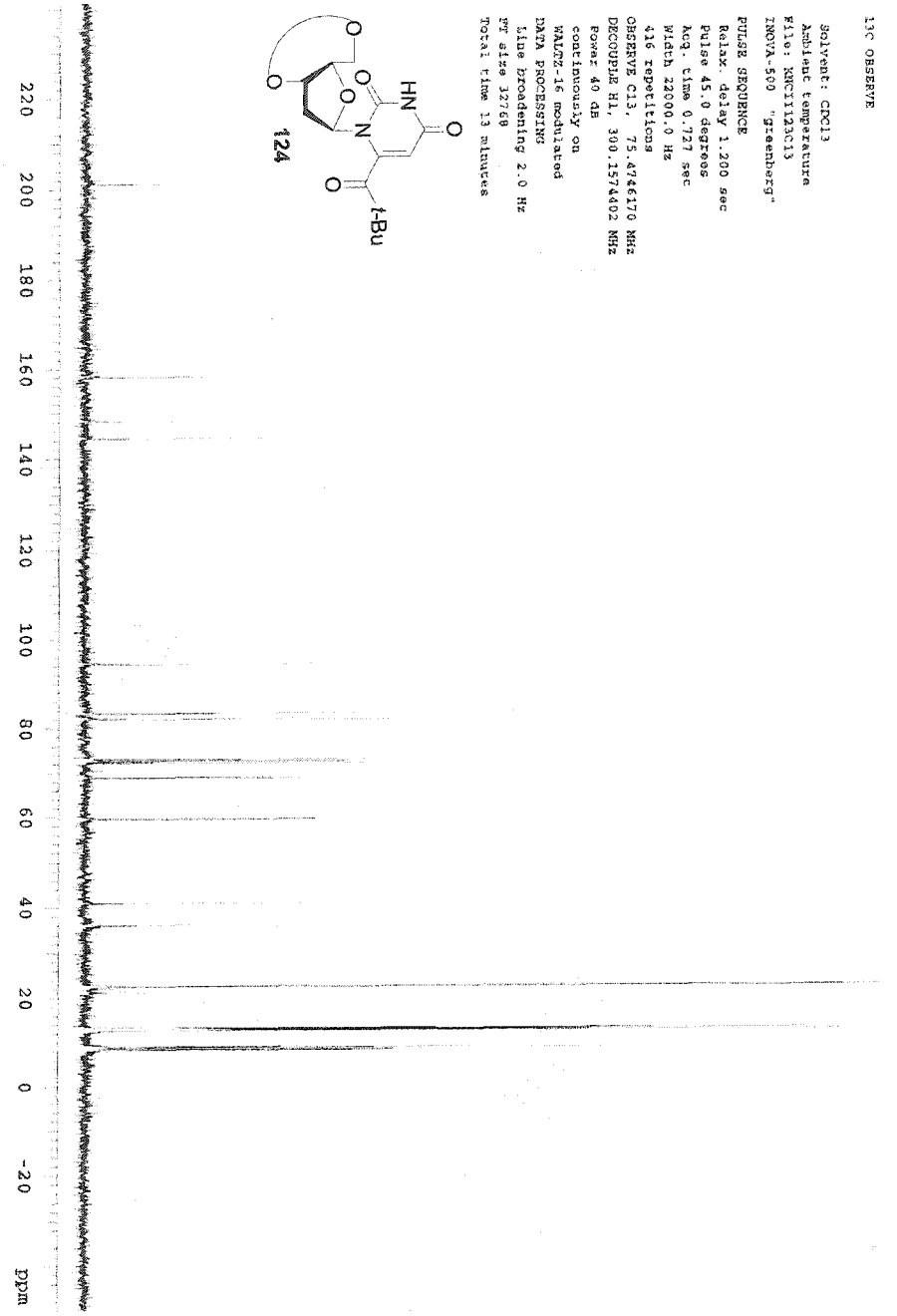

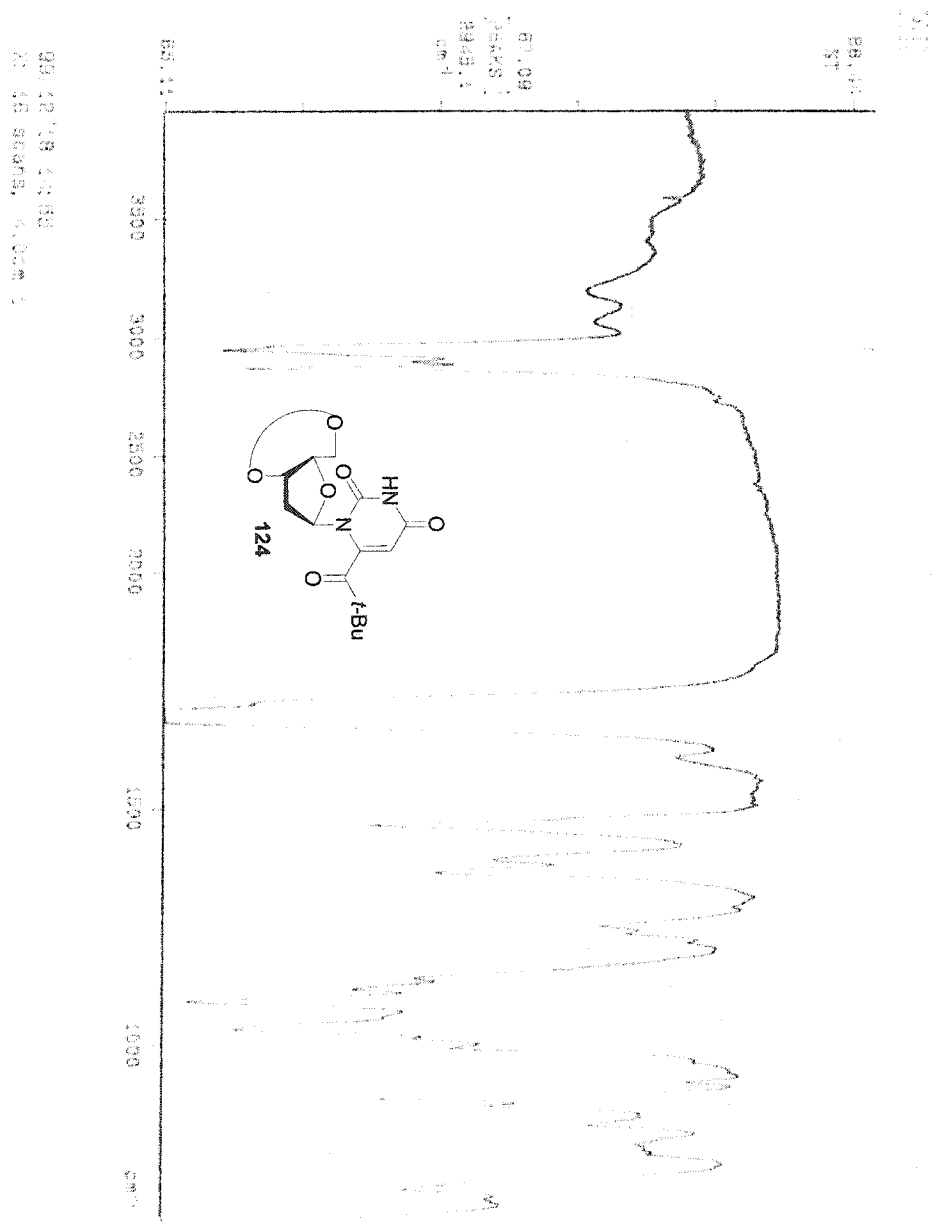

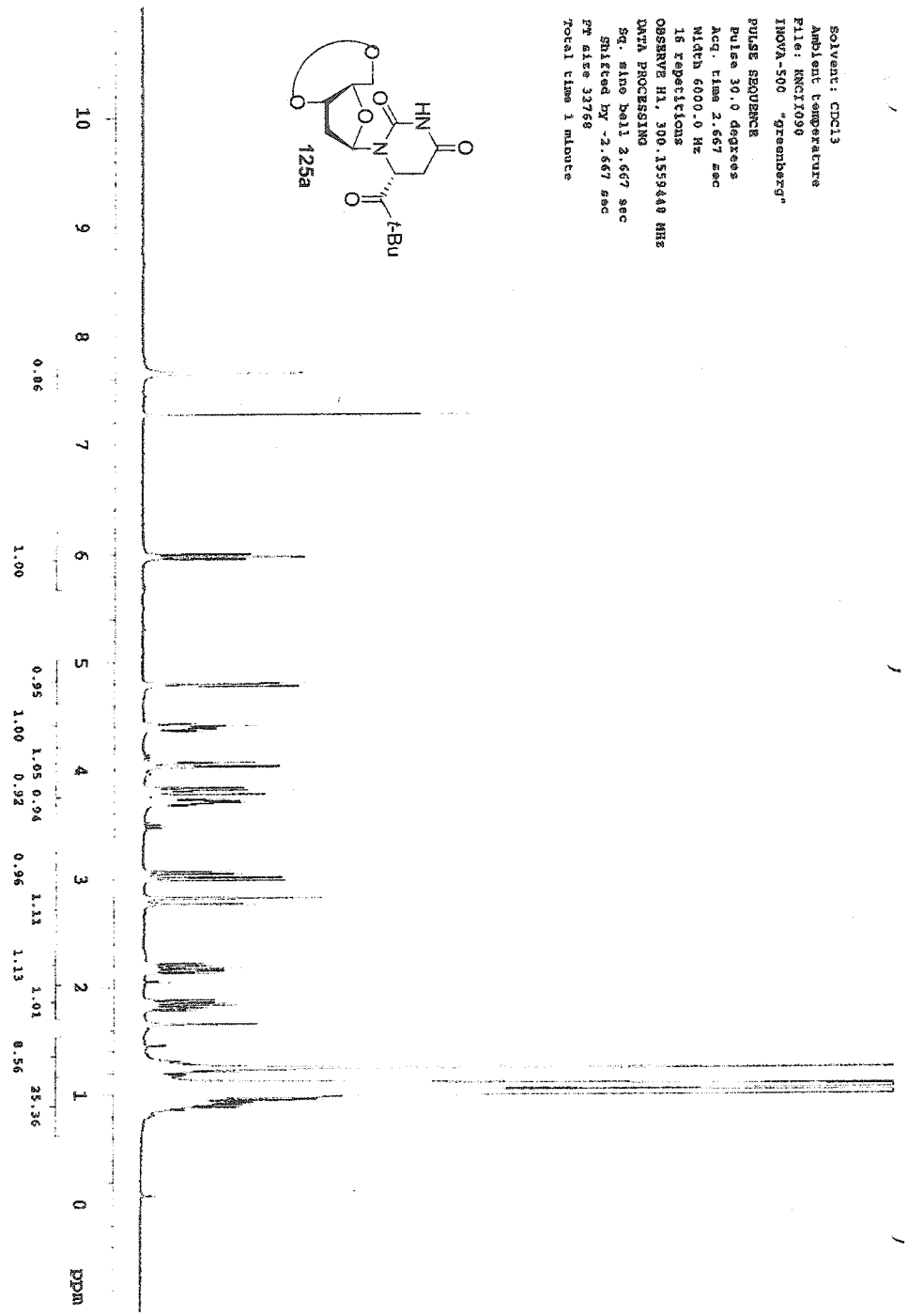

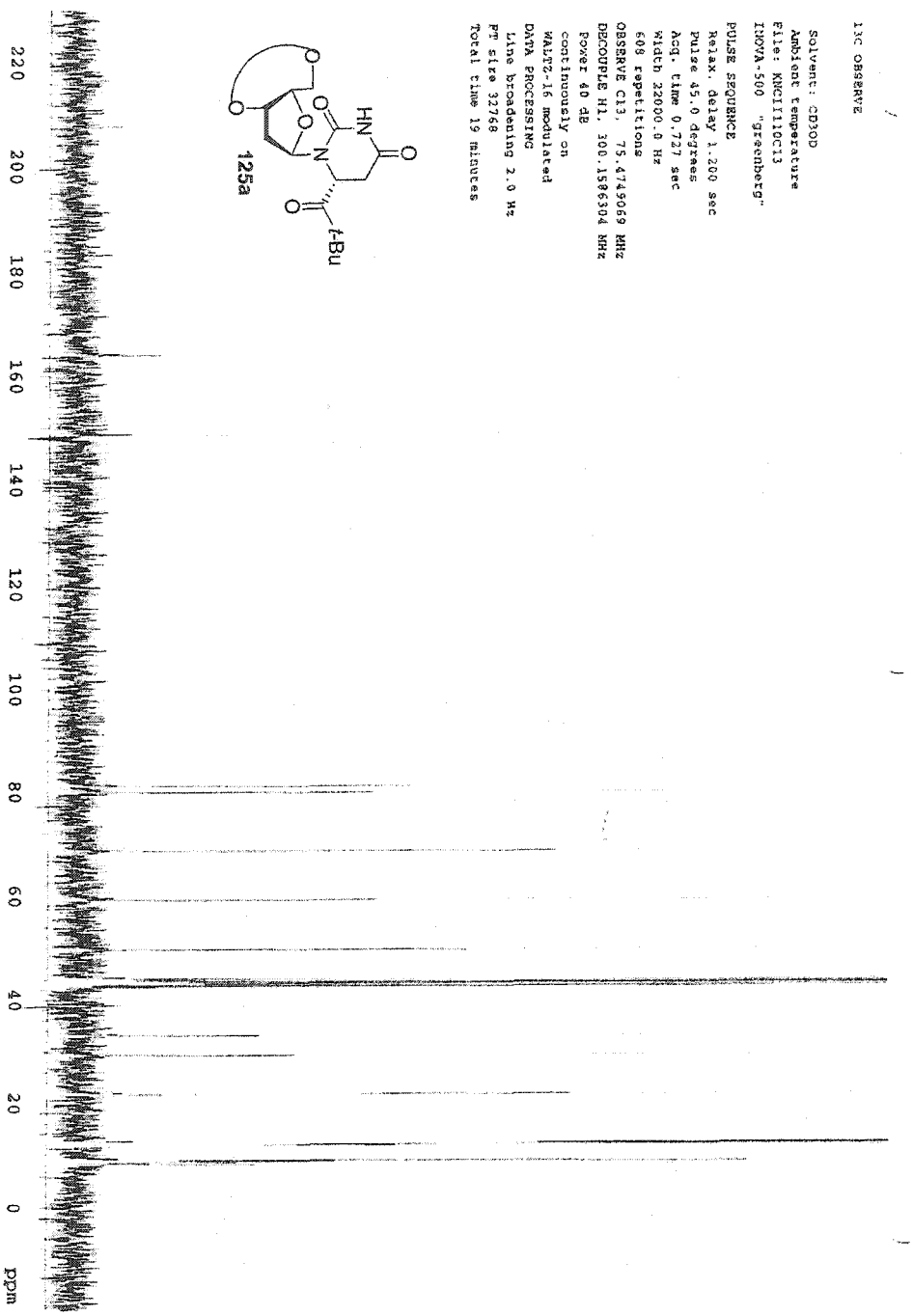

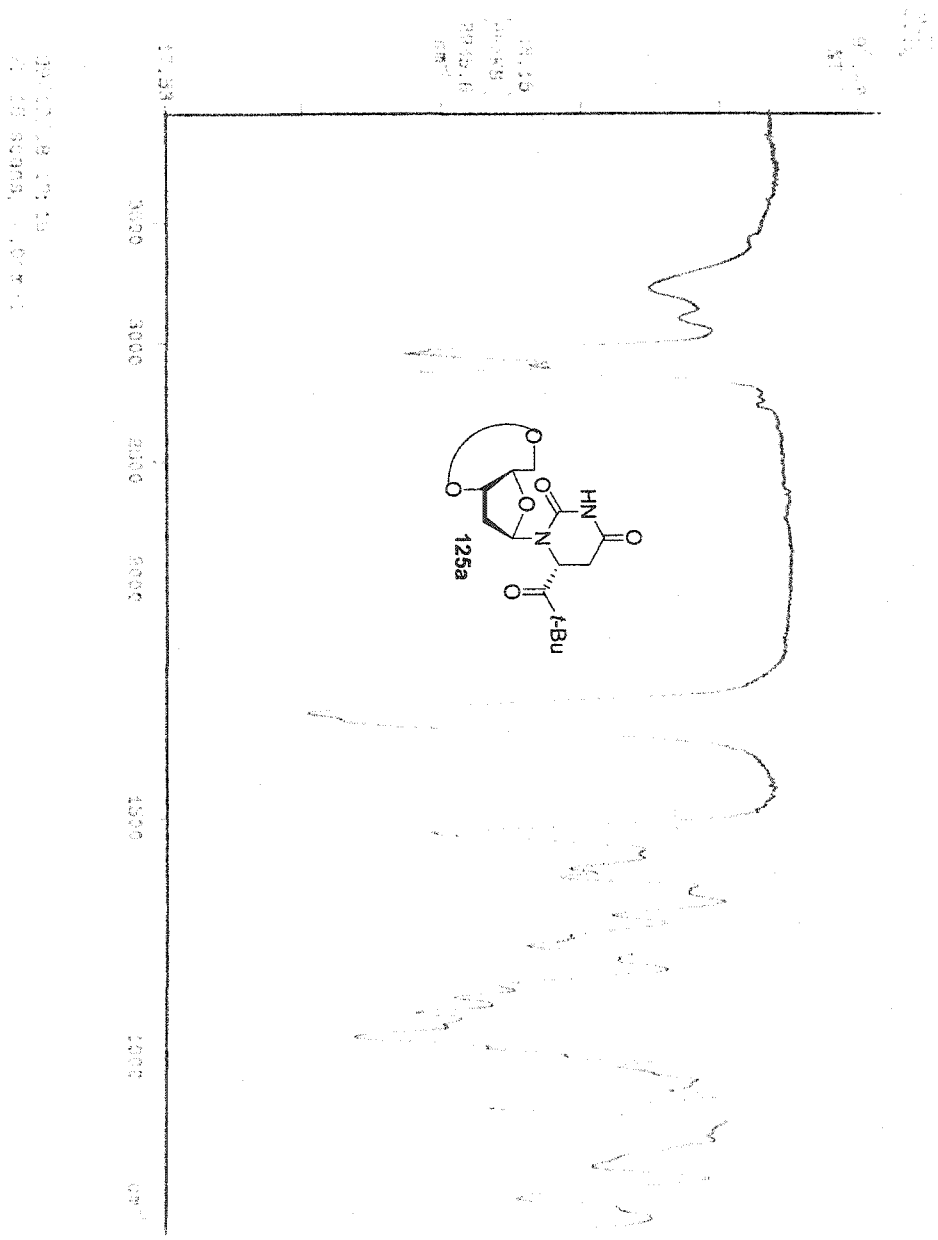

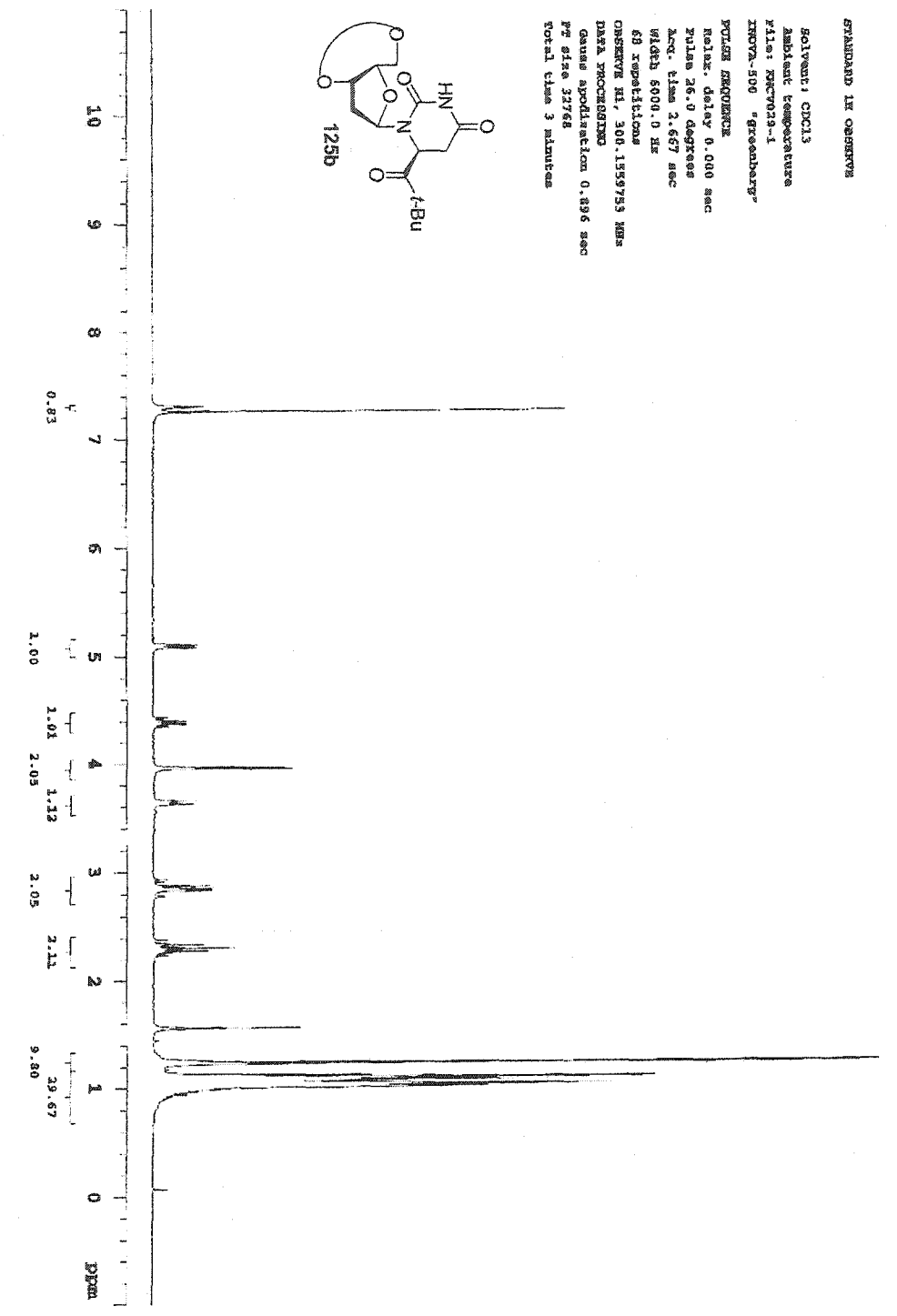

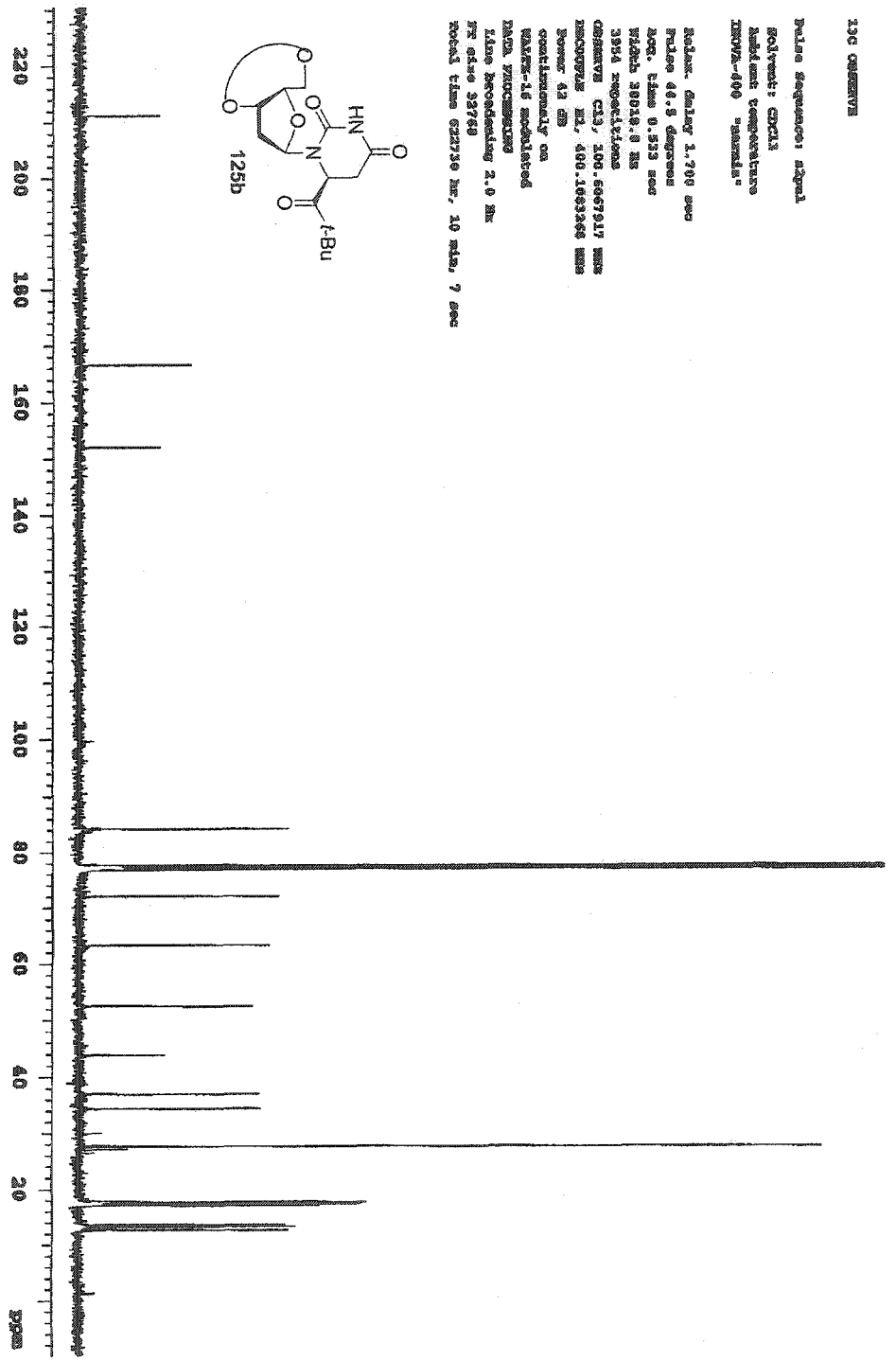

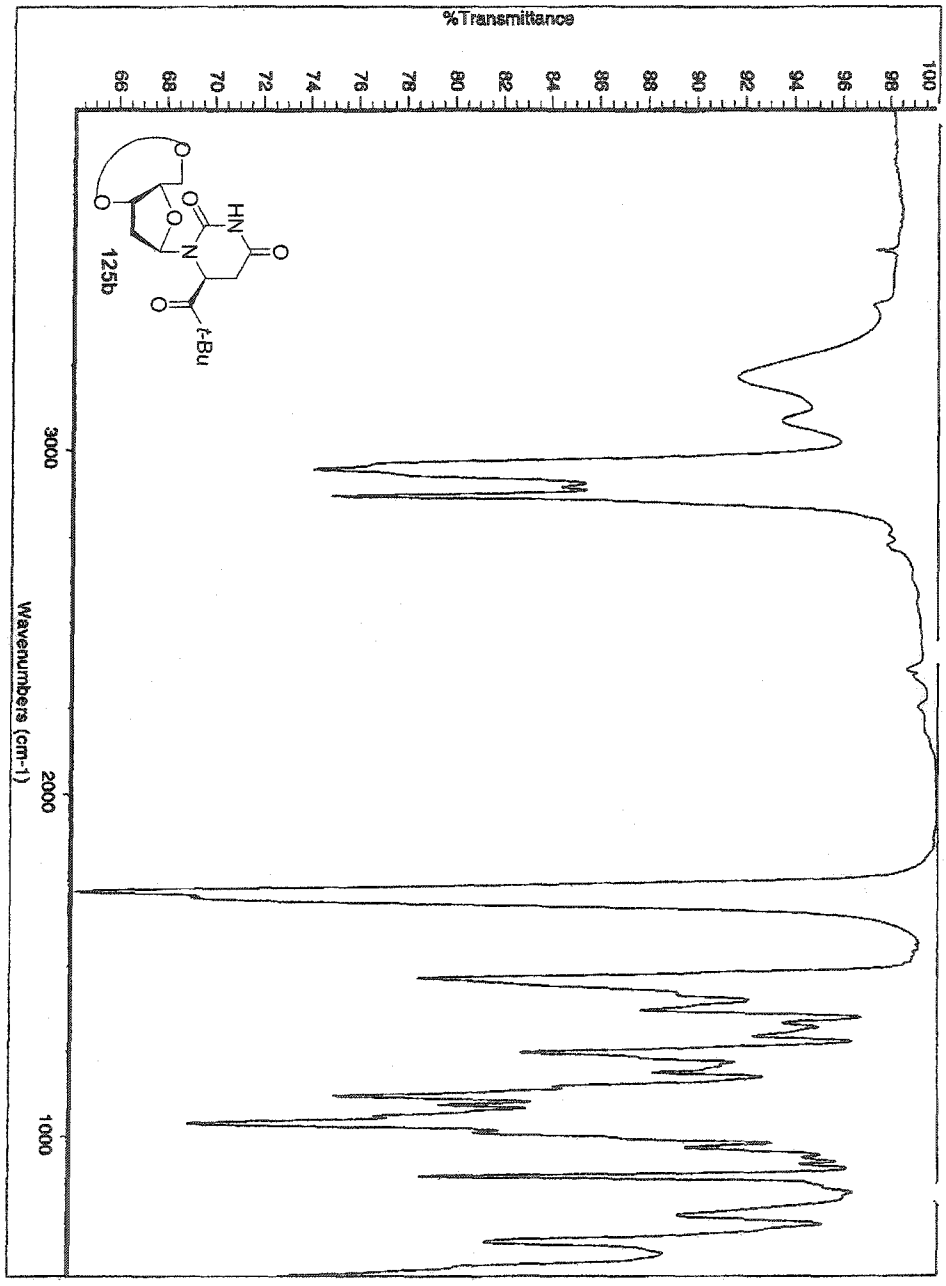

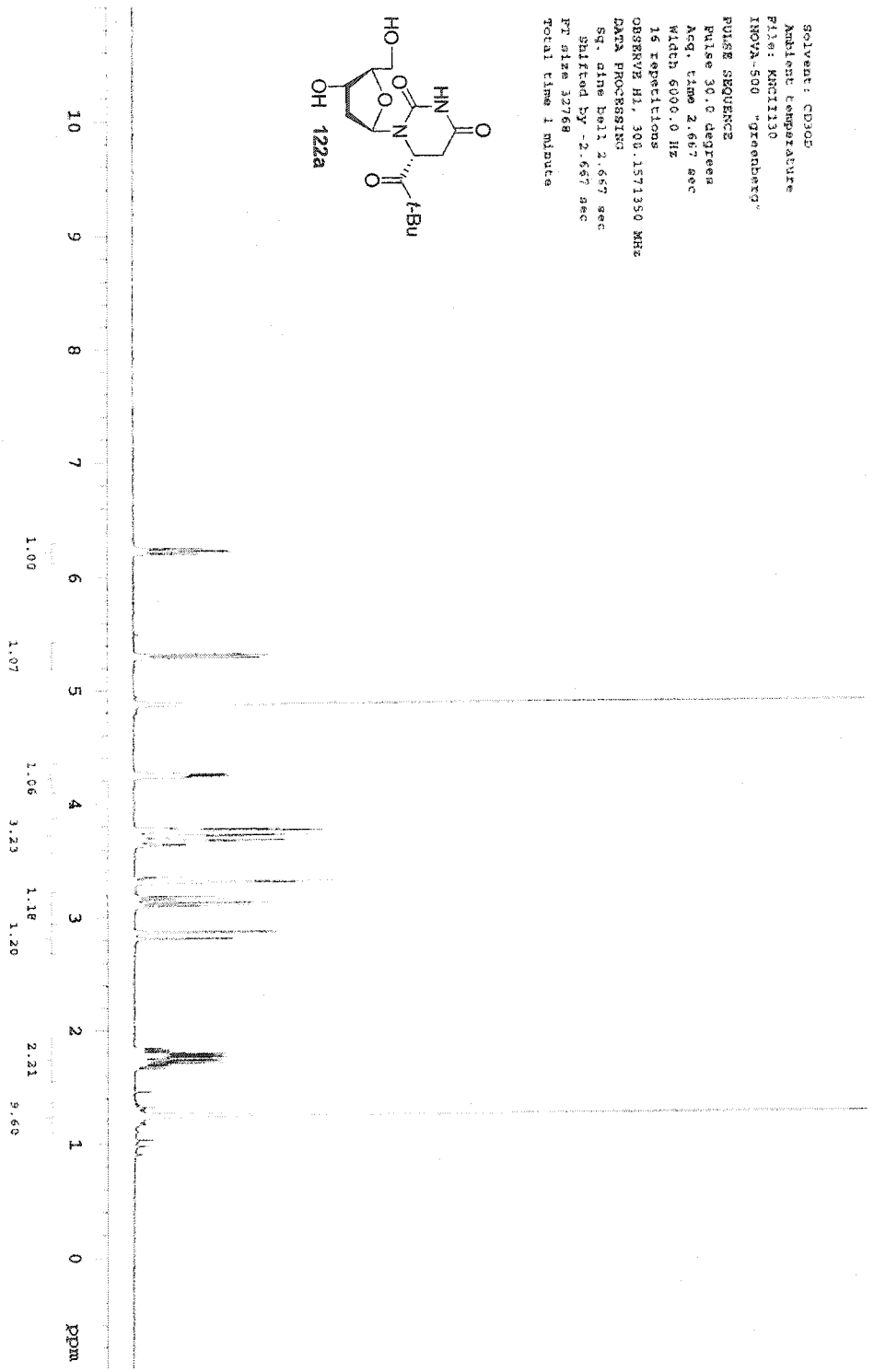

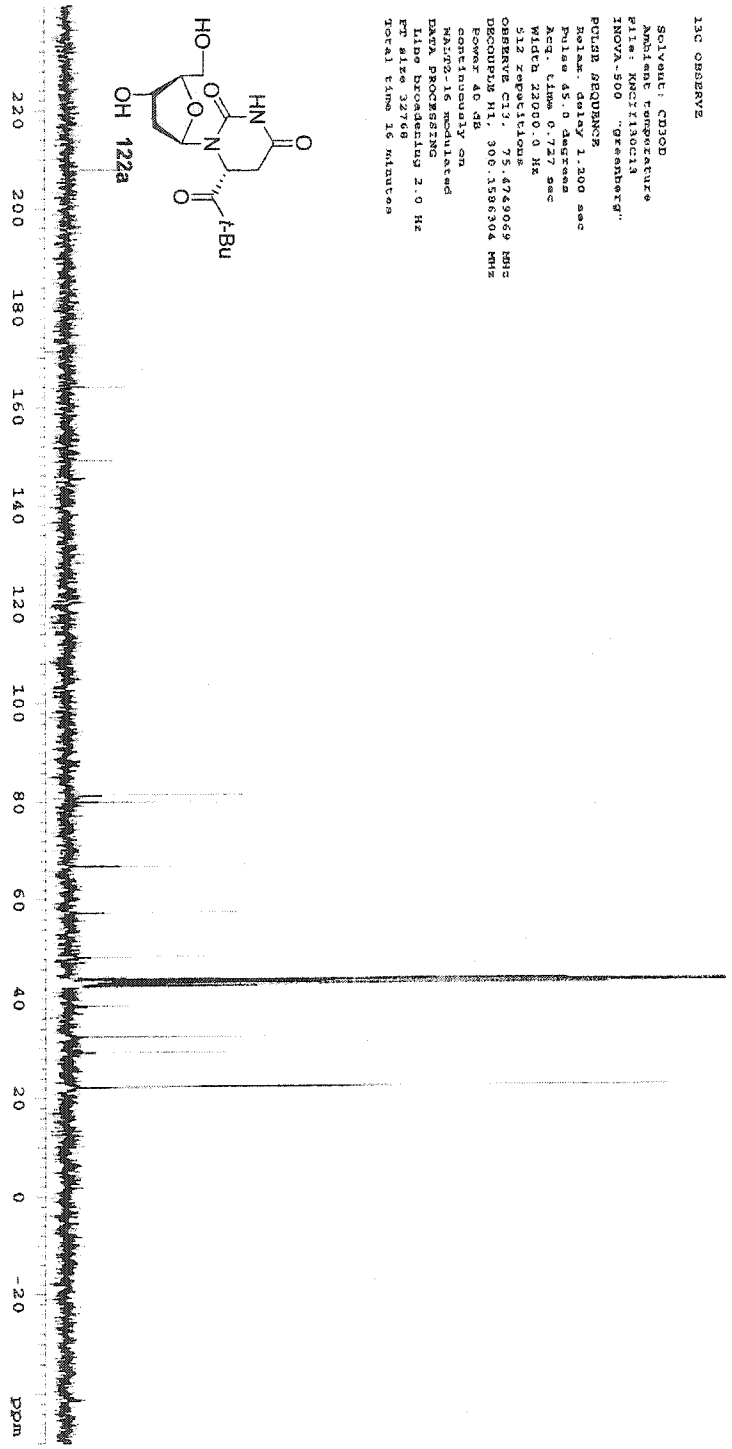

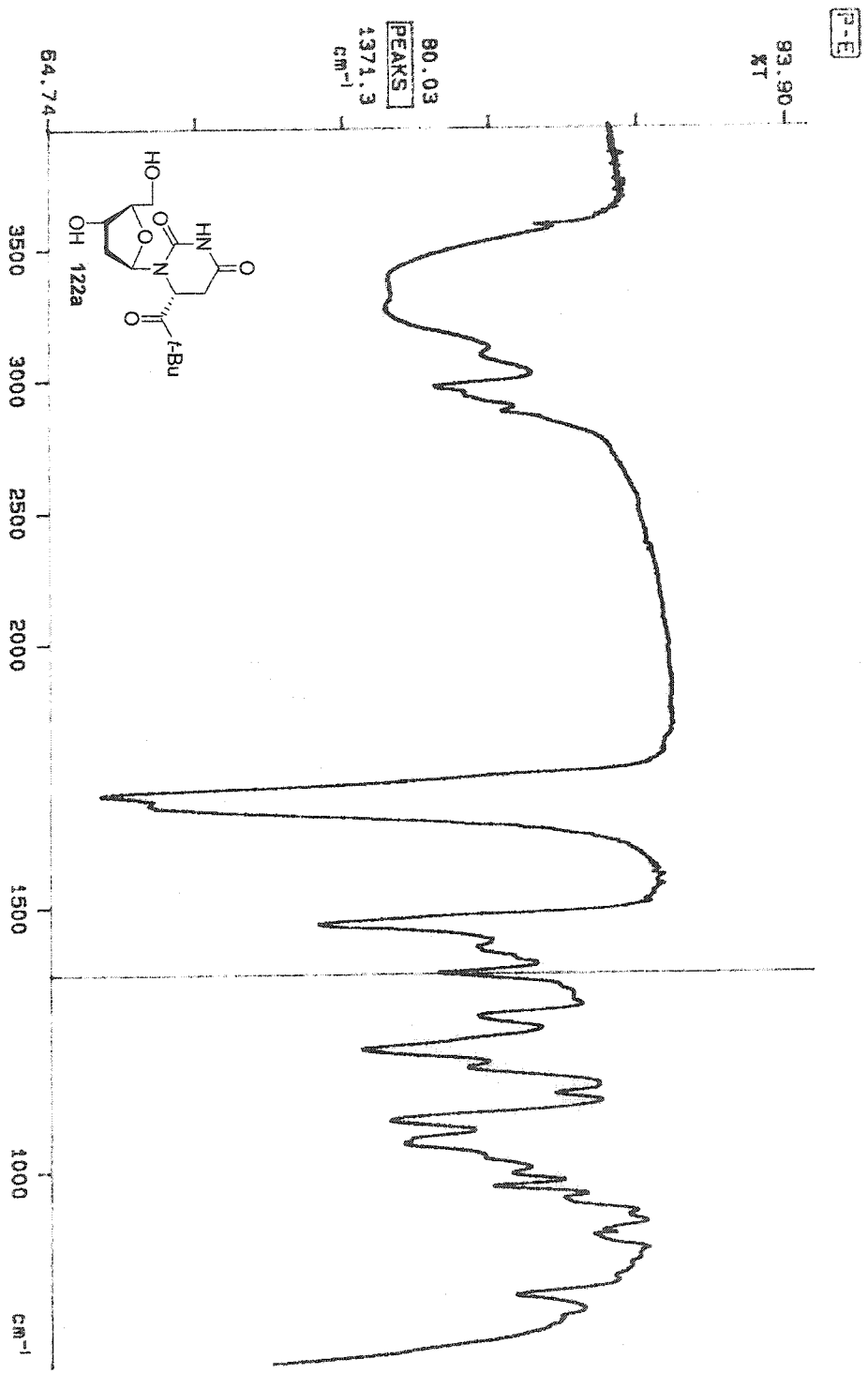

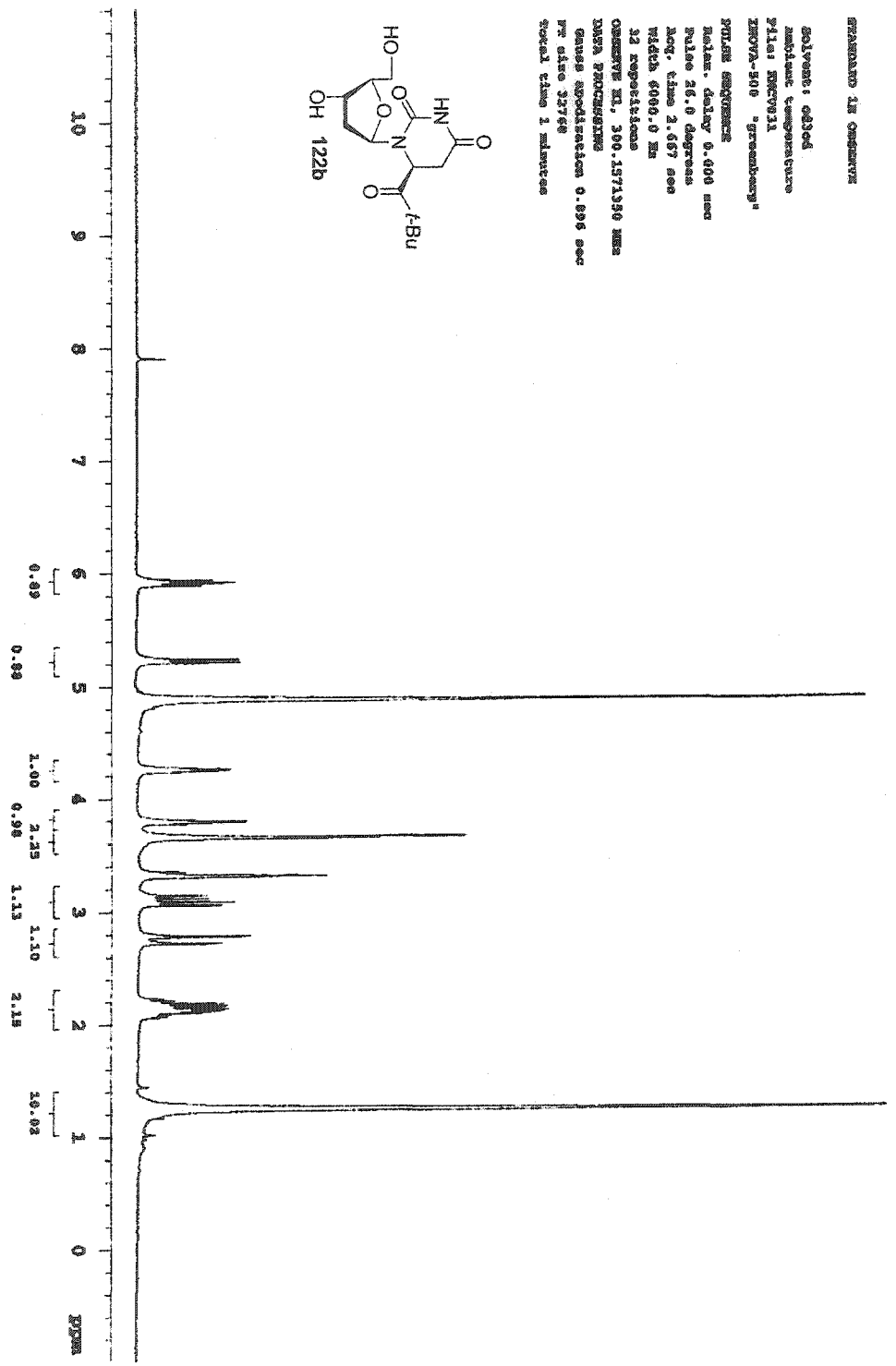

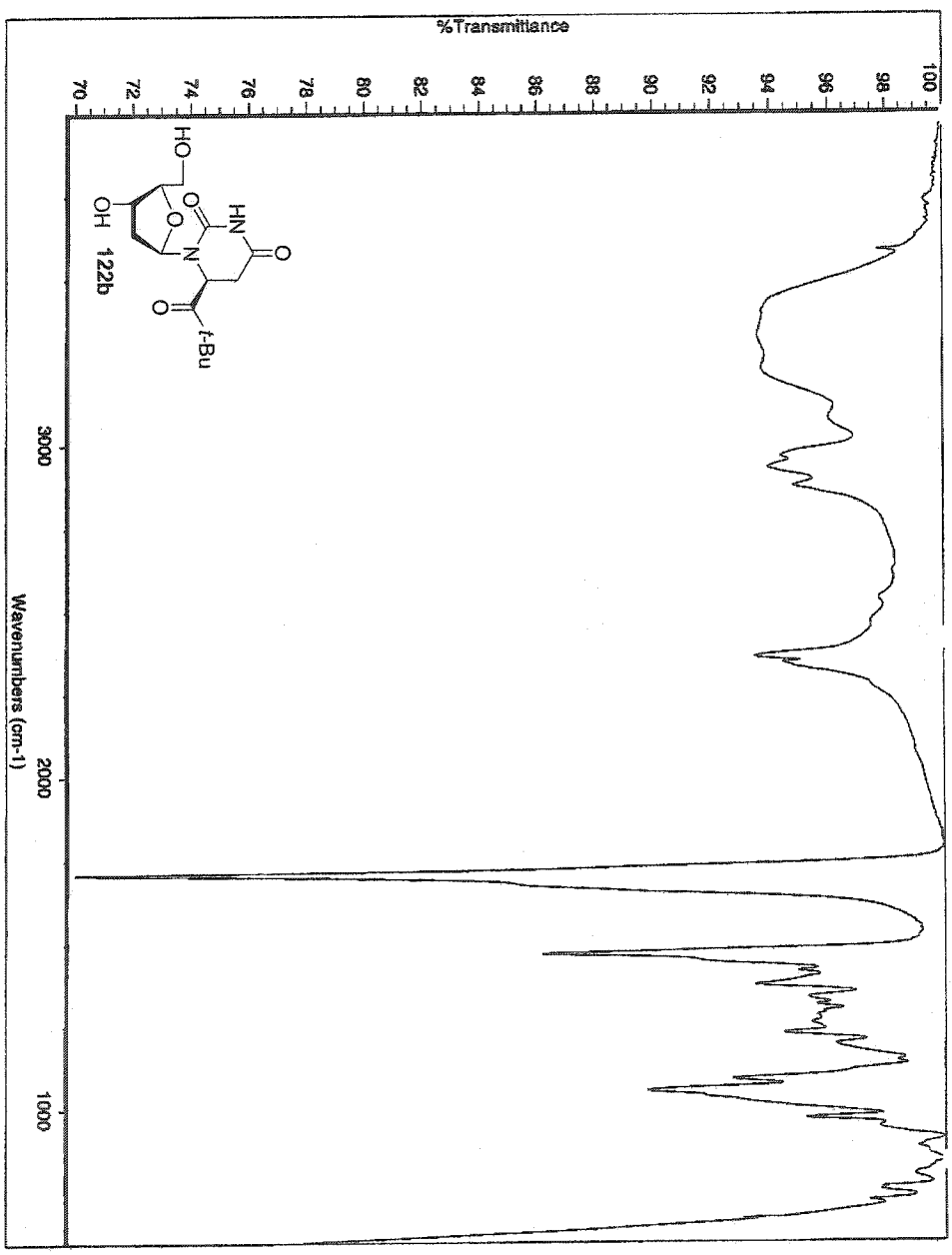

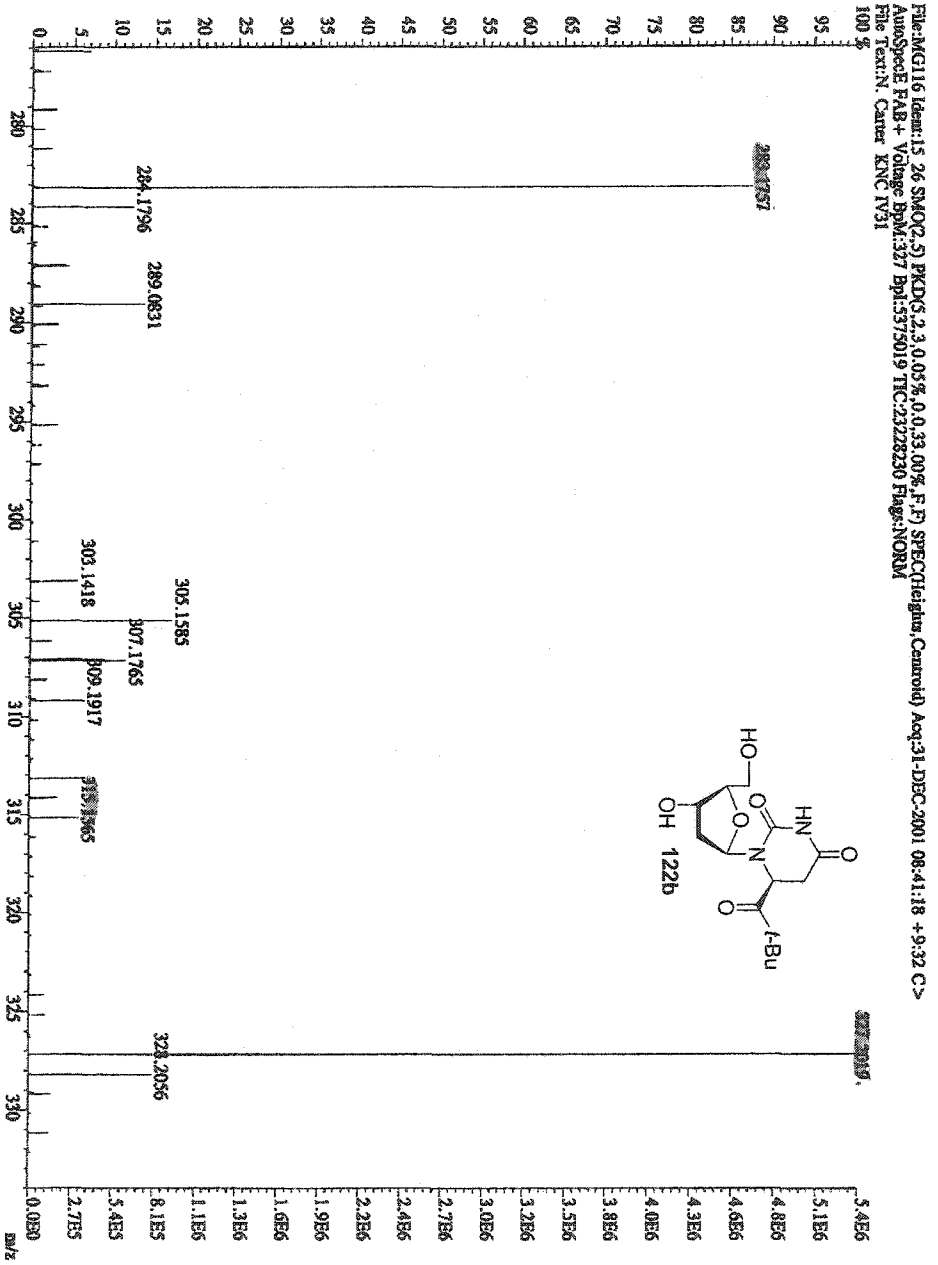

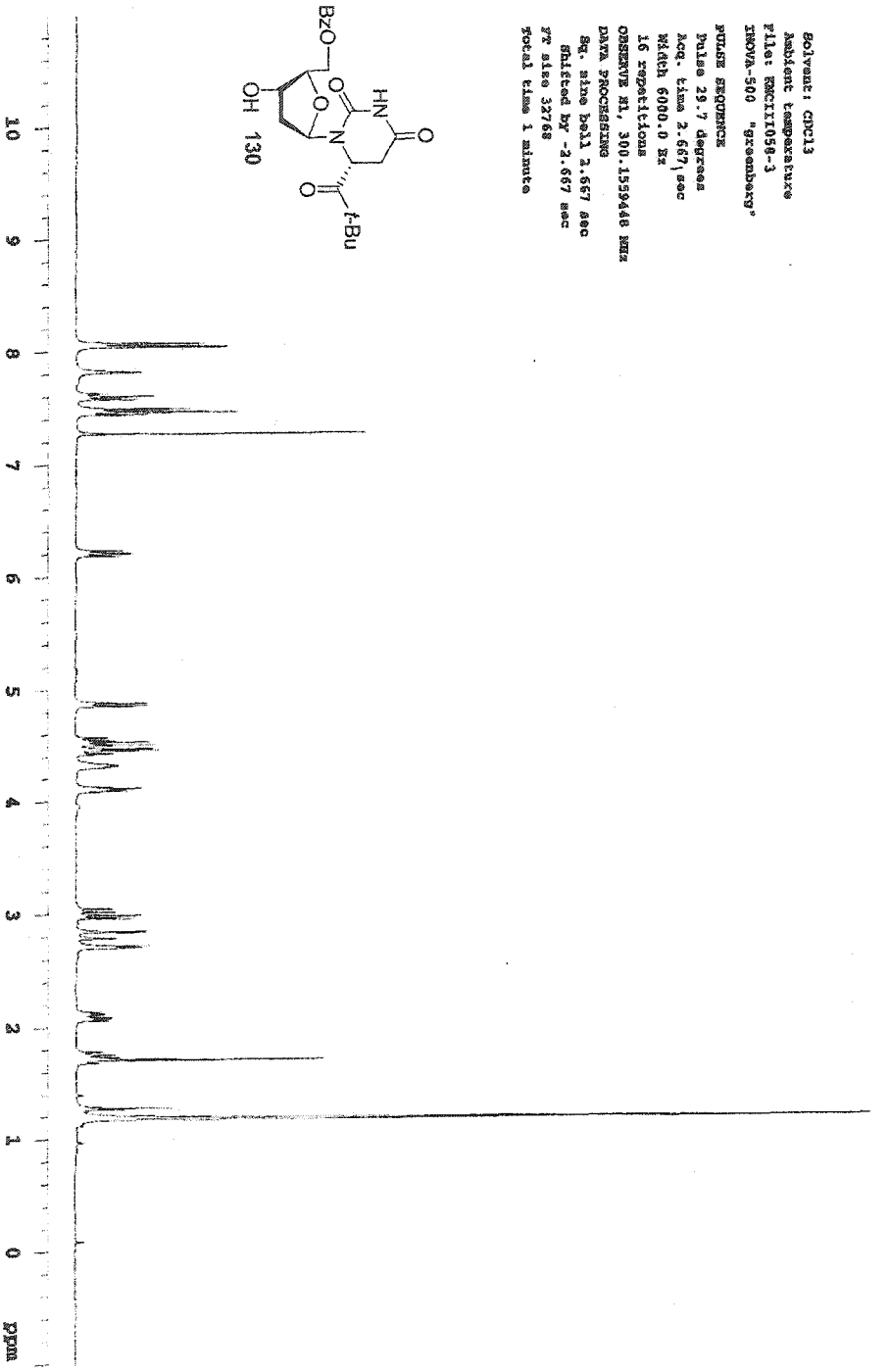

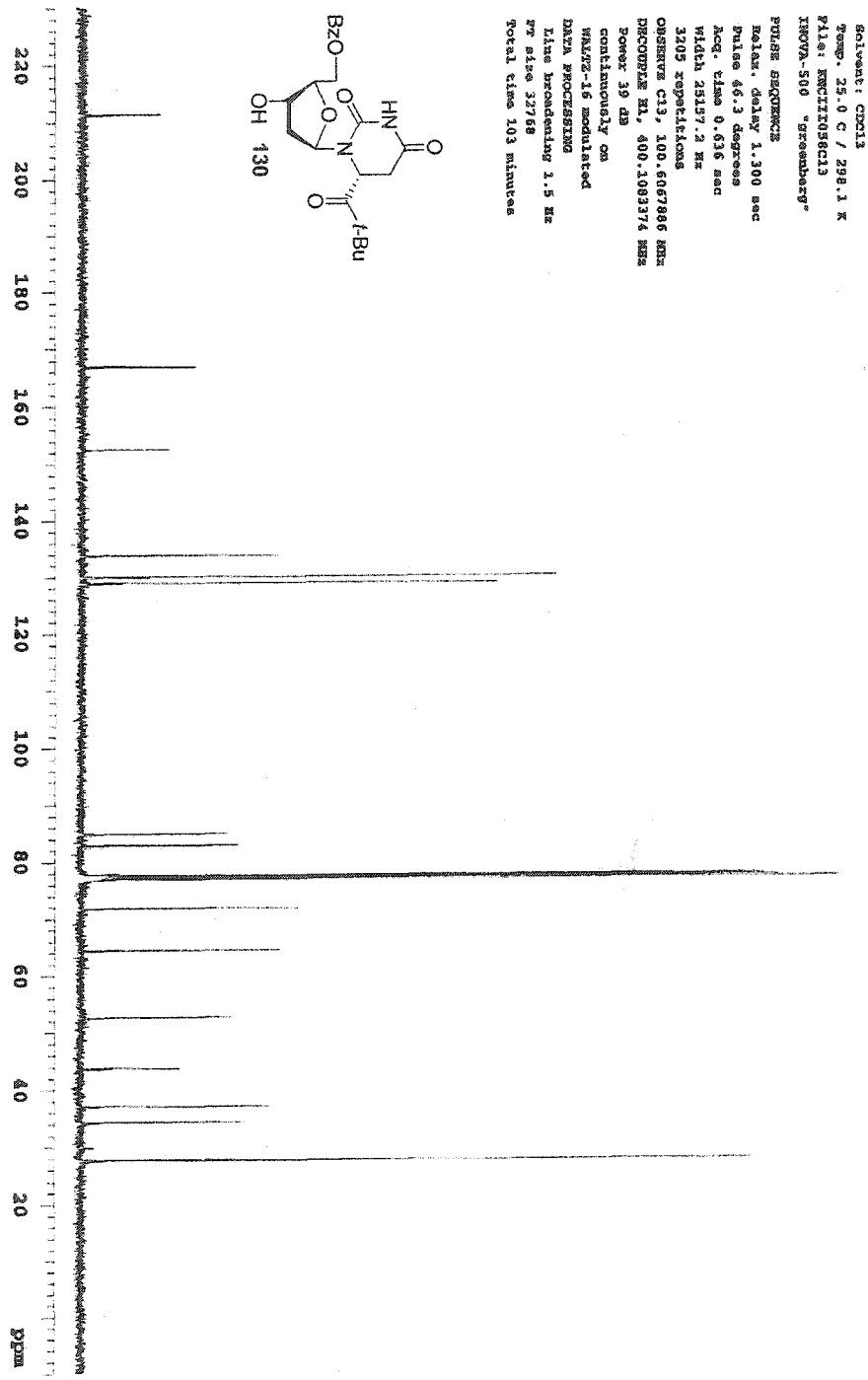

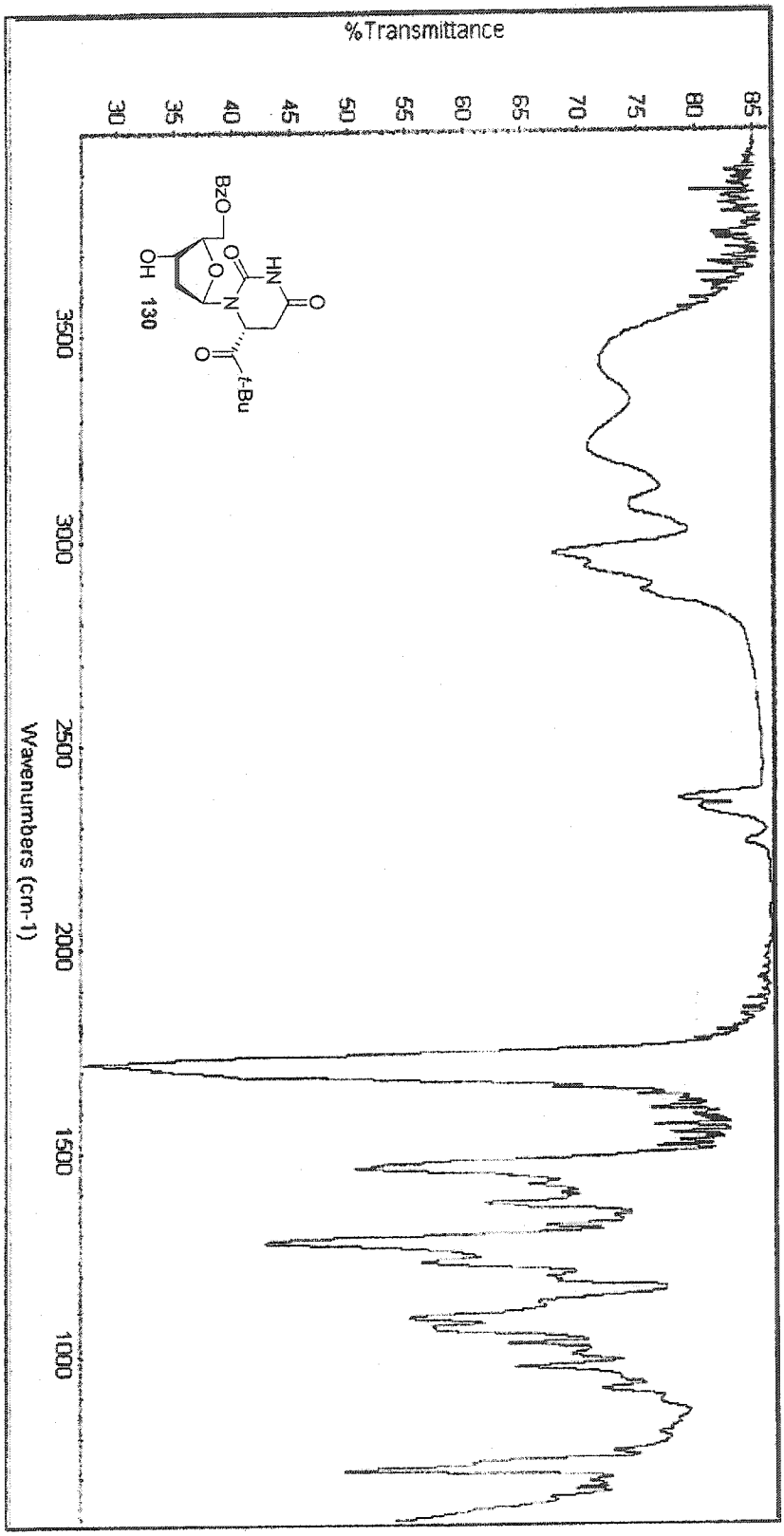

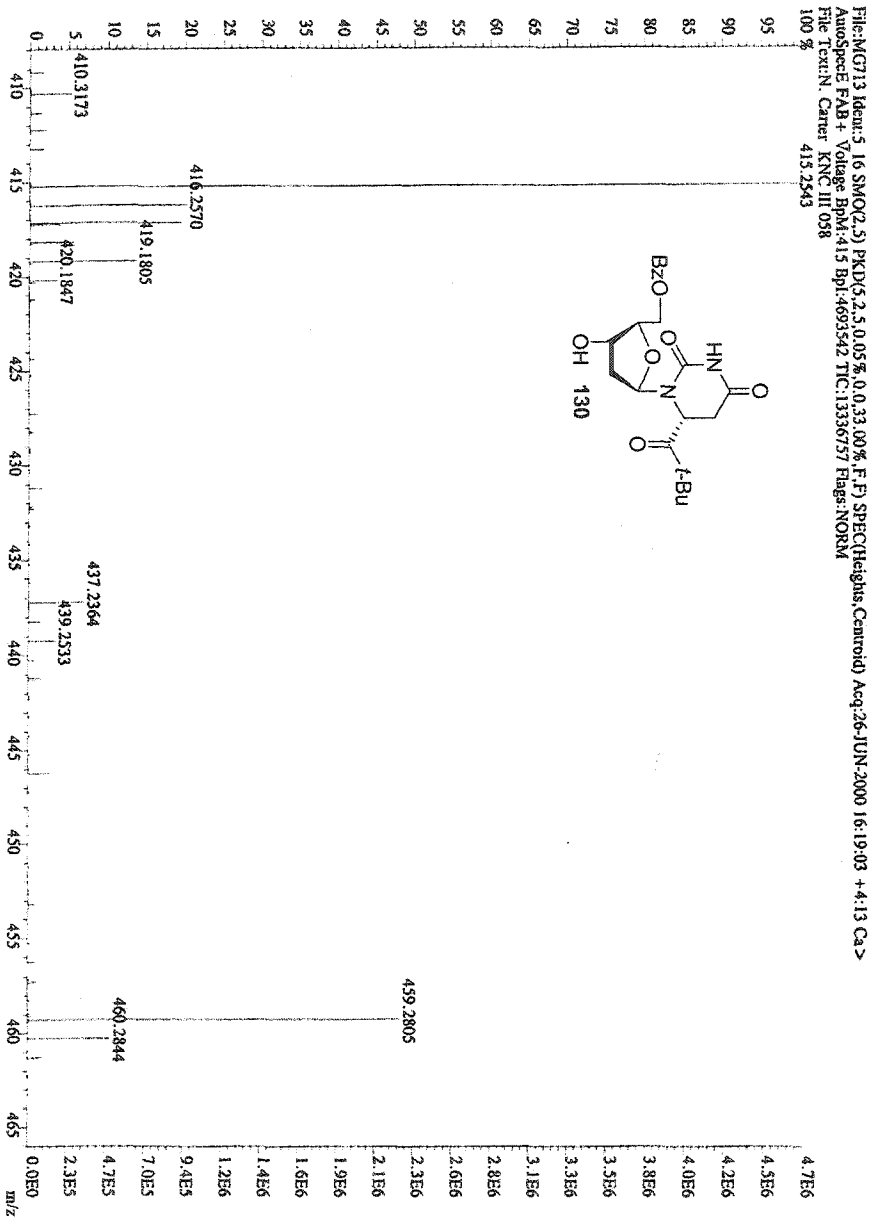

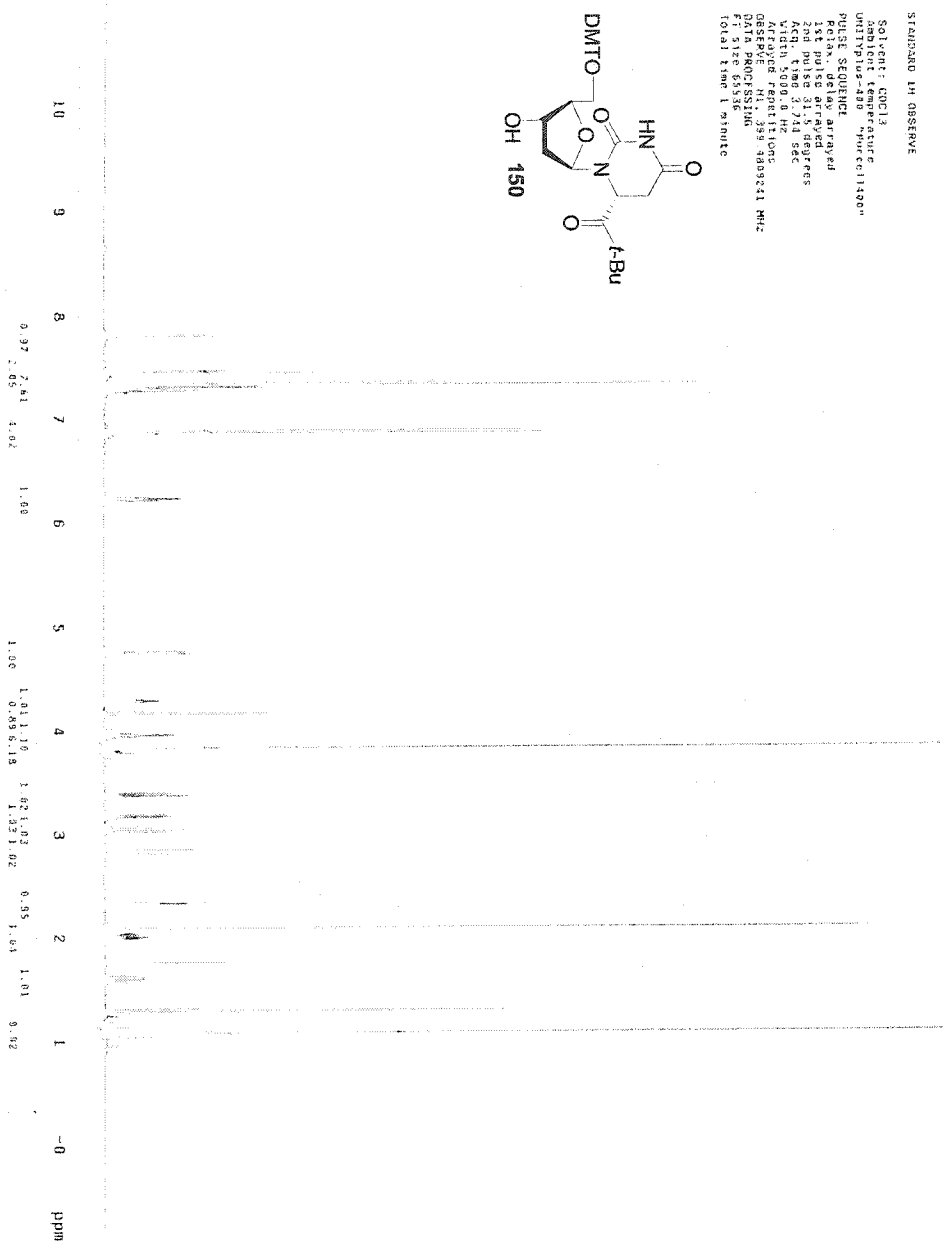

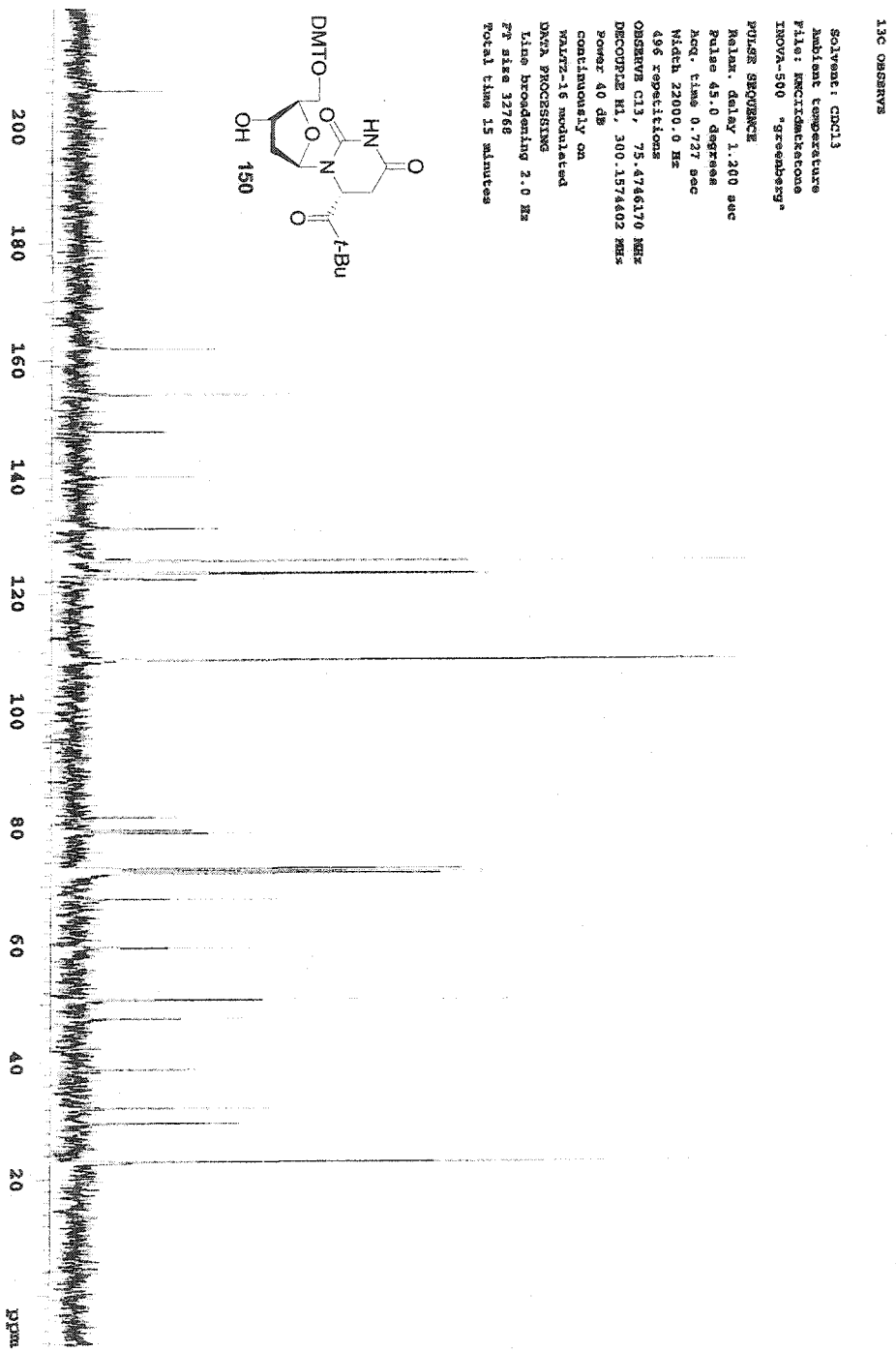

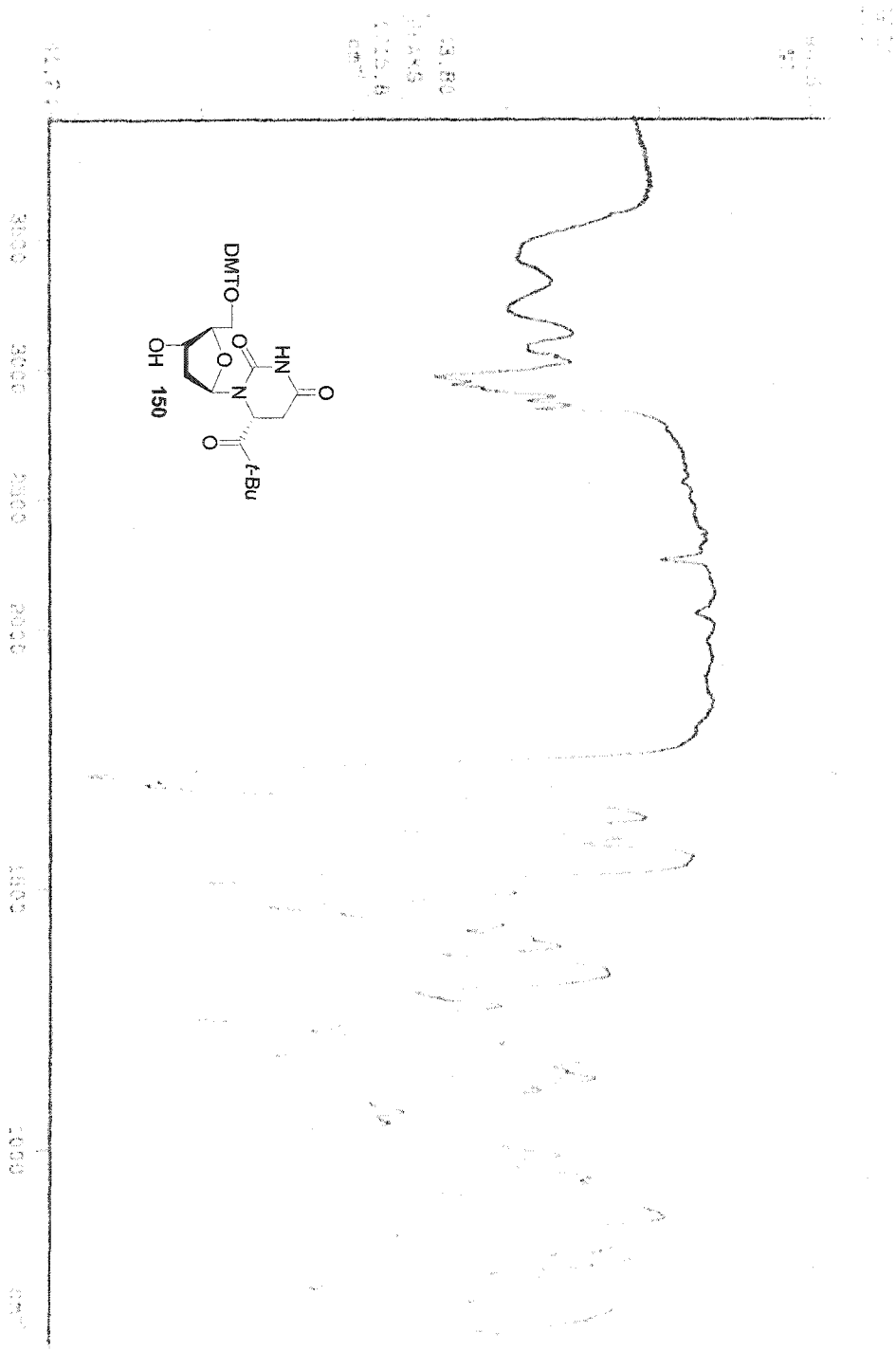

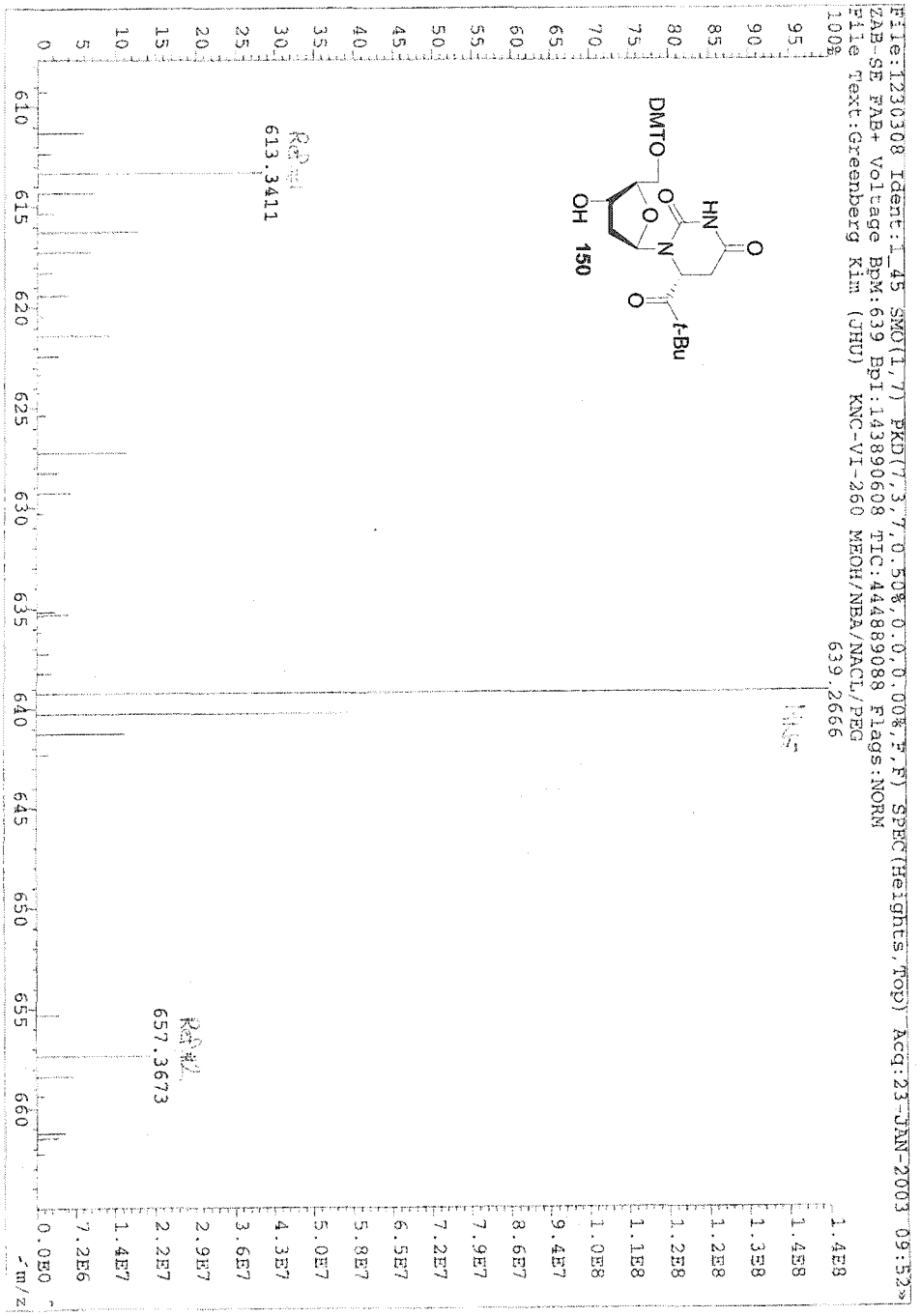

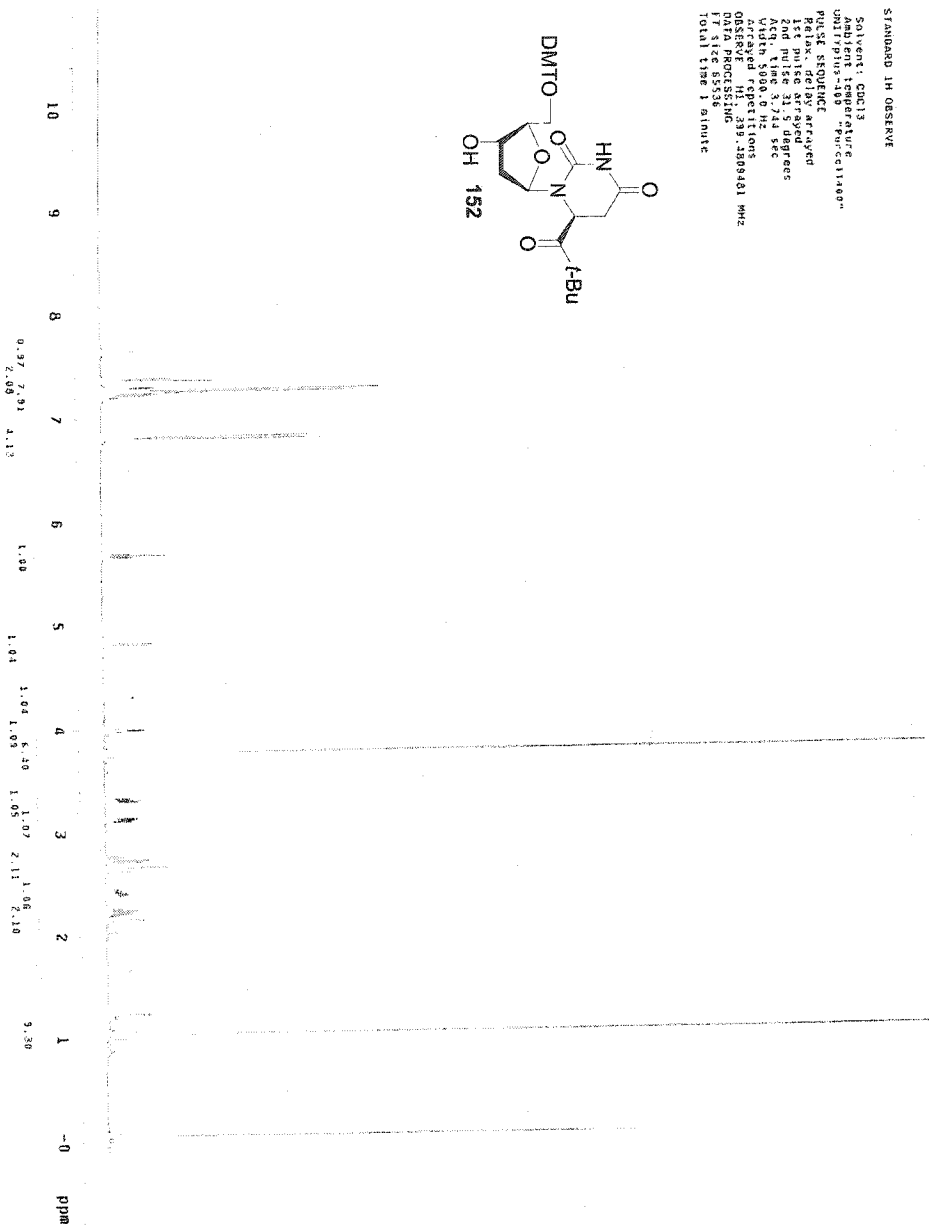

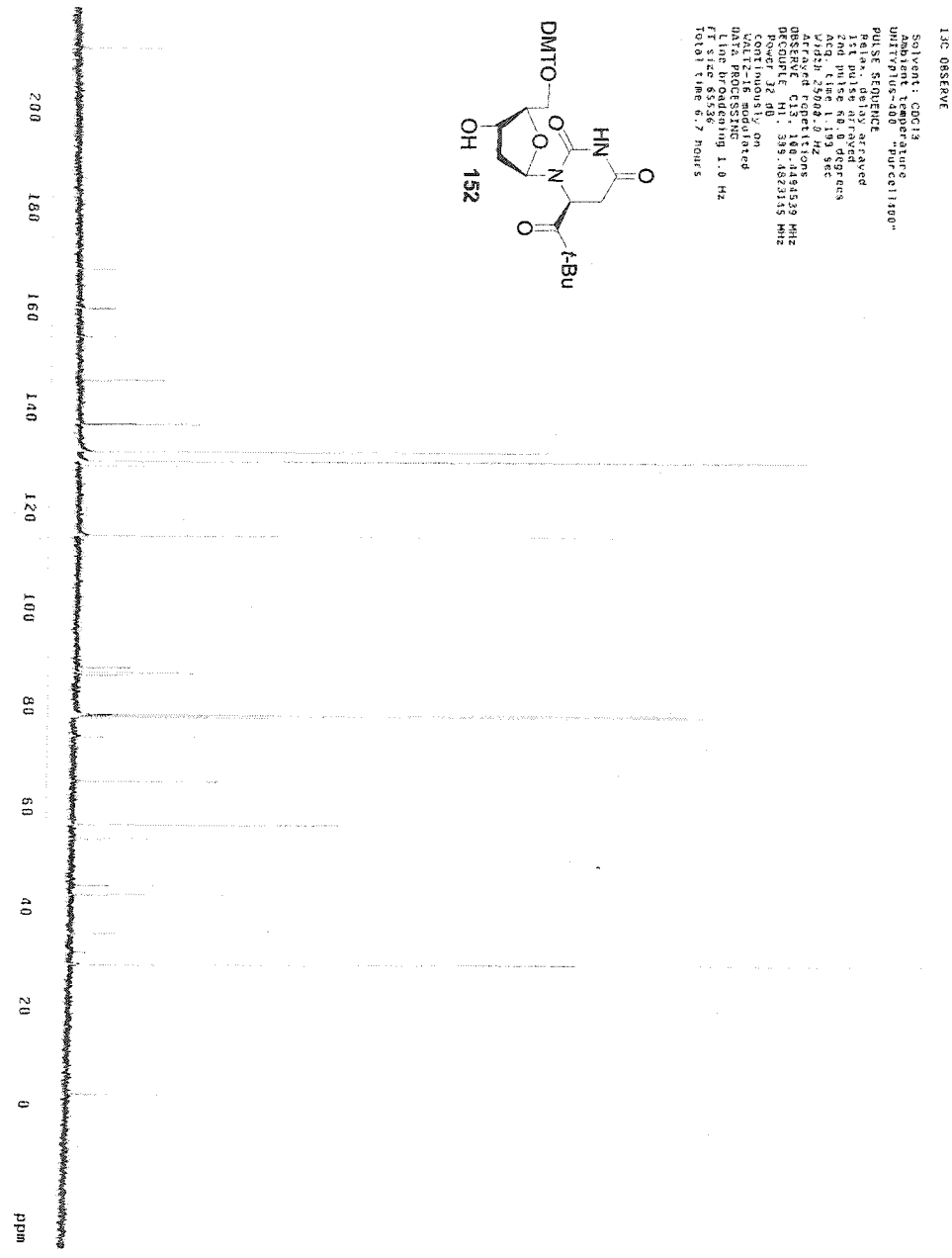

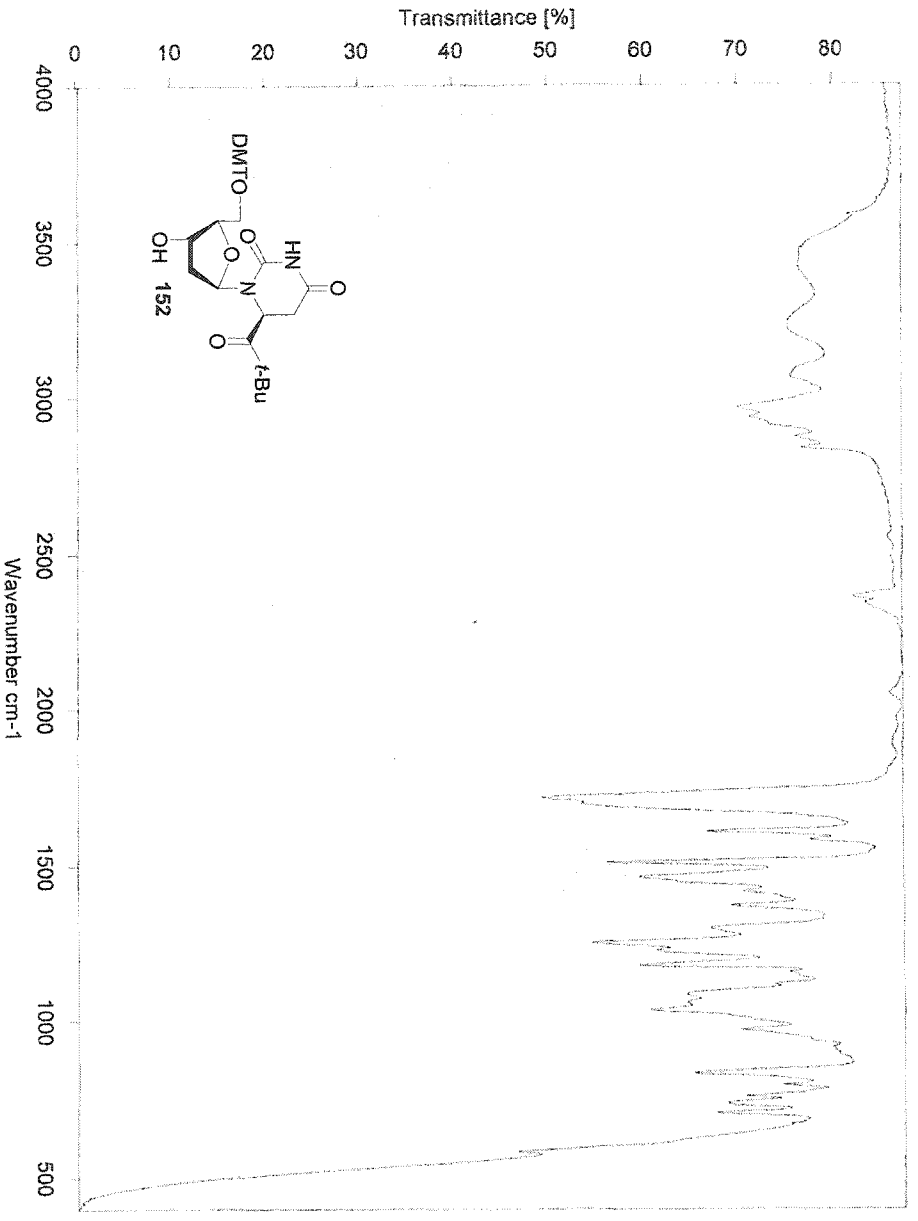

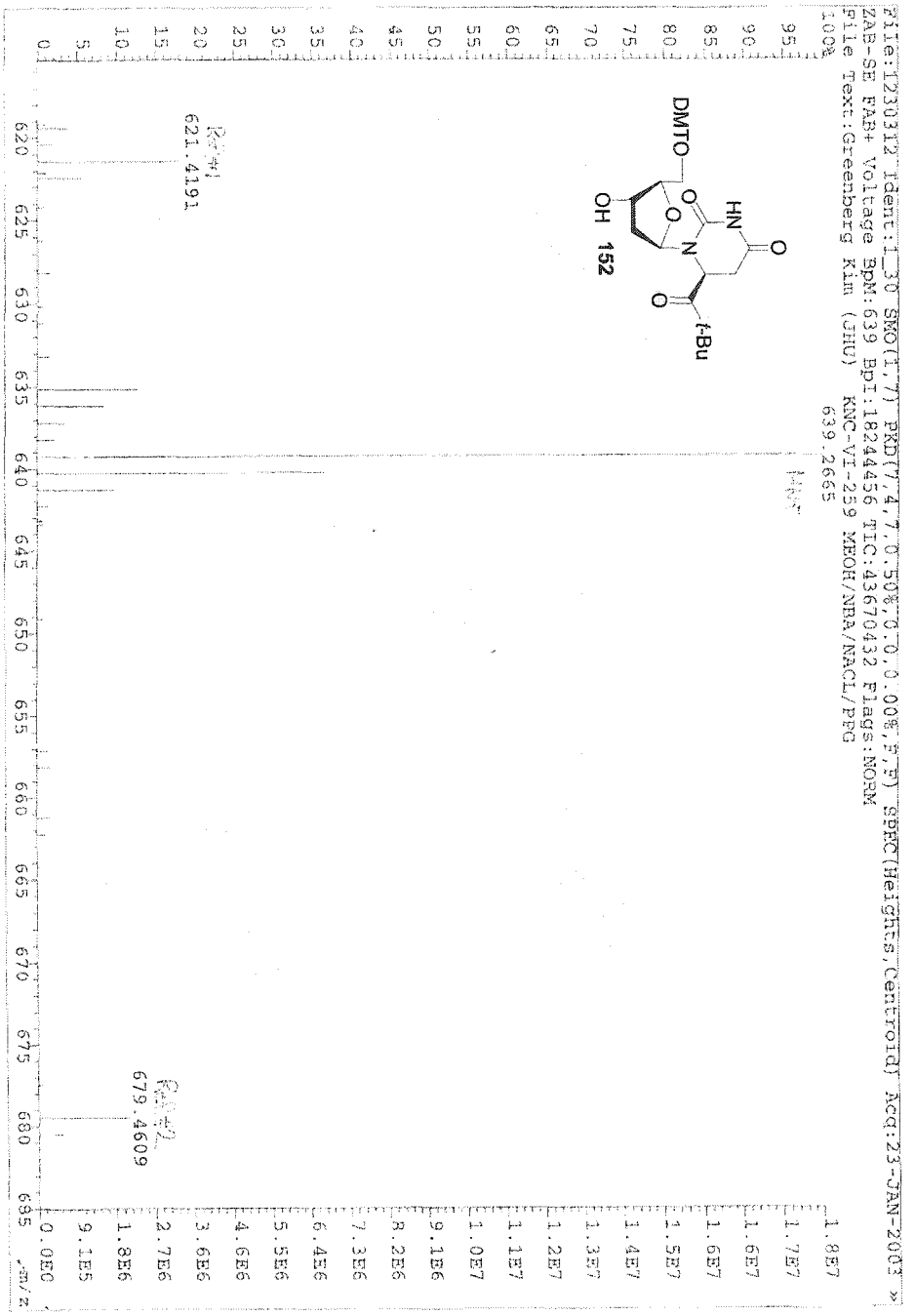

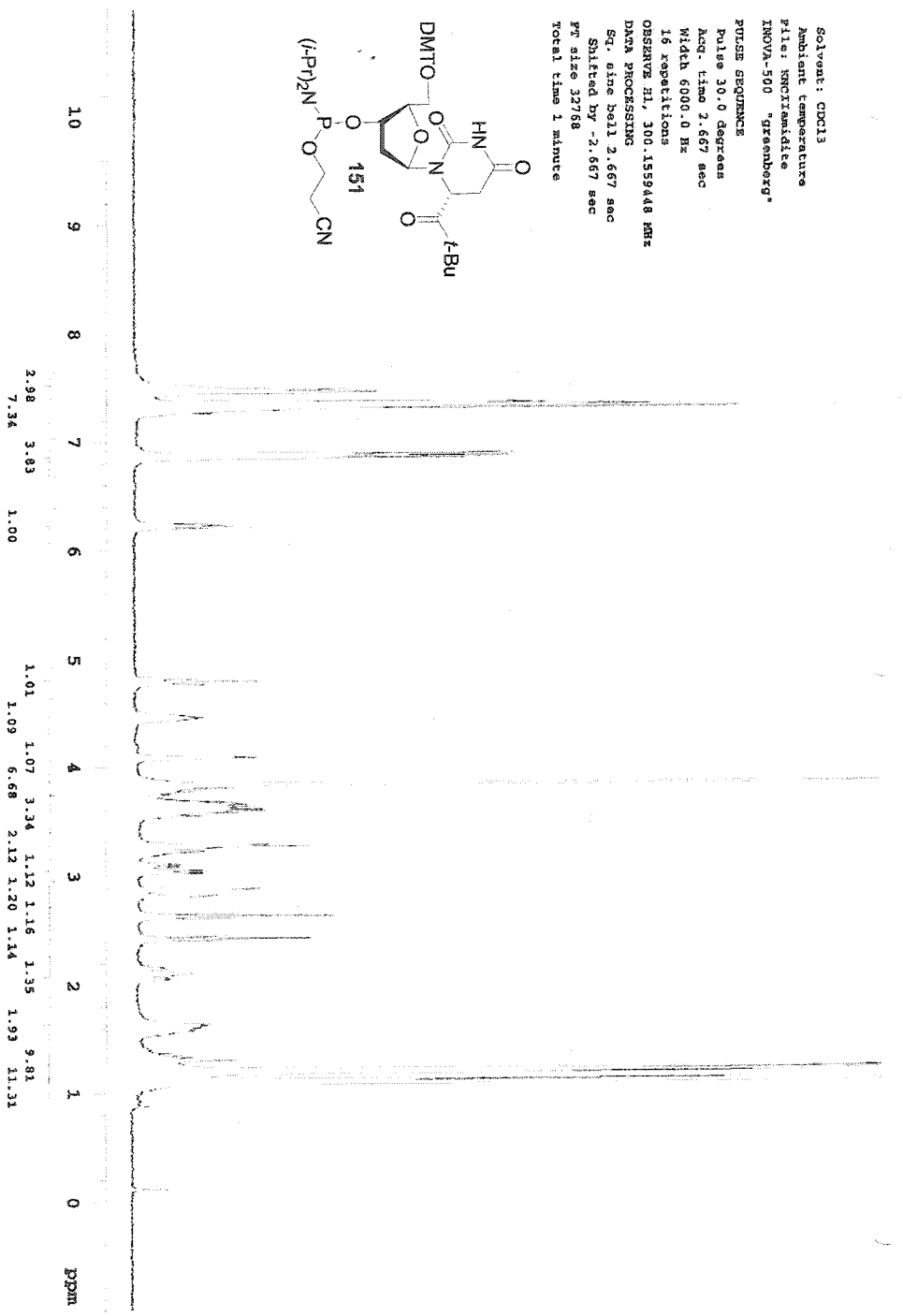

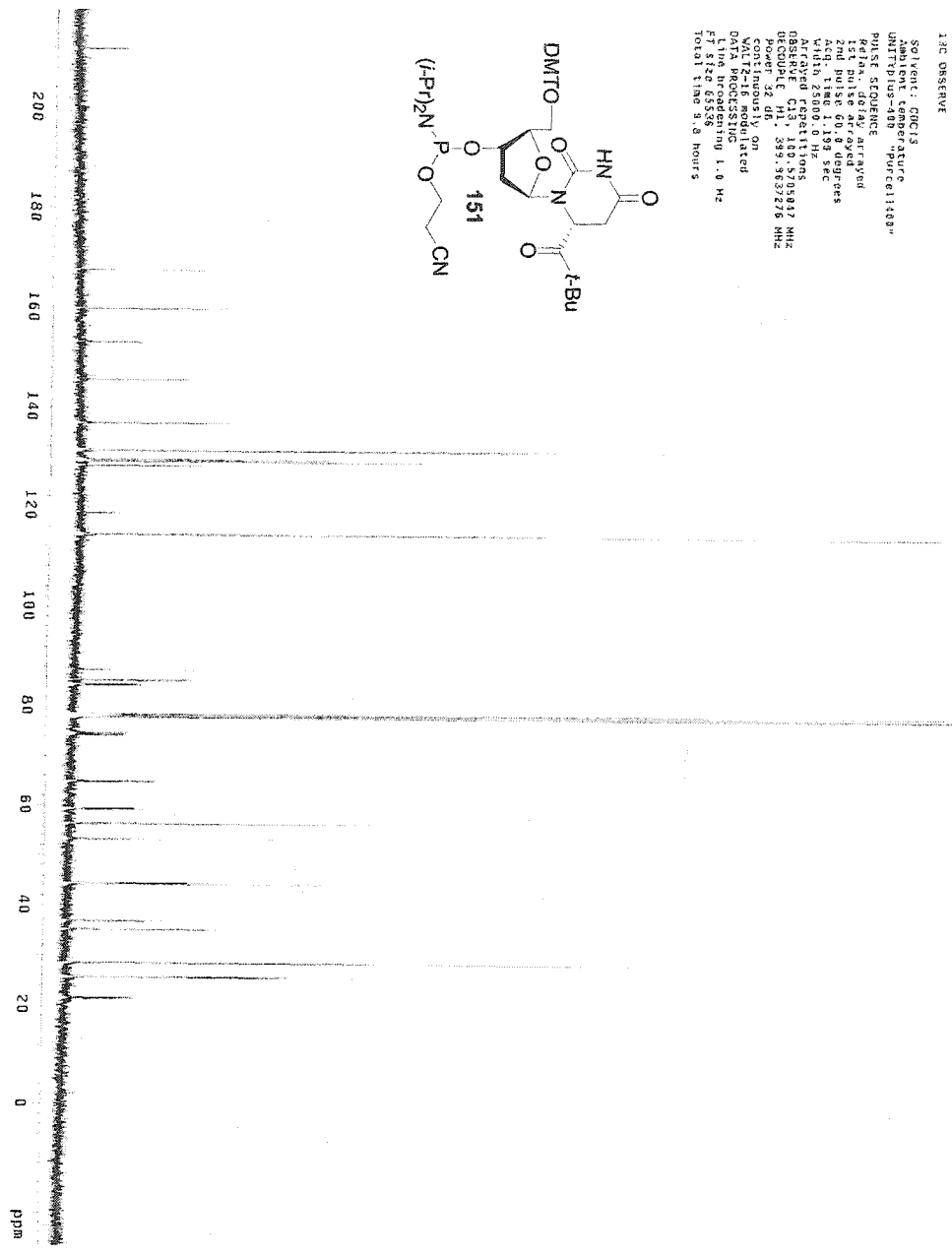

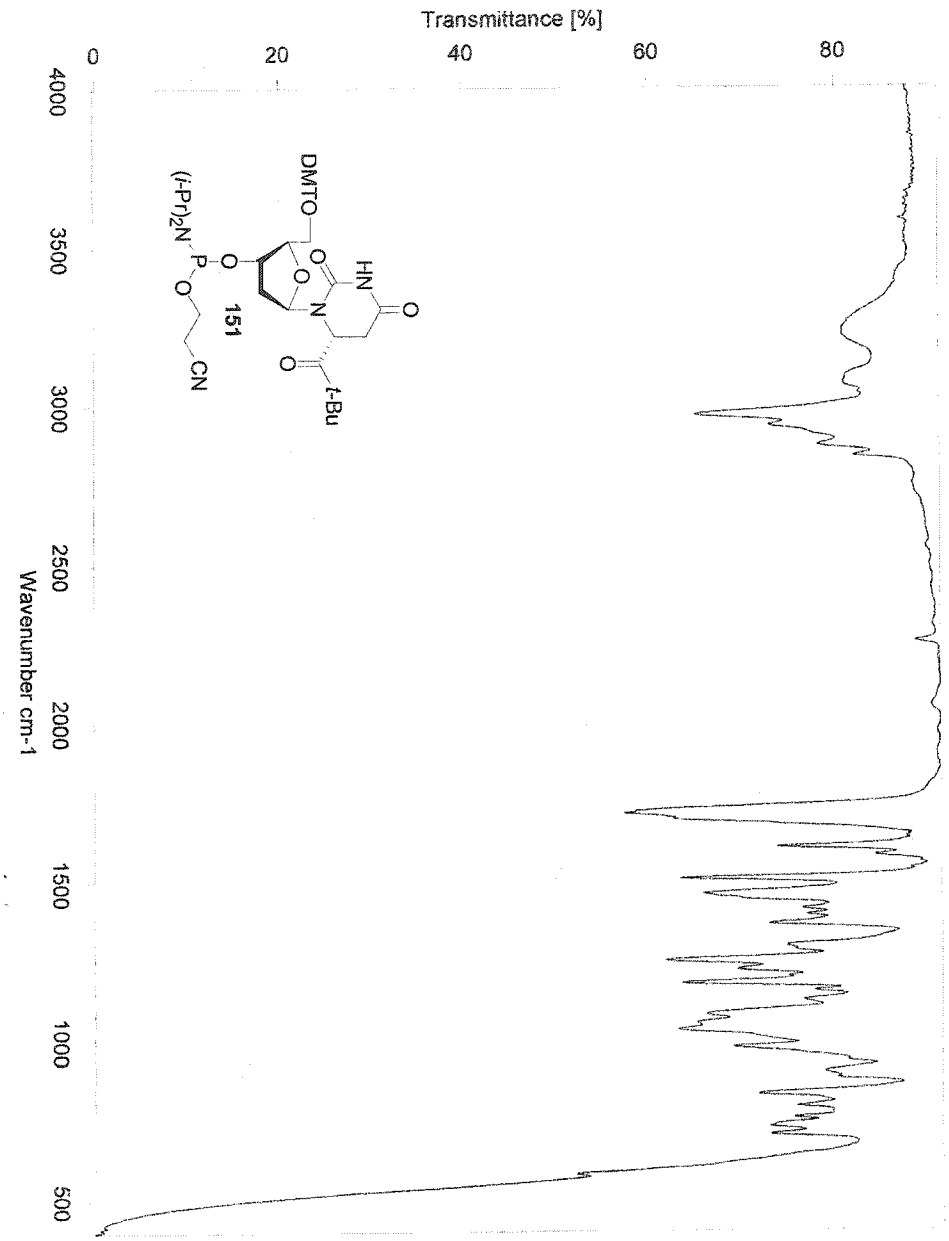

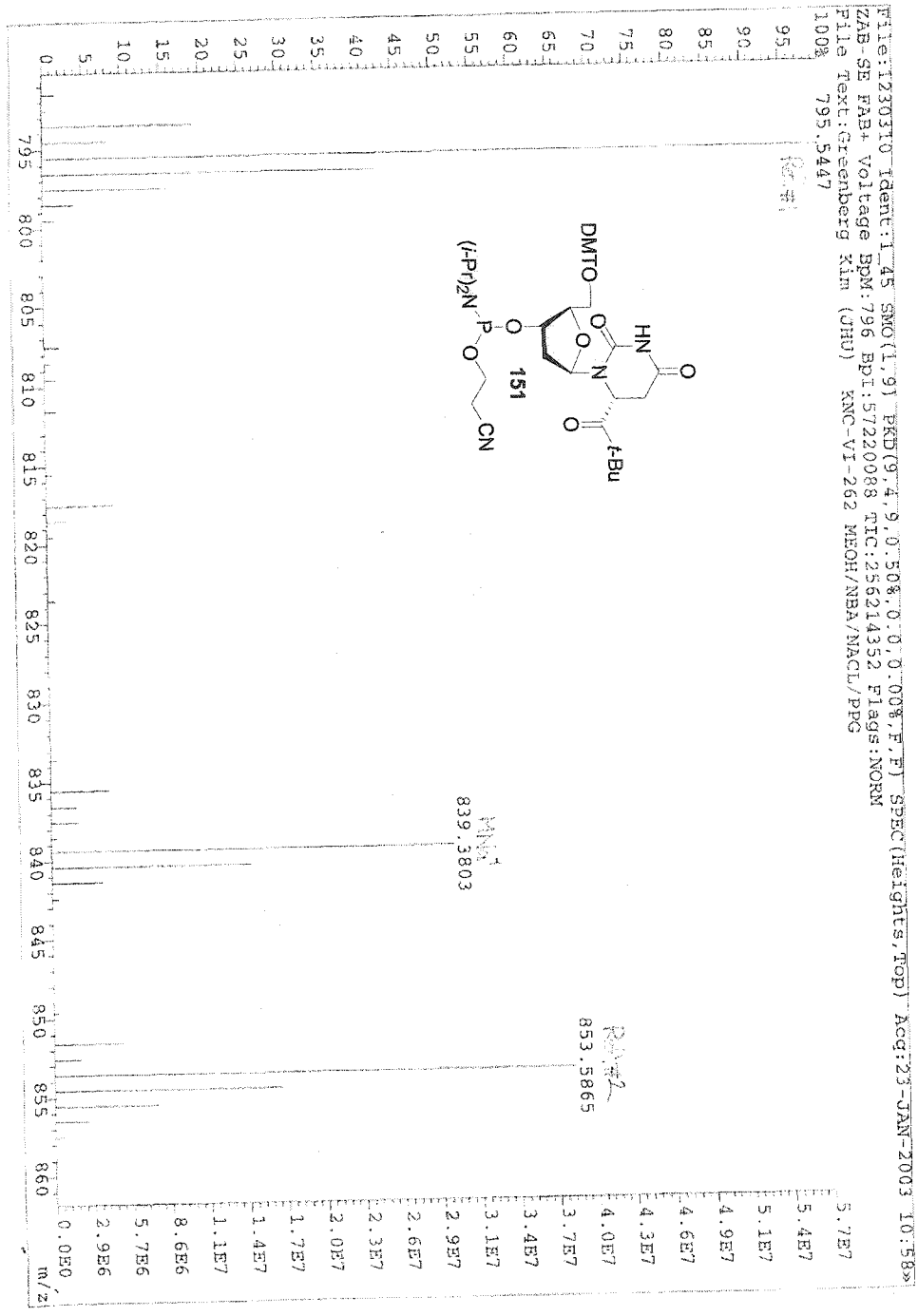

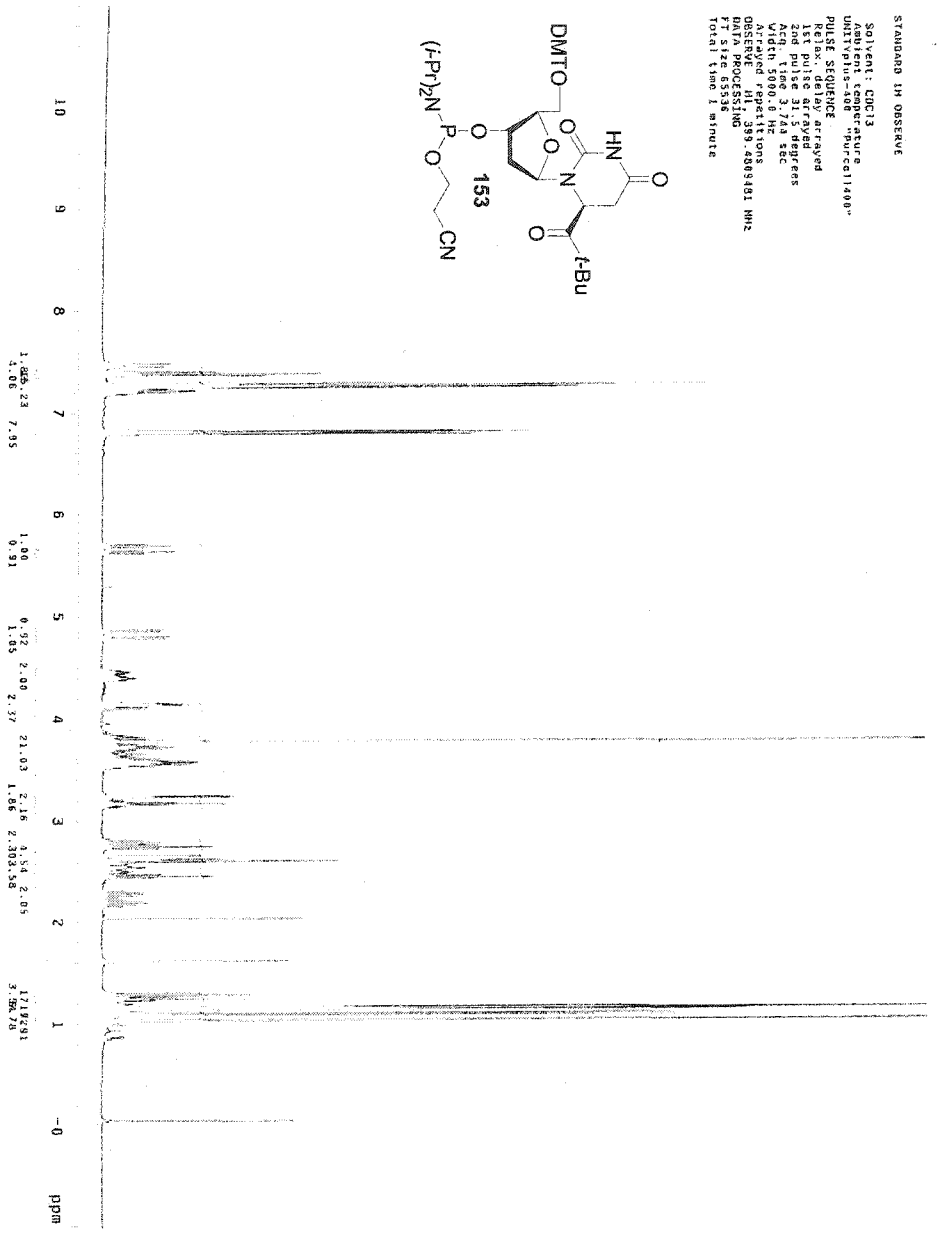

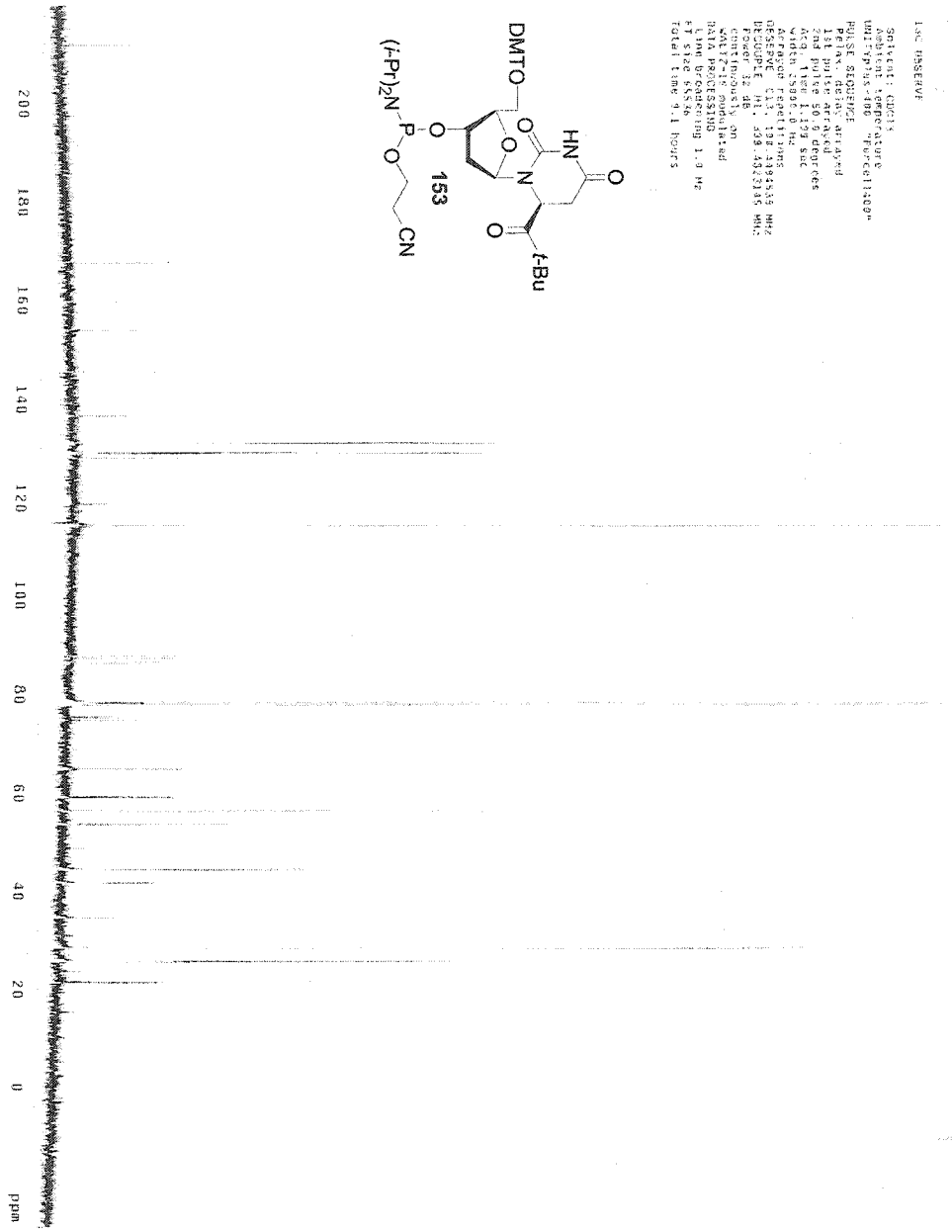

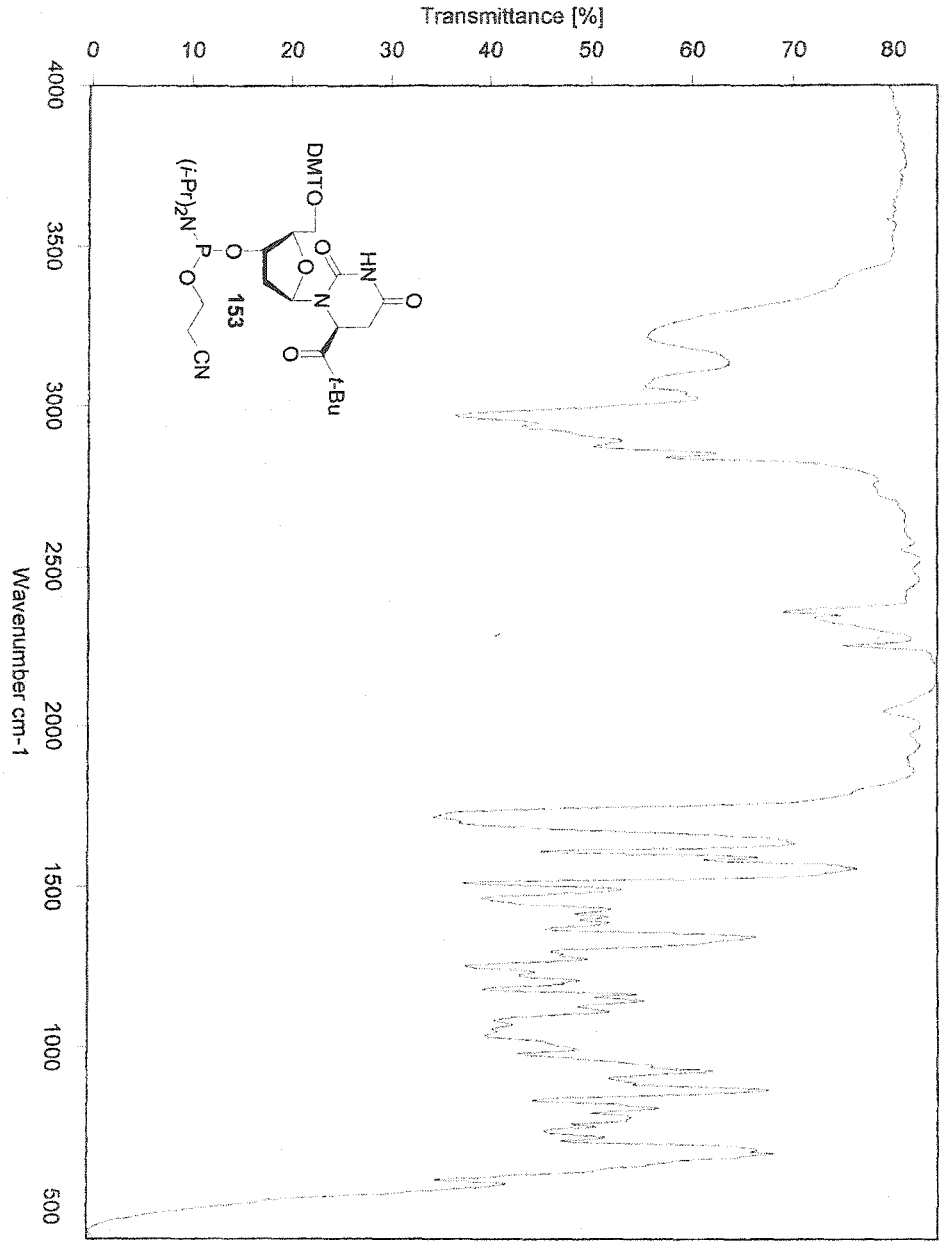

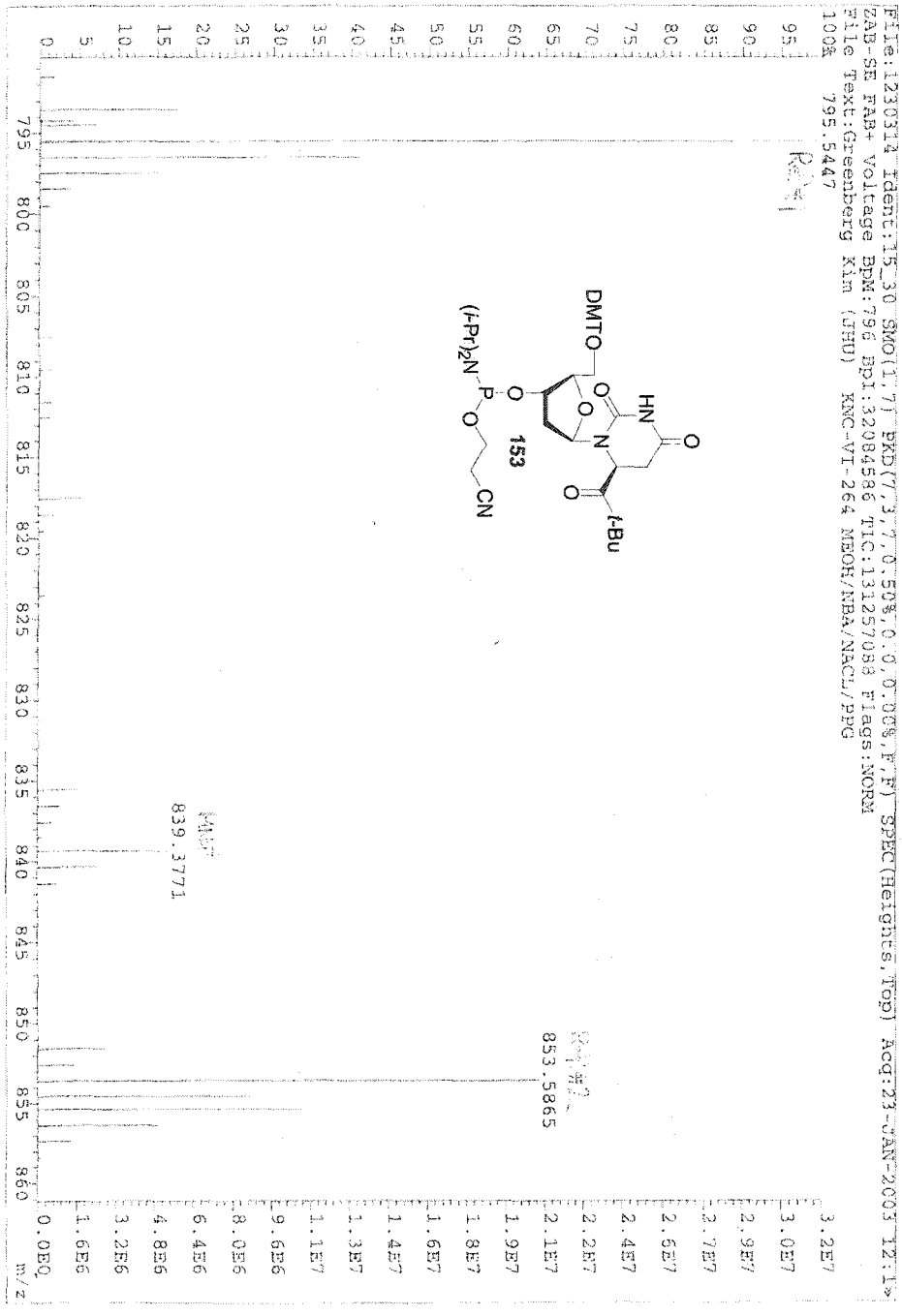

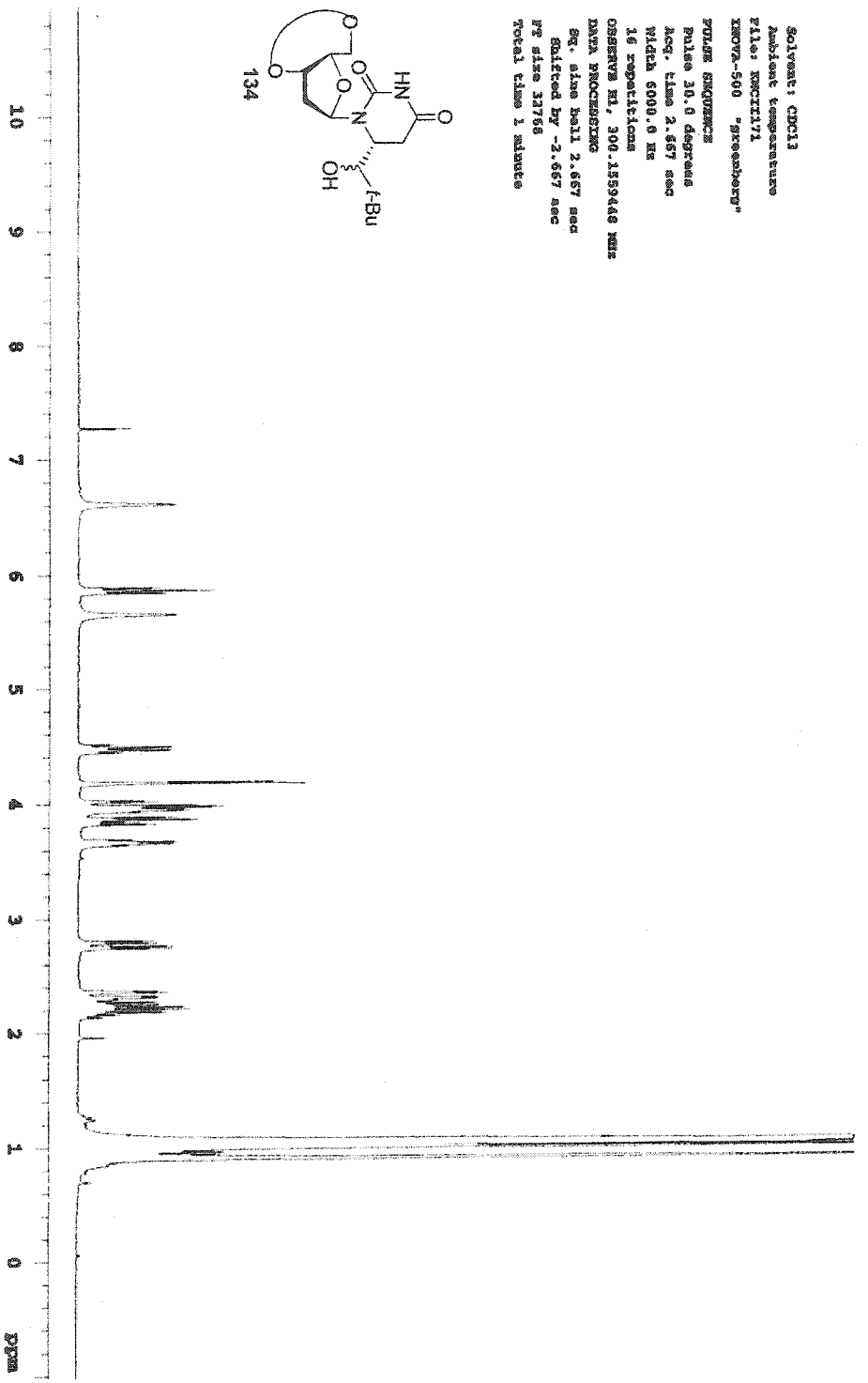

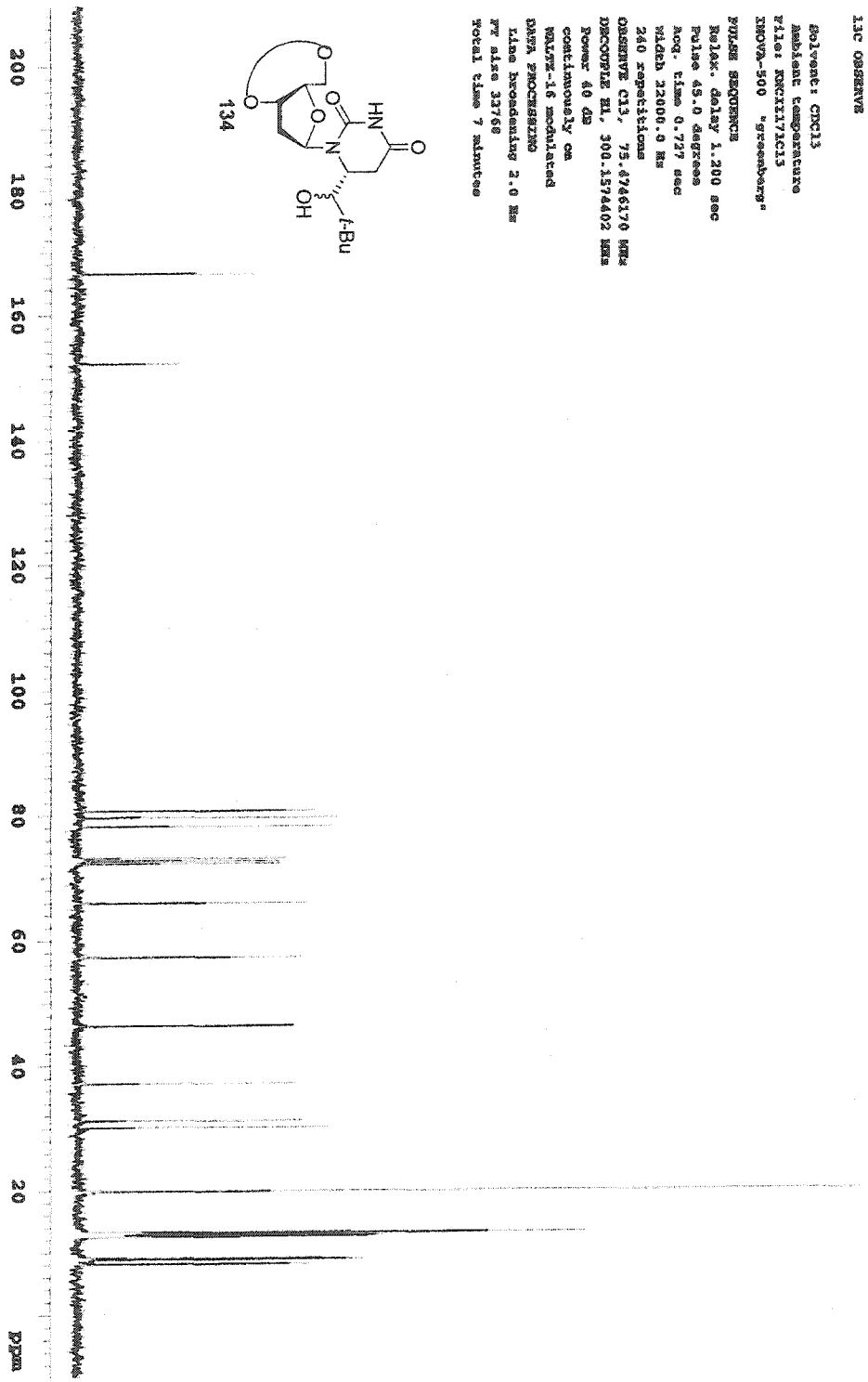

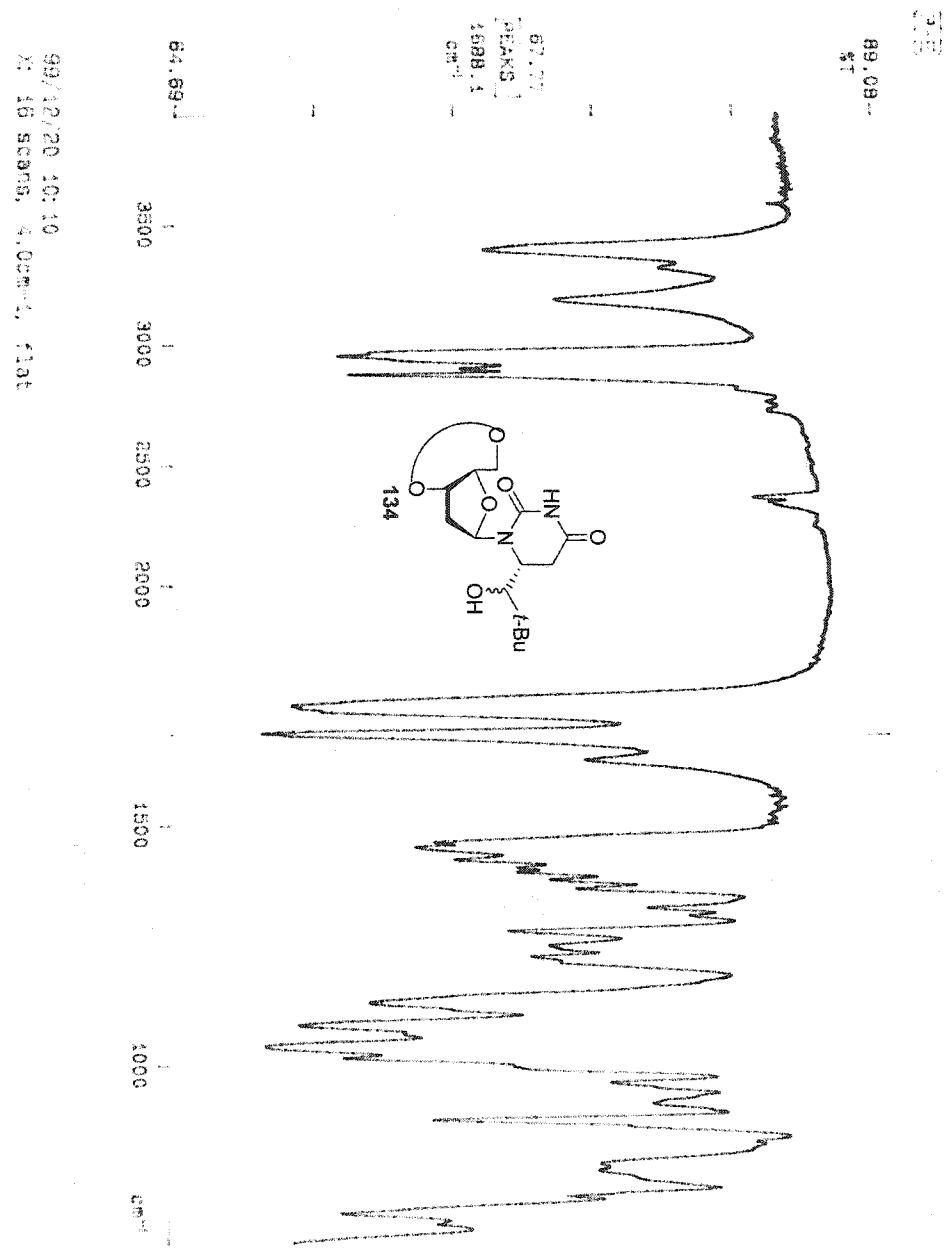

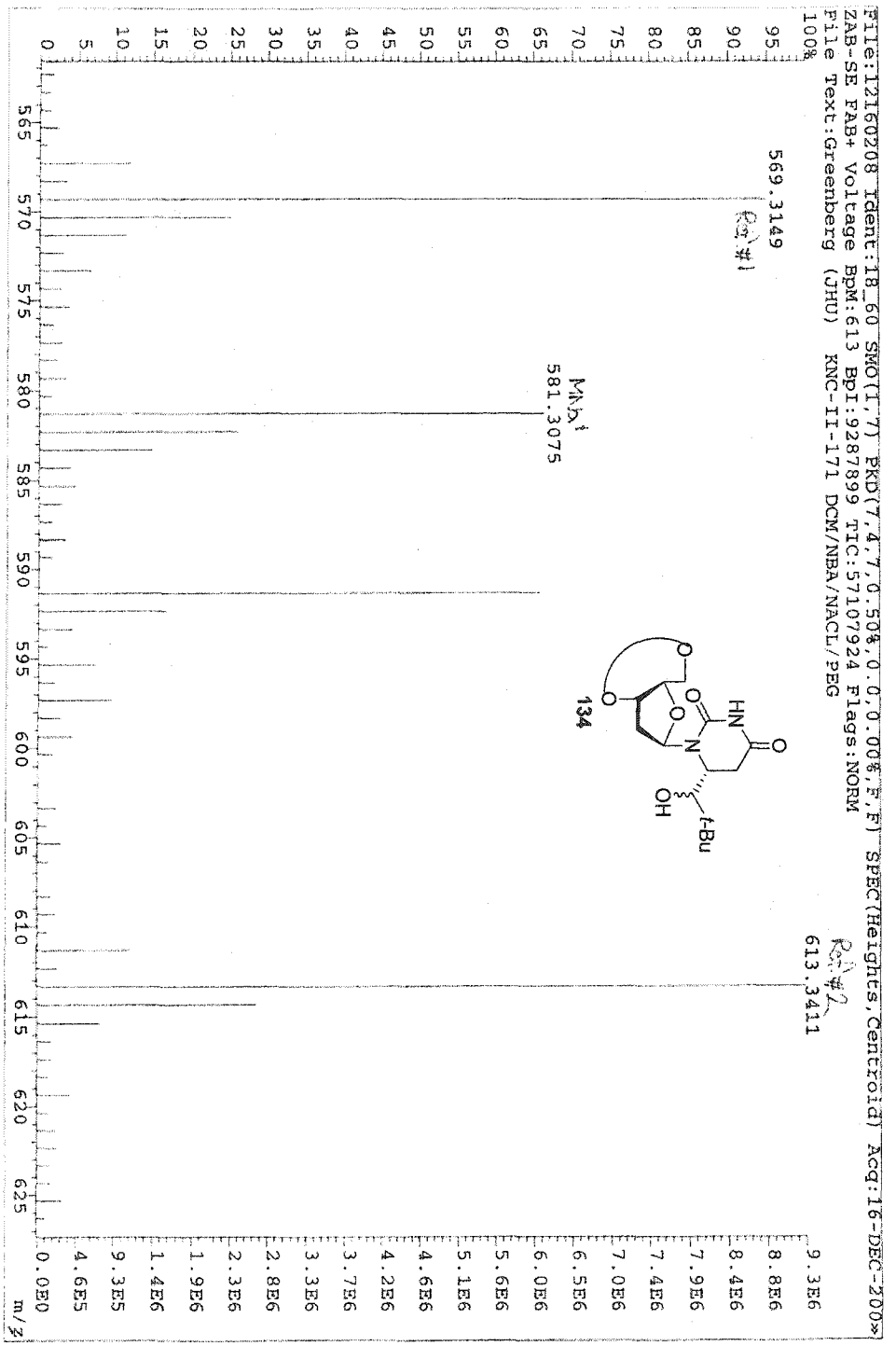

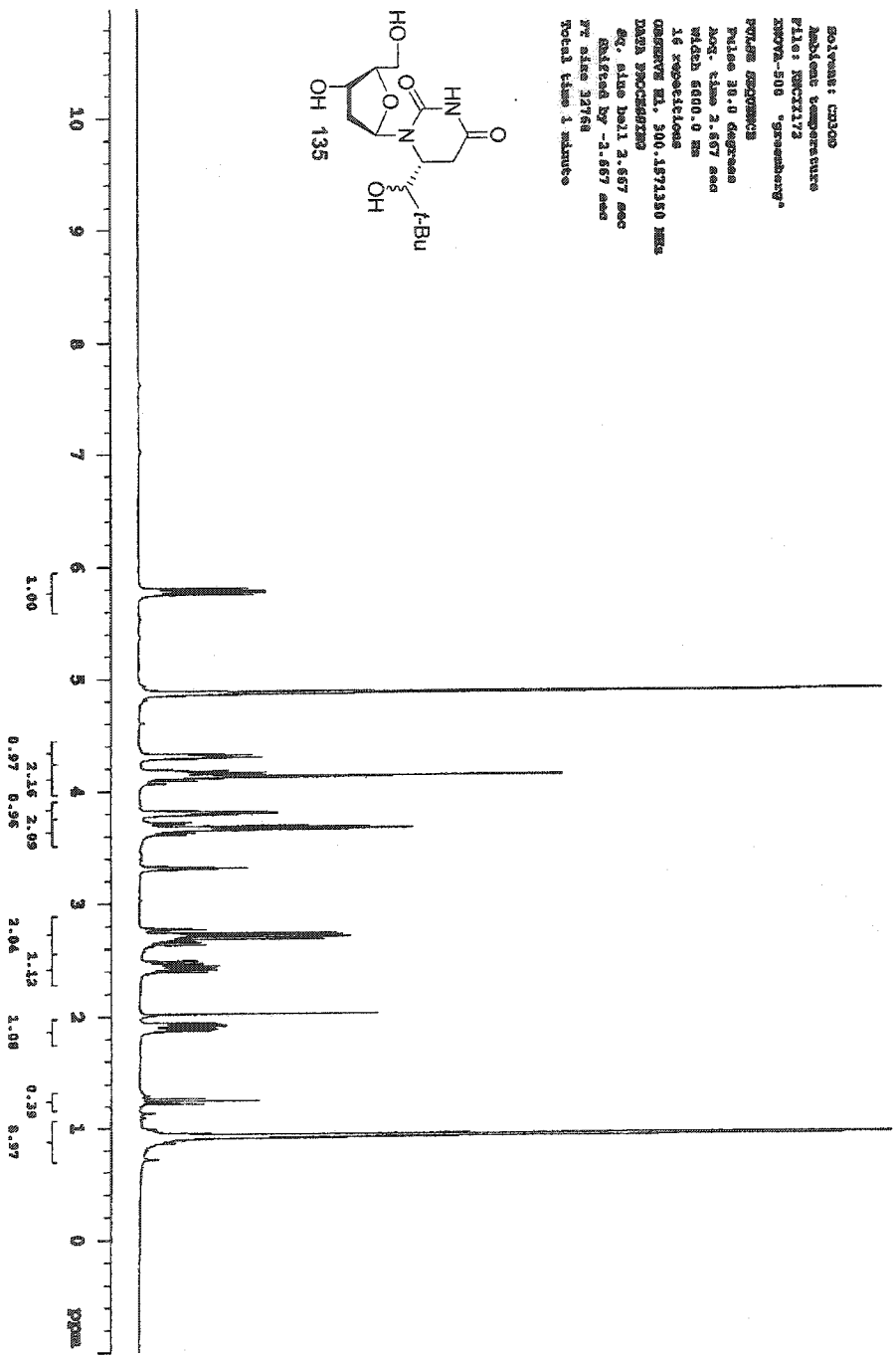

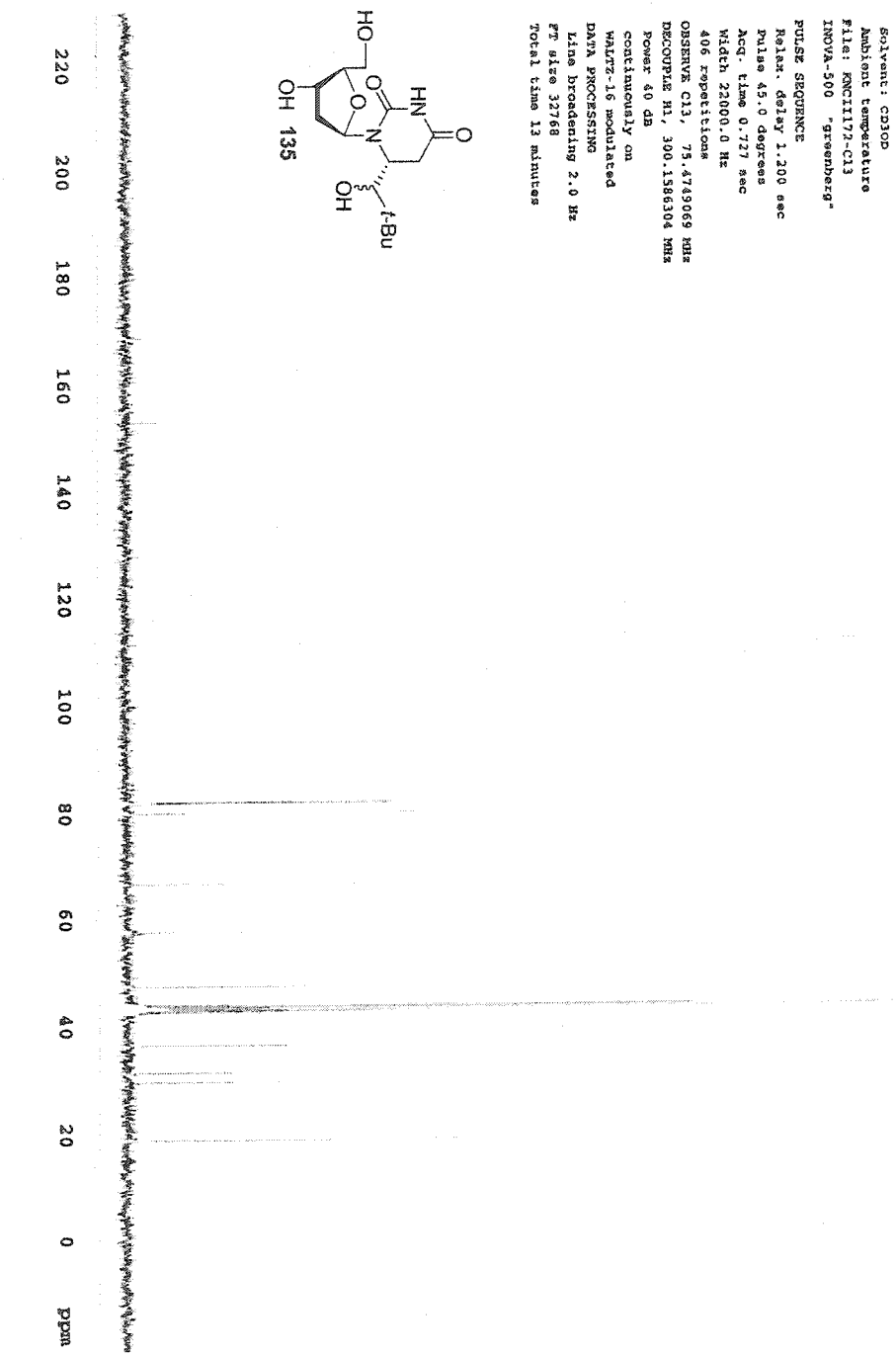

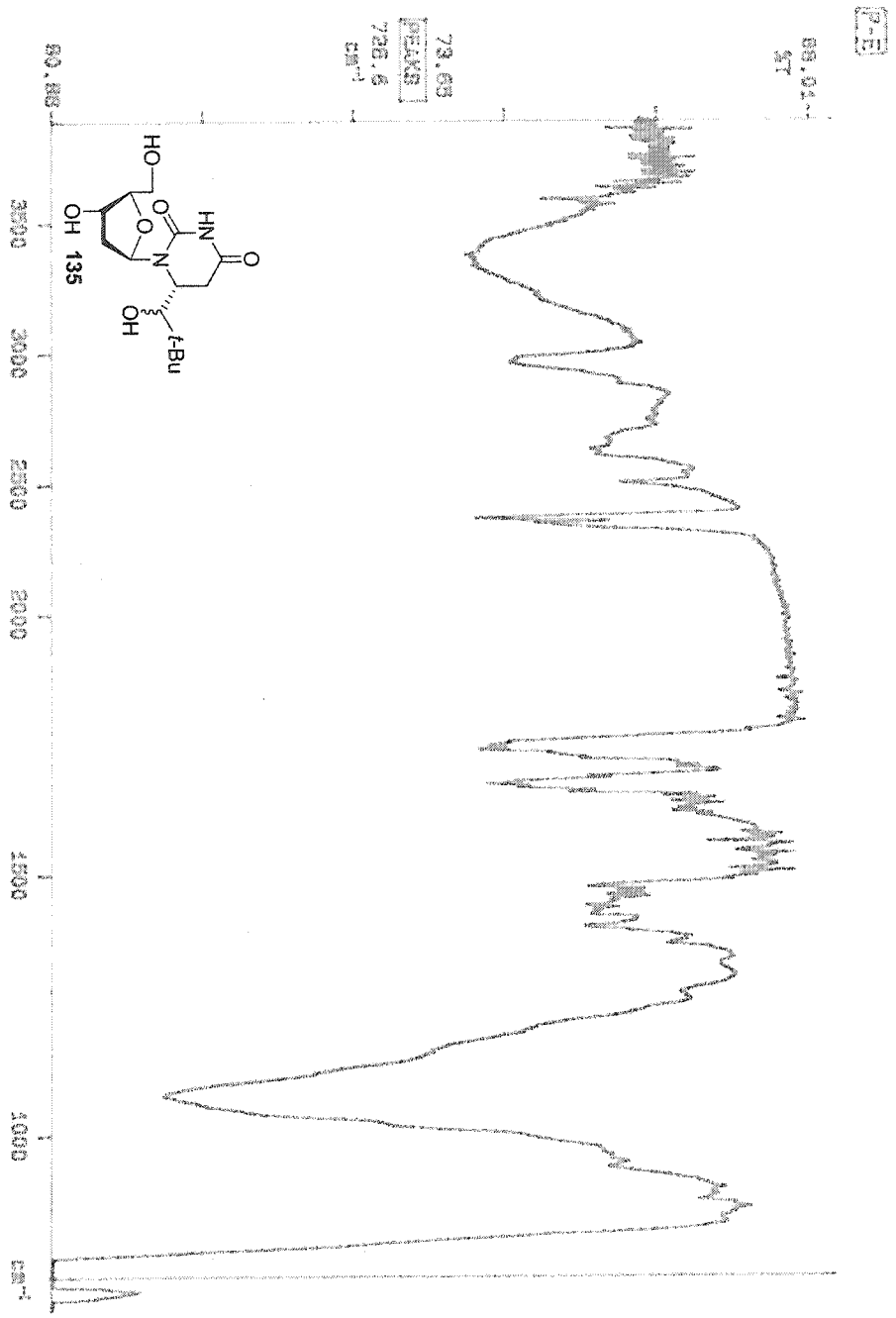

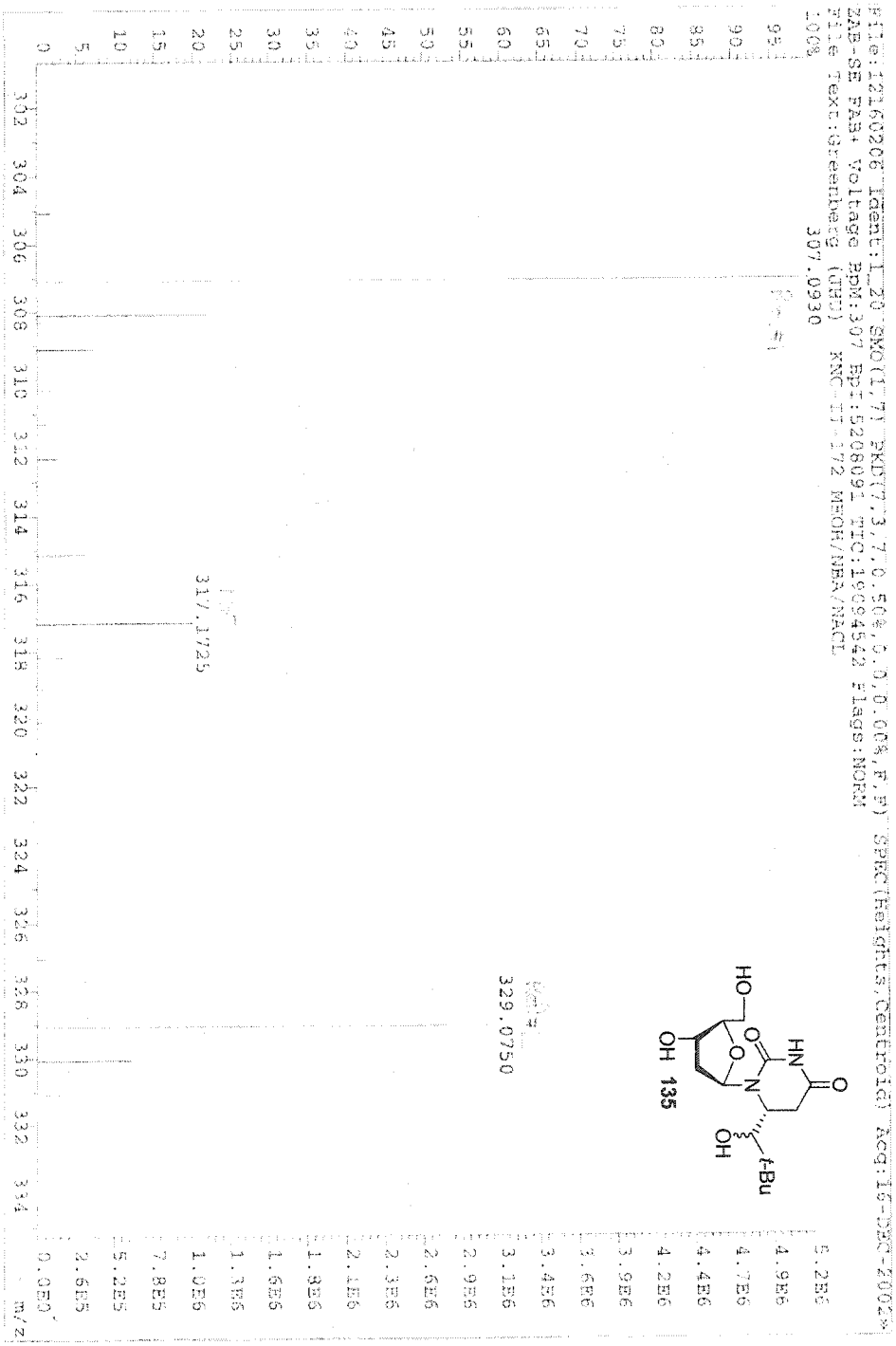

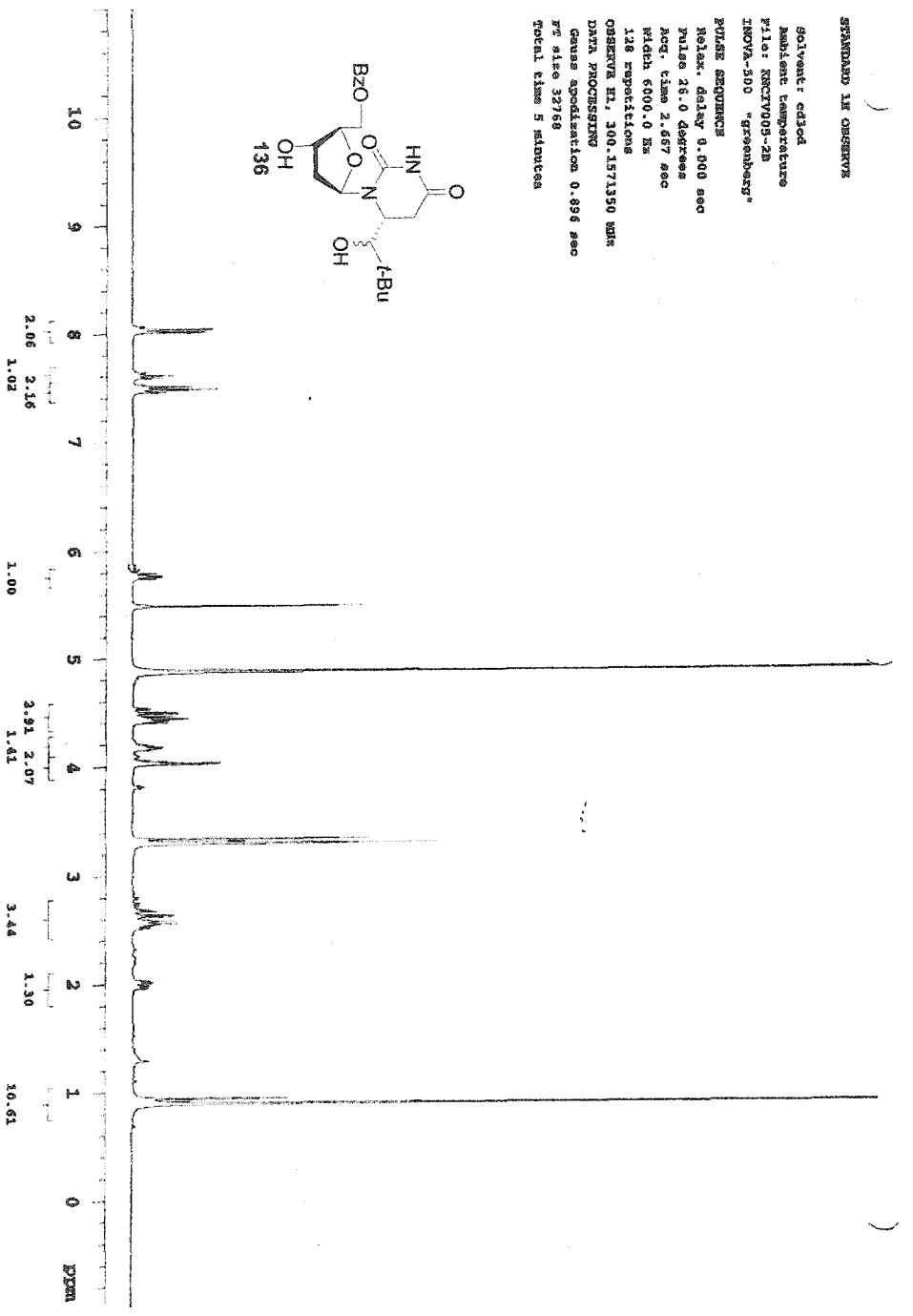

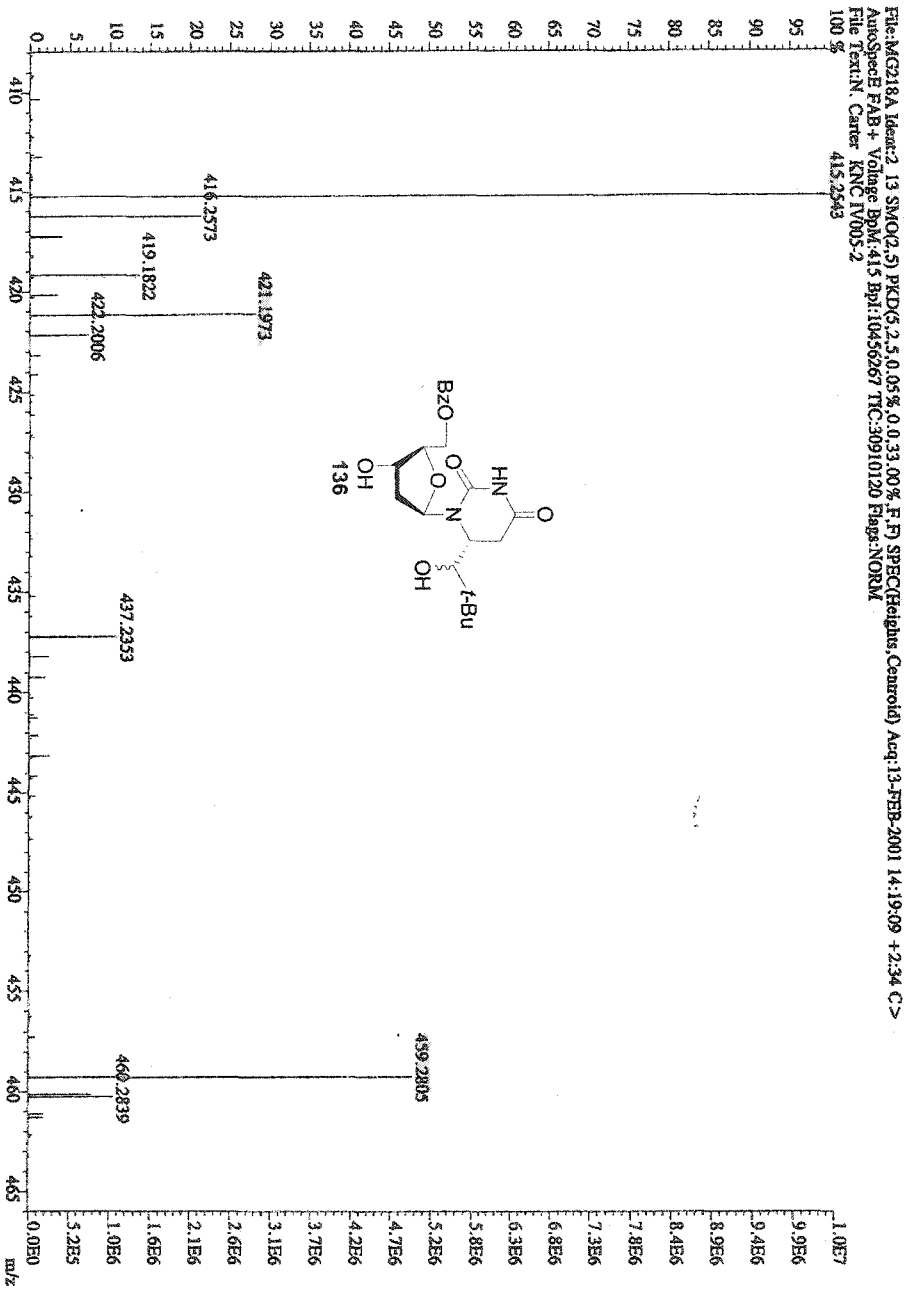

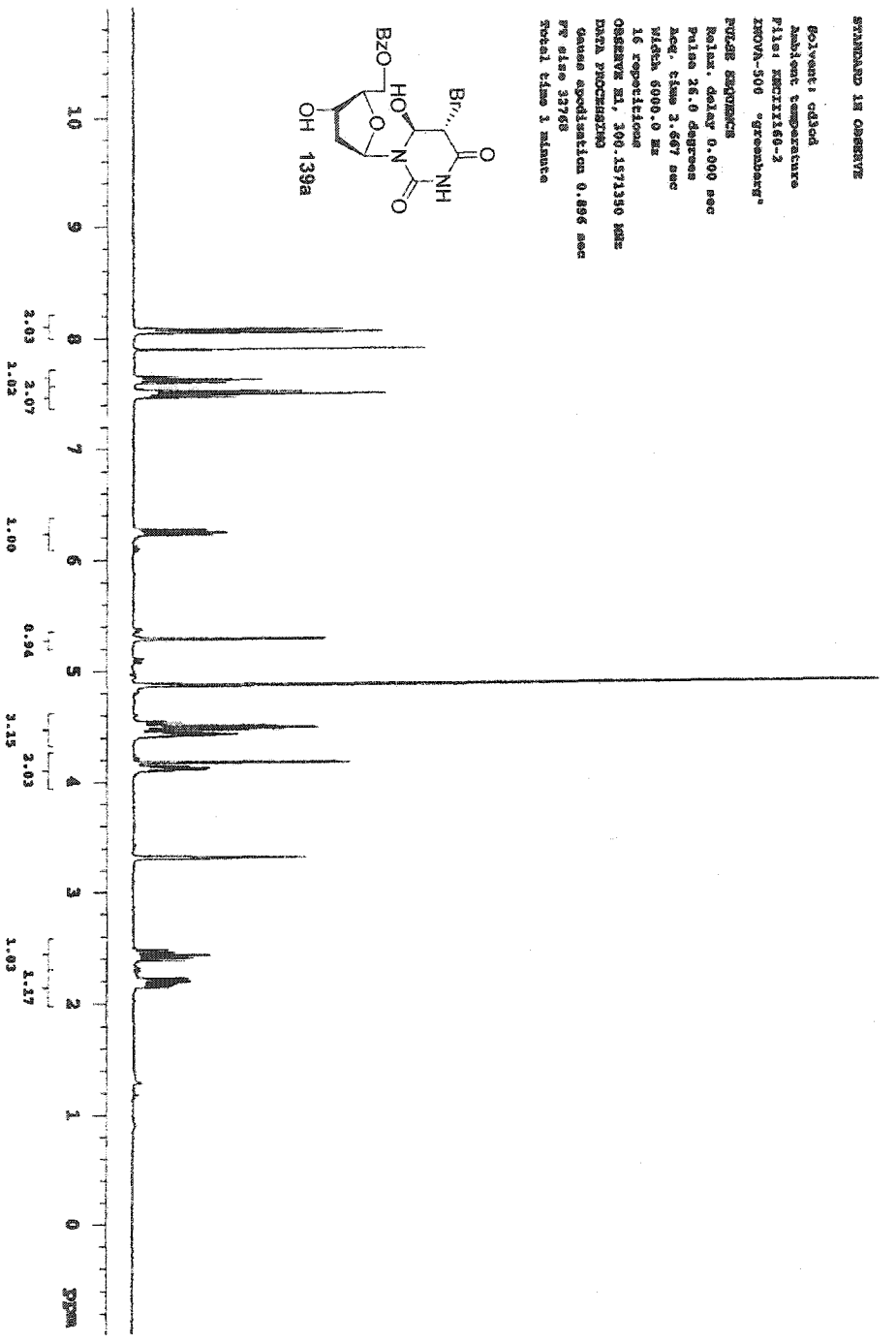

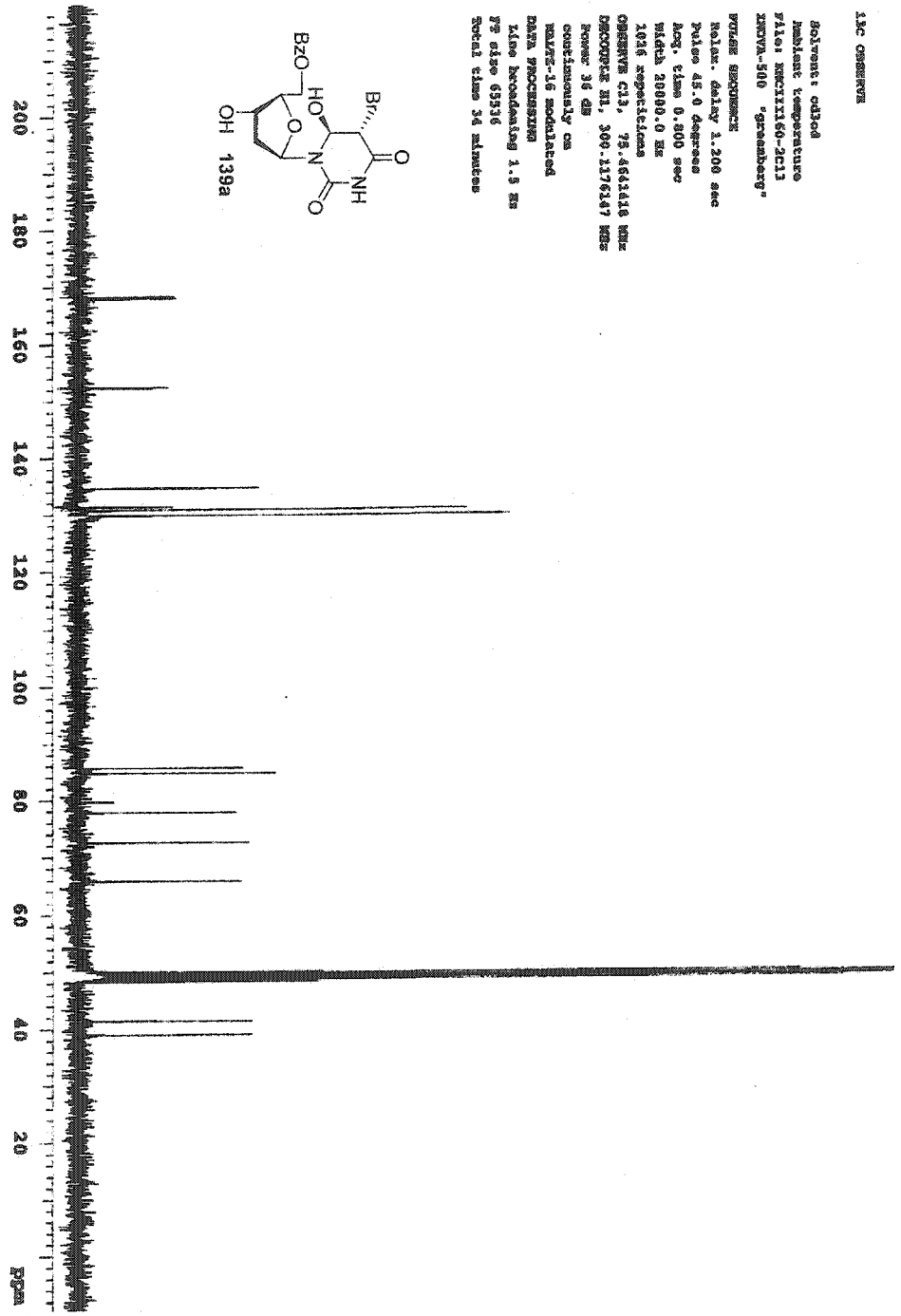

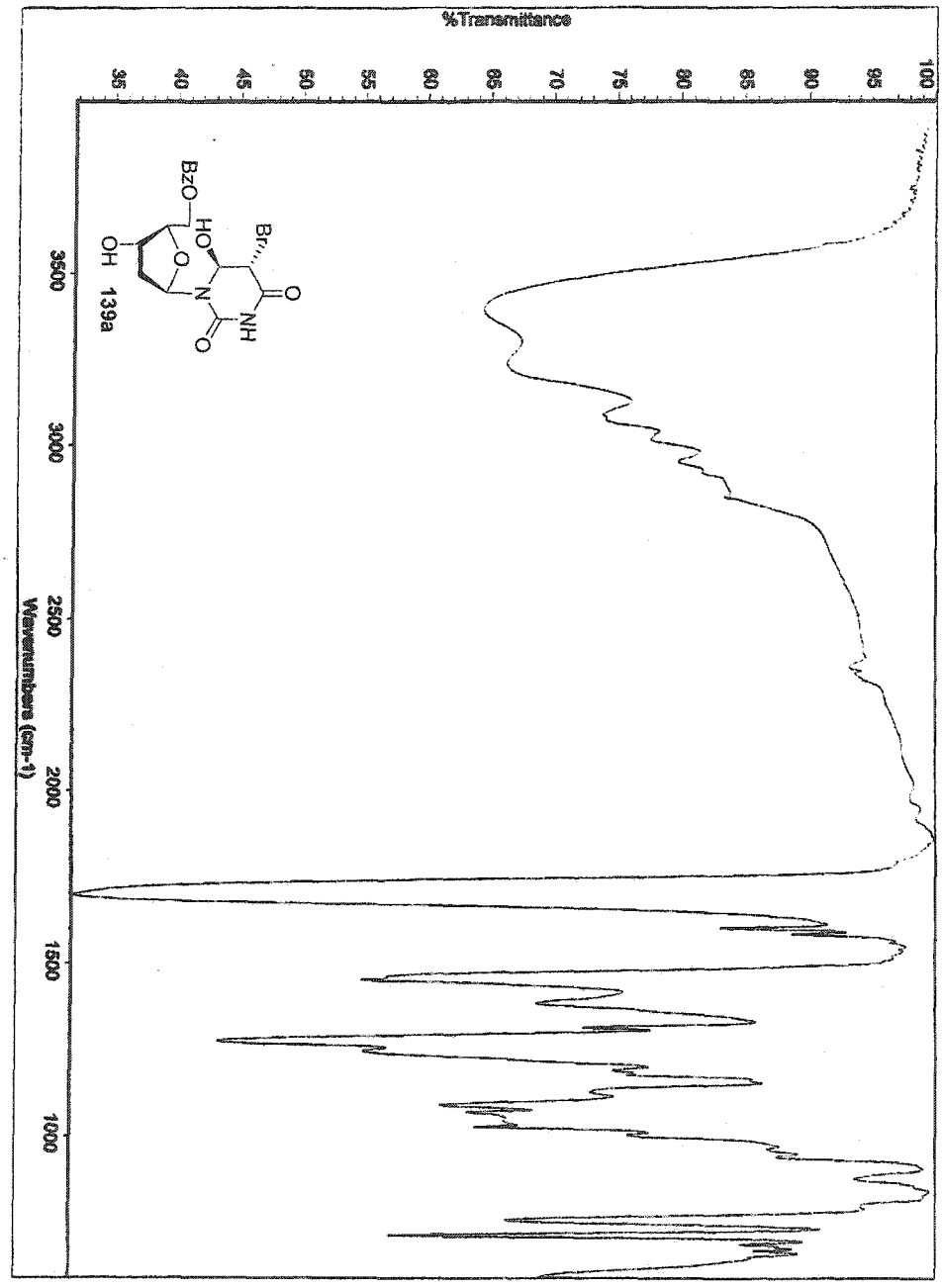

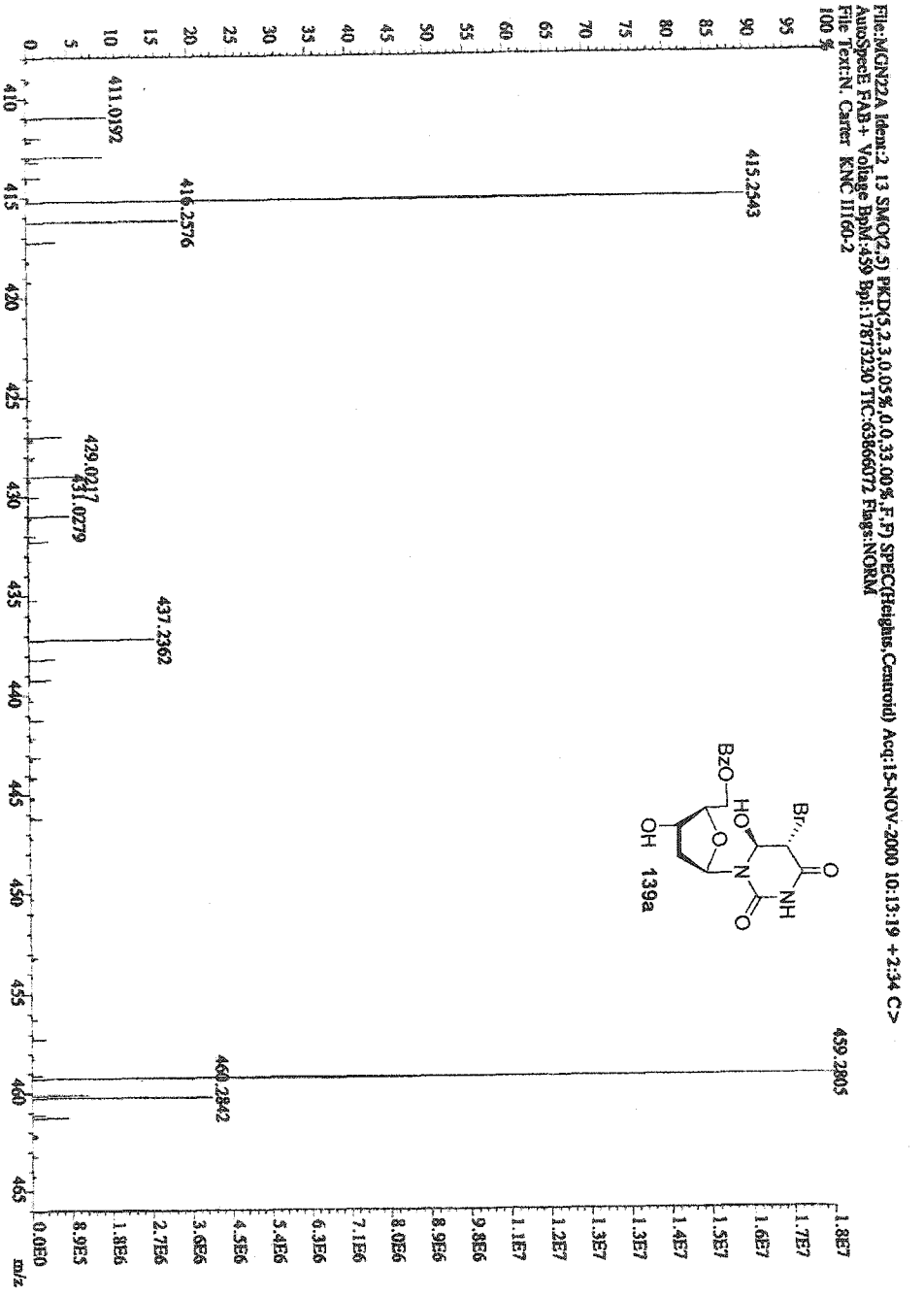

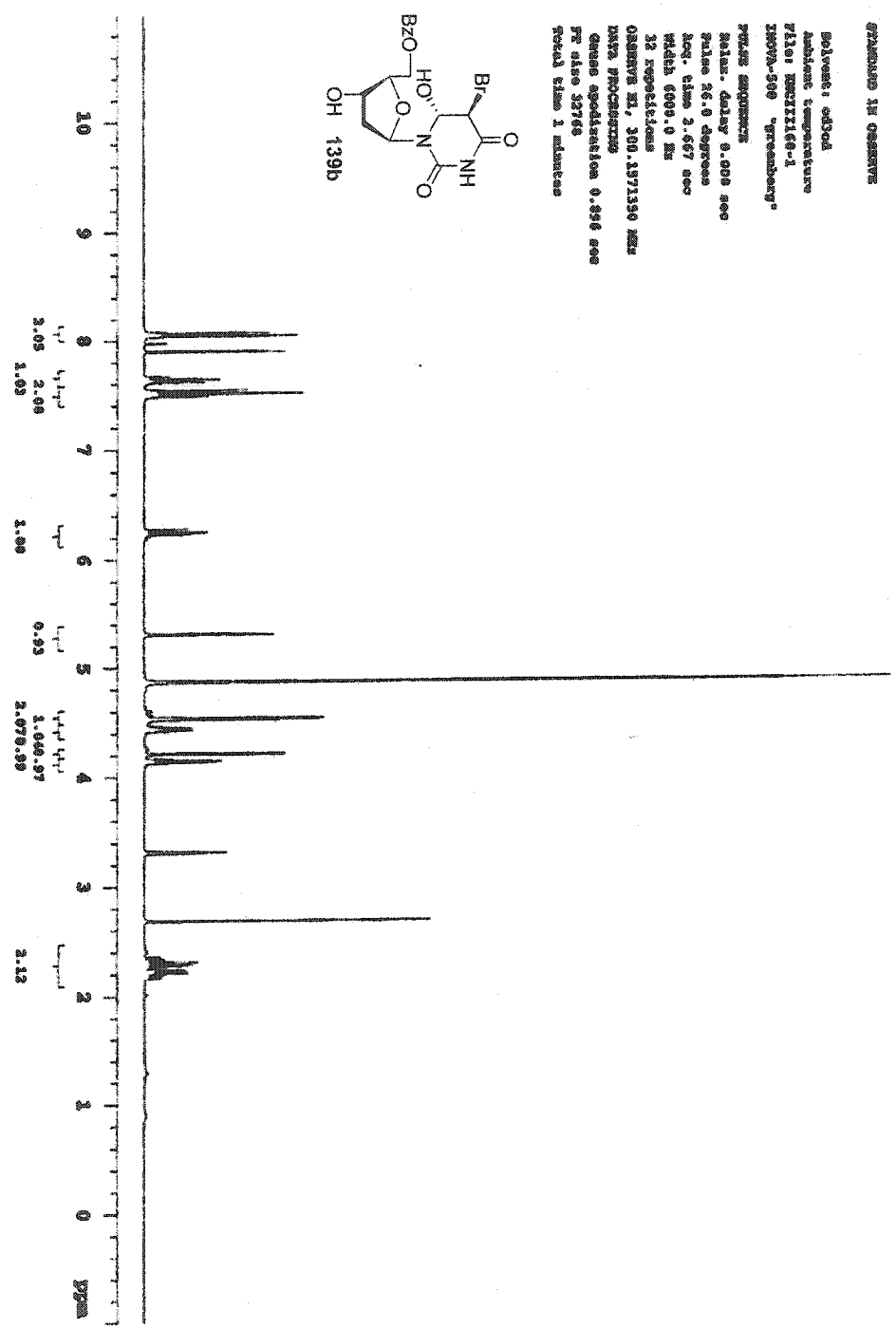

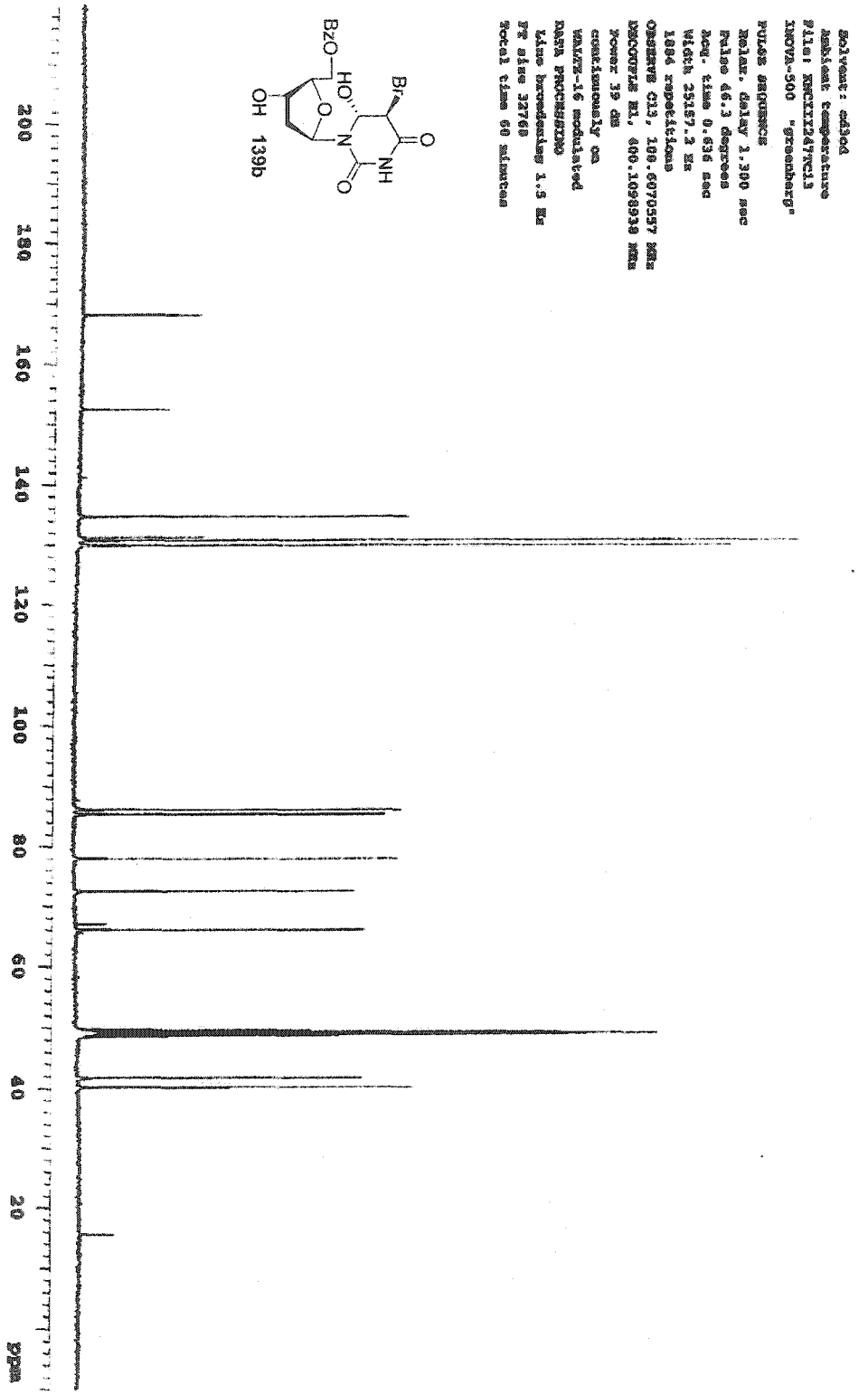

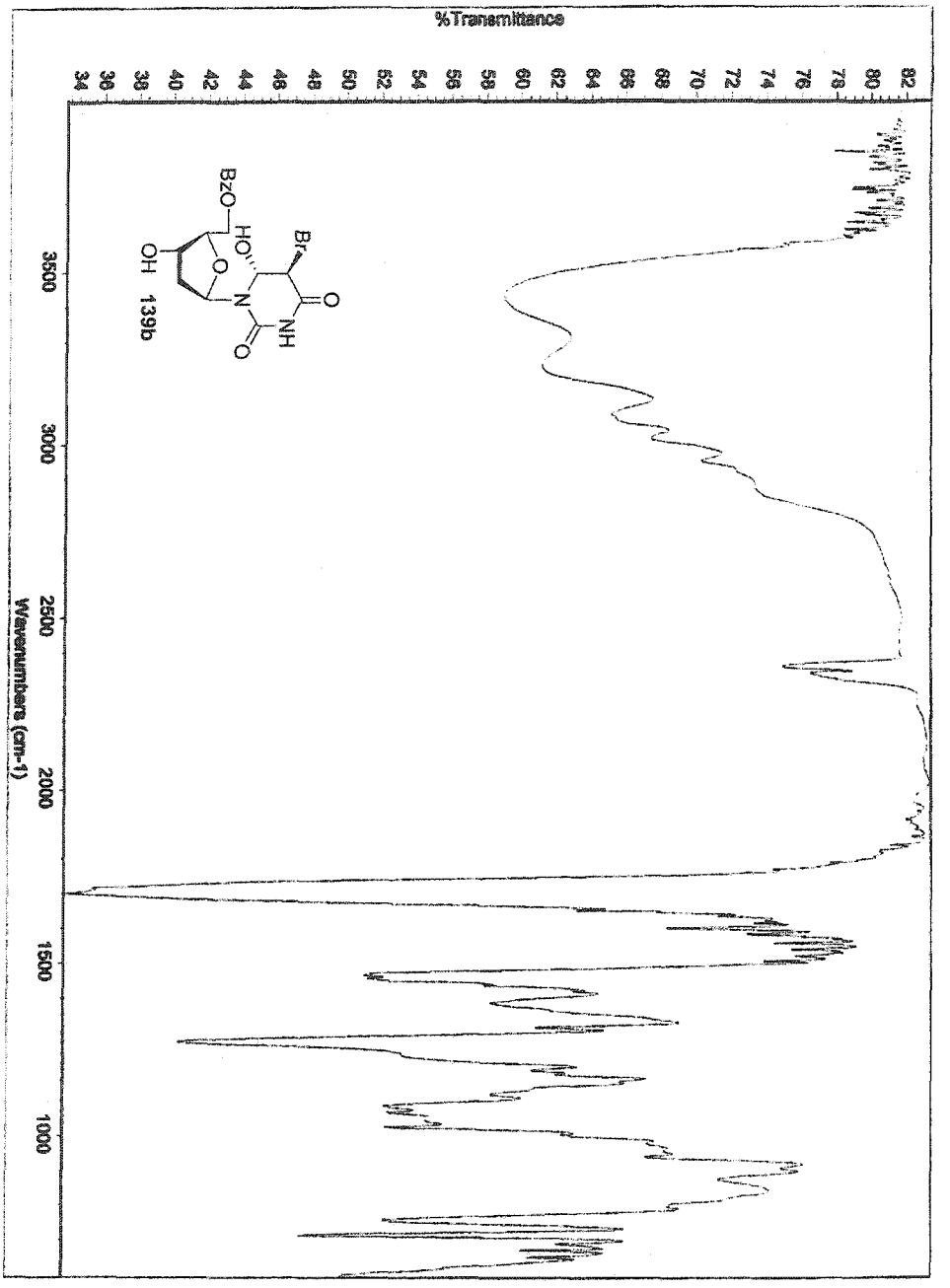

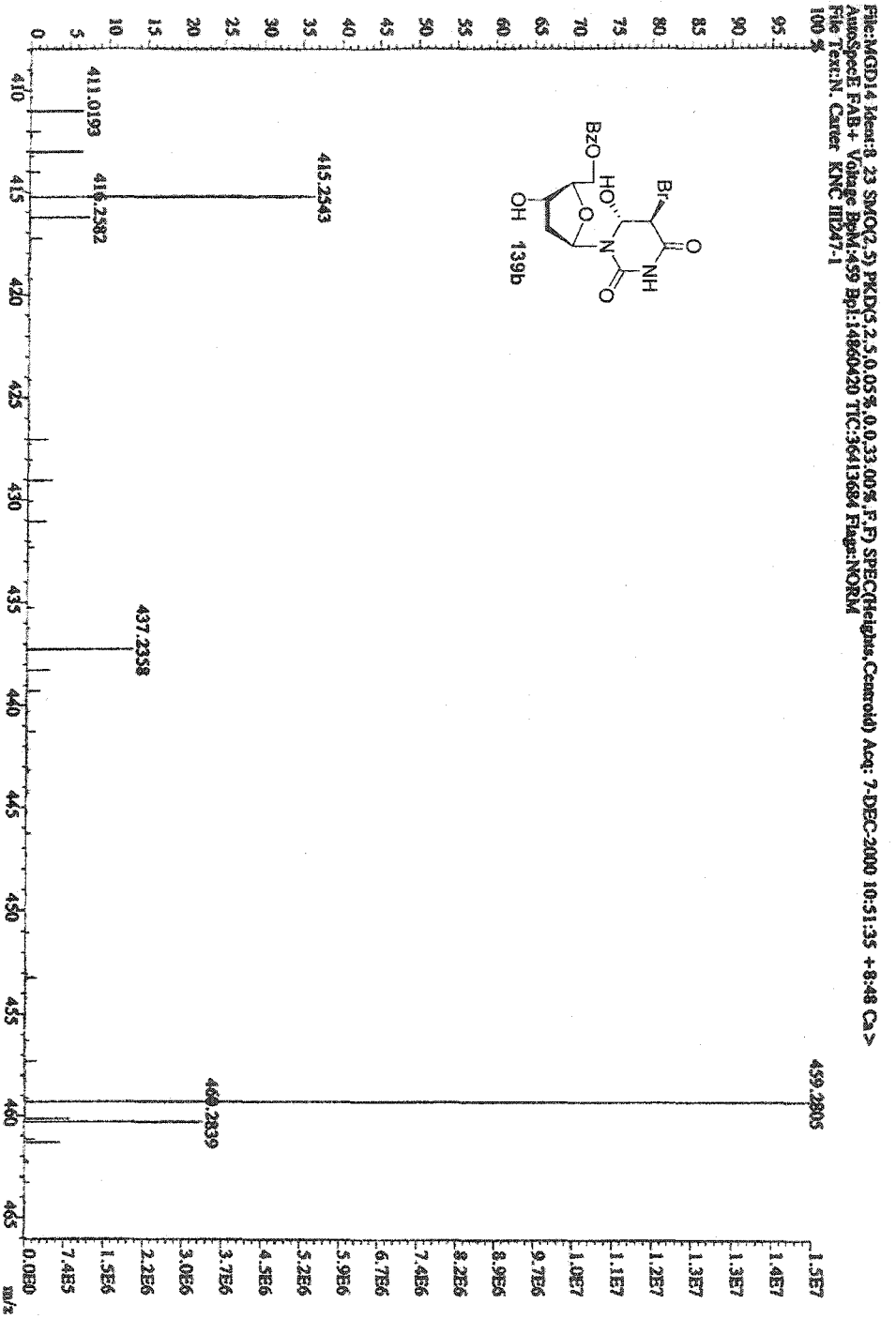

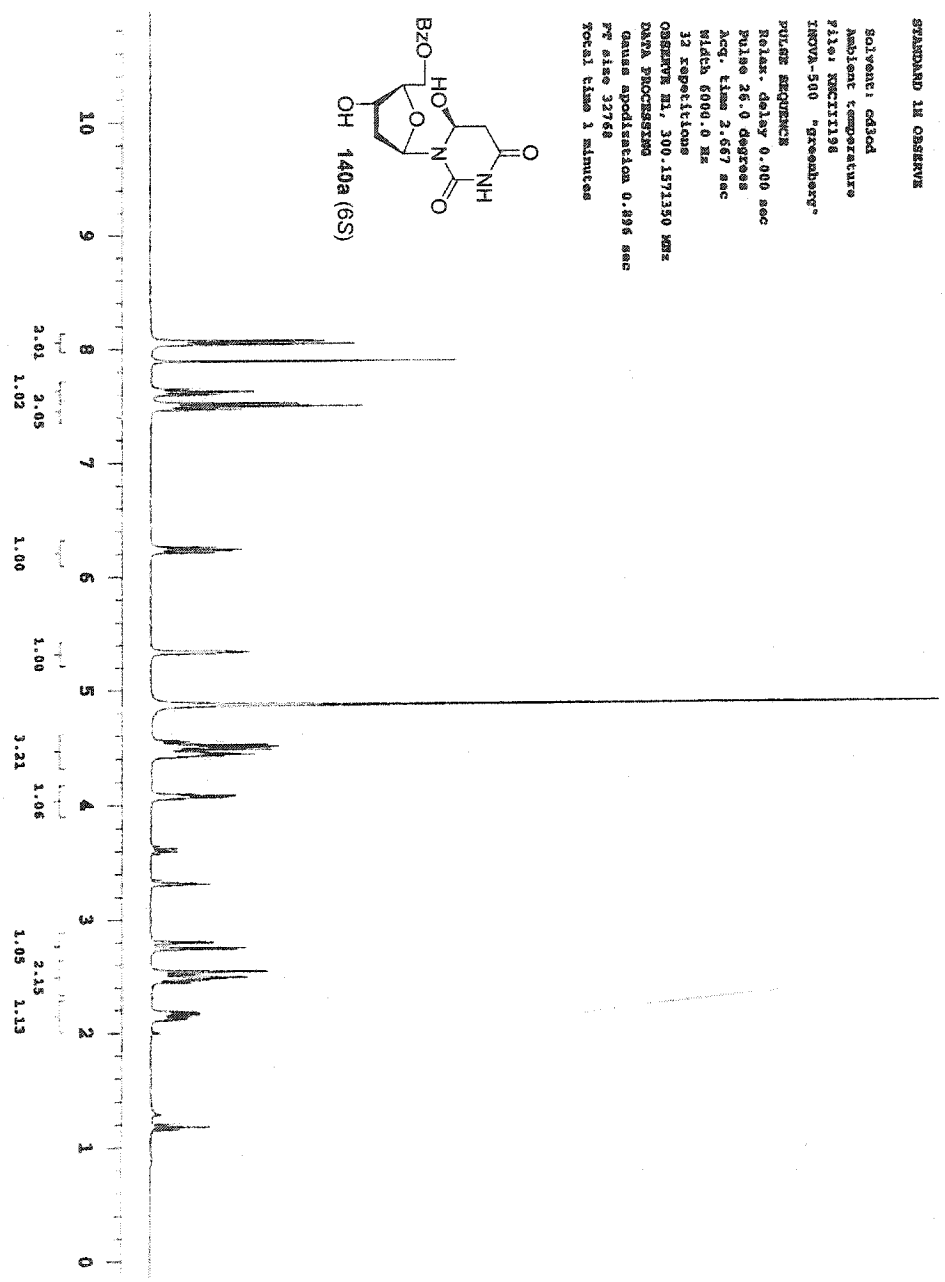

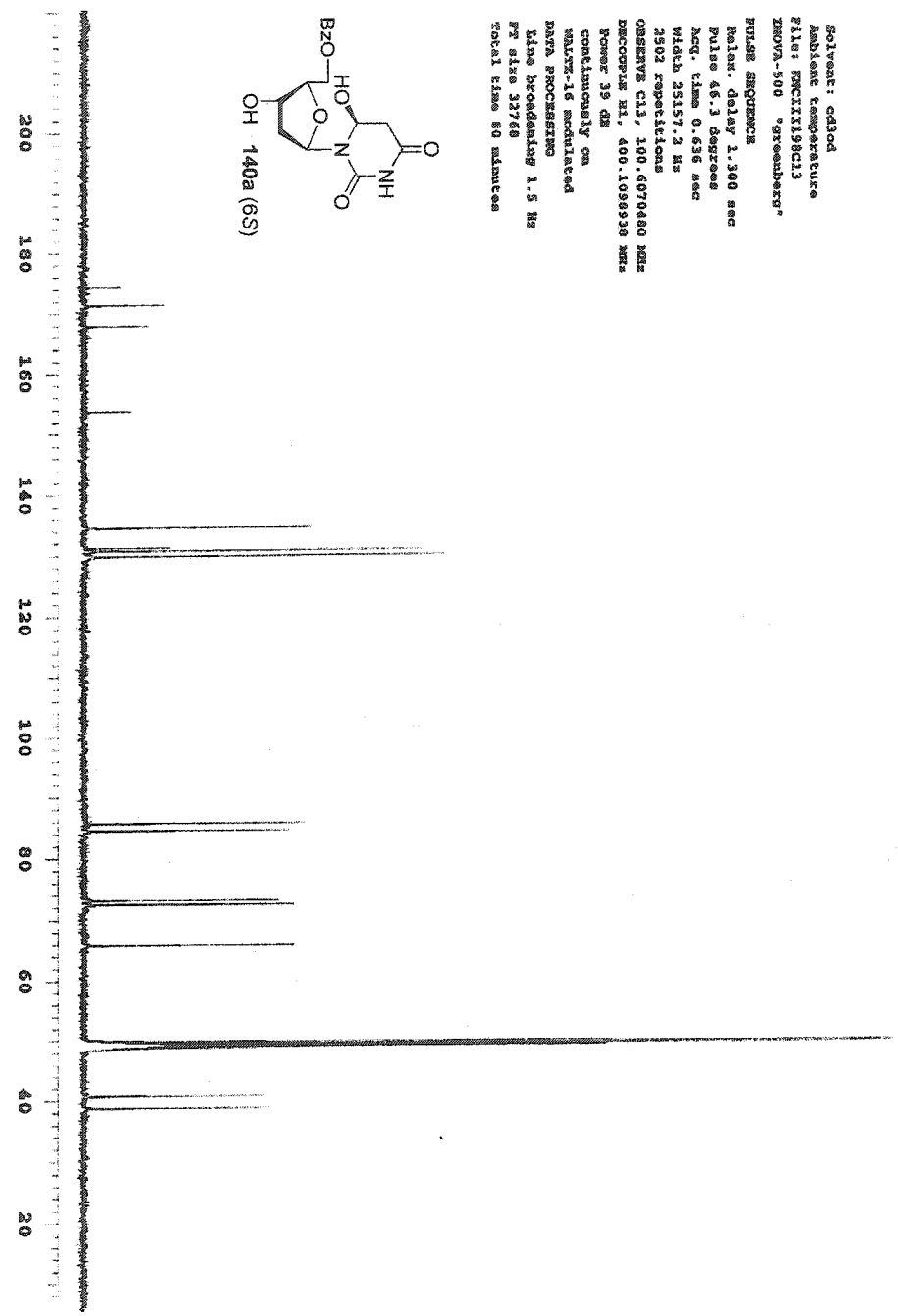

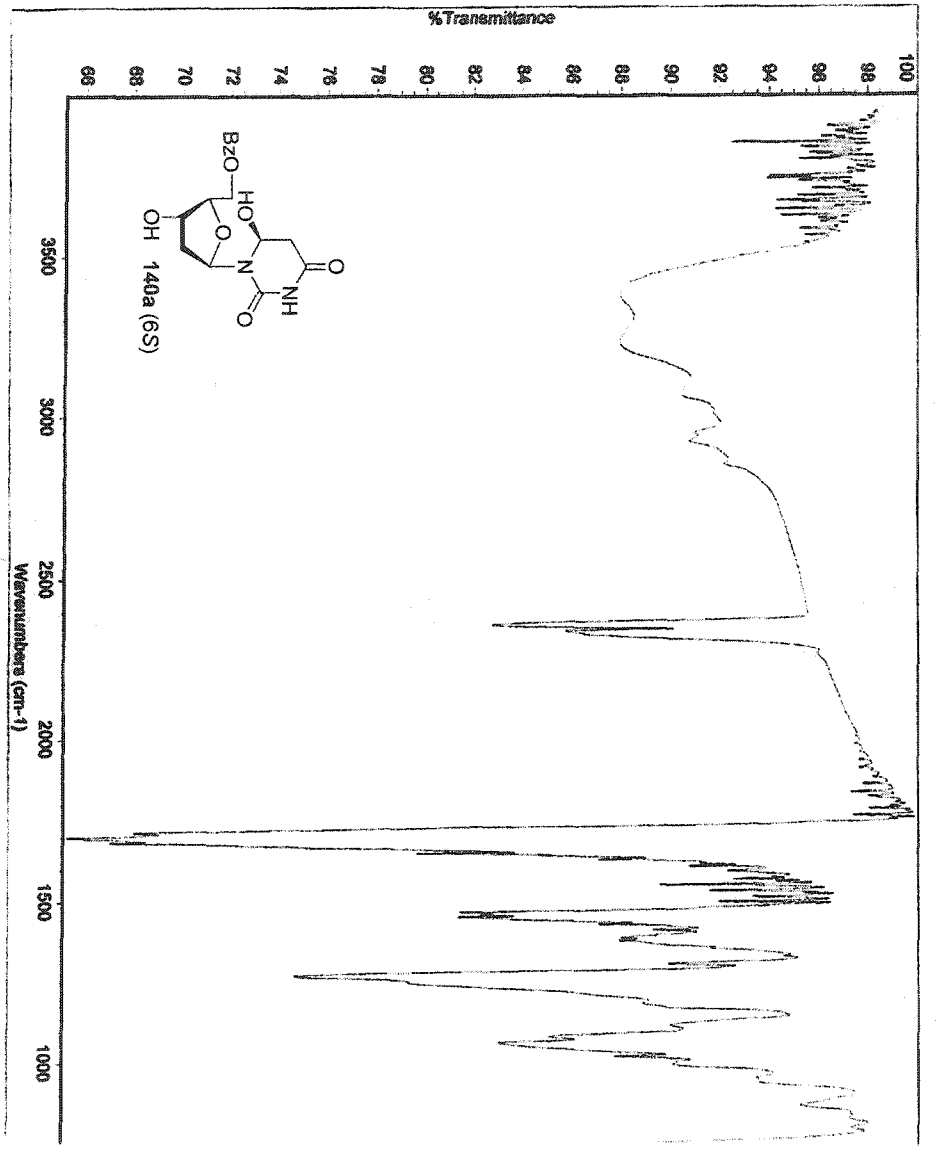

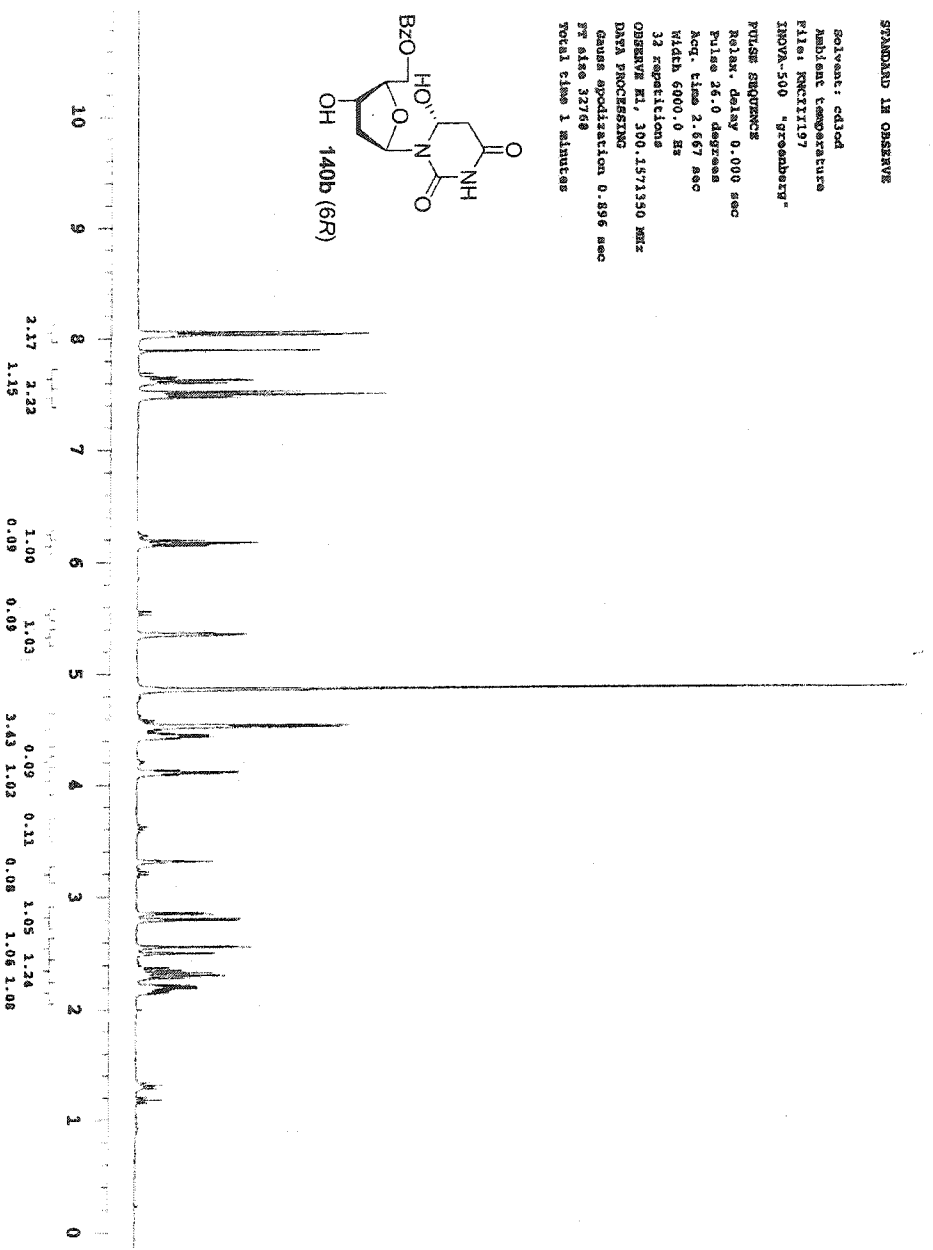

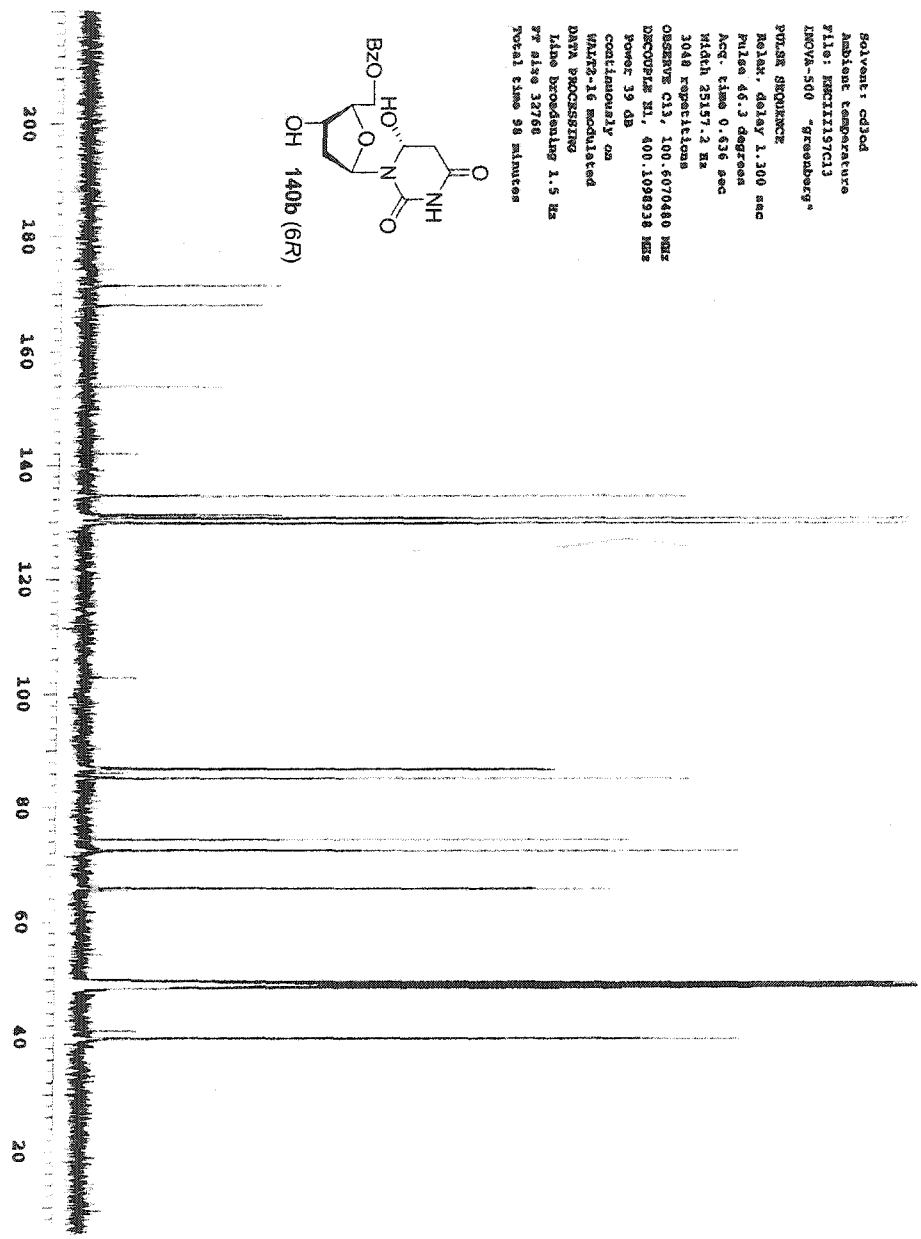

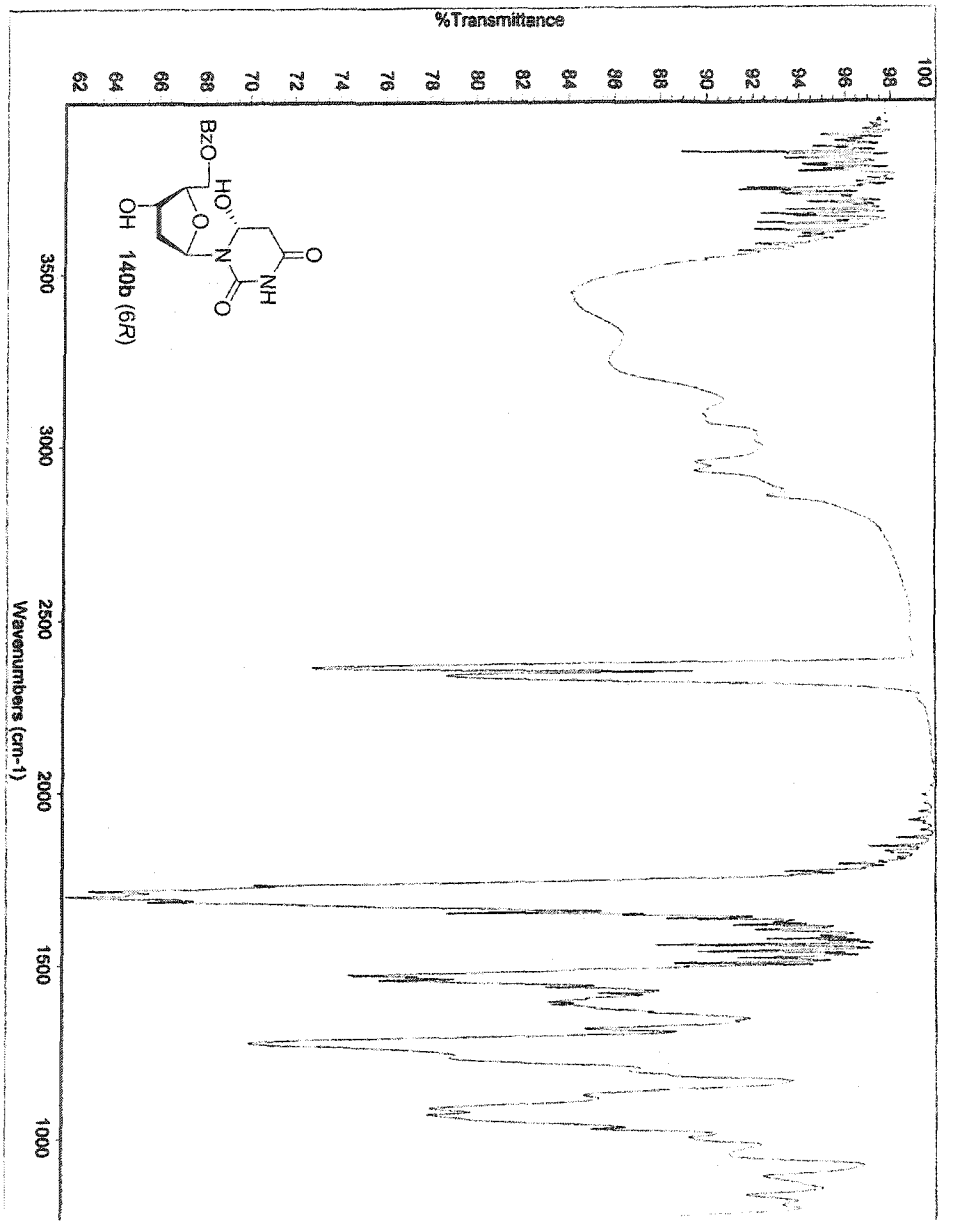

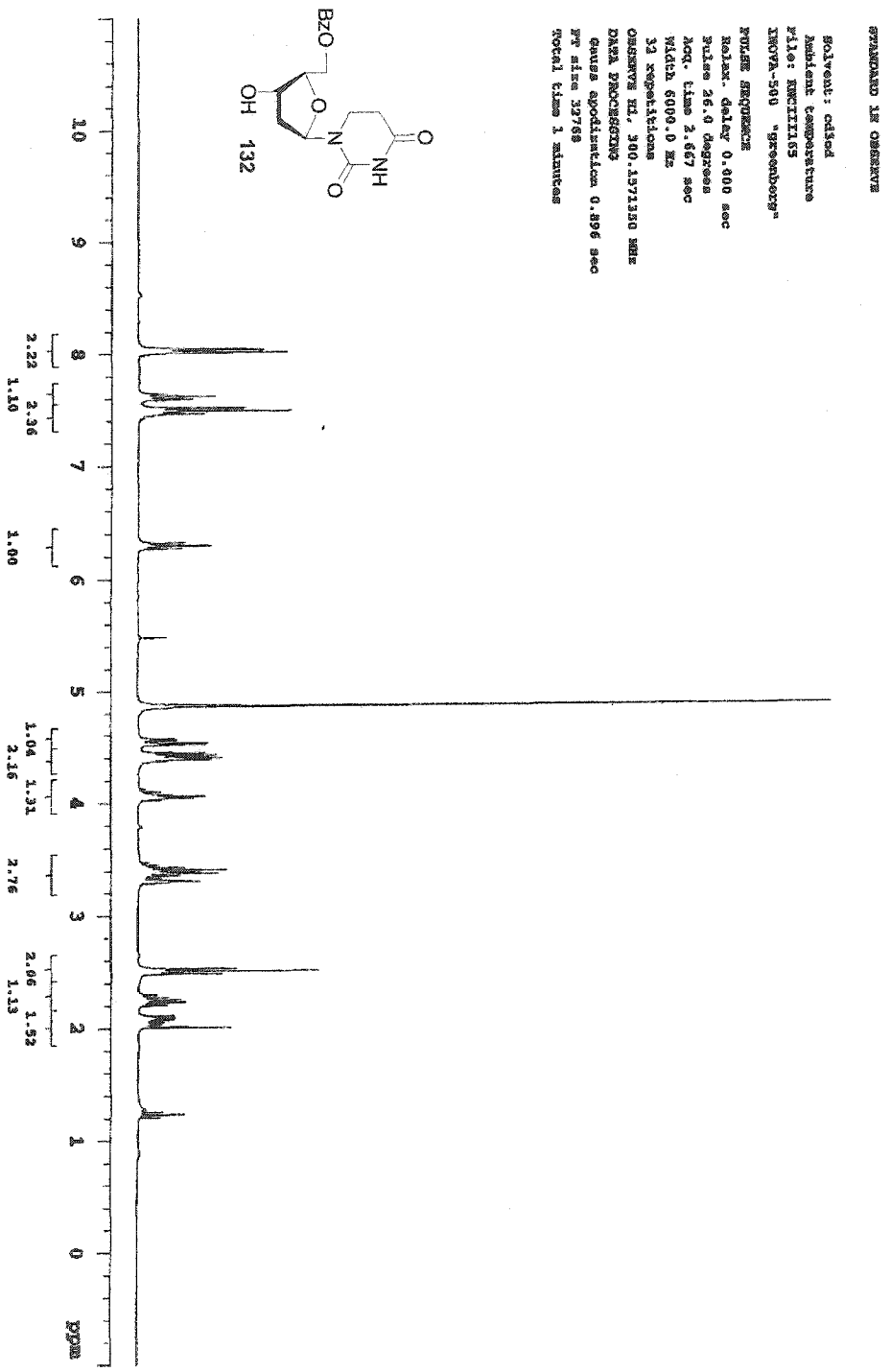

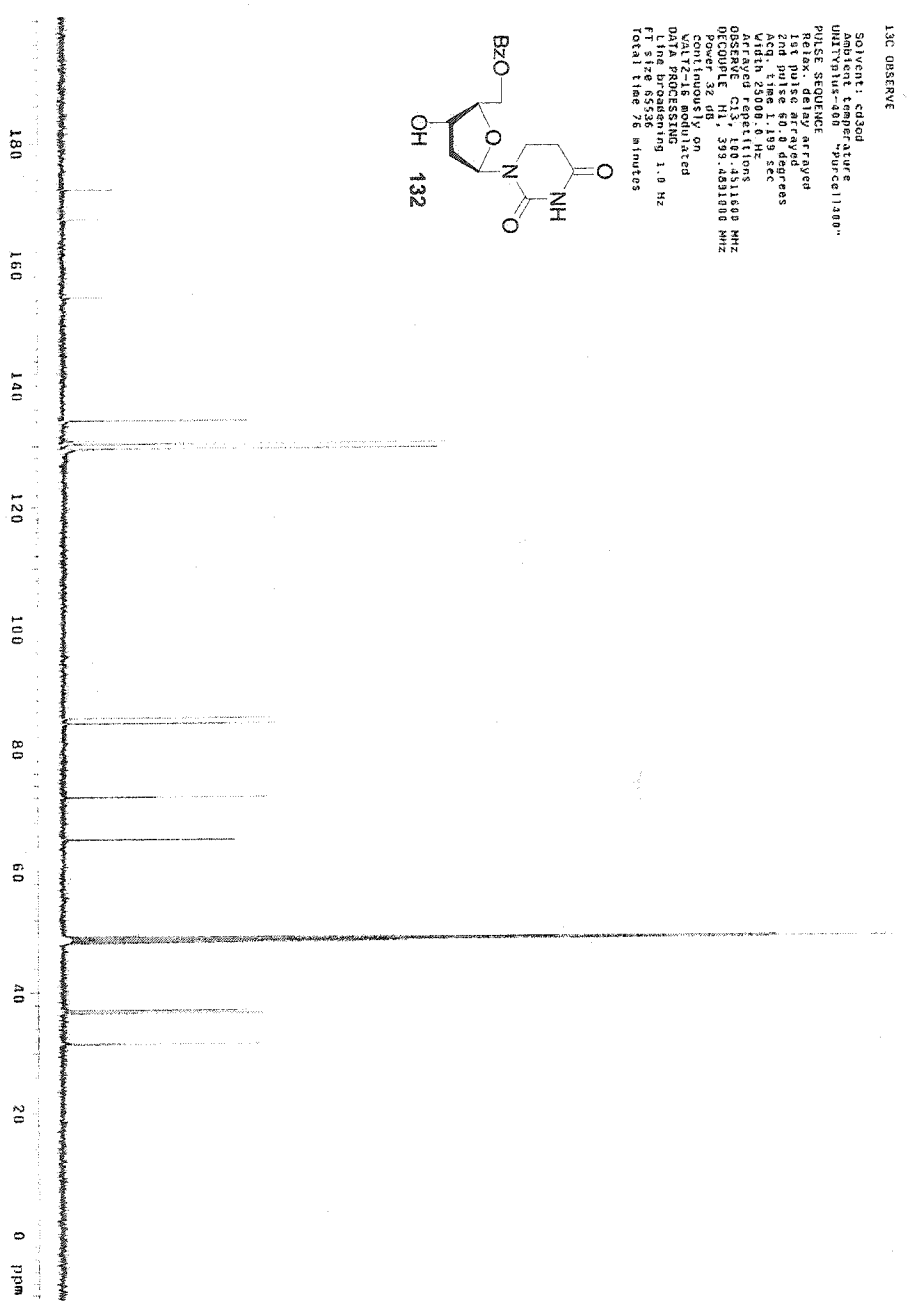

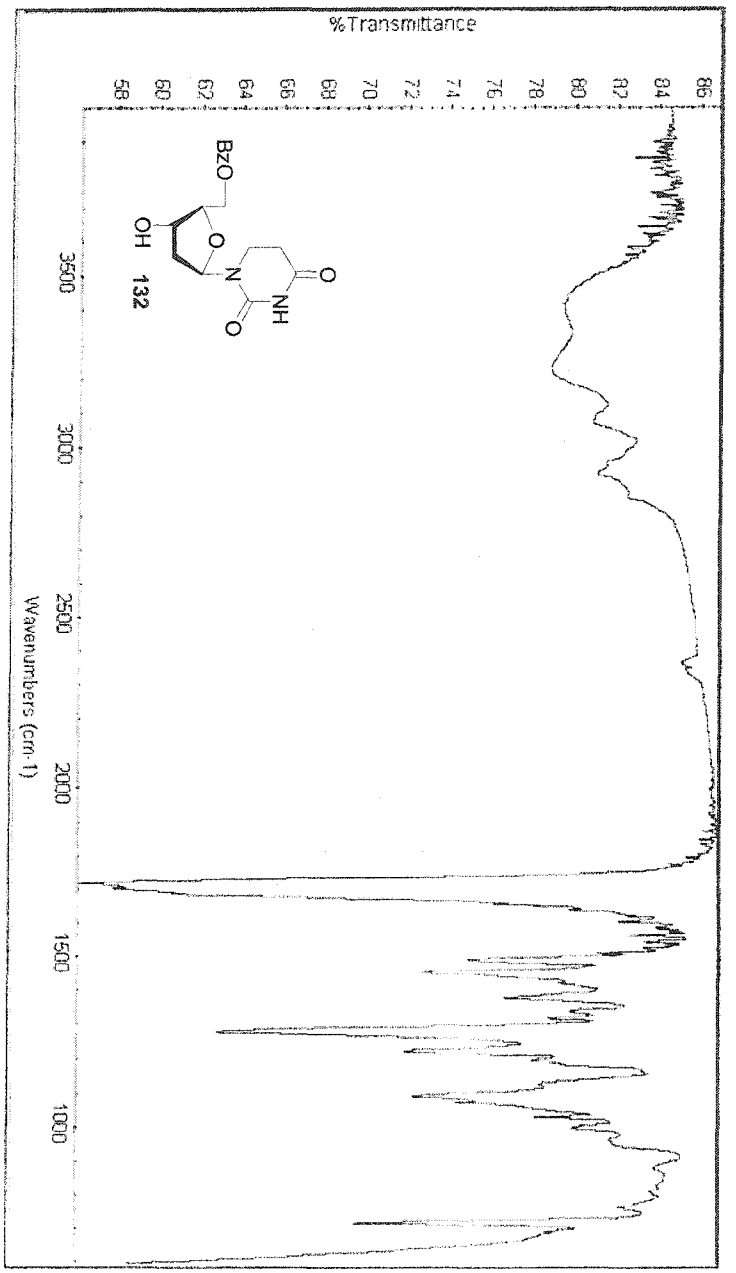

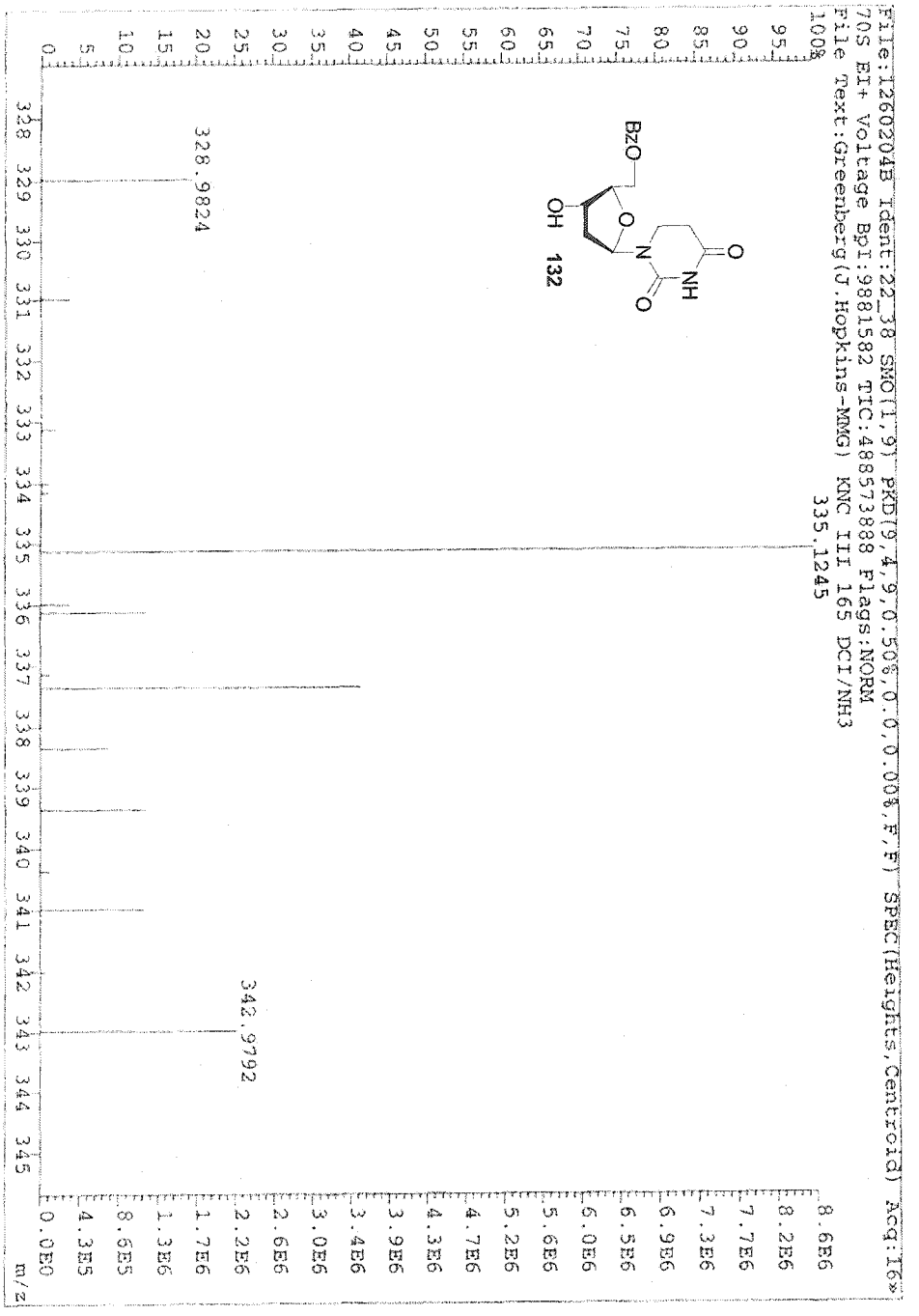

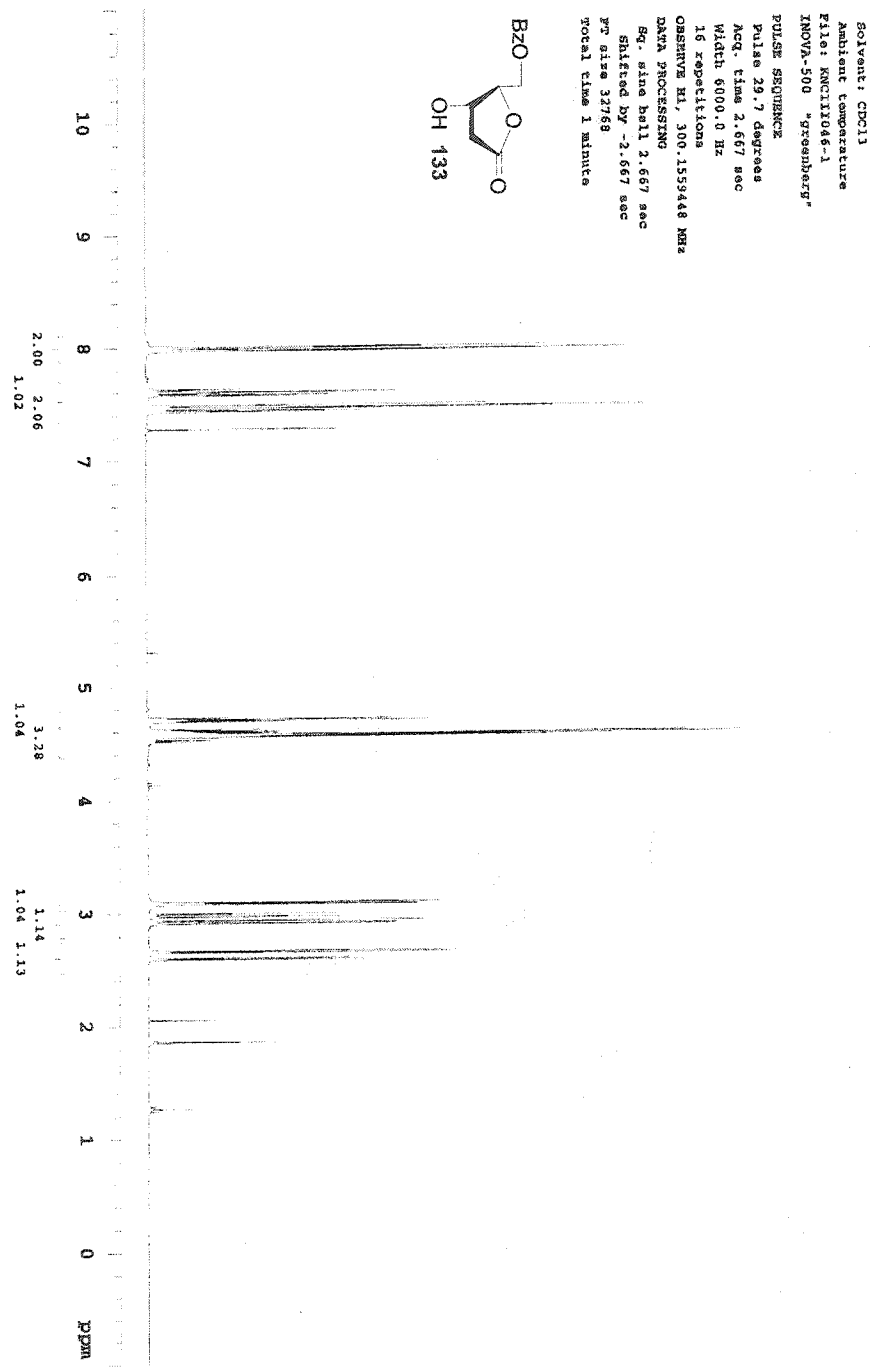

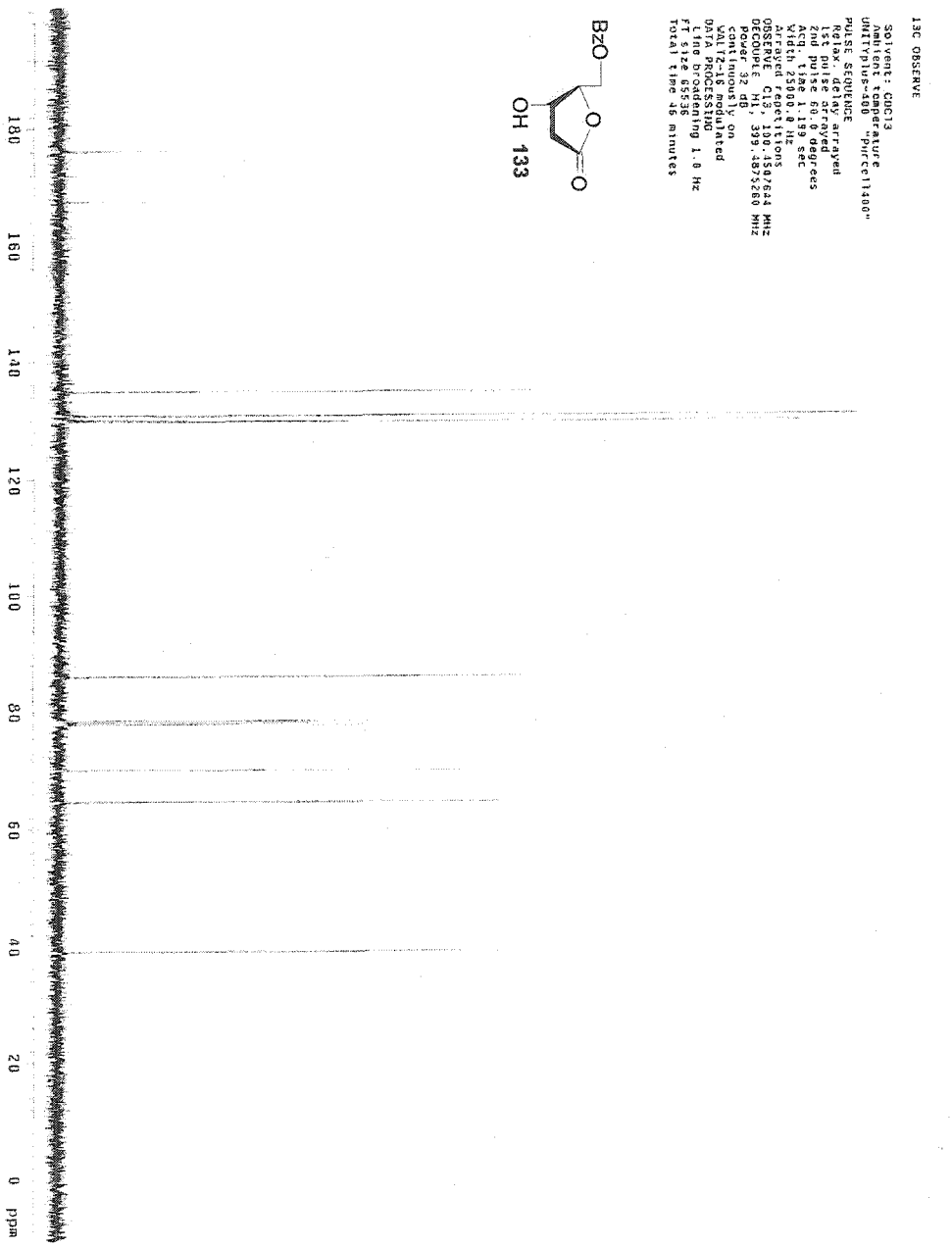

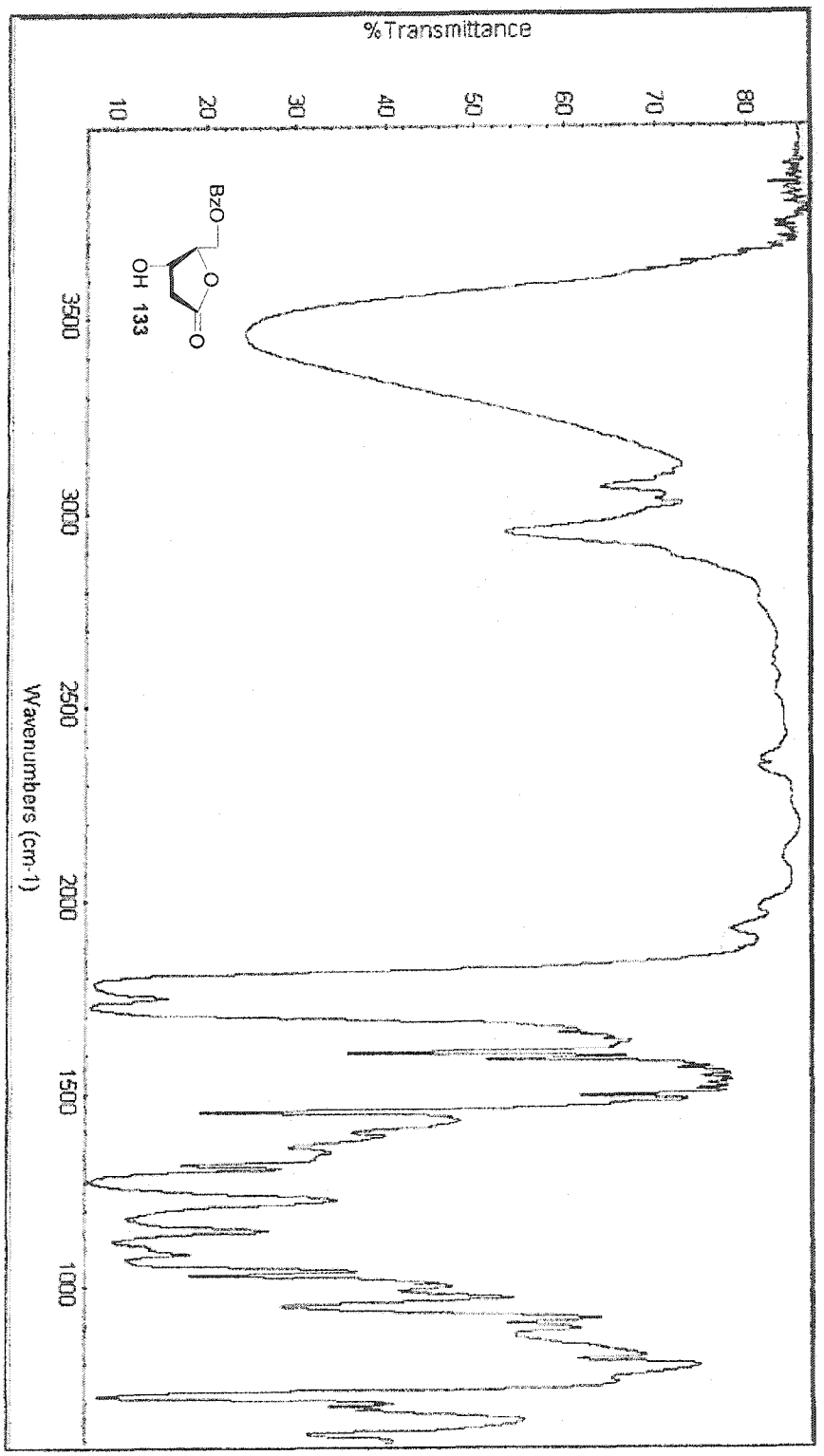

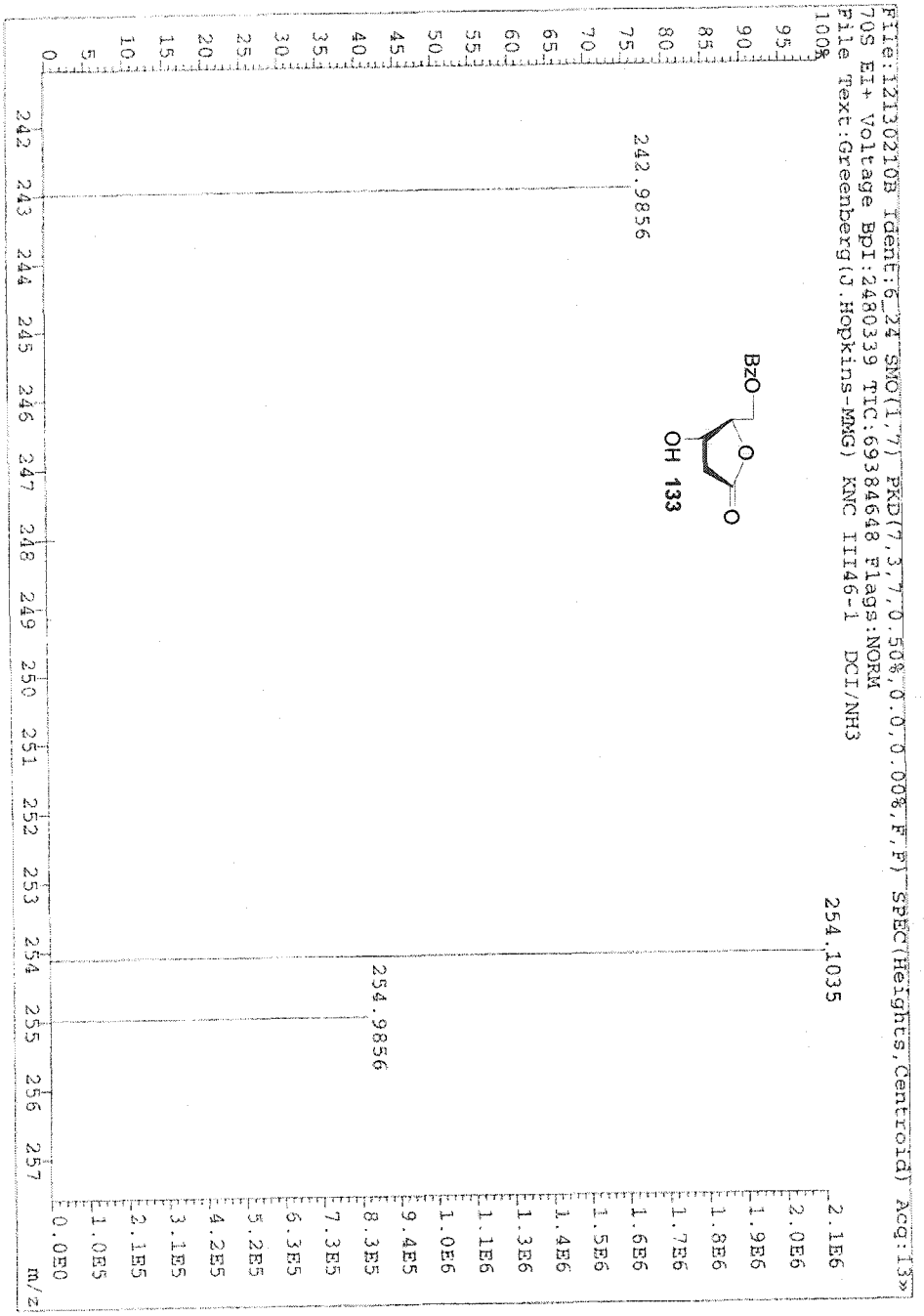

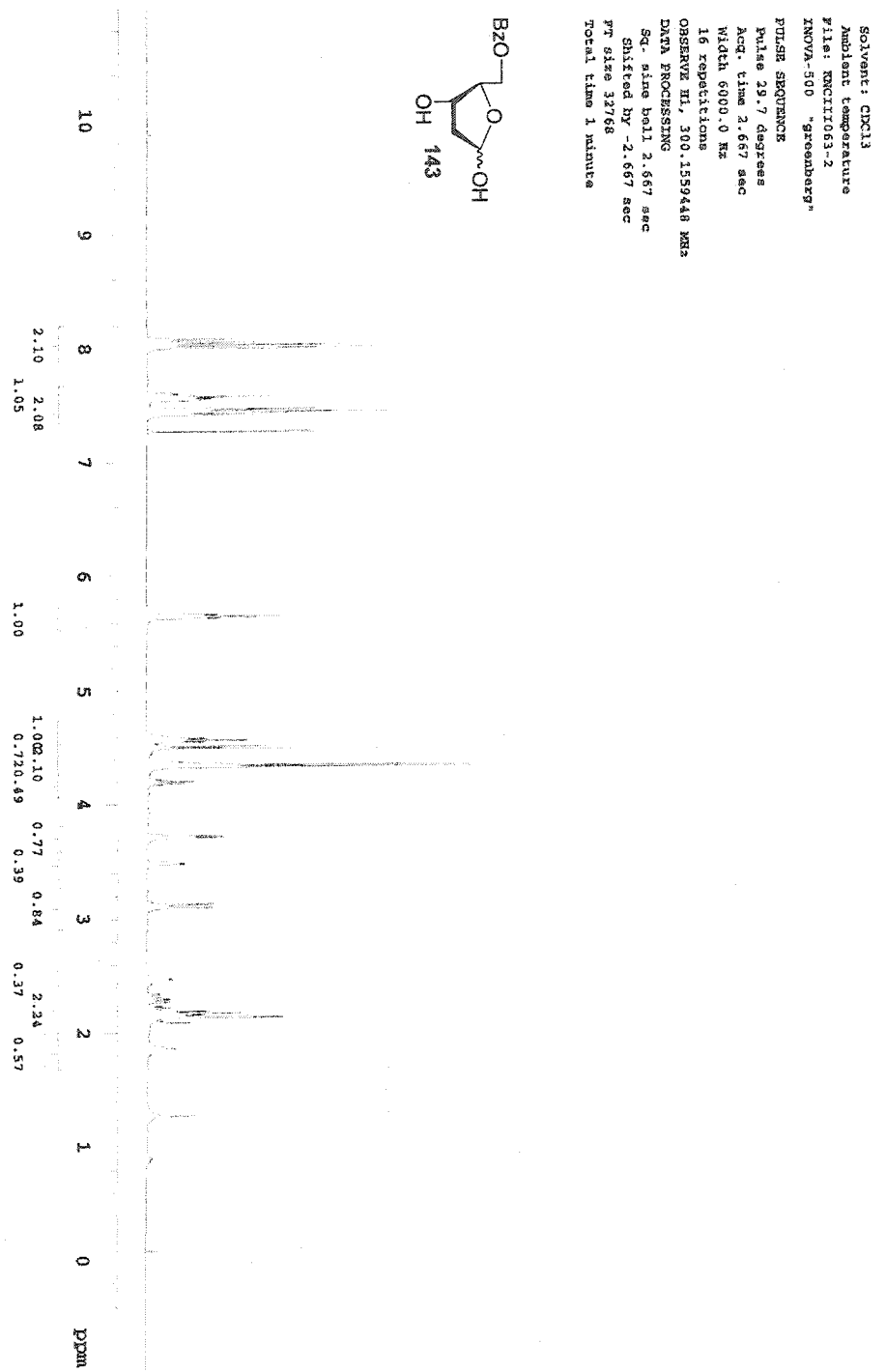

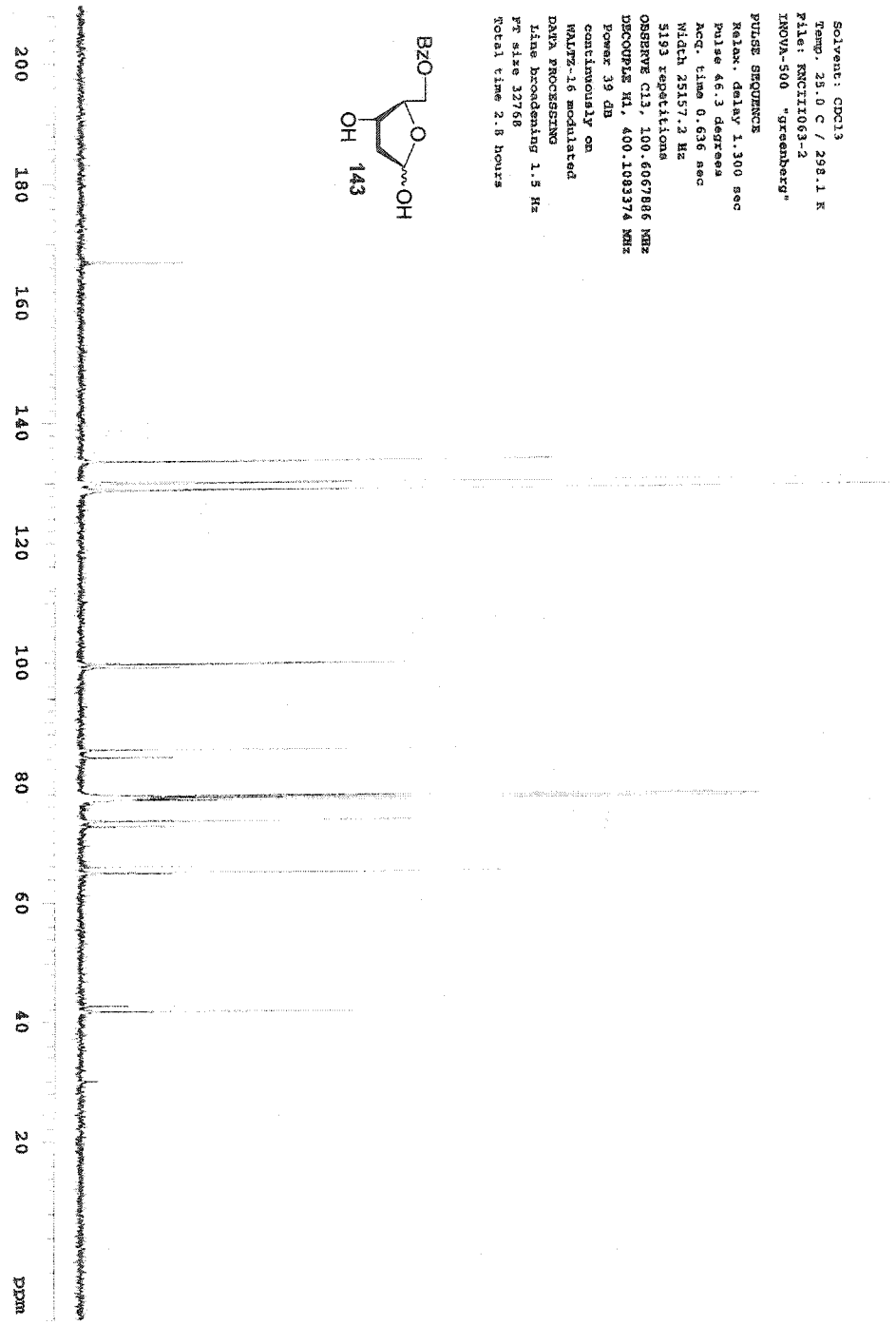

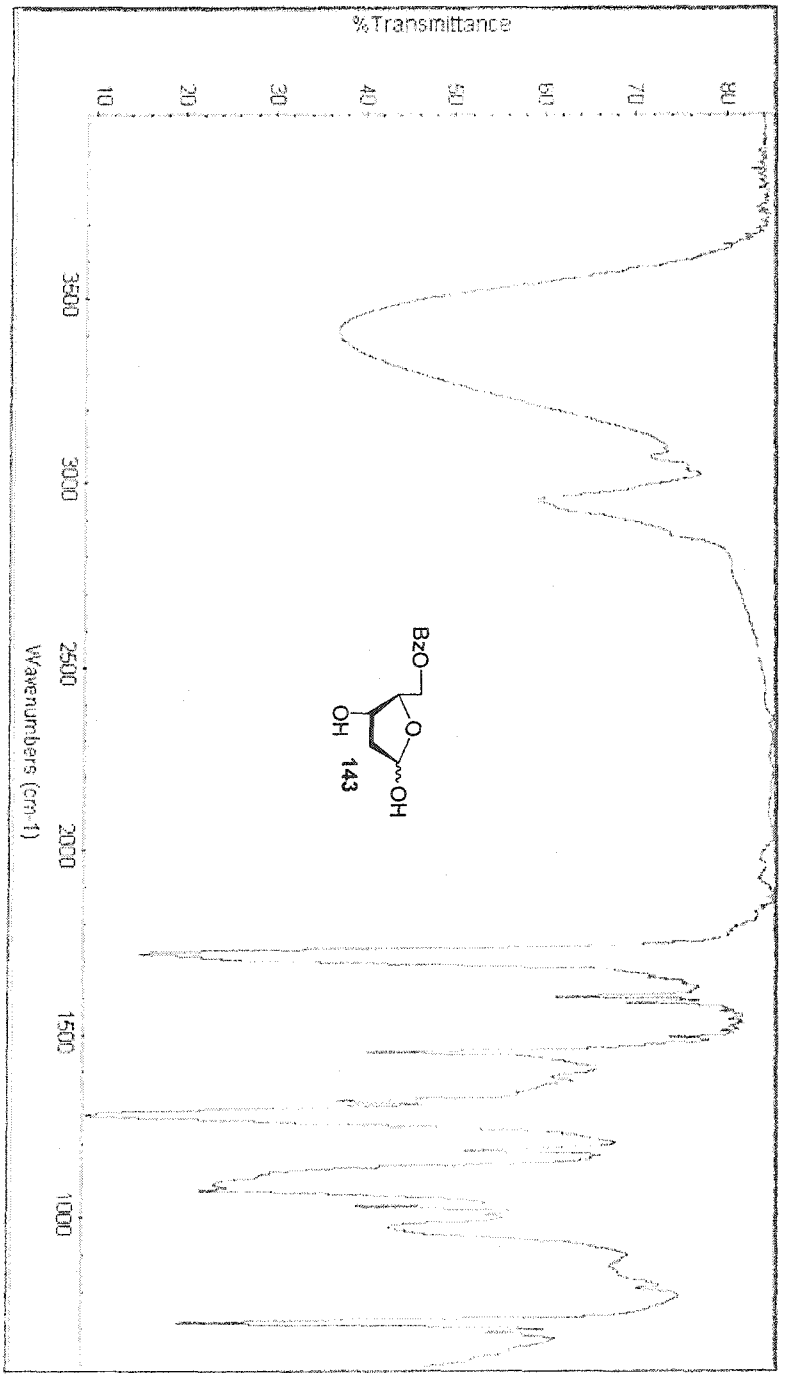

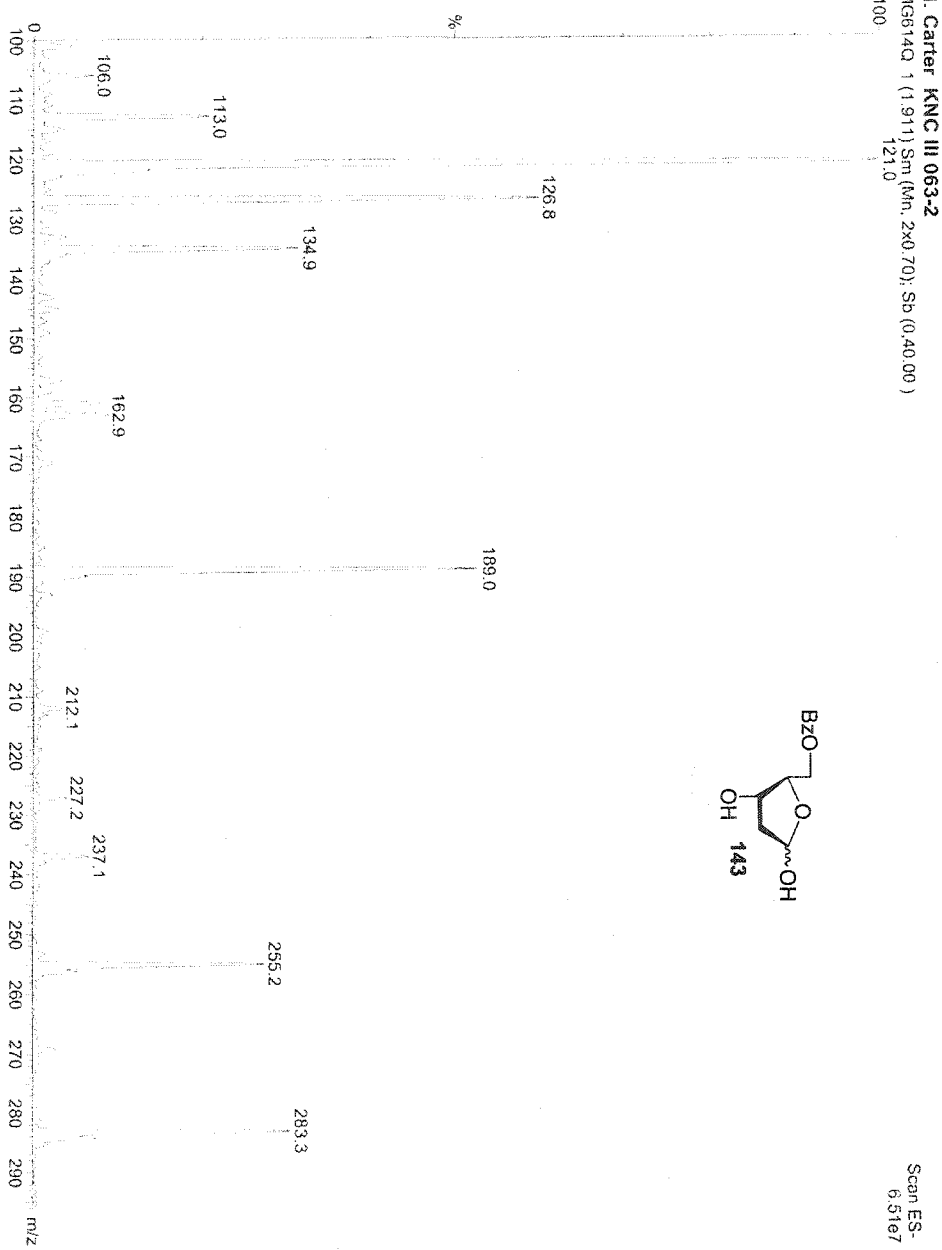

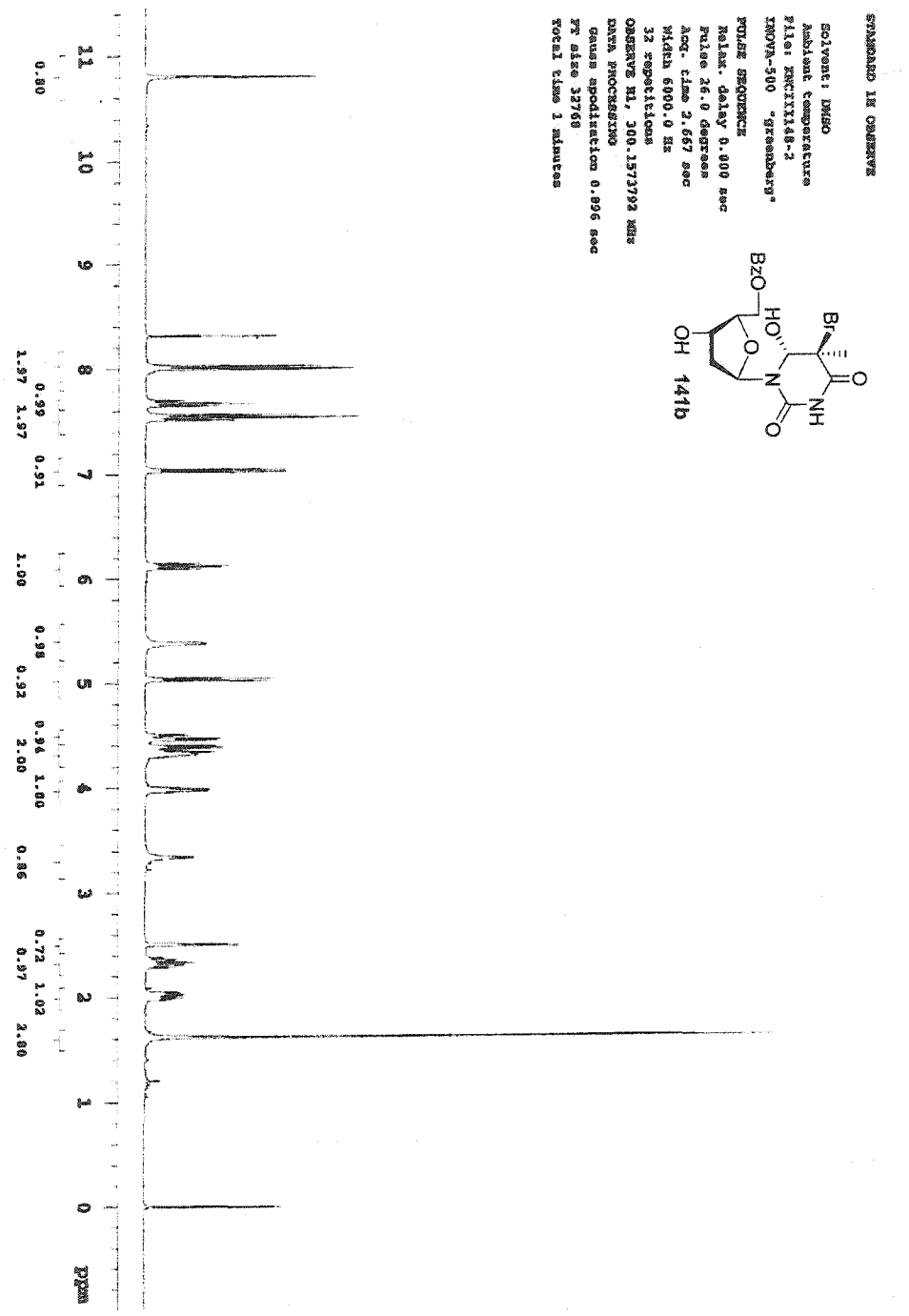

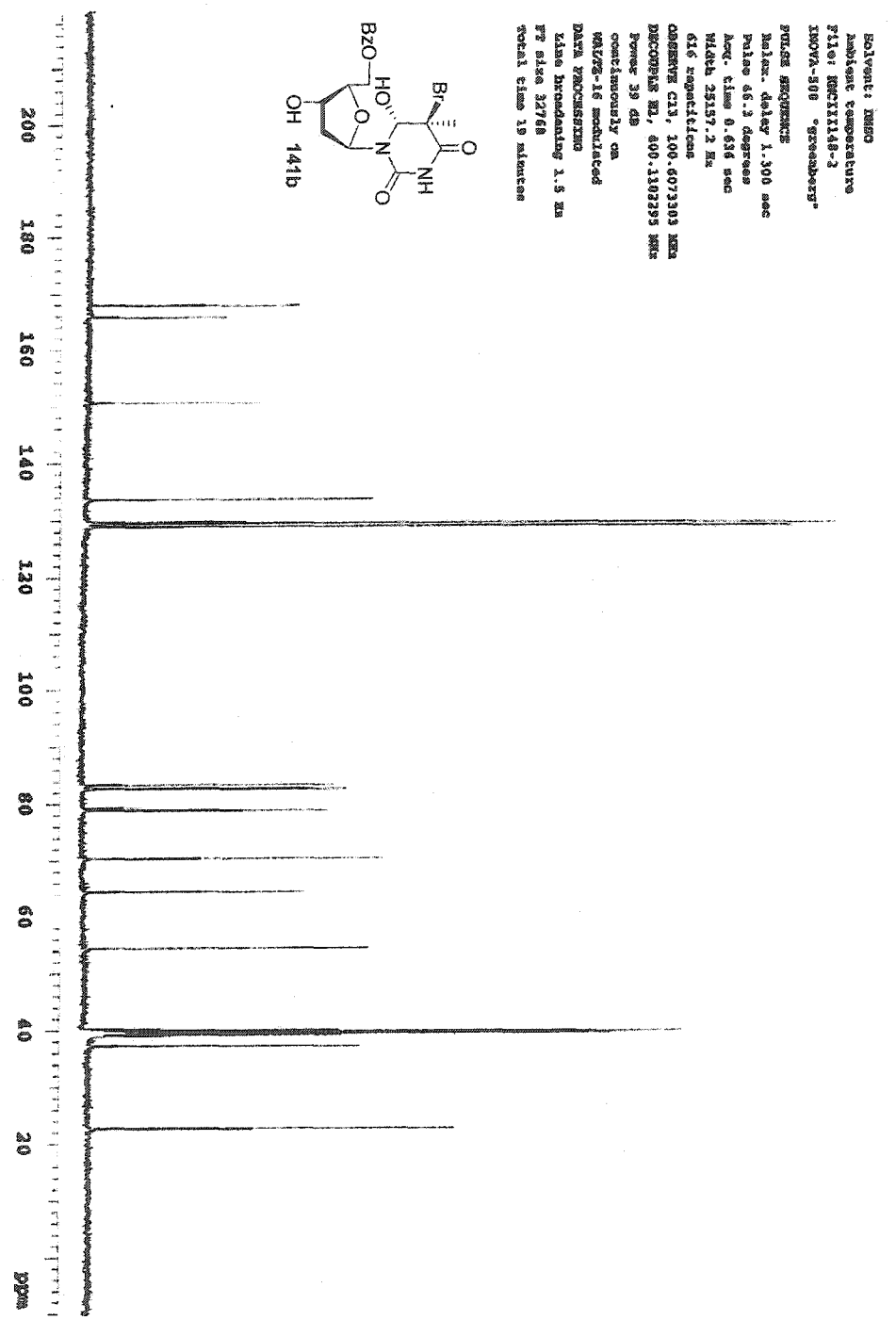

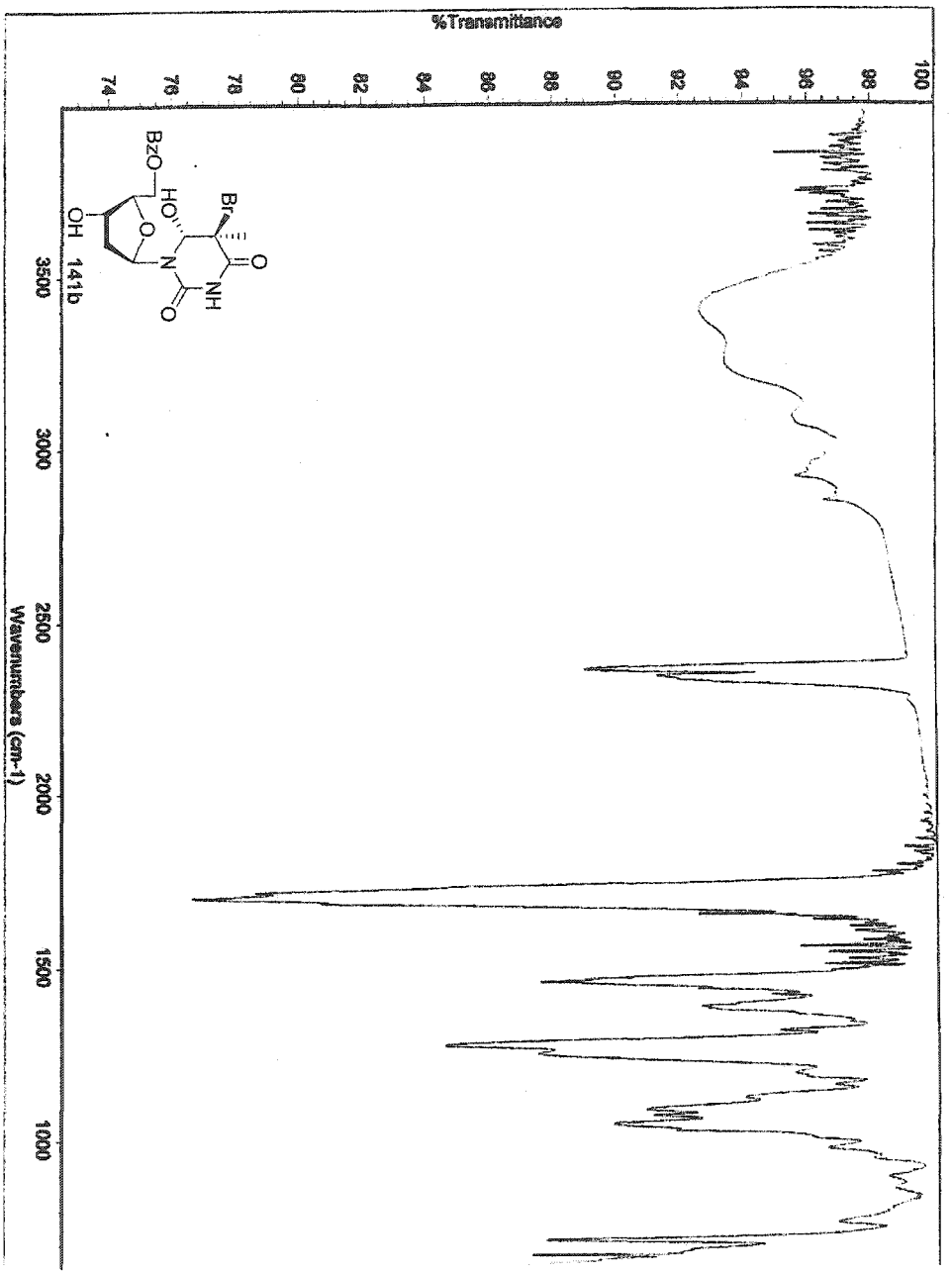

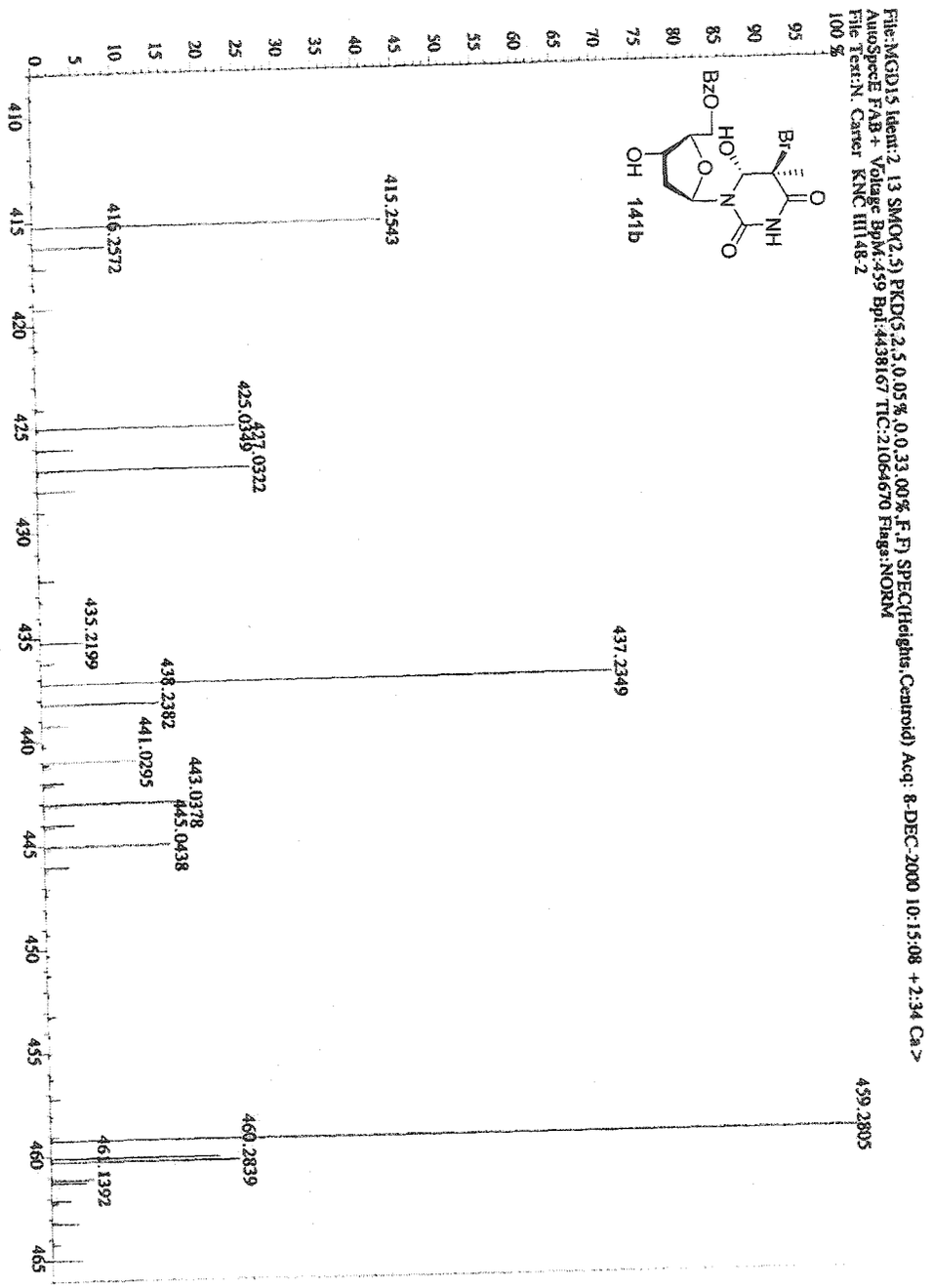

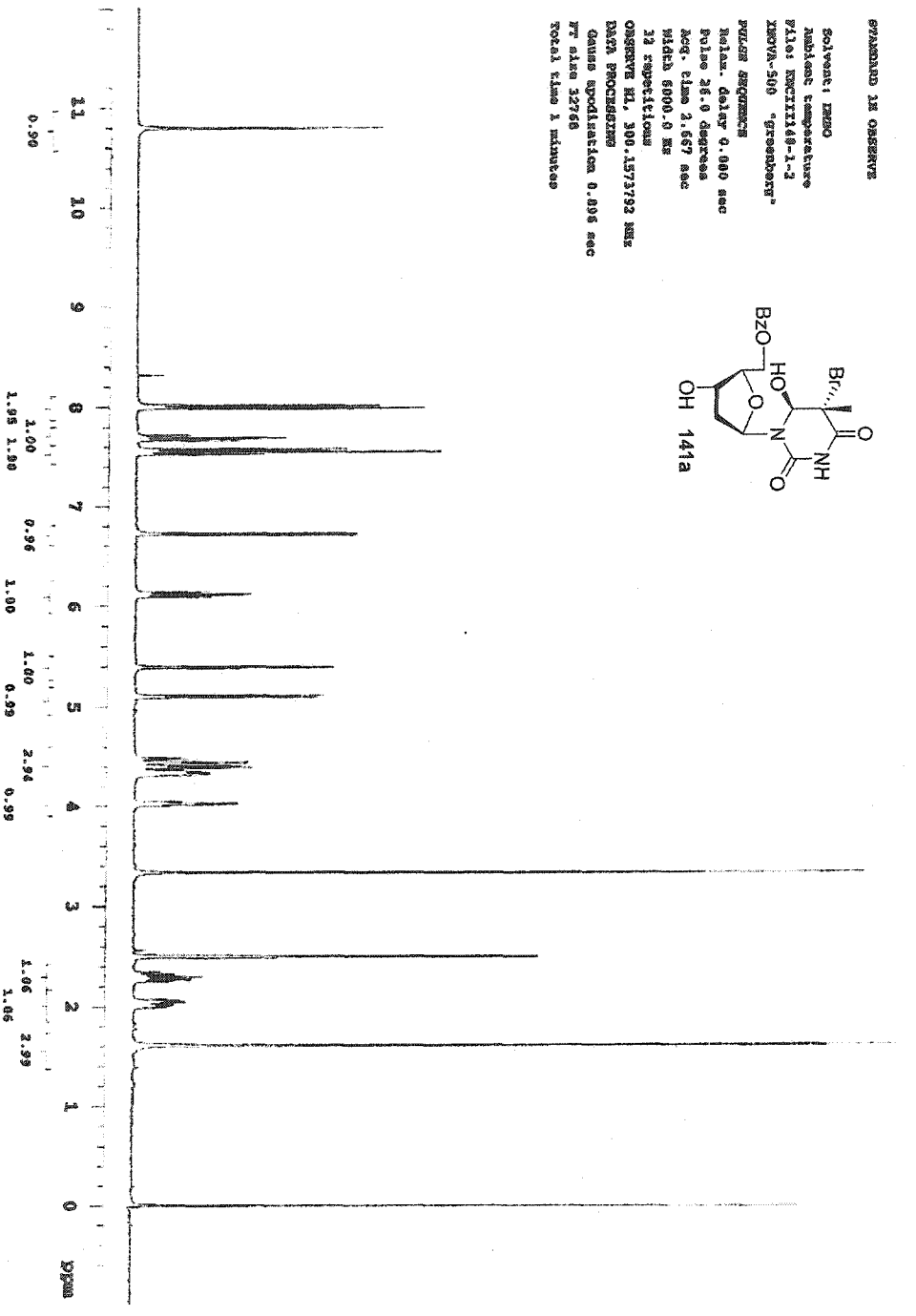

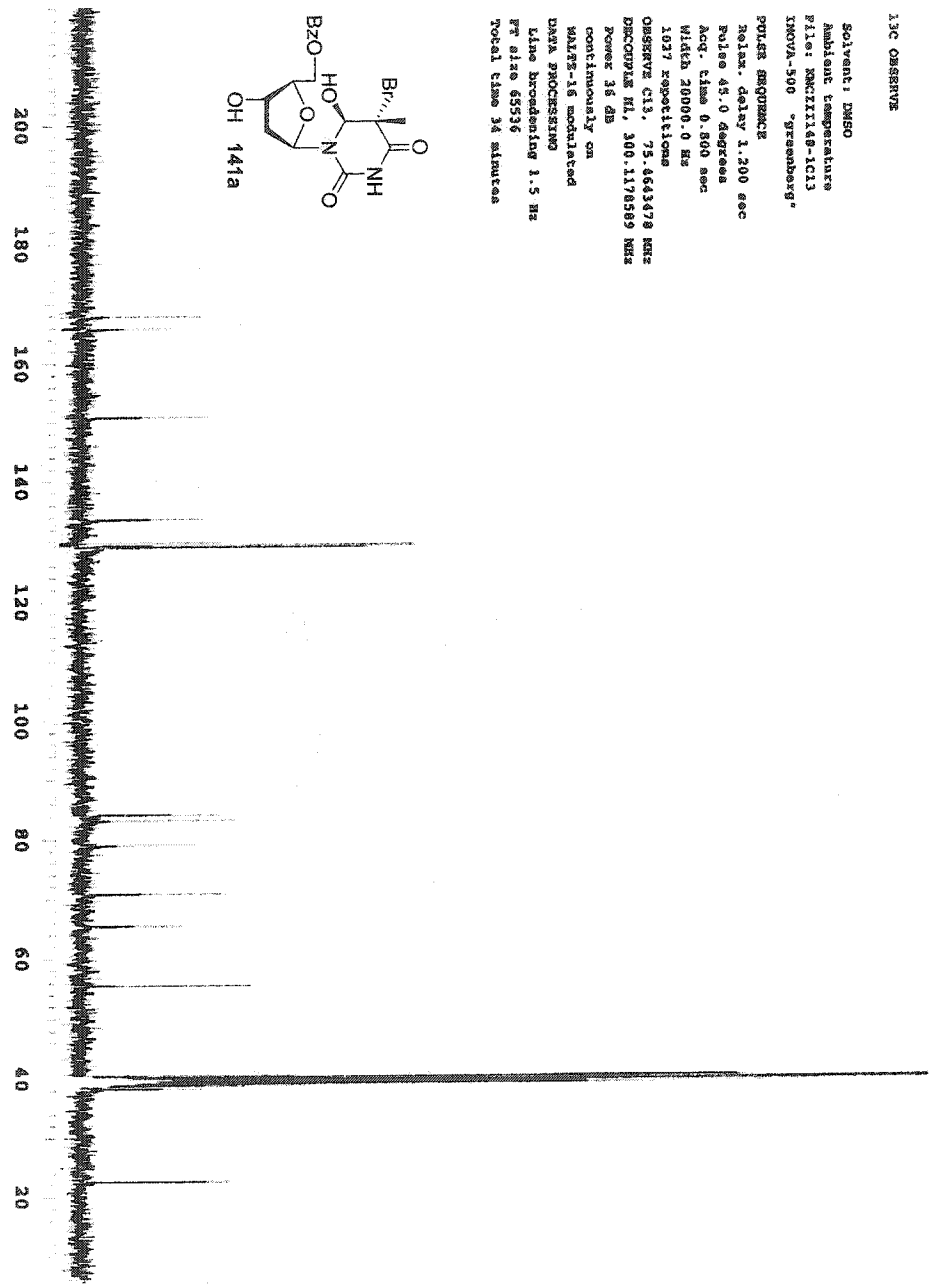

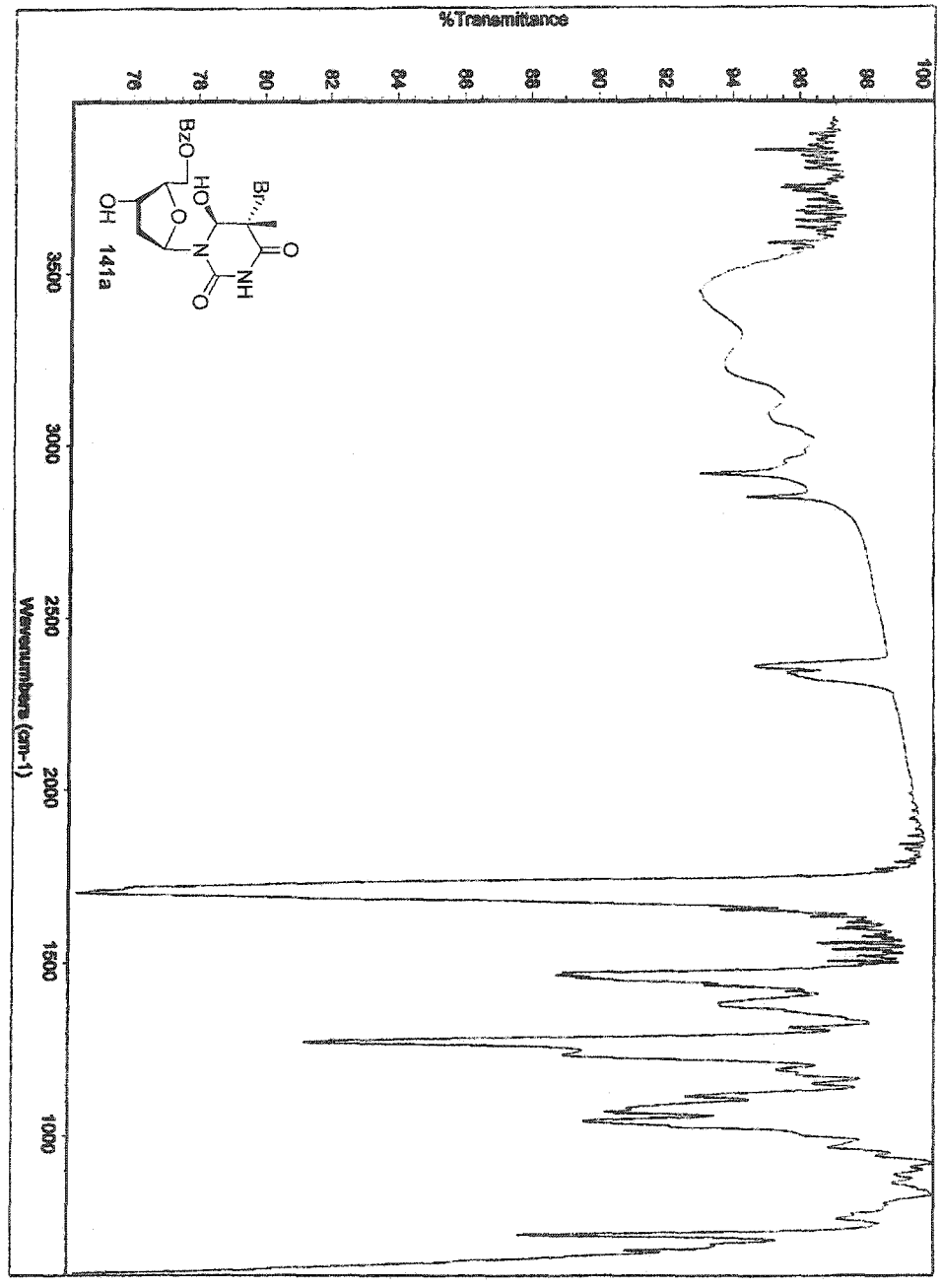

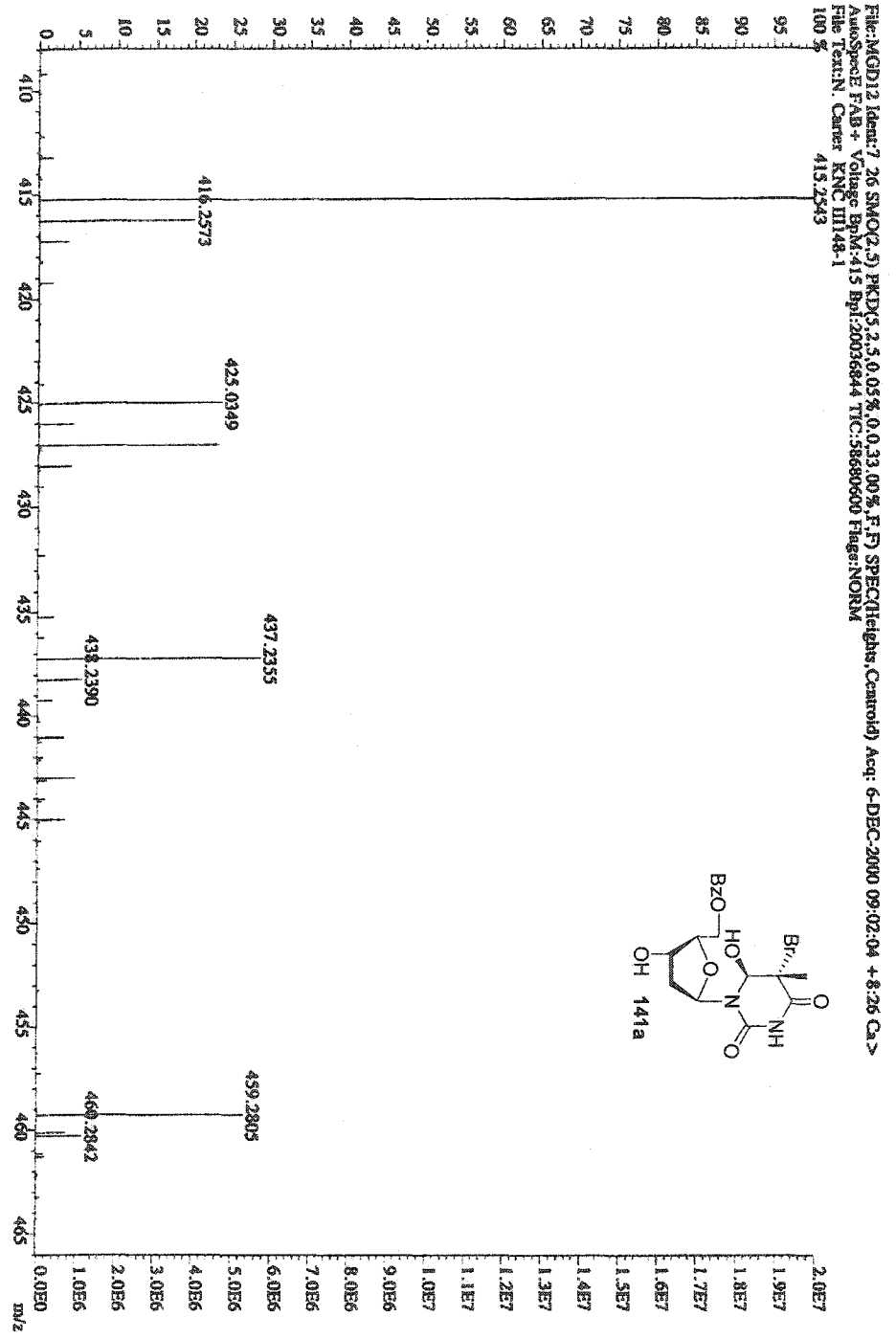

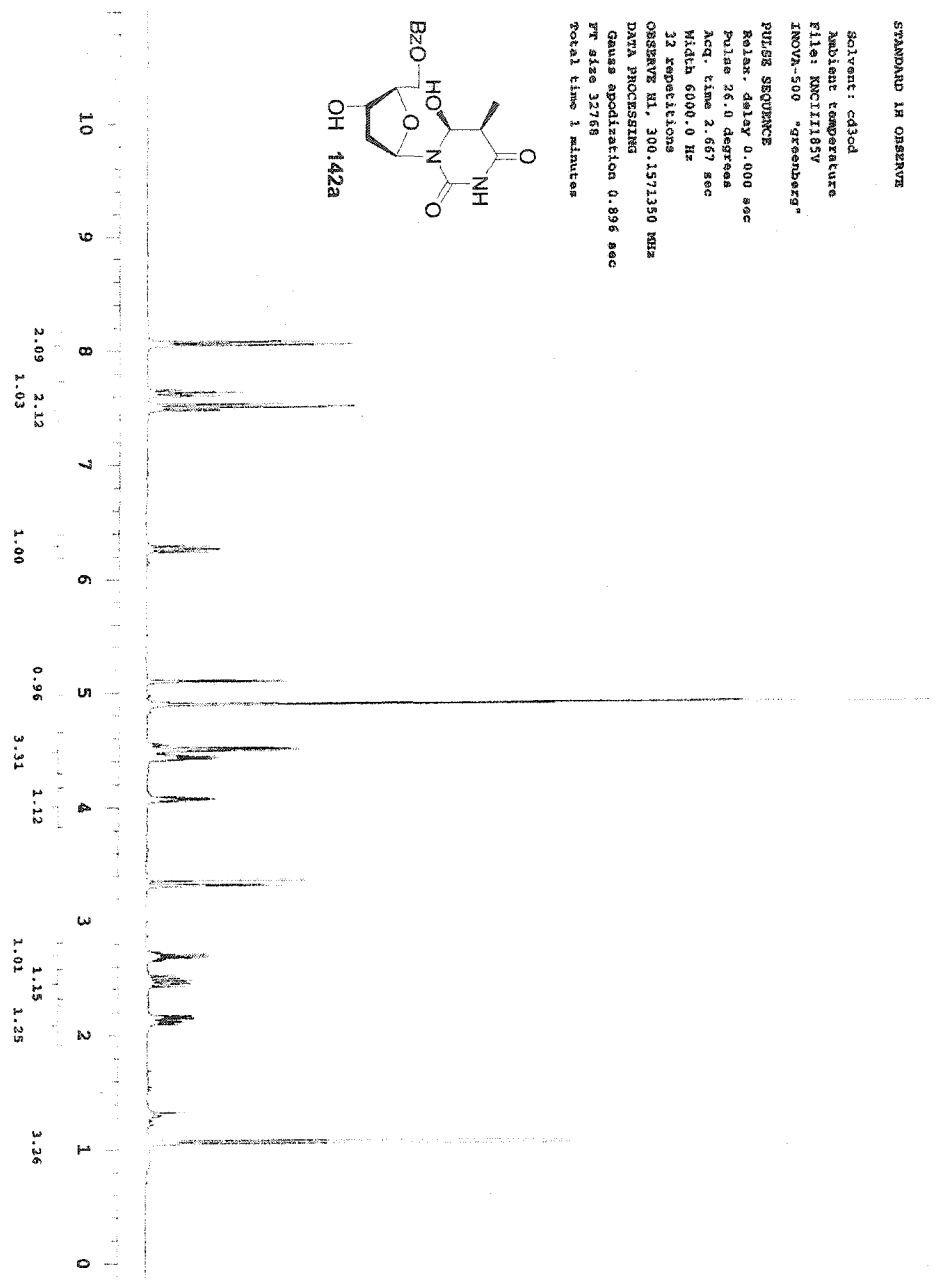

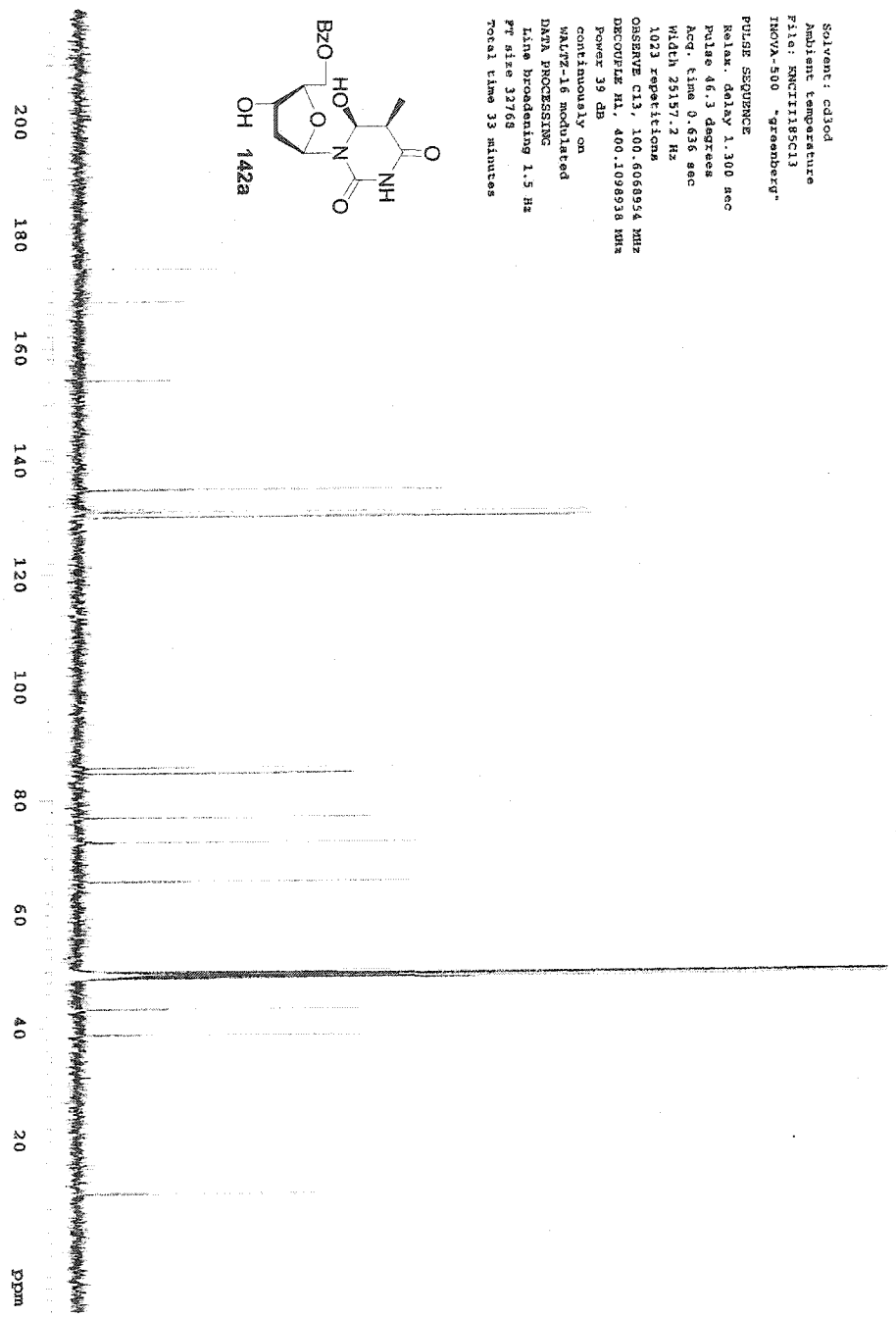

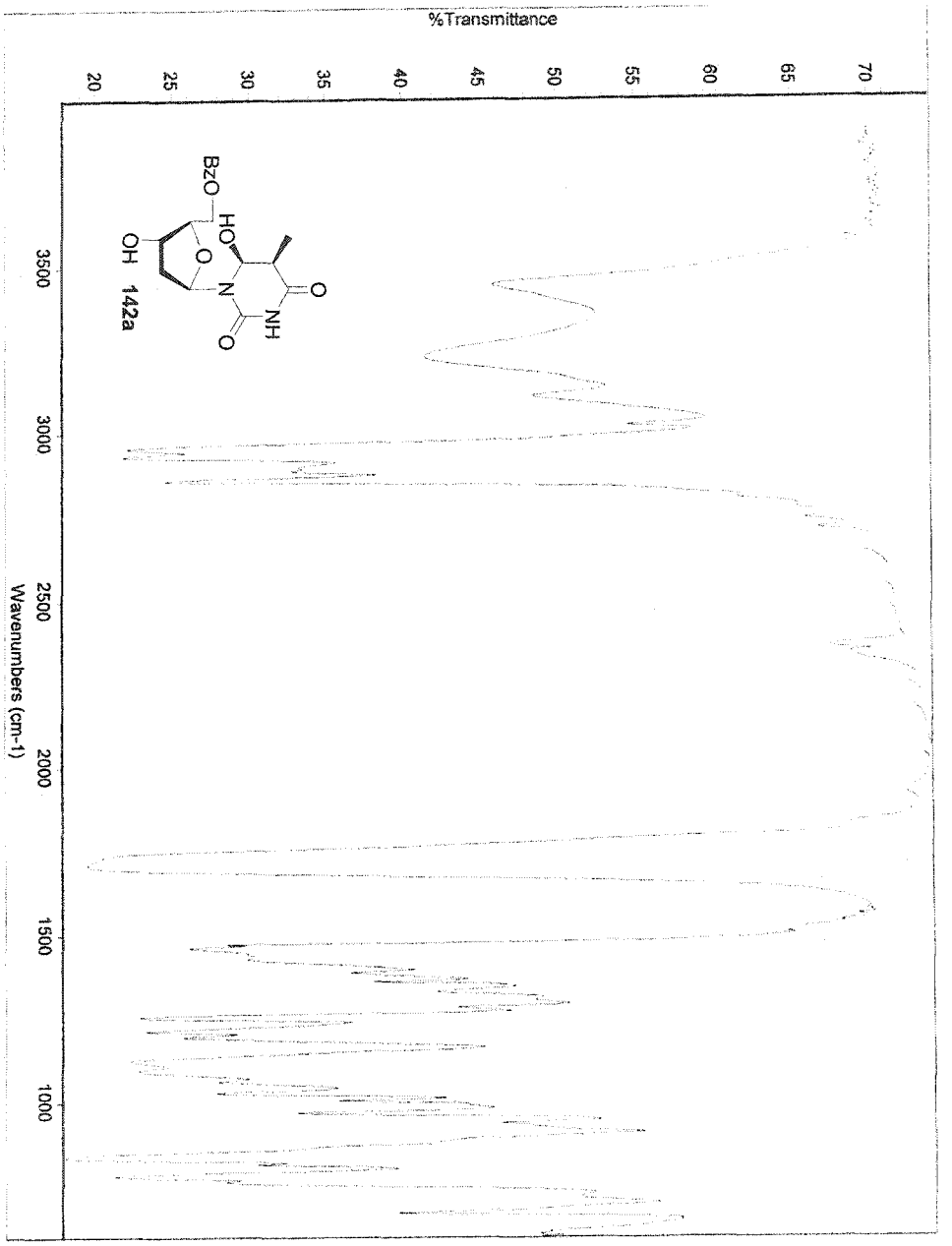

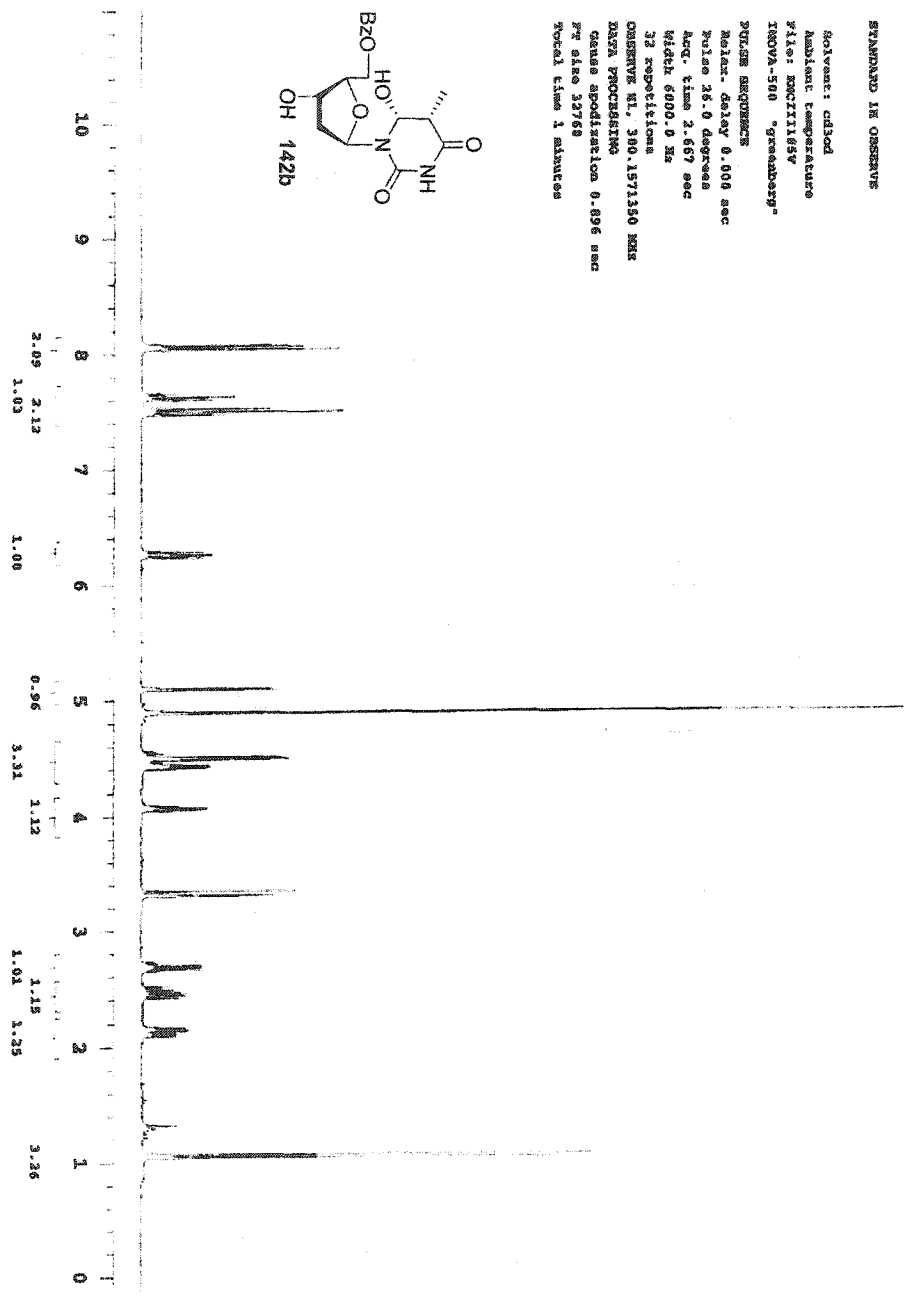

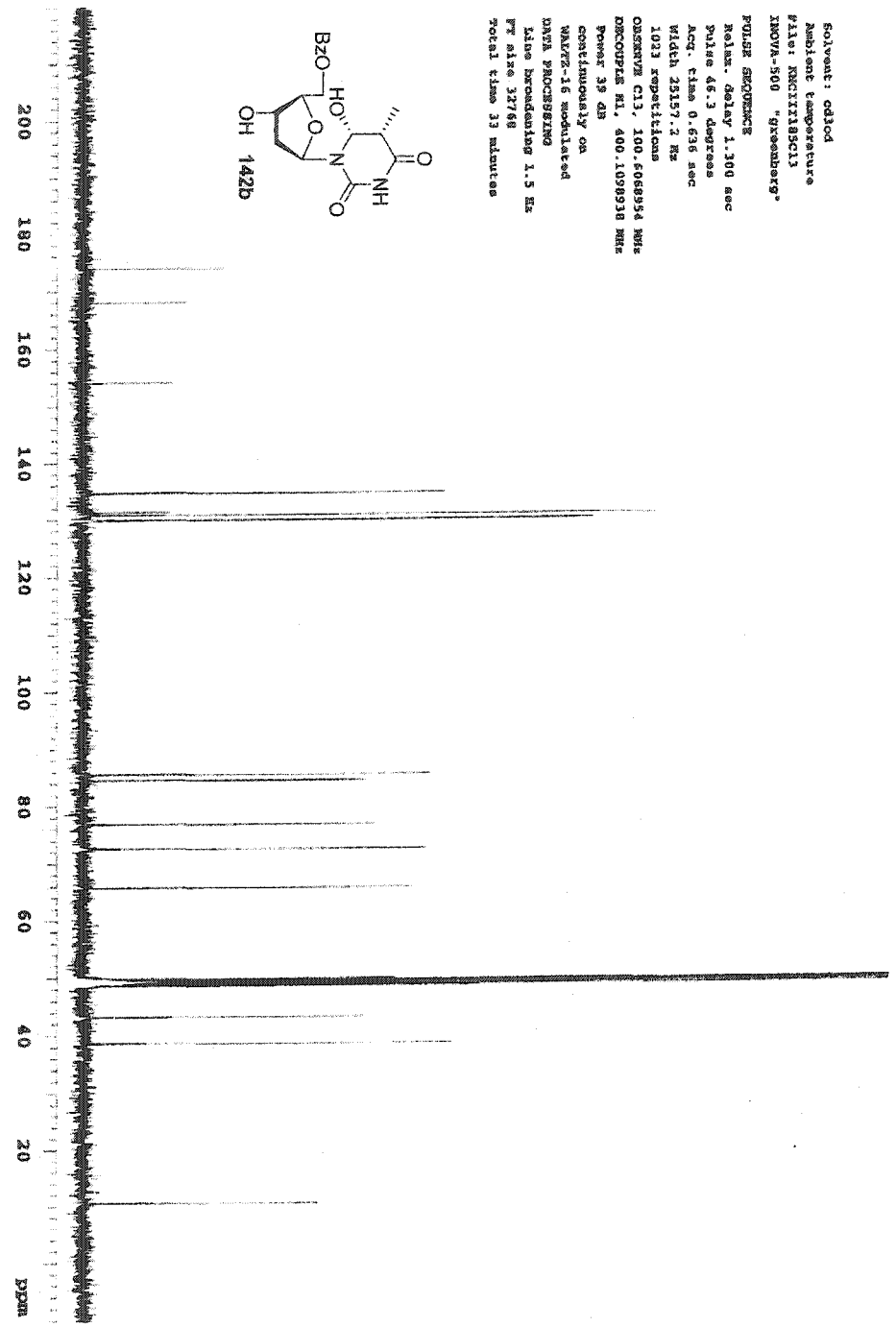

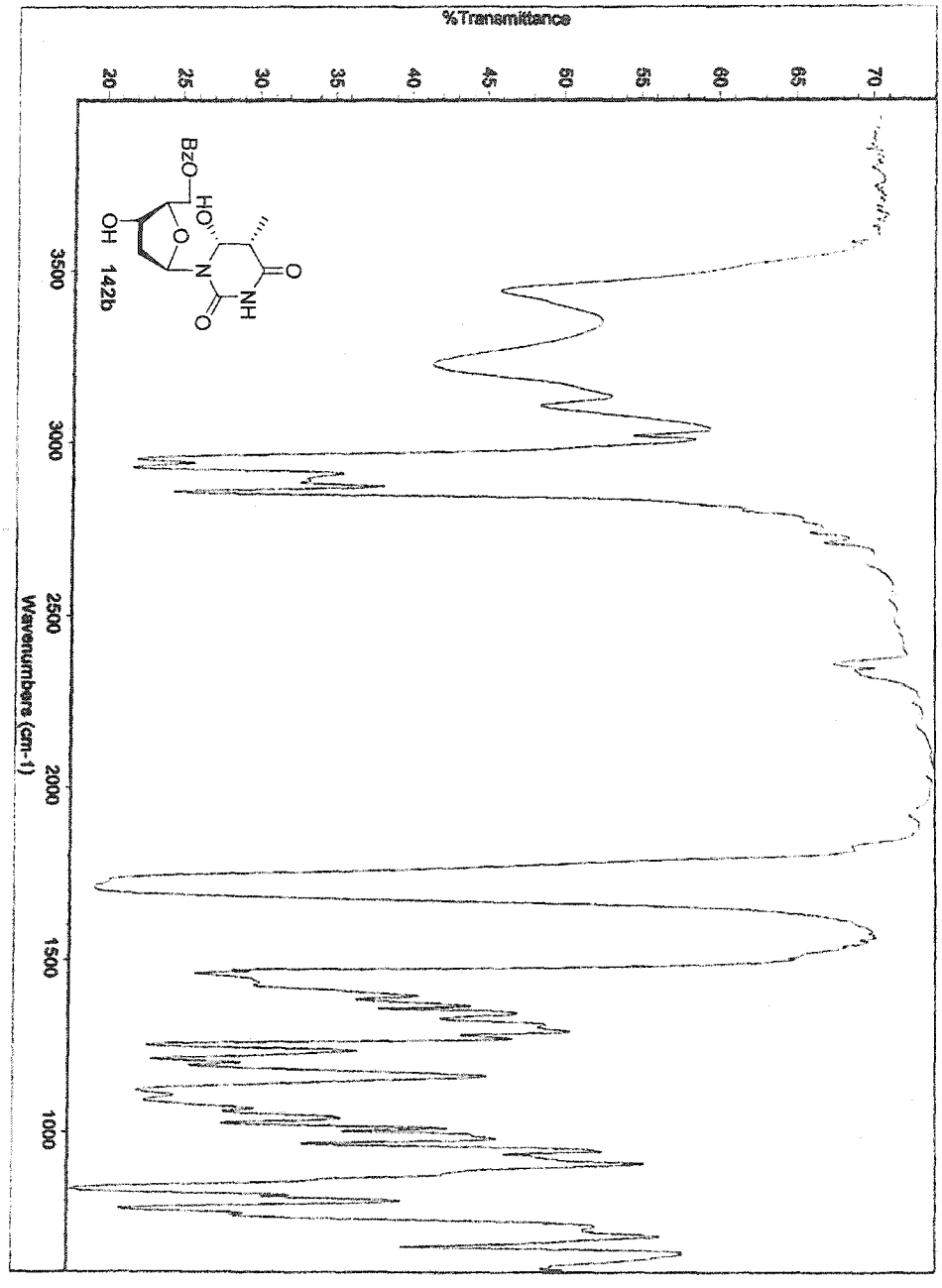

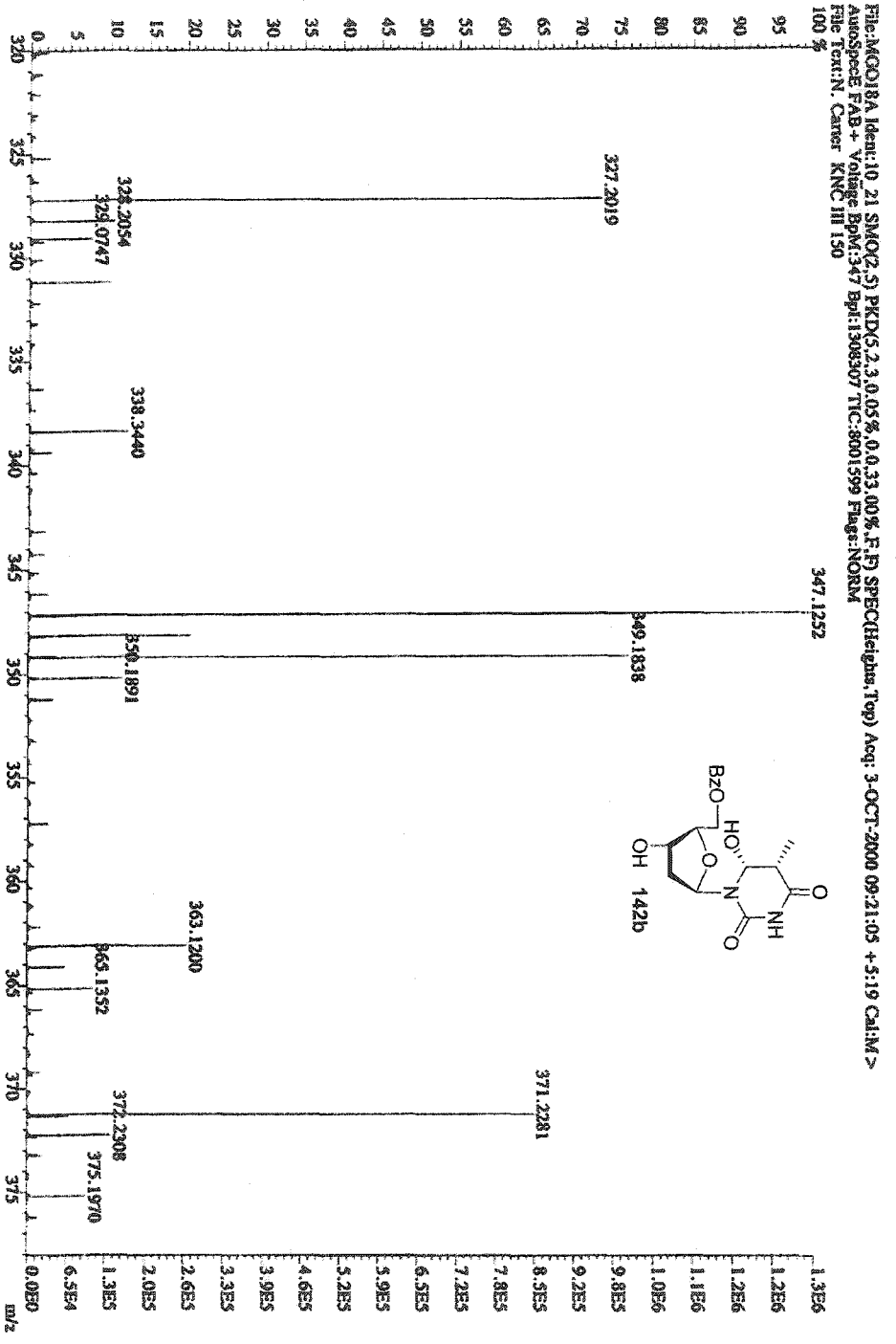

Appendix C: Electrospray Mass Spectra

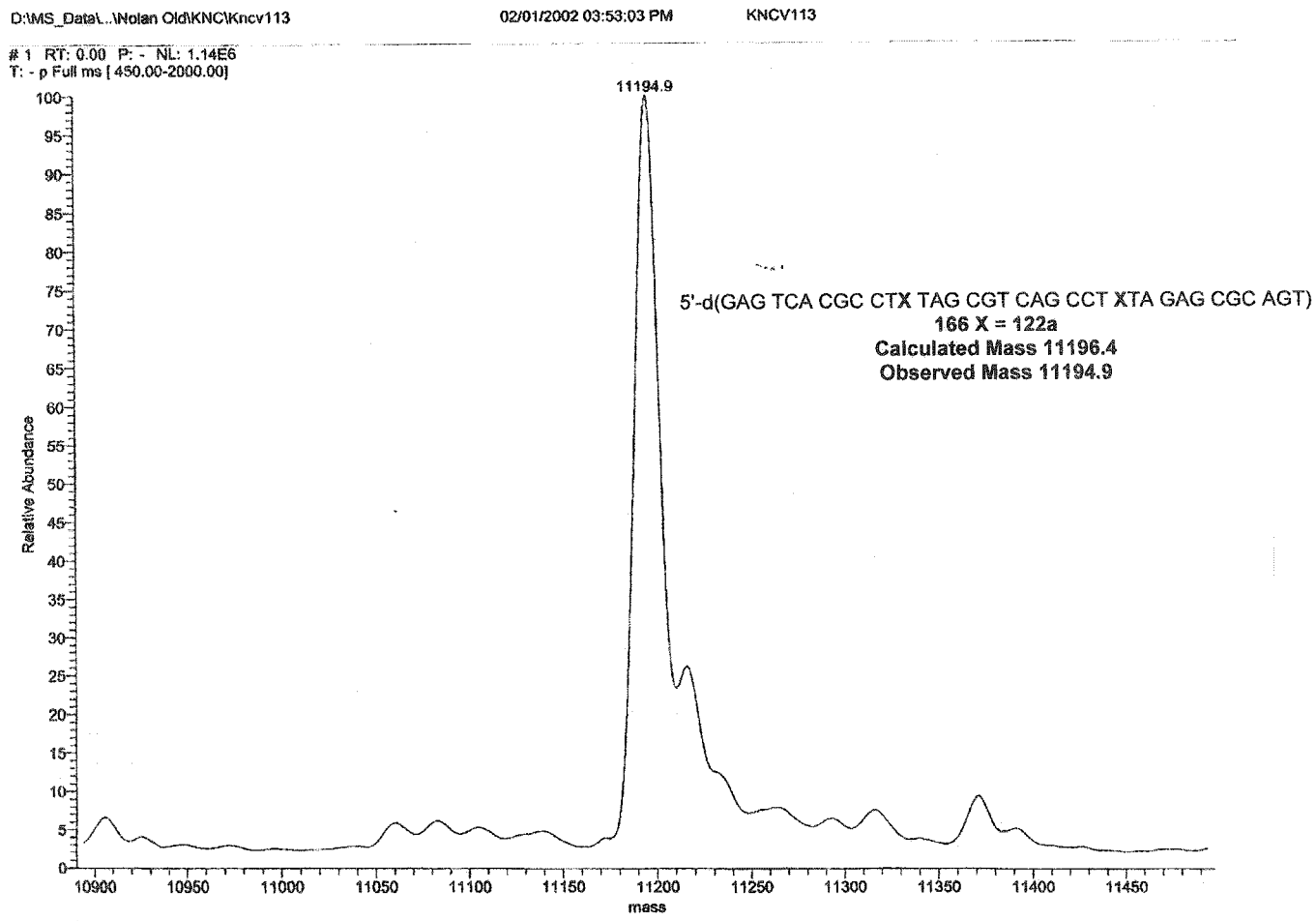

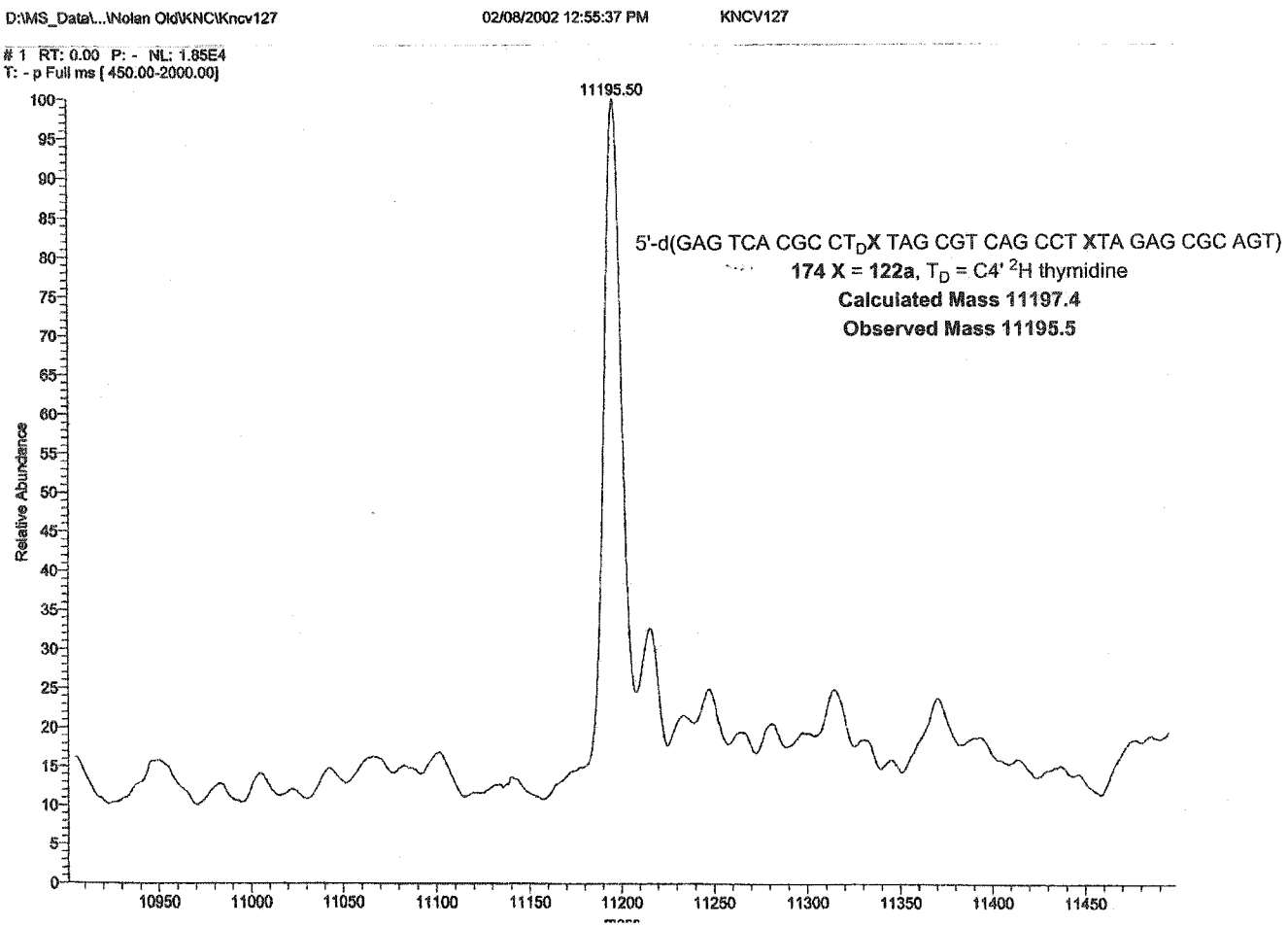

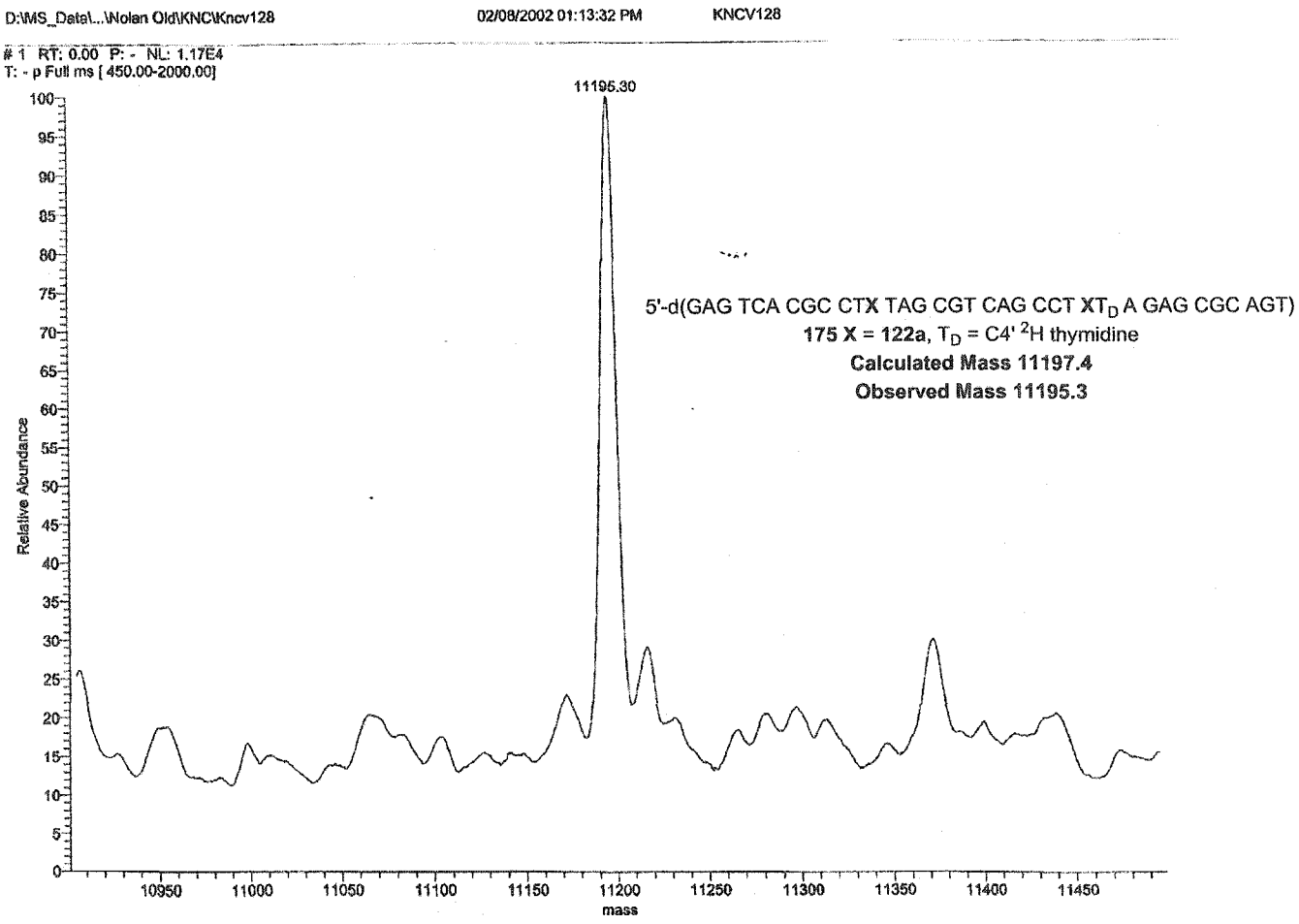

Appendix D: MALDI-TOF Mass Spectra

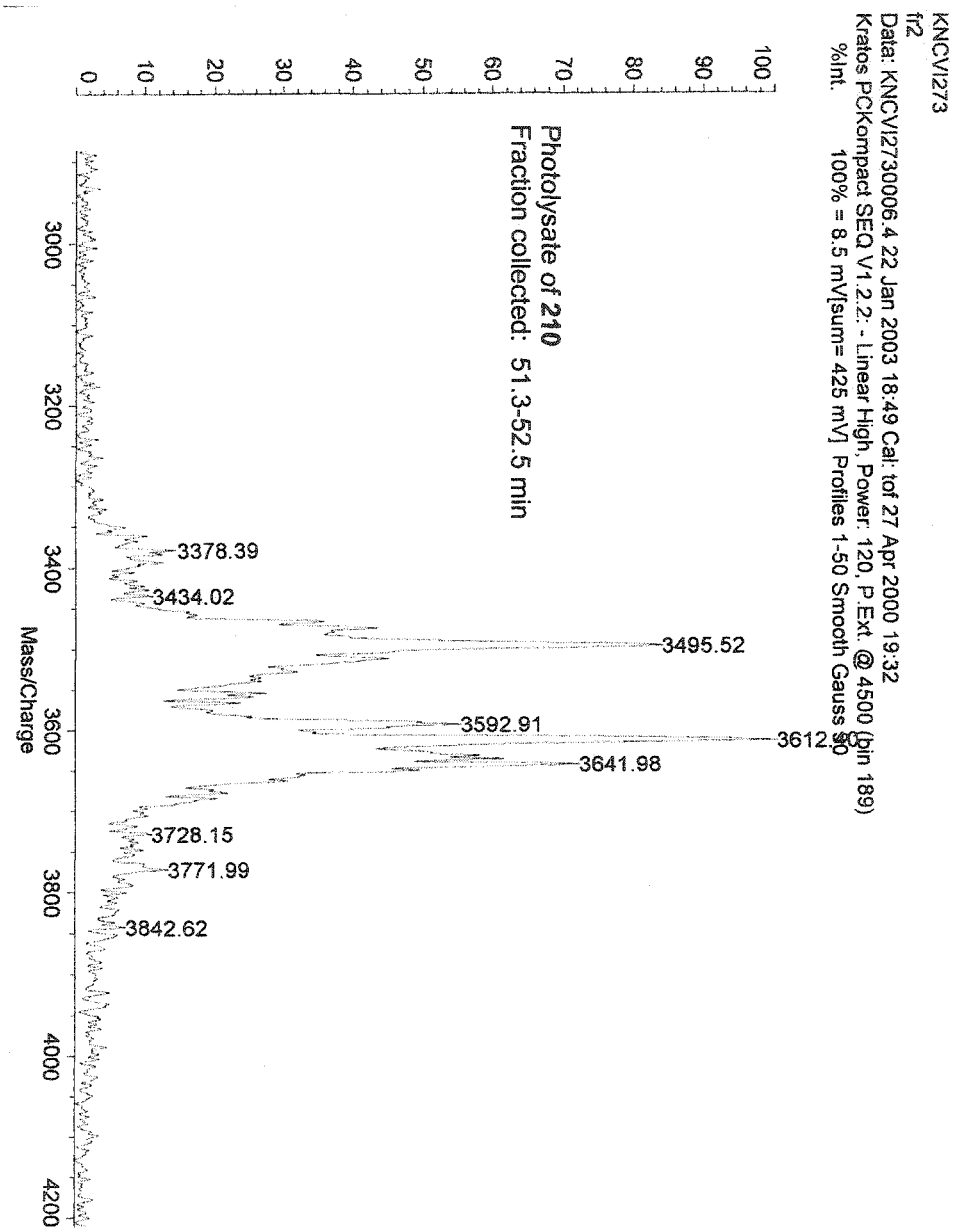

KNCVI273
fr3
Data: KNCVI2730011.6 22 Jan 2003 18:57 Cal: tof 27 Apr 2000 19:32
Kratos PCKompact SEQ V1.2.2: - Linear High, Power: 130, P.Ext. @ 4500 (bin 189)
%Int. 100% = 118 mV[sum= 5908 mV] Profiles 1-50 Smooth Gauss 30

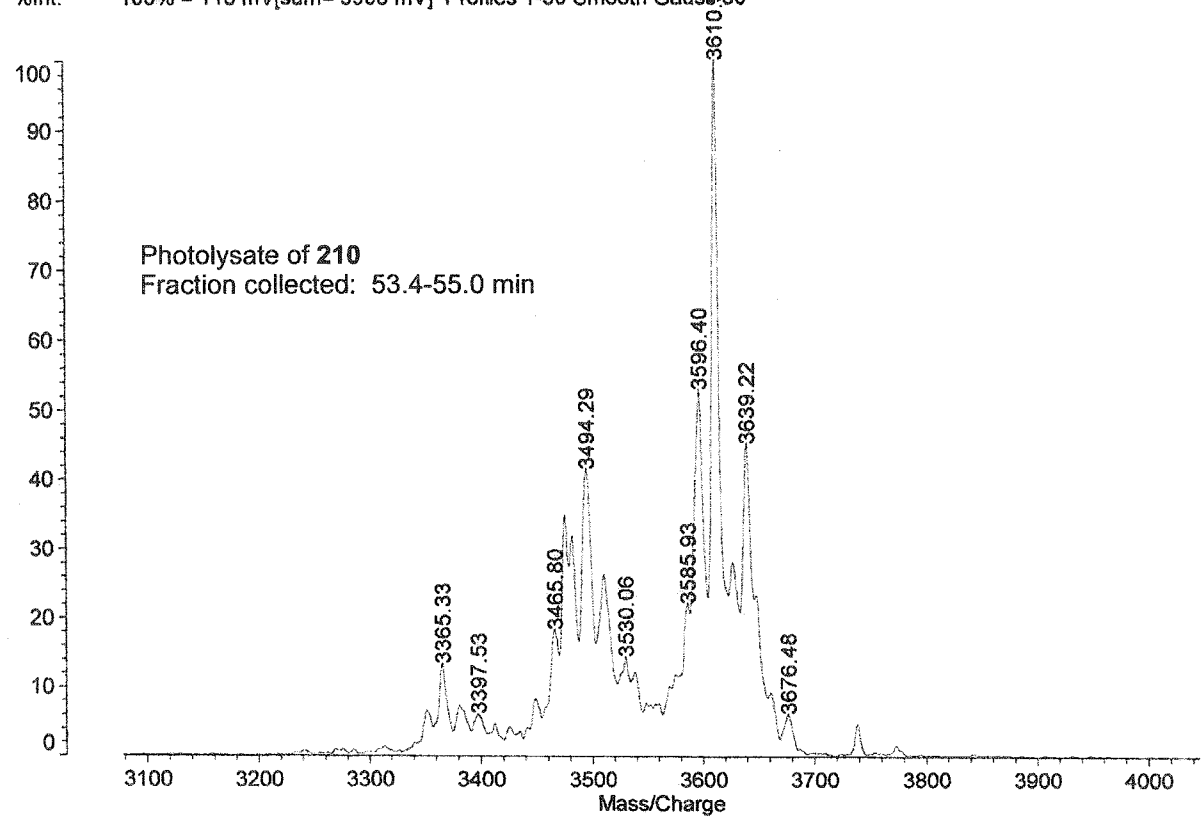

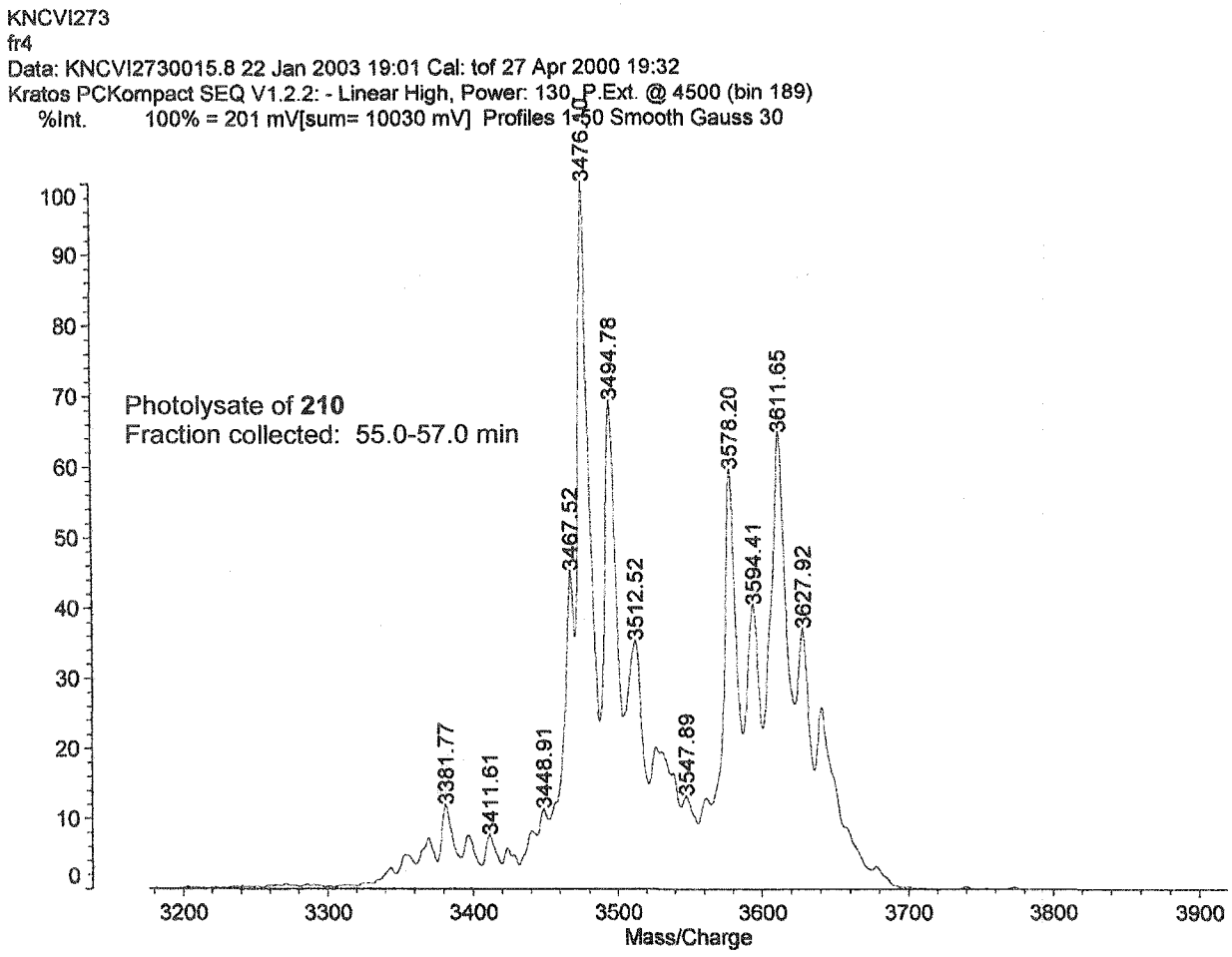

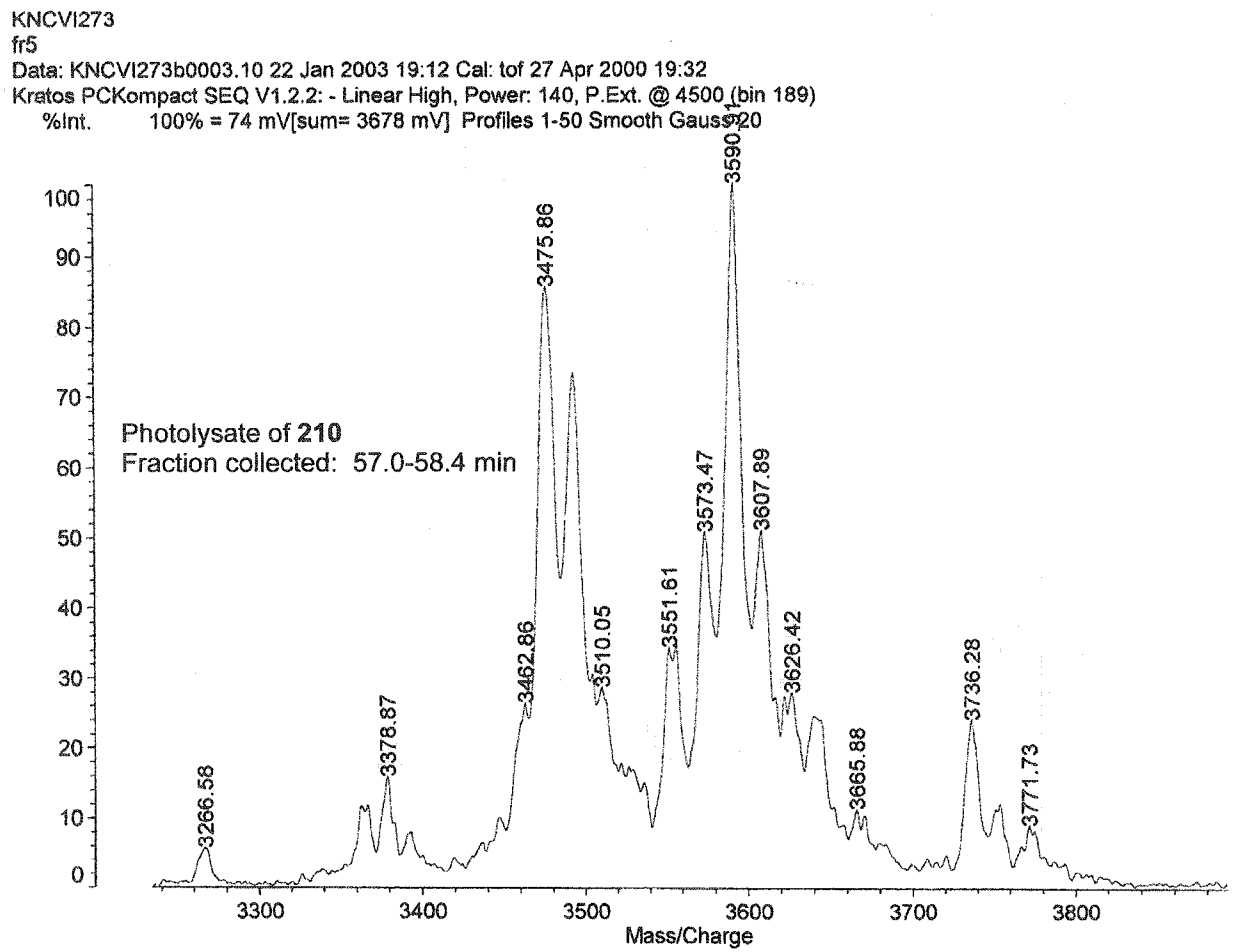

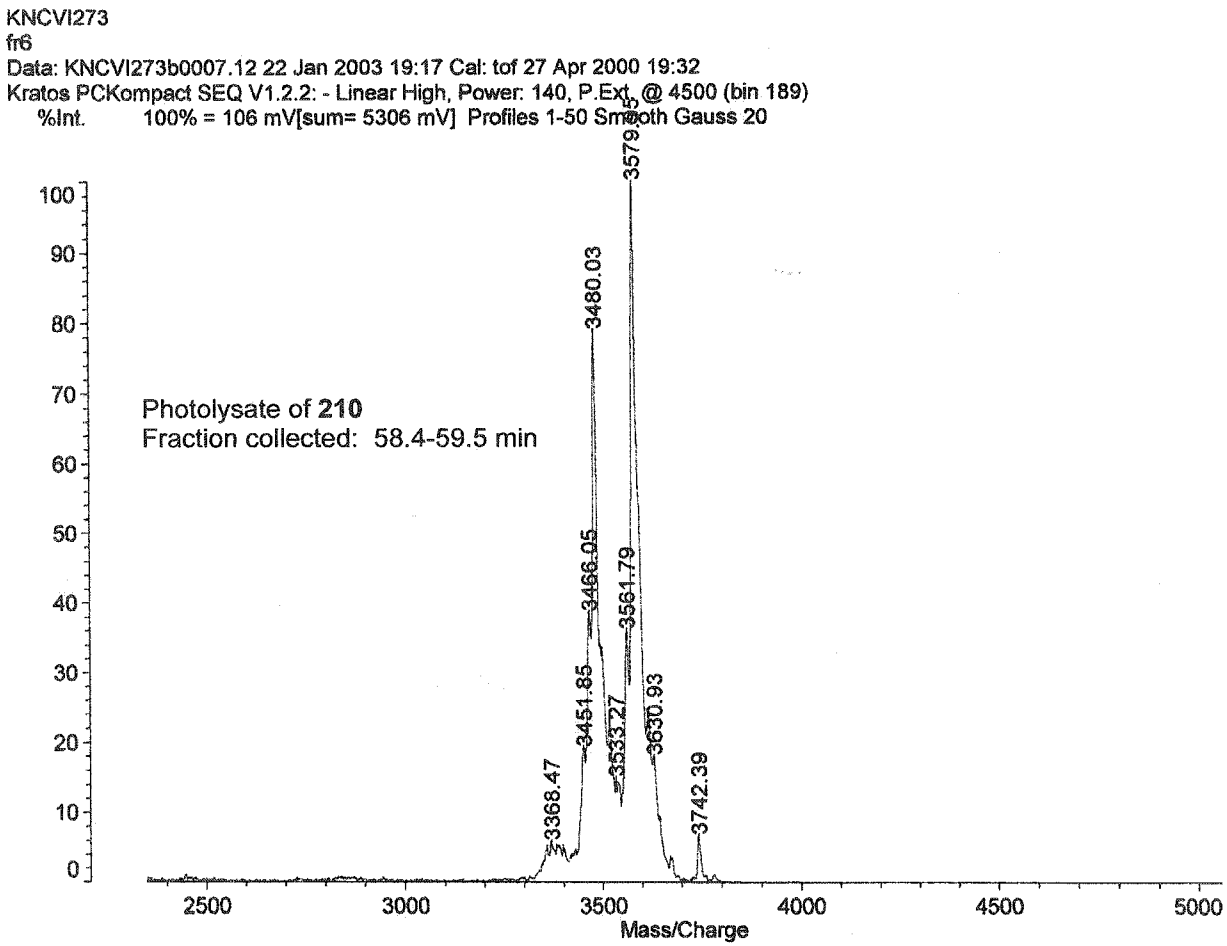

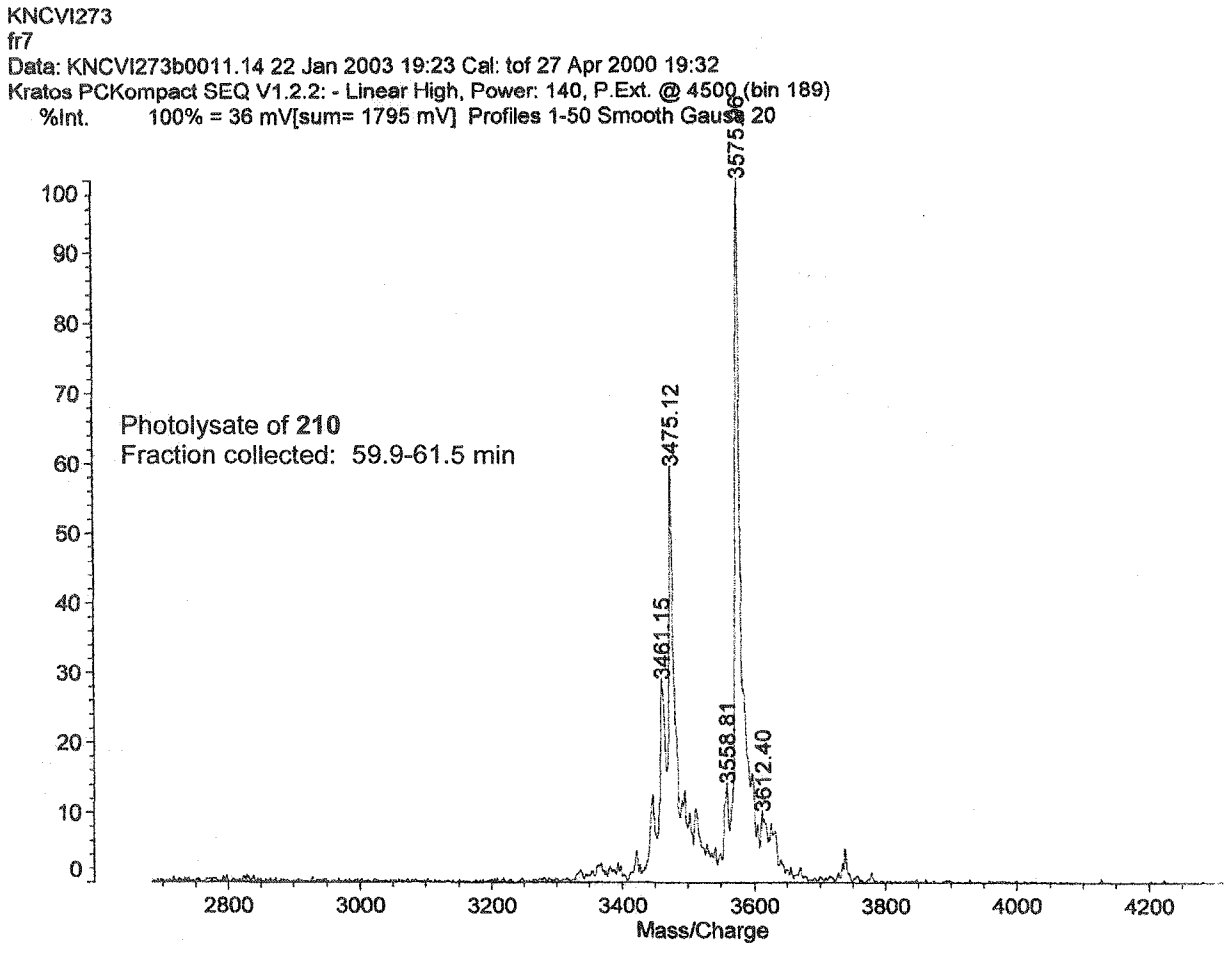

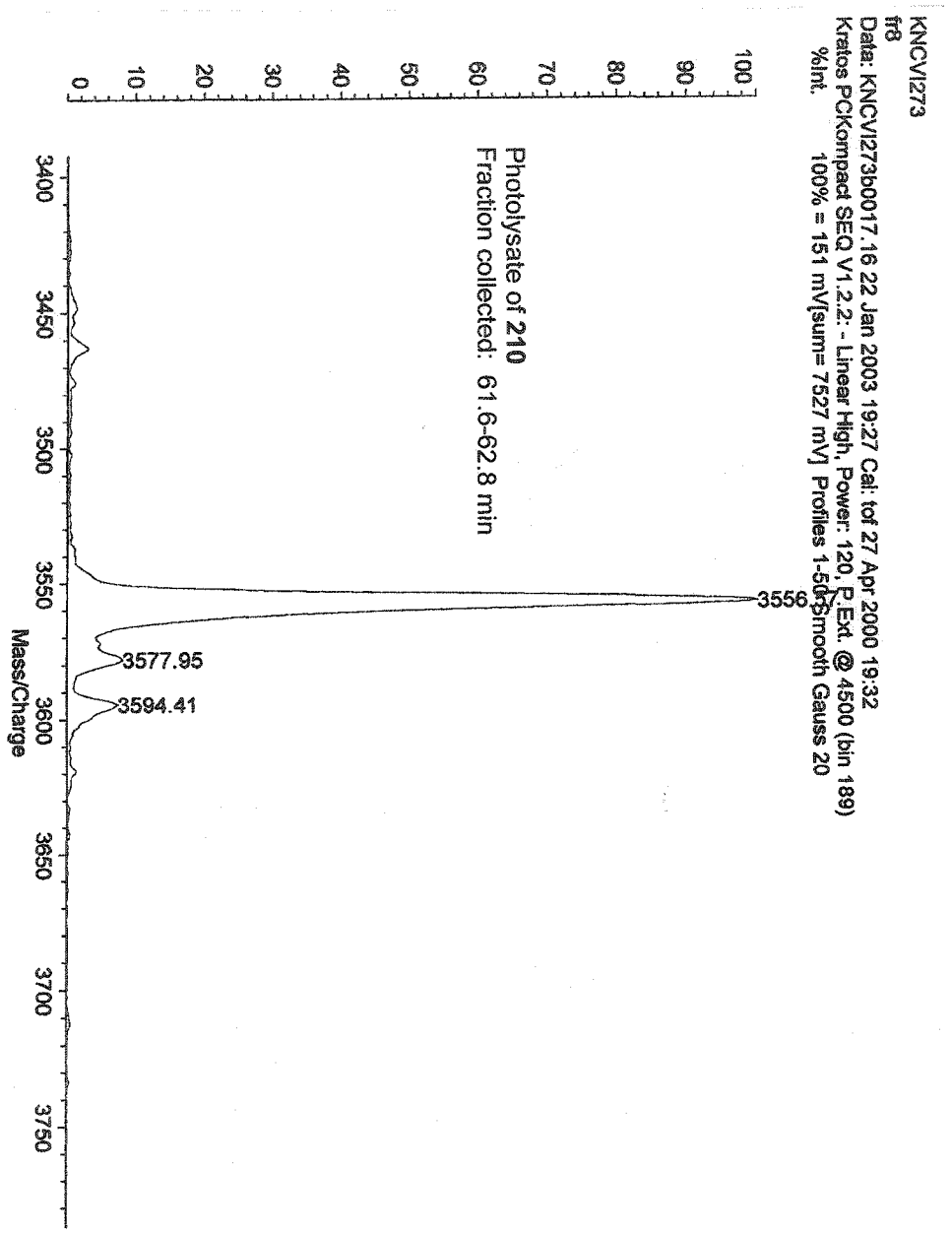

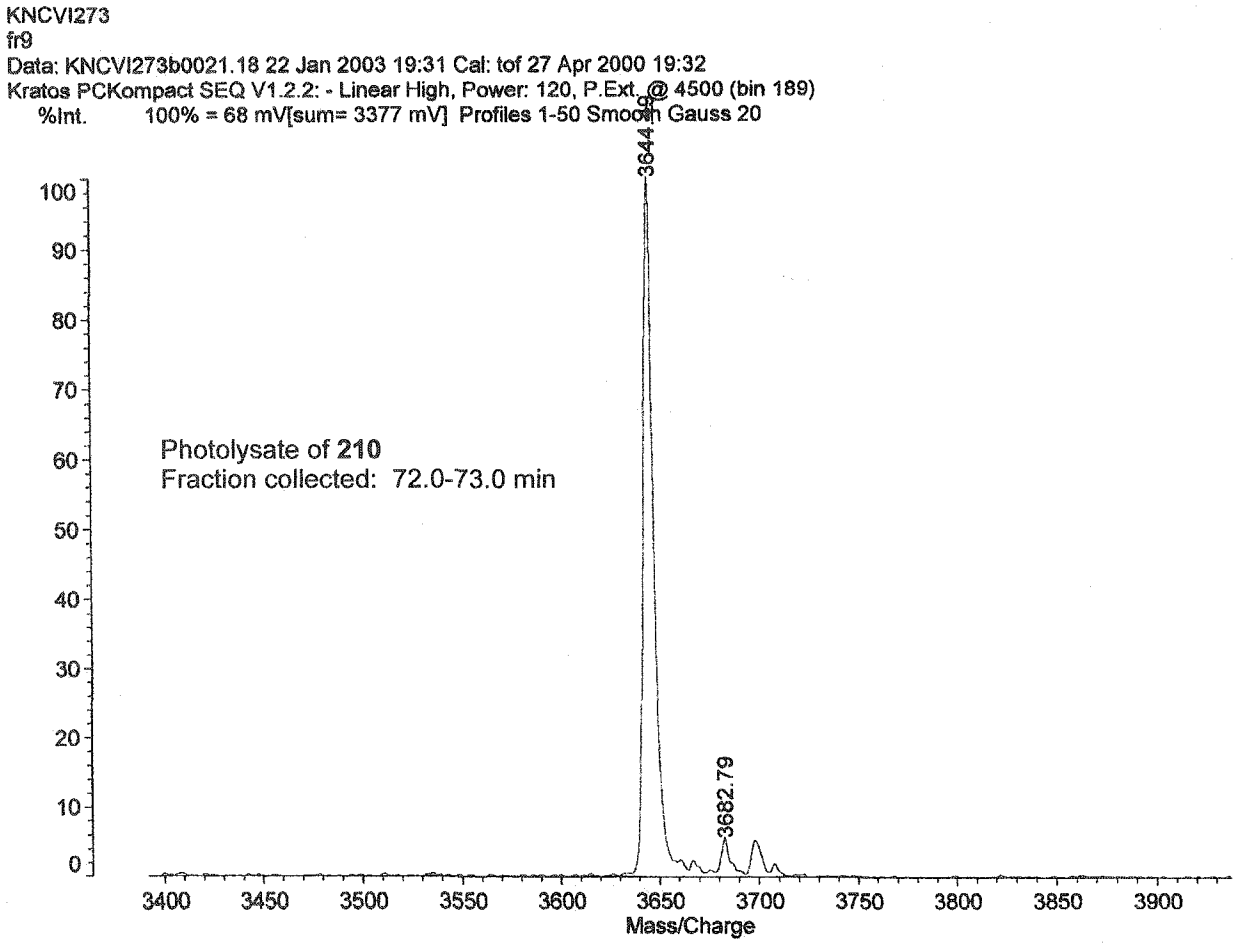

KNC7056
Fr4
Data: KNC0056.3 12 May 103 17:24 Cal: Nolan 12 May 103 16:03
Kratos Kompact MALDI 4 V5.2.1: - Linear High Power: 165, tDE @ 2000 (bin 78)

%Int. 100% =3 mV[sum= 130 mV] Profiles 1-40 Smooth Av 10 -Baseline 30

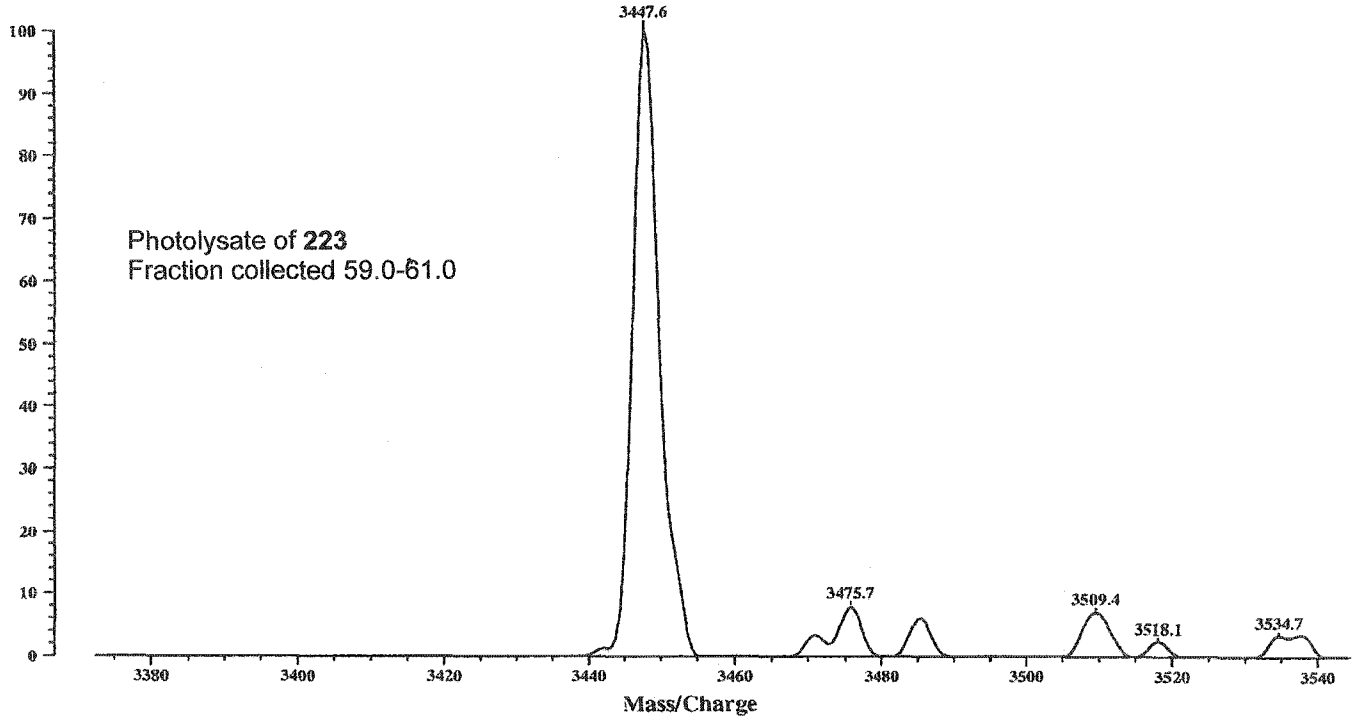

KNC7056
Fr6
Data: KNC0066.7 12 May 103 17:44 Cal: Nolan 12 May 103 16:03
Kratos Kompact MALDI 4 V5.2.1: - Linear High Power: 165, tDE @ 2000 (bin 78)

%Int. 100% =10 mV[sum= 532 mV] Profiles 1-50 Smooth Av 10 -Baseline 30

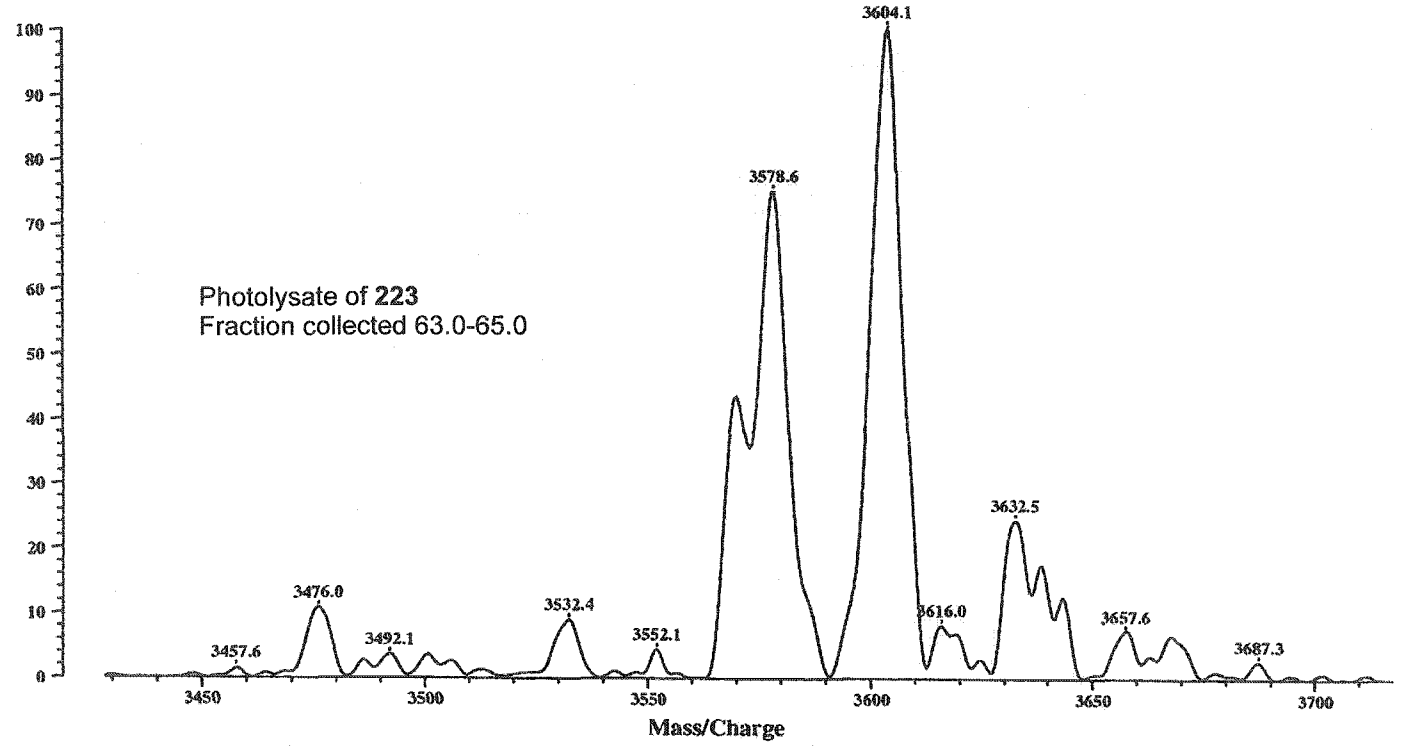

KNC7056
Fr7
Data: KNC0070.9 12 May 103 17:54 Cal: Nolan 12 May 103 16:03
Kratos Kompact MALDI 4 V5.2.1: - Linear High Power: 165, tDE @ 2000 (bin 78)

%Int. 100% =104 mV[sum= 5213 mV] Profiles 1-50 Smooth Av 10 -Baseline 30

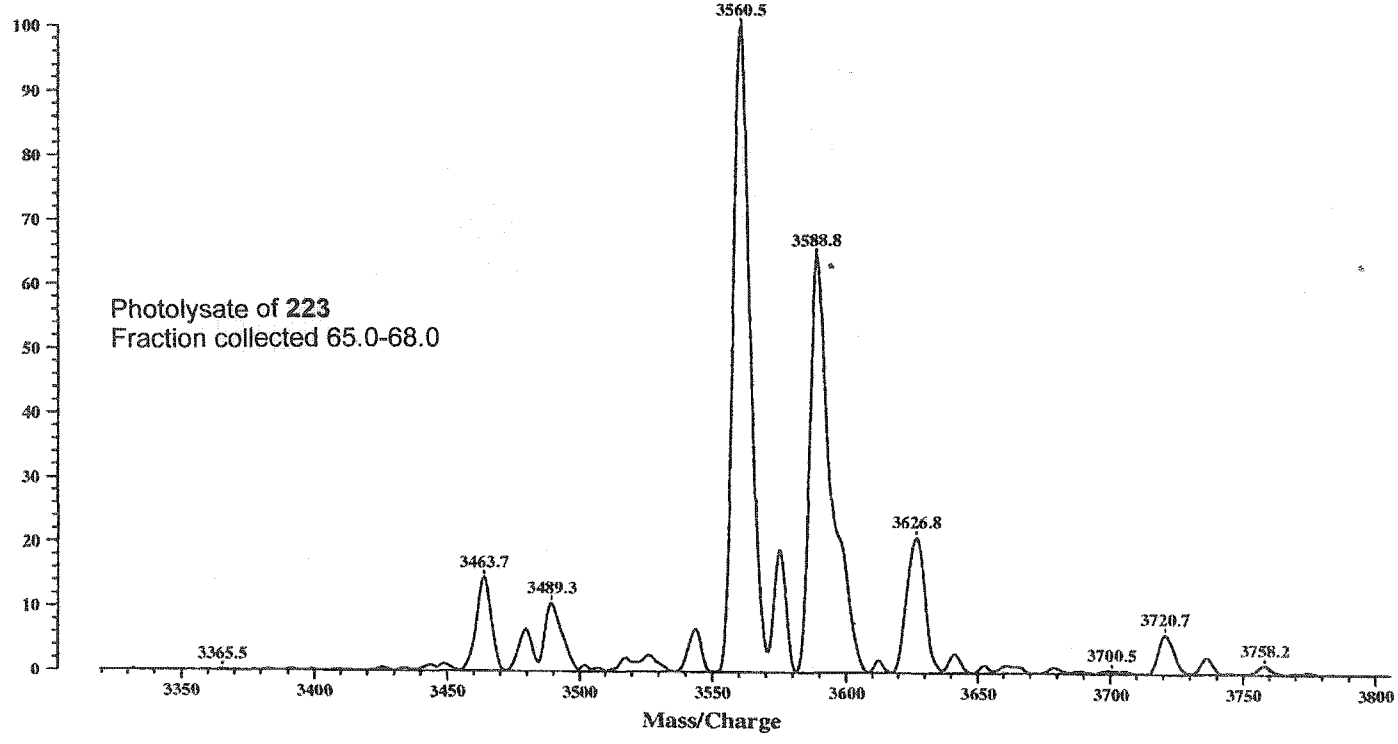

KNC7056
Fr8
Data: KNC0074.11 12 May 103 18:04 Cal: Nolan 12 May 103 16:03
Kratos Kompact MALDI 4 V5.2.1: - Linear High Power: 165, tDE @ 2000 (bin 78)

%Int. 100% =50 mV[sum= 2525 mV] Profiles 1-50 Smooth Av 10 -Baseline 30

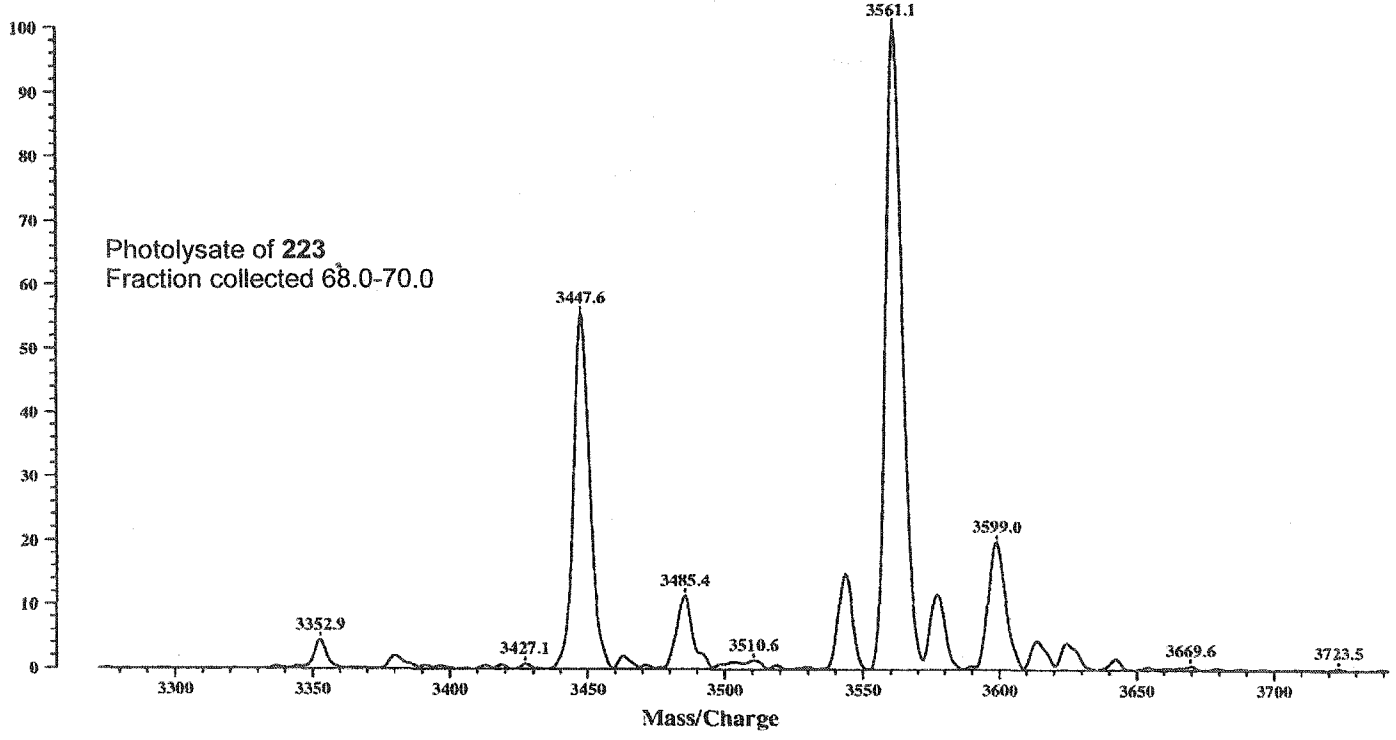

KNC7056
Fr9
Data: KNC0079.13 12 May 103 18:19 Cal: Nolan 12 May 103 16:03
Kratos Kompact MALDI 4 V5.2.1: - Linear High Power: 165, tDE @ 2000 (bin 78)

%Int. 100% =185 mV[sum= 9257 mV] Profiles 1-50 Smooth Av 10 -Baseline 30

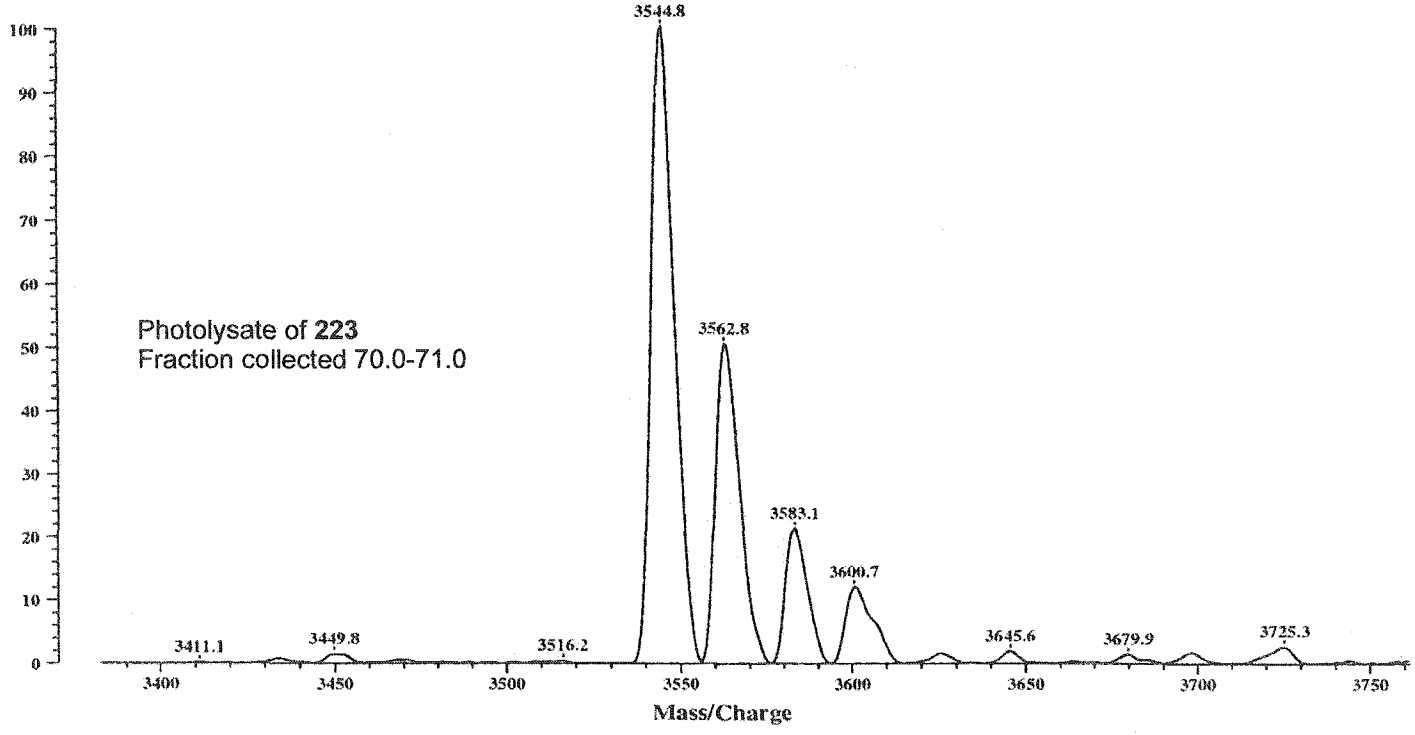

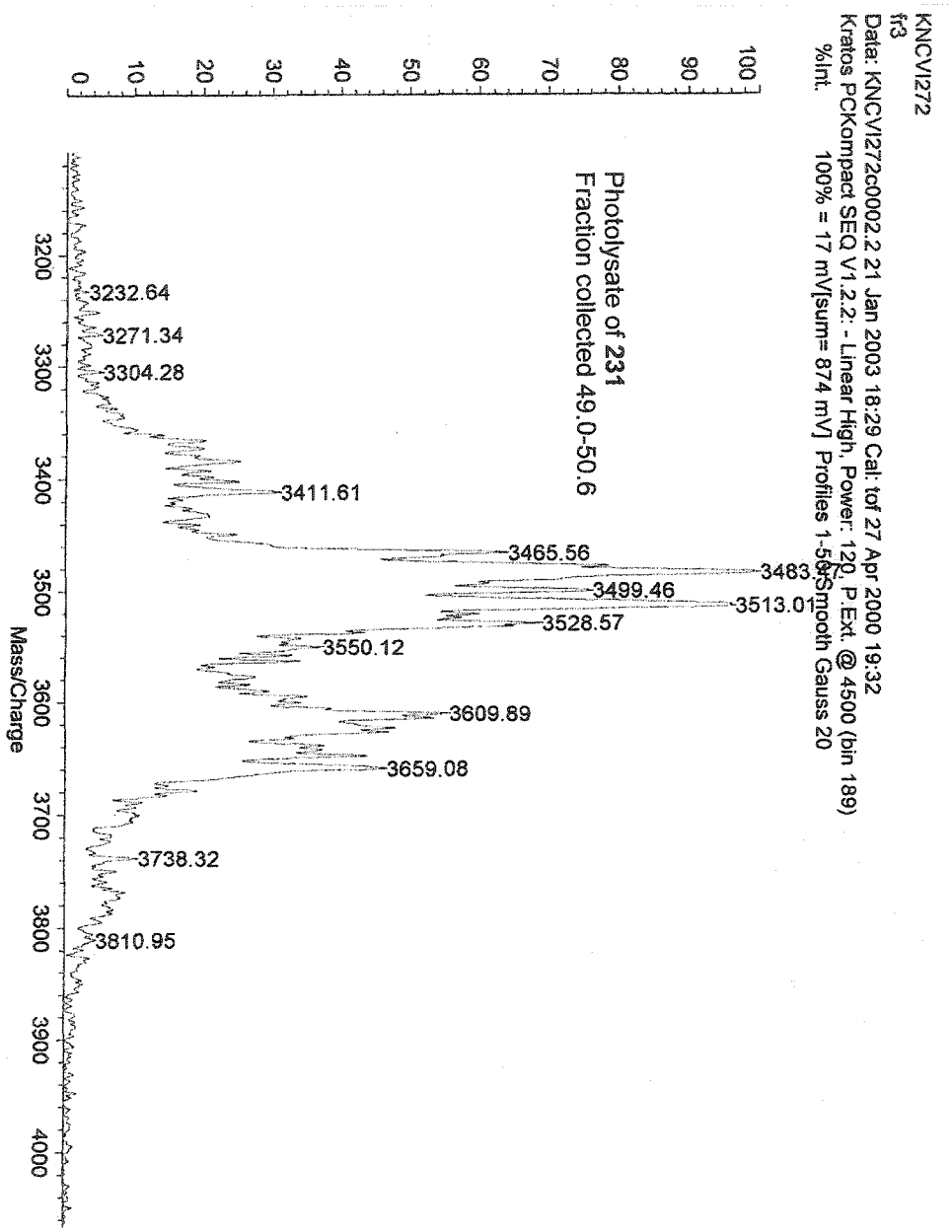

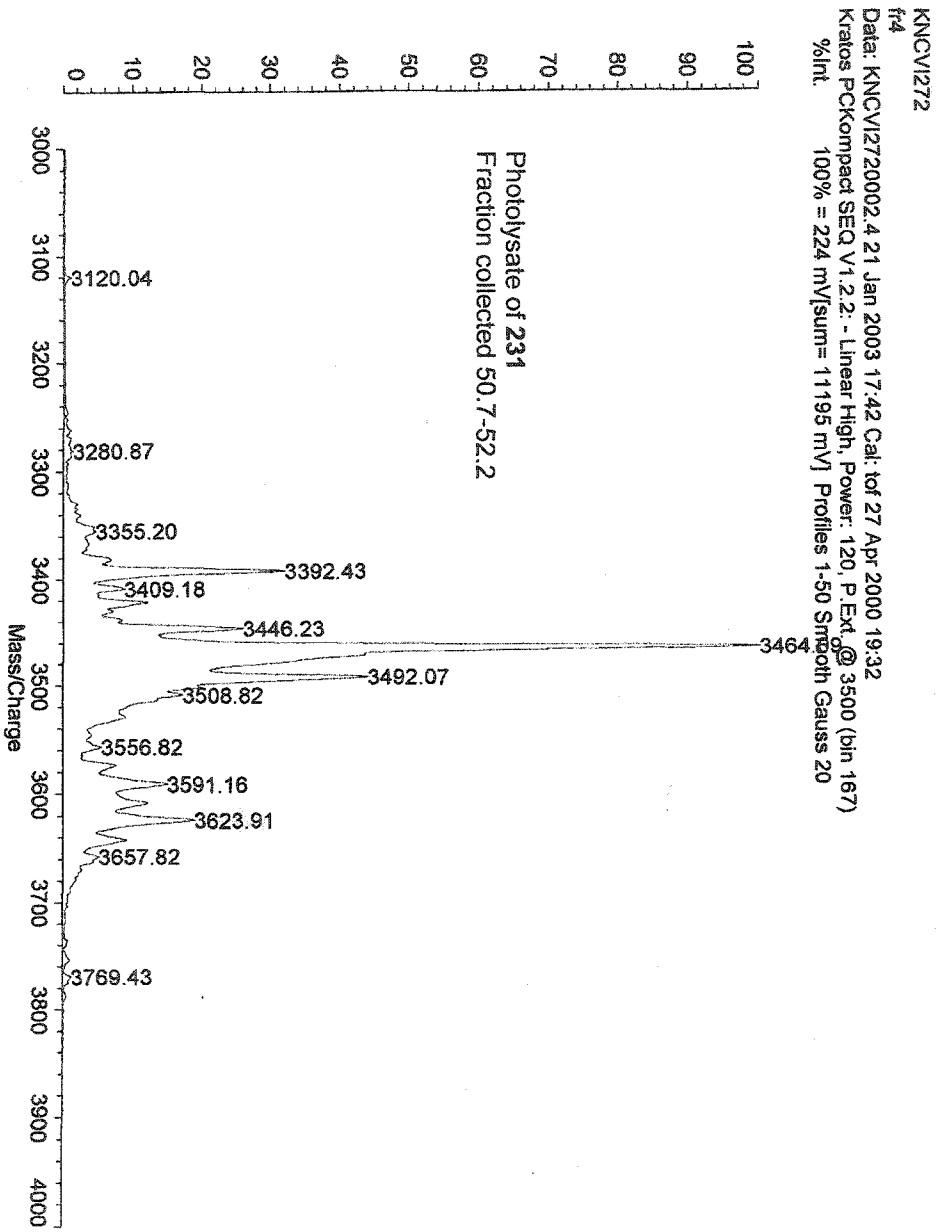

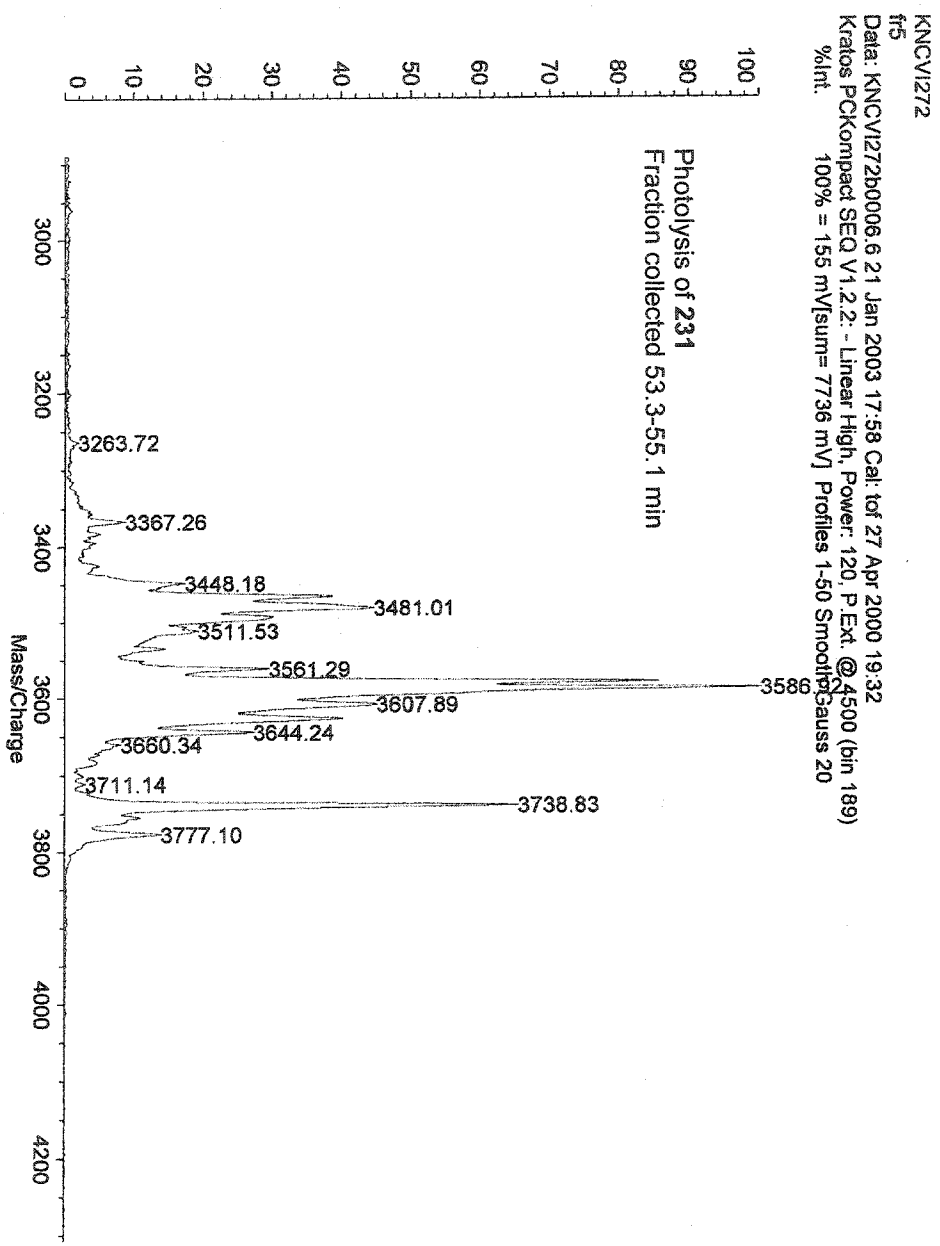

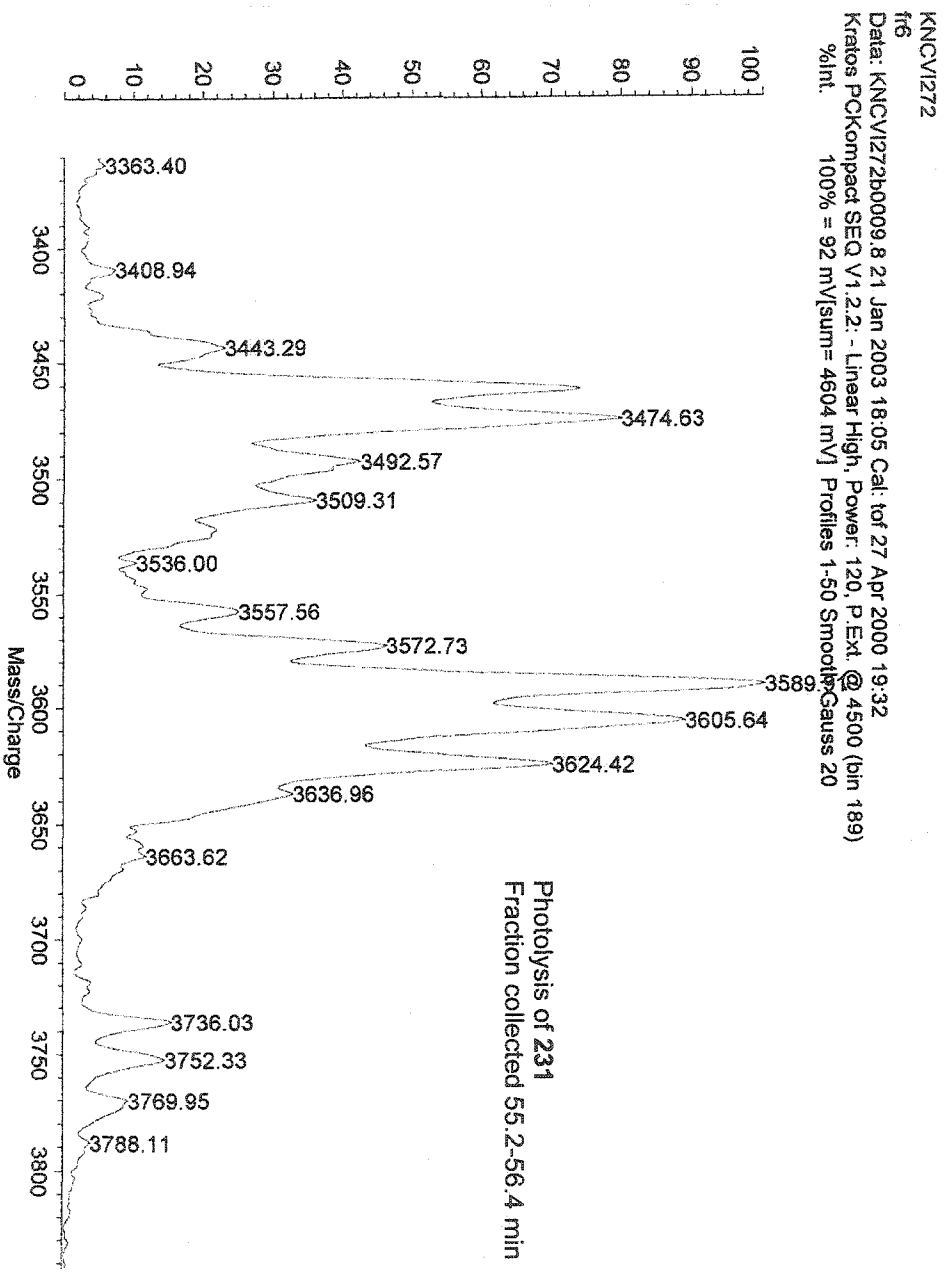

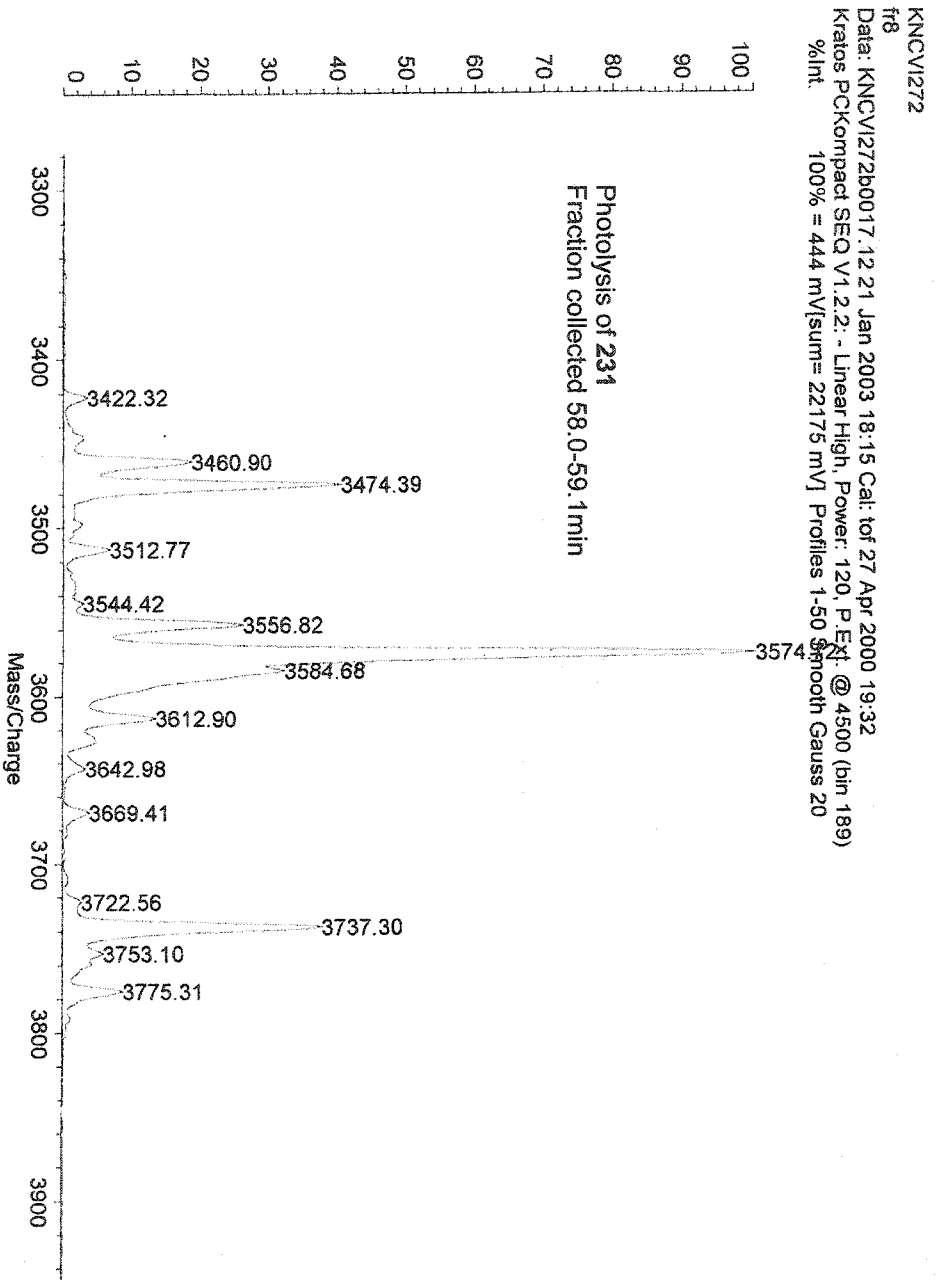

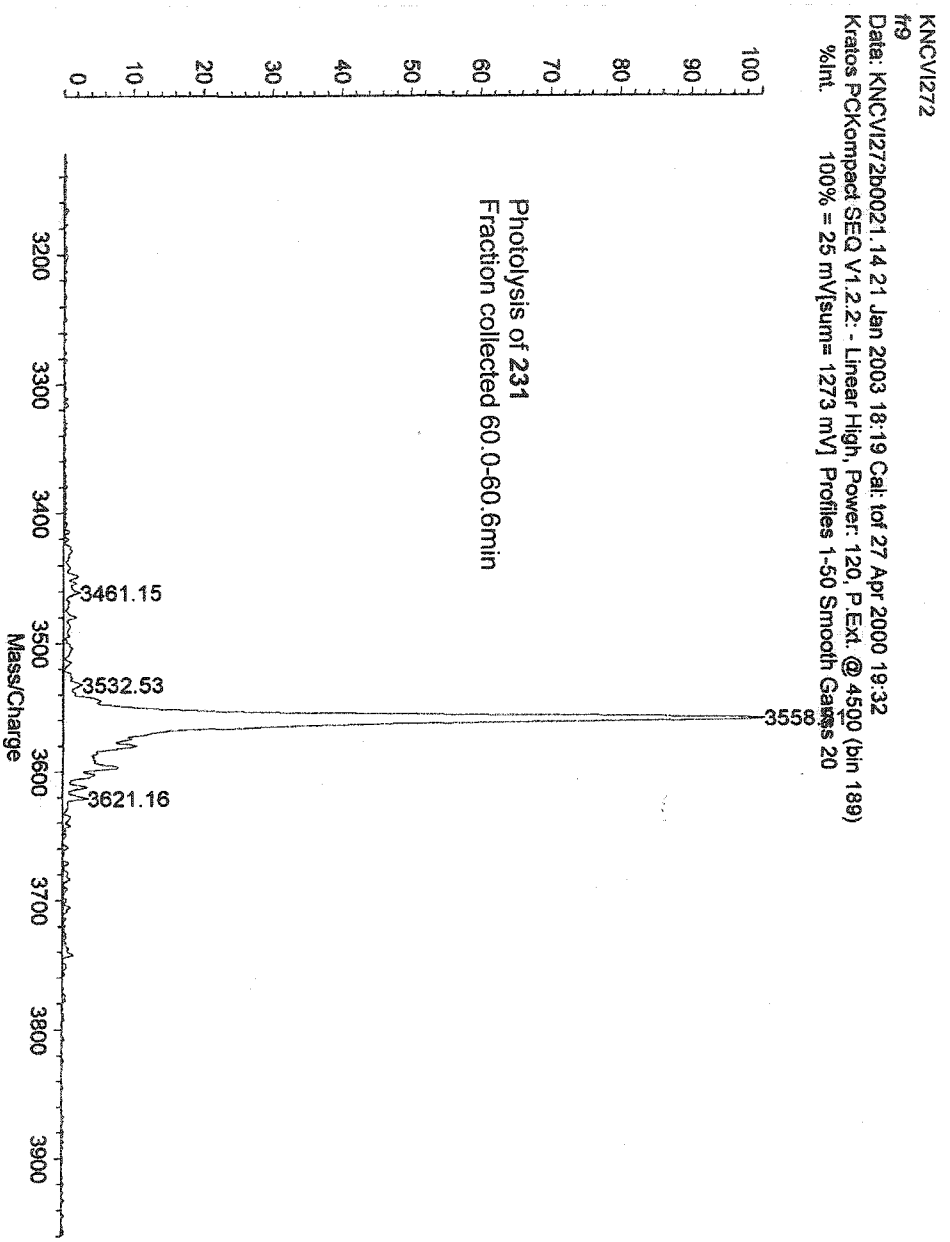

Appendix E: Supplementary Data Tables

Supplementary Table. The distribution of alkali-labile lesions in 5'-^{32}P-154[a]

Oxygen[b]	Site	Percentage of total lesions (NaOH)[c]	Percentage of total lesions (Piperidine)[d]	Piperidine induced lesions/ NaOH induced lesions[e]	Experiment
-	T_{17}	ND	11 ± 1	-	V060
	122a	ND	53 ± 6	-	
	T_{15}	ND	26 ± 2	-	
	dC_{14}	ND	10 ± 1	-	
	T_{17}	ND	11 ± 4	-	V064
	122a	ND	52 ± 13	-	
	T_{15}	ND	27 ± 7	-	
	dC_{14}	ND	10 ± 1	-	
	T_{17}	ND	12 ± 1	-	V076
	122a	ND	47 ± 4	-	
	T_{15}	ND	32 ± 4	-	
	dC_{14}	ND	9.0 ± 1.1	-	

Supplementary Table. The distribution of alkali-labile lesions in 5'-^{32}P-**154**[a]

Oxygen[b]	Site	Percentage of total lesions (NaOH)[c]	Percentage of total lesions (Piperidine)[d]	Piperidine induced lesions/ NaOH induced lesions[e]	Experiment
+	T_{17}	ND	5.0 ± 0.1	-	V058
	122a	ND	29 ± 1	-	
	T_{15}	ND	46 ± 1	-	
	dC_{14}	ND	20 ± 2	-	
	T_{17}	ND	5.0 ± 1.2	-	V060
	122a	ND	34 ± 3	-	
	T_{15}	ND	46 ± 4	-	
	dC_{14}	ND	15 ± 3	-	
	T_{17}	ND	5.0 ± 0.8	-	V063
	122a	ND	34 ± 2	-	
	T_{15}	ND	45 ± 4	-	
	dC_{14}	ND	16 ± 1	-	
	T_{17}	ND	5.0 ± 1.0	-	V064
	122a	ND	32 ± 2	-	
	T_{15}	ND	45 ± 3	-	
	dC_{14}	ND	18 ± 2	-	
	T_{17}	ND	7.2 ± 2.0	-	V070
	122a	ND	29 ± 1	-	
	T_{15}	ND	46 ± 1	-	
	dC_{14}	ND	18 ± 2	-	
	T_{17}	-	4.0 ± 0.3	-	VII024
	122a	25 ± 3	30 ± 1	3.9 ± 0.3	
	T_{15}	52 ± 8	48 ± 4	2.9 ± 0.4	
	dC_{14}	23 ± 4	18 ± 1	2.5 ±0.3	
	T_{17}	-	4.0 ± 0.9	-	VII046
	122a	25 ± 5	36 ± 4	5.6 ± 1.1	
	T_{15}	53 ± 6	48± 7	3.4 ±0.4	
	dC_{14}	22 ±5	12 ± 2	2.1 ± 0.5	

Supplementary Table. The distribution of alkali-labile lesions in 3'-^{32}P-**154**[a]

Oxygen[b]	Site	Percentage of total lesions (NaOH)[c]	Percentage of total lesions (Piperidine)[d]	Piperidine induced lesions/ NaOH induced lesions[e]	Experiment
-	dA_{18}	ND	14 ± 2	-	V193
	T_{17}	ND	16 ± 4	-	
	122a	ND	70 ± 6	-	
	T_{15}	ND	-	-	
+	dA_{18}	ND	6.0 ± 0.4	-	V193
	T_{17}	ND	33 ± 2	-	
	122a	ND	46 ± 2		
	T_{15}	ND	15 ± 2		
	dA_{18}	-	6.0 ± 1.7	-	VII024
	T_{17}	-	28 ± 6	-	
	122a	45 ± 7	46 ± 8	1.21 ± 0.16	
	T_{15}	55 ± 7	20 ± 3	3.29 ± 0.62	

Supplementary Table. The distribution of alkali-labile lesions in 5'-^{32}P-**159**

Oxygen[b]	Site	Percentage of total lesions (NaOH)[c]	Percentage of total lesions (Piperidine)[d]	Piperidine induced lesions/ NaOH induced lesions[e]	Experiment
-	T_{17}	ND	25 ± 3	-	V061
	122a	ND	54 ± 5	-	
	T_{15}	ND	14 ± 7	-	
	dC_{14}	ND	7.0 ± 0.6	-	
	T_{17}	ND	19 ± 3	-	V065
	122a	ND	61 ± 4	-	
	T_{15}	ND	11 ± 7	-	
	dC_{14}	ND	9.0 ± 1.0	-	
	T_{17}	ND	28 ± 9	-	V079
	122a	ND	52 ± 3	-	
	T_{15}	ND	15 ± 2	-	
	dC_{14}	ND	5.0 ± 0.5	-	

Supplementary Table. The distribution of alkali-labile lesions in 5'-^{32}P-**159**

Oxygen[b]	Site	Percentage of total lesions (NaOH)[c]	Percentage of total lesions (Piperidine)[d]	Piperidine induced lesions/ NaOH induced lesions[e]	Experiment
+	T_{17}	ND	8.0 ± 1.1	-	V061
	122a	ND	39 ± 2	-	
	T_{15}	ND	39 ± 4	-	
	dC_{14}	ND	14 ± 2	-	
	T_{17}	ND	9.0 ± 0.1	-	V065
	122a	ND	49 ± 4	-	
	T_{15}	ND	34 ± 3	-	
	dC_{14}	ND	8.0 ± 0.1	-	
	T_{17}	ND	8.0 ± 0.7	-	V071
	122a	ND	38 ± 2	-	
	T_{15}	ND	38 ± 1	-	
	dC_{14}	ND	16 ± 1	-	
	T_{17}	ND	8.0 ± 0.4	-	VI078
	122a	ND	47 ± 2	-	
	T_{15}	ND	32 ± 2	-	
	dC_{14}	ND	13 ± 1	-	
	T_{17}	ND	7.0 ± 1.1	-	VI025
	122a	ND	46 ± 3	-	
	T_{15}	ND	37 ± 2	-	
	dC_{14}	ND	10 ± 1	-	
	T_{17}	-	6.0 ± 1.3	-	VI034
	122a	52 ± 5	43 ± 3	2.53 ± 0.16	
	T_{15}	35 ± 4	41 ± 5	3.54 ± 0.44	
	dC_{14}	13 ± 2	10 ± 2	2.27 ± 0.49	
	T_{17}	-	5.0 ± 0.9	-	VI031
	122a	56 ± 14	50 ± 4	1.82 ± 0.38	
	T_{15}	33 ± 6	35 ± 2	2.18 ± 0.25	
	dC_{14}	11 ± 2	10 ± 1	1.64 ± 0.19	

Supplementary Table. The distribution of alkali-labile lesions in 3'-^{32}P-**159**

Oxygen[b]	Site	Percentage of total lesions (NaOH)[c]	Percentage of total lesions (Piperidine)[d]	Piperidine induced lesions/ NaOH induced lesions[e]	Experiment
-	dA_{18}	ND	15 ± 2	-	V194
	T_{17}	ND	26 ± 7	-	
	122a	ND	59 ± 10	-	
	T_{15}	ND	-	-	
	dA_{18}	ND	13 ± 1.1	-	V086
	T_{17}	ND	39 ± 6	-	
	122a	ND	48 ± 5		
	T_{15}	ND	-		
+	dA_{18}	ND	7.0 ± 1.4	-	V194
	T_{17}	ND	35 ± 6	-	
	122a	ND	48 ± 8		
	T_{15}	ND	10 ± 2		
	dA_{18}	-	6.0 ± 0.5	-	VI085
	T_{17}	-	49 ± 1.3	-	
	122a	69 ± 24	41 ± 2	0.76 ± 0.14	
	T_{15}	31 ± 9	4.0 ± 0.1	3.74 ± 1.00	
	dA_{18}	-	5.0 ±0.5	-	VI285
	T_{17}	-	41 ± 4	-	
	122a	73 ± 6	49 ± 2	0.74 ± 0.21	
	T_{15}	27 ± 4	5.0 ± 1.1	2.69 ± 0.23	
	dA_{18}	-	6.0 ± 0.9	-	VI287
	T_{17}	-	35 ± 6	-	
	122a	72 ± 16	52 ± 6	0.98 ± 0.23	
	T_{15}	28 ± 7	7.0 ± 1.4	2.78 ± 0.47	
	dA_{18}	-	6.0 ± 0.7	-	VII006
	T_{17}	-	32 ± 5	-	
	122a	56 ± 11	48 ± 4	2.47 ± 0.34	
	T_{15}	44 ±10	14 ± 2	0.84 ±0.21	

Supplementary Table. The effect of GSHOEt upon piperidine-lablity in the aerobic photolysates of 5'-^{32}P-**154**.[a]

[GSHOEt]	% Cleavage					Experiment
(μM)	T_{17}	**122a**	T_{15}	dC_{14}	Total	V063
-	2.8 ± 0.4	18 ± 0.1	24 ± 2	9.1 ± 0.4	54 ± 3	
5	2.5 ± 0.2	17 ± 0.7	18 ± 0.8	6.8 ± 0.6	45 ± 2	
50	2.8 ± 0.5	18 ± 0.2	7.8 ± 0.8	3.3 ± 0.4	31 ± 0.8	
500	2.9 ± 0.1	19 ± 0.9	3.6 ± 0.2	1.4 ± 0.1	27 ± 0.7	
5000	2.2 ± 0.2	22 ± 4	3.2 ± 0.2	1.1 ± 0.2	28 ± 4	
-	3.9 ± 0.3	16 ± 0.5	24 ± 0.3	9.7 ± 1.1	54 ± 0.3	V070
5	2.6 ± 0.2	15 ± 3	16 ± 8	5.4 ± 2.7	39 ± 14	
50	1.4 ± 0.2	18 ± 1	8.9 ± 1.6	2.5 ± 0.4	30 ± 3	
500	1.1 ±0.1	22 ± 0.4	6.1 ± 0.5	1.6 ± 0.1	31 ± 2	
5000	1.7 ± 0.1	23 ± 0.2	5.8 ± 0.3	1.3 ± 0.2	32 ± 0.1	

[a] % Cleavages are calculated as a function of total DNA per lane.

Supplementary Table. The effect of GSHOEt upon piperidine-lablity in the aerobic photolysates of 5'-^{32}P-**159**.[a]

[GSHOEt]	% Cleavage					Experiment
(μM)	T_{17}	**122a**	T_{15}	dC_{14}	Total	V062
-	3.5 ± 0.1	19 ± 4	17 ± 10	5.8 ± 4	45 ± 17	
5	4.3 ± 0.2	20 ± 1	18 ± 1	5.4 ± 0.1	48 ± 2	
50	4.7 ± 0.8	24 ± 2	11 ± 2	3.4 ± 1.0	44 ± 2	
500	2.2 ± 0.4	22 ± 1	5.8 ± 0.3	1.9 ± 0.1	32 ± 1	
5000	1.3 ± 0.2	24 ± 0.4	4.3 ± 0.2	1.4 ± 0.2	31 ± 0.6	
-	4.2 ± 0.3	19 ± 0.7	20 ± 0.5	7.9 ± 0.6	50 ± 1	V071
5	4.5 ± 0.2	18 ± 0.5	16 ± 3	5.3 ± 0.6	43 ± 4	
50	3.1 ± 0.3	18 ± 1	10 ± 0.6	3.5 ± 0.2	34 ± 0.3	
500	2.9 ± 0.5	21 ± 1	8.4 ± 0.3	2.1 ± 0.3	34 ± 2	
5000	1.7 ± 0.4	22 ± 1	7.0 ± 0.1	1.8 ± 0.1	32 ± 2	

[a] % Cleavages are calculated as a function of total DNA per lane.

Supplementary Table. The effect of GSHOEt upon piperidine-lablity in the degassed photolysates of 5'-^{32}P-**154**.[a]

[GSHOEt]	% Cleavage					Experiment
(μM)	T_{17}	**122a**	T_{15}	dC_{14}	Total	V076
-	2.8 ± 0.2	11 ± 1	7.2 ± 0.8	1.9 ± 0.2	23 ± 0.1	
5	3.0 ± 0.1	9.5 ± 0.1	6.7 ± 0.2	2.3 ± 0.1	22 ± 0.4	
50		11 ± 1	2.6 ± 0.3	1.9 ± 0.1	14 ± 2	
500		11 ± 2	2.1 ± 0.6	0.85 ± 0.1	14 ± 3.2	
5000		12 ± 0.1	2.3 ± 0.4	1.1 ± 0.2	15 ± 0.6	

[a] % Cleavages are calculated as a function of total DNA per lane.

Supplementary Table. The effect of GSHOEt upon piperidine-lablity in the degassed photolysates of 5'-^{32}P-**159**.[a]

[GSHOEt]	% Cleavage					Experiment
(μM)	T_{17}	**122a**	T_{15}	dC_{14}	Total	V079
-	8.6 ± 2.9	16 ± 0.5	4.7 ± 0.6	1.6 ± 0.1	31 ± 2	
5	4.5 ± 2.0	14 ± 0.7	3.9 ± 0.1	1.7 ± 0.2	24 ± 1	
50	2.4 ± 1.1	13 ± 1	3.7 ± 0.2	1.4 ± 0.2	21 ± 1	
500	-	12 ± 2	3.0 ± 0.8	1.4 ± 0.4	16 ± 3	
5000	-	12 ± 1	2.6 ± 0.2	1.4 ±0.1	16 ± 2	

[a] % Cleavages are calculated as a function of total DNA per lane.

Supplementary Table. Isotope Effects for C1' Hydrogen Atom Abstraction.

DNA	Base Treatment	Isotope Effect	Experiment
167 (ss)	Piperidine	1.85 ± 0.33	V293
		1.65 ± 0.30	VI004
		1.54 ± 0.18	V139
170 (ds)		1.98 ± 0.45	V294
		2.09 ± 0.40	VI005
167 (ss)	NaOH	4.06 ± 0.67	VI057
		4.56 ± 1.57	VI063
170 (ds)		4.32 ± 0.59	VI049
		4.42 ± 0.97	VI069
168 (ss)	Piperidine	1.11 ± 0.19	V140
170 (ds)		1.07 ±0.16	V148

Supplementary Table. Isotope Effects for C4' Hydrogen Atom Abstraction.

DNA	Base Treatment	Isotope Effect	Experiment
174 (ss)	Piperidine	2.02 ± 0.46	V267
		2.35 ± 0.45	V269
176 (ds)		1.28 ± 0.18	VI131
		1.89 ± 0.25	VI102
174 (ss)	NaOH	2.01 ± 0.52	VI058
		2.41 ± 0.76	VI064
176 (ds)		1.46 ± 0.38	VI052
		1.74 ± 0.34	VI070
		1.67 ± 0.33	VI131
175 (ss)	Piperidine	1.30 ± 0.13	V280
		1.10 ± 0.18	V287
177 (ds)		1.26 ± 0.20	V281
		1.16 ± 0.19	V288

Supplementary Table. Isotope Effects for C5' Hydrogen Atom Abstraction.

DNA	Base Treatment	Isotope Effect	Experiment
181 (ss)	Piperidine	0.76 ± 0.13	VI032
		0.59 ± 0.09	VI171
		0.67 ± 0.11	VI162
183 (ds)		0.78 ± 0.26	VI022
		0.78 ± 0.16	VI033
181 (ss)	NaOH	0.91 ± 0.08	VI171
		1.09 ± 0.16	VI162
182 (ss)	Piperidine	1.13 ± 0.29	VI041
184 (ds)		0.99 ± 0.15	VI033

Supplementary Table. NaOH and piperidine lability in aerobic photolysates of 5'-^{32}P-**188**.

Site	Percentage of total lesions (NaOH)[b]	Percentage of total lesions (Piperidine)[c]	Piperidine induced lesions/ NaOH induced lesions[d]	Experiment
T_{17}	-	3.0 ± 0.1	-	V210
122a	20 ± 3	32 ± 0.5	3.1 ± 0.3	
dHT_{15}	65 ± 7	52 ± 0.8	1.5 ± 0.1	
dC_{14}	15 ± 1	13 ± 0.5	1.5 ± 0.9	
T_{17}	24 ± 9	3.0 ± 0.3		VI031
122a	63 ± 2	37 ± 1	2.5 ± 0.1	
dHT_{15}	13 ± 1	51 ± 2	1.3 ± 0.1	
dC_{14}	-	9.0 ± 0.4	1.2 ± 0.1	

Supplementary Table. NaOH and piperidine lability in aerobic photolysates of 5'-^{32}P-**189**.

Site	Percentage of total lesions (NaOH)[b]	Percentage of total lesions (Piperidine)[c]	Piperidine induced lesions/ NaOH induced lesions[d]	Experiment
dHT_{17}		14 ± 1	-	VI078
122a	24 ± 8	30 ± 3	5.0 ± 1.2	
T_{15}	47 ± 14	37 ± 4	3.3 0.8	
dC_{14}	29 ± 6	20 ± 8	2.7 ± 0.3	
dHT_{17}	-	14 ± 2	-	VI082
122a	34 ± 11	35 ± 5	3.4 ± 0.9	
T_{15}	40 ± 14	34 ± 3	2.9 ± 0.3	
dC_{14}	26 ± 10	17 ± 6	2.2 ± 0.4	

Supplementary Table. NaOH and piperidine lability in aerobic photolysates of 5'-^{32}P-**190**.

Site	Percentage of total lesions (NaOH)[b]	Percentage of total lesions (Piperidine)[c]	Piperidine induced lesions/ NaOH induced lesions[d]	Experiment
dHT_{17}	-	5.0 ± 1.0	-	VI277
122a	19 ± 5	30 ± 4	2.6 ± 0.6	
dHT_{15}	62 ± 13	50 ± 4	1.4 ± 0.2	
dC_{14}	19 ± 4	15 ± 1	1.4 ± 0.3	
dHT_{17}	-	10 ± 1	-	VI284
122a	30 ± 5	31 ± 2	2.3 ± 0.4	
dHT_{15}	54 ± 6	44 ± 5	1.5 ± 0.1	
dC_{14}	16 ± 3	15 ± 2	1.6 ± 0.6	

Supplementary Table. NaOH and piperidine lability in aerobic photolysates of 3'-^{32}P-**188**.

Site	Percentage of total lesions (NaOH)[b]	Percentage of total lesions (Piperidine)[c]	Piperidine induced lesions/ NaOH induced lesions[d]	Experiment
T_{17}	-	32 ± 3	-	VI053
122a	30 ± 6	47 ± 3	3.8 ± 0.6	
dHT_{15}	70 ± 18	32 ± 3	0.74 ± 0.19	
T_{17}	-	30 ± 4	-	VI126
122a	43 ± 17	53 ± 9	4.3 ± 0.4	
dHT_{15}	57 ± 23	17 ± 5	1.0 ± 0.3	

Supplementary Table. NaOH and piperidine lability in aerobic photolysates of 3'-^{32}P-**189**.

Site	Percentage of total lesions (NaOH)[b]	Percentage of total lesions (Piperidine)[c]	Piperidine induced lesions/ NaOH induced lesions[d]	Experiment
dA_{18}	-	12 ± 3	-	VI085
dHT_{17}	25 ± 5	45 ± 5	7.8 ± 1.4	
122a	41 ± 6	29 ± 8	3.1 ± 0.9	
T_{15}	34 ± 12	14 ± 2	1.8 ± 0.7	
dA_{18}	-	11 ± 2	-	VI086
dHT_{17}	21 ± 8	46 ± 8	12 ± 4	
122a	52 ± 27	30 ± 3	3.0 ± 0.6	
T_{15}	27 ± 6	14 ± 2	2.7 ± 0.4	

Supplementary Table. NaOH and piperidine lability in aerobic photolysates of 3'-^{32}P-**190**.

Site	Percentage of total lesions (NaOH)	Percentage of total lesions (Piperidine)	Piperidine induced lesions/ NaOH induced lesions	Experiment
dA_{18}	-	6.0 ± 0.9	-	VI285
dHT_{17}	13 ± 5	44 ± 1	16 ± 5	
122a	34 ± 28	17 ± 3	2.2 ± 0.6	
dHT_{15}	53 ± 12	33 ± 4	2.8 ± 0.5	
dA_{18}	-	6.0 ± 1.1	--	VI287
dHT_{17}	16 ± 2	34 ± 3	7.5 ± 2.6	
122a	35 ± 8	21 ± 2	2.1 ± 0.3	
dHT_{15}	49 ± 10	39 ± 2	2.8 ± 0.4	

Supplementary Table. NaOH and piperidine lability in aerobic photolysates of 5'-^{32}P-**203**.

Site	Percentage of total lesions (NaOH)	Percentage of total lesions (Piperidine)	Piperidine induced lesions/ NaOH induced lesions	Experiment
dU_{17}	-	6.0 ± 0.7	-	VII25
122a	21 ± 6	26 ± 1	5.2 ± 1.1	
T_{15}	49 ± 13	46 ± 2	3.9 ± 0.8	
dC_{14}	30 ± 7	22 ± 1	3.2 ± 0.5	
dU_{17}	-	6.0 ± 0.6	-	VII34
122a	18 ± 3-	27 ± 1	4.1 ± 0.6	
T_{15}	54 ± 8	49 ± 1	2.5 ± 0.2	
dC_{14}	28 ± 5	18 ± 0.5	1.8 ± 0.2	

Supplementary Table. NaOH and piperidine lability in aerobic photolysates of 3'-^{32}P-**203**.

Site	Percentage of total lesions (NaOH)	Percentage of total lesions (Piperidine)	Piperidine induced lesions/ NaOH induced lesions	Experiment
dA_{18}	-	4.0 ± 0.6	-	VII001
dU_{17}	-	11 ± 1	-	
122a	41 ± 6	49 ± 5	4.8 ± 0.4	
T_{15}	59 ± 11	36 ± 5	2.4 ± 0.4	
dA_{18}	-	3.0 ± 0.4	-	VII006
dU_{17}	-	5.0 ± 1.0	-	
122a	62 ± 10	55 ± 1	3.0 ± 0.3	
T_{15}	38 ± 7	37 ± 2	3.3 ± 0.5	

Supplementary Table. The effect of D_2O upon piperidine lability in aerobic photolysates of 5'-^{32}P-**241**.[a]

Solvent	% Cleavage				
	dG_{17}	**122a**	dG_{15}	dC_{14}	Total
H_2O	4.9 ± 0.2	5.8 ± 0.3	7.4 ±0.6	0.52 ± 0.05	19 ±1
D_2O	4.6 ± 0.7	5.2 ±0.1	5.9 ± 0.3	0.49 ± 0.04	16 ± 1

[a] % Cleavages are calculated as a function of total DNA per lane.

Supplementary Table. The effect of D_2O upon piperidine lability in aerobic photolysates of 3'-^{32}P-**241**.[a]

Solvent	% Cleavage				
	dA_{18}	dG_{17}	**122a**	dG_{15}	Total
H_2O	0.54 ±0.04	15 ± 1	7.2 ± 0.6	2.1 ± 0.2	25 ± 1
D_2O	0.68 ± 0.10	15 ± 2	7.1 ± 1.3	2.6 ± 0.3	26 ± 2

[a] % Cleavages are calculated as a function of total DNA per lane.